



FRIEDRICH-SCHILLER- UNIVERSITÄT JENA

Friedrich-Schiller-Universität Jena

Chemisch-Geowissenschaftliche Fakultät

Organic redox-active materials for redox-flow batteries

Dissertation

(kumulativ)

zur Erlangung des akademischen Grades

doctor rerum naturalium (Dr. rer. nat.)

vorgelegt dem Rat der Chemisch-Geowissenschaftlichen Fakultät

der Friedrich-Schiller-Universität Jena

von Diplom-Chemiker Tino Hagemann

geboren am 06.04.1989 in Apolda

Gutachter:

- | | |
|---------------------------------|-------------------------------------|
| 1. Prof. Dr. Ulrich S. Schubert | Friedrich-Schiller-Universität Jena |
| 2. Prof. Dr. Andrea Balducci | Friedrich-Schiller-Universität Jena |

Tag der öffentlichen Verteidigung: 18.05.2018

Table of Content

Documentation of Authorship	4
1 Introduction	11
2 Flow batteries – General principles and rise of the organic active materials	15
2.1 General working principle of flow batteries and performance parameters.....	15
2.2 “The metal age” – metal-based flow batteries	18
2.3 “Rise of the organics” – organic-based flow batteries	20
3 Bipolar organic redox-active materials for application in symmetric redox- flow batteries.....	23
3.1 Nitronyl nitroxide containing redox-active material.....	23
3.2 TCAA derivative as redox-active material	27
4 A combined polymer/low-molar-mass-based aqueous redox-flow battery	33
5 Polymer-based redox-active materials for flow batteries	41
5.1 Poly(boron-dipyrromethene)s as potential bipolar polymer-based redox- active material	41
5.2 Statistically distributed linear TEMPO copolymers as cathode active material in a poly(TEMPO)/zinc hybrid-flow battery	44
5.3 Block copolymer micelles with a TEMPO-corona as cathode active material in a poly(TEMPO)/zinc hybrid-flow battery	48
6 Summary	53
7 Zusammenfassung.....	58
8 References	63
List of abbreviations	69
Curriculum vitae.....	71
Publication list	72
Acknowledgements / Danksagung.....	74
Declaration of Authorship / Selbstständigkeitserklärung	76

Documentation of Authorship

This section contains a list of individual authors' contributions to the publications reprinted in this thesis.

P1) "Redox-flow batteries: From metals to organic redox-active materials" J. Winsberg, ¹ T. Hagemann, ² T. Janoschka, ³ M. D. Hager, ⁴ U. S. Schubert, ⁵ <i>Angew. Chem. Int. Ed.</i> 2017 , 56, 686–711.					
Author	1	2	3	4	5
Conception of the manuscript	X	X		X	
Preparation of the manuscript	X	X	X		
Correction of the manuscript				X	X
Supervision of T. Hagemann				X	X
Suggestion crediting publication equivalents		0.5			

This publication has been also used in the cumulative PhD thesis of J. Winsberg; T. Janoschka. T. Hagemann and J. Winsberg contributed equally.

P2) "A bipolar nitronyl nitroxide small molecule for an all-organic redox-flow battery" T. Hagemann, ¹ J. Winsberg, ² B. Häupler, ³ T. Janoschka, ⁴ J. J. Gruber, ⁵ A. Wild, ⁶ U. S. Schubert, ⁷ <i>NPG Asia Mater.</i> 2017 , 9, e340.							
Author	1	2	3	4	5	6	7
Conceptual contribution	X						
Synthesis	X				X		
Electrochemical characterization	X	X					
Battery tests	X	X					
Correction of the manuscript		X	X	X	X	X	X
Supervision of T. Hagemann						X	X
Suggestion crediting publication equivalents	1.0						

This publication has been also used in the cumulative PhD thesis of J. Winsberg.

P3) "Synthesis and Electrochemical Study of a TCAA Derivative – A potential bipolar redox-active material" T. Hagemann, ¹ J. Winsberg, ² A. Wild, ³ U. S. Schubert, ⁴ <i>Electrochim. Acta.</i> 2017 , 228, 494–502.				
Author	1	2	3	4
Conceptual contribution	X			
Synthesis	X			
Electrochemical characterization	X	X		
Correction of the manuscript		X	X	X
Supervision of T. Hagemann			X	X
Suggestion crediting publication equivalents	1.0			

P4) "An aqueous all-organic RFB employing a (2,2,6,6-tetramethylpiperidin-1-yl)oxyl-containing polymer as catholyte and dimethyl viologen dichloride as anolyte" T. Hagemann, ¹ J. Winsberg, ² M. Grube, ³ I. Nischang, ⁴ T. Janoschka, ⁵ N. Martin, ⁶ M. D. Hager, ⁷ U. S. Schubert, ⁸ <i>J. Power Sources</i> 2018 , 378, 546–554.								
Author	1	2	3	4	5	6	7	8
Conceptual contribution	X				X	X		
Synthesis	X							
Characterization	X		X	X				
Electrochemical characterization	X							
Battery performance investigations	X	X						
Correction of the manuscript		X	X	X	X	X	X	X
Supervision of T. Hagemann							X	X
Suggestion crediting publication equivalents	1.0							

P5) “Poly(TEMPO)/zinc hybrid-flow battery: A novel, “green,” high voltage, and safe energy storage system” J. Winsberg, ¹ T. Janoschka, ² S. Morgenstern, ³ T. Hagemann, ⁴ S. Muench, ⁵ G. Hauffman, ⁶ J.-F. Gohy, ⁷ M. D. Hager, ⁸ U. S. Schubert, ⁹ <i>Adv. Mater.</i> 2016 , 28, 2238–2243.										
Author	1	2	3	4	5	6	7	8	9	
Conceptual contribution	X									
Polymer synthesis		X	X							
Electrochemical characterization	X			X	X					
Battery tests	X									
Correction of the manuscript		X		X	X		X	X	X	
Supervision of J. Winsberg								X	X	
Suggestion crediting publication equivalents				0.25						

This publication has been also used in the cumulative PhD thesis of J. Winsberg.

P6) “Polymer/zinc hybrid-flow battery using block copolymer micelles featuring a TEMPO corona as catholyte” J. Winsberg, ¹ S. Muench, ² T. Hagemann, ³ S. Morgenstern, ⁴ T. Janoschka, ⁵ M. Billing, ⁶ F. H. Schacher, ⁷ G. Hauffman, ⁸ J.-F. Gohy, ⁹ S. Hoeppener, ¹⁰ M. D. Hager, ¹¹ U. S. Schubert, ¹² <i>Polym. Chem.</i> 2016 , 7, 1711–1718.												
Author	1	2	3	4	5	6	7	8	9	10	11	12
Conceptual contribution	X											
Polymer synthesis								X	X			
Electrochemical characterization	X	X	X	X								
Battery tests	X											
TEM imaging										X		
DLS analysis	X					X	X					
Correction of the manuscript		X	X		X		X		X	X	X	X
Supervision of J. Winsberg											X	X
Suggestion crediting publication equivalents			0.25									

This publication has been also used in the cumulative PhD thesis of J. Winsberg.

P7) “Poly(boron-dipyrromethene) – A redox-active polymer class for polymer redox-flow batteries” J. Winsberg, ¹ T. Hagemann, ² S. Muench, ³ C. Friebe, ⁴ B. Häupler, ⁵ T. Janoschka, ⁶ S. Morgenstern, ⁷ M. D. Hager, ⁸ U. S. Schubert, ⁹ <i>Chem. Mater.</i> 2016 , 28, 3401–3405.									
Author	1	2	3	4	5	6	7	8	9
Conceptual contribution	X								
Polymer syntheses	X					X	X		
Electrochemical characterization	X	X	X	X					
Battery tests	X								
Correction of the manuscript		X	X	X	X	X		X	X
Supervision of J. Winsberg								X	X
Suggestion crediting publication equivalents		0.25							

This publication has been also used in the cumulative PhD thesis of J. Winsberg.

Jena, den

Erklärung zu den Eigenanteilen des Promovenden/der Promovendin sowie der weiteren Doktoranden/Doktorandinnen als Koautoren an den Publikationen und Zweitpublikationsrechten bei einer kumulativen Dissertation

Für alle in dieser kumulativen Dissertation verwendeten Manuskripte liegen die notwendigen Genehmigungen der Verlage („Reprint permissions“) für die Zweitpublikation vor.

Die Co-Autoren der in dieser kumulativen Dissertation verwendeten Manuskripte sind sowohl über die Nutzung, als auch über die oben angegebenen Eigenanteile informiert und stimmen dem zu (es wird empfohlen, diese grundsätzliche Zustimmung bereits mit Einreichung der Veröffentlichung einzuholen bzw. die Gewichtung der Anteile parallel zur Einreichung zu klären).

Die Anteile des Promovenden/der Promovendin sowie der weiteren Doktoranden/Doktorandinnen als Koautoren an den Publikationen und Zweitpublikationsrechten bei einer kumulativen Dissertation sind in der Anlage aufgeführt.

Name des Promovenden/der Promovendin	Datum	Ort	Unterschrift
--------------------------------------	-------	-----	--------------

Dipl.-Chem. Tino Hagemann

Ich bin mit der Abfassung der Dissertation als publikationsbasiert, d.h. kumulativ, einverstanden und bestätige die vorstehenden Angaben. Eine entsprechend begründete Befürwortung mit Angabe des wissenschaftlichen Anteils des Doktoranden/der Doktorandin an den verwendeten Publikationen werde ich parallel an den Rat der Fakultät der Chemisch-Geowissenschaftlichen Fakultät richten.

Name Erstbetreuer(in)	Datum	Ort	Unterschrift
Prof. Dr. U. S. Schubert			

1 Introduction

In 2016 the global electricity production was about 24,350 TWh,^[1] whereby the main part (almost 40% in 2014) was generated by coal-fired power stations, followed in some distance by gas, hydroelectric, nuclear and oil plants.^[2] In addition to this, the greenhouse gas emissions are highest for coal plants with an average life-cycle emission rate of 1 kg carbon dioxide (CO₂) per kWh of generated electricity.^[3-6] Therefore, starting from the industrial era, the carbon dioxide concentration within the atmosphere rose dramatically since the first measurements in 1750 from 277 ppm to 406 ppm in May 2017.^[7, 8] Unfortunately, the climate change is mainly a result of the greenhouse gas emissions, in particular of CO₂.^[6, 9-12] In recent years this has resulted in a rethinking of the world energy production towards renewable energy resources such as solar and geothermal energy as well as hydropower, wind power, and biomass, in order to reduce the CO₂ emissions.^[13-17] In particular Germany, which decided by law (Erneuerbare Energien Gesetz) for 2030 and 2050 a minimum proportion of renewable energy for the generation of electricity of 50% and 80%, respectively, promote this “Energiewende”.^[18, 19] In 2015, 29% of the total gross electricity generation are covered by renewable energies in the European Union,^[20] while the global shares of electricity generation from renewable resources lies at 24.5%.^[21] However, according to the International Energy Outlook 2016 (IEO2016), the renewable resources with an increase of 2.9% per year are the fastest growing sources. This is urgently required because the IEO2016 estimates a growth of the net electricity production of 69% by 2040, which means numerical 36,500 TWh.^[22] Today, hydropower is the primary and with a worldwide share of 71% (equal to about 16% of total electricity production) the most widely used renewable energy source.^[23] Nevertheless, hydroelectricity as well as geothermal energy requires necessarily some principal conditions like certain geographical circumstances and are, therefore, limited for a use in all parts of the world.^[14, 17, 24] Due to the fact that for the mentioned reasons a further growth of hydroelectricity is restricted (growth rate of 2.7% in 2015), in particular the rapidly emerging solar energy and wind power (growth rate of 28% and 17%, respectively, in 2015) will become the most important and widely used renewable energy resources in future.^[17, 21, 24] Unfortunately, today’s electricity grids are constructed for electric power systems, which utilizing fossil fuels and feature the simple working principle burning fuel to generate power on demand. However, they are not suitable for an intermittent

electricity generation, which depends on weather, time of day and year, by wind and solar power.^[16, 24-26] Accordingly, during the sunny midday time and windy days surplus electricity (production surpass the energy demand) is available, while at a “Dunkelflaute” (cloudy and windless periods) little or no energy is produced.^[6, 19, 27-29] Another difficulty to manage is that most of the renewable resources are locally limited and often far apart from load centers. Furthermore, in recent times common power plants (output >1 GW) are increasingly substituted by decentralized power systems like wind turbines (output up to 2.5 MW) and roof top photovoltaics (output of in maximum 10 kW).^[13, 19, 30] Taking all these circumstances, the actual electricity grids have to be refined to “green” future grids to render the “Energiewende” successfully. These so called “smart grids” have to unite the intermittent renewable energy production, decentralized small scale power plants, a intelligent (demand) energy management and low-cost energy storage.^[6, 13, 16, 26, 31] Potential energy storage technologies are pumped hydro and compressed air, thermal storage, flywheels, superconducting magnetic energy storage as well as electrochemical energy storage.^[6, 24, 26, 29, 31, 32] Secondary batteries in which electrical energy is stored as chemical energy, are besides supercapacitors, a prevalent type of electrochemical energy storage.^[6, 29, 33] The development of secondary batteries starts in the middle of the 19th century with lead acid (Gaston Planté in 1860),^[34] leading over nickel/cadmium (1899),^[29] sodium/sulfur (Ford in the late 1960s)^[6, 35] and nickel/metal hydride (mid 1980s)^[29] to Li ion (early 1970s),^[36] which are still the most used systems.^[6, 29, 37] However, these systems exhibit serious drawbacks like a short lifetime, serveral safety concerns and exessive costs.^[37] Redox-flow batteries (RFBs), on the other hand, are a comperative newer and unfamiliar technology,^[37] but display significant benefits concerning their lifetime, expenses, safety aspects, modularity, transportability and flexible applicability.^[13, 37, 38] Furthermore, RFBs are due to various reasons a most promising technology for storage of wind and solar power: This kind of secondary battery, which is technically akin to electrochemically regenerative fuel cells, can be precisely adjusted to the generator unit. Contrary to other electrochemical storage systems, RFBs can additionally be scaled independently from each other in capacity as well as power, simply by separate dimensioning of the volume of the external electrolyte reservoirs (tanks) and the electrochemical cell (stack). Furthermore, RFBs are able to store electricity in kWh to MWh scale in the short- to medium term (seconds to few hours) and can be sited almost

anywhere, consequently also in decentralized regions and, therefore, perfectly meet the requirements profile of a within the “Energiewende” required energy storage device.^[6, 13, 24, 29, 30, 32, 37, 39]

Common RFBs, like the commercially available all-vanadium redox-flow battery (VRFB),^[40-42] the Fe/Cr^[43-45] system and the zinc/bromine^[46-48] hybrid-flow battery (HFB), normally utilize critical and high-priced metal salts, hazardous and corrosive acidic electrolytes (sulfuric acid) and furthermore high-priced ion-exchange membranes such as Nafion[®] (DuPont, USA).^[13, 39, 49-51] For these reasons, these systems will highly probably not become a profound “green” energy-storage solution in future and, therefore, outline just the early stage of commercialization. Nevertheless, in particular the zinc/bromine HFB, offers a developmental potential. Because the utilization of the zinc(II)/zinc(0) redox couple as anode active material exhibit certain benefits like environmental friendliness, a low price of the raw material and a low endangerment, which, however, due to the usage of a toxic and harmful halogen such as bromine or polyiodide as cathode active material, and required complexing agents, are seriously restricted.^[49, 52-55] Though, these limitations can be overcome by the usage of convenient and ideally environmentally sustainable as well as cost-effectively redox-active organic charge-storage materials, whose solubility and electrochemical properties can be adjusted by the aimed introduction of substituents and functional groups, instead of inorganic halogens.^[13, 49, 52, 56] Further, to eliminate the other drawbacks of the common metal-based RFBs, the development of all-organic flow batteries, employing low-cost organic low-molar-mass compounds or polymers as charge-storage materials, aqueous electrolyte systems and inexpensive membranes.^[13, 39, 49, 57] In particular, organic symmetric RFBs, virtually a VRFB analog,^[42] which utilize one bipolar organic material as catholyte and anolyte respectively, are due to the simplified cell design, the considerably less synthesis effort and the resulting prevention of cross-contamination, are of great interest.^[57-60] Since, at the beginning of this thesis no highly qualified organic charge-storage material are known, new redox-active organic materials have to be investigated and evaluated in detail to ensure their suitability for application in a RFB.

In this thesis, low-molar-mass- as well as polymer-based organic charge-storage materials for the usage in all-organic symmetric redox-flow batteries are described. Also, an all-organic combined RFB (polymer and low-molar-mass-compound as active

materials) and zinc/organic hybrid-flow batteries are described. Adapted to the requirements of the respective kind of flow battery, tailor-made redox-active organic materials (in terms of their solubility as well as electrochemical properties) were synthesized for aqueous and non-aqueous electrolyte systems. In **Chapter 3** two bipolar low-molar-mass compounds, a nitronyl nitroxide containing and a 2,3,7,8-tetracyano-1,4,5,6,9,10-hexazaanthracene (TCAA) derivative, were investigated in detail concerning their suitability as charge-storage materials for an application in a non-aqueous symmetric RFB.

Besides redox-active low-molar-mass compounds, which are distinguished by none or less synthesis effort, good viscosities and solubilities, redox-active organic polymers are highly interesting as charge-storage materials. Due to their large size, polymer-based active materials allow the usage of inexpensive porous separators instead of the common used high-priced ion-exchange membranes. Take advantage of the benefits of both systems seems obvious. As a consequence, **Chapter 4** deals with a combined all-organic aqueous RFB, whereby for the first time a polymer as well as a low-molar-mass-compound as active materials were utilized. Furthermore, to achieve maximum long-term cycling stability and the preferably best battery performance, essential key factors of a flow battery like the suitability of the separator, the concentration of the supporting electrolyte and the flow rate of the electrolytes were investigated.

In **Chapter 5** the focus is on polymer-based flow batteries. In this context (2,2,6,6-tetramethylpiperidine-1-yl)oxyl (TEMPO) containing co-polymers as catholyte with zinc as anode were investigated in detail in poly(TEMPO)/zinc hybrid-flow batteries. Furthermore, polymers containing the potential bipolar boron-dipyrromethenes (BODIPYs) as redox-active units, are investigated regarding their applicability in symmetric polymer-based redox-flow batteries (pRFBs).

2 Flow batteries – General principles and rise of the organic active materials

Parts of this chapter have been published in **P1**) J. Winsberg, T. Hagemann, T. Janoschka, M. D. Hager, U. S. Schubert, *Angew. Chem. Int. Ed.* **2017**, 56, 686-711.

2.1 General working principle of flow batteries and performance parameters

In general, redox-flow batteries (RFBs) consist of two crucial components (**Figure 2.1a**): The electrochemical cell and two external electrolyte reservoirs (storage tanks). The electrochemical cell in turn involves two electrodes, which are detached by a separator. Between these components a electrolyte solution, containing the redox-active charge-storage materials, which are in their charged as well as discharged form in solution (this is why they were defined as anolyte and catholyte, respectively), is recirculated through pumps. Therefore, the utilized electrodes only supply the active area for the redox process, instead as usual participating in it. Nevertheless, they have to fulfill essential criteria such as a high electrical conductivity as well as specific surface area, chemical inertness towards the employed electrolytes and furthermore stability in the utilized operating potential range of the flow battery.^[61-63]

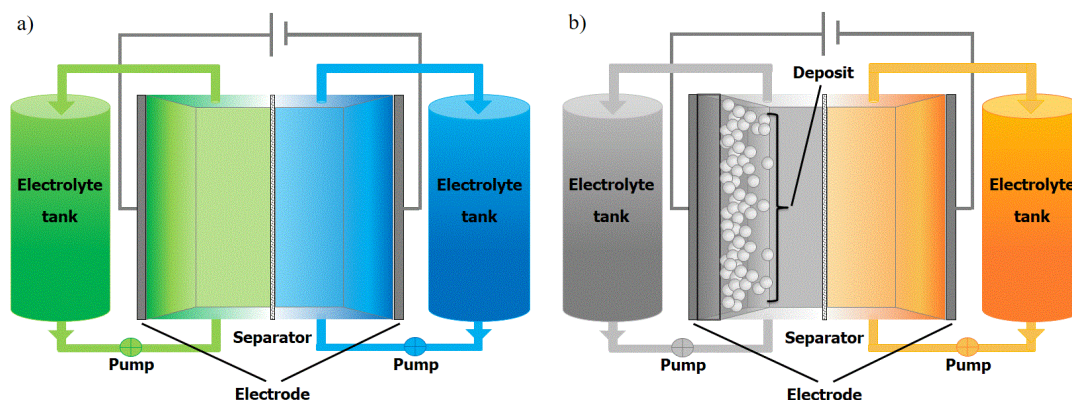


Figure 2.1: (a) Schematic representation of a redox-flow battery, which consists of an electrochemical cell with two compartments, detached by a membrane. The electrolytes are circulated by pumps between the electrochemical cell and the storage tanks. (b) Schematic representation of a hybrid-flow battery, a special type of flow batteries, whereby at least one redox-active material is electroplated in the charging/discharging process on one electrode.

To avoid an inappropriate mixture of both electrolytes the employed separator, another essential factor of a RFB, must be impermeable to the charge-storage material, but at the same time highly permeable for the supporting electrolyte (conducting salt) ions.^{[37,}

^{38]} Beside the charge-storage materials the separator represents the main cost element of

a flow battery,^[64] and furthermore feature a decisive effect of the battery performance parameters like lifetime (mechanical and chemical inertness), current and energy density.

In the particular case that one of the two half-cells contains a gaseous material such as hydrogen or exhibit at least one redox pair with a solid redox state this kind of flow battery is named hybrid-flow battery (HFB, **Figure 2.1b**). Thereby, the solid active material, commonly a metal like zinc or a metal oxide (*e.g.*, PbO₂) is electroplated on a anode or cathode, respectively, while charging/discharging but in the reversal process dissolves again. However, the possible formation of metallic dendritic structures from the metal deposition could cause restrictions of the battery performance (capacity, power density, stable battery cycling). Therefore, the design of the flow cell has to be adjusted to this specific circumstances.^[37, 65]

Besides the fundamental components such as electrodes and separator (detailed consideration in **Chapter 4**) several key factors like the utilized electrolyte system (aqueous or non-aqueous media), the concentration of the conducting salt, the flow rate of the electrolytes and above all the charge-storage material have a decisive effect on the performance of the flow battery. The battery performance can be determined by specific parameters such as the volumetric capacity (*C*), current (*J*) and energy density (*E*), coulombic (*CE*), voltage (*VE*) and energy efficiency (*EE*), which are particularly influenced by the active material. For example the volumetric capacity (Eq. 1, in Ah L⁻¹) is significant characterized by the number of transferred electrons (*n*) during the redox process and the quantity of the redox-active material in the electrolyte. By use of the volumetric capacity and the voltage (*U*) the energy density (Eq. 2, in Wh L⁻¹) can be calculated.

$$C = \frac{m \cdot n \cdot F}{M \cdot V} \quad (1)$$

$$E = C \cdot U \quad (2)$$

C = volumetric capacity, *m* = mass, *n* = number of electrons, *F* = Faraday's constant, *M* = molar mass, *V* = volume; *E* = energy density, *U* = voltage.

Ideally the energy density should be as high as possible. To achieve this, the charge-storage material has to feature a high volumetric capacity, what can be reached by a low-molar-mass of the compound or monomer and the transfer of more than only one

electron during the redox process, a high cell voltage and a high solubility in the applied solvent. On the other hand, the current density (J , Eq. 3, in A cm^{-2}), which affect the charge and discharge time of the flow battery, is defined by the applied current (I) and the membrane area (A).

$$J = \frac{I}{A} \quad (3)$$

The current density is affected by the kinetics of the redox reactions and the electrolyte system. Aqueous systems display compared to non-aqueous systems higher conductivities and consequently higher applicable current densities.^[52] Furthermore, the coulombic (Eq. 4, in %) and voltage efficiency (Eq. 5, in %) delivers valuable data about the electrical quality of the battery. Their product results the energy efficiency (Eq. 6, in %).

$$CE = \eta_c = \frac{Q_D}{Q_C} \quad (4)$$

$$VE = \eta_V = \frac{\frac{\int_0^{T_D} E_D(t) dt}{T_D}}{\frac{\int_0^{T_C} E_C(t) dt}{T_C}} = \frac{\overline{E}_D}{\overline{E}_C} \quad (5)$$

$$EE = \eta_{EE} = \eta_c \cdot \eta_V \quad (6)$$

η = efficiency; Q = charge; T = time for charging/discharging; E = potential. Subscripts: C = charging, D = discharging.

The CE is the ratio of the amount of charge applied during the discharge process (Q_D) and the amount of charge applied during the charge process (Q_C) of the same cycle. Ideal values for the CE are equal or superior to 99%. Lower values are a indication for undesired side reaction of the charge-storage material or electrolyte or of a membrane crossover of the active material. The VE , however, is calculated at constant current by the quotient of the mean discharging voltage (\overline{E}_D) and the mean charging voltage (\overline{E}_C) and is influenced by several overpotentials such as the polarization, ohmic and diffusion overpotential.^[66-68]

To achieve the best battery performance all these factors need to be considered and a suitable combination has to be developed. Starting with the electrolyte system, whereby an aqueous system is preferred due to the high ionic conductivity. However, by the utilization of organic charge-storage materials in aqueous media several disadvantages occur like the usually low solubility in water and the limited potential window of water. In organic solvents these problems do not occur, but they feature otherwise only a low conductivity which restricted the current rating. Also the choice of the charge-storage material, whereby a organic-based is preferred, is subjected to several key factors such as highly stable and reversible redox reactions, high solubility in the applied solvent, high volumetric capacity, low viscosity and furthermore economic as well as environmental aspects.

2.2 “The metal age” – metal-based flow batteries

The history of RFBs dates back to the year 1949, when Kangro patented the first flow battery, which used in one embodiment $\text{Cr}(\text{SO}_4)_2$ in 2 M sulfuric acid as catholyte and anolyte, respectively, and in an other embodiment a $\text{Cr}(\text{SO}_4)_2$ as anode and TiCl_4 as cathode active material.^[69, 70] Since 1973 the National Aeronautics and Space Administration (NASA) under Hagedorn and Thaller investigated RFBs, employing the $\text{Cr}^{3+}/\text{Cr}^{2+}$ as anolyte and the $\text{Fe}^{3+}/\text{Fe}^{2+}$ redox pair as catholyte, dissolved in acidified electrolytes, intensively as stationary energy storage systems. Unfortunately, the reported 1 kW/13 kWh redox system exhibited a fast capacity decay and, therefore, a restricted battery performance. This was caused by a crossover of the active materials across the used anion-exchange membrane, because at this time suitable membranes were not commercially available wherefore own manufactured membranes, which did not meet the demands, had to be employed.^[44, 71] In 1986, Skyllas-Kazacos *et al.* developed the VRFB, which represents since then the most advanced and dominant RFB technology. As redox-active material only vanadium, in particular the redox couples $\text{V}^{3+}/\text{V}^{2+}$ as anolyte and $\text{V}^{5+}/\text{V}^{4+}$ as catholyte, fully dissolved in all four oxidations stages in aqueous sulfuric acid solution, is utilized. Nevertheless, the VRFB features several serious problems such as the high material cost of vanadium (mining and purification), the common used expensive cation-exchange membranes and the temperature dependent solubility of the redox-active species, which restricts the energy density as well as the operation range. Therefore, a progressive commercialization is rather difficult.^[37, 42, 72]

Another commercially available flow battery is the Zn/Br₂ HFB. The original concept of a zinc/halogen HFB was already developed in the 1880s, with a zinc/chlorine battery by Renard in 1884 and just one year later with a zinc/bromine battery by Bradley and finally in the 1970s and 1980s further developed by Exxon and Gould Inc.. As described above, during charging in the negative half-cell the solved Zn²⁺_(aq) is reduced to the solid Zn⁰, which is electroplated on the anode, whereas in the other half-cell Br⁻ is oxidized to bromine. However, bromine in its liquid as well as gaseous state is extremely toxic and hazardous, which imply serious limitations. As a consequence, complexing agents like quaternary ammonium salts are added to form quaternary ammonium bromides to minimize the concentration of liquid bromine and to reduce the bromine vapor pressure.^[37, 46-48] Beside these flow batteries, the Fe/Zn and all-iron system are already under the development by companies, and furthermore a high number of other metal-based active materials like Ru,^[73, 74] Zn/Ni,^[75] Zn/Ce,^[76] Ti/Fe,^[77] Mn³⁺/Mn²⁺,^[78] Pb/PbO₂,^[79-82] Cu/PbO₂,^[83] all-Cu,^[84] all-U,^[85] all-Cr,^[86] and Li^[87-89] were investigated regarding their applicability in the recent years.

Despite all their benefits, the classic metal-based flow batteries will most likely not be the future energy storage systems of choice. Because they contain high-priced metal salts (e.g., vanadium), corrosive acidic electrolytes (e.g., sulfuric acid), harmful and toxic halogens like bromine or polyiodide and expensive ion-exchange membranes such as Nafion[®]. Moreover it should be taken into account that the relative amount of the needed metals in the lithosphere does not represent their effective availability, because they are usually obtained as products of ore mining. Additionally, the crucial high purity requirements of the utilized active materials further increases the costs. Beyond, they are commonly quarry in the developing countries, where insufficient civil and environmental standards are associated with mining and disposal.^[37, 56, 57] In comparison the costs of the raw materials utilized in the Zn/Br₂ HFB are relatively low, but as mentioned before the toxicity of the bromine and the mandatory required complexing agents caused disadvantages.^[52-55] In particular the total costs of RFBs, which are comprised of electrolyte costs (includes redox-active material, supporting electrolyte, solvent and eventually required additives), systems cost (power electronics, battery management system, pumps) stacks (e.g., separator and felt), installations and long-time running maintenance costs, are one of the most critical factors for a further commercialization. Cost analyses, for example from Darling *et al.*,^[64] prove that the

majority of costs are caused by the redox-active material itself and the utilized membrane. Based on the many drawbacks of metal-based systems, the current research focuses on the development of an aqueous all-organic RFB utilizing low-cost membranes and sustainable, inexpensive organic charge-storage materials.

2.3 “Rise of the organics” – organic-based flow batteries

Through the use of low-cost and sustainable organic charge-storage materials, which can be obtained by petrochemistry or renewable sources, organic-based flow batteries represents a considerable improvement of social, environmental and economic aspects.^[53, 90] In particular, when the primary materials are cost-efficient, no or only minor synthetic effort is necessary and a sophisticated purification process can be avoided, organic redox-active materials can display significant cost advantage in respect to metal-based charge-storage materials.^[57] For instance, Huskinson *et al.* performed a brief cost calculation for their reported anthraquinone disulphonate/bromine system, which yields a redox-active material price of \$27 per kWh, which is considerably less compared to the material price of \$81 per kWh for the state-of-the-art vanadium systems.^[90] Another major benefit of organic charge-storage materials is the capability to adjust their redox properties and/or solubility by introduction of functional groups and substituents.^[56, 57, 91, 92] For example, through the introduction of electron-withdrawing and electron-donating functional groups the original redox potential of the charge-storage material can be tuned to exploit the electrochemical stability window of the utilized aqueous or non-aqueous solvent. In some cases, also the fundamental electrochemical stability of the redox reaction and/or the long-term stability of the redox-active material can be improved.^[91-93] In addition, also the solubility of the active material in the preferred polar solvent (aqueous or aprotic polar organics) can be increased significantly by the introduction of polar groups, *e.g.*, the use of a tetraethylene glycol chain enhanced the solubility of a nitronyl nitroxide containing active material in acetonitrile of up to 3.8 molal.^[57] Generally, this method enable a solubility of organic-based redox-active material in aqueous solvents of over 1 M.^[90]

The utilization of organic redox-active materials indirectly leads to a further cost savings, because low-molar-mass compounds enable the application of more cost-effective non-perfluorinated ion-exchange membranes and polymers the use of simple inexpensive porous separators like dialysis membranes instead of the commonly

employed high-priced perfluorinated cation-exchange membranes.^[49, 52, 57, 92, 94-98] Based on these numerous benefits, in recent years the “rise of organics” in flow batteries started initially as ingredients such as organic additives^[99, 100] as well as organic ligands in redox-active metal-ligand complexes^[73, 101] and finally leading in form of low-molar-mass and polymer-based redox-active materials (examples are summarized in **Figure 2.2**) to several semi-organic,^[52, 95, 97, 102-104] metal-free organic/inorganic^[90, 105] and all-organic RFBs.^[49, 57, 60, 92, 96, 106, 107]

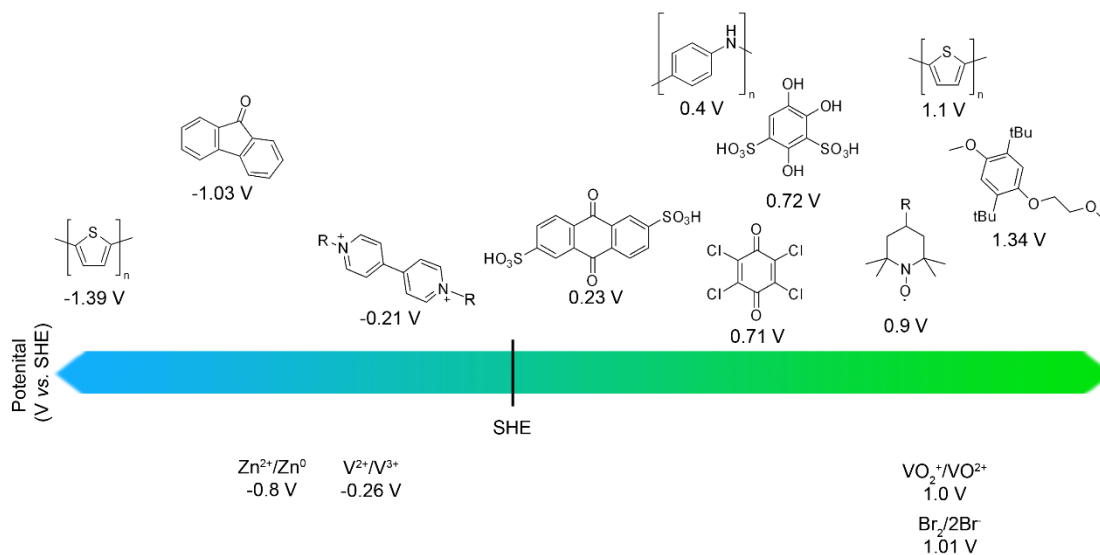


Figure 2.2: Schematic overview of selected appropriate organic and inorganic redox-active materials and their redox potentials (recalculated to a SHE reference if measured against another reference electrode).^[60, 90, 98, 102, 104, 108-112] Conversion factors: SHE to AgCl/Ag = +0.197 V, SHE to SCE = +0.241 V, SHE to Fc⁺/Fc = +0.750 V.^[113] SHE: standard hydrogen electrode, SCE: standard calomel electrode, Fc: ferrocene.

Nevertheless, there are currently some challenges in organic charge-storage materials, which need to be solved in future. For example the minor long-term stability, compared to common employed metal salts, as well as the moderate solubility and consequently energy density in aqueous media. This can be realized through the development of highly soluble (at least 2 M) organic active materials, which undergo no side reactions, feature highly reversible redox couples and no functional groups tend to unwanted reaction such as hydrolysis of ester, as well as the optimization of the electrolyte. Beside the improvement of the solubility, also the utilization of organic bipolar materials with a high potential difference or materials which transferred more than usual one electron, can lead to an increase in the energy density.

At the moment, (2,2,6,6-tetramethylpiperidin-1-yl)oxyl (TEMPO) derivatives as catholyte and viologen as well as anthraquinone derivatives as anolyte seems to be due

to their good chemical reversibility, their fast reaction kinetics and economical aspects (*e.g.*, the price of 4-HO-TEMPO is around \$5 to 6 kg⁻¹)^[114] the most promising organic charge-storage materials for RFB application. However, some factors like the solubility in the charged/discharged state must be further improved. Additionally, more redox-active materials must be investigated and evaluated for their suitability as charge-storage materials in RFBs.

3 Bipolar organic redox-active materials for application in symmetric redox-flow batteries

Parts of this chapter have been published in **P2)** T. Hagemann, J. Winsberg, B. Häupler, T. Janoschka, J. J. Gruber, A. Wild, U. S. Schubert, *NPG Asia Mater.* **2017**, 9, e340. **P3)** T. Hagemann, J. Winsberg, A. Wild, U. S. Schubert, *Electrochim. Acta.* **2017**, 228, 494-502.

In context of the “rise of organic charge-storage materials” various polymer- as well as low-molar-mass-based materials have been investigated and reported. Usually, these active materials feature one reversible redox process, whereupon they are, depending on their redox potentials, utilized either as catholyte or as anolyte. Unlike, bipolar organic redox-active materials feature two reversible redox couples and can be, therefore, used simultaneously both as cathode and as anode material in a symmetric RFB. Up to now, bipolar charge-storage materials were only investigated by Oh *et al.*,^[60] Potash *et al.*^[58] and Duan *et al.*^[59] Besides the fact, that such a organic symmetric RFB represents virtually a VRFB equivalent,^[42] several advantages like a simplified cell design, less effort on synthesis as well as electrolyte engineering and particularly a avoidance of cross-contamination arise.^[13, 56-60]

3.1 Nitronyl nitroxide containing redox-active material

Stable nitroxide radicals such as TEMPO, which derivatives are currently the most suitable organic catholyte materials, represent an interesting class of potential charge-storage materials for RFB application. In particular nitronyl nitroxide (NN) radicals represent, due to their high chemical and electrochemical reversibility of both redox couples (bipolar character) as well as the high difference of both redox potentials, a promising representative for further research in the field of flow batteries. In the development of a appropriate low-molar-mass NN derivative, attention should be paid to a specific structural requirement that must be fulfilled, namely the introduction of an phenyl ring at the 2-position of the NN (**Scheme 3.1**). This moiety indeed reduces the volumetric capacity, but without the aromatic moiety NNs exhibit only a deficient chemical stability in solution in the presence of air.^[115-117] Although water is the preferred solvent, his restricted potential window prevent a utilization of NN containing active materials in aqueous electrolyte systems. However, the majority of aromatic NNs feature a insufficient solubility in organic polar solvents such as acetonitrile or carbonate based solvents, which are preferred for application in RFBs.

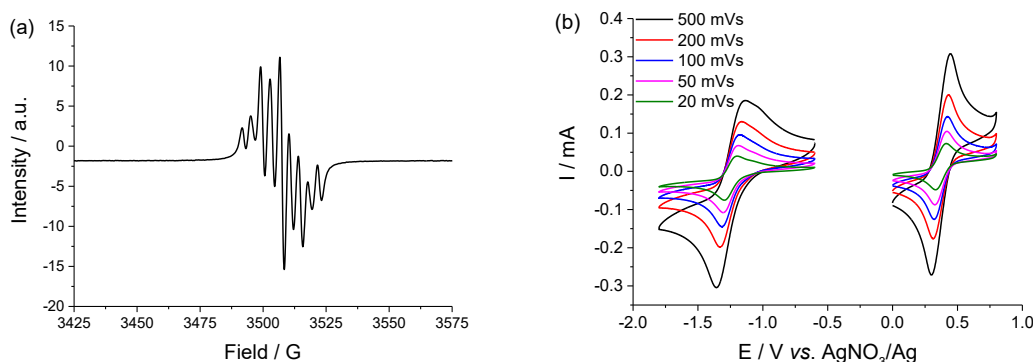


Figure 3.1: Electrochemical characterization of **4**: (a) EPR spectrum of **4** obtained in 10^{-4} M toluene solution, (b) cyclic voltammogram obtained for 2.1 mM acetonitrile solution of **4** with 0.1 M TBAPF₆ as supporting electrolyte at different scan rates.

Cyclic voltammetry (CV) measurements (**Figure 3.1b**) in acetonitrile solution and 0.1 M TBAPF₆ as supporting electrolyte exhibited quasi-reversible redox reactions of the NN⁺ (oxoammonium cation)/NN redox pair at $E_{1/2} = 0.37$ V and the NN/NN⁻ (aminoxyl anion) redox pair at $E_{1/2} = -1.25$ V vs. AgNO₃/Ag. The obtained redox potentials led to a cell voltage of 1.62 V. Furthermore, on the basis of a diffusion-controlled behavior (peak current grows linearly with the square root of the scan rate) the diffusion coefficient (D) for both redox couples could be calculated from the CV curves by using the Randles-Sevcik equation. The obtained values of 1.08×10^{-5} and 0.81×10^{-5} cm² s⁻¹ for both the NN⁺/NN and NN/NN⁻ redox pair are similar to these yielded by rotating disk electrode (RDE) measurements (in acetonitrile containing 0.1 M TBAPF₆) with 3.45×10^{-6} and 4.74×10^{-6} cm² s⁻¹ for the reduction and oxidation reaction, respectively. Further evaluation of the RDE measurements *via* Koutecký-Levich analysis and Tafel analysis yields for the well-defined redox reaction of the NN⁺/NN redox pair an electron-transfer rate constant (k^0) of 1.42×10^{-2} cm s⁻¹ as well as a transfer coefficient (α) of 0.59, which is nearby the value of an ideal reversible redox reaction of 0.5.

To evaluate the applicability of compound **4** as bipolar redox-active material a static test cell was manufactured. The static battery, utilizing an anion-exchange membrane (AEM) fumasep[®] FAP-PK-3130 and a 16 mM (32 mM active NN units) solution of **4** in acetonitrile with 0.5 M TBAPF₆ as conducting salt as anolyte and catholyte respectively, was charged/discharged for 75 consecutive cycles at a current density of 1 mA cm⁻². Well-defined charging plateaus at 1.67 V and discharging plateaus at 1.45 V (**Figure 3.2a**), coulombic efficiencies of up to 95% and a maximal discharge

capacity of 0.53 mAh (Figure 3.2b) were achieved as well as a voltage efficiency of 86% and an energy efficiency of 82%, which were representatively calculated for the 75th cycle.

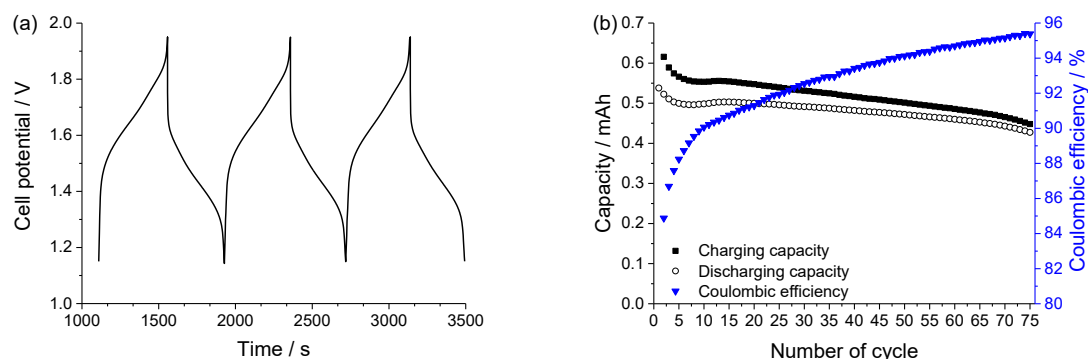


Figure 3.2: Static 5 cm² test cell, employing the FAP-PK-3130 AEM, with 16 mM (32 mM NN units) of **4** in acetonitrile and 0.5 M TBAPF₆ as anolyte and catholyte, respectively (with a theoretical charge-storage capacity of 0.88 Ah L⁻¹ for both solutions), 4 mL electrolyte per half-cell; (a) exemplary 3rd to 5th charge/discharge cycle at a current density of 1 mA cm⁻², (b) coulombic efficiency, charge and discharge capacity at a current density of 1 mA cm⁻².

Furthermore, to study the influence of the current density on the electrical performance of the battery a pumped flow cell comprised a 16 mM (32 mM active NN units) solution of **4** in acetonitrile with 0.5 M TBAPF₆, both as anolyte and catholyte, was charged/discharged in a voltage window of 1.10 to 1.95 V (Figure 3.3).

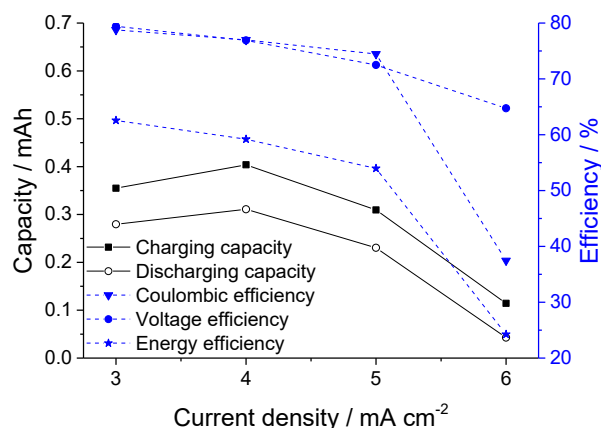


Figure 3.3: Electric performance of a pumped 5 cm² test cell with 16 mM (32 mM NN units) in acetonitrile and 0.5 M TBAPF₆ as anolyte and catholyte, respectively (with a theoretical capacity of 0.83 Ah L⁻¹ for both solutions) including capacity, coulombic, voltage and energy efficiency depending on the current density (10 mL electrolyte per half-cell; flow rate adjusted to 10 mL min⁻¹; FAP-PK-3130 AEM).

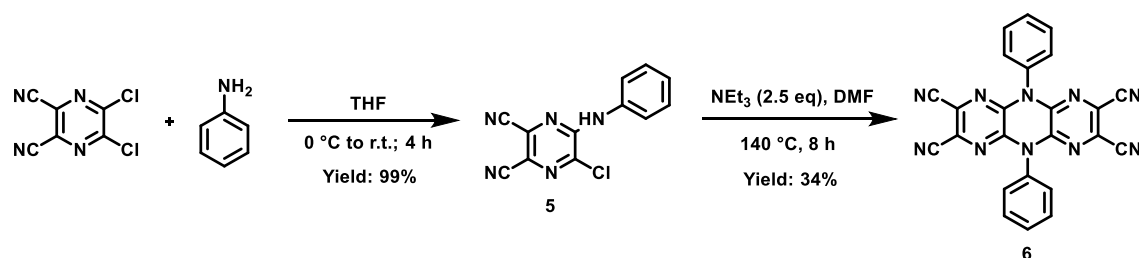
Four current densities (3, 4, 5 and 6 mA cm⁻²) could be applied, whereby a stable capacity retention and efficiencies at current densities of 3, 4 and 5 mA cm⁻² were achieved. Indeed only moderate coulombic and voltage efficiencies of around 80%,

which causes energy efficiencies of around 60%, were reached. Owing to the low conductivity of organic solvents higher current densities could not be applied and already at a current density of 6 mA cm^{-2} the charge and discharge capacity as well as the efficiencies drops significantly.

Moreover, a pumped flow cell with a higher active material concentration of 0.1 M (0.2 M NN units) **4** and 0.5 M TBAPF₆ in acetonitrile was charged/discharged for 20 consecutive cycles at a current density of 6 mA cm^{-2} featuring a theoretical capacity of 5.4 Ah L^{-1} and consequently an energy density of the electrolyte system of 4.1 Wh L^{-1} .

3.2 TCAA derivative as redox-active material

Another interesting substance class of potential bipolar charge-storage materials for application in symmetric RFBs are the 2,3,7,8-tetracyano-1,4,5,6,9,10-hexaza-anthracene (TCAA) derivatives. Compared to the NN containing compound **4**, investigated in **Chapter 3.1**, the TCAAs have the benefit of a even higher redox voltage of around 2.9 V (NN derivative **4** 1.62 V) and a less synthesis effort (**Scheme 3.2**).



Scheme 3.2: Schematic representation of the straightforward two-step synthesis route to compound **6**.

First mentioned in 1993,^[120] the synthesis and first fundamental investigations of TCAA derivatives were reported by Jaung *et al.*^[121] Starting from the affordable and commercially available 2,3-dichloro-5,6-dicyanopyrazine by adding two equivalents of an amine a monosubstituted 2-arylamino-3-chloro-5,6-dicyanopyrazines such as compound **5** (**Scheme 3.2**) can be synthesized in high yields *via* a nucleophilic substitution reaction. The following intermolecular cyclization (usually in dimethylformamide with triethylamine as base) yield a 5,10-disubstituted-2,3,7,8-tetracyano-5,10-dihydrodipyrazino[2,3-*b*:2',3'-*e*]pyrazine, *e.g.*, the derivative **6** (**Scheme 3.2**). Based on these straightforward synthesis, in particular through the nucleophilic substitution reaction in step one, electron-withdrawing or electron-donating functional groups and/or solubility promoting substituents can easily and purposeful be introduced to adjust the redox behavior and/or solubility of the TCAA. So far, the redox properties of these substance class are only incompletely explored. As a consequence, in

order to evaluate TCAAs as potential bipolar redox-active materials for an application in RFBs, the electrochemical behavior of derivative **6** was investigated in detail. Previously, to obtain a fundamental understanding of the redox potentials of the two redox couples and also the structure of **6** in its oxidized and reduced form density functional theory (DFT) calculations were performed (**Figure 3.4**).

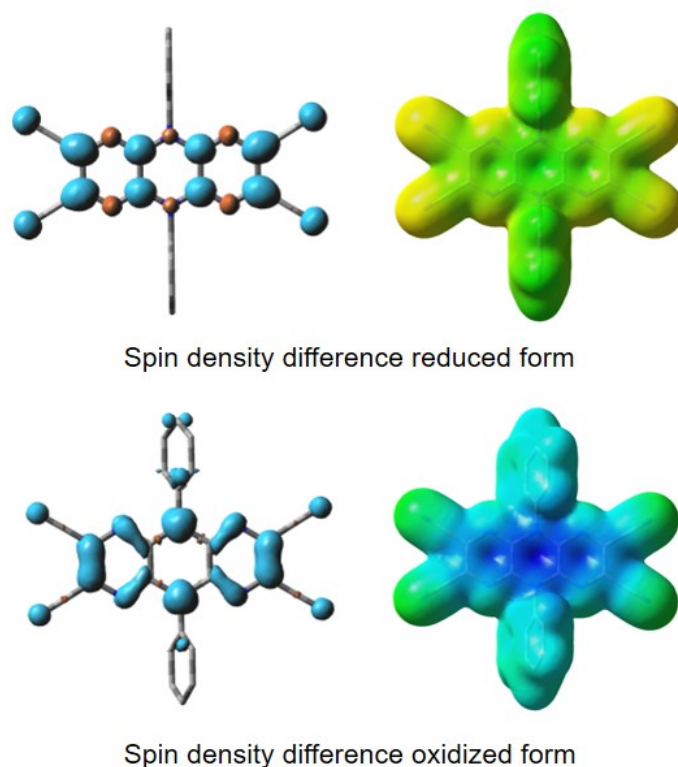


Figure 3.4: Schematic representation of the spin density difference of the reduced species (above) and the oxidized species (below), drawn at an isovalue of 0.002 (left) and with the electrostatic potential (−0.3 to 0.3) mapped onto the total density, drawn at an isovalue of 0.005 (right), which were determined by DFT using the Gaussian09 program package (Version A.02).^[122] The hybrid functional B3LYP^[123, 124] was selected in combination with the 6-31G* basis set. For all calculation, the solvent environment was modelled for acetonitrile using the implemented polarization continuum model (PCM).^[125, 126]

Figure 3.4 shows the calculated distribution of the spin density of the reduced species (above) and the oxidized species (below), which is in each case (independent from the manner of presentation) relatively even spread over the whole molecule. This behavior revealed a principle stability of both redox states, because no position in molecule **6** feature a higher reactivity (identifiable due to a high or low spin density). Nevertheless, it is noteworthy to mention that there is a possibility of a radical recombination in the reduced species, which counteracts the stability of this redox state. Furthermore, the absolute redox potentials referenced vs. Fc^+/Fc in acetonitrile with $E_{1/2} = 1.52$ V for the oxidation and re-reduction and $E_{1/2} = -1.29$ V for the reduction and re-oxidation were calculated.

To determine the real redox potentials CV measurements of derivative **6** with 0.1 M TBAPF₆ conducting salt, dissolved in acetonitrile were performed. The cyclic voltammogram (**Figure 3.5**) show a quasi-reversible oxidation/re-reduction at $E_{1/2} = 1.42$ V as well as a quasi-reversible reduction/re-oxidation at $E_{1/2} = -1.49$ V vs. Fc⁺/Fc, which are quite similar to the beforehand calculated values.

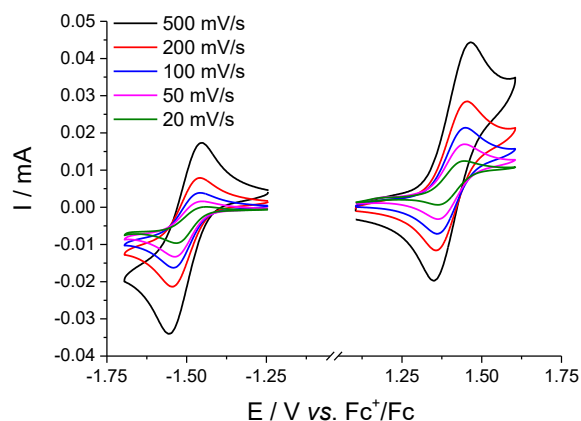


Figure 3.5: Cyclic voltammogram obtained for 3.8 mM acetonitrile solution of **6** with 0.1 M TBAPF₆ at different scan rates.

Further analyses of the obtained results exposes for both redox pairs a diffusion-controlled behavior (lineary relation of the peak currents and the square root of the scan rate), whereby by using the Randles-Sevcik equation the diffusion coefficient (D) of the oxidation/re-reduction $4.1 \times 10^{-5} \text{ cm}^2 \text{ s}^{-1}$ and reduction/re-oxidation $2.6 \times 10^{-5} \text{ cm}^2 \text{ s}^{-1}$ were calculated. Also the number of transferred electrons (n) for both redox processes of **6** were determined by CV (measurements with IR drop compensation), resulting on the assumption of a non ideal reversible redox reactions, for both oxidation and reduction a one electron process.

Additionally, advanced cyclic voltammetry (CVA) measurements (**Figure 3.6**) in acetonitrile solution with 0.1 M TBAPF₆ were performed to study the chemical reversibility of both redox processes and to detect potential side reactions in a surrounding which is closer to a battery operation. While the CVA for the oxidation/re-reduction redox pair ($E_{1/2} = 1.39$ V vs. Fc⁺/Fc, **Figure 3.6a**) exhibited no essential differences compared to the original spectrum (**Figure 3.5**, right), the cyclic voltammogram received for the reduction/re-oxidation redox pair ($E_{1/2} = -1.51$ V vs. Fc⁺/Fc, **Figure 3.6b**) display a new signal at -1.69 V and, therefore, crucial differences to the initially cyclic voltammogram (**Figure 3.5**, left). Particularly visible at lower scan rates (50 and 100 mV/s) the TCAA derivative **6** appears to undergo under simulated

battery conditions a further reduction and re-oxidation reaction, which indicates a non stable redox behavior of this redox pair.

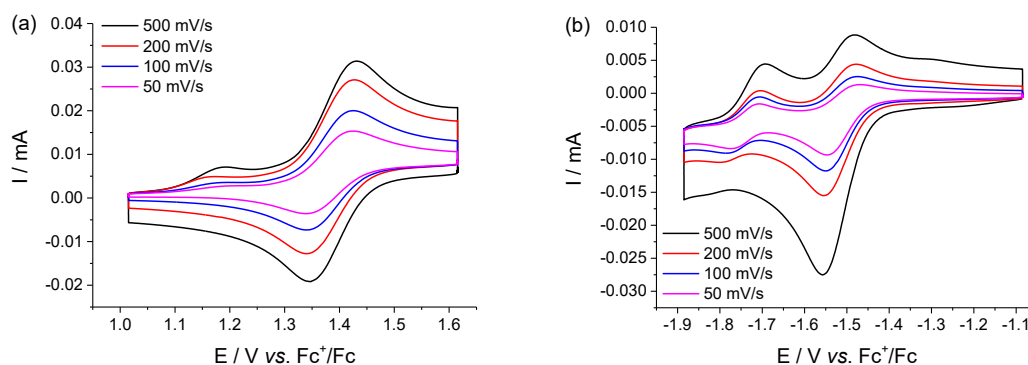


Figure 3.6: Cyclic voltammogram obtained for 2.5 mM acetonitrile solution of **6** with 0.1 M TBAPF₆ as conducting salt at different scan rates, measured *via* an advanced CV method (hold time of five minutes at each scan rate): (a) Oxidation and re-reduction as well as (b) reduction and re-oxidation.

To confirm these results and further explore the chemical reversibility of both redox pairs UV–vis–NIR spectroelectrochemical measurements (**Figure 3.7**) *vs.* a AgNO₃/Ag pseudoreference electrode (-0.084 V *vs.* Fc⁺/Fc) in a highly diluted acetonitrile solution of **6** with 0.1 M TBAPF₆ were performed. As expected from the previous CVA measurements, the investigation of the oxidation of **6** at potentials up to 1.5 V *vs.* AgNO₃/Ag (**Figure 3.7a**), whereby over the subsequent re-reduction at 0.2 V the original absorbance spectrum are qualitatively restored, suggesting a good chemical reversibility of this redox process.

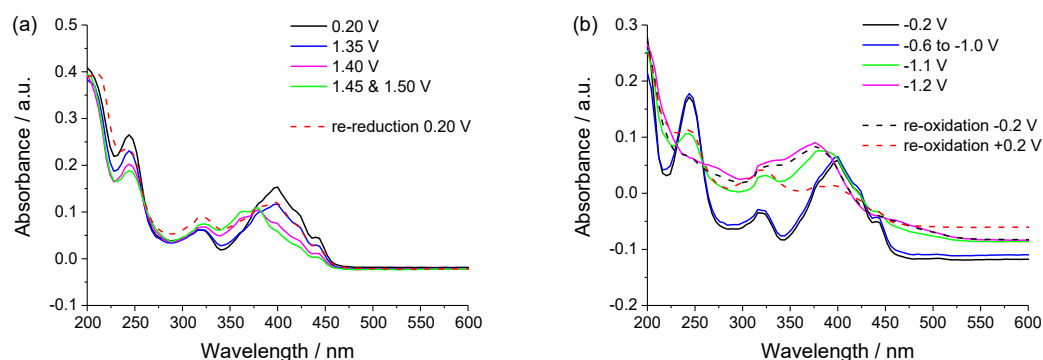


Figure 3.7: UV–vis–NIR spectroelectrochemical measurements of **6** in acetonitrile with 0.1 M TBAPF₆ as conducting salt (E *vs.* AgNO₃/Ag, about -0.084 V *vs.* Fc⁺/Fc). (a) Oxidation reaction and (b) reduction reaction.

Against this, for the reduction reaction of **6** at potentials up to -1.2 V (**Figure 3.7b**) the initial absorbance spectrum could not be restored during the following re-oxidation at -0.2 V. Only at a re-oxidation at 0.2 V the original signals could roughly be recovered.

But there are still differences, which indicate side reactions for this redox pair and therefore verified the results of the CVA measurements.

Nonetheless, the redox properties, in particular the diffusion behavior and the kinetics of the electron transfer, were further investigated *via* RDE measurements of **6** in acetonitrile solution with 0.1 M TBAPF₆. Both, the oxidation/re-reduction (**Figure 3.8a**) and the reduction/re-oxidation redox pair (**Figure 3.8b**) exhibit a diffusion-controlled behavior with a calculated diffusion coefficient (D) of $1.42 \times 10^{-5} \text{ cm}^2 \text{ s}^{-1}$ and $9.43 \times 10^{-6} \text{ cm}^2 \text{ s}^{-1}$, respectively, which are in the same magnitude as the calculated values obtained from CV measurements as well as diffusion coefficient of comparable organic charge-storage materials known from literature.^[57, 90, 127-129]

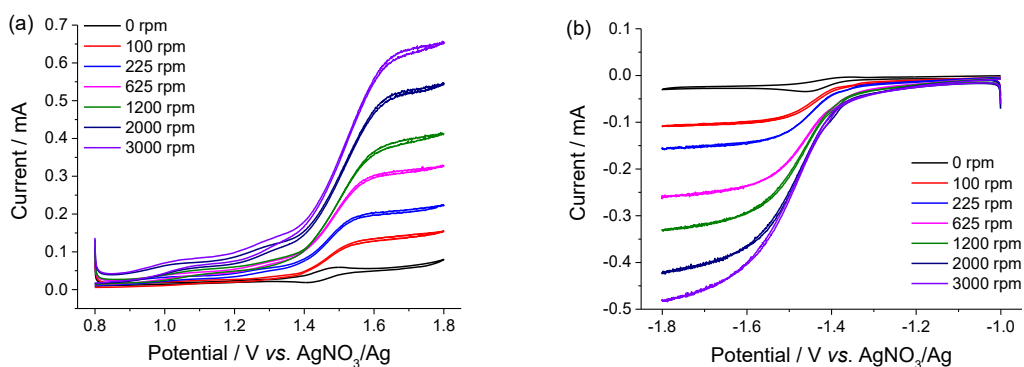


Figure 3.8: Rotating disk electrode measurement of **6** ($2 \times 10^{-3} \text{ mol L}^{-1}$) vs. a AgNO_3/Ag pseudoreference electrode ($-0.084 \text{ V vs. Fc}^+/\text{Fc}$) with 0.1 M TBAPF₆ in acetonitrile, scan rate 5 mV s^{-1} , at rotating rates from 0 to 3000 rpm, (a) Oxidation and re-reduction and (b) reduction and re-oxidation.

The subsequently performed Koutecký-Levich analysis unveil for both redox reactions mass-transport-independent currents and the Tafel analysis show an electron-transfer rate constant (k^0) of $1.08 \times 10^{-2} \text{ cm s}^{-1}$ as well as a transfer coefficient α of 0.86 for the oxidation/re-reduction and an electron-transfer rate constant (k^0) of $1.00 \times 10^{-2} \text{ cm s}^{-1}$ as well as a transfer coefficient α of 0.65, which is close to the α -value of an ideal reversible redox reaction of 0.5, for the reduction/re-oxidation redox pair.

In conclusion, the promising electrochemical properties of **6** such as a high redox voltage of 2.91 V as well as electrochemically stable quasi-reversible redox reactions, which are initially determined *via* DFT calculation and further validated *via* CV measurements, could not decisive verified by further extensive electrochemical investigations *via* UV-vis-NIR spectroelectrochemical, CVA and RDE measurements. Although, the oxidation and re-reduction reaction feature a electrochemically quasi-

reversible and diffusion-controlled behavior, advanced CV as well as UV–vis–NIR spectroelectrochemical measurements suggest under simulate battery conditions a non stable redox behavior of the reduction/re-oxidation redox couple. Therefore, no charge/discharge experiments in a symmetric flow battery setup with derivative **6** as catholyte and anolyte, respectively, were performed. Based on the determined principle applicability of this substance class as charge-storage materials future studies will focus on the introduction of suitable substituents or functional groups to achieve also a stable quasi-reversible redox behavior of the reduction/re-oxidation reaction and to improve the solubility of the TCAA derivatives in the preferred organic solvents.

4 A combined polymer/low-molar-mass-based aqueous redox-flow battery

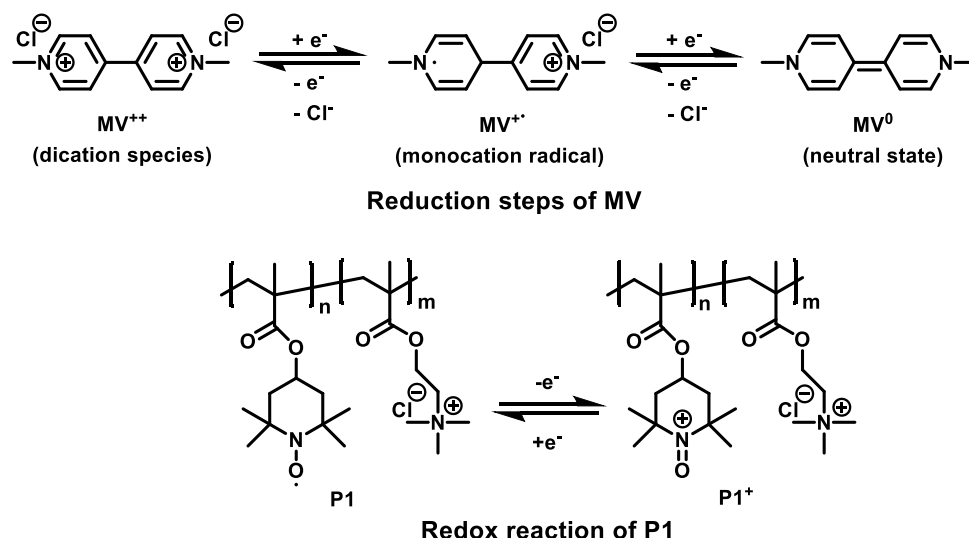
Parts of this chapter have been published in **P4**) T. Hagemann, J. Winsberg, M. Grube, I. Nischang, T. Janoschka, N. Martin, M. D. Hager, U. S. Schubert, *J. Power Sources* **2018**, 378, 546-554.

As already described in **Chapter 2** the current research in the field of flow batteries concentrates on the development of an aqueous RFB utilizing low-cost membranes and safe, sustainable and inexpensive organic redox-active materials. At the moment, for aqueous electrolyte systems, TEMPO derivatives as catholyte and viologen derivatives as anolyte are due to economical aspects as well as their high chemical reversibility and fast reaction kinetics the most promising organic charge-storage materials. Therefore, in the last years several high performance aqueous all-organic RFBs with TEMPO/viologen derivatives as redox-active materials were reported, *e.g.*, Janoschka *et al.*^[49] described a novel organic RFB utilizing TEMPO- and viologen-containing polymers in pH-neutral aqueous sodium chloride solution, which enable the use of cost-effective dialysis membranes. Also low-molar-mass based viologen and TEMPO derivatives such as the *N,N'*-dimethyl-4,4'-bipyridinium dichloride (**MV**) as well as the 4-HO-TEMPO^[107] and TEMPTMA^[96] were successfully applied in all-organic aqueous RFBs.^[49, 96, 107]

With the aim to unite the various advantages of the polymer- and low-molar-mass-based system like low costs, good electrochemical performance and long-term stability a combined all-organic RFB, utilizing for the first time a combination of a polymer and a low-molar-mass compound as active materials, were developed. In an aqueous sodium chloride solution the TEMPO-containing copolymer poly(2,2,6,6-tetramethyl-piperidinyloxy-4-yl methacrylate-*co*-[2-(methacryloyloxy) ethyl] trimethyl ammonium chloride) (**P1**) was used as catholyte and the low-molar-mass **MV** as anolyte.

While the **MV** was synthesized according to literature,^[96, 130] **P1**, which was originally prepared by Janoschka *et al.*,^[49] was provided as aqueous solution (capacity of 8.3 Ah L⁻¹) as industrial sample by Polymaterials AG (Germany). For further application the aqueous solution was dialyzed (with a molecular weight cut-off (MWCO) of the dialysis membrane of 1,000 g mol⁻¹) against water and lyophilized to yield **P1** as an orange powder. Asymmetric-flow field-flow fractionation (AF4) was used to determine the number average molar mass ($M_n = 20,600$ g mol⁻¹) as well as the

dispersity ($D = 1.71$). The absolute spin-activity of 6.93×10^{17} spins mg^{-1} and, consequently, a capacity of 30 ± 3 mA h g^{-1} was determined by EPR spectroscopy.



Scheme 4.1: Schematic representation of the two possible reduction steps of MV^{++} (above) and the redox reaction of **P1** (below).

Since the redox behavior of viologen (**Scheme 4.1**, above) and TEMPO (**Scheme 4.1**, below) derivatives are well-known only fundamental electrochemical investigations *via* cyclic voltammetry (**Figure 4.1**) were conducted.

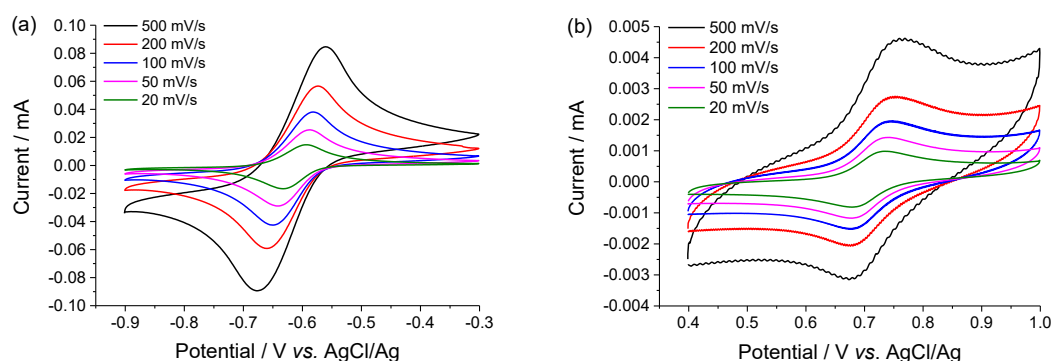


Figure 4.1: Cyclic voltammogram at different scan rates obtained for a 1 M aqueous NaCl solution of (a) 10 mM **MV** and (b) of 5 mM **P1**.

The CV measurements (**Figure 4.1a**) of 10 mM **MV** in 1 M NaCl_{aq} solution display for the $\text{MV}^{++}/\text{MV}^{+\bullet}$ redox pair, which is in contrast to the second redox pair ($\text{MV}^{+\bullet}/\text{MV}^0$) usable for battery application,^[131, 132] a chemical reversible reduction/re-oxidation at $E_{1/2} = -0.6$ V vs. AgCl/Ag. The subsequently performed CVA measurement under conditions which are more akin to these in a battery setup, exhibited no essential differences to the original voltammogram. The cyclic voltammogram (**Figure 4.1b**) obtained for 5 mM **P1** in 1 M NaCl_{aq} solution show for the TEMPO/TEMPO⁺ redox

pair a chemical reversible oxidation and re-reduction at $E_{1/2} = 0.7 \text{ V vs. AgCl/Ag}$. The following performed CVA measurements exhibited no significant differences to the initially voltammogram and, therefore, a good chemical reversibility also under simulated battery conditions.

After the validation of the electrochemical properties of **MV** and **P1** a combined aqueous all-organic RFB was fabricated. To achieve the highest possible battery performance several key factors like the type of anion-exchange membrane, concentration of the conducting salt, the behavior without the utilization of any conducting salt, and the influence of the flow rate of the electrolytes were investigated in detail. In particular the membrane has a crucial impact on the performance parameters such as lifetime, current and energy density. For these reasons, and for economic aspects,^[64] the utilized membrane should ideally be tailor-made for an application in RFBs and feature a low ohmic resistance in the used electrolyte, a good mechanical stability and chemical inertness, which is essential to achieve a long lifetime,^[13] and, to allow a high counterion mobility, a good permeability for the supporting electrolyte ions. Furthermore, the separator has to prevent a crossover of the active materials to achieve high coulombic efficiencies and a low capacity retention over long-term operation. While the usually employed perfluorinated Nafion[®] membranes involve excessive costs and the affordable dialysis membranes cannot be used, because they are impractical for low-molar-mass compound like **MV**, four different less expensive fumasep[®] anion-exchange membranes, because both utilized redox-active materials display at least one positive charge in all occurring redox-states, were chosen for all battery tests. The employed FAA-3-PE30, FAP-PK-3130, FAS-30 and FAA-3-50 AEM differ in the reinforcement, the thickness (dry) and the area resistance (Cl⁻ form). Consecutively the applicability of the four AEMs was examined in a pumped 5 cm² test cell, which was charged/discharged in a voltage window of 0.80 to 1.35 V, with 0.5 M **MV** and **P1** both in a 1.5 M NaCl_{aq} solution as anolyte and catholyte, respectively. Thereby, the electric cell resistance was determined by electrochemical impedance spectroscopy (EIS) and the influence of the various current densities on the battery performance was studied (**Figure 4.2**). The FAS-30 and the FAA-3-50 AEM exhibited with 3.32 and 1.67 $\Omega \text{ cm}^2$, respectively, the lowest area resistance of the four membranes and, consequently, the best ion mobility. Therefore, nine different current densities from 1 up to 16 mA cm⁻² could be applied for these two

AEM, whereas on the contrary for the FAA-3-PE30 and the FAP-PK-3130, which exhibited a higher area resistances of 9.62 and 7.77 $\Omega \text{ cm}^2$, respectively, lower maximal current densities of only 8 and 12 mA cm^{-2} could be applied.

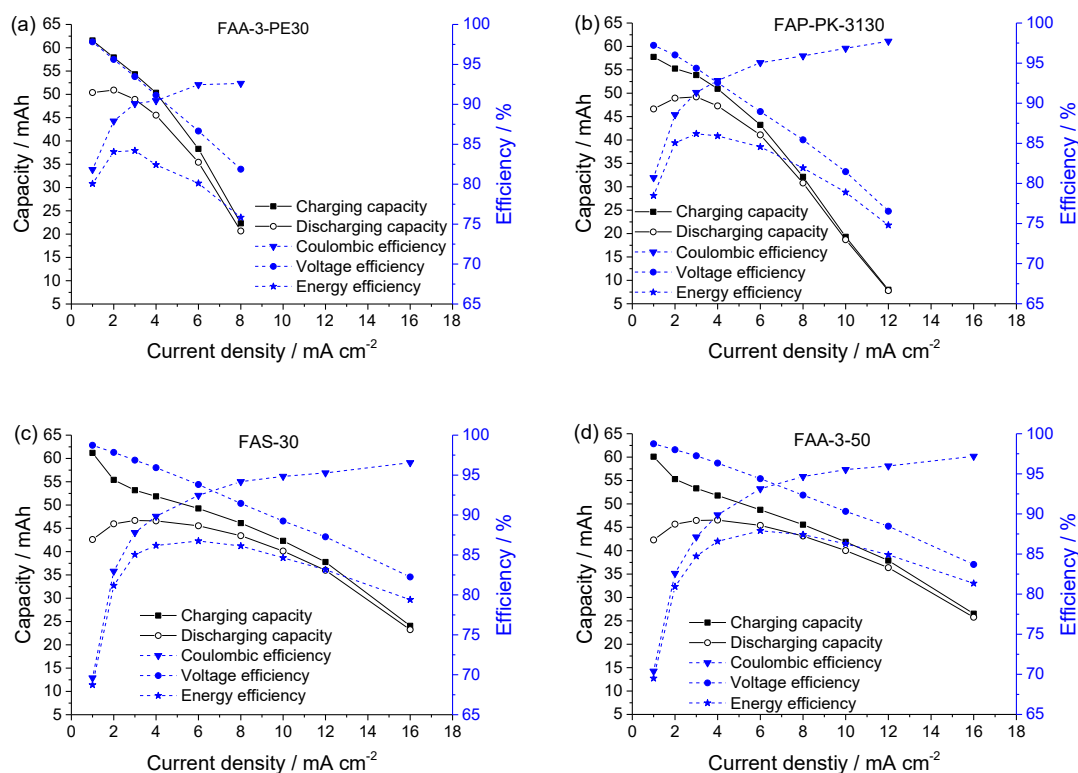


Figure 4.2: Electric performance of a pumped 5 cm² test cell with 0.5 M MV and P1 both in 1.5 M NaCl_{aq} as anolyte and catholyte, respectively (theoretical charge-storage capacity of 6.5 Ah L⁻¹), including capacity, coulombic, voltage and energy efficiency depending on the current density (10 mL electrolyte per half-cell, flow rate adjusted to 16 mL min⁻¹); (a) FAA-3-PE30, (b) FAP-PK-3130, (c) FAS-30 and (d) FAA-3-50 AEM.

However, the achieved charging and discharging capacities as well as the coulombic, voltage and energy efficiencies are comparable for all AEMs (Figure 4.2a-d). The pumped test cells, employing the FAS-30 (Figure 4.2c) and FAA-3-50 AEM (Figure 4.2d) feature at current densities in the range of 1 to 10 mA cm⁻² with discharging capacities of up to 47 mAh, coulombic efficiencies of up to 97% and energy efficiencies of 80 to 87% (except for a current density of 1 mA cm⁻²) the best battery performance. Nevertheless, also the pumped tests cells with FAA-3-PE30 (Figure 4.2a) and FAP-PK-3130 AEM (Figure 4.2b) reached at current densities of 1 to 6 mA cm⁻² with discharging capacities of 51 and 50 mAh, respectively, good results. In conclusion, all four used AEMs are suitable for an application in this combined aqueous all-organic RFB, but the FAA-3-50 AEM is, due to obtained performance parameters as well as the lowest measured electric cell resistance, the preferred membrane.

Afterwards, the impact of the supporting electrolyte (conducting salt), which are utilized for charge balancing and to increase the conductivity of the electrolyte solution,^[13] on the performance of this combined aqueous RFB was investigated. Owing to safety and economic aspects sodium chloride is the most preferred conducting salt for aqueous electrolyte systems. Due to the use of **MV**, which contains chloride counterions with a high mobility,^[96] it is an interesting issue if in this case the utilization of a supporting electrolyte is generally necessary. To verify this, a pumped test cells without additional conducting salt was manufactured and the influence on the current rating was investigated (**Figure 4.3**).

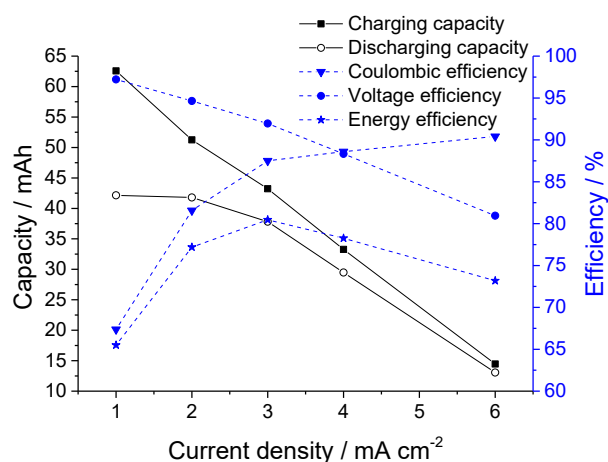


Figure 4.3: Electric performance of a pumped 5 cm² test cell, employing the FAA-3-50 AEM with 0.5 M **MV** and **P1** both in aqueous solution as anolyte and catholyte, respectively (theoretical charge-storage capacity of 6.7 Ah L⁻¹), including capacity, coulombic, voltage and energy efficiency depending on the current density (10 mL electrolyte per half-cell, flow rate adjusted to 16 mL min⁻¹).

The achieved performance parameters (**Figure 4.3**) such as the applicable current densities of up to 6 mA cm⁻² with discharging capacities of up to 42 mAh and coulombic efficiencies of up to 91% are significantly worse than those of the same flow cell (**Figure 4.2d**) using additional 1.5 M NaCl as supporting electrolyte. Furthermore, a three times higher area resistance (10.1 Ω cm²) was measured, which implicates poorer ion mobility. For this reason, it is highly advisable to use a conducting salt such as NaCl for this combined aqueous RFB. To identify the most favorable concentration of the used supporting electrolyte a pumped flow cell with electrolyte solutions comprising 0 to 5 M NaCl was cycled and the electric cell as well as the area resistance was investigated. **Figure 4.4** display that with increasing concentration of the conducting salt up to 1.5 M the electric cell resistance and subsequently the area resistance nearly linearly decreases. At NaCl concentrations above 1.5 M up to 3 M the electric cell resistance and, thus, the area resistance remained nearly constant. At higher

concentrations over 3 M both resistances rises again marginal, which results to a simultaneous rise in the viscosity of the aqueous NaCl solution.

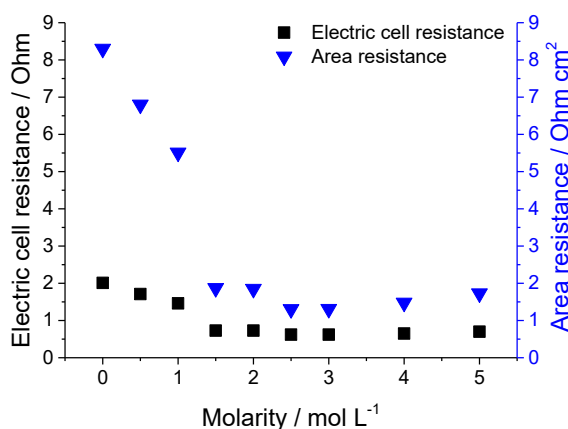


Figure 4.4: Electric cell and area resistance of a 5 cm² test cell as a function of the used concentration of the aqueous NaCl solution (0 to 5 M NaCl, 10 mL solution per half-cell, flow rate adjusted to 16 mL min⁻¹, FAA-3-50 AEM).

With increasing viscosity an interference of the ions with each other occur, whereby their mobility declines. At a NaCl concentration of 1.5 M the best accordance between a high counterion mobility and viscosity of the electrolyte solution could be achieved. Hence, for all battery tests a 1.5 M aqueous NaCl solution was utilized as electrolyte.

Another important influence parameter, which has so far not been investigated, is the optimization of the flow conditions. Principally, the overall efficiency and the performance parameters of the pumped flow cell, compared to a static setup, is significantly better. This is caused to the fact that in a static battery setup the available electrolyte volume can only partially be used and, furthermore, only a limited quantity of the active materials diffuses to a active electrode area. To study the impact of the flow conditions on the battery performance, the influence of different electrolyte flow rates on the discharge capacity of a test cell, which was charged/discharged in a voltage window of 0.80 to 1.35 V at a current density of 10 mA cm⁻², was investigated. Initially, the flow rate of both anolyte and catholyte solution were increased from 4 mL min⁻¹ up to 16 mL min⁻¹ (**Figure 4.5**), which corresponds to a full exchange of the electrolyte solution inside the 5 cm² test cell of two to eight times per minute. But the effect on the overall efficiency and the battery performance, representative evident from the slightly rise of the discharge capacity (**Figure 4.5**), is comparatively moderate. Also at further experiments, whereby the flow rate of the anolyte and the catholyte were changed independently of each other (one electrolyte flow rate was set at a constant rate

of 4 mL min^{-1} while the other electrolyte flow rate was altered), the discharge capacity only marginal increases. This demonstrates that the impact of the flow rate in relation to other factors like the utilized AEM or the concentration of the conducting salt is less significant.

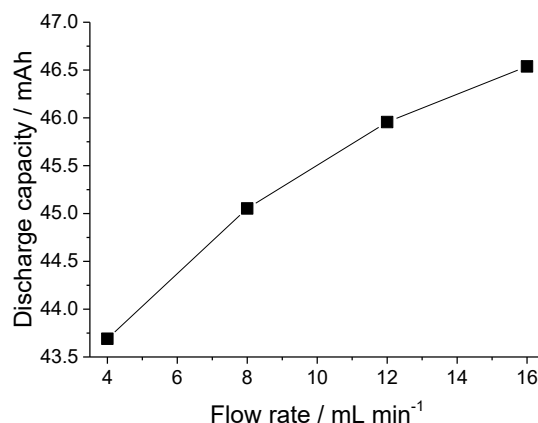


Figure 4.5: Discharge capacity of a pumped 5 cm^2 test cell, employing the FAA-3-50 AEM, with 0.5 M MV and **P1**, both in $1.5 \text{ M NaCl}_{\text{aq}}$ solution as anolyte and catholyte, respectively (theoretical charge-storage capacity of 6.7 Ah L^{-1} , 10 mL electrolyte per half-cell), as a function of the utilized electrolyte flow rate at a current density of 10 mA cm^{-2} .

Finally, based on the results of the previous studies, a long-term cycling stability test over 500 consecutive charge/discharge cycles in a pumped flow cell employing a FAA-3-50 AEM, with 0.5 M MV and **P1** each in a $1.5 \text{ M NaCl}_{\text{aq}}$ solution in a voltage window of 0.80 to 1.35 V at a constant flow rate of 16 mL min^{-1} and a current density of 5 mA cm^{-2} was performed.

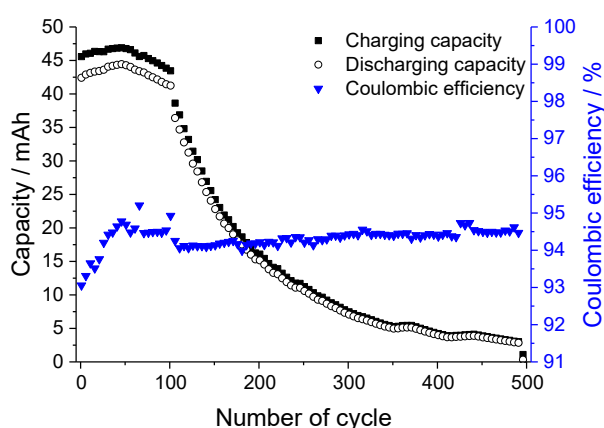


Figure 4.6: Long-term cycling stability test in a pumped electrochemical 5 cm^2 test cell, employing a FAA-3-50 AEM, with 0.5 M MV and **P1** both in $1.5 \text{ M NaCl}_{\text{aq}}$ solution (theoretical charge-storage capacity 6.7 Ah L^{-1} , 10 mL electrolyte per half-cell, constant flow rate of 16 mL min^{-1}): charging/discharging capacity and coulombic efficiency over 500 consecutive cycles at a constant current density of 5 mA cm^{-2} .

Figure 4.6 displays a stable battery cycling for 100 consecutive charge and discharge cycles with a maximal achieved discharge capacity of 44.4 mAh, which corresponds to approximately 66% of the theoretical possible discharge capacity of 67 mAh. With an overall energy density of this electrolyte system of 3.8 W h L^{-1} , coulombic efficiencies up to 95%, and, exemplarily calculated for the 100th cycle, a voltage efficiency of 91% as well as an energy efficiency of 85%, were reached. However, over the next 400 cycles the discharge capacity drop rapidly to 2.8 mAh, which correlates to a capacity retention of only 6%.

An investigation of the osmotic pressure of the catholyte as well as anolyte in an osmosis chamber proved the observation that this significant capacity decay after 100 cycles is caused by an osmotic process. Due to a osmotic pressure difference between these two electrolytes, water flows over time from the **P1** containing half-cell through the semipermeable AEM to the **MV** containing half-cell, whereby after the 100th cycle the solubility limit of **P1** was reached and this active material precipitated on the surface of the electrode, finally resulting in a drastic decrease of the capacity.

5 Polymer-based redox-active materials for flow batteries

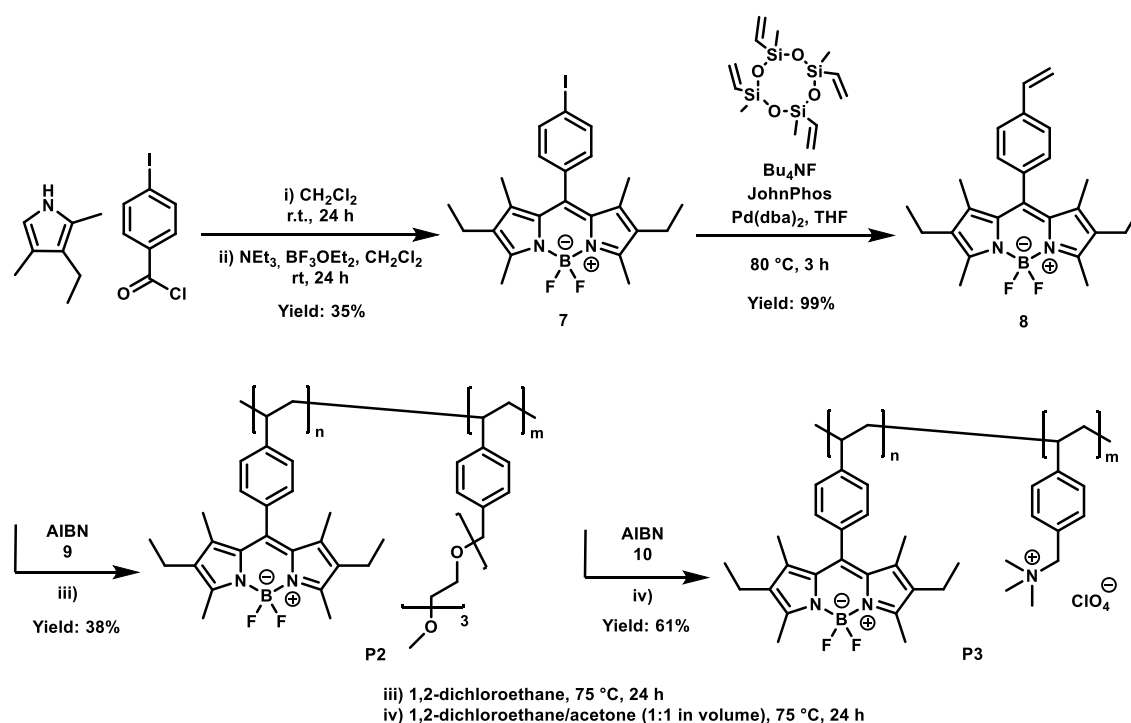
Parts of this chapter have been published in **P5**) J. Winsberg, T. Janoschka, S. Morgenstern, T. Hagemann, S. Muench, G. Hauffman, J.-F. Gohy, M. D. Hager, U. S. Schubert, *Adv. Mater.* **2016**, 28, 2238-2243. **P6**) J. Winsberg, S. Muench, T. Hagemann, S. Morgenstern, T. Janoschka, M. Billing, F. H. Schacher, G. Hauffman, J.-F. Gohy, S. Hoeppener, M. D. Hager, U. S. Schubert, *Polym. Chem.* **2016**, 7, 1711-1718. **P7**) J. Winsberg, T. Hagemann, S. Muench, C. Friebe, B. Häupler, T. Janoschka, S. Morgenstern, M. D. Hager, U. S. Schubert, *Chem. Mater.* **2016**, 28, 3401-3405.

Unlike low-molar-mass charge-storage materials described in **Chapter 3** polymer-based active materials with high molar-masses and linear or special shaped architectures enable the use of simple, low priced and robust porous separators such as dialysis membranes instead of the usually employed more expensive ion-exchange membranes.^[49, 52, 57, 92, 94-98]

5.1 Poly(boron-dipyrromethene)s as potential bipolar polymer-based redox-active material

Certain boron-dipyrromethenes (BODIPYs), a substance class well-known as chemosensors and laser dyes, feature two chemical reversible redox processes and therefore represents potential bipolar charge-storage materials for an application in an polymer-based symmetric all-organic RFB. To develop suitable derivatives, tailor-made BODIPY-containing copolymers (poly(BODIPY-*co*-TEGSt) **P2** and poly(BODIPY-*co*-TASSt) **P3**) were prepared *via* a free radical copolymerization of the styrene-based, alkyl-functionalized BODIPY monomer **8** with the solubility promoting comonomers (vinylbenzyl)triethyleneglycol monomethylether (TEGSt) **9** and (vinylbenzyl)trimethylammonium perchlorate (TASSt) **10** (**Scheme 5.1**). The use of a alkyl-functionalized BODIPY was necessary, because only a entire substitution of all hydrogen atoms of the BODIPY core insure a chemically reversibility of the redox processes.

Size-exclusion chromatography (SEC) was utilized to determine the number average molar mass (**P2** $M_n = 17 \text{ kg mol}^{-1}$, **P3** $M_n = 4 \text{ kg mol}^{-1}$) as well as the dispersity (**P2** $\bar{D} = 2.3$, **P3** $\bar{D} = 1.5$) of both copolymers. The composition of both copolymers was determined by ^1H NMR spectroscopy, yielding a molar ratio of 0.20. Before the preparation of copolymer **P2** and **P3** the BODIPY monomer **8** was electrochemical investigated *via* CV and UV-vis-NIR spectroelectrochemical measurements. Both exhibited a chemical reversibility of the BODIPY⁺/BODIPY and BODIPY/BODIPY⁻ redox pair.



Scheme 5.1: Schematic representation of the synthesis of the BODIPY monomer **8** as well as the preparation of the copolymers **P2** and **P3**.

The cyclic voltammogram of **8**, obtained in propylene carbonate with 0.1 M TBAClO_4 , show two quasi-reversible redox reactions at -1.51 V and at 0.69 V vs. AgNO_3/Ag . Subsequently measured CVs of **P2** (Figure 5.1a) and **P3** (Figure 5.1b) confirm the redox properties and also display two quasi-reversible redox reactions with peak splits of 90 mV (**P2**) and 100 mV (**P3**).

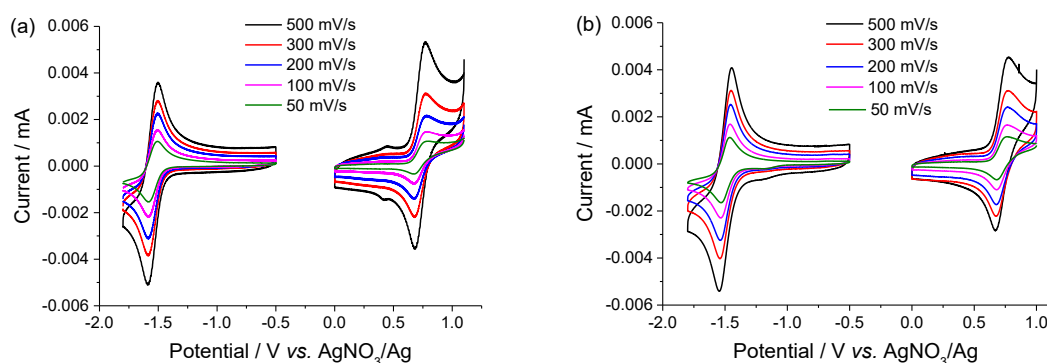


Figure 5.1: Cyclic voltammograms of (a) **P2** and (b) **P3**, each in propylene carbonate with 0.1 M TBAClO_4 as conducting salt at different scan rates.

Unfortunately, further analyses revealed that **P2** is not ideally suited as cathode redox-active material, because the oxidation/re-reduction redox pair do not feature a diffusion-

controlled behavior. Therefore, the usability of **P2** as anode redox-active material was investigated in an all-organic pRFB with poly(TEMPO-*co*-PEGMA) (**P4**, PEGMA = poly(ethyleneglycol)methacrylate), which was synthesized according to Janoschka *et al.*,^[133] as cathode redox-active material. In a static custom-made PTFE (polytetrafluoroethylene) trough, employing a size-exclusion membrane (MWCO of 1,000 g mol⁻¹), **P2** and **P4** each in propylene carbonate with 0.5 M TBAClO₄ as electrolytes, were charged and discharged in a voltage window of 1.40 to 2.15 V for 100 consecutive cycles (**Figure 5.2b**).

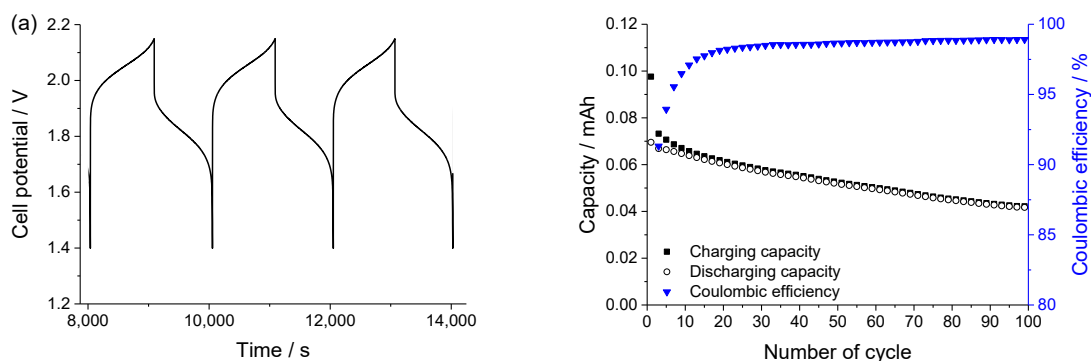


Figure 5.2: Static electrochemical test in a custom-made PTFE trough, employing a size-exclusion membrane (MWCO of 1,000 g mol⁻¹), with **P2** and **P4** in propylene carbonate and 0.5 M TBAClO₄ as anolyte and catholyte, respectively (1 mL electrolyte per section, electrolyte energy density 0.5 Wh L⁻¹), (a) representative 3rd to 5th charge/discharge cycle, (b) long-term cycling stability test with a constant current of 0.25 mA.

This all-organic non-aqueous polymer-based battery exhibit well-defined charge and discharge plateaus at 2.04 V and 1.82 V (**Figure 5.2a**), a maximal discharge capacity of 0.07 mAh, a high coulombic efficiency of up to 99%, a voltage efficiency of 89%, and a energy efficiency of 88%. After the long-term cycling stability test a capacity retention of 70% was achieved, which proved the suitability of **P2** as anode redox-active material for RFB application.

In contrast, further analyses of the CV measurements revealed for the BODIPY copolymer **P3** a fundamental applicability as bipolar charge-storage material, but due to the polarity of the comonomer **10** copolymer **P3** appears more appropriate as cathode redox-active material. Therefore, an all-organic pRFB utilizing both synthesized BODIPY copolymers **P2** and **P3** in propylene carbonate with 0.5 M TBAClO₄ as anolyte and catholyte, respectively, was manufactured (**Figure 5.3**).

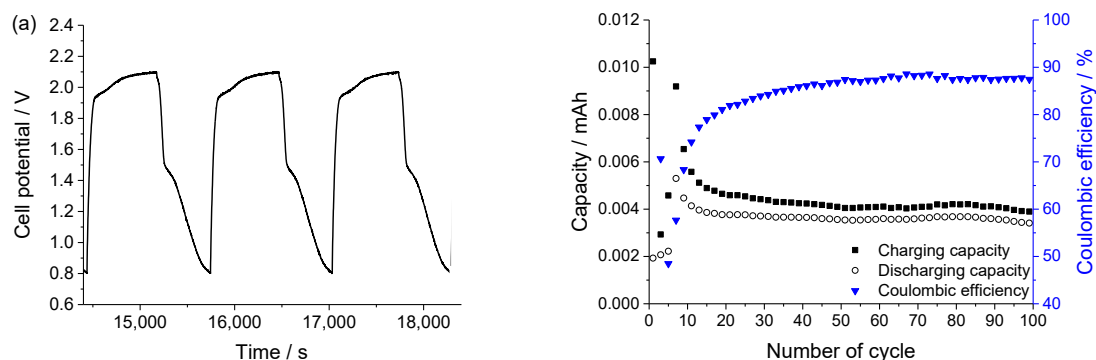


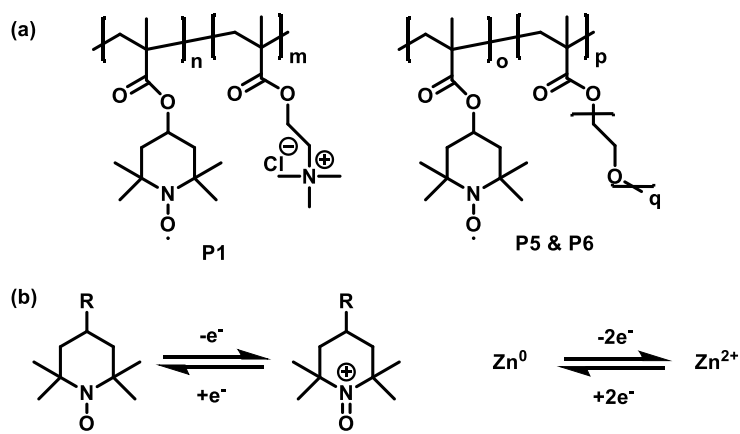
Figure 5.3: Static electrochemical test in a custom-made PTFE trough, employing a size-exclusion membrane (MWCO of $1,000 \text{ g mol}^{-1}$), with **P2** and **P3** in propylene carbonate and 0.5 M TBAClO₄ as anolyte and catholyte, respectively (1 mL electrolyte per section, energy density 0.5 Wh L^{-1}), (a) representative 13th to 15th charge/discharge cycle, (b) long-term cycling stability test with a constant current of 0.25 mA.

This all-BODIPY battery, investigated in a custom-made PTFE trough, display flat charge plateaus at 2.06 V, meanwhile the average discharge voltage was 1.28 V (**Figure 5.3a**), with coulombic efficiencies of up to 89% and a voltage efficiency of 62%, resulting in a energy efficiency of 55%. After a discharge capacity decay of around 30% over the first ten cycles, the discharge capacity remained constant at approximately 0.0037 mAh during the subsequent 90 cycles (**Figure 5.3b**). This stable battery cycling proved the suitability of BODIPY copolymer **P2** as anode and BODIPY copolymer **P3** as cathode charge-storage material. However, a battery utilizing only one bipolar BODIPY copolymer simultaneous both as anolyte and catholyte could not be demonstrated so far.

5.2 Statistically distributed linear TEMPO copolymers as cathode active material in a poly(TEMPO)/zinc hybrid-flow battery

Since TEMPO derivatives, as discussed in **Chapter 2** and **Chapter 4**, represent the most promising organic cathode active materials for an application in flow batteries, three different types of linear TEMPO-containing copolymers (**P1**, **P5** and **P6**, **Scheme 5.2**, **Table 5.1**) were synthesized according to Janoschka *et al.*^[133] and their suitability as cathode redox-active material in a poly(TEMPO)/zinc hybrid-flow battery was investigated in detail. Different comonomers (METAC = [2-(methacryloyloxy)-ethyl] trimethylammonium chloride) and two PEGMAs (poly(ethyleneglycol)-methacrylate) with number average molar masses (M_n) of 450 g mol^{-1} and 950 g mol^{-1}

were copolymerized with the TEMPO methacrylate to increase the solubility of the respective copolymers in aqueous and non-aqueous media (**Table 5.2**).



Scheme 5.2: Schematic representation of (a) the structure of the TEMPO copolymers **P1**, **P5** and **P6**, (b) the redox mechanism of TEMPO derivatives and zinc.

Table 5.1: Weight average molar masses, dispersities, composition and radical content of **P1**, **P5** and **P6**.

Polymer	Weight average molar mass (M_w) / kg mol ⁻¹	Dispersity (\bar{D})	Molar ratio (TEMPO:comonomer)	Radical content / mole fraction
P1	37 ^a	2.4	1:1 ^c	0.28 ^f (theoretical value 0.50)
P5	70 ^b	1.3	3.5:1 ^d	0.77 ^f (theoretical value 0.77)
P6	54 ^b	2.6	1:1 ^e	0.49 ^f (theoretical value 0.50)

M_w obtained via (a) AF4, (b) size-exclusion chromatography: DMAc + 0.21% LiCl, poly(styrene) standard; comonomers: (c) METAC, (d) PEGMA $M_n = 450$ g mol⁻¹, (e) PEGMA $M_n = 950$ g mol⁻¹, (f) calculated from the spin count obtained via ESR spectroscopy.

Table 5.2: Composition and energy density of poly(TEMPO)-based catholytes **A** to **D**.

Catholyte	Polymer	Solvent	Conducting salt	Energy density / Wh L ⁻¹ ^b
A	P1	water	0.71 M NaCl, 0.08 M ZnCl ₂ , 0.08 M NH ₄ Cl	0.94
B	P6	water	1.0 M ZnCl ₂ , 1.0 M NH ₄ Cl	2.04
C	P5	EC/DMC/DEC ^a	0.75 M Zn(ClO ₄) ₂ ×6H ₂ O	3.97
D	P5	EC/DMC/DEC ^a	0.5 M Zn(ClO ₄) ₂ ×6H ₂ O	0.59

(a) Mixture (1:1:1 in volume), (b) energy density was calculated by the following equation: Energy density = (volumetric capacity × open circuit voltage at 50% state of charge (carbonate based electrolytes: 1.3 V, aqueous electrolyte: 1.7 V))/2.

For the HFB setup zinc foil was employed as anode and zinc salt both as conducting salt and anode active material. A dialysis membrane ($\text{MWCO} = 1,000 \text{ g mol}^{-1}$) was used to separate both half-cell compartments. Since, poly(TEMPO-*co*-METAC) **P1** precipitates in concentrated solutions of several applied zinc salts (*e.g.*, ZnCl_2 , $\text{Zn}(\text{ClO}_4)_2$, $\text{Zn}(\text{NO}_3)_2$, ZnSO_4) only a two-time molar excess (relating to the TEMPO moieties) of zinc chloride and in addition sodium chloride as well as ammonium chloride both as supporting electrolyte and additive, were utilized. Initially, to investigate the electrochemical behavior of zinc and **P1**, CV measurements of a 0.1 M $\text{ZnCl}_{2\text{aq}}$ 0.01 M **P1** solution were performed and exhibited a quasi-reversible redox reaction at a half-wave potential of 0.70 V *vs.* AgCl/Ag for the TEMPO/TEMPO⁺ redox pair (**Figure 5.4a**, blue line) as well as a peak separation of 0.53 V *vs.* AgCl/Ag (scan rate 50 mV s⁻¹) for the Zn(II)/Zn(0) redox pair (**Figure 5.4a**, black line). The special shape of the cyclic voltammogram (**Figure 5.4a**) is typical for zinc, because of the electrodeposition at potentials below -1.26 V and a following dissolution at potentials above -1.1 V *vs.* AgCl/Ag.

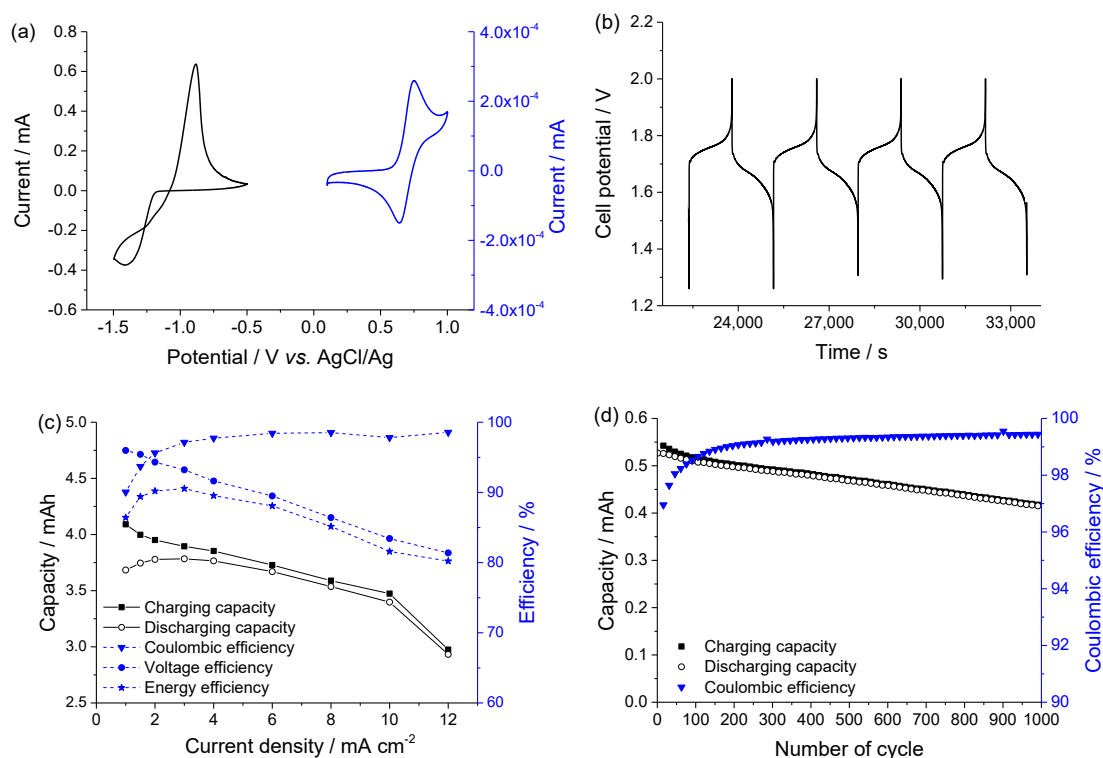


Figure 5.4: (a) Cyclic voltammogram of a 0.1 M $\text{ZnCl}_{2\text{aq}}$ 0.01 M **P1** solution at a scan rate of 50 mV s⁻¹; Manufactured aqueous pumped electrochemical 5 cm² test cell utilizing catholyte **A** (volumetric capacity of 1.1 Ah L⁻¹, 8 mL per half-cell, flow rate adjusted to 20 mL min⁻¹), (b) exemplary charge/discharge cycles at a current density of 2 mA cm⁻², (c) capacity, coulombic, voltage and energy efficiency as function of the applied current density, (d) long-term cycling stability test of a static 5 cm² test cell utilizing catholyte **A** at a current density of 2 mA cm⁻².

The subsequently manufactured aqueous HFB employing catholyte **A** exhibited well-defined charging and discharging plateaus with a narrow potential drop (**Figure 5.4b**), coulombic efficiencies of up to 99% (**Figure 5.4c**) and an overall energy density of 0.94 Wh L^{-1} . Current densities of up to 12 mA m^{-2} (**Figure 5.4c**) could be used, with almost consistent discharging capacity for current densities from 1 to 10 mA m^{-2} . A long-term stability test over 1,000 consecutive charging and discharging cycles in a static HFB setup (**Figure 5.4d**) at a current density of 2 mA m^{-2} exhibited a discharging capacity retention of nearly 79% and, therefore, a good chemical reversibility of catholyte **A**. Another aqueous HFB utilizing catholyte **B** show a maximum material activity of 87.6% with a overall energy density of 2.04 Wh L^{-1} . Compared to catholyte **A** higher current densities of up to 20 mA m^{-2} could be applied.

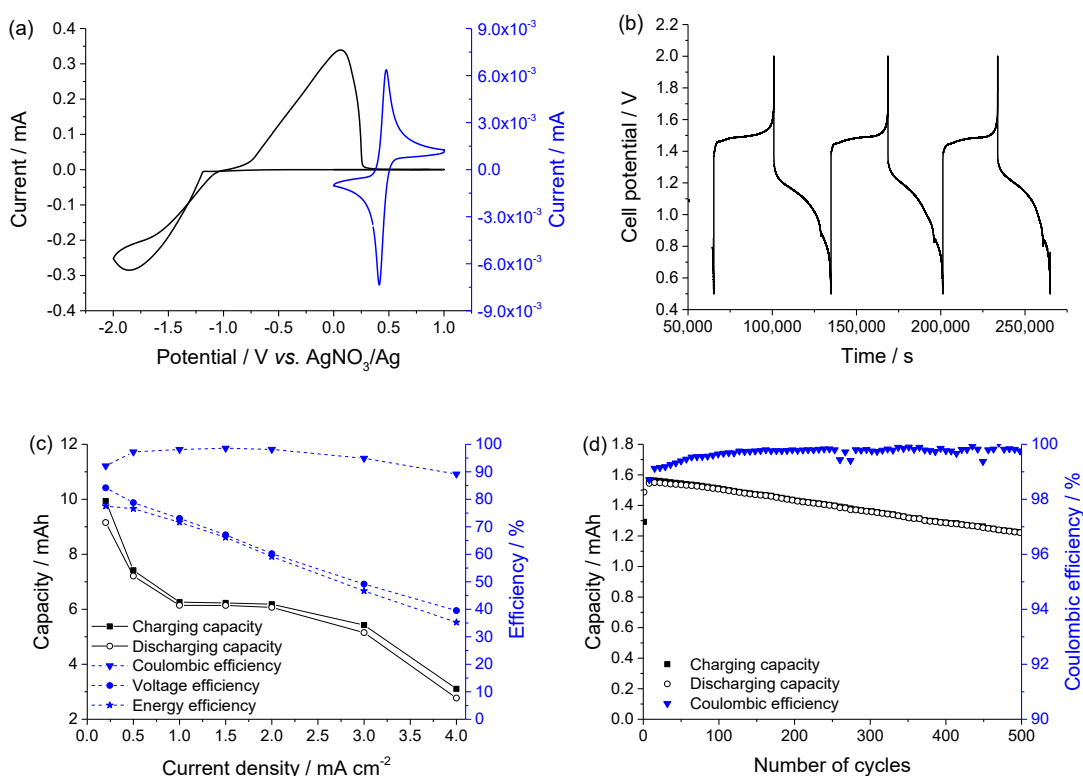


Figure 5.5: (a) Cyclic voltammogram of 0.1 M $\text{Zn}(\text{ClO}_4)_2 \cdot 6\text{H}_2\text{O}$ (black line) and 0.01 M **P5** in EC/DMC/DEC (1:1:1 in volume) at a scan rate of 50 mV s^{-1} ; (b) exemplary charge/discharge cycles of a pumped non-aqueous electrochemical 5 cm^2 test cell utilizing catholyte **C** (volumetric capacity of 6.1 Ah L^{-1} , 8 mL per half-cell, flow rate adjusted to 20 mL min^{-1}) at a current density of 1 mA cm^{-2} , (c) electrical performance: capacity, coulombic, voltage and energy efficiency as function of the applied current density of a pumped HFB utilizing catholyte **D** (volumetric capacity of 0.91 Ah L^{-1} , 8 mL per half-cell, flow rate adjusted to 20 mL min^{-1}), (d) long-term cycling stability test of a static non-aqueous 5 cm^2 test cell utilizing catholyte **D** at a current density of 1.4 mA cm^{-2} .

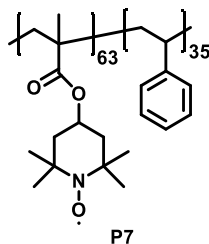
Since poly(TEMPO-*co*-PEGMA) **P5** featured a deficient solubility in aqueous media, organic electrolyte systems (catholyte **C**, **D**) were used. CV measurements of 0.01 M **P5** in a mixture of EC/DMC/DEC (1:1:1 in volume) at a scan rate 50 mV s^{-1} revealed also

a quasi-reversible redox reaction for the TEMPO/TEMPO⁺ redox pair at a half-wave potential of 0.44 V vs. AgNO₃/Ag (**Figure 5.5a**, blue line) with a peak split of 63 mV. For the Zn(II)/Zn(0) redox pair a comparable wide peak separation of 1.8 V vs. AgNO₃/Ag (**Figure 5.5a**, black line) was found. Further RDE measurements of **P5** in Zn(ClO₄)₂ revealed a diffusion-controlled behavior ($D = 1.65 \times 10^{-7} \text{ cm}^2 \text{ s}^{-1}$), a electron-transfer rate constant (k^0) of $9.93 \times 10^{-2} \text{ cm s}^{-1}$ and a transfer coefficient α of 0.44, which is close to an ideal reversible redox reaction of 0.5. Afterwards the usability of **P5** was investigated in a non-aqueous HFB with zinc-foil as anode, 0.75 M Zn(ClO₄)₂×6H₂O dissolved in a mixture of EC/DMC/DEC (1:1:1 in volume) as anolyte as well as catholyte **C** and **D**. A pumped HFB with catholyte **C** exhibited reversible charge/discharge plateaus (**Figure 5.5b**) with an – in comparison to the aqueous electrolyte systems – large potential drop of 350 mV. This marked difference is caused by the higher cell resistance of 27.30 Ω (1.35 Ω for aqueous HFB employing catholyte **B**), which was determined by EIS (prior to cycling), as well as the kinetically limited redox reaction of the Zn(II)/Zn(0) redox couple in organic electrolytes. Utilizing catholyte **D**, the electrical performance of this HFB was investigated. Current densities from 0.25 to 4 mA cm⁻² could be applied (**Figure 5.5c**), whereby coulombic efficiencies above 89% and a material activity of 99% (at a current density of 0.5 mA cm⁻²) were achieved. Indeed, with increasing current densities the discharge capacity decreased and stayed up to 3 mA cm⁻² at a level of approximately 6 mAh. In a static setup a long-term stability test over 500 consecutive charging and discharging cycles was performed. High coulombic efficiencies above 99.7% and a capacity retention of 81% (**Figure 5.5d**) were reached.

5.3 Block copolymer micelles with a TEMPO-corona as cathode active material in a poly(TEMPO)/zinc hybrid-flow battery

One future challenge of polymer-based RFBs, which must be addressed is the improvement of the electrolyte viscosity which is, due to the use of polymeric redox-active materials, very high compared to those of low-molar-mass-based RFBs. Unfortunately, a high viscosity leads to a decline in the ion mobility and the efficiency, which negatively impacts the performance of the battery.^[133] By the use of special shaped polymers with dendrimeric or micellar structures instead of the commonly linear polymers, the electrolyte viscosity can be reduced. For this purpose, a tailor-made block

copolymer PTMA₆₃-*b*-PS₃₅ (**P7**, **Scheme 5.3**, PTMA = poly(TEMPO methacrylate), PS = polystyrene) was synthesized according to literature procedures,^[133, 134] and afterwards used as cathode redox-active material in a poly(TEMPO)/Zn HFB. The copolymer **P7** was characterized *via* ¹H NMR and EPR spectroscopy to determine the average degree of polymerization of each block (number in the subscript) and the absolute spin-activity (spin count of $1.7 \times 10^{18} \text{ mg}^{-1}$ corresponds to a radical content of 82%), respectively.



Scheme 5.3: Schematic representation of the utilized block copolymer PTMA₆₃-*b*-PS₃₅.

SEC measurements revealed a number average molar mass (M_n) of 41 kg mol^{-1} (PS standard) and a dispersity (D) of 1.1. Due to the fact, that **P7** comprise a polar TEMPO block as well as unpolar styrene block, the copolymer when dissolved in polar organic carbonates aggregates into micellar structures, most likely with a PS core and a PTMA corona.^[135] Subsequently, the electrochemical behavior was investigated *via* CV measurements with 0.01 M **P7** in a mixture of EC/DMC/DEC (1:1:1 in volume) at a scan rate of 50 mV s^{-1} . The cyclic voltammogram exhibited a quasi-reversible redox reaction of the TEMPO⁺/TEMPO redox pair at a half-wave potential of 0.4 V with a peak split of 90 mV (**Figure 5.6a**, blue line) as well as a large peak separation of 2.1 V *vs.* AgNO₃/Ag for the Zn(II)/Zn(0) redox pair (**Figure 5.6a**, black line). To study the kinetics of the redox reaction of **P7**, RDE measurements in EC/DMC/DEC (1:1:1 in volume) with 0.1 M Zn(ClO₄)₂·6H₂O were performed, whereby a diffusion-controlled behavior, a diffusion coefficient (D) of $1.8 \times 10^{-7} \text{ cm}^2 \text{ s}^{-1}$ and a electron-transfer rate constant (k^0) of $7 \times 10^{-4} \text{ cm s}^{-1}$ was determined.

A non-aqueous poly(TEMPO)/Zn HFB employing a dialysis membrane (MWCO of $1,000 \text{ g mol}^{-1}$) as separator, zinc foil as anode and a 0.5 M solution of Zn(ClO₄)₂·6 H₂O both as conducting salt and anode active material in EC/DMC/DEC (1:1:1 in volume), was manufactured to investigate the suitability of **P7** as cathode redox-active material. With a maximal solubility of 13 mg mL^{-1} in the utilized electrolyte, an overall energy density of 0.8 Wh L^{-1} was achieved. The pumped HFB exhibit in a voltage range

between 0.5 to 2.0 V well-defined charge and discharge plateaus (**Figure 5.6b**) but also a large voltage drop of 280 mV, which is caused by the high cell resistance of $29\ \Omega$ (determined by EIS). In a subsequent experiment (**Figure 5.6c**), the impact of the current density on the performance of the battery was investigated. Owing to the restricted ionic conductivity of non-aqueous electrolyte system only current densities from 0.2 to $5\ \text{mA cm}^{-2}$ could be applied, whereby the coulombic efficiencies always remained above 90% (maximum of 98% at $2\ \text{mA cm}^{-2}$). At $0.2\ \text{mA cm}^{-2}$ a maximal discharge capacity of 8.7 mAh, which corresponds to a material utilization of 93%, was achieved. However, with increasing current densities the discharge capacity decline, but remain between 1 to $3\ \text{mA cm}^{-2}$ constant at 6.1 mAh (**Figure 5.6c**).

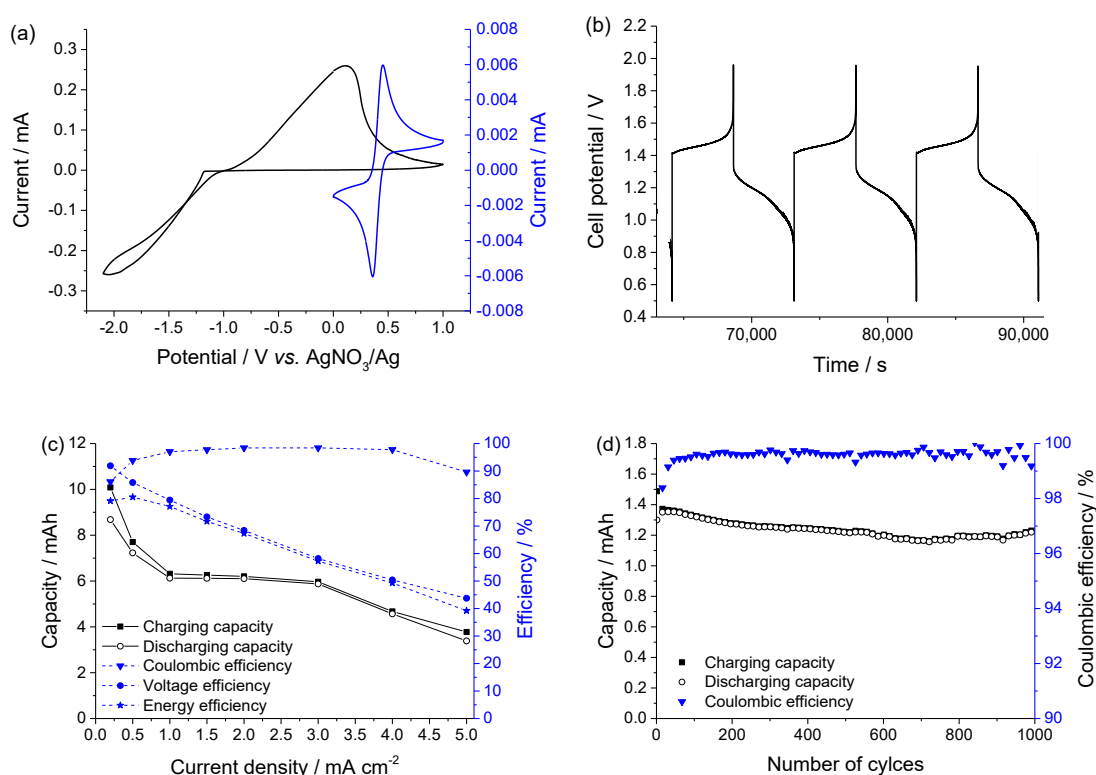


Figure 5.6: (a) Cyclic voltammogram of 0.01 M **P7** in EC/DMC/DEC (1:1:1 in volume) with 0.1 M $\text{Zn}(\text{ClO}_4)_2 \cdot 6\text{H}_2\text{O}$ as conducting salt at a scan rate of $50\ \text{mV s}^{-1}$; Pumped electrochemical $5\ \text{cm}^2$ test cell with **P7** as cathode redox-active material in EC/DMC/DEC (1:1:1 in volume) and 0.5 M $\text{Zn}(\text{ClO}_4)_2 \cdot 6\ \text{H}_2\text{O}$ both as conducting salt and anode active material (volumetric capacity of $1.2\ \text{Ah L}^{-1}$, 8 mL per half-cell, flow rate adjusted to $20\ \text{mL min}^{-1}$), (b) exemplary charge and discharge cycles at a current density of $1\ \text{mA cm}^{-2}$, (c) electrical performance as a function of different current densities, (d) long-term cycling stability test in a static $5\ \text{cm}^2$ test cell at a constant current density of $1.5\ \text{mA cm}^{-2}$.

Finally, the long-term cycling stability was investigated in static setup at a constant current density of $1.5\ \text{mA cm}^{-2}$. Over 1,000 consecutive charging and discharging cycles a great discharge capacity retention of 95% with coulombic efficiencies of up to 99.8% was reached (**Figure 5.6d**), yielding an excellent reversibility as well as stability for the used redox couples.

The proposition made at the beginning that the utilization of specially shaped polymers leads to a reduction of the electrolyte viscosity was proven by rheological measurements (**Figure 5.7a**), which revealed a non-Newtonian, shear thinning behavior for the in previous HFB experiments utilized PTMA₆₃-*b*-PS₃₅ (**P7**) containing catholyte. For comparison, a catholyte comprising a statistically distributed linear P(TMA-*co*-PEGMA) copolymer with an equal ratio of TEMPO active units and comonomer, exhibit a higher dynamic viscosity, which confirmed that a micellar structure improve the overall viscosity.

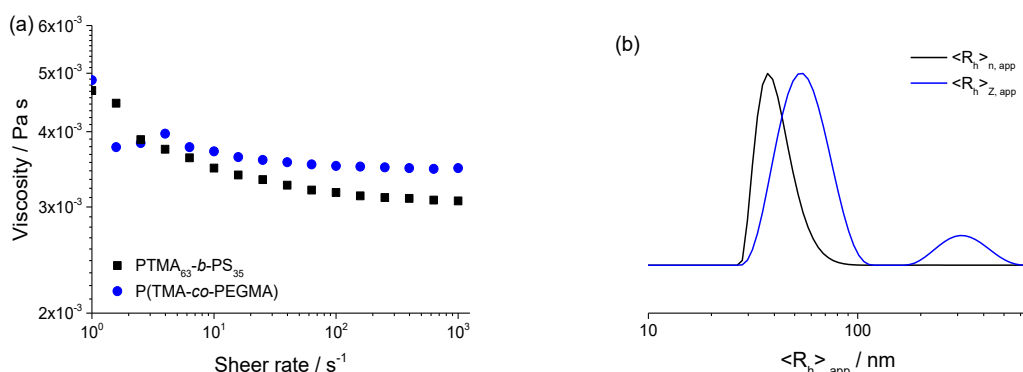


Figure 5.7: (a) Rheological measurements of PTMA₆₃-*b*-PS₃₅ (**P7**) and P(TMA-*co*-PEGMA) (both 13 mg mL⁻¹) in a mixture of EC/DMC/DEC (1:1:1 in volume) with 0.5 M Zn(ClO₄)₂×6 H₂O as conducting salt, (b) dynamic light scattering (DLS) measurement of charged PTMA₆₃-*b*-PS₃₅ (**P7**, 13 mg mL⁻¹) micelles in a mixture of EC/DMC/DEC (1:1:1 in volume), caused by the clouding within the electrolyte a characterization of the uncharged PTMA₆₃-*b*-PS₃₅ micelles was not practicable; $\langle R_h \rangle_{n, app}$: mean number weighted distribution, $\langle R_h \rangle_{z, app}$: mean intensity weighted distribution.

Finally, the structure of the completely charged catholyte (*via* chronoamperometry at 1.9 V) was examined by dynamic light scattering (DLS) measurements (**Figure 5.7b**).

At an average apparent hydrodynamic radius ($R_{h,app}$) of 40 nm one population of micelles was discovered. Additionally, at the intensity weighted distribution ($R_{z,app}$) two more micelle populations, a single micelle at a radius of 55 nm and secondary agglomerates at 310 nm were detected. Subsequently performed transmission electron microscopy (TEM) images (**Figure 5.8**) verified these observations. Furthermore, a large amount of sheet like structures were detected for the clouded uncharged catholyte (**Figure 5.8a**), but also individual micellar structures (**Figure 5.8b**). Unlike, the imaging of the catholyte in the charged state (**Figure 5.8c, d**) exhibited a large number of individual micellar structures, typically with a diameter in the range of 50 to 75 nm. With a higher optical resolution the core-corona structure of a individual micelles as well as secondary agglomerates with a diameter of ~300 nm were detected.

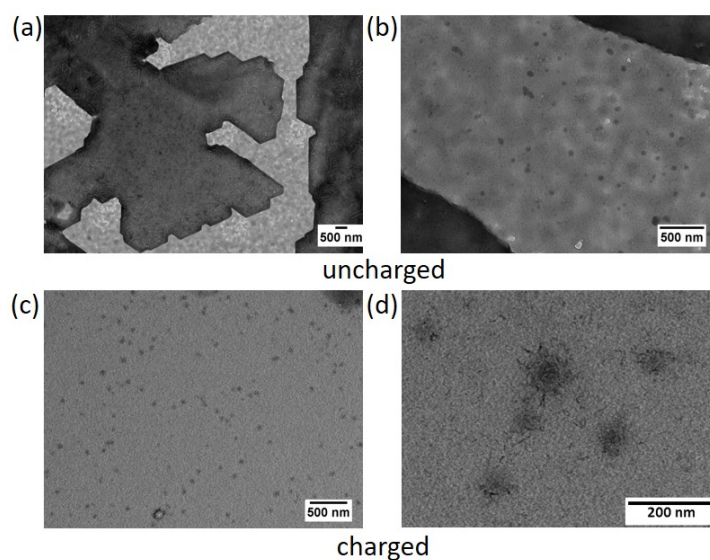


Figure 5.8: Transmission electron microscopy (TEM) images of uncharged (above) and charged (below) PTMA₆₃-*b*-PS₃₅ (**P7**, 13 mg mL⁻¹) in a mixture of EC/DMC/DEC (1:1:1 in volume) with 0.5 M Zn(ClO₄)₂·6 H₂O as conducting salt, (a) imaging of the uncharged catholyte, (b) zoom-in **Figure 5.8a**, (c) imaging of the charged catholyte, (d) zoom-in **Figure 5.8c**.

With the obtained results from the HFB tests as well as the special micellar architecture, the TEMPO-containing copolymer **P7** showed a high potential as charge-storage material for flow battery applications.

6 Summary

As a result of climate change, which is mainly caused by greenhouse gas emissions, in particular of CO₂, the world energy production is shifting increasingly towards renewable energy solutions such as photovoltaics and geothermal energy as well as wind power, biomass and hydroelectricity. Due to certain restrictions of hydroelectricity and geothermal energy, in particular, solar energy and wind power, will become the most important renewable energy resources in future. Unfortunately, today's electricity grids are not suitable for these intermittent electricity generation. Therefore, to render the "Energiewende" successfully they have to be advanced to so called "smart grids", which combine an intermittent renewable energy production and decentralized small scale power plants with low-cost energy storage technologies. In particular redox-flow batteries (**Figure 6.1**), which can be precisely adapted to the generator unit, are due to certain benefits like lifetime, safety and economical aspects, transportability, modularity and flexible applicability well suited for the storage of wind and solar electricity.

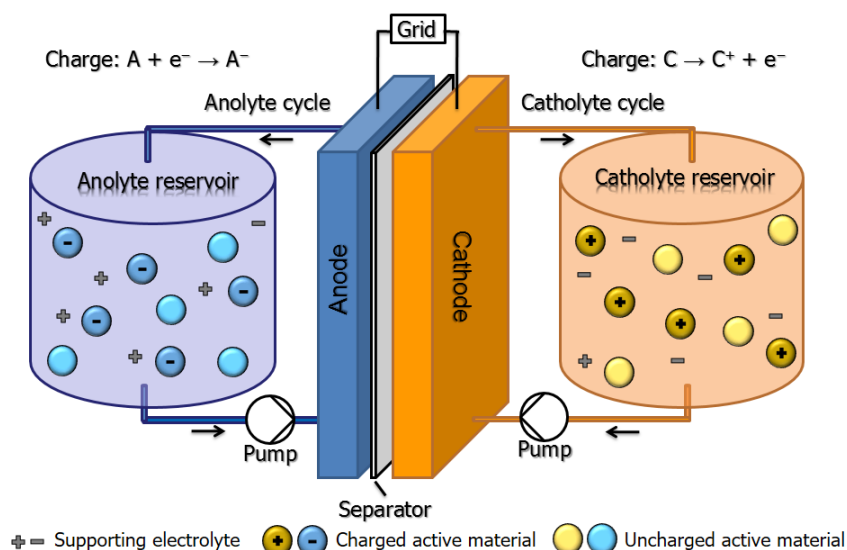


Figure 6.1: Schematic representation of the principle structure of a redox-flow battery, which consists of two external reservoirs for the storage of the charged/discharged electrolytes, pumps for circulating the electrolytes through the system, an electrochemical cell with two compartments detached by a separator and a connection to the grid.

Additionally, flow batteries feature an independent scalability of capacity and power, simply by the separate sizing of the volume of the external reservoirs and the size of the electrochemical cell. However, commercially available state-of-the-art metal-based systems like the all-vanadium RFB feature serious drawbacks such as the use of high-cost metal salts, hazardous and highly corrosive acidic electrolyte solutions as well as expensive perfluorinated membranes. The development of an all-organic RFB,

Summary

preferably in a safe aqueous electrolyte systems, utilizing sustainable and economic organic charge-storage materials as well as affordable membranes can overcome these disadvantages. In particular, the redox-active material represents one of the most important factors in terms of the costs and performance of the flow battery. Organic active materials, when the raw materials are affordable, no or minor synthesis effort is required and a complicated purification process can be avoided, feature a substantial price advantage compared to metal-based materials. Furthermore, the solubility as well as the redox properties of organics can be adapted by introduction of specific substituents or functional groups. Therefore, within this thesis, low-molar-mass as well as polymeric organic redox-active materials for aqueous and non-aqueous electrolyte systems were synthesized and their applicability as charge-storage materials in a flow battery were investigated in detail. In particular, bipolar active materials, which feature two reversible redox pairs and can, therefore, simultaneously be utilized both as cathode and as anode material were extensively studied. Furthermore, for the first time a combination of an organic low-molar-mass- and a polymer-based active material was implemented. Also tailor-made (2,2,6,6-tetramethyl-piperidin-1-yl)oxyl (TEMPO)-containing copolymers, in one instance a special shaped copolymer with a micellar structure, were prepared and utilized in a hybrid-flow battery (HFB). An overview of the investigated redox-active materials and their redox potentials are given in

Figure 6.2.

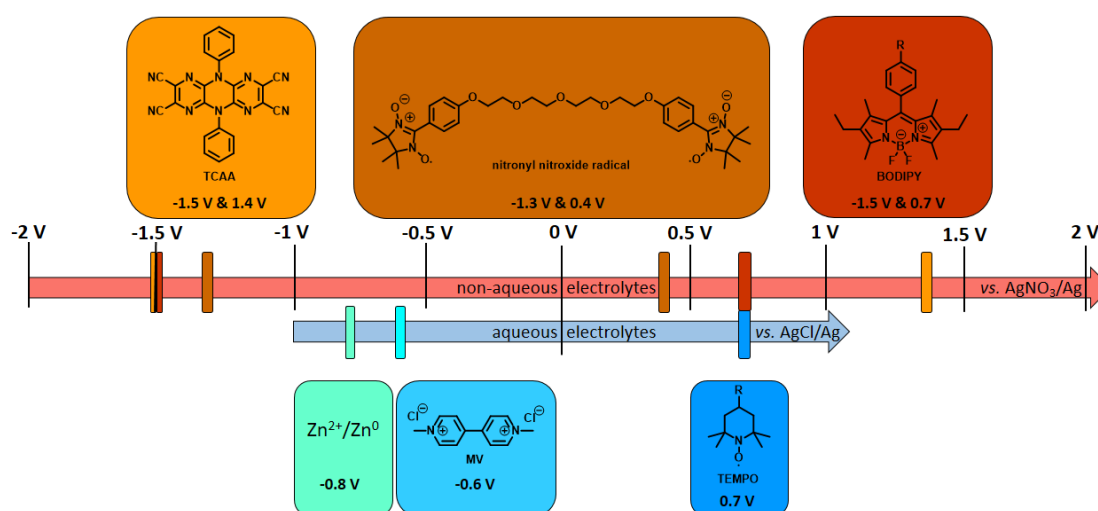


Figure 6.2: Schematic representation of the low-molar-mass- and polymer-based redox-active materials, which were investigated in this thesis, and their redox potential. The stated redox potentials were measured (depending on the used electrolyte system) vs. AgNO₃/Ag (non-aqueous system) or AgCl/Ag (aqueous system).

Summary

The development of a symmetric RFB, which represents virtually an all-vanadium redox-flow battery equivalent, is of high interest due to certain benefits such as a less effort on synthesis and engineering of the electrolyte, a simplified cell design and primarily an avoidance of cross-contamination. For this purpose, three different bipolar redox-active materials, a nitronyl nitroxide (NN) radical **4**, a 2,3,7,8-tetracyano-1,4,5,6,9,10-hexazaanthracene (TCAA) derivative **6** and two boron-dipyrromethene (BODIPY) containing copolymers **P2** and **P3** were synthesized. An utilization of these materials in the preferred aqueous electrolyte system was not possible because of the limited potential window of water (-1.5 to 1.5 V).

The NN containing compound **4** exhibited a quasi-reversible oxidation ($E_{1/2} = 0.37$ V *vs.* AgNO_3/Ag) and reduction reaction ($E_{1/2} = -1.25$ V *vs.* AgNO_3/Ag) as well as a diffusion-controlled behavior. A static battery setup exhibited a stable cycling over 75 consecutive charge/discharge cycles with coulombic efficiencies of up to 95% and a voltage efficiency of 86%.

The TCAA derivatives represents another substance class of potential bipolar active materials and are highly interesting due to their high redox voltage of around 3 V. Since this substance class was up to now only rudimentary investigated, a low-molar-mass derivative **6** was synthesized and extensively studied, to evaluate his potential as bipolar redox-active material. Initially performed density functional theory (DFT) calculations and cyclic voltammetry (CV) measurements revealed a quasi-reversible redox reactions at a half-wave potential of 1.42 V and -1.49 V *vs.* Fc^+/Fc . However, further studies (UV-vis-NIR spectroelectrochemistry and rotating disk electrode (RDE) measurements) exhibited for the reduction/re-oxidation redox pair a non stable redox behavior, which prevent a utilization of **6** in a symmetric RFB. Nevertheless, an introduction of other substituents to stabilize the reduced species can enable an applicability of TCAA derivatives as active material in a RFB.

Also BODIPY derivatives feature under specific structural conditions two chemical reversible redox processes. Therefore, two styrene-based BODIPY-containing copolymers **P2** and **P3** were synthesized. CV and UV-vis-NIR spectroelectrochemical measurements revealed a chemical reversibility of the $\text{BODIPY}^+/\text{BODIPY}$ and the $\text{BODIPY}/\text{BODIPY}^-$ redox couple at a half-wave potential at -1.51 V and 0.69 V *vs.* AgNO_3/Ag , respectively. Unfortunately, further analyses exhibited for **P2** a none ideal applicability as cathode redox-active material. Since **P3** caused by the polarity of the

Summary

comonomer, appears more suited as cathode active material, an all-BODIPY battery with **P2** as anode and **P3** as cathode redox-active material was manufactured and displayed over 100 cycles a stable battery cycling with coulombic efficiencies of up to 89%. Nevertheless, up to now a flow battery with only one bipolar BODIPY copolymer could not be demonstrated.

Also, for the first time, a combined aqueous all-organic RFB, utilizing the copolymer poly(2,2,6,6-tetramethyl-piperidinyloxy-4-yl methacrylate-co-[2-(methacryloyloxy)ethyl] trimethyl ammonium chloride) (**P1**) as catholyte as well as the low-molar-mass *N,N'*-dimethyl-4,4'-bipyridinium dichloride (**MV**) as anolyte, was developed. In order to achieve the best possible battery performance key factors such as the type of the used anion-exchange membrane, the influence of the electrolyte flow rate as well as the concentration of the conducting salt was investigated. Finally, on the basis of the achieved information, a pumped test cell was manufactured and exhibited over 100 cycles a stable performance with an overall energy density of 3.6 W h L^{-1} , coulombic efficiencies up to 95%, and voltage efficiencies of up to 91%.

Furthermore, two novel and “green” organic/inorganic poly(TEMPO)/zinc hybrid-flow batteries (HFB) were developed, utilizing inexpensive TEMPO-containing copolymers as cathode active materials. Initially three different types of statistically distributed linear copolymers **P1**, **P5** and **P6** were synthesized by a free radical copolymerization. An aqueous HFB comprising the water soluble **P1** and a low-cost dialysis membrane, with zinc foil as anode and zinc salt as conducting salt as well as anode active material, respectively, was cycled for 1,000 consecutive charge/discharge cycles at a current density of 2 mA m^{-2} and revealed with a discharging capacity retention of 79% a good chemical reversibility as well as long-term stability. In contrast **P5**, which feature otherwise than **P1** and **P6** only a low solubility in aqueous media, was utilized in a non-aqueous HFB. A material activity of 99% and a coulombic efficiency above 89% were achieved.

The use of special shaped polymers such as micellar or dendrimeric architectures can significantly reduce the electrolyte viscosity. Therefore, the tailor-made block copolymer PTMA₆₃-*b*-PS₃₅ (**P7**), featuring a micellar structure, which was proved *via* rheological and dynamic light scattering (DLS) measurements, was synthesized and investigated in a non-aqueous poly(TEMPO)/Zn HFB. A long-term stability test in a static setup over 1,000 consecutive charge/discharge cycles, whereby a coulombic

Summary

efficiency of up to 99.8% and a discharge capacity retention of 95% was reached, revealed a excellent reversibility for the employed micellar TEMPO-containing catholyte.

In summary, flow batteries display a great potential as future energy-storage system of choice. In particular, organic-based flow batteries feature, compared to the classic metal-based systems, several benefits concerning costs, social and environmental aspects as well as specific performance parameters. Another important advantage is the possibility to adapt the redox properties and/or solubility of the organic active materials by the introduction of substituents or functional groups. For these named reasons, a variety of semi- and all-organic flow batteries were developed and reported in literature in the last years. However, there are still several challenges which need to be met. Consequently, future research should be focused on the improvement of the solubility in their uncharged as well as charged state, and the reversibility of the redox couples of the used active materials to increase the energy density and the lifetime, respectively. Furthermore the overall cost should be further reduced, for example due to the use of simple low-priced separators, water as solvent as well as sodium chloride as conducting salt and earth-abundant metals or in particular organics as active materials.

7 Zusammenfassung

Aufgrund des Klimawandels, der hauptsächlich durch die Emission von Treibhausgasen, allen voran durch CO_2 , verursacht wurde, hat ein Umdenken bei der weltweiten Energieproduktion hin zu erneuerbaren Energien wie zum Beispiel Solar- und Windenergie, Geothermie, Biomasse und Wasserkraft stattgefunden. Vor allem Solar- und Windenergie, da sie im Gegensatz zur Geothermie und Wasserkraft keinen Einschränkungen unterliegen, werden in Zukunft die bedeutendsten erneuerbaren Energiequellen darstellen. Allerdings sind die bestehenden Stromnetze nicht für diese periodische Stromerzeugung geeignet. Um die Energiewende erfolgreich durchführen zu können muss eine Weiterentwicklung der existierenden Stromnetze hin zu sogenannten “smart grids”, die eine periodische regenerative Stromerzeugung, dezentralisierte kleinere Kraftwerke sowie preiswerte Energiespeicherung miteinander kombinieren, erfolgen.

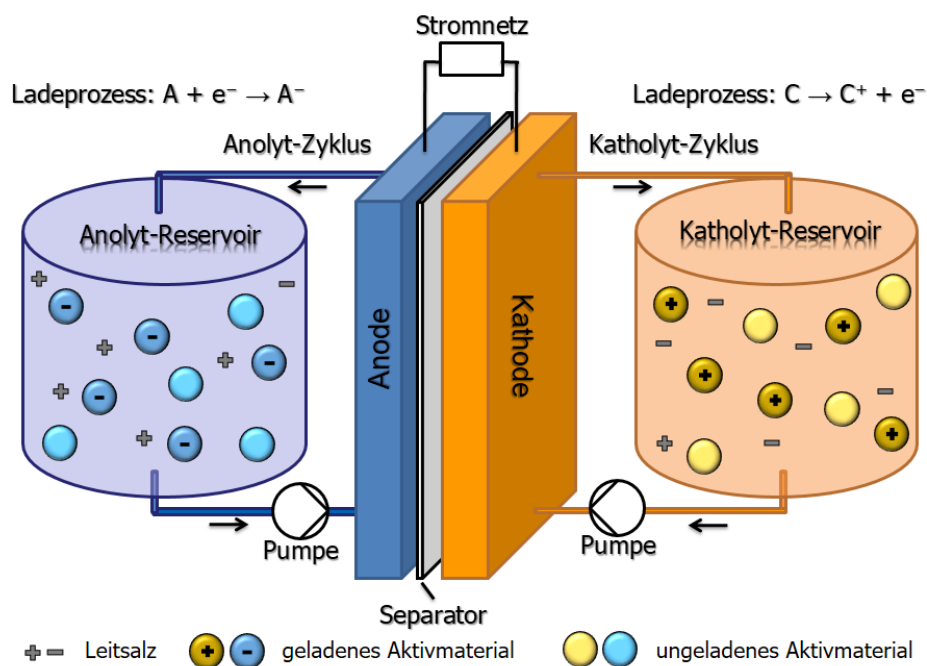


Abbildung 7.1: Schematische Darstellung des Aufbaus einer Redox-Flow Batterie, bestehend aus zwei externen Vorratsbehältern für die geladenen/ungeladenen Elektrolyte, Pumpen welche die Elektrolyte durch das System zirkulieren, einer elektrochemischen Zelle mit zwei Halbzellen, die durch einen Separator getrennt sind, sowie einer Verbindung zu einem Stromnetz.

Besonders die Redox-Flow-Batterie (**Abbildung 7.1**) ist durch bestimmte Vorteile, wie beispielsweise ihre lange Lebenszeit, Wirtschaftlichkeit, Transportierbarkeit, Modularität sowie einer flexiblen Anwendbarkeit, besonders geeignet für die Speicherung von Solar- und Windstrom. Darüber hinaus verfügen Flow-Batterien durch separate Skalierbarkeit des Volumens der externen Vorratsbehälter und der Größe der

elektrochemischen Zelle über eine unabhängige Skalierbarkeit in Kapazität und Leistung. Jedoch weisen die kommerziell erhältlichen, metallbasierten Systeme einige entscheidende Nachteile auf, wie z.B. die Verwendung von teuren Metallsalzen und perfluorierten Membranen sowie gefährliche und hochkorrosive Elektrolytlösungen. Die Entwicklung einer voll-organischen RFB, bevorzugt in einem wässrigen Elektrolytssystem, die nachhaltige und ökonomische organische Materialien zur Ladungsspeicherung sowie erschwingliche Membranen verwendet, kann potentiell diese Nachteile überwinden. Besonders die redoxaktiven Materialien stellen in Bezug auf die Kosten sowie die Leistungsfähigkeit einer Flow-Batterie einen entscheidenden Einflußfaktor dar. Organische Aktivmaterialien, falls die Rohstoffe preiswert sind, kein oder nur ein geringer Synthesaufwand nötig ist und darüberhinaus ein komplexer Reinigungsprozess vermieden werden kann, weisen gegenüber metallbasierten Aktivmaterialien einen erheblichen Kostenvorteil auf. Zusätzlich können die Löslichkeit und die Redox Eigenschaften organischer Materialien durch die Einführung geeigneter Substituenten oder funktioneller Gruppen gezielt eingestellt werden. Daher wurden im Rahmen dieser Doktorarbeit niedermolekulare sowie polymerbasierte organische redoxaktive Materialien für wässrige und nicht wässrige Elektrolytsysteme hergestellt und ihre Anwendbarkeit als Aktivmaterial in einer Flow-Batterie detailliert untersucht. Ein Überblick über die untersuchten redoxaktiven Materialien und deren Redoxpotentiale ist in **Abbildung 7.2** gegeben.

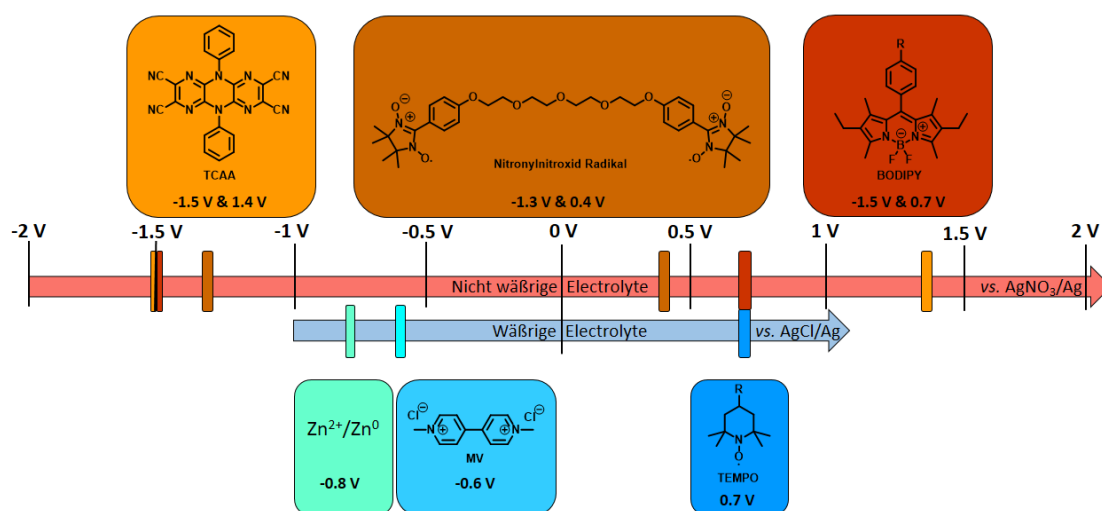


Abbildung 7.2: Schematische Darstellung der im Rahmen dieser Doktorarbeit untersuchten niedermolekularen und polymerbasierten redoxaktiven Materialien sowie deren Redoxpotentiale. Die angegebenen Redoxpotentiale wurden (in Abhängigkeit vom verwendeten Elektrolytsystem) gegen AgNO₃/Ag (nicht wässrige Systeme) oder AgCl/Ag (wässrige Systeme) gemessen.

Besonders intensiv wurden bipolare Aktivmaterialien, welche zwei reversible Redoxpaare besitzen und daher gleichzeitig sowohl als Kathoden- als auch als Anodenmaterial verwendet werden können, studiert. Außerdem wurde erstmals eine Kombination eines organischen niedermolekularen redoxaktiven Materials und einem redoxaktiven Polymer umgesetzt. Desweiteren wurden maßgeschneiderte Copolymere mit 2,2,6,6-Tetramethylpiperidinyloxyl (TEMPO) als redoxaktive Einheit, in einem Fall sogar mit einer speziellen mizellaren Struktur, hergestellt und in einer Hybrid-Flow-Batterie (HFB) untersucht.

Die Entwicklung einer symmetrischen RFB ist aufgrund gewisser Vorteile wie z.B. einem geringeren Aufwand bei der Synthese und der Entwicklung der Elektrolyte, ein vereinfachtes Zelldesign und vor allem eine Vermeidung einer Kreuzkontaminationen von hohem Interesse. Darum wurden drei verschiedene bipolare redoxaktive Materialien, ein Nitronylnitroxid (NN)-Radikal **4**, ein 2,3,7,8-Tetracyano-1,4,5,6,9,10-hexazaanthracen (TCAA)-Derivat **6** sowie zwei Borondipyrrromethen (BODIPY) Copolymere **P2** und **P3** hergestellt und anschließend detailliert erforscht. Eine Verwendung dieser Materialien in einem wässrigen Elektrolytsystem war wegen des begrenzten Potentialfensters von Wasser ($-1,5$ bis $1,5$ V) nicht möglich.

Das Nitronylnitroxidderivat **4** zeigte eine quasi-reversible Oxidations- ($E_{1/2} = 0,37$ V gegen AgNO_3/Ag) und Reduktionsreaktion ($E_{1/2} = -1,25$ V gegen AgNO_3/Ag) sowie ein diffusionskontrolliertes Verhalten. In einer ungepumpten Batterie konnte über 75 aufeinanderfolgenden Lade-/Entladezyklen ein stabiles Verhalten demonstriert werden. Dabei wurden Coulomb-Effizienzen von bis zu 95% und Spannungs-Effizienzen von bis zu 86% erzielt. TCAA-Derivate, eine weitere Substanzklasse potentiell bipolarer Aktivmaterialien, sind insbesondere durch ihre sehr hohe Redox-Spannung von etwa 3 V interessant. Da diese Substanzklasse bislang nur ansatzweise erforscht ist, wurde ein niedermolekulares Derivat **6** hergestellt und explizit im Hinblick auf sein Potential als bipolares redoxaktives Material untersucht. Die zu Beginn durchgeführten Dichtefunktionaltheorie (DFT)-Berechnungen sowie Cyclovoltammetrie (CV)-Messungen ergaben zwei quasi-reversible Redoxreaktion bei einem Halbstufenpotential von 1,42 V und $-1,49$ V gegen Fc^+/Fc . Allerdings offenbarten weitere Untersuchungen durch UV-vis-NIR-Spektroelektrochemie und rotierende Scheibenelektroden (RDE)-Messungen ein instabiles Redoxverhalten für das Reduktions-/Re-oxidations-Redoxpaar. Um diese Substanzklasse als bipolares Aktivmagterial zu verwenden muss

also zunächst die reduzierter Spezies, z.B. durch die Einführung geeigneter Substituenten, stabilisiert werden. Unter bestimmten strukturellen Voraussetzungen besitzen auch BODIPY-Derivate zwei chemisch reversible Redoxprozesse. Daher wurden zwei styrolbasierte BODIPY Copolymere **P2** und **P3** hergestellt. CV- und UV-vis-NIR-spektroelektrochemische Messungen zeigten eine chemische Reversibilität des BODIPY⁺/BODIPY- sowie des BODIPY/BODIPY⁻-Redoxpaares bei einem Halbstufenpotential von -1,51 V bzw. 0,69 V gegen AgNO₃/Ag. Unglücklicherweise offenbarten weitere Analysen von **P2** keine ideale Eignung als Kathodenmaterial. Da **P3** aufgrund der Polarität seines Comonomers sich besser als Kathodenmaterial eignet wurde schließlich eine Batterie mit zwei BODIPY Copolymeren, **P2** und **P3**, hergestellt. Über 100 aufeinanderfolgenden Zyklen, mit Coulomb-Effizienzen von bis zu 89%, konnte ein stabiler Betrieb der Batterie gezeigt werden. Jedoch gelang es bislang noch nicht eine voll-organische Flow-Batterie, die nur ein bipolares BODIPY-Copolymer gleichzeitig als Anoden- und Kathodenmaterial verwendet, zu entwickeln.

Zum ersten Mal wurde auch eine kombinierte voll-organische RFB entwickelt, die sowohl ein Polymer, das Poly(2,2,6,6-tetramethylpiperidinyloxy-4-ylmethacrylat-co-[2-(methacryloyloxy)ethyl] trimethylammoniumchlorid) (**P1**) als Katholyt, sowie das niedermolekulare *N,N'*-Dimethyl-4,4'-bipyridiniumdichlorid (**MV**) als Anolyt verwendet. Um die bestmögliche Batterieleistung zu erzielen, wurden verschiedenen wichtige Faktoren wie die Art der verwendeten Anionenaustauschermembran, die Fließgeschwindigkeit des Elektrolyten sowie die Konzentration des Leitsalzes untersucht. Die letztendlich auf der Grundlage der erhaltenen Informationen gefertigte gepumpte Testzelle zeigte über 100 Zyklen eine stabile Leistung mit einer Energiedichte von 3,6 W h L⁻¹, einer Coulomb-Effizienz von bis zu 95% und eine Spannungs-Effizienz von bis zu 91%.

Neben den bereits genannten Systemen wurden zwei neue „grüne“ organisch/anorganische Poly(TEMPO)/Zink HFBs, die kostengünstige TEMPO Copolymere als Kathodenmaterial verwenden, entwickelt. Zunächst wurden drei verschiedenartige statistisch verteilte lineare Copolymere **P1**, **P5** und **P6** mittels freier radikalischer Copolymerisation hergestellt. Eine wässrige HFB, mit Zinkfolie als Anode, Zinksalz als Leitsalz sowie Anodenmaterial, dem wasserlöslichen **P1** als Kathodenmaterial sowie einer günstigen Dialysemembran, zeigte bei einer Stromdichte von 2 mA m⁻² über 1000 aufeinanderfolgende Ladungs-/Entladungszyklen einen Erhalt der

ursprünglichen Entladungskapazität von 79% und somit eine gute chemische Reversibilität sowie Langzeitstabilität. Da das Copolymer **P5** im Gegensatz zu **P1** und **P6** nur eine geringe Löslichkeit in Wasser aufweist, wurde es in einer nicht wässrigen HFB eingesetzt. Dabei konnte eine Materialaktivität von 99% und eine Coulomb-Effizienz von über 89% erreicht werden. Durch die Verwendung von Polymeren mit speziellen Architekturen, wie z.B. mizellaren oder dendrimeren Strukturen, kann die Elektrolytviskosität deutlich verringert werden. Aus diesem Grund wurde das maßgeschneiderte Blockcopolymer PTMA₆₃-*b*-PS₃₅ (**P7**) mit einer mizellaren Struktur, die durch rheologische und dynamische Lichtstreuungs (DLS)-Messungen nachgewiesen wurde, hergestellt und in einer nicht wässrigen Poly(TEMPO)/Zn HFB untersucht. Ein Langzeitstabilitätstest in einem ungepumpten Setup über 1000 aufeinanderfolgenden Lade-/Entladezyklen zeigte eine Coulomb-Effizienz von bis zu 99,8%, einen Erhalt der ursprünglichen Entladungskapazität von 95% und demzufolge eine ausgezeichnete Reversibilität für das verwendete mizellare Copolymer-Kathodenmaterial.

Zusammenfassend lässt sich sagen, dass Flow-Batterien ein großes Potenzial als zukünftige Energiespeichersystem der Wahl haben. Insbesondere organische Flow-Batterien weisen im Vergleich zu den klassischen metallbasierten Systemen einige Vorteile in Bezug auf Kosten, soziale und umweltbezogene Aspekte sowie spezifische Leistungsparameter auf. Ein weiterer großer Vorteil ist die Möglichkeit, die Redox Eigenschaften und/oder die Löslichkeit von organischen Aktivmaterialien durch die Einführung von Substituenten oder funktionellen Gruppen gezielt einzustellen. Allerdings gibt es noch einige Herausforderungen die bewältigt werden müssen. Infolgedessen sollte sich die zukünftige Forschung auf die Verbesserung der Löslichkeit der Aktivmaterialien in ihrem ungeladenen sowie geladenen Zustand, und die Reversibilität ihrer Redoxpaare fokussieren, um die Energiedichte bzw. die Lebensdauer zu erhöhen. Darüber hinaus sollten die Gesamtkosten signifikant weiter reduziert werden, zum Beispiel durch den Einsatz einfacher, preisgünstiger Separatoren, Wasser als Lösungsmittel sowie Natriumchlorid als Leitsalz, und durch auf der Erde in genügendem Maße vorkommende Metalle oder insbesondere durch organische Stoffe als Aktivmaterialien.

8 References

- [1] Enerdata, Global Energy Statistical Yearbook 2017, <https://yearbook.enerdata.net/world-electricity-production-map-graph-and-data.html#world-electricity-production-map-graph-and-data.html>, **2017** (last accessed 11.09.17).
- [2] T. S. P. Data Portal, Breakdown of Electricity Generation by Energy Source, <http://www.tsp-data-portal.org/Breakdown-of-Electricity-Generation-by-Energy-Source#tspQvChart>, **2016** (last accessed 11.04.17).
- [3] P. J. Meier, P. P. H. Wilson, G. L. Kulcinski, P. L. Denholm, *Energy Policy* **2005**, 33, 1099-1108.
- [4] Z. J. N. Steinmann, A. Venkatesh, M. Hauck, A. M. Schipper, R. Karuppiah, I. J. Laurenzi, M. A. J. Huijbregts, *Environ. Sci. Technol.* **2014**, 48, 5282-5289.
- [5] Y. Zhang, J. McKechnie, D. Cormier, R. Lyng, W. Mabee, A. Ogino, H. L. MacLean, *Environ. Sci. Technol.* **2010**, 44, 538-544.
- [6] Z. Yang, J. Zhang, M. C. W. Kintner-Meyer, X. Lu, D. Choi, J. P. Lemmon, J. Liu, *Chem. Rev.* **2011**, 111, 3577-3613.
- [7] C. Le Quéré, R. Moriarty, R. M. Andrew, J. G. Canadell, S. Sitch, J. I. Korsbakken, P. Friedlingstein, G. P. Peters, R. J. Andres, T. A. Boden, R. A. Houghton, J. I. House, R. F. Keeling, P. Tans, A. Arneeth, D. C. E. Bakker, L. Barbero, L. Bopp, J. Chang, F. Chevallier, L. P. Chini, P. Ciais, M. Fader, R. A. Feely, T. Gkritzalis, I. Harris, J. Hauck, T. Ilyina, A. K. Jain, E. Kato, V. Kitidis, K. Klein Goldewijk, C. Koven, P. Landschützer, S. K. Lauvset, N. Lefèvre, A. Lenton, I. D. Lima, N. Metzl, F. Millero, D. R. Munro, A. Murata, J. E. M. S. Nabel, S. Nakaoka, Y. Nojiri, K. O'Brien, A. Olsen, T. Ono, F. F. Pérez, B. Pfeil, D. Pierrot, B. Poulter, G. Rehder, C. Rödenbeck, S. Saito, U. Schuster, J. Schwinger, R. Séférian, T. Steinhoff, B. D. Stocker, A. J. Sutton, T. Takahashi, B. Tilbrook, I. T. van der Laan-Luijkx, G. R. van der Werf, S. van Heuven, D. Vandemark, N. Viovy, A. Wiltshire, S. Zaehle, N. Zeng, *Earth Syst. Sci. Data* **2015**, 7, 349-396.
- [8] P. Tans, R. Keeling, NOAA ESRL DATA: Recent Global CO₂, <https://www.esrl.noaa.gov/gmd/ccgg/trends/global.html>, **2017** (last accessed 11.09.17).
- [9] J. T. Houghton, L. G. M. Filho, B. A. Callander, N. Harris, A. Kattenberg, K. Maskell, *Climate Change 1995: The Science of Climate Change*, Cambridge Univ. Press, **1996**.
- [10] P. M. Cox, R. A. Betts, C. D. Jones, S. A. Spall, I. J. Totterdell, *Nature* **2000**, 408, 184-187.
- [11] S. Solomon, G.-K. Plattner, R. Knutti, P. Friedlingstein, *Proc. Natl. Acad. Sci.* **2009**, 106, 1704-1709.
- [12] P. Friedlingstein, R. A. Houghton, G. Marland, J. Hackler, T. A. Boden, T. J. Conway, J. G. Canadell, M. R. Raupach, P. Ciais, C. Le Quere, *Nature Geosci.* **2010**, 3, 811-812.
- [13] J. Winsberg, T. Hagemann, T. Janoschka, M. D. Hager, U. S. Schubert, *Angew. Chem. Int. Ed.* **2017**, 56, 686-711.
- [14] D. Cook, B. Davidsdottir, J. G. Petursson, *Renew. Sust. Energ. Rev.* **2015**, 49, 211-220.
- [15] O. Edenhofer, K. Seyboth, F. Creutzig, S. Schlömer, *Annu. Rev. Environ. Resour.* **2013**, 38, 169-200.

References

- [16] S. Weitemeyer, D. Kleinhans, T. Vogt, C. Agert, *Renew. Energ.* **2015**, 75, 14-20.
- [17] N. Armaroli, V. Balzani, *Angew. Chem. Int. Ed.* **2007**, 46, 52-66.
- [18] Z. Abdmouleh, R. A. M. Alammari, A. Gastli, *Renew. Sust. Energ. Rev.* **2015**, 45, 249-262.
- [19] H. Wirth, Fraunhofer Institut for Solar Energy Systems ISE, <https://www.ise.fraunhofer.de/en/publications/veroeffentlichungen-pdf-dateien-en/studien-und-konzeptpapiere/recent-facts-about-photovoltaics-in-germany.pdf>, **2016** (last accessed 11.09.17).
- [20] Eurostat. Electricity generated from renewable sources, http://ec.europa.eu/eurostat/statistics-explained/index.php/Energy_from_renewable_sources#cite_note-2, **2017** (last accessed 11.09.17).
- [21] Renewables 2017 Global Status Report, http://www.ren21.net/wp-content/uploads/2017/06/17-8399_GSR_2017_Full_Report_0621_Opt.pdf, **2017** (last accessed 11.09.17).
- [22] International Energy Outlook 2016, <https://www.eia.gov/outlooks/ieo/electricity.php>, **2017** (last accessed 11.09.17).
- [23] World Energy Council, <https://www.worldenergy.org/data/resources/resource/hydropower/>, **2017** (last accessed 11.09.17).
- [24] A. Sternberg, A. Bardow, *Energy Environ. Sci.* **2015**, 8, 389-400.
- [25] P. Cappers, J. MacDonald, C. Goldman, O. Ma, *Energy Policy* **2013**, 62, 1031-1039.
- [26] C. Budischak, D. Sewell, H. Thomson, L. Mach, D. E. Veron, W. Kempton, *J. Power Sources* **2013**, 225, 60-74.
- [27] P. Denholm, M. O'Connell, G. Brinkman, J. Jorgenson, *Overgeneration from Solar Energy in California: A Field Guide to the Duck Chart*, National Renewable Energy Laboratory, **2015**.
- [28] B. Burger, Fraunhofer-Institut für Solare Energiesysteme ISE, <http://www.ise.fraunhofer.de/de/downloads/pdf-files/data-nivc-/stromproduktion-aus-solar-und-windenergie-2014.pdf>, **2015** (last accessed 11.09.17).
- [29] M. S. Whittingham, *Proceedings of the IEEE* **2012**, 100, 1518-1534.
- [30] P. Alstone, D. Gershenson, D. M. Kammen, *Nature Clim. Change* **2015**, 5, 305-314.
- [31] B. Dunn, H. Kamath, J.-M. Tarascon, *Science* **2011**, 334, 928-935.
- [32] M. Skyllas-Kazacos, M. H. Chakrabarti, S. A. Hajimolana, F. S. Mjalli, M. Saleem, *J. Electrochem. Soc.* **2011**, 158, R55-R79.
- [33] P. C. B. Daniel H. Doughty, Abbas A. Akhil, Nancy H. Clark, and John D. Boyes, *Electrochem. Soc. Interface* **2010**, 49-53.
- [34] A. J. Salkind, A. G. Cannone, F. A. Trumbure (ed. D. Linden, T. B. Reddy) *Handbook of Batteries*, 3rd ed., McGraw-Hill, New-York **2002**, Chap. 23, 23.21-23.88.
- [35] J. T. Kummer, N. Weber, DE 1671760, **1968**.
- [36] D. Linden, T. B. Reddy (ed. D. Linden, T. B. Reddy) *Handbook of Batteries*, 3rd ed., McGraw-Hill, New-York **2002**, Chap. 14, 14.11-14.106.
- [37] G. L. Soloveichik, *Chem. Rev.* **2015**, 115, 11533-11558.
- [38] C. Ponce de León, A. Frías-Ferrer, J. González-García, D. A. Szánto, F. C. Walsh, *J. Power Sources* **2006**, 160, 716-732.
- [39] P. Alotto, M. Guarnieri, F. Moro, *Renew. Sust. Energ. Rev.* **2014**, 29, 325-335.
- [40] S. Roe, C. Menictas, M. Skyllas-Kazacos, *J. Electrochem. Soc.* **2016**, 163, A5023-A5028.

References

- [41] M. Skyllas-Kazacos, L. Cao, M. Kazacos, N. Kausar, A. Mousa, *ChemSusChem* **2016**, 9, 1521-1543.
- [42] M. Skyllas-Kazacos, M. Rychcik, R. G. Robins, A. G. Fane, *J. Electrochem. Soc.* **1986**, 133, 1057-1058.
- [43] H. L. Thaller, US 3996064, **1976**.
- [44] N. H. Hagedorn, L. H. Thaller, *NASA-TEM-82854 Design Flexibility of Redox Flow Systems*, **1982**.
- [45] M. Lopez-Atalaya, G. Codina, J. R. Perez, J. L. Vazquez, A. Aldaz, *J. Power Sources* **1992**, 39, 147-154.
- [46] C. S. Bradley, US 312802, **1885**.
- [47] D. J. Eustace, US 4064324, **1977**.
- [48] D. J. Eustace, *J. Electrochem. Soc.* **1980**, 127, 528-532.
- [49] T. Janoschka, N. Martin, U. Martin, C. Friebe, S. Morgenstern, H. Hiller, M. D. Hager, U. S. Schubert, *Nature* **2015**, 527, 78-81.
- [50] A. Crawford, V. Viswanathan, D. Stephenson, W. Wang, E. Thomsen, D. Reed, B. Li, P. Balducci, M. Kintner-Meyer, V. Sprenkle, *J. Power Sources* **2015**, 293, 388-399.
- [51] V. Viswanathan, A. Crawford, D. Stephenson, S. Kim, W. Wang, B. Li, G. Coffey, E. Thomsen, G. Graff, P. Balducci, M. Kintner-Meyer, V. Sprenkle, *J. Power Sources* **2014**, 247, 1040-1051.
- [52] J. Winsberg, T. Janoschka, S. Morgenstern, S. Muench, T. Hagemann, G. Hauffman, J.-F. Gohy, M. D. Hager, U. S. Schubert, *Adv. Mater.* **2016**, 28, 2238-2243.
- [53] K. Lin, Q. Chen, M. R. Gerhardt, L. Tong, S. B. Kim, L. Eisenach, A. W. Valle, D. Hardee, R. G. Gordon, M. J. Aziz, M. P. Marshak, *Science* **2015**, 349, 1529-1532.
- [54] M. E. Easton, P. Turner, A. F. Masters, T. Maschmeyer, *RSC Adv.* **2015**, 5, 83674-83681.
- [55] J.-D. Jeon, H. S. Yang, J. Shim, H. S. Kim, J. H. Yang, *Electrochim. Acta* **2014**, 127, 397-402.
- [56] T. Hagemann, J. Winsberg, A. Wild, U. S. Schubert, *Electrochim. Acta* **2017**, 228, 494-502.
- [57] T. Hagemann, J. Winsberg, B. Häupler, T. Janoschka, J. J. Gruber, A. Wild, U. S. Schubert, *NPG Asia Mater* **2017**, 9, e340.
- [58] R. A. Potash, J. R. McKone, S. Conte, H. D. Abruña, *J. Electrochem. Soc.* **2016**, 163, A338-A344.
- [59] W. Duan, R. S. Vemuri, J. D. Milshtein, S. Laramie, R. D. Dmello, J. Huang, L. Zhang, D. Hu, M. Vijayakumar, W. Wang, J. Liu, R. M. Darling, L. Thompson, K. Smith, J. S. Moore, F. R. Brushett, X. Wei, *J. Mater. Chem. A* **2016**, 4, 5448-5456.
- [60] S. H. Oh, C. W. Lee, D. H. Chun, J. D. Jeon, J. Shim, K. H. Shin, J. H. Yang, *J. Mater. Chem. A* **2014**, 2, 19994-19998.
- [61] X. Sun, T. Souier, M. Chiesa, A. Vassallo, *Electrochim. Acta* **2014**, 148, 104-110.
- [62] G. Nikiforidis, W. A. Daoud, *J. Electrochem. Soc.* **2015**, 162, A809-A819.
- [63] P. Trogadas, O. O. Taiwo, B. Tjaden, T. P. Neville, S. Yun, J. Parrondo, V. Ramani, M.-O. Coppens, D. J. L. Brett, P. R. Shearing, *Electrochem. Commun.* **2014**, 48, 155-159.
- [64] R. M. Darling, K. G. Gallagher, J. A. Kowalski, S. Ha, F. R. Brushett, *Energy Environ. Sci.* **2014**, 7, 3459-3477.

References

- [65] P. K. Leung, C. Ponce-de-León, C. T. J. Low, F. C. Walsh, *Electrochim. Acta* **2011**, 56, 6536-6546.
- [66] A. Weber, M. Mench, J. Meyers, P. Ross, J. Gostick, Q. Liu, *J. Appl. Electrochem.* **2011**, 41, 1137-1164.
- [67] J.-Y. Chen, C.-L. Hsieh, N.-Y. Hsu, Y.-S. Chou, Y.-S. Chen, *Energies* **2014**, 7, 5863.
- [68] K. Bromberger, J. Kaunert, T. Smolinka, *Energy Technol.* **2014**, 2, 64-76.
- [69] W. Kangro, DE 914264, **1949**.
- [70] W. Kangro, DE 1006479, **1957**.
- [71] N. H. Hagedorn, *NASA TM-83677 Redox Storage System Development Project*, **1984**.
- [72] M. Skyllas-Kazacos, R. G. Robins, AU 575247, **1986**.
- [73] M. H. Chakrabarti, R. A. W. Dryfe, E. P. L. Roberts, *Electrochim. Acta* **2007**, 52, 2189-2195.
- [74] M. H. Chakrabarti, E. P. L. Roberts, C. Bae, M. Saleem, *Energy Convers. Manage.* **2011**, 52, 2501-2508.
- [75] J. Cheng, L. Zhang, Y.-S. Yang, Y.-H. Wen, G.-P. Cao, X.-D. Wang, *Electrochem. Commun.* **2007**, 9, 2639-2642.
- [76] P. K. Leung, C. Ponce-de-León, C. T. J. Low, A. A. Shah, F. C. Walsh, *J. Power Sources* **2011**, 196, 5174-5185.
- [77] R. F. Savinell, C. C. Liu, R. T. Galasco, S. H. Chiang, J. F. Coetzee, *J. Electrochem. Soc.* **1979**, 126, 357-360.
- [78] F.-Q. Xue, Y.-L. Wang, W.-H. Wang, X.-D. Wang, *Electrochim. Acta* **2008**, 53, 6636-6642.
- [79] A. Hazza, D. Pletcher, R. Wills, *PCCP* **2004**, 6, 1773-1778.
- [80] D. Pletcher, R. Wills, *PCCP* **2004**, 6, 1779-1785.
- [81] A. Hazza, D. Pletcher, R. Wills, *J. Power Sources* **2005**, 149, 103-111.
- [82] D. Pletcher, H. Zhou, G. Kear, C. T. J. Low, F. C. Walsh, R. G. A. Wills, *J. Power Sources* **2008**, 180, 621-629.
- [83] J. Pan, Y. Sun, J. Cheng, Y. Wen, Y. Yang, P. Wan, *Electrochem. Commun.* **2008**, 10, 1226-1229.
- [84] L. Sanz, D. Lloyd, E. Magdalena, J. Palma, K. Kontturi, *J. Power Sources* **2014**, 268, 121-128.
- [85] T. Yamamura, Y. Shiokawa, H. Yamana, H. Moriyama, *Electrochim. Acta* **2002**, 48, 43-50.
- [86] C. Bae, E. P. L. Roberts, M. H. Chakrabarti, M. Saleem, *Int. J. Green Energy* **2011**, 8, 248-264.
- [87] M. Duduta, B. Ho, V. C. Wood, P. Limthongkul, V. E. Brunini, W. C. Carter, Y.-M. Chiang, *Adv. Energy Mater.* **2011**, 1, 511-516.
- [88] Y. Zhao, H. R. Byon, *Adv. Energy Mater.* **2013**, 3, 1630-1635.
- [89] Y. Yang, G. Zheng, Y. Cui, *Energy Environ. Sci.* **2013**, 6, 1552-1558.
- [90] B. Huskinson, M. P. Marshak, C. Suh, S. Er, M. R. Gerhardt, C. J. Galvin, X. Chen, A. Aspuru-Guzik, R. G. Gordon, M. J. Aziz, *Nature* **2014**, 505, 195-198.
- [91] B. Häupler, A. Wild, U. S. Schubert, *Adv. Energy Mater.* **2015**, 1402034.
- [92] J. Winsberg, T. Hagemann, S. Muench, C. Friebe, B. Häupler, T. Janoschka, S. Morgenstern, M. D. Hager, U. S. Schubert, *Chem. Mater.* **2016**, 28, 3401-3405.
- [93] K. M. Pelzer, L. Cheng, L. A. Curtiss, *J. Phys. Chem. C* **2017**, 121, 237-245.
- [94] X. Li, H. Zhang, Z. Mai, H. Zhang, I. Vankelecom, *Energy Environ. Sci.* **2011**, 4, 1147-1160.

References

- [95] J. Winsberg, S. Muench, T. Hagemann, T. Janoschka, S. Morgenstern, M. Billing, F. H. Schacher, G. Hauffman, J.-F. Gohy, S. Hoeppener, M. Hager, U. S. Schubert, *Polym. Chem.* **2016**, 7, 1711-1718.
- [96] T. Janoschka, N. Martin, M. D. Hager, U. S. Schubert, *Angew. Chem. Int. Ed.* **2016**, 55, 14427-14430.
- [97] T. Sukegawa, I. Masuko, K. Oyaizu, H. Nishide, *Macromolecules* **2014**, 47, 8611-8617.
- [98] Y. Zhao, S. Si, C. Liao, *J. Power Sources* **2013**, 241, 449-453.
- [99] Q. Lai, H. Zhang, X. Li, L. Zhang, Y. Cheng, *J. Power Sources* **2013**, 235, 1-4.
- [100] Y. H. Wen, H. M. Zhang, P. Qian, H. T. Zhou, P. Zhao, B. L. Yi, Y. S. Yang, *J. Electrochem. Soc.* **2006**, 153, A929-A934.
- [101] J.-H. Kim, K. J. Kim, M.-S. Park, N. J. Lee, U. Hwang, H. Kim, Y.-J. Kim, *Electrochem. Commun.* **2011**, 13, 997-1000.
- [102] Y. Xu, Y. Wen, J. Cheng, G. Cao, Y. Yang, *Electrochem. Commun.* **2009**, 11, 1422-1424.
- [103] W. Wang, W. Xu, L. Cosimbescu, D. Choi, L. Li, Z. Yang, *Chem. Commun.* **2012**, 48, 6669-6671.
- [104] X. Wei, W. Xu, M. Vijayakumar, L. Cosimbescu, T. Liu, V. Sprenkle, W. Wang, *Adv. Mater.* **2014**, 26, 7649-7653.
- [105] Q. Chen, M. R. Gerhardt, L. Hartle, M. J. Aziz, *J. Electrochem. Soc.* **2016**, 163, A5010-A5013.
- [106] Z. Li, S. Li, S. Liu, K. Huang, D. Fang, F. Wang, S. Peng, *Electrochem. Solid-State Lett.* **2011**, 14, A171-A173.
- [107] T. Liu, X. Wei, Z. Nie, V. Sprenkle, W. Wang, *Adv. Energy Mater.* **2016**, 6, 1501449.
- [108] Y. Xu, Y.-H. Wen, J. Cheng, G.-P. Cao, Y.-S. Yang, *Electrochim. Acta* **2010**, 55, 715-720.
- [109] K. Takechi, Y. Kato, Y. Hase, *Adv. Mater.* **2015**, 27, 2501-2506.
- [110] J. Huang, L. Cheng, R. S. Assary, P. Wang, Z. Xue, A. K. Burrell, L. A. Curtiss, L. Zhang, *Adv. Energy Mater.* **2015**, 5, 1401782.
- [111] X. Wei, W. Xu, J. Huang, L. Zhang, E. Walter, C. Lawrence, M. Vijayakumar, W. A. Henderson, T. Liu, L. Cosimbescu, B. Li, V. Sprenkle, W. Wang, *Angew. Chem. Int. Ed.* **2015**, 54, 8684-8687.
- [112] Y. K. Zeng, T. S. Zhao, L. An, X. L. Zhou, L. Wei, *J. Power Sources* **2015**, 300, 438-443.
- [113] L. R. F. A. J. Bard, *Electrochemical Methods*, 2nd ed., Wiley, New York **2001**.
- [114] https://www.alibaba.com/product-detail/4-Hydroxy-Tempo_60504037183.html?spm=a2700.7724857.main07.9.2bd13975WADEcC&s=p, **2017**, (last accessed 11.09.2017).
- [115] E. F. Ullman, J. H. Osiecki, D. G. B. Boocock, R. Darcy, *J. Amer. Chem. Soc.* **1972**, 94, 7049-7059.
- [116] E. F. Ullman, L. Call, J. H. Osiecki, *J. Org. Chem.* **1970**, 36, 3623-3631.
- [117] L. Dulog, J. S. Kim, *Makromol. Chem.* **1989**, 190, 2609-2614.
- [118] Y. Nakano, T. Yagyu, T. Hirayama, A. Ito, K. Tanaka, *Polyhedron* **2005**, 24, 2141-2147.
- [119] H. Nishide, Y. Hozumi, T. Nii, E. Tsuchida, *Macromolecules* **1997**, 30, 3986-3991.
- [120] D. Hou, M. Matsuoka, *Dyes and Pigments* **1993**, 22, 57-68.
- [121] J.-Y. Jaung, K. Fukunishi, M. Matsuoka, *J. Heterocycl. Chem.* **1997**, 34, 653-657.

References

- [122] M. J. Frisch, G. W. Trucks, H. B. Schlegel, G. Scuseria, M. A. E.; Robb, J. R. Cheeseman, G. Scalmani, V. Barone, B. Mennucci, G. A. Petersson, H. Nakatsuji, M. Caricato, X. Li, H. P. Hratchian, A. F. Izmaylov, J. Bloino, G. Zheng, J. L. Sonnenberg, M. Hada, M. Ehara, K. Toyota, R. Fukuda, J. Hasegawa, M. Ishida, T. Nakajima, Y. Honda, O. Kitao, H. Nakai, T. Vreven, J. Montgomery, J. A., J. Peralta, F. E.; Ogliaro, M. Bearpark, J. J. Heyd, E. Brothers, K. N. Kudin, V. N. Staroverov, R. Kobayashi, J. Normand, K. Raghavachari, A. Rendell, J. C. Burant, S. S. Iyengar, J. Tomasi, M. Cossi, N. Rega, N. J. Millam, M. Klene, J. E. Knox, J. B. Cross, V. Bakken, C. Adamo, J. Jaramillo, R. Gomperts, R. E. Stratmann, O. Yazyev, A. J. Austin, R. Cammi, C. Pomelli, J. W. Ochterski, R. L. Martin, K. Morokuma, V. G. Zakrzewski, G. A. Voth, P. Salvador, J. J. Dannenberg, S. Dapprich, A. D. Daniels, Ö. Farkas, J. B. Foresman, J. V. Ortiz, J. Cioslowski, D. J. Fox, Revision A.02 ed., Gaussian, Inc., Wallingford, CT, **2010**.
- [123] A. D. Becke, *J. Chem. Phys.* **1993**, *98*, 5648-5652.
- [124] C. T. Lee, W. T. Yang, R. G. Parr, *Physical Review B* **1988**, *37*, 785-789.
- [125] E. Cancès, B. Mennucci, J. Tomasi, *J. Chem. Phys.* **1997**, *107*, 3032-3041.
- [126] J. Tomasi, B. Mennucci, R. Cammi, *Chem. Rev.* **2005**, *105*, 2999-3093.
- [127] B. Yang, L. Hooper-Burkhardt, F. Wang, G. K. Surya Prakash, S. R. Narayanan, *J. Electrochem. Soc.* **2014**, *161*, A1371-A1380.
- [128] S. Zhang, X. Li, D. Chu, *Electrochim. Acta* **2016**, *190*, 737-743.
- [129] F. R. Brushett, J. T. Vaughey, A. N. Jansen, *Adv. Energy Mater.* **2012**, *2*, 1390-1396.
- [130] C. Yang, M.-S. Wang, L.-Z. Cai, X.-M. Jiang, M.-F. Wu, G.-C. Guo, J.-S. Huang, *Inorg. Chem. Commun.* **2010**, *13*, 1021-1024.
- [131] K. Murugavel, *Polym. Chem.* **2014**, *5*, 5873-5884.
- [132] C. L. Bird, A. T. Kuhn, *Chem. Soc. Rev.* **1981**, *10*, 49-82.
- [133] T. Janoschka, S. Morgenstern, H. Hiller, C. Friebe, K. Wolkersdorfer, B. Häupler, M. D. Hager, U. S. Schubert, *Polym. Chem.* **2015**, *6*, 7801-7811.
- [134] G. Hauffman, J. Rolland, J.-P. Bourgeois, A. Vlad, J.-F. Gohy, *J. Polym. Sci., Part A: Polym. Chem.* **2013**, *51*, 101-108.
- [135] G. Hauffman, Q. Maguin, J.-P. Bourgeois, A. Vlad, J.-F. Gohy, *Macromol. Rapid Commun.* **2014**, *35*, 228-233.

List of abbreviations

AEM	Anion-exchange membrane
AF4	Asymmetric flow field-flow fractionation
BODIPY	Boron-dipyrromethene
CE	Coulombic efficiency
CV	Cyclic voltammetry
CVA	Advanced cyclic voltammetry
\bar{D}	Dispersity
DEC	Diethyl carbonate
DFT	Density functional theory
DLS	Dynamic light scattering
DMAc	<i>N,N</i> -Dimethylacetamide
DMC	Dimethyl carbonate
E	Energy density
EC	Ethylene carbonate
EE	Energy efficiency
EIS	Electrochemical impedance spectroscopy
EPR	Electron paramagnetic resonance
HFB	Hybrid-flow battery
IR	Internal resistance
METAC	[2-(Methacryloyloxy)ethyl]trimethylammonium chloride)
MV	<i>N,N'</i> -dimethyl-4,4'-bipyridinium dichloride
M_n	Number average molar mass
M_w	Weight average molar mass
MWCO	Molecular weight cut-off
NASA	National Aeronautics and Space Administration
NMR	Nuclear magnetic resonance
NN	Nitronyl nitroxide
P	Poly
PEGMA	Poly(ethylene glycol)methacrylate
pRFB	Polymer-based redox-flow battery
PS	Polystyrene

List of abbreviations

PTFE	Polytetrafluoroethylene
PTMA	Poly(TEMPO methacrylate)
RDE	Rotating disk electrode
RFB	Redox-flow battery
SEC	Size-exclusion chromatography
TAS _t	(Vinylbenzyl)trimethylammonium perchlorate
TBAPF ₆	Tetrabutylammonium hexafluorophosphate
TCAA	2,3,7,8-Tetracyano-1,4,5,6,9,10-hexazaanthracene
TEGSt	(Vinylbenzyl)triethyleneglycol monomethylether
TEM	Transmission electron microscopy
TEMPO	(2,2,6,6-Tetramethylpiperidin-1-yl)oxyl
TEMPTMA	<i>N,N,N</i> -2,2,6,6-Heptamethylpiperidinyloxy-4-ammonium chloride
TMA	TEMPO methacrylate
UV-vis-NIR	Ultraviolet-visible-near infrared
VE	Voltage efficiency
VRFB	All-vanadium redox-flow battery
4-HO-TEMPO	4-Hydroxy-TEMPO

Curriculum vitae



06.04.1989	Born in Apolda, Germany
08/1995 – 06/1999	State Primary School Wickerstedt
08/1999 – 06/2007	University entrance certification at Gymnasium Bergschule Apolda
07/2007 – 03/2008	Basic military service at the Offiziersanwärterbataillon Hammelburg and Panzeraufklärer in Gotha
04/2008 – 09/2008	Employment by Grosse-Immobilien-Dienstleistungen GbR
10/2008 – 10/2012	Study of chemistry at the Friedrich-Schiller-University Jena, Germany
11/2012 – 07/2013	Diploma thesis in the group of Prof. Dr. Wolfgang Weigand: “Neuartige Metallkomplexe mit modifizierten DTPA-Derivaten”
07/2013	Diploma
since 08/2013	PhD student at the Laboratory of Macromolecular and Organic Chemistry (IOMC) at the Friedrich-Schiller-University Jena at the group of Prof. Dr. Ulrich S. Schubert

Jena, den

.....

Tino Hagemann

Publication list

Peer-reviewed publications

- [1] J. Greiser, **T. Hagemann**, T. Niksch, P. Traber, S. Kupfer, S. Gräfe, H. Görls, W. Weigand, M. Freesmeyer “Synthesis and Characterization of GaIII, InIII and LuIII Complexes of a Set of dtpa Bis-Amide Ligands”, *Eur. J. Inorg. Chem.* **2015**, 4125-4137.
- [2] B. Häupler, **T. Hagemann**, C. Friebe, A. Wild, U. S. Schubert, “Dithiophenedione-Containing Polymers for Battery applications”, *ACS Appl. Mater. Interfaces* **2015**, 7, 3473-3479.
- [3] J. Winsberg, T. Janoschka, S. Morgenstern, **T. Hagemann**, S. Muench, G. Hauffman, J.-F. Gohy, M. D. Hager, U. S. Schubert, “Poly(TEMPO)/Zinc Hybrid-Flow Battery: A Novel, “Green,” High Voltage, and Safe Energy Storage System”, *Adv. Mater.* **2016**, 28, 2238-2243.
- [4] J. Winsberg, S. Muench, **T. Hagemann**, S. Morgenstern, T. Janoschka, M. Billing, F. H. Schacher, G. Hauffman, J.-F. Gohy, S. Hoepfener, M. D. Hager, U. S. Schubert, “Polymer/Zinc Hybrid-Flow Battery Using Block Copolymer Micelles Featuring a TEMPO Corona as Catholyte”, *Polym. Chem.* **2016**, 7, 1711-1718.
- [5] J. Winsberg, **T. Hagemann**, S. Muench, C. Friebe, B. Häupler, T. Janoschka, S. Morgenstern, M. D. Hager, U. S. Schubert, “Poly(boron-dipyrromethene) – A Redox-Active Polymer Class for Polymer Redox-Flow Batteries”, *Chem. Mater.* **2016**, 28, 3401-3405.
- [6] **T. Hagemann**, J. Winsberg, B. Häupler, T. Janoschka, J. J. Gruber, A. Wild, U. S. Schubert, “Bipolar Nitronyl Nitroxide Small Molecule for an All-Organic Redox-Flow Battery”, *NPG Asia Mater.* **2017**, 9, 340.
- [7] **T. Hagemann**, J. Winsberg, A. Wild, U. S. Schubert, “Synthesis and Electrochemical Study of a TCAA Derivative – A Potential Bipolar Redox-Active Material”, *Electrochem. Acta.* **2017**, 228, 494-502.

- [8] J. Winsberg, **T. Hagemann**, T. Janoschka, M. D. Hager, U. S. Schubert, “Redox-Flow Batteries: From Metals to Organics”, *Angew. Chem. Int. Ed.* **2017**, 56, 686-711; *Angew. Chem.* **2017**, 129, 702-729.
- [9] **T. Hagemann**, J. Winsberg, M. Grube, I. Nischang, T. Janoschka, N. Martin, M. D. Hager, U. S. Schubert, “An Aqueous All-Organic RFB Employing a (2,2,6,6-Tetramethylpiperidin-1-yl)oxyl-containing Polymer as Catholyte and Dimethyl Viologen Dichloride as Anolyte”, *J. Power Sources* **2018**, 378, 546-554.

Acknowledgements / Danksagung

This thesis would not have been possible without the continuous help, support and advice of several people. First of all, I would like to thank Prof. Dr. Ulrich S. Schubert for the opportunity to perform this work in his research group that constitutes the foundation for this thesis. He offered me a current and interesting interdisciplinary research topic and the freedom to put my own ideas into practice.

Furthermore, I would like to thank Dr. Martin D. Hager for providing a substantial base regarding scientific advices, taking care of material support and his help in the scientific publication process.

In addition a large number of colleagues supported me over the last years and therefore I would like to say personally thanks to all of you:

First and foremost to Dr. Mark Billing, Dr. Kevin Barthelmes and Dr. Andreas Wild, without them I would not have successfully concluded the chemistry studies or writing this thesis. Furthermore, the three of them became real friends to me, which means in my opinion more than any academic degree.

Tobias Janoschka for introducing me into the topic, supporting me during the development of this thesis and for correction of all our common publications. I would like to thank Dr. Jan Winsberg, my fellow in misery over the last years, for improvement of my english knowlegde during the preparation of all our common publications and the fun we had together. Dr. Christian Friebe and Christian Stolze for their support with electrochemical measurements. Sabine Morgenstern, my working-wife, Kristin Schreyer and Maria Strumpf, the good souls of all the labs I have worked in.

I also would like to thank the administrative team consisting of Franca Frister and Sylvia Braunsdorf, who kept the place running all the time as well as Dr. Uwe Köhn for his safety instructions and for handling all my chemical orders as fast as possible.

Also thanks to all other group members and technical staff who cannot be listed all individually, but have helped me a lot in the last years.

At the end I grateful thank my mother and my maternal grandparents for their support throughout my entire life. In particular my granddad, who was always a role model for me and who taught me that I can achieve everything alone by willpower.

Acknowledgements / Danksagung

Furthermore, I would like to thank all my friends and buddies from my “Herzensverein” SV Eintracht Wickerstedt as well as USV Erfurt, for those lots of moments of joy that make life worth living. In particular Rainer and Marcus, whom I can blindly trust from an early age.

Declaration of Authorship / Selbstständigkeitserklärung

Ich erkläre, dass ich die vorliegende Arbeit selbstständig und unter Verwendung der angegebenen Hilfsmittel, persönlichen Mitteilungen und Quellen angefertigt habe.

I certify that the work presented here is, to the best of my knowledge and belief, original and the result of my own investigations, except as acknowledged, and has not been submitted, either in part or whole, for a degree at this or any other university.

Jena, den

.....

Tino Hagemann

Publication P1

Redox-flow batteries: From metals to organic redox-active materials

J. Winsberg, T. Hagemann, T. Janoschka, M. D. Hager, U. S. Schubert,
Angew. Chem. Int. Ed. **2017**, 56, 686-711.



Redox-Flow Batteries

International Edition: DOI: 10.1002/anie.201604925

German Edition: DOI: 10.1002/ange.201604925

Redox-Flow Batteries: From Metals to Organic Redox-Active Materials

Jan Winsberg⁺, Tino Hagemann⁺, Tobias Janoschka, Martin D. Hager, and Ulrich S. Schubert*

Keywords:

electrochemistry · energy storage ·
organic active materials ·
organic electrolytes ·
redox-flow batteries



Research on redox-flow batteries (RFBs) is currently experiencing a significant upturn, stimulated by the growing need to store increasing quantities of sustainably generated electrical energy. RFBs are promising candidates for the creation of smart grids, particularly when combined with photovoltaics and wind farms. To achieve the goal of “green”, safe, and cost-efficient energy storage, research has shifted from metal-based materials to organic active materials in recent years. This Review presents an overview of various flow-battery systems. Relevant studies concerning their history are discussed as well as their development over the last few years from the classical inorganic, to organic/inorganic, to RFBs with organic redox-active cathode and anode materials. Available technologies are analyzed in terms of their technical, economic, and environmental aspects; the advantages and limitations of these systems are also discussed. Further technological challenges and prospective research possibilities are highlighted.

1. Introduction

The global energy demand is fulfilled mainly by the production of electricity from fossil fuel and nuclear-based power plants. These conventional energy production plants have typical power outputs of over 1 GW, but are far from being sustainable. Fossil fuels have been exploited on a large scale since the start of the industrial revolution in the 19th century.^[1] Since then, the concentration of carbon dioxide in the atmosphere has increased from 280 ppm to over 401 ppm in December 2015.^[2] CO₂, as well as other greenhouse gases, seems to be the main origin of climate change.^[3–5] Additionally, coal-fired power plants emit a multitude of different toxic heavy metals and fine dust.^[6,7] Although nuclear power plants were once proposed to be the main alternative to fossil fuel based plants to reduce CO₂ emissions but, from the point-of-view of a responsibly acting society, they should not be utilized for electricity generation.^[8–11] In fact, we need to change our energy production to “green” and renewable sources, such as geothermal and solar energy, hydroelectricity, and wind power. However, geothermal energy and hydroelectricity are associated with other disadvantages (e.g. limited availability or massive ecological impact) and are limited to certain geographical conditions.^[12,13] The utilization of solar energy and wind power, thus, seems to be the most promising alternative.^[14,15]

A large number of new power plants using solar energy and wind power were built in the last few years throughout the world and a major expansion is planned until 2020 and 2050, respectively.^[16] Furthermore, a second trend to local small-scale energy production by photovoltaics is recognizable.^[17] Unlike before, electricity is now generated discontinuously—depending on the weather—and in a more decentralized manner, often on a kW scale. Today's electricity grids are not designed for this kind of energy production.^[18] Conventional power plants produce a stable base load over a long period of time. In contrast, energy production from wind power and solar energy is intermittent and energy demand can diverge from energy production. Intelligent

storage technologies are required to overcome temporal deviations in energy production and consumption.^[19] Only with the combination of renewable power sources and energy storage systems, connected as a smart grid, can the turnaround in energy policy (“Energiewende”) be successful.^[20]

Possible storage technologies are pumped hydro, compressed air, thermal, flywheel, superconducting magnetic, electric double layer, and electrochemical energy storage systems.^[21] Typical sizes of photovoltaics range between 1 kW (small-scale roof-top system) up to 550 MW (Topaz Solar Farm, California, USA), and wind turbines typically produce a power of 2.5 MW (up to even 7.5 MW for the newest generation of large wind turbines). With this power range in mind, RFBs seem to be an ideal storage technology for wind and solar electricity.

From the Contents

1. Introduction	687
2. General Principles of Flow Batteries	687
3. History: The Metal Age	692
4. Rise of the Organic Active Materials	693
5. Photoelectrochemical Redox-Flow Batteries (Photo-RFBs)	705
6. Conclusion and Future Challenges	707

[*] J. Winsberg,^[†] T. Hagemann,^[†] T. Janoschka, Dr. M. D. Hager, Prof. Dr. U. S. Schubert
Lehrstuhl für Organische und Makromolekulare Chemie (IOMC)
Friedrich-Schiller-Universität Jena
Humboldtstrasse 10, 07743 Jena (Germany)
E-mail: ulrich.schubert@uni-jena.de

J. Winsberg,^[†] T. Hagemann,^[†] T. Janoschka, Dr. M. D. Hager, Prof. Dr. U. S. Schubert
Center for Energy and Environmental Chemistry Jena (CEEC Jena)
Friedrich-Schiller-Universität Jena
Philosophenweg 7a, 07743 Jena (Germany)

[†] These authors contributed equally to this work.

Supporting information for this article (an extended data table of utilized redox-active materials) can be found under: <http://dx.doi.org/10.1002/anie.201604925>.

© 2016 The Authors. Published by Wiley-VCH Verlag GmbH & Co. KGaA. This is an open access article under the terms of the Creative Commons Attribution Non-Commercial NoDerivs License, which permits use and distribution in any medium, provided the original work is properly cited, the use is non-commercial, and no modifications or adaptations are made.

2. General Principles of Flow Batteries

The central components of redox-flow batteries are an electrochemical cell and two tanks. The electrochemical cell contains two electrodes and a separator. An electrolyte solution is circulated between these components by pumps. The redox-active cathode and anode materials are not formed as solid electrodes, but are dissolved in the electrolyte, for which reason it is named as either the catholyte or anolyte. The separator is permeable to the supporting electrolyte (a conducting salt), but impermeable to the redox-active material. This setup, similar to fuel cells, enables the power and capacity of the battery to be scaled independently from each other. A schematic representation is provided in Figure 1 a. A hybrid-flow battery (HFB) is a similar type of flow battery. It features at least one redox couple with a solid redox state (Figure 1 b). This active material is electroplated on an electrode during charging and dissolved again in the electrolyte in the subsequent discharging process. This cell design must be adopted, as the electroplated metal often forms dendritic structures, which may cause a short-circuit or puncture the membrane.^[22]

The electrical performance of the battery is affected by many parameters and can be measured by the following benchmarks. The volumetric capacity of the electrolyte indicates the amount of charge that can be stored in a certain amount of electrolyte [Eq. (1)]. The redox-active material can

$$C = \frac{m \cdot n \cdot F}{M \cdot V} \quad (1)$$

be dissolved, but particles, gases, or ionic liquids can also be utilized. Thus, the volumetric capacity is dependent on the amount of redox-active material and the number of electrons that participate in the redox process. The unit most used for the volumetric capacity is Ah L^{-1} . The energy density includes the voltage between the utilized redox couples and is, thus, measured in Wh L^{-1} [Eq. (2)].

$$E = C \cdot U \quad (2)$$

C = volumetric capacity, m = mass, n = number of electrons, F = Faraday's constant, M = molar mass, V = volume, E = energy density, and U = voltage.



Jan Winsberg studied Business Chemistry at the Heinrich Heine University Düsseldorf, Germany, where he obtained his BSc and MSc in the field of macromolecular chemistry. He joined the group of Prof. Schubert as a PhD student in 2013, where he develops organic redox-active materials for redox-flow batteries.



Martin D. Hager completed his PhD in 2007 at the Friedrich Schiller University Jena in the group of Prof. Dr. Elisabeth Klemm, working on conjugated (rod-coil) polymers for polymer solar cells. After postdoctoral research at the TU Eindhoven, in 2008 he became a group leader in the group of Prof. Schubert at the FSU Jena. His research interests include reversible polymer systems for self-healing applications, conjugated polymers for solar cells, as well as redox-active polymers for batteries (from small printable devices to large redox-flow-batteries).



Tino Hagemann studied Chemistry at the Friedrich Schiller University Jena, Germany. He obtained his diploma in chemistry in the field of complex chemistry and in 2013 he joined the group of Prof. Schubert as a PhD student, where he develops organic electrolytes for redox-flow batteries.



Ulrich S. Schubert was born in Tübingen (Germany) in 1969. He studied chemistry in Frankfurt and Bayreuth (Germany) and at the Virginia Commonwealth University, Richmond (USA). His PhD was performed at the Universities of Bayreuth and South Florida. After postdoctoral research with Prof. J.-M. Lehn at the University of Strasbourg (France), he moved to the TU Munich (Germany), where he habilitated in 1999. From 1999 to 2000 he was Professor at the University of Munich, and from 2000 to 2007 Full Professor at the TU Eindhoven. Since 2007, he has been a Full Professor at the Friedrich Schiller University Jena.



Tobias Janoschka studied Chemistry and Business Administration at the Friedrich Schiller University in Jena, Germany. He joined the group of Prof. Schubert as a PhD student in 2011 with a scholarship from the "Fonds der Chemischen Industrie", specializing in organic and macromolecular synthesis. His current focus is on innovative electro-active materials for redox-flow batteries.

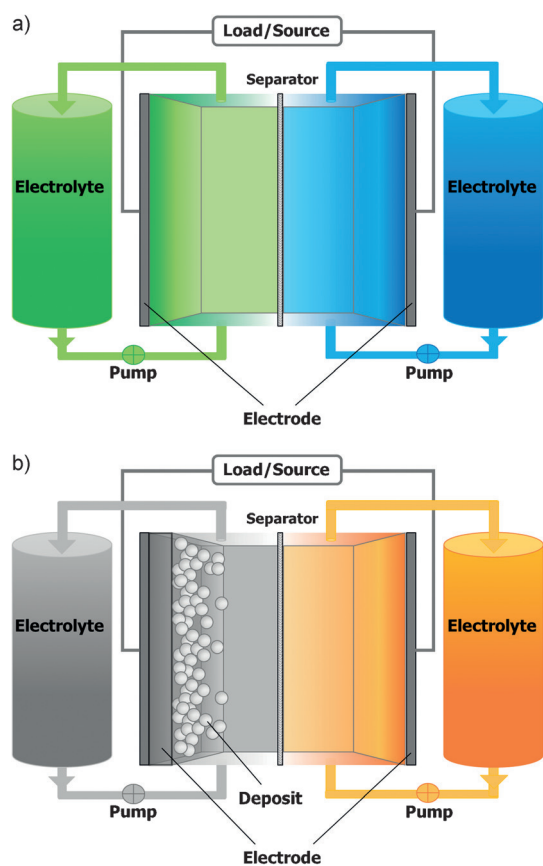


Figure 1. a) Schematic representation of a redox-flow battery (RFB). The battery consists of an electrochemical cell with two compartments and a separator in between. The electrolyte is circulated between the cell and the storage tanks by pumps. b) Schematic representation of a hybrid-flow battery (HFB). A material is electroplated in the charging process on one electrode.

The current density has a direct impact on the charging/discharging time of the battery, and is related to the membrane area of the electrochemical cell. An often used unit is mA cm^{-2} , which translates to power density mW cm^{-2} if the voltage is taken into account.

The coulombic efficiency (CE), sometimes referred to as the faradaic or current efficiency, and the voltage efficiency (VE) are two important indicators of the electrical quality of a flow battery. The CE relates the charge applied in the charging procedure to the retained charge in the discharging procedure of the same charge/discharge cycle [Eq. (3)].

$$CE = \eta_c = \frac{Q_D}{Q_C} \quad (3)$$

Coulombic efficiencies $< 99\%$ are an indication of crossover of the redox-active material through the membrane into the opposite half-cell or irreversible side reactions of the redox-active material or the electrolyte itself, for example, hydrogen formation.

$$VE = \eta_v = \frac{\int_0^{T_D} E_D(t) dt}{T_D} = \frac{\bar{E}_D}{\frac{\int_0^{T_C} E_C(t) dt}{T_C} = \bar{E}_C} \quad (4)$$

$$EE = \eta_{EE} = \eta_C \cdot \eta_V \quad (5)$$

η = efficiency, subscripts: C = charging, D = discharging, Q = charge, T = time for charging/discharging, and E = potential.

VE is the ratio between the mean discharging voltage and the mean charging voltage at constant current [Eq. (4)]. The difference between these mean values is caused by a variety of overpotentials. The diffusion, polarization, and ohmic overpotential are decisive for flow batteries.^[23–25] The VE decreases as the current density increases. The multiplication of CE by VE yields the energy efficiency [EE; Eq. (5)], which is a measure of the applied and retained energy. Typical EE values of RFBs are in the range of 50 to 90 %, depending on the applied current density and material quality.

2.1. Redox-Active Materials

The redox-active charge-storage material has a significant impact on the performance of a flow battery. Its reaction kinetics have an influence on the applicable current density, and the viscosity of the electrolyte is also affected by the redox-active material and its concentration. A general decrease in performance can be observed at higher viscosities, as the charge-carrier mobility within the electrolyte is reduced and the energy requirement for electrolyte circulation is increased. The employed active materials are often metal-based redox couples dissolved in aqueous media, but a greatly increasing number of charge-storage materials based on organic redox-active molecules have been reported recently.^[199,200] Some of these organic materials are not soluble in water and, thus, the utilization of an organic solvent is required. Organic aprotic solvents show a better electrochemical stability and a wider potential window than protic solvents such as water. This can lead to batteries with higher energy densities, as redox couples with an elevated voltage can be used. However, the ion conductivity in organic solvents is much lower, which limits applicable current densities. This effect is partially mitigated by a higher voltage (power density). Some organic materials are soluble in water, particularly if the molecule contains polar substituents. Thus, high current densities are applicable, but the voltage between the two redox couples is restricted. Hence, an “L” shape in Figure 2 is clearly visible, which illustrates the limitations of current flow-battery technologies.

A variety of organic molecules have been investigated as charge-storage materials in polymer-based organic batteries, for example, stable NO radicals, carbonyl compounds, and organosulfur compounds.^[26] These studies can be used as the starting point for the development of suitable organic materials tailored for applications in RFBs. These materials, which can be obtained by synthetic approaches, have to feature at least two stable and (electro)chemically reversible redox states. Starting materials can be obtained from petrochemistry or, in the best case, by extraction from renewable

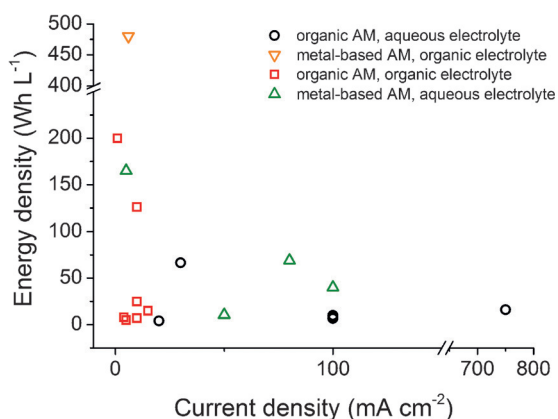


Figure 2. Energy density versus current density of selected RFB systems (AM = active material).

sources, white biotechnology, as well as in the future by power-to-X technologies. Nevertheless, the exploitation of organic starting materials is not limited to certain geographical areas, but can be performed globally if an independent procurement of organic raw materials is possible. In particular, Europe, being poor in numerous critical raw materials, might profit from its strong chemical industry, which can produce organic active materials on a large scale. Another advantage is the flexibility of organic materials. Solubility, chemical reversibility, and redox potential can be tuned by modification of the organic core component with particular functional groups to improve the battery performance. The reversibility of the utilized redox couples are of particular interest, since the (electro)chemical reversibility determines the number of possible charge/discharge cycles of a flow battery.

2.2. Separators

An ideal separator of a flow battery keeps the redox-active couples completely apart, but is permeable to the supporting electrolyte ions to enable charge balance.^[27] The selectivity of the separator is crucial, as a cross-contamination of catholyte and anolyte leads to reduced efficiencies and, in the case of asymmetric electrolytes, a long-term decay of capacity.^[28] A limited number of flow batteries can be used without a separator, for example, flow batteries with two solid electrodes or batteries with a gas diffusion electrode.^[29,30] A wide range of separators were investigated over the last few years: perfluorinated and non-perfluorinated ion-exchange membranes (e.g. Nafion) are often used.^[31] In flow batteries, where solvated polymeric species or particles are the utilized active material, porous separators, such as dialysis membranes or simple microporous PP/PE foils, can be used.^[32–37] Furthermore, the modification of polymer-based membranes with coatings of inorganic particles, for example, was reported to increase the selectivity of the separator.^[38]

A low resistance of the separator is essential for good performance parameters of the battery. The mechanical firmness and chemical inertness are of great importance for

the long-term performance stability.^[39] The “fouling” of a membrane gradually reduces the performance values of an RFB. It develops by attractive interactions between the membrane and the electrolyte, which causes an accumulation of these compounds on the surface or within the pores of the membrane. This can lead to reduced selectivity (retention of the active materials) up to the point of complete clogging of the separator.^[40]

Flow batteries with different solvents for the anolyte and catholyte require the utilization of separators that completely isolate the two compartments, for example, Li in propylene carbonate (anolyte) and TEMPO in water (catholyte). Ceramic membranes, which are conductive for a single ion, are utilized for this purpose. A significant drawback of this membrane technology is the restricted ion conductivity, which leads to limited applicable current densities.^[41]

2.3. Electrodes

The electrodes of RFBs do not take part in the redox reactions of the cathode- and anode-active material, but provide the active surface for the reactions of the redox couples dissolved in the catholyte and anolyte, respectively. They have to feature an excellent electrical conductivity,^[42] high specific surface area, stability in the applied operating potential range of the RFB, and chemical inertness against the often highly corrosive electrolytes.^[43,44] The corrosion process of an electrode—for example, CO₂ evolution in all-vanadium RFBs—decreases the performance characteristics of the electrode.^[44–46] In addition, electrodes should facilitate a good wettability of the electrolyte and enable high reaction kinetics of the utilized redox couples. Depending on the applied active material, this can be accomplished by activation or modification of the electrode by oxidation, doping, or addition of nanomaterials.^[47–56] Solutions of organic compounds in water show a surfactant-like behavior and a low surface tension. This results in a good wettability behavior, even without electrode modification.^[34] Frequently used electrodes are graphite felt and carbon paper, but advanced electrodes were also fabricated from, for example, carbon nanotubes, which catalyze the redox reactions.^[57] Electrodes consisting of metal mesh/foam are also used and can be coated with, for example, platinized Ti or IrO₂.^[58–60] A common side reaction during operation of aqueous batteries is the water-splitting reaction. An ideal electrode utilized in aqueous-based electrolytes prevents the evolution of hydrogen and oxygen, which is a main cause for charge imbalance and efficiency losses. However, hydrogen evolution is not limited to aqueous electrolytes, but is possible in all protic solvents. For example, Suarez et al. reported sufficient inhibition of H₂ generation on a graphite felt electrode that was coated with Bi nanoparticles.^[61] This effect is accompanied with a slightly shifted potential of the vanadium reduction to higher potentials; presumably caused by a catalytic effect. However, the optimization of the electrodes has been investigated only for inorganic active materials. Therefore, there is a great need for research to optimize the electrodes for organic active materials.

2.4. Advantages and Challenges of Flow Batteries

Flow batteries offer a variety of benefits. The power and capacity of the system can be scaled independently from each other by separate sizing of the tank volume and the cell stacks (reaction cells). This allows an exact adaption to the associated generator unit. Flow batteries can switch between charging and discharging within a fraction of a second, but are actually designed for storing electricity for several hours.^[21] In addition, modularized flow batteries, in the form of shipping containers, can be moved and set up as “mobile” energy-storage devices.^[62] In this way, the electrical power supply in decentralized regions, for example in developing countries, could be ensured.^[17] Common flow batteries rely on aqueous electrolytes that are not flammable, and a safe battery operation is guaranteed. The lifetime exceeds that of lead-acid and lithium ion/polymer batteries significantly. These advantages can be utilized for application possibilities, such as, peak shaving, as well as load and frequency balancing.^[63] The increasing amount of electricity generated from renewable sources, such as wind power and solar energy, can lead to peaks in the energy production. For example, a significant increase in electricity produced from photovoltaics is observable around midday. In contrast, the energy demand is relatively low at this time compared to the evening. Electricity production from wind energy can exceed the energy demand considerably in stormy periods.^[64] These phenomena can be monitored in the energy profile.^[65–68] Flow batteries can be used to flatten these profiles (peak shaving). When viewing the system as a whole, large energy-storage devices reduce the risk of black-outs caused by net frequency exceedances by intercepting over-production.^[64,69] For this purpose, enormous energy-storage devices have to be developed that have lifetimes of at least 20 years, to offer cost-efficient and reliable energy storage. In contrast to the proof-of-principle small-scale flow batteries, these large-scale systems are operated in a different manner. Whereas laboratory-scale tests are often performed under extreme conditions to study the material's properties, practical applications rely on milder conditions to extend the material's lifetime. Large-scale systems have to deal with the hydraulic and electric cascading of numerous cell stacks and intelligent battery management systems. The development effort for these complex systems is very high, since a variety of components and peripheral devices have to be harmonized and coordinated.^[70] Further challenges are the relatively low volumetric energy density compared to lithium ion/polymer and lead-acid batteries. Current commercially available all-vanadium RFB (VRFB) systems feature an energy density of 25 Wh L^{-1} ,^[71] with conventional storage technologies such as lead-acid (40 Wh kg^{-1} , 100 Wh L^{-1}) and lithium ion/polymer (180 Wh kg^{-1} , 100 Wh L^{-1}) easily outperforming this value.^[72] Hence, the space requirement of flow batteries is rather large to be competitive in the field of overall capacity. However, flow batteries have a better volumetric capacity than pumped hydro storage, the technology mostly used in the USA.^[73]

The acquisition and working costs are one of the most significant drivers that determines market penetration. The

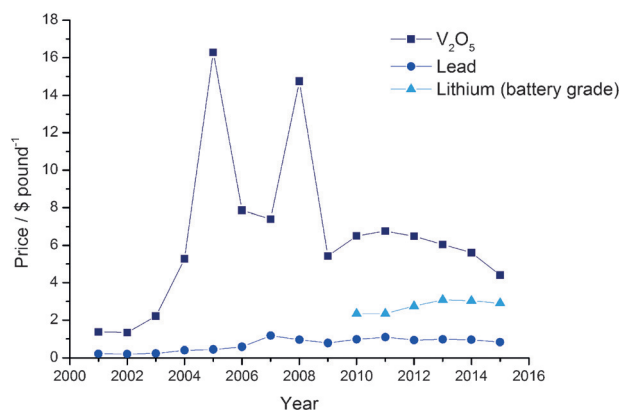


Figure 3. Commodity prices of Li (battery grade), Pb, and V₂O₅ (standard grade). Data obtained from the U.S. geological survey.

commodity price of vanadium is strongly dependent on the amount of high-performance steel produced and is, relatively high compared to lead and lithium (Figure 3). Additionally, a remarkable fluctuation was observed between 2004 and 2009, which can be expected to recur with new economic growth in China within the next few years.

The Advanced Research Projects Agency-Energy (ARPA-E) of the Department of Energy (DOE) set a capital cost target of $\$100 \text{ kW}^{-1} \text{ h}^{-1}$ for one hour of storage for market penetration.^[74] An important advantage of RFBs that utilize organic charge-storage materials is a possible cost benefit over metal-based RFBs. Several cost analyses were performed, amongst others, by Darling et al. that illustrate that the two primary cost drivers are the price of the active material itself and the price of the utilized membrane.^[75–77] As a consequence, the production costs for the organic active material have to be as low as possible. This requires low-cost starting materials, simple chemical reactions with full conversion, and no necessary purification steps. A basic calculation was performed by Huskinson et al., which found redox-active material prices of $\$27 \text{ kW}^{-1} \text{ h}^{-1}$ for the anthraquinone disulfonate/bromide system in contrast to $\$81 \text{ kW}^{-1} \text{ h}^{-1}$ for vanadium systems.^[78] In terms of the utilized separator, perfluorinated proton exchange membranes have the highest costs, followed by ion-exchange membranes, and finally porous separators having the lowest costs. Thus, the application of polymer-based organic charge-storage materials is attractive.^[34] In addition, it was found that flow batteries using electrolytes based on organic solvents are far from being cost-competitive.^[75] Hence, water in combination with sodium chloride as the supporting electrolyte is the recommended electrolyte, both from a cost and also a safety point of view.

The common flow-battery systems (VRFB, Fe/Cr, and Zn/Br₂) illustrate evident concerns regarding the environmental or social impact in the case of the production of the primary materials, damage, or disposal. For example, ore mining may be executed in developing countries with unsatisfactory social and environmental standards (e.g. zinc mining in China) or the utilized electrolytes may reveal significant hazards.^[23,34,79]

Furthermore, the overall efficiency of flow batteries is reduced by the control systems as well as the permanently

operating pumps, which circulate the electrolytes between the electrochemical cell and the storage tanks. An active temperature management, which is necessary in VRFBs, can have an additional effect on the overall efficiency.^[62]

The significant challenge for organic charge-storage materials is the long-term stability of the electrolyte. In contrast to metals, which form stable ions, organic compounds tend to undergo side reactions when they are either oxidized or reduced; in particular, if radical ions are formed. Reactions with the electrolyte can also be observed. For example, the widely used redox-active cathode material TEMPO undergoes disproportionation reactions at pH values lower 2.5 and the oxoammonium cation is not stable in basic media. Thus, a long lifecycle of the active materials can only be reached under optimized conditions.

Electrolytes based on metal redox-active materials can be galvanically recycled. Thermal recycling seems to be the best option for electrolytes based on organic active materials.

3. History: "The Metal Age"

A brief summary of flow batteries based on metal redox-active materials is presented in this section; a much more detailed overview is given, for example, by Yu and co-workers,^[80] Soloveichik,^[81] Skyllas-Kazacos et al.,^[82] and Noack et al.^[83]

The first battery type similar to today's flow batteries was patented by Kangro in 1949.^[84] This system employed $\text{Cr}_2(\text{SO}_4)_3$ as the cathode and anode active material and 2 M sulfuric acid as the supporting electrolyte, and yielded a cell voltage of 1.75 V.^[85] TiCl_4 , Ti/Fe , Ti/Cr , Ti/Cl_2 , and Cr/Fe were also proposed as redox-active materials.^[84–86] The National Aeronautics and Space Administration (NASA) reported an Fe/Cr system in the 1970s, which gained much attention.^[87] The employed redox couples were $\text{Fe}^{3+}/\text{Fe}^{2+}/\text{Cr}^{3+}/\text{Cr}^{2+}$ solvated in an acidified electrolyte. A 1 kW/13 kWh demonstrator was fabricated that worked in combination with a photovoltaic array. Unfortunately, this RFB system suffered from fast capacity decay caused by crossover of the redox-active species across the utilized anion-exchange membrane. As a consequence of this, mixed electrolytes were utilized in following studies. At that time, no satisfactory membrane was commercially available and custom-made membranes could not meet the requirements in terms of resistivity and selectivity. A decade later Skyllas-Kazacos and Robins patented the VRFB.^[88] This system utilizes the redox couples $\text{VO}_2^+/\text{VO}^{2+}/\text{V}^{3+}/\text{V}^{2+}$, and an open circuit voltage (OCV) of 1.3 V was reached.^[89] The origin of the aqueous Zn/Br_2 battery goes back to a patent of Bradley from 1885.^[90] The first hybrid-flow batteries were developed by Exxon and Gould Inc. in the 1970s and 1980s, respectively.^[91,92] ZnBr_2 is employed as the redox-active material. During the charging process, $\text{Zn}^{2+}_{(\text{aq})}$ is reduced to $\text{Zn}^0_{(\text{s})}$ and a deposit is formed on the electrode (electroplating). At the counter electrode, Br^- is oxidized to elemental bromine. Complexing agents, for example, quaternary ammonium salts are added to reduce the hazard of liquid or gaseous bromine.^[93,94] The Fe/Cr , Zn/Br_2 , all-vanadium, Fe/Zn , and all-iron flow batteries are either

already commercially available or under development by several companies. A wide range of other metal-based redox-active materials were investigated on a laboratory scale over the last few years. For example, Zn/Ce ,^[59,95] Zn/Ni ,^[29] Ru ,^[96,97] $\text{UO}_2^+/\text{U}^{3+}$,^[98] $\text{Mn}^{3+}/\text{Mn}^{2+}$,^[99] all- Cu ,^[100] Pb/PbO_2 ,^[101] Ti/Fe ,^[102] Cu/PbO_2 ,^[103] and Li ^[104–106] were all investigated. Besides these metal-based systems, the metal-free H/Br flow battery also represents a promising system.^[30,81,83,107,108]

3.1. Current Trends in Metal RFBs

Despite the fact that the systems described previously were already proposed several decades ago, they are still the subject of current research. A lot of interesting technologies have been reported over the last few months. Li et al. increased the energy density of VRFBs by utilizing a mixed HCl and H_2SO_4 supporting electrolyte, and increased the solubility of vanadium to 2.5 M (energy density ca. 40 WhL^{-1}).^[109] The group of Skyllas-Kazacos reported a high energy density VRFB.^[70] Typical concentrations of the redox-active vanadium were in the range of 1.6 and 2 M in commercial systems. Supersaturated solutions were obtained by the addition of inorganic additives; 1 wt % H_3PO_4 and 2 wt % $(\text{NH}_4)_2\text{SO}_4$ were added to obtain 3 M vanadium solutions. This system is a significant advancement and increases the theoretical capacity to 80 AhL^{-1} . However, a material utilization of only 62 % was reached in charge/discharge experiments, thus leading to an achievable capacity of 49.6 AhL^{-1} .^[70]

An ambipolar Zn/polyiodide HFB with a superior energy density of 167 WhL^{-1} was reported by Wang and co-workers.^[110] The authors utilized a 5 M ZnI_2 solution both as the catholyte and anolyte. Publications on the iron/chromium RFBs have decreased significantly in recent years. Nevertheless, the EnerVault Corporation installed a 250 kW/1 MWh facility in California, USA, in summer 2015.

Lithium-flow batteries represent an emerging topic in the scientific community that tries to combine the benefits of Li-ion batteries and flow batteries. The main benefit is an elevated cell potential in the range of 2.5 to 3 V, which is possible because of the utilization of an organic solvent. Chen et al. reported a non-aqueous sulfur-impregnated carbon composite dispersion as the catholyte and combined it with a $\text{Li}_{(\text{s})}$ anode.^[111] This setup leads to an average discharging voltage of 2 V and an immense volumetric capacity of 294 AhL^{-1} .

A similar design was reported by Mubeen et al.^[112] Here, the concept of a carbon particle based cathode was extended by the utilization of a carbon particle based anode, where $\text{Zn}^{2+}/\text{Zn}^0$ was the anode active material. Several cathode active materials were investigated: Cu , MnO , Br , and again S .

Huang et al. reported a lithium iodide HFB with a potential energy density of 670 WhL^{-1} . However, only a flow battery with an energy density of about 0.4 WhL^{-1} has so far been realized.^[113]

Metal-air flow batteries are of great interest, as they promise high energy and low-cost battery systems. A lithium-air battery was reported, in which an ionic liquid was used.^[114]

The vanadium-air redox-flow battery (VARFB) or vanadium-oxygen fuel cell (VOFC) increases the energy density significantly compared to VRFBs.^[115–119] The common anodic redox-reaction of V^{3+}/V^{2+} is utilized in combination with an oxygen cathode.

Wei et al. reported an aqueous, pH-neutral Fe/S flow battery.^[120] This battery features 1M solutions of Na_2S_2 and $K_3Fe(CN)_6$ as the catholyte and anolyte, respectively, which leads to a capacity of 11.7 Ah L^{-1} . A drawback of this battery system is the limited cell voltage of 0.91 V. However, this system represents a notable innovation regarding the acquisition costs compared to VRFBs, which are stated to be only one third of those of vanadium in terms of raw material cost per kWh.

Manohar et al. presented an $FeCl_2$ hybrid-flow battery with an improved efficiency. This system employed the redox couples $Fe^{3+}/Fe^{2+}/Fe^{2+}/Fe^0$ with a standard redox-cell potential of 1.2 V. Hydrogen evolution is problematic in iron chloride batteries and drastically reduces the efficiency of the battery. The authors suppressed this process by utilizing ascorbic acid and $InCl_3$ as additives as well as an increased pH value of 2.^[121]

Gong et al. reported a Zn/Fe HFB with system capital costs of $100\text{ \$ kW}^{-1}\text{ h}^{-1}$.^[74] The system features a volumetric capacity of 12 Ah L^{-1} and utilizes $FeCl_2$ and $Na_2[Zn(OH)_4]$ as the catholyte and anolyte, respectively.

Some of these systems show several problems in relation to the environmental and sociopolitical impact, or the system design is too complicated for large-scale batteries. The compatibility of flow batteries with these considerations can be improved by the utilization of regenerative and non-corrosive electrolytes. As a consequence, the implementation of organic redox-active species is a first move in this direction. Moreover, the utilization of organic materials can reduce the acquisition costs per kWh compared to cost-intensive metals. The utilization of organic redox-active materials in flow-battery applications will be discussed in detail in the following section.

4. Rise of the Organic Active Materials

As already mentioned, conventional metal-based flow batteries have several drawbacks, which limit their commercial success. However, the development of RFBs based on inexpensive and sustainable redox-active organic materials can overcome these drawbacks.

When we use the term “organic” or “all-organic” in association with flow batteries, we refer only to the redox-active materials utilized and not to the solvent or the supporting electrolyte, which can be water or any organic solvent capable of dissolving the organic redox-active material.

Intensive research on the use of RFBs as flexible and scalable energy-storage systems came to the conclusion that future RFB systems, irrespective of their use for domestic or large-scale application, have to utilize noncorrosive, safe, and especially low-cost charge-storage materials.^[34, 122, 123] In the last decade the first steps were taken by the utilization of

organic additives such as complexing agents,^[124, 125] followed by metal-ligand complexes with organic ligands as charge-storage materials,^[58, 96] and subsequently to flow batteries with an inorganic and an organic active material.^[32, 126] In recent years, organic/halogen,^[78, 127] and all-organic RFBs were developed.^[128, 129] Organic compounds offer the potential to overcome several metal-related problems and may lead to sophisticated high-performing RFBs for tomorrow's electricity grids. For that purpose, new organic redox-active charge-storage materials have to be discovered and investigated for application in RFBs. These materials can be low-molar-mass compounds (molar mass $< 1000\text{ g mol}^{-1}$ and ≤ 2 repeating redox-active units) or redox-active polymers, both with well-defined electrochemical properties. Selected examples are summarized in Figure 4.

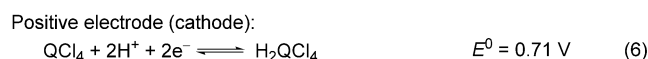
4.1. Flow Batteries with Organic/Inorganic Redox-Active Materials

These RFBs utilize one redox-active organic material and a second inorganic species for the charge-storage process. This classification refers only to the active material employed. Other components, such as solvents, metal-based supporting electrolytes, and additives of any kind, are excluded.

4.1.1. Flow Batteries with Low-Molar-Mass Organic/Inorganic Redox-Active Materials

4.1.1.1. Quinone-Based Redox-Active Materials

The first organic/inorganic flow battery was developed by Xu et al. in 2009.^[131] The single-flow cadmium/chloranil flow battery utilized Cd^0 as the anode-active material and an acidic $CdSO_4$ solution as the anolyte. The insoluble tetrachloro-*p*-benzoquinone (chloranil, QCl_4) was utilized as the organic cathode.



The authors fabricated a small test cell consisting of a QCl_4 /carbon black cathode, a copper foil as the current collector, and an aqueous electrolyte consisting of 0.5M $CdSO_4$, 1M $(NH_4)_2SO_4$, and 0.5M H_2SO_4 . The insolubility of QCl_4 , H_2QCl_4 , and Cd^0 meant that the single-flow battery could be operated without utilization of a membrane. The fabricated battery revealed an average charge voltage of 1.18 V and an average discharge voltage of 0.97 V at a current density of 10 mA cm^{-2} . The coulombic efficiency reached 99% with an energy efficiency of 82% over the first 100 charge/discharge cycles.

The reported single-flow battery has the advantage of being membrane-free and, therefore, saving investment costs. The requirement of a strongly acidic electrolyte for the chloranil cathode, however, can be seen as a drawback.

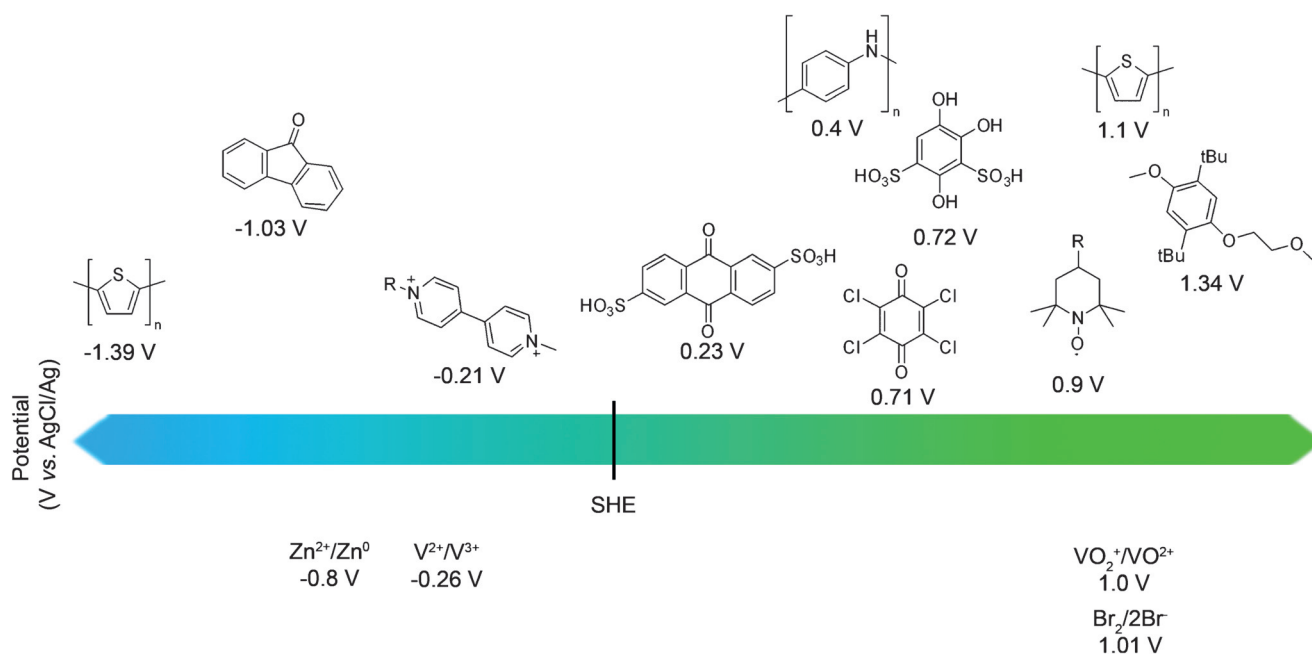
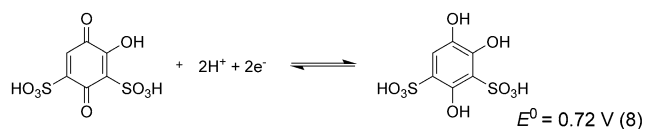


Figure 4. Schematic overview of selected organic/inorganic active materials and their redox potentials; recalculated to a SHE reference if measured against another reference electrode. Conversion factors: SHE to AgCl/Ag = +0.197 V, SHE to SCE = +0.241 V, SHE to Fc^+/Fc = +0.750 V;^[130] SHE: standard hydrogen electrode, SCE: standard calomel electrode, Fc: ferrocene.^[35,41,78,126,131–137]

In a subsequent study, the authors reported a lead/4,5-dibenzoquinone-1,3-benzenedisulfonate (tiron) HFB.^[133] The test cell, equipped with a Nafion 115 membrane, utilized 0.25 M tiron in 3 M H_2SO_4 as the cathode material and a $\text{Pb}^{2+}/\text{Pb}^0$ hybrid anode.

Positive electrode (cathode):



Negative electrode (anode):

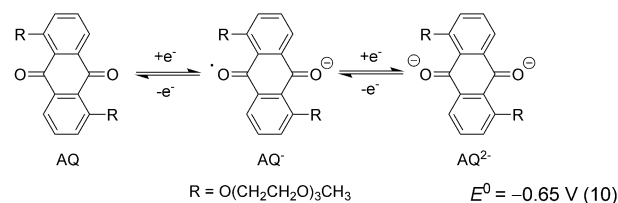


The charge/discharge test indicated an irreversible reaction at an elevated cell voltage and a low coulombic efficiency of 38 % in the first cycle. An average coulombic efficiency of 93 % and an average energy efficiency of 82 % were achieved over the following nine cycles. The cycling of the battery was performed at 10 mA cm^{-2} and the energy density was calculated to be 2.8 Wh L^{-1} . Similar to chloranil, the electrochemical behavior of tiron is strongly pH-dependent and the reported HFB can only be operated with electrolytes below pH 4. Furthermore, tiron exhibited an electrochemical hydroxylation during the first electrolysis, which causes a part of the active material to undergo an irreversible side reaction.

In 2012, Wang et al. reported an organic/inorganic HFB based on an anthraquinone derivative with methoxytriethyleneglycol substituents (15D3GAQ) dissolved in propylene carbonate as the organic cathode material, lithium as the anode, and LiPF_6 as the supporting electrolyte.^[138]

Anthraquinone derivatives are well-known as organic cathode materials for lithium-ion batteries and, therefore, the redox mechanism has been extensively investigated.^[139–143] The ethylene glycol moieties promote solubility, in particular in non-aqueous polar solvents, and a concentration of 0.25 M has been reached.

Positive electrode (cathode):



Negative electrode (anode):



The electrochemical performance of 15D3GAQ was investigated in a static test cell, equipped with a porous polypropylene separator and 0.25 M 15D3GAQ and 1 M LiPF_6 in propylene carbonate as the supporting electrolyte and anode-active material, respectively. The static cell was charged and discharged in the range of 1.8 and 2.8 V, and demonstrated an energy efficiency of 82 % and a theoretical specific discharge energy density of 25 Wh L^{-1} over nine cycles. A current density of 0.1 mA cm^{-2} was applied in the first cycle, but was raised progressively up to 10 mA cm^{-2} .^[138] Nevertheless, an optimization of the electrolyte is necessary to overcome an observed decline in the discharge capacity, caused by side reactions between anthraquinone and the carbonate-based solvents.

As a consequence of the considerable potential of anthraquinones as organic redox-active materials, Bachman et al. investigated the redox chemistry, the influence of substituents on the redox potential, and the solvation free energy of about 50 anthraquinone derivatives by density functional theory (DFT) calculations.^[145] The study revealed that a complete methylation of the anthraquinone core decreases the reduction potential by 0.47 V and that the introduction of oxymethyldioxolane substituents (with a similar reduction window and adequate oxidative stability) enhances the solvation energy.^[145]

In a preliminary study, Quan et al. used conducting cyclic voltammetry measurements to investigate the electrochemical properties of anthraquinone in buffered and unbuffered aqueous solution at different pH values.^[146] In these studies, quinoidic structures revealed promising properties for charge-storage applications in flow batteries. The solubility could be ensured by the choice of suitable substituents, and the redox potential can be adjusted in the same manner.

In 2015, Lin et al. reported an alkaline quinone flow battery by utilizing commercially available 2,6-dihydroxyanthraquinone (2,6-DHAQ, Figure 5) and ferrocyanide/ferricyanide.^[147]

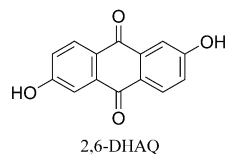


Figure 5. Schematic representation of the chemical structure of 2,6-dihydroxyanthraquinone (2,6-DHAQ).

This system represents an improvement over the organic/halogen aqueous RFB (Huskinson et al.,^[78] a detailed description can be found in Section 4.2). The ferrocyanide/ferricyanide replaced the dangerous $\text{Br}_2/2\text{Br}^-$ redox couple. In contrast to this, ferrocyanide/ferricyanide has a low toxicity and is nonvolatile. The authors claimed on the basis of these characteristics that the reported RFB can be used as a cost-efficient,

nontoxic, nonflammable, and safe energy-storage system. However, the strongly alkaline electrolyte is also highly corrosive (pH 14; 1M KOH).

The introduced electron-donating hydroxy groups in the 2,6-DHAQ reduce the reduction potential and increase the battery voltage.^[78,147] Furthermore, the hydroxy groups are deprotonated in alkaline solution, which improves the solubility up to 0.6M in a 1M KOH solution at room temperature. The reduction potential is independent of the pH value above pH 12. Hence, the reversibility of the redox reaction was investigated by cyclic voltammetry at pH 14, and displayed a rapid kinetic rate constant and two one-electron reductions separated by 60 mV.

The electrochemical performance was investigated in a flow cell containing a Nafion 212 membrane, 0.5M 2,6-DHAQ dipotassium salt in 1M KOH solution as the anolyte, and 0.4M $\text{K}_4\text{Fe}(\text{CN})_6$ in 1M KOH solution as the catholyte; this performance correlates to an energy density of 6.8 Wh L^{-1} . A constant current density of 100 mA cm^{-2} was applied, and 100 charge/discharge cycles with a current efficiency above 99% and a steady energy efficiency of 84% were measured (Figure 6).^[147]

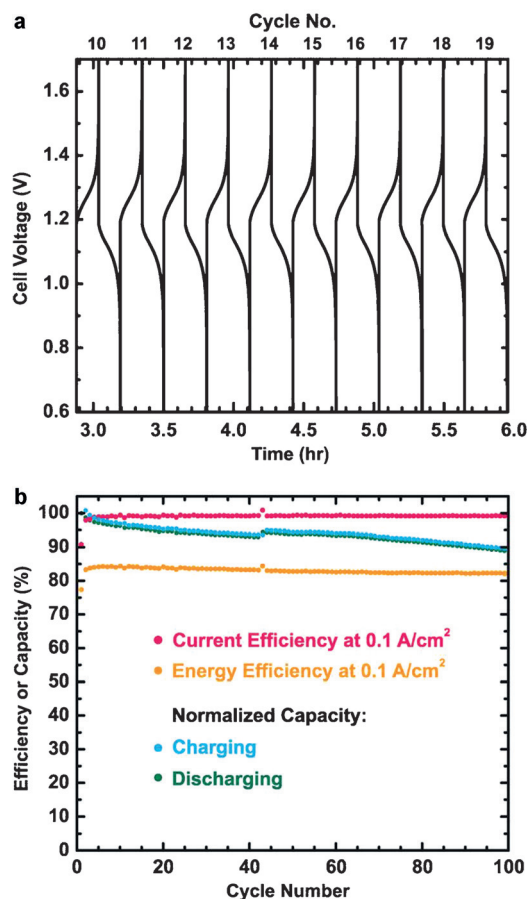


Figure 6. Cell cycling performance of the alkaline quinone flow battery. a) Representative voltage versus time curves during 100 charge/discharge cycles at 0.1 A cm^{-2} , recorded between the 10th and 19th cycles. b) Capacity retention, current efficiency, and energy efficiency values of 100 cycles. Normalized capacity is evaluated on the basis of the capacity of the first charge and discharge cycle.^[147]

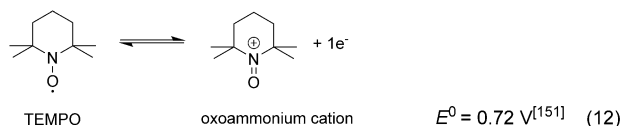
4.1.1.2. TEMPO-Based Redox-Active Materials

Wei et al. reported in 2014 a lithium HFB containing 2,2,6,6-tetramethylpiperidine-1-oxyl (TEMPO) as the organic active material.^[126] TEMPO is a stable, heterocyclic nitroxide radical that had already been explored as a redox-active material for semiorganic lithium and all-organic radical batteries.^[148–150]

Cyclic voltammetry studies of TEMPO with LiPF_6 as the conductive salt, dissolved in ethylene carbonate (EC)/propylene carbonate (PC)/ethyl methyl carbonate (EMC; weight ratio of 4:1:5), demonstrated highly reversible redox reactions and a one-electron transfer for the nitroxide radical/oxoammonium cation redox couple [Eq. (12)].

To investigate the electrochemical performance of TEMPO in a flow-battery environment, a non-aqueous hybrid Li/TEMPO flow cell with a hybrid anode of lithium foil and graphite felt, a polyethylene-based porous separator, and graphite felt as the cathode was fabricated. Furthermore, a fluoroethylene carbonate (FEC) additive was added to protect the Li anode. TEMPO, dissolved in a mixture of EC/PC/EMC (weight ratio of 4:1:5), as well as LiPF_6 as support-

Positive electrode (cathode):



Negative electrode (anode):



ing electrolyte and anode active material, was added to both cell compartments, but only circulated on the cathode side.

Battery tests with various concentrations of TEMPO (0.1M, 0.8M, 1.5M, and 2.0M) were performed. One hundred consecutive charge/discharge cycles were demonstrated at a TEMPO concentration of 0.1M in 1.0M LiPF₆ EC/PC/EMC with 15 wt % FEC additive at a current density of 5 mA cm⁻². Thereby, an energy efficiency of 86 %, a coulombic efficiency of 99 %, a voltage efficiency of 87 %, and an average capacity retention of 99.8 % per cycle were achieved. At the same current density, but with 0.8M TEMPO in 1.2M LiPF₆ with 15 wt % FEC additive, the performance in terms of the stability was reduced and a theoretical energy density of 64 Wh L⁻¹ during the first 30 cycles was achieved.^[126]

The obtained results, in particular for higher concentrations up to 2.0M TEMPO, with a theoretical energy density of 126 Wh L⁻¹ surpass the performance of other conventional aqueous and non-aqueous RFBs.^[129,152–154] These high energy densities are facilitated by the large difference in the redox potentials, which lead to a system voltage of 3.5 V.^[126]

The authors reported a high solubility of TEMPO up to 5.2M in the solvent mixture, which offers the possibility to further increase the energy density.^[126] However, the viscosity of the electrolyte also rises as the concentration increases, and results in a high power demand of the pumps for circulating the electrolytes. Thus, the overall system efficiency of a practical RFB is significantly lowered. Furthermore, such high energy densities at a limited maximal current density are not practical in the everyday use of a flow battery, since the cell stack would need to be prohibitively large.

Takechi et al. discussed that a concentration higher than 2.0M is difficult to obtain for redox-active organic materials in aqueous and non-aqueous solvents, and came to the conclusion that the use of an ionic liquid could overcome this limitation and enable higher maximal theoretical energy densities.^[41] The TEMPO derivative 4-methoxy-2,2,6,6-tetramethylpiperidine-1-oxyl [MeO-TEMPO, redox mechanism in Eq. (12)] was selected as the organic redox-active compound and lithium bis(trifluoromethanesulfonyl)imide (LiTFSI) as the supporting electrolyte. The TFSI anion exhibits an uncommon plasticizing effect and induces the formation of a supercooled liquid.

A mixture of MeO-TEMPO and LiTFSI (MTLT) in a molar ratio of 1:1 features a “self-melting behavior and formed a smooth viscous liquid”.^[41] MTLT (1:1) showed the best energy density, but also had a significant viscosity (η) above 10 Pas at room temperature, which is caused by the concentration of the redox-active material, and is 500 times higher than the viscosity of classical electrolytes applied in

VRFBs.^[155,156] The viscosity was reduced by the addition of water to the molten MTLT (1:1), thereby enabling application in RFBs. MTLT (1:1) plus 17 wt % H₂O exhibited a viscosity of 72 mPas and a conductivity (σ) of 3.1 mS cm⁻¹. However, the capacity was lowered to 1.11 mAh.

The system was chosen as the catholyte for further investigations in flow-cell tests. A hybrid battery with a lithium ion conducting glass ceramic (LIC-GC) membrane and lithium metal as the anode was constructed. MTLT (1:1) plus 17 wt % of H₂O was utilized as the catholyte and 1M LiTFSI in propylene carbonate as the anolyte. A non-pumped battery showed over 20 charge/discharge cycles at a current density of 0.1 mA cm⁻² with a charge/discharge capacity of 93 % and 92 %, a coulombic efficiency of 99 %, a capacity retention of 84 %, a calculated energy density of 200 Wh L⁻¹, and a specific energy of 155 Wh kg⁻¹, which are the highest energy densities achieved for organic/inorganic flow batteries to date. The charge/discharge tests in a flow battery revealed a steady capacity retention with a broad range of flow rates at restricted current densities from 0.1 to 1 mA cm⁻².^[41] In particular, this limited current rating, which is induced by the LIC-GC separator and the carbonate-based organic anolyte, prevents commercialization of this system.

4.1.1.3. Alkoxybenzene-Based Redox-Active Materials

Huang et al. reported redox-active low-molar-mass compounds as cathode materials for non-aqueous RFBs in 2014.^[134] Based on the general structure of dimethoxy-di-*tert*-butylbenzene (Figure 7), which is responsible for the electrochemical properties and stability, oligoethylene oxide chains were introduced to increase the moderate solubility (ca. 0.4M) in carbonate-based polar solvents and, consequently, the energy density.

Besides the better solubility, the authors also observed an alteration of the physical properties at room temperature, from a solid state (DBBB) over a semi-liquid (ANL-10) to liquid (ANL-8, ANL-9). This enables new possibilities to significantly increase the energy density. The utilization of a supporting electrolyte, which is soluble in the charge-storage material, would allow the solvent to be replaced.

The three charge-storage materials (ANL-8, ANL-9, and ANL-10) were investigated by cyclic voltammetry in propylene carbonate with 0.2M LiBF₄ and exhibited a good electro-

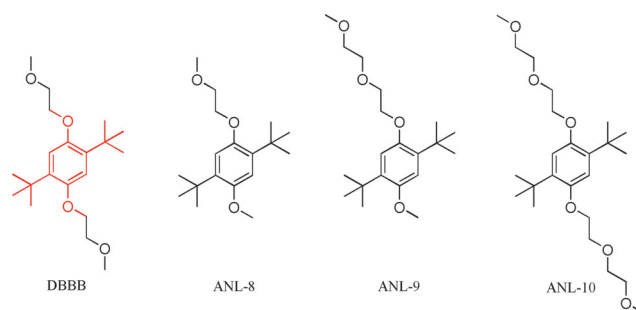


Figure 7. Chemical structures of 2,5-di-*tert*-butyl-1,4-bis(2-methoxyethoxy)benzene (DBBB) and modified derivatives ANL-8, ANL-9, and ANL-10.

chemical reversibility and redox potentials of around 4.0 V versus Li^+/Li . However, ANL-8 features a diffusion coefficient of the same order of magnitude as vanadium,^[157,158] DBBB,^[159,160] and several quinone derivatives.^[78,161] The battery tests were performed with 1 mM ANL-8 plus 0.5 M LiBF_4 as a conducting salt, dissolved in propylene carbonate, at a constant charging current of 0.4 mA in a bulk-electrolysis cell, where an energy density of 0.05 Wh L^{-1} for the catholyte could be achieved. The obtained voltage, energy efficiency, and capacity profiles revealed a deviant behavior at the first cycle, which indicates a side reaction during the first charging process. The energy efficiency of the first cycle was only 37 %, whereas the value for the following cycles was 81 %.^[134]

Huang et al. also investigated several other 1,4-dimethoxybenzene derivatives as redox-active materials for non-aqueous RFBs in a subsequent study.^[162] Starting from 2,5-di-*tert*-butyl-1,4-bis(2-methoxyethoxy)benzene (DBBB), well-known as a material for protection against overcharging in lithium-ion batteries,^[163] the authors modified the sterically demanding substituent groups to increase the solubility. Five substituted 1,4-dimethoxybenzene derivatives were generated and further investigated. Cyclic voltammetry measurements showed that 2,3-dimethyl-1,4-dimethoxybenzene (23DDB) and 2,5-dimethyl-1,4-dimethoxybenzene (25DDB, Figure 8) underwent quasireversible redox reactions and a one-electron transfer.

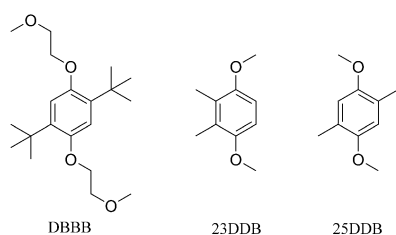


Figure 8. Chemical structures of 2,5-di-*tert*-butyl-1,4-bis(2-methoxyethoxy)benzene (DBBB), 2,3-dimethyl-1,4-dimethoxybenzene (23DDB), and 2,5-dimethyl-1,4-dimethoxybenzene (25DDB).

Thus, 23DDB and 25DDB were further explored through galvanostatical cycling in a bulk electrolysis cell. The utilized electrolytes contained 1 mM redox-active material and 0.5 M LiTFSI dissolved in polycarbonate. The corresponding electrolytes were charged/discharged from 0 to 50 % state of charge (SOC) over 100 cycles at a charging current of 0.4 mA.

The calculated energy density of 0.05 Wh L^{-1} for the cathode material as well as the charge and discharge capacities illustrate the drawbacks of these two derivatives. These studies showed that 50 % of 25DDB and 50 % of 23DDB turned irreversibly into a non-rechargeable species after approximately 48 cycles and 15 cycles, respectively. Accordingly, the average coulombic efficiency of 25DDB is about 90 % for the first 40 cycles and of 23DDB between 75 and 80 % for the first 20 cycles.^[162] In contrast to the good electrochemical properties of these alkoxybenzenes seen from CV measurements, the battery tests revealed several concerns regarding the chemical reversibility of the active

material. Therefore, their general suitability as active materials is questionable.

In contrast, TEMPO-containing organic/inorganic flow batteries showed elevated energy densities (64 to 200 Wh L^{-1} , for the cathode materials), which was facilitated by the utilization of a Li_{S} anode and an electrolyte based on an organic carbonate. However, the current rating was restricted and safety concerns remain. In contrast, the quinone battery has excellent current ratings, but a limited energy density. However, the safety aspect is improved.

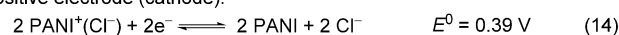
On the basis of these results, anthraquinone and TEMPO derivatives are the most promising organic charge-storage materials because of their interesting redox potentials, good chemical reversibility, and fast kinetics. However, future challenges concern the development of suitable substituents to further improve the performance and the solubility of these redox-active units for RFB applications.

4.1.2. Flow Batteries with Polymer-Based Organic/Inorganic Redox-Active Materials

A significant drawback of common RFBs is the often utilized and expensive Nafion ion-exchange membrane. The application of polymers with sufficiently high molar masses and linear, starlike, hyperbranched, or cyclic architectures instead of low-molar-mass compounds as organic redox-active materials allow the use of cost-efficient size-exclusion/dialysis membranes and microporous separators.^[32–36]

In 2013, Zhao et al. reported the first polymer-based HFB, which utilized polyaniline (PANI) particles as the charge-storage material. The authors constructed a HFB based on a zinc plate as the anode, a cost-efficient polypropylene microporous separator, and a flowing PANI microparticle suspension in ZnCl_2 and NH_4Cl as the catholyte.^[35]

Positive electrode (cathode):



Negative electrode (anode):



The fabricated flow battery was operated for 32 charge/discharge cycles. Current densities in the range of 10 to 30 mA cm^{-2} were applied, whereby a linear decrease in the achieved capacity with increasing current densities was observed. Coulombic efficiencies of 97 % and a decrease in the discharge capacity retention of 0.07 % per cycle were obtained. Furthermore, the calculated maximal theoretical energy density of 66.5 Wh L^{-1} exceeds the value of about 25 Wh L^{-1} of conventional VRFBs.^[35,109] However, the charge/discharge cycling at a current density of 20 mA cm^{-2} with an average discharge voltage of 1.1 V and a discharge capacity density of 115.2 mAh g^{-1} (150 g L^{-1} PANI suspension) reaches a maximal energy density of 9.5 Wh L^{-1} . Furthermore, coulombic efficiencies of over 100 % were achieved in some experiments. The authors ascribed this phenomenon to the oxidation of the PANI particles by

atmospheric oxygen. In the discharging procedure, these chemically oxidized particles can be reduced by consumption of the supporting electrolyte $\text{Zn}^{2+}_{(\text{aq})}$. Hence, a long-term decline in the battery performance is apparent. In addition, the application of a conductive polymer as the charge-storage material is not favored, as the redox potential of the polymer changes with the degree of oxidation (level of charging). This leads to steep potential curves in a battery application. The redox system was improved in a following study by using Ag-doped PANI particles.^[165]

Nagarjuna et al. presented a poly(vinylbenzylethylviologen) nonconductive polymer as the cathode material for non-aqueous flow batteries in 2014.^[36] The authors synthesized five vinylbenzylethylviologen polymers with molar masses (M_n) of 21, 104, 158, 233, and 318 kg mol^{-1} . These redox-active polymers (RAPs) featured a good solubility (above 2.1 M per repeating unit) in non-aqueous solvents such as acetonitrile or propylene carbonate, as well as chemically reversible redox reactions in cyclic voltammetry measurements. The authors employed a Celgard microporous trilayer PE/PP separator and observed, at cell-operating conditions, a polymer cross-over of 7% for the RAP with a molar mass of 318 kg mol^{-1} over a period of 6 h.

The electrochemical performance was investigated by using a non-aqueous redox-flow-cell configuration, which contained a metal oxide auxiliary electrode. The utilized flow-cell setup was not completely charged/discharged and demonstrated a charge capacity of 44% and a coulombic efficiency of above 45% at a C rate of 1/10.

In the same year, Sukegawa et al. described a 2,2,6,6-tetramethylpiperidin-1-oxyl (TEMPO) substituted bottle-brush polymer with a well-defined size as a potential catholyte for flow-battery applications.^[166] Bottlebrush polymers feature a lower viscosity than linear polymers with the same molar mass. Furthermore, the structure of a bottlebrush polymer is spatially tunable, for example, by the ratio of the length of the side chain and the main chain. The authors synthesized the target polymer poly(norbornene)-*g*-poly(4-methacryloyloxy-2,2,6,6-tetramethylpiperidine-1-oxyl) (PNB-*g*-PTMA) by a “grafting-through” technique.

The fabricated half-cell included a single flow channel, an AgCl/Ag reference electrode, and a carbon mesh current collector as the working electrode. 0.1 M PNB-*g*-PTMA ($M_n = 2.2 \times 10^5 \text{ g mol}^{-1}$) plus 0.1 M *n*-tetrabutylammonium perchlorate as a supporting electrolyte dissolved in ethylene carbonate/diethyl carbonate (1:1 in volume) were constantly circulated through the system. A half-cell charge/discharge experiment revealed a plateau potential at 1.0 V versus AgCl/Ag and a charge capacity utilization of 95% at a C-rate of 1. Furthermore, 1% of the utilized polymer passed through the porous separator over a period of 24 h.

The reported PNB-*g*-PTMA bottlebrush polymer is a notable innovation in the field of polymer-based RFBs (pRFB) and is designed, in particular, to counteract the increased viscosity of the electrolyte, one of the greatest challenges pRFBs have to overcome. However, the solubility has to be further increased to improve the energy density of this system. Similar concepts should be applied to water-soluble polymers.

In 2016, Winsberg et al. reported a novel, “green” poly-(TEMPO)/zinc semiorganic HFB.^[32,33] The authors combined the benefits of the zinc/halogen flow battery with those of an all-organic polymer RFB,^[34] which uses low-cost organic polymers as redox-active materials as well as a simple size-exclusion membrane as separator. Compared to recently reported zinc-halogen HFBs, this battery shows significant improvements in terms of corrosion and environmental impact. Three TEMPO-containing polymers were applied, one P(TMA-*co*-METAC) and two P(TMA-*co*-PEGMA)s (TMA = TEMPO methacrylate, METAC = [2-(methacryloyloxy)ethyl]trimethylammonium chloride, PEGMA = poly(ethylene glycol) methacrylate) with various monomer to co-monomer ratios, as redox-active materials in carbonate-based and aqueous electrolyte systems. A hybrid flow battery was constructed with a dialysis membrane as the separator, zinc foil as the anode, and P(TMA-*co*-PEGMA) as the cathode active material. The supporting electrolyte and anolyte used was $\text{Zn}(\text{ClO}_4)_2 \times 6\text{H}_2\text{O}$ in ethylene carbonate (EC)/dimethyl carbonate (DMC)/diethyl carbonate (DEC; v:v:v, 1:1:1). A stable charge/discharge cycling was performed over 500 cycles and revealed an average capacity decay of 0.04% per cycle and coulombic efficiencies of >99.7%. Current densities in the range of 0.5 to 4 mA cm^{-2} were applied. Here, a linear decrease in the energy efficiency with increasing current density was observed. The authors demonstrated a maximum capacity of 6.1 Ah L^{-1} .

Battery tests in aqueous electrolyte systems were performed to reach higher applicable current densities. The utilized aqueous catholyte contained P(TEMPO-*co*-METAC) as the cathode active material plus 0.71 M NaCl, 0.08 M ZnCl_2 , and 0.08 M NH_4Cl as the supporting electrolyte. Current densities up to 12 mA cm^{-2} and an energy density of 1.9 Wh L^{-1} were reached. Additionally, the coulombic efficiency with a maximum of 99% at 12 mA cm^{-2} always remained above 90% and the energy efficiency always above 80%. A good long-term stability with 1000 consecutive charge/discharge cycles, with an initial discharge capacity retention of 79%, were achieved (Figure 9).

Current densities up to 20 mA cm^{-2} and an energy density of 4.1 Wh L^{-1} were achieved with an aqueous catholyte containing P(TEMPO-*co*-PEGMA) plus 1.0 M ZnCl_2 and 1.0 M NH_4Cl as the supporting electrolyte. A material activity of 88% was reached, and the coulombic efficiency stayed mostly above 90% at various current densities. However, a linear decrease in the capacity occurred at increasing current densities.

This organic/inorganic HFB permits a stable potential window of up to 2 V (OCV 1.7 V) in an aqueous electrolyte system. Furthermore, contamination with oxygen is unproblematic and an expensive process to render the HFB inert is unnecessary.

In a following study the authors demonstrated the application of core-corona micelles with a TEMPO-containing corona as the cathode active material.^[33] The application of a micellar catholyte reduced the viscosity compared to the previously reported linear TEMPO-containing polymers. Again, a stable battery cycling was demonstrated over 1000 consecutive charge/discharge cycles with 95% retention of

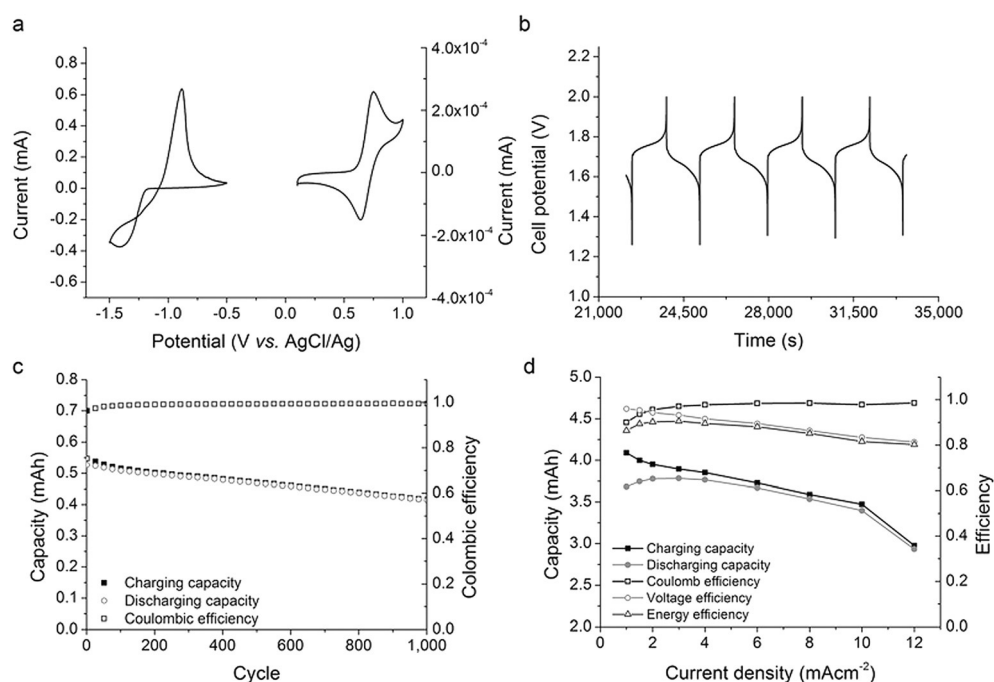


Figure 9. a) Cyclic voltammogram of an aqueous solution of 0.1 M zinc chloride and 0.01 M poly(TEMPO). Scan rate: 50 mV s⁻¹. b) Exemplary charging/discharging curves at a current density of 2 mA cm⁻², aqueous catholyte; polymer solution in NaCl, ZnCl₂, NH₄Cl with a capacity of 1.1 Ah L⁻¹, flow rate: 20 mL min⁻¹. c) Long-term stability test, cycling of a static cell. d) Electrical performance: capacity, coulombic, voltage, and energy efficiency depending on the applied current density.^[32]

initial discharge capacity and applicable current densities in the range of 0.2 to 5 mA cm⁻². The battery featured an energy density of 0.8 Wh L⁻¹.

From these described polymer-based organic/inorganic flow batteries, the combination of zinc/organic polymer^[32,33,35] shows the greatest potential for further developments. As mentioned before, TEMPO-based redox-active materials,^[32,33,166] in particular, are promising charge-storage materials because of their well-defined redox behavior. The good long-term stability is ensured by the hindered recombination of two TEMPO moieties because of steric effects, the delocalization of the radical electron, and an unfavored NO–ON bond formation.

In contrast to RFBs based on low-molar-mass organic charge-storage materials, polymer-based RFBs allow the utilization of cost-efficient size-exclusion (dialysis) membranes and microporous separators. Nevertheless, potential challenges such as an increased synthesis effort, solubility, and viscosity properties have to be addressed in future studies.

4.2. Redox-Flow Batteries Based on Organic/Halogen Redox-Active Materials

These RFB systems operate without the utilization of any metal as the redox-active material. The first was reported by Huskinson et al. in 2014.^[78] It is based on 9,10-anthraquinone-2,7-disulfonic acid (AQDS) in H₂SO₄ as the anolyte and Br₂/2Br⁻ in HBr as the catholyte (Figure 10). The employed flow-

cell setup contained a Nafion 212 proton-exchange membrane, 3 M HBr and 0.5 M Br₂ as the catholyte, and 1 M AQDS in 1 M H₂SO₄ as the anolyte.

The charge/discharge experiment, conducted at 40 °C, revealed a stable performance over 20 cycles, a discharge capacity retention of 99%, and a current efficiency of around 99% at a current density of 500 mA cm⁻². The applied electrolyte had a calculated energy density of 9.4 Wh L⁻¹. These results, which are comparable with those of the quinone-based organic/inorganic flow battery,^[147] illustrate that anthraquinones represent a promising organic anode material for RFB applications. Their synthesis from inexpensive starting materials is straightforward and

Positive electrode (cathode):



Negative electrode (anode):



can be easily scaled up. Furthermore, AQDS undergoes a very fast and chemically reversible two-electron two-proton reduction in sulfuric acid. A kinetic rate constant (k_0) of $7.2 \times 10^{-3} \text{ cm s}^{-1}$ was measured, which is very high compared to the corresponding values of other metal-based redox-active materials used in flow-battery applications.^[23] The utilized AQDS has a solubility of greater than 1 M at pH 0, which can be increased by the introduction of functional groups, such as hydroxy groups. Nevertheless, the described quinone/hydroquinone redox couple also shows some drawbacks, such as limited solubility in aqueous media. Furthermore, the necessity to conduct the battery tests at a temperature of 40 °C increases the energy demand and lowers the over-all efficiency of the system.

In a following study, the authors described in detail the cycling performance of this flow battery.^[168] The initially applied Nafion 212 membrane was replaced by a Nafion 115 membrane and the electrolyte contained 1 M AQDS in 1 M H₂SO₄ as the anolyte (100 mL) as well as 3 M HBr and 0.5 M Br₂ as the catholyte (120 mL). At a current density of 250 mA cm⁻², the flow cell exhibited an average discharge capacity retention of nearly 100% per cycle over 106 cycles.

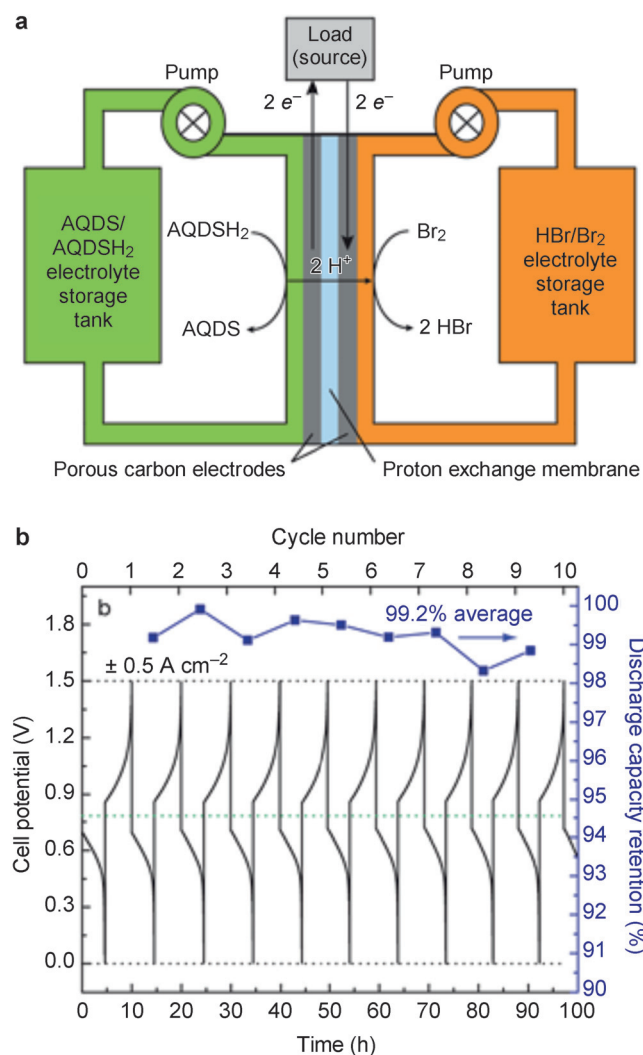


Figure 10. a) Schematic diagram of a cell. The discharge mode is shown; the arrows are reversed for the electrolysis/charge mode. AQDSH₂ refers to the reduced form of AQDS. b) Constant-current cycling at 0.5 A cm⁻² at 40 °C using a 3 M HBr, 0.5 M Br₂ solution on the positive side and a 1 M AQDS, 1 M H₂SO₄ solution on the negative side; the discharge capacity retention is indicated for each cycle.^[78]

At a current density of 750 mA cm⁻², the flow cell was cycled 750 times and revealed an average current efficiency of 98 % as well as an average discharge capacity retention of nearly 100 % per cycle.

In 2015, Chen et al. also reported a quinone/bromide RFB based on the cell design developed by Huskinson et al.^[127] In contrast to the earlier study,^[78] baked (400 °C in air for 24 h) SGL carbon paper (ca. 400 μm thick) was utilized instead of pretreated Toray carbon paper (7.5 μm thick, uncompressed) as electrodes to enhance the power output. The cell operated at 40 °C using AQDS in 1 M H₂SO₄ as the anolyte and 3 M HBr together with 2 M Br₂ as the catholyte. Although the anolyte and the anode compartments were not altered, the composition of the catholyte was modified. The redox potential and, thus, the cell voltage could be increased by reducing the concentration of HBr or enhancing the Br₂ concentration.

Adversely, a decrease in the HBr concentration led to an increase in the membrane and electrolyte resistance and additionally to a high rate of bromine crossover. The described flow cell revealed a short-circuit current density above 4000 mA cm⁻² at 90 % SOC and a peak galvanic power density of 1 W cm⁻².^[127] These data represent a significant improvement in reference to the published results of Huskinson et al.^[78] Furthermore, the achieved peak galvanic power density of 1.0 W cm⁻² is 75 % higher than the maximum values of previously published VRFBs.^[169]

In a subsequent study, Chen et al. also reported a cycling analysis of the quinone/bromide RFB.^[170] The authors used 1 M AQDS in 1 M H₂SO₄ as the anolyte (25 mL) and 3.5 M HBr in combination with 0.5 M Br₂ as the catholyte. The battery tests were performed at 30 °C, with current densities in the range of 100 to 1000 mA cm⁻² with the aim of investigating the impact of the current density on the voltage polarization, charge capacity, as well as, current, voltage, and energy efficiency. Since the focus was on the organic redox-active anode material, a significant excess of the active species on the cathode side was employed, which led to a ratio of positive to negative charge capacity of 5:36. The authors observed linear polarization curves at current densities up to 250 mA cm⁻² at a SOC in the range of 10 to 90 %. The overvoltage increased as the current density increased, and resulted in an earlier accomplished voltage limit, which led to a decrease in the utilized charge/discharge capacity. Leakage of the anolyte, destruction of the redox-active anode material, and the Br₂ crossover also resulted in a decrease in the charge/discharge capacity. Thus, 40 % of the theoretical capacity was achievable at a current density of 1000 mA cm⁻². On the basis of the obtained results, Chen et al. were able to explain the relationship between current density and coulombic, voltage, and energy efficiency through established equations.

Zhang et al. reported in 2016 an improvement to Li's^[171] investigated 3D numerical model and simulation study of the quinone/bromide RFB.^[172] A 3D non-isothermal transient model with added graphite plates as well as a temperature field was utilized to investigate the influence of current, temperature, and electrolyte flow rate on the battery performance of the quinone/bromide RFB. The flow-cell setup was designed in accordance with that of Huskinson et al.^[78] Battery tests were simulated with current densities in the range of 50 to 400 mA cm⁻² with the aim of investigating the impact of the current density on the battery performance. Furthermore, battery tests were performed with a current density of 200 mA cm⁻² and 500 mA cm⁻² to compare the obtained computational results with experimental data; a good comparability was found. The investigated 3D model showed a strong influence of the flow channel structure and temperatures > 30 °C on the battery performance.

As mentioned before, anthraquinone derivatives revealed excellent properties as charge-storage materials in battery applications. However, the solubility needs to be increased to 2 M and bromine needs to be replaced by a safer organic cathode active material in future studies.

4.3. Redox-Flow Batteries with Organic Redox-Active Materials for the Catholyte and Anolyte

As previously discussed, the focus of research in the field of flow batteries should be the development of a RFB using noncorrosive, safe, and in particular low-cost redox-active organic charge-storage materials.^[34] Thereby, promising redox-active low-molar-mass compounds as well as redox-active polymers are of interest. Both systems have inherent advantages; small molecules have the advantages of little or no synthetic effort, potential high solubilities, and good diffusion coefficients, whereas polymers offer the prospect of using more cost-efficient and robust separators compared to ion-selective membranes.

The development of a so-called all-organic equivalent to a VRFB with a bipolar redox-active material is of high interest, because this material would be able to undergo oxidation as well as reduction reactions and could, therefore, be applied as both the cathode- and anode-active material. This feature would reduce the synthesis effort of the whole process and potentially overcome the problem of cross-contamination, since a slow mixing of the electrolytes would only lead to a reduced coulombic efficiency but not to a continuously decreasing charge/discharge capacity.^[28]

4.3.1. Redox-Flow Batteries with Low-Molar-Mass Organic Redox-Active Materials

4.3.1.1. Symmetric Redox-Flow Batteries with Bipolar Organic Redox-Active Materials

In 2011, Rasmussen investigated pyrazine-based cyanoazacarbon derivatives as potential bipolar organic redox-active materials.^[173] Cyclic voltammetry measurements of the derivative 9,10-butyl-2,3,6,7-tetracyano-1,4,5,8,9,10-hexaanthracene revealed a chemical reversibility for the oxidation as well as the reduction reaction, and a possible cell potential of nearly 3 V.

A few years later, Potash et al. reported a symmetric redox-flow battery, which utilizes diaminoanthraquinones (DAAQs) as bipolar redox-active materials.^[28] Several commercially available DAAQs were investigated by cyclic voltammetry, with the DAAQ derivative Disperse Blue 134 (DB-134) showing a good reversibility in both the oxidation and reduction reactions. Therefore, this material was further investigated in a glass H-cell, where the compartments were separated by a glass frit with medium porosity. Solutions with a concentration of 50 mM DB-134 and 100 mM tetrabutylammoniumperchlorate in acetonitrile/toluene (v/v; 3:2) were charged/discharged at a current of 2 mA. The authors demonstrated three charge/discharge cycles with a subsequent reversal of polarization. Depending on the cycling method, a coulombic efficiency in the range of 85 and 61 %, a voltage efficiency between 53 and 45 %, and an energy efficiency in the range of 43 and 28 % were achieved. The continuous decrease can be explained by a slow degradation of the redox-active DB-134. The observed energy density was 0.94 WhL⁻¹.^[28] These moderate results of the battery tests are induced by the limited solubility of the utilized DB-134 in

the electrolyte, the observed crossover through the porous glass frit, and the incomplete inert battery setup.

In 2016, Duan et al. published an alternative approach to a non-aqueous symmetric redox-flow battery by using the commercially available 2-phenyl-4,4,5,5-tetramethylimidazoline-1-oxyl oxide (PTIO, Figure 11), a nitronyl nitroxide radical, as the bipolar organic redox-active material.^[174]

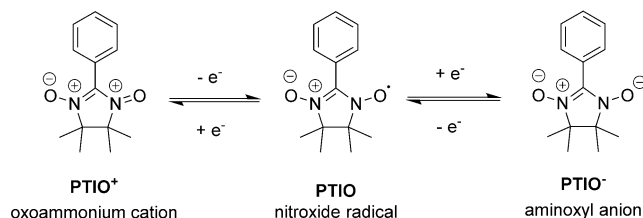


Figure 11. Electrochemical reactions of PTIO.

Compounds containing nitronyl nitroxides were first described in 1968 by Osiecki et al., and subsequently investigated electrochemically in detail and used in several magnetic applications.^[175–183]

PTIO, as a novel charge-storage material for RFBs, features a potential high solubility of about 2.6 M in acetonitrile. However, a flow cell with a PTIO concentration > 0.5 M has not been realized so far. Furthermore, a crossover of the redox-active material through the separator, which limits the CE, and a high viscosity of the electrolyte was observed. The state of charge and the concentration of PTIO was monitored by FTIR spectroscopy. The cycling performance of a flow cell that utilized a Daramic porous separator and 0.5 M PTIO with 1 M TBAPF₆/acetonitrile as the supporting electrolyte was investigated. The test cell completed over 15 cycles at a current density of 20 mA cm⁻² at a coulombic efficiency of about 90 %, a voltage efficiency of 67 %, an energy efficiency of 60 %, and an energy density of 9 WhL⁻¹ during charge as well as 5 WhL⁻¹ during discharge. These results are far better than the values of the symmetric redox-flow battery reported by Potash et al.^[28]

However, independent of the utilized PTIO concentration, the demonstrated flow cells show a continuous capacity loss, probably because of an electrolyte imbalance and/or chemical instability of the charged redox-active material.

4.3.1.2. Asymmetric Redox-Flow Batteries with Organic Redox-Active Materials in Organic Electrolytes

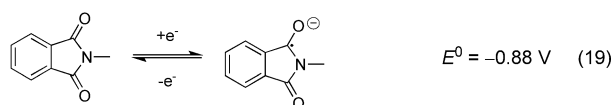
In 2011, Li et al. reported the first RFB with two redox-active organic compounds, TEMPO and *N*-methylphthalimide, as the cathode and anode active material.^[129]

Cyclic voltammetry measurements showed quasireversible redox reactions for both compounds with a voltage of approximately 1.6 V. The authors performed battery tests with a test cell containing a Nepem 117 cation-exchange membrane by using 0.1 M TEMPO and 0.1 M *N*-methylphthalimide, both dissolved in anhydrous acetonitrile plus 1 M NaClO₄ supporting electrolyte, as the catholyte and anolyte, respectively. The static test cell was operated at a current

Positive electrode (cathode):



Negative electrode (anode):



density of 0.35 mA cm^{-2} . The coulombic efficiency exceeded 90 % and an energy density of 1.7 Wh L^{-1} was achieved during the first 20 charge/discharge cycles.

The increased voltage of 1.6 V in comparison to VRFBs represents a significant advantage and illustrates the flexibility of all-organic RFBs. However, the capacity and current rating of this system are restricted by the organic electrolyte.

In 2012, Brushett et al. reported a non-aqueous RFB by using 2,5-di-*tert*-butyl-1,4-bis(2-methoxyethoxy)benzene (DBBB) and 2,3,6-trimethylquinoxaline (TMeQ) as redox-active materials.^[159] The fundamental electrochemical properties of these compounds were investigated by cyclic voltammetry and revealed a high redox reversibility at around 4 V versus Li^+/Li for DBBB and two reversible redox reactions at 2.48 and 2.8 V versus Li^+/Li for the TMeQ. The authors developed a “proof-of-concept coin-cell flow battery” to verify the feasibility of these redox-active molecules for application in a RFB. This setup, normally appropriate for lithium-ion/thin-film battery tests, contained a Nafion 117 membrane with 0.05 M DBBB and 0.05 M TMeQ in 0.2 M LiBF_4 dissolved in propylene carbonate as the catholyte and anolyte, respectively. As a consequence of the unoptimized cell design and the limited solubility of DBBB, the maximum observed capacity of this coin-cell test device was 0.6 Ah L^{-1} at a current density of $0.0625 \text{ mA cm}^{-2}$.^[159] This is much lower than the high capacity of common VRFBs.^[70] A battery cycling was performed over 30 cycles, and coulombic efficiencies of around 70 % and energy efficiencies of around 37 % were achieved.^[159]

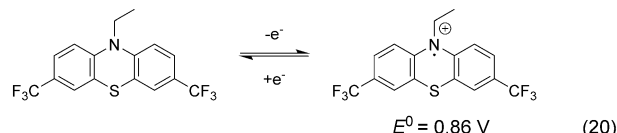
The alkoxybenzenes DBBB and the previously discussed ANL-8,^[134] 23DBB, and 25DB,^[162] all showed rather poor results in regard to solubility and chemical reversibility. As a result, their utilization in flow batteries is not reasonable and future research should focus on different active materials.

Despite this limited performance, Su and co-workers also investigated DBBB as a redox-active cathode material for non-aqueous RFBs.^[160] Based on the results from Brushett et al.,^[159] the authors developed an automated electrolyte preparation as well as a characterization platform, which allowed combinatorial screening of a large number of electrolytes, including the redox-active DBBB, several alkali ion salts as supporting electrolytes, and organic carbonates as solvents. The highest solubility ($>0.5 \text{ M}$) and also ionic conductivity ($>5 \text{ mS cm}^{-1}$) were achieved for a solvent mixture of linear and cyclic carbonates with lithium hexafluorophosphate (LiPF_6) as supporting electrolyte and bis(trifluoromethane)sulfonamide lithium (LiTFSI) as an additive.^[160] However, the ionic conductivity is significantly higher in

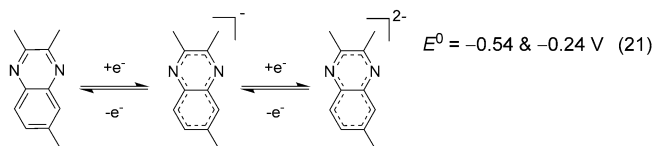
aqueous solution than in organic solvents. For example, the TEMPO/methylviologen system in aqueous solution exhibits an ionic conductivity of about 100 mS cm^{-1} .^[135] Thus, aqueous organic RFBs seem to be a better alternative to the non-aqueous organic systems.

Kaur et al. reported in 2015 the phenothiazine derivative 3,7-bis(trifluoromethyl)-*N*-ethylphenothiazine (BCF3EPT) as an organic cathode material and 2,3,6-trimethylquinoxaline (TMeQ) as an anode material.

Positive electrode (cathode):



Negative electrode (anode):

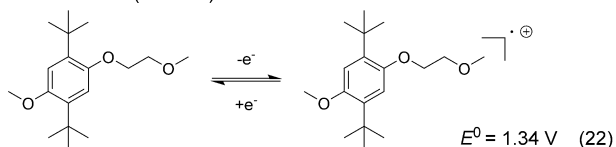


The cell performance was investigated by using a static Swagelok cell, in combination with a Nafion 117 membrane and 0.2 M LiBF_4 in propylene carbonate as the supporting electrolyte. The static Swagelok cell with 0.05 M BCF3EPT/TMeQ showed a coulombic efficiency of approximately 92 % and an energy density of around 0.84 Wh L^{-1} . The battery cycling experiment revealed that this flow cell lost nearly all of its capacity after 100 consecutive charge/discharge cycles. A second battery with an increased capacity (0.15 M of each redox-active species) demonstrated a stable performance over 60 cycles. Thereby, an average charge/discharge capacity of 0.44 and 0.37 mAh g^{-1} , a coulombic efficiency of almost 89 %, and an energy density of approximate 2.5 Wh L^{-1} were achieved. However, a battery with an increased concentration of 0.35 M showed a rapidly decreasing charge/discharge capacity that decreased to zero after 20 cycles.^[184]

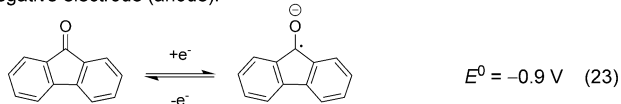
The current system exhibits some serious drawbacks such as the restricted solubility of the TMeQ anolyte and the non-optimized membrane selection, which results in a crossover of the organic compounds. Furthermore, it was observed that the utilized BCF3EPT catholyte undergoes a second irreversible oxidation in the charging procedure, which leads to a decrease in the overall capacity. Additionally, an adverse side reaction of the anode active material cannot be excluded, thereby rendering this material, up to now, questionable for RFB applications.

Wei et al. reported another non-aqueous RFB with ANL-8 and 9-fluorenone (FL) as the cathode and anode material, respectively.^[136] These two small molecules demonstrated good solubility, or in the case of ANL-8 (which is liquid at room temperature) good miscibility with several organic solvents, and well-defined electrochemical properties. To investigate the performance of the ANL-8/FL battery, a test cell was fabricated with a Daramic microporous

Positive electrode (cathode):



Negative electrode (anode):



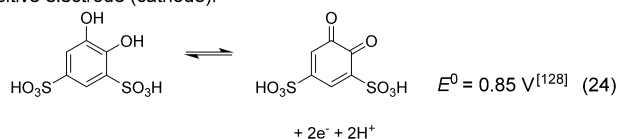
polyethylene/silica separator, 0.5 M FL, and 0.5 M ANL-8 in acetonitrile with 1.0 M tetraethylammonium bis(trifluoromethylsulfonyl)imide as the conducting salt. Over 100 charge/discharge cycles, at a current density of 15 mA cm^{-2} , the flow cell demonstrated a cell voltage of $> 2 \text{ V}$, coulombic efficiencies of 86 %, a voltage efficiency of 83 %, and an energy efficiency of 71 %. The theoretical energy density was 15 Wh L^{-1} , of which 73 % could be utilized.

The achieved performance parameters are much higher than those for the reported system by Brushett et al.^[159] and Li et al.^[129] Despite this, a demonstration of a stable charge/discharge capacity retention over a few cycles was not possible and a constant decrease over 100 cycles starting from 5.8 to 1.2 Ah L^{-1} was observed, which represents a loss of nearly 80 %. Similar to the previously discussed studies with ANL-8 and DBBB, the unsuitability of alkoxybenzenes is affirmed.

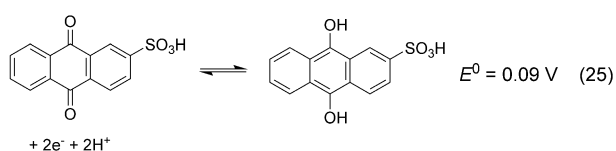
4.3.1.3. Asymmetric Redox-Flow Batteries with Organic Redox-Active Materials in Aqueous Electrolytes

In 2014, Yang et al. reported the first aqueous all-organic RFB. They used a water-soluble 1,2-benzoquinone-3,5-disulfonic acid (BQDS) as the organic cathode active material and anthraquinone-2-sulfonic acid (AQS) as well as anthraquinone-2,6-disulfonic acid as the organic anode active material.^[128]

Positive electrode (cathode):



Negative electrode (anode):

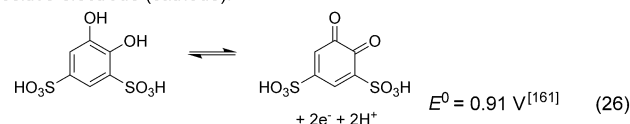


The authors developed a redox-flow cell with a membrane electrode assembly, which was fabricated from coated carbon

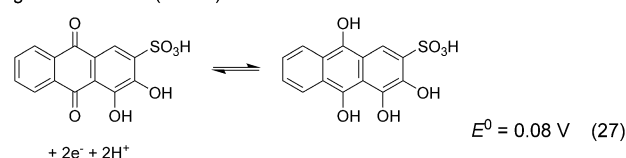
paper electrodes and a Nafion 117 membrane. The flow cell contained 0.2 M BQDS and 0.2 M AQS in 1 M H_2SO_4 as the catholyte and anolyte, respectively. The electrolytes had a calculated energy density of 1.25 Wh L^{-1} . A charge/discharge experiment was conducted over 12 cycles at a current density of 10 mA cm^{-2} , whereby a capacity retention of 90 % was reached.^[128] Limiting factors of these organic charge-storage materials are their moderate solubility in aqueous media and the observed mass transport of the reactants. These factors and the non-optimized battery setup lead to a restriction of the possible current density. The reported system can be seen as an improvement compared to the AQDS/bromide RFB in terms of safety, as the toxic bromine catholyte is replaced by BQDS. However, the capacity and the electrical performance are significantly inferior.

Zhang et al. reported an aqueous RFB with the already known water-soluble 1,2-benzoquinone-3,5-disulfonic acid (BQDS) as the catholyte and an inexpensive anthraquinone derivative, 3,4-dihydroxy-9,10-anthraquinone-2-sulfonic acid (ARS), as the anolyte.^[128,161]

Positive electrode (cathode):



Negative electrode (anode):

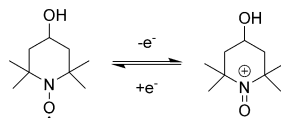


Both charge-storage materials are commercially available. Electrochemical investigations showed that ARS exhibits a two-electron redox process and that the redox reactions of both molecules are highly reversible. The utilized laboratory flow cell comprised copper plates as current collectors and a Nafion 212 proton-exchange membrane. Charge/discharge measurements with 0.05 M BQDS and 0.05 M ARS in 1 M H_2SO_4 as the catholyte and anolyte, respectively, were performed with various current densities of 20, 30, and 60 mA cm^{-2} to investigate the cell performance. Three charge/discharge cycles with an average discharge capacity of 90 mAh^{-1} , a calculated discharge capacity retention of around 98 %, as well as a coulombic efficiency of 99 % were achieved. The maximal power density of 10.6 mW cm^{-2} was accomplished at 80 % SOC at a current density of 60 mA cm^{-2} .^[161]

The authors obtained good coulombic efficiencies through fast charging and slow discharging cycling, but the unoptimized flow-cell setup led to a voltage loss. Furthermore, the observed energy density of 0.4 Wh L^{-1} and the current density is limited by the restricted solubility of the utilized redox-active molecules, especially of the ARS.

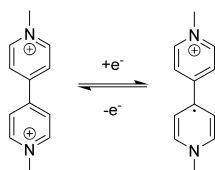
At the end of 2015, Liu et al. described an aqueous RFB with 4-hydroxy-2,2,6,6-tetramethylpiperidine-1-oxyl (4-HO-TEMPO) and methylviologen (MV) as the organic redox-active catholyte and anolyte, respectively. The authors applied the derivative 4-HO-TEMPO instead of common TEMPO as the cathode active material because of its higher water solubility of up to 2.1 M.^[135] However, the solubility of 4-HO-TEMPO in NaCl solution is only approximately 0.5 M.

Positive electrode (cathode):



$$E^0 = 0.80 \text{ V} \quad (28)$$

Negative electrode (anode):



$$E^0 = -0.45 \text{ V} \quad (29)$$

NaCl was utilized as the supporting electrolyte and an anion-exchange membrane allowed selective transport of chloride ions. CV and RDE measurements showed that MV and 4-HO-TEMPO displayed chemically reversible and diffusion-controlled redox reactions. Battery tests were performed at room temperature at concentrations of 0.1 M and 0.5 M of the redox-active material in aqueous 1.0 M or 1.5 M solution of NaCl at current densities in the range of 20 to 100 mA cm⁻². 72 % of the theoretical capacity at a current density of 60 mA cm⁻² was utilized. A voltage efficiency of 62 %, an energy efficiency of 63 %, and a coulombic efficiency above 99 % were achieved over 100 charge/discharge cycles. The theoretic energy density of this system was 8.4 Wh L⁻¹ (Figure 12).^[135]

The reported flow battery exhibited a moderate energy density and good coulombic efficiencies. However, the voltage efficiency and, thus, the energy efficiency strongly limit the performance of this system. One of the benefits is the low price and commercial availability of the employed active materials. The major problem, which affects the long-term usability of this system, is the side reaction of the 4-HO-TEMPO. The oxoammonium cation [which is generated in the charging procedure; Eq. (28)] is capable of oxidizing alcohols, thereby leading to a self-oxidation of 4-HO-TEMPO to 4-keto-TEMP-hydroxylamine.^[185]

The development of RFBs with inexpensive and sustainable organic redox-active materials as well as low-cost membranes may overcome the existing drawbacks of inorganic RFBs, such as the VRFB. In particular, a symmetric RFB with an organic bipolar redox-active material could represent an organic alternative to state-of-the-art VRFBs. Nevertheless, research in this field is in its infancy and needs further intensive investigations on potential organic bipolar redox-active materials. A bipolar material that can be utilized in the electrochemical window of water is of particular

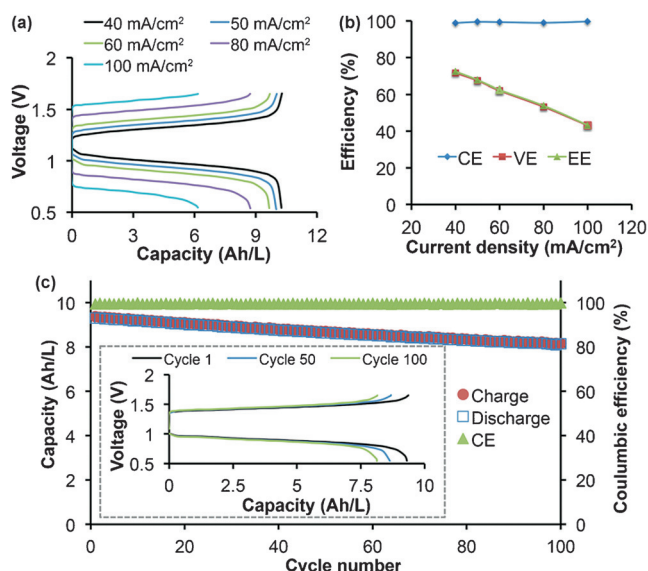


Figure 12. a) Representative charge and discharge profiles of the MV/4-HO-TEMPO RFB (0.5 M) at cycling rates from 20 to 100 mA cm⁻². b) Plots of Coulombic efficiency, voltage efficiency, and energy efficiency versus current density of the cell. c) Capacity and coulombic efficiency versus cycling numbers of the cell at 60 mA cm⁻². Conditions: anolyte, 0.5 M MV in 1.5 M NaCl aqueous solution; catholyte, 0.5 M 4-HO-TEMPO in 1.5 M NaCl aqueous solution; flow rate, 20 mL min⁻¹.^[135]

interest. Asymmetric RFBs are also an interesting topic for further developments so as to increase the capacity and, thus, the energy density. The choice of the right charge-storage materials and highly selective membranes already allows good long-term capacity retentions and low crossover reactions to be achieved.

4.3.2. Redox-Flow Batteries with Polymer-Based Organic Active Materials

The first polymer-based non-aqueous symmetric RFB was reported by Oh et al. in 2014. The authors fabricated an electrolyte based on a suspension of polythiophene (PT) particles, where PT serves as the bipolar redox-active material.^[132] A high stability of the redox reactions and pronounced n-doping and p-doping was exhibited. The observed electrochemical redox processes at -2.0 and 0.5 V versus Ag⁺/Ag enabled a high cell potential of 2.5 V. The performance of these bipolar redox-active conductive particles was investigated in a flow-cell setup with an anion-exchange membrane and carbon black as the conductive additive. Polythiophene microparticles (8.41 g L⁻¹) were dispersed in a solution of 1 M tetraethylammonium tetrafluoroborate (TEABF₄) in propylene carbonate. At a current density of 0.5 mA cm⁻², the flow battery demonstrated a stable charge/discharge behavior over 20 cycles with a high energy efficiency of 61 % and a maximal observed energy density of 2.7 Wh L⁻¹.^[132] Besides the advantage that the conjugated polymer particles lead to a decrease in the electric resistance inside the cell, the application of conjugated polymer particles led to some major drawbacks, such as

steep potential curves and the possibility of clogged flow channels as a result of agglomerated particles.

Water offers several advantages over organic electrolyte solvents: It is nonflammable, inexpensive, and allows for high ion mobility, for example, low ohmic resistance. For this reason, Janoschka et al. evaluated numerous water-soluble polymers (polymethacrylates and polystyrenes) for application in an aqueous RFB.^[186] A special focus was on their rheological, thermal, and electrochemical properties with a target of < 20 mPas to ensure the efficient operation of a pumped RFB. A novel battery type to replace common ion-exchange membranes and highly corrosive, acidic electrolyte solutions with inexpensive dialysis membranes and pH-neutral sodium chloride solutions was reported by using optimized polymers, which employ TEMPO and viologen as the redox-active moieties (Figure 13).^[34,186]

The dialysis membrane showed a good retention of the redox-active materials and a low resistance of $1.14 \Omega \text{ cm}^2$, which is in the range of Nafion. The high ion mobility in water led to current densities of up to 100 mA cm^{-2} being attained. The long-term stability of the system was demonstrated in a static test cell by repeated charging/discharging over 10 000 cycles with 80 % capacity retention. Furthermore, a pumped flow cell with an increased volumetric capacity of 10 Ah L^{-1} demonstrated a capacity retention of around 80 % after 95 consecutive charge/discharge cycles. The faster fade in capacity can be explained by a side reaction, possibly induced by oxygen. Although this novel system may lay the foundation for a new RFB working principle (polymer plus dialysis

membrane), capacity limitations of currently 10 Wh L^{-1} still need to be overcome, for example, by substituting linear for hyperbranched polymers.

Winsberg et al. reported a poly(boron dipyrromethene)-based flow battery.^[187] Boron dipyrromethenes (BODIPYs) are frequently used as chemosensors and laser dyes. Besides their special optical properties, several BODIPYs feature chemically reversible oxidation and reduction reactions, which render them a potential bipolar redox-active material for flow-battery applications and, thus, an organic alternative to VRFBs (Figure 14).

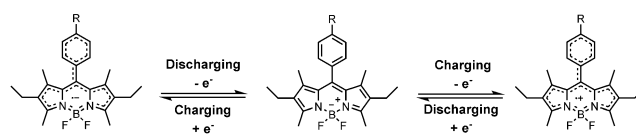


Figure 14. Redox mechanism of the utilized BODIPY derivative.

The authors synthesized styrene-based polymers with pendant BODIPY moieties and fabricated an organic solution-based battery by using polymeric TEMPO as the catholyte and a BODIPY copolymer as the anolyte. This battery featured a mean discharging voltage of 1.82 V and 100 consecutive charge/discharge cycles with 70 % retention of the initial discharge capacity. A second battery that featured two different BODIPY copolymers, one as the catholyte and a second as the anolyte, revealed a mean charging voltage of 2.06 V but only a mean discharging voltage of 1.28 V. Nevertheless, a stable battery cycling was observed for 90 consecutive charge/discharge cycles. A bipolar polymer, which can be used both in the catholyte and anolyte, has so far not been reported.

5. Photoelectrochemical Redox-Flow Batteries (Photo-RFBs)

RFBs are utilized as a buffer for intermittent electric energy. Electricity which is produced by wind power or solar energy is converted into chemical energy and stored for a certain amount of time. Photo-RFBs render this detour via electrical energy unnecessary, since light is directly stored as chemical energy. The development of highly efficient photoelectrodes and their integration into RFB technologies may result in the use of conventional photo-

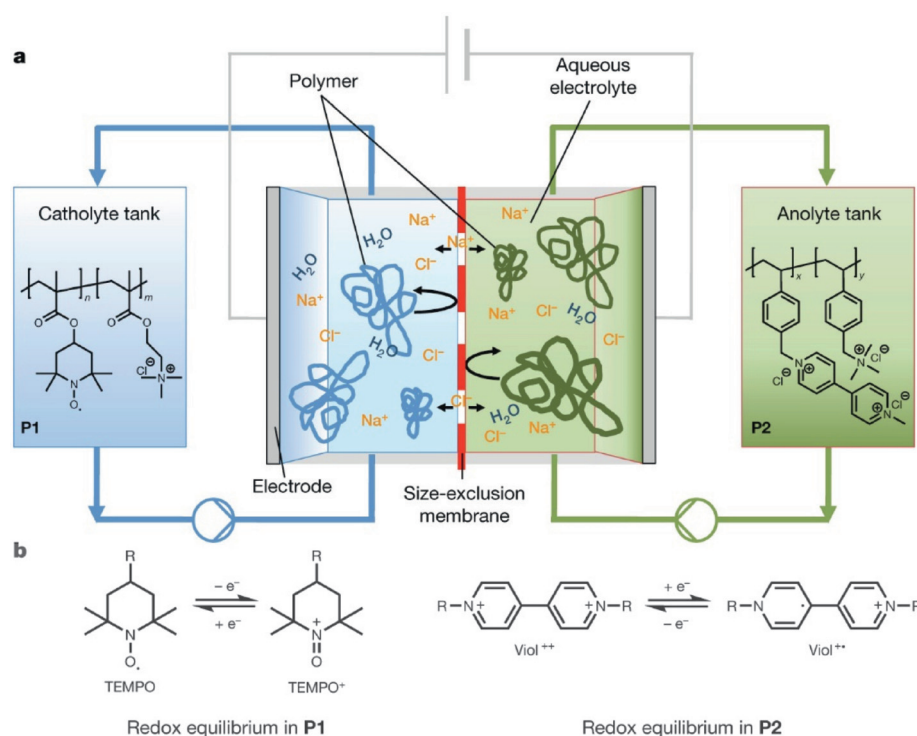


Figure 13. a) Schematic representation of a polymer-based RFB consisting of an electrochemical cell and two electrolyte reservoirs. The anolyte and catholyte cycle are separated by a semipermeable size-exclusion membrane, which retains the redox-active macromolecules while allowing small salt ions to pass. b) Fundamental electrode reactions of P1 (TEMPO radical) and P2 (viologen).^[34]

voltaic systems and batteries becoming obsolete, thereby leading to a more cost-efficient and simpler all-in-one system.

The design of a photo-RFB is very similar to that of regular RFBs, but differs in the additional utilization of a photoelectrode, which is typically fabricated from conductive glass coated with a photocatalyst. A schematic representation is shown in Figure 15.

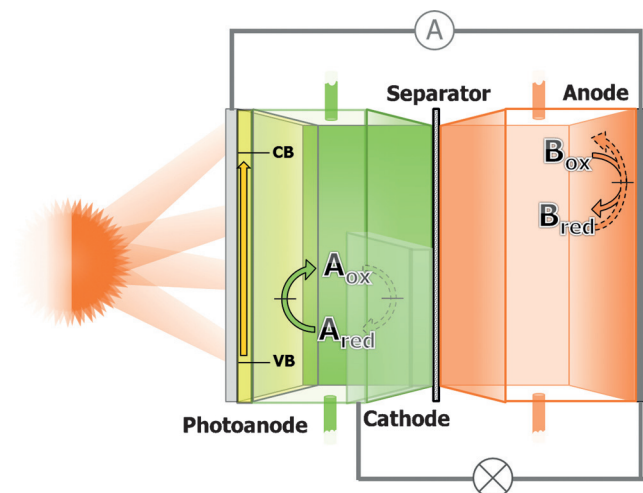


Figure 15. Schematic representation of a photoelectrochemical redox-flow battery.

The charging process is dependent on the photoanode. This electrode is mandatory for the light-harvesting process, as incident light generates electron-hole pairs, which induce the oxidation of the catholyte at the interface between the catholyte and photoanode.^[188] Simultaneously, the anolyte is reduced by the transferred electron. The subsequent discharging procedure is the same as in regular RFBs.

5.1. Photoelectrochemical Redox-Flow Batteries with Asymmetric Electrolytes

The group of Gao and co-workers proposed this technology first and combined the classical dye-sensitized solar cell (DSSC, Grätzel cell) with the flow-battery technology.^[189] FTO glass coated with TiO_2 and a ruthenium dye were utilized as the photoanode and the redox couple I_3^-/I^- as the catholyte. A Li^+ glass ceramic separator prevented electrolyte crossover and allowed charge equalization through the Li conductivity.

In a first publication, the anolyte contained decamethylferrocene, which led to an average discharging voltage of 0.33 V in the dark and a photocharging voltage of around 0.55 V. A maximum discharge capacity was reached with 53.3 mAh L^{-1} , which corresponds to a material utilization of 24% after an illumination time of 2400 s and 48% of the photocharge capacity.^[189] In a second publication, the anolyte was replaced by an aqueous Li_2WO_4 solution.^[190] This led to an elevated average discharging voltage of 0.45 V and a photocharge plateau voltage of 0.76 V.^[190] In a third study,

quinoxaline derivatives were employed as the anode-active material and represent a first approach for the application of organic active materials in solar rechargeable RFBs.^[191] As for the Li_2WO_4 system, charging voltages of 0.78 V and average discharging voltages of 0.45 V were achieved.

Gao et al. successfully demonstrated the possibility of combining a DSSC with a RFB. However, the presented systems have to overcome several challenges, since capacities, cell voltages, and applicable current densities are not competitive with state-of-the-art RFBs.

An improvement to these systems was reported by Wu et al., by using solid lithium as the anode.^[192] In addition, guanidine thiocyanate and chenodeoxycholic acid were used as additives to improve the wettability on the hydrophobic dye-sensitized TiO_2 photoanode. The advantages of this system are the elevated charging and discharging voltages of 3.55 V and 3.35 V, respectively, and the ability to use a highly concentrated aqueous catholyte with a concentration of 2.0 M LiI. Consequently, the electrolyte revealed a theoretical capacity of 35.7 Ah L^{-1} . After 16.8 h, the battery was charged to 91% of its theoretical capacity and 25 charge/discharge cycles were demonstrated. The low photocharging rate is equally considered a drawback.

The photocharging capability of organic/inorganic RFBs with the anthraquinone derivative AQDS as the anode-active material and either ferrocyanide or bromide as the cathode-active material was demonstrated recently.^[193,194] Wedge et al. used a hematite photoanode annealed with polyaniline for the oxidation of ferrocyanide.^[193] An unbiased photocharging was possible up to a state of charge of 12%.

Liao et al. used a dual silicon photoelectrochemical cell in an AQDS/bromide RFB.^[194] The photocathode consisted of $\text{C}/\text{TiO}_2/\text{Ti}/\text{n}^+\text{-Si}$ and the photoanode of $\text{Pt}/\text{p}^+\text{-Si}$. A high conversion efficiency of 6% was achieved with these optimized photoelectrodes. The battery was self-charged to 0.8 V and a discharge capacity of 730 mAh L^{-1} was reached after photocharging for 2 h. The authors demonstrated constant capacity retention over ten consecutive charge/discharge cycles, which makes this system the most advanced photo-RFB so far.

5.2. Solar Chargeable All-Vanadium Redox-Flow Batteries

A few studies describe the solar charging of VRFBs with photoanodes in which TiO_2 and WO_3 as well as CdS are used.^[195–198] However, electrical efficiencies are, to date, only moderate. Furthermore, a degradation of some photoanodes was observed in the highly acidic electrolyte.^[197]

Current photo-RFB technologies are still in their infancy. Research should address the interaction between the photoelectrode and the active material by matching their redox potentials in relation to the conduction band of the semiconductor. Organic active materials can represent an ideal class of materials, since the redox potentials can be fine-tuned by variation of the substituents.

6. Conclusion and Future Challenges

Flow batteries are, in our opinion, the battery technology with the greatest potential to be one of the key elements in the energy transition to a sustainable electricity supply. The current redox couples and electrolytes in VRFB, Fe/Cr, and Zn/Br₂ systems represent only an intermediate step to nontoxic and noncorrosive electrolytes, which rely on organic or earth-abundant active materials. Improvements can be achieved by addressing the following challenges:

An increase in the energy density can be accomplished by utilizing redox-active materials with an elevated solubility of at least 2 M, which can be achieved by intelligent design of the molecules. Of particular interest are organic materials capable of transferring more than just one electron, as well as bipolar materials with a large difference between their redox potentials. The exact adjustment of the redox potential of the active material and the expanded potential window of water, by exploiting the overpotential of the electrode, can also significantly increase the energy density. Further approaches include the utilization of water-miscible liquid organic materials or decreasing the molar mass of a single molecule to decrease the solvent/active material mass ratio and, hence, to increase the solubility.

Suspension-based systems or ionic-liquid electrolytes have in fact the highest energy densities, but suffer enormously from minimum applicable current densities and their application is, therefore, not reasonable. For the same reason, the application of high-voltage systems, which require an organic solvent, is not desirable for large stationary battery systems. An elevated energy density would be desirable, as the space requirement of the battery and likewise the operating costs would decrease.

An increase in the current density can be achieved by accelerating the kinetic reactions on the electrodes. This can be realized by choosing appropriate electrode materials and/or their activation/modification. The modification of the electrodes is a completely novel approach, particularly for organic compounds. However, organic systems (e.g. quinones) already have advantages over vanadium-based systems in terms of their reaction kinetics. The applied membrane also has a significant impact on the current capability. In this context, the membrane should feature an ohmic resistance as low as possible and should allow a high counterion mobility. Membrane-free systems utilizing, for example, immiscible electrolytes could also lead to improvements.

Furthermore, the current density can be increased by reducing the viscosity of the electrolyte and thus enable accelerated charge-carrier transport. In regard to polymeric systems, this is achievable by utilizing (hyper)branched architectures.

An increase in the lifetime can be realized by the utilization of highly reversible redox couples, which undergo no side reactions and offer thousands of charge/discharge cycles. Therefore, systems that just transfer an electron but do not undergo a conformational change have the potential to be more stable. In addition, pH-sensitive molecules or redox reactions should be omitted. This includes the absence of functional groups prone to hydrolysis, such as esters. The

temperature stability of organic redox couples in flow batteries at temperatures in the range of 50 to 70 °C has been barely investigated, but it is of high importance as organic compounds can undergo side reactions when a certain activation energy is exceeded.

The long life cycle of the electrodes can be improved by not utilizing strongly acidic conditions. The selectivity of the membrane also has a significant impact on the long-term retention of capacity. Highly selective membranes are required for the preservation of this performance characteristic. Membranes that are designed, in particular, for flow-battery applications are not commercially available. However, calculating a lifetime of 20 years with a capacity retention of 80 % and one charge/discharge cycle per day, the crossover of cathode and anode active material must not exceed 0.002 % per cycle. This illustrates why the development of bipolar organic active materials is highly attractive.

An increase in the overall system efficiency can be accomplished by expanding the temperature range in which no precipitation of either active material or supporting electrolyte occurs. This is also required for common metal-based RFBs (e.g. VRFBs, Fe/Cr, and Zn/Br₂) and would consequently reduce the energy demand for heating or cooling the electrolyte. The utilization of additives or the selection of active materials and supporting electrolytes with excellent solubility could allow this target to be met.

A decrease in the costs is an important, if not the most important, driving force to enable market penetration for RFBs. This goal can be accomplished by the utilization of organic materials or earth-abundant metals for the charge-storage process. Furthermore, the utilization of simple separators instead of complex ion-selective membranes would reduce the costs, likewise the utilization of water as solvent.

Concerning these requirements, key performance indicators such as leveled cost of energy (\$ MW⁻¹ h⁻¹) or costs per surface power density (\$ m² W⁻¹) seem to be reasonable assessment criteria. The duration of use has to be included in this calculation, as most RFBs have extended lifetimes compared to lead or lithium ion batteries.

In summary, research and development should focus on aqueous redox- and hybrid-flow batteries, which utilize organic active materials. In this case, highly soluble organic compounds, which can be produced with minimal effort in high yields, are favored to enable the efficient production of large-scale systems with capacities in the range of MWh. Additionally, a special focus on the system safety, in regard to the flammability and toxicity is required. In particular, for household-sized RFBs, which can be used in combination with decentralized roof-top photovoltaic electricity production, safe battery systems are absolute necessary. The HFB technology systems comprising a Zn anode should be investigated further, since this metal expands the usable voltage range in water and can be acquired at low cost.

Therefore, we suggest focusing on TEMPO as the organic cathode material for aqueous flow batteries. 4-HO-TEMPO can be purchased at prices of \$5–6 kg⁻¹, and its solubility in water can be increased by alteration of the substituent in the 4-position. TEMPO has a high oxidation potential near the

upper limit of the potential window of water and reveals chemically reversible redox reactions in a pH range of 3 to 7. Viologen and anthraquinone species are suitable anode active materials which have good chemical reversibility and fast reaction kinetics. However, the solubility of either their uncharged state (e.g. AQDS) or charged state (e.g. dimethylviologen) has to be increased. Both molecules can be purchased at affordable costs, with dimethylviologen having the lower reduction potential at the bottom end of the water potential window.

We also see a backlog in membrane development, as most utilized membranes are designed for applications in fuel cells and not in RFBs. The utilization of biotechnology or extraction from renewable natural sources to obtain organic redox-active materials would further improve the environmental impact of RFBs.

Acknowledgements

We acknowledge the European Regional Development Fund (EFRE), the Thuringian Ministry for Economic Affairs, Science and Digital Society (TMWWdG), the Federal Ministry for Economic Affairs and Energy (BMWi), the Central Innovation Programme for SMEs (ZIM), and the Fonds der Chemischen Industrie (FCI).

How to cite: *Angew. Chem. Int. Ed.* **2017**, *56*, 686–711
Angew. Chem. **2017**, *129*, 702–729

- [1] P. M. Vitousek, H. A. Mooney, J. Lubchenco, J. M. Melillo, *Science* **1997**, *277*, 494–499.
- [2] P. Tans, R. Keeling, July 8, 2015 ed., NOAA, <http://www.esrl.noaa.gov/gmd/ccgg/trends/>, **2015**.
- [3] S. Solomon, G.-K. Plattner, R. Knutti, P. Friedlingstein, *Proc. Natl. Acad. Sci. USA* **2009**, *106*, 1704–1709.
- [4] P. M. Cox, R. A. Betts, C. D. Jones, S. A. Spall, I. J. Totterdell, *Nature* **2000**, *408*, 184–187.
- [5] J. T. Houghton, L. G. M. Filho, B. A. Callander, N. Harris, A. Kattenberg, K. Maskell, *Climate Change 1995: The Science of Climate Change*, Cambridge Univ. Press, Cambridge, **1996**.
- [6] M. S. Reddy, S. Basha, H. V. Joshi, B. Jha, *J. Hazard. Mater.* **2005**, *123*, 242–249.
- [7] C. Tebert, Quecksilber-Emissionen aus Kohlekraftwerken, Ökopool GmbH, **2016**.
- [8] I. Dincer, *Renewable Sustainable Energy Rev.* **2000**, *4*, 157–175.
- [9] H. Lund, *Energy* **2007**, *32*, 912–919.
- [10] G. Katata, M. Chino, T. Kobayashi, H. Terada, M. Ota, H. Nagai, M. Kajino, R. Draxler, M. C. Hort, A. Malo, T. Torii, Y. Sanada, *Atmos. Chem. Phys.* **2015**, *15*, 1029–1070.
- [11] F. von Hippel, R. Ewing, R. Garwin, A. Macfarlane, *Nature* **2012**, *485*, 167–168.
- [12] D. Cook, B. Davidsdottir, J. G. Petursson, *Renewable Sustainable Energy Rev.* **2015**, *49*, 211–220.
- [13] D. M. Rosenberg, R. A. Bodaly, P. J. Usher, *Global Environ. Change* **1995**, *5*, 127–148.
- [14] O. Edenhofer, K. Seyboth, F. Creutzig, S. Schlömer, *Annu. Rev. Environ. Resour.* **2013**, *38*, 169–200.
- [15] S. Weitemeyer, D. Kleinhans, T. Vogt, C. Agert, *Renewable Energy* **2015**, *75*, 14–20.
- [16] Z. Abdmouleh, R. A. M. Alammari, A. Gastli, *Renewable Sustainable Energy Rev.* **2015**, *45*, 249–262.
- [17] P. Alstone, D. Gershenson, D. M. Kammen, *Nat. Clim. Change* **2015**, *5*, 305–314.
- [18] P. Cappers, J. MacDonald, C. Goldman, O. Ma, *Energy Policy* **2013**, *62*, 1031–1039.
- [19] B. Dunn, H. Kamath, J.-M. Tarascon, *Science* **2011**, *334*, 928–935.
- [20] C. Budischak, D. Sewell, H. Thomson, L. Mach, D. E. Veron, W. Kempton, *J. Power Sources* **2013**, *225*, 60–74.
- [21] P. Alotto, M. Guarnieri, F. Moro, *Renewable Sustainable Energy Rev.* **2014**, *29*, 325–335.
- [22] P. K. Leung, C. Ponce-de-León, C. T. J. Low, F. C. Walsh, *Electrochim. Acta* **2011**, *56*, 6536–6546.
- [23] A. Weber, M. Mench, J. Meyers, P. Ross, J. Gostick, Q. Liu, J. Appl. Electrochem. **2011**, *41*, 1137–1164.
- [24] J.-Y. Chen, C.-L. Hsieh, N.-Y. Hsu, Y.-S. Chou, Y.-S. Chen, *Energies* **2014**, *7*, 5863.
- [25] K. Bromberger, J. Kaunert, T. Smolinka, *Energy Technol.* **2014**, *2*, 64–76.
- [26] S. Muench, A. Wild, C. Friebe, B. Haeupler, T. Janoschka, U. S. Schubert, *Chem. Rev.* **2016**, *116*, 9438–9484.
- [27] R. Darling, K. Gallagher, W. Xie, L. Su, F. Brushett, *J. Electrochem. Soc.* **2016**, *163*, A5029–A5040.
- [28] R. A. Potash, J. R. McKone, S. Conte, H. D. Abruña, *J. Electrochem. Soc.* **2016**, *163*, A338–A344.
- [29] J. Cheng, L. Zhang, Y.-S. Yang, Y.-H. Wen, G.-P. Cao, X.-D. Wang, *Electrochem. Commun.* **2007**, *9*, 2639–2642.
- [30] W. A. Braff, M. Z. Bazant, C. R. Buie, *Nat. Commun.* **2013**, *4*, 2346.
- [31] X. Li, H. Zhang, Z. Mai, H. Zhang, I. Vankelecom, *Energy Environ. Sci.* **2011**, *4*, 1147–1160.
- [32] J. Winsberg, T. Janoschka, S. Morgenstern, S. Muench, T. Hagemann, G. Hauffman, J.-F. Gohy, M. D. Hager, U. S. Schubert, *Adv. Mater.* **2016**, *28*, 2238–2243.
- [33] J. Winsberg, S. Muench, T. Hagemann, T. Janoschka, S. Morgenstern, M. Billing, F. H. Schacher, G. Hauffman, J.-F. Gohy, S. Hoepfner, M. D. Hager, U. S. Schubert, *Polym. Chem.* **2016**, *7*, 1711–1718.
- [34] T. Janoschka, N. Martin, U. Martin, C. Friebe, S. Morgenstern, H. Hiller, M. D. Hager, U. S. Schubert, *Nature* **2015**, *527*, 78–81.
- [35] Y. Zhao, S. Si, C. Liao, *J. Power Sources* **2013**, *241*, 449–453.
- [36] G. Nagarjuna, J. Hui, K. J. Cheng, T. Lichtenstein, M. Shen, J. S. Moore, J. Rodríguez-López, *J. Am. Chem. Soc.* **2014**, *136*, 16309–16316.
- [37] L. W. Hruska, R. F. Savinell, *J. Electrochem. Soc.* **1981**, *128*, 18–25.
- [38] Z. Yuan, X. Zhu, M. Li, W. Lu, X. Li, H. Zhang, *Angew. Chem. Int. Ed.* **2016**, *55*, 3058–3062; *Angew. Chem.* **2016**, *128*, 3110–3114.
- [39] J. Drillkens, D. Schulte, D. U. Sauer, *ECS Trans.* **2010**, *28*, 167–177.
- [40] M. Vijayakumar, M. S. Bhuvaneshwari, P. Nachimuthu, B. Schwenzer, S. Kim, Z. Yang, J. Liu, G. L. Graff, S. Thevuthasan, J. Hu, *J. Membr. Sci.* **2011**, *366*, 325–334.
- [41] K. Takechi, Y. Kato, Y. Hase, *Adv. Mater.* **2015**, *27*, 2501–2506.
- [42] X. Sun, T. Souier, M. Chiesa, A. Vassallo, *Electrochim. Acta* **2014**, *148*, 104–110.
- [43] G. Nikiforidis, W. A. Daoud, *J. Electrochem. Soc.* **2015**, *162*, A809–A819.
- [44] P. Trogadas, O. O. Taiwo, B. Tjaden, T. P. Neville, S. Yun, J. Parrondo, V. Ramani, M.-O. Coppens, D. J. L. Brett, P. R. Shearing, *Electrochem. Commun.* **2014**, *48*, 155–159.
- [45] H. Liu, Q. Xu, C. Yan, *Electrochem. Commun.* **2013**, *28*, 58–62.
- [46] P. K. Leung, C. Ponce-de-León, F. J. Recio, P. Herrasti, F. C. Walsh, *J. Appl. Electrochem.* **2014**, *44*, 1025–1035.
- [47] B. Li, M. Gu, Z. Nie, X. Wei, C. Wang, V. Sprenkle, W. Wang, *Nano Lett.* **2014**, *14*, 158–165.

- [48] Z. González, A. Sánchez, C. Blanco, M. Granda, R. Menéndez, R. Santamaría, *Electrochem. Commun.* **2011**, *13*, 1379–1382.
- [49] W. H. Wang, X. D. Wang, *Electrochim. Acta* **2007**, *52*, 6755–6762.
- [50] Z. He, L. Dai, S. Liu, L. Wang, C. Li, *Electrochim. Acta* **2015**, *176*, 1434–1440.
- [51] A. M. Pezeshki, J. T. Clement, G. M. Veith, T. A. Zawodzinski, M. M. Mench, *J. Power Sources* **2015**, *294*, 333–338.
- [52] G. Nikiforidis, W. A. Daoud, *Electrochim. Acta* **2015**, *168*, 394–402.
- [53] G. Nikiforidis, Y. Xiang, W. A. Daoud, *Electrochim. Acta* **2015**, *157*, 274–281.
- [54] J.-Z. Chen, W.-Y. Liao, W.-Y. Hsieh, C.-C. Hsu, Y.-S. Chen, *J. Power Sources* **2015**, *274*, 894–898.
- [55] T.-M. Tseng, R.-H. Huang, C.-Y. Huang, K.-L. Hsueh, F.-S. Shieu, *J. Electrochem. Soc.* **2013**, *160*, A1269–A1275.
- [56] K. J. Kim, M.-S. Park, Y.-J. Kim, J. H. Kim, S. X. Dou, M. Skyllas-Kazacos, *J. Mater. Chem. A* **2015**, *3*, 16913–16933.
- [57] Y. Munaiah, S. Suresh, S. Dheenadayalan, V. K. Pillai, P. Ragupathy, *J. Phys. Chem. C* **2014**, *118*, 14795–14804.
- [58] J.-H. Kim, K. J. Kim, M.-S. Park, N. J. Lee, U. Hwang, H. Kim, Y.-J. Kim, *Electrochem. Commun.* **2011**, *13*, 997–1000.
- [59] P. K. Leung, C. Ponce-de-León, C. T. J. Low, A. A. Shah, F. C. Walsh, *J. Power Sources* **2011**, *196*, 5174–5185.
- [60] M. Rychcik, M. Skyllas-Kazacos, *J. Power Sources* **1987**, *19*, 45–54.
- [61] D. J. Suárez, Z. González, C. Blanco, M. Granda, R. Menéndez, R. Santamaría, *ChemSusChem* **2014**, *7*, 914–918.
- [62] M. Skyllas-Kazacos, M. H. Chakrabarti, S. A. Hajimolana, F. S. Mjalli, M. Saleem, *J. Electrochem. Soc.* **2011**, *158*, R55–R79.
- [63] P. Leung, X. Li, C. Ponce-de-León, L. Berlouis, C. T. J. Low, F. C. Walsh, *RSC Adv.* **2012**, *2*, 10125–10156.
- [64] D. D. Banham-Hall, G. A. Taylor, C. A. Smith, M. R. Irving, *IEEE Trans. Power Syst.* **2012**, *27*, 1690–1697.
- [65] P. Denholm, M. O'Connell, G. Brinkman, J. Jorgenson, *Over-generation from Solar Energy in California: A Field Guide to the Duck Chart*, National Renewable Energy Laboratory, **2015**.
- [66] H. Wirth, *Recent Facts about Photovoltaics in Germany*, Fraunhofer Institut for Solar Energy Systems ISE, **2016**.
- [67] B. Burger, *Stromerzeugung aus Solar- und Windenergie im Jahr 2014*, Fraunhofer Institut for Solar Energy Systems ISE, **2015**.
- [68] Z. Yang, J. Zhang, M. C. W. Kintner-Meyer, X. Lu, D. Choi, J. P. Lemmon, J. Liu, *Chem. Rev.* **2011**, *111*, 3577–3613.
- [69] J. A. Short, D. G. Infield, L. L. Freris, *IEEE Trans. Power Syst.* **2007**, *22*, 1284–1293.
- [70] S. Roe, C. Menictas, M. Skyllas-Kazacos, *J. Electrochem. Soc.* **2016**, *163*, A5023–A5028.
- [71] W. Wang, Q. Luo, B. Li, X. Wei, L. Li, Z. Yang, *Adv. Funct. Mater.* **2013**, *23*, 970–986.
- [72] P. Poizot, F. Dolhem, *Energy Environ. Sci.* **2011**, *4*, 2003–2019.
- [73] C.-J. Yang, R. B. Jackson, *Renewable Sustainable Energy Rev.* **2011**, *15*, 839–844.
- [74] K. Gong, X. Ma, K. M. Conforti, K. J. Kuttler, J. B. Grunewald, K. L. Yeager, M. Z. Bazant, S. Gu, Y. Yan, *Energy Environ. Sci.* **2015**, *8*, 2941–2945.
- [75] R. M. Darling, K. G. Gallagher, J. A. Kowalski, S. Ha, F. R. Brushett, *Energy Environ. Sci.* **2014**, *7*, 3459–3477.
- [76] A. Crawford, V. Viswanathan, D. Stephenson, W. Wang, E. Thomsen, D. Reed, B. Li, P. Balducci, M. Kintner-Meyer, V. Sprenkle, *J. Power Sources* **2015**, *293*, 388–399.
- [77] V. Viswanathan, A. Crawford, D. Stephenson, S. Kim, W. Wang, B. Li, G. Coffey, E. Thomsen, G. Graff, P. Balducci, M. Kintner-Meyer, V. Sprenkle, *J. Power Sources* **2014**, *247*, 1040–1051.
- [78] B. Huskinson, M. P. Marshak, C. Suh, S. Er, M. R. Gerhardt, C. J. Galvin, X. Chen, A. Aspuru-Guzik, R. G. Gordon, M. J. Aziz, *Nature* **2014**, *505*, 195–198.
- [79] X. Zhang, L. Yang, Y. Li, H. Li, W. Wang, B. Ye, *Environ. Monit. Assess.* **2012**, *184*, 2261–2273.
- [80] Y. Zhao, Y. Ding, Y. Li, L. Peng, H. R. Byon, J. B. Goodenough, G. Yu, *Chem. Soc. Rev.* **2015**, *44*, 7968–7996.
- [81] G. L. Soloveichik, *Chem. Rev.* **2015**, *115*, 11533–11558.
- [82] M. Skyllas-Kazacos, L. Cao, M. Kazacos, N. Kausar, A. Mousa, *ChemSusChem* **2016**, *9*, 1521–1543.
- [83] J. Noack, N. Roznyatovskaya, T. Herr, P. Fischer, *Angew. Chem. Int. Ed.* **2015**, *54*, 9776–9809; *Angew. Chem.* **2015**, *127*, 9912–9947.
- [84] W. Kangro, DE914264, **1949**.
- [85] W. Kangro, H. Pieper, *Electrochim. Acta* **1962**, *7*, 435–448.
- [86] W. Kangro, DE1006479, **1957**.
- [87] N. H. Hagedorn, NASA TM-83677 Redox Storage System, **1984**.
- [88] M. Skyllas-Kazacos, R. G. Robins, AU 575247, **1986**.
- [89] M. Skyllas-Kazacos, M. Rychcik, R. G. Robins, A. G. Fane, *J. Electrochem. Soc.* **1986**, *133*, 1057–1058.
- [90] C. S. Bradley, US 312802, **1885**.
- [91] D. J. Eustace, US 4064324, **1977**.
- [92] D. Linden, T. B. Reddy, *Handbook of Batteries*, McGraw-Hill, New York, **2002**.
- [93] M. d. Rossi, US 3738870, **1973**.
- [94] K. J. Cathro, K. Cedzynska, D. C. Constable, P. M. Hoobin, *J. Power Sources* **1986**, *18*, 349–370.
- [95] R. Clarke, B. Dougherty, S. Harrison, P. Millington, S. Mohanta, US 0202925 A1, **2004**.
- [96] M. H. Chakrabarti, R. A. W. Dryfe, E. P. L. Roberts, *Electrochim. Acta* **2007**, *52*, 2189–2195.
- [97] M. H. Chakrabarti, E. P. L. Roberts, C. Bae, M. Saleem, *Energy Convers. Manage.* **2011**, *52*, 2501–2508.
- [98] T. Yamamura, Y. Shiokawa, H. Yamana, H. Moriyama, *Electrochim. Acta* **2002**, *48*, 43–50.
- [99] F.-Q. Xue, Y.-L. Wang, W.-H. Wang, X.-D. Wang, *Electrochim. Acta* **2008**, *53*, 6636–6642.
- [100] L. Sanz, D. Lloyd, E. Magdalena, J. Palma, K. Kontturi, *J. Power Sources* **2014**, *268*, 121–128.
- [101] D. Pletcher, R. Wills, *Phys. Chem. Chem. Phys.* **2004**, *6*, 1779–1785.
- [102] R. F. Savinell, C. C. Liu, R. T. Galasco, S. H. Chiang, J. F. Coetzee, *J. Electrochem. Soc.* **1979**, *126*, 357–360.
- [103] J. Pan, Y. Sun, J. Cheng, Y. Wen, Y. Yang, P. Wan, *Electrochem. Commun.* **2008**, *10*, 1226–1229.
- [104] M. Duduta, B. Ho, V. C. Wood, P. Limthongkul, V. E. Brunini, W. C. Carter, Y.-M. Chiang, *Adv. Energy Mater.* **2011**, *1*, 511–516.
- [105] Y. Zhao, H. R. Byon, *Adv. Energy Mater.* **2013**, *3*, 1630–1635.
- [106] Y. Yang, G. Zheng, Y. Cui, *Energy Environ. Sci.* **2013**, *6*, 1552–1558.
- [107] N. Singh, E. W. McFarland, *J. Power Sources* **2015**, *288*, 187–198.
- [108] K. T. Cho, P. Ridgway, A. Z. Weber, S. Haussener, V. Battaglia, V. Srinivasan, *J. Electrochem. Soc.* **2012**, *159*, A1806–A1815.
- [109] L. Li, S. Kim, W. Wang, M. Vijayakumar, Z. Nie, B. Chen, J. Zhang, G. Xia, J. Hu, G. Graff, J. Liu, Z. Yang, *Adv. Energy Mater.* **2011**, *1*, 394–400.
- [110] B. Li, Z. Nie, M. Vijayakumar, G. Li, J. Liu, V. Sprenkle, W. Wang, *Nat. Commun.* **2015**, *6*, 6303.
- [111] H. Chen, Q. Zou, Z. Liang, H. Liu, Q. Li, Y.-C. Lu, *Nat. Commun.* **2015**, *6*, 5877.
- [112] S. Mubeen, Y.-s. Jun, J. Lee, E. W. McFarland, *ACS Appl. Mater. Interfaces* **2016**, *8*, 1759–1765.
- [113] Q. Huang, J. Yang, C. B. Ng, C. Jia, Q. Wang, *Energy Environ. Sci.* **2016**, *9*, 917–931.
- [114] S. Monaco, F. Soavi, M. Mastragostino, *J. Phys. Chem. Lett.* **2013**, *4*, 1379–1382.

- [115] J. G. Austing, C. N. Kirchner, E.-M. Hammer, L. Komsiyyska, G. Wittstock, *J. Power Sources* **2015**, 273, 1163–1170.
- [116] J. G. Austing, C. N. Kirchner, L. Komsiyyska, G. Wittstock, *J. Power Sources* **2016**, 306, 692–701.
- [117] C. Menictas, M. Skyllas-Kazacos, *J. Appl. Electrochem.* **2011**, 41, 1223–1232.
- [118] H. Kaneko, A. Negishi, K. Nozaki, K. Sato, M. Nakajima, US 5318865A, **1994**.
- [119] J. Noack, C. Cremers, D. Bayer, J. Tübke, K. Pinkwart, *J. Power Sources* **2014**, 253, 397–403.
- [120] X. Wei, G.-G. Xia, B. Kirby, E. Thomsen, B. Li, Z. Nie, G. G. Graff, J. Liu, V. Sprenkle, W. Wang, *J. Electrochem. Soc.* **2016**, 163, A5150–A5153.
- [121] A. K. Manohar, K. M. Kim, E. Plichta, M. Hendrickson, S. Rawlings, S. R. Narayanan, *J. Electrochem. Soc.* **2016**, 163, A5118–A5125.
- [122] M. Armand, J. M. Tarascon, *Nature* **2008**, 451, 652–657.
- [123] C. J. Barnhart, S. M. Benson, *Energy Environ. Sci.* **2013**, 6, 1083–1092.
- [124] Q. Lai, H. Zhang, X. Li, L. Zhang, Y. Cheng, *J. Power Sources* **2013**, 235, 1–4.
- [125] Y. H. Wen, H. M. Zhang, P. Qian, H. T. Zhou, P. Zhao, B. L. Yi, X. S. Yang, *J. Electrochem. Soc.* **2006**, 153, A929–A934.
- [126] Y. Wei, W. Xu, M. Vijayakumar, L. Cosimbescu, T. Liu, V. Sprenkle, W. Wang, *Adv. Mater.* **2014**, 26, 7649–7653.
- [127] Q. Chen, M. R. Gerhardt, L. Hartle, M. J. Aziz, *J. Electrochem. Soc.* **2016**, 163, A5010–A5013.
- [128] B. Yang, L. Hoober-Burkhardt, F. Wang, G. K. S. Prakash, S. R. Narayanan, *J. Electrochem. Soc.* **2014**, 161, A1371–A1380.
- [129] Z. Li, S. Li, S. Liu, K. Huang, D. Fang, F. Wang, S. Peng, *Electrochem. Solid-State Lett.* **2011**, 14, A171–A173.
- [130] A. J. Bard, L. R. Faulkner, *Electrochemical Methods*, 2nd ed., Wiley, New York, **2001**.
- [131] Y. Xu, Y. Wen, J. Cheng, G. Cao, Y. Yang, *Electrochem. Commun.* **2009**, 11, 1422–1424.
- [132] S. H. Oh, C. W. Lee, D. H. Chun, J. D. Jeon, J. Shim, K. H. Shin, J. H. Yang, *J. Mater. Chem. A* **2014**, 2, 19994–19998.
- [133] Y. Xu, Y.-H. Wen, J. Cheng, G.-P. Cao, Y.-S. Yang, *Electrochim. Acta* **2010**, 55, 715–720.
- [134] J. Huang, L. Cheng, R. S. Assary, P. Wang, Z. Xue, A. K. Burrell, L. A. Curtiss, L. Zhang, *Adv. Energy Mater.* **2015**, 5, 1401782.
- [135] T. Liu, X. Wei, Z. Nie, V. Sprenkle, W. Wang, *Adv. Energy Mater.* **2016**, 6, 1501449.
- [136] X. Wei, W. Xu, J. Huang, L. Zhang, E. Walter, C. Lawrence, M. Vijayakumar, W. A. Henderson, T. Liu, L. Cosimbescu, B. Li, V. Sprenkle, W. Wang, *Angew. Chem. Int. Ed.* **2015**, 54, 8684–8687; *Angew. Chem.* **2015**, 127, 8808–8811.
- [137] Y. K. Zeng, T. S. Zhao, L. An, X. L. Zhou, L. Wei, *J. Power Sources* **2015**, 300, 438–443.
- [138] W. Wang, W. Xu, L. Cosimbescu, D. Choi, L. Li, Z. Yang, *Chem. Commun.* **2012**, 48, 6669–6671.
- [139] H. Alt, H. Binder, A. Köhling, G. Sandstede, *Electrochim. Acta* **1972**, 17, 873–887.
- [140] T. Le Gall, K. H. Reiman, M. C. Grossel, J. R. Owen, *J. Power Sources* **2003**, 119–121, 316–320.
- [141] Z. Song, H. Zhan, Y. Zhou, *Chem. Commun.* **2009**, 448–450.
- [142] Z. Lei, W. Wei-kun, W. An-bang, Y. Zhong-bao, C. Shi, Y. Yu-sheng, *J. Electrochem. Soc.* **2011**, 158, A991–A996.
- [143] W. Xu, A. Read, P. K. Koech, D. Hu, C. Wang, J. Xiao, A. B. Padmaperuma, G. L. Graff, J. Liu, J.-G. Zhang, *J. Mater. Chem.* **2012**, 22, 4032–4039.
- [144] S. P. Ong, V. L. Chevrier, G. Hautier, A. Jain, C. Moore, S. Kim, X. Ma, G. Ceder, *Energy Environ. Sci.* **2011**, 4, 3680–3688.
- [145] J. E. Bachman, L. A. Curtiss, R. S. Assary, *J. Phys. Chem. A* **2014**, 118, 8852–8860.
- [146] M. Quan, D. Sanchez, M. F. Wasylkiw, D. K. Smith, *J. Am. Chem. Soc.* **2007**, 129, 12847–12856.
- [147] K. Lin, Q. Chen, M. R. Gerhardt, L. Tong, S. B. Kim, L. Eisenach, A. W. Valle, D. Hardee, R. G. Gordon, M. J. Aziz, M. P. Marshak, *Science* **2015**, 349, 1529–1532.
- [148] H. Nishide, S. Iwasa, Y.-J. Pu, T. Suga, K. Nakahara, M. Satoh, *Electrochim. Acta* **2004**, 50, 827–831.
- [149] Y. Liang, Z. Tao, J. Chen, *Adv. Energy Mater.* **2012**, 2, 742–769.
- [150] T. Janoschka, M. D. Hager, U. S. Schubert, *Adv. Mater.* **2012**, 24, 6397–6409.
- [151] M. C. Krishna, D. A. Grahame, A. Samuni, J. B. Mitchell, A. Russo, *Proc. Natl. Acad. Sci. USA* **1992**, 89, 5537–5541.
- [152] A. E. S. Sleightholme, A. A. Shinkle, Q. Liu, Y. Li, C. W. Monroe, L. T. Thompson, *J. Power Sources* **2011**, 196, 5742–5745.
- [153] A. A. Shinkle, A. E. S. Sleightholme, L. D. Griffith, L. T. Thompson, C. W. Monroe, *J. Power Sources* **2012**, 206, 490–496.
- [154] T. Herr, J. Noack, P. Fischer, J. Tübke, *Electrochim. Acta* **2013**, 113, 127–133.
- [155] G. Oriji, Y. Katayama, T. Miura, *Electrochim. Acta* **2004**, 49, 3091–3095.
- [156] Y. Wen, H. Zhang, P. Qian, P. Zhao, H. Zhou, B. Yi, *Acta Phys.-Chim. Sin.* **2006**, 22, 403–408.
- [157] E. Sum, M. Rychcik, M. Skyllas-Kazacos, *J. Power Sources* **1985**, 16, 85–95.
- [158] E. Sum, M. Skyllas-Kazacos, *J. Power Sources* **1985**, 15, 179–190.
- [159] F. R. Brushett, J. T. Vaughey, A. N. Jansen, *Adv. Energy Mater.* **2012**, 2, 1390–1396.
- [160] L. Su, M. Ferrandon, J. A. Kowalski, J. T. Vaughey, F. R. Brushett, *J. Electrochem. Soc.* **2014**, 161, A1905–A1914.
- [161] S. Zhang, X. Li, D. Chu, *Electrochim. Acta* **2016**, 190, 737–743.
- [162] J. Huang, L. Su, J. A. Kowalski, J. L. Barton, M. Ferrandon, A. K. Burrell, F. R. Brushett, L. Zhang, *J. Mater. Chem. A* **2015**, 3, 14971–14976.
- [163] L. Zhang, Z. Zhang, P. C. Redfern, L. A. Curtiss, K. Amine, *Energy Environ. Sci.* **2012**, 5, 8204–8207.
- [164] Lutfullah, H. S. Dunsmore, R. Paterson, *J. Chem. Soc. Faraday Trans. 1* **1976**, 72, 495–503.
- [165] S. Wu, Y. Zhao, D. Li, Y. Xia, S. Si, *J. Power Sources* **2015**, 275, 305–311.
- [166] T. Sukegawa, I. Masuko, K. Oyaizu, H. Nishide, *Macromolecules* **2014**, 47, 8611–8617.
- [167] H. D. Inerowicz, W. Li, I. Persson, *J. Chem. Soc. Faraday Trans.* **1994**, 90, 2223–2234.
- [168] B. Huskinson, M. P. Marshak, M. R. Gerhardt, M. J. Aziz, *ECS Trans.* **2014**, 61, 27–30.
- [169] M. L. Perry, R. M. Darling, R. Zaffou, *ECS Trans.* **2013**, 53, 7–16.
- [170] Q. Chen, L. Eisenach, M. J. Aziz, *J. Electrochem. Soc.* **2016**, 163, A5057–A5063.
- [171] X. Li, *Electrochim. Acta* **2015**, 170, 98–109.
- [172] D. Chu, X. Li, S. Zhang, *Electrochim. Acta* **2016**, 190, 434–445.
- [173] P. G. Rasmussen, US 8080327 B1, **2011**.
- [174] W. Duan, R. S. Vemuri, J. D. Milshtein, S. Laramie, R. D. Dmello, J. Huang, L. Zhang, D. Hu, M. Vijayakumar, W. Wang, J. Liu, R. M. Darling, L. Thompson, K. Smith, J. S. Moore, F. R. Brushett, X. Wei, *J. Mater. Chem. A* **2016**, 4, 5448–5456.
- [175] J. H. Osiecki, E. F. Ullman, *J. Am. Chem. Soc.* **1968**, 90, 1078–1079.
- [176] T. Sukegawa, A. Kai, K. Oyaizu, H. Nishide, *Macromolecules* **2013**, 46, 1361–1367.
- [177] J. Lee, E. Lee, S. Kim, G. S. Bang, D. A. Shultz, R. D. Schmidt, M. D. E. Forbes, H. Lee, *Angew. Chem. Int. Ed.* **2011**, 50, 4414–4418; *Angew. Chem.* **2011**, 123, 4506–4510.

- [178] R. Ziesel, G. Ulrich, R. C. Lawson, L. Echegoyen, *J. Mater. Chem.* **1999**, 9, 1435–1448.
- [179] E. Coronado, C. Gimenez-Saiz, M. Nicolas, F. M. Romero, E. Rusanov, H. Stoeckli-Evans, *New J. Chem.* **2003**, 27, 490–497.
- [180] Y. Nakano, T. Yagyu, T. Hirayama, A. Ito, K. Tanaka, *Polyhedron* **2005**, 24, 2141–2147.
- [181] A. Caneschi, D. Gatteschi, N. Laloti, C. Sangregorio, R. Sessoli, G. Venturi, A. Vindigni, A. Rettori, M. G. Pini, M. A. Novak, *Angew. Chem. Int. Ed.* **2001**, 40, 1760–1763; *Angew. Chem.* **2001**, 113, 1810–1813.
- [182] S. Y. Zhou, X. Li, T. Li, L. Tian, Z. Y. Liu, X. G. Wang, *RSC Adv.* **2015**, 5, 17131–17139.
- [183] L.-L. Li, S. Liu, Y. Zhang, W. Shi, P. Cheng, *Dalton Trans.* **2015**, 44, 6118–6125.
- [184] A. P. Kaur, N. E. Holubowitch, S. Ergun, C. F. Elliott, S. A. Odom, *Energy Technol.* **2015**, 3, 446.
- [185] E. Fritz-Langhals, *Org. Process Res. Dev.* **2005**, 9, 577–582.
- [186] T. Janoschka, S. Morgenstern, H. Hiller, C. Friebe, K. Wolkersdörfer, B. Häupler, M. D. Hager, U. S. Schubert, *Polym. Chem.* **2015**, 6, 7801–7811.
- [187] J. Winsberg, T. Hagemann, S. Muench, C. Friebe, B. Häupler, T. Janoschka, S. Morgenstern, M. D. Hager, U. S. Schubert, *Chem. Mater.* **2016**, 28, 3401–3405.
- [188] D. Sengupta, P. Das, B. Mondal, K. Mukherjee, *Renewable Sustainable Energy Rev.* **2016**, 60, 356–376.
- [189] P. Liu, Y.-l. Cao, G.-R. Li, X.-P. Gao, X.-P. Ai, H.-X. Yang, *ChemSusChem* **2013**, 6, 802–806.
- [190] N. F. Yan, G. R. Li, X. P. Gao, *J. Mater. Chem. A* **2013**, 1, 7012–7015.
- [191] N. F. Yan, G. R. Li, X. P. Gao, *J. Electrochem. Soc.* **2014**, 161, A736–A741.
- [192] M. Yu, W. D. McCulloch, D. R. Beauchamp, Z. Huang, X. Ren, Y. Wu, *J. Am. Chem. Soc.* **2015**, 137, 8332–8335.
- [193] K. Wedege, J. Azevedo, A. Khataee, A. Bentien, A. Mendes, *Angew. Chem. Int. Ed.* **2016**, 55, 7142–7147; *Angew. Chem.* **2016**, 128, 7258–7263.
- [194] S. Liao, X. Zong, B. Seger, T. Pedersen, T. Yao, C. Ding, J. Shi, J. Chen, C. Li, *Nat. Commun.* **2016**, 7, 11474.
- [195] Z. Wei, D. Liu, C. Hsu, F. Liu, *Electrochem. Commun.* **2014**, 45, 79–82.
- [196] D. Liu, Z. Wei, C.-j. Hsu, Y. Shen, F. Liu, *Electrochim. Acta* **2014**, 136, 435–441.
- [197] J. Azevedo, T. Seipp, J. Burfeind, C. Sousa, A. Bentien, J. P. Araújo, A. Mendes, *Nano Energy* **2016**, 22, 396–405.
- [198] Z. Peimanifard, S. Rashid-Nadimi, *J. Power Sources* **2015**, 300, 395–401.
- [199] T. Janoschka, N. Martin, M. D. Hager, U. S. Schubert, *Angew. Chem. Int. Ed.* **2016**, DOI: 10.1002/anie.201606472; *Angew. Chem.* **2016**, DOI: 10.1002/ange.201606472.
- [200] J. Winsberg, C. Stolze, S. Muench, F. Liedl, M. D. Hager, U. S. Schubert, *ACS Energy Lett.* **2016**, DOI: 10.1021/acsenenergy-lett.6b00413.

Received: May 19, 2016

Revised: July 11, 2016

Published online: November 7, 2016

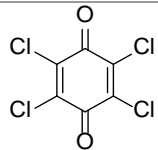
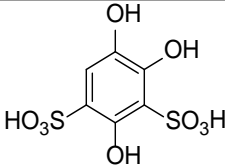
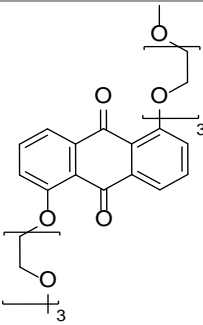
Supporting Information

Redox-Flow Batteries: From Metals to Organic Redox-Active Materials

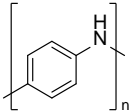
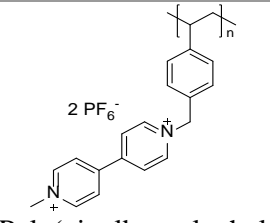
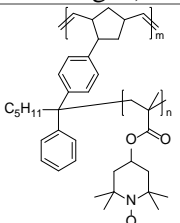
*Jan Winsberg⁺, Tino Hagemann⁺, Tobias Janoschka, Martin D. Hager, and Ulrich S. Schubert**

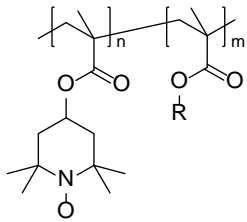
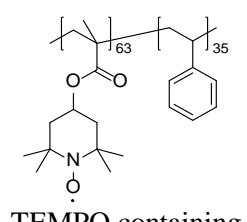
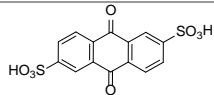
anie_201604925_sm_miscellaneous_information.pdf

Extended Data Table: Utilized redox-active materials.

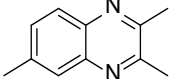
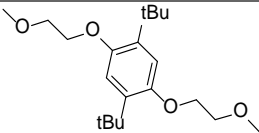
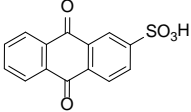
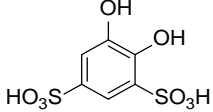
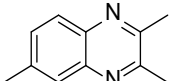
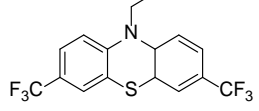
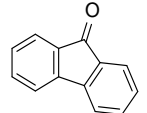
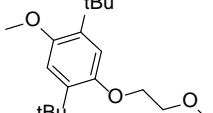
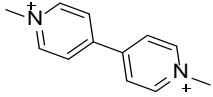
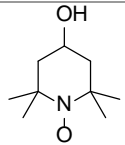
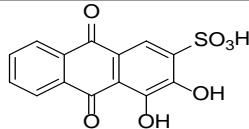
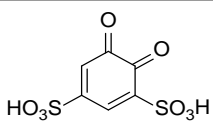
Anode	Cathode	Electrolyte	Theoretical cell voltage / V	Current density / mA cm ⁻²	Theoretic energy density / Wh L ⁻¹	Maximal observed energy density / Wh L ⁻¹	Cycles reported	Membrane	Ref.
1. Flow batteries utilizing organic/inorganic redox-active materials									
Cd/CdSO ₄ (single flow)	 Chloranil	H ₂ SO ₄ / (NH ₄) ₂ SO ₄ / CdSO ₄	1.14	10	-	-	100	None	[131]
Pb/PbSO ₄	 Tiron	H ₂ SO ₄	1.1	10	-	2.8	10	Nafion 115	[133]
Li	 15D3GAQ	LiPF ₆ /PC	2.3	0.1 to 10	25	25 ^a	9 to 40	PP separator	[138]

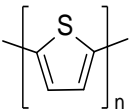
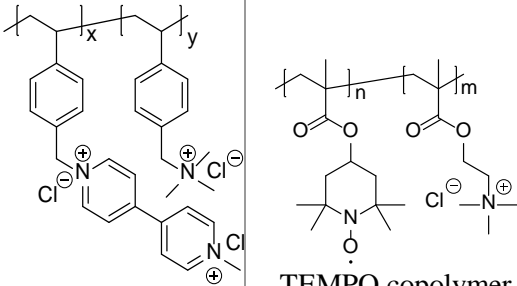
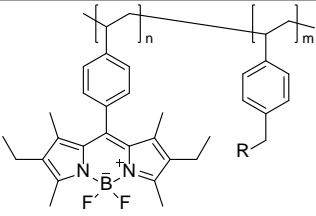
[illegible]

Anode	Cathode	Electrolyte	Theoretical cell voltage / V	Current density / mA cm ⁻²	Theoretic energy density / Wh L ⁻¹	Maximal observed energy density / Wh L ⁻¹	Cycles reported	Membrane	Ref.
Zn	 PANI	ZnCl ₂ /NH ₄ Cl	1.1	10 to 30	66.5	9.5	32	PP micro porous membrane	[35]
LiNi _{0.33} Mn _{0.33} Co _{0.33} O ₂	 Poly(vinylbenzyl ethyl viologen)	LiBF ₄ /CH ₃ CN	1.11	0.2 mA (current)	15.5 ^a (14 Ah L ⁻¹ volumetric energy density)	15.5 ^a	11	PP/PE separator	[36]
Half-cell only	 Poly(norbornene)-g-poly(4-methacryloyloxy-2,2,6,6-tetramethylpiperidin-1-oxyl) (PNB-g-PTMA)	(C ₄ H ₉) ₄ NClO ₄ /EC/DEC	Half-cell-only	-	-	0.94 ^a	2	PP/PE separator	[166]

Anode	Cathode	Electrolyte	Theoretical cell voltage / V	Current density / mA cm ⁻²	Theoretic energy density / Wh L ⁻¹	Maximal observed energy density / Wh L ⁻¹	Cycles reported	Membrane	Ref.
Hybrid Zn(II)/Zn(0)	 TEMPO containing polymers	Zn(ClO ₄) ₂ × 6H ₂ O/ EC/DMC/ DEC or ZnCl ₂ , NH ₄ Cl/wat er or NaCl, ZnCl ₂ , NH ₄ Cl/wat er	1.69	0.5 to 20	8.1	4.1	1,000	Dialysis membrane (regenerated cellulose, MWCO of 1.000 g mol ⁻¹)	[32]
Hybrid Zn(II)/Zn(0)	 TEMPO containing polymers	Zn(ClO ₄) ₂ × 6H ₂ O/ EC/DMC/ DEC or ZnCl ₂ , NH ₄ Cl/wat er or NaCl, ZnCl ₂ , NH ₄ Cl/wat er	1.69	0.5 to 20	1.6	0.8	1,000	Dialysis membrane (regenerated cellulose, MWCO of 1.000 g mol ⁻¹)	[33]
3. RFBs based on organic/halogen redox-active materials									
 AQDS (ADQSH ₂)	Br ₂	HBr/H ₂ SO ₄ (aq)	0.81	200 to 500	-	9.4	15	Nafion 212	[78]
AQDS (ADQSH ₂)	Br ₂	HBr/H ₂ SO ₄ (aq)	0.85	250 to 750	-	9.4	106 to 750	Nafion 115	[168]

Anode	Cathode	Electrolyte	Theoretical cell voltage / V	Current density / mA cm ⁻²	Theoretic energy density / Wh L ⁻¹	Maximal observed energy density / Wh L ⁻¹	Cycles reported	Membrane	Ref.
AQDS (ADQSH ₂)	Br ₂	HBr/H ₂ SO ₄ (aq)	0.85	>4000	-	-	-	Nafion 212	[127]
AQDS (ADQSH ₂)	Br ₂	HBr/H ₂ SO ₄ (aq)	0.75	100 to 1000	-	5.2	5 to 40	Nafion 115	[170]
4. RFBs utilizing low molar mass organic redox-active materials for catholyte and anolyte									
		CH ₃ CN/TE ABF ₄ or EC/PC/ TEABF ₄	~2.8		-	-	-	PP separator	[173]
		CH ₃ CN/ toluene	1.76; 2.72 (for the 1 st and 2 nd respective oxidations and reductions)	0.67 (2 mA charging current)	-	1.00	6	Medium porosity glass frit	[28]
		CH ₃ CN	1.73	20	9 (during charging) 5 (during discharging)	8.00	15, 35, 100	Daramic porous separator	[174]
		NaClO ₄ / CH ₃ CN	1.6	0.35	-	1.7	20	Nepem 117	[129]

Anode	Cathode	Electrolyte	Theoretical cell voltage / V	Current density / mA cm ⁻²	Theoretic energy density / Wh L ⁻¹	Maximal observed energy density / Wh L ⁻¹	Cycles reported	Membrane	Ref.
 TMeQ	 DBBB	LiBF ₄ /PC	1.12; 1.44 (TMeQ shows two reversible redox events)	0.0625	-	1.1	30	Nafion 117	[159]
 AQS	 BQDS	H ₂ SO _{4(aq)}	0.97	2 to 10	-	1.25	12	Nafion 117	[128]
 TMeQ	 BCF3EPT	LiBF ₄ /PC	1.1; 1.4 (TMeQ shows two reversible redox events)	0.14 (0.1 mA charging current)	-	0.84 to 5.91	50 to 100	Nafion 117	[184]
 FL	 ANL-8	TEA-TFSI/CH ₃ CN	2.37	10 to 15	15 (for charging) 11 (for discharging)	13.63	100	Micro porous PE/silica separator	[136]
 Methyl viologen	 4-HO-TEMPO	NaCl/H ₂ O	1.25	20 to 100	8.4	6.9	100	“Selemin” AEM	[199]
 ARS	 BQDS	H ₂ SO _{4(aq)}	0.83	20 to 60	-	0.38	3	Nafion 212	[161]

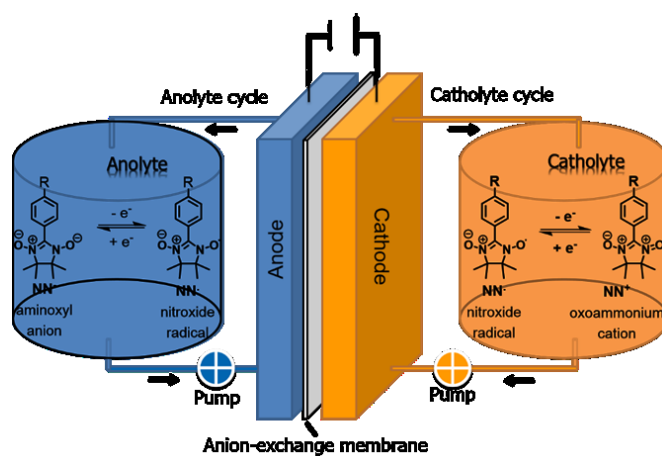
Anode	Cathode	Electrolyte	Theoretical cell voltage / V	Current density / mA cm ⁻²	Theoretic energy density / Wh L ⁻¹	Maximal observed energy density / Wh L ⁻¹	Cycles reported	Membrane	Ref.
5. RFBs utilizing polymer-based organic redox-active materials for catholyte and anolyte									
 Poly(thiophene) microparticles		TEABF ₄ /P C	2.5	0.5 to 5 (static cell); 0.2 to 1 (pumped cell)	-	3.2 (static cell); 2.7 (pumped cell)	30 (static cell); 20 (pumped cell)	FAP-PP-375 AEM	[132]
 Viologen copolymer TEMPO copolymer		NaCl/H ₂ O	1.1	20 (static cell) 20 to 100 (pumped cell)	10.8	5.5	10,000 (static cell) ~95 (pumped cell)	Cellulose-based dialyses membrane	[34, 186]
 R = solubility promoting substituent Poly(BODIPY)		PC	2.2 V	0.25 mA (current)	0.3	0.07	100	Cellulose-based dialyses membrane	[187]

a) The energy density was calculated excluding the anolyte, due to a hybrid flow setup. In case no further information like the capacity [Ah L⁻¹] are available, the maximal observed energy density [Wh L⁻¹] was calculated by the following equation: energy density = (concentration of the electrolyte solution × 26.8 Ah L⁻¹ for one-electron redox-reaction × average cell voltage [V])/2.

Publication P2

A bipolar nitronyl nitroxide small molecule for an all-organic redox-flow battery

T. Hagemann, J. Winsberg, B. Häupler, T. Janoschka, J. J. Gruber, A. Wild, U. S. Schubert,
NPG Asia Mater. **2017**, 9, e340.



ORIGINAL ARTICLE

A bipolar nitronyl nitroxide small molecule for an all-organic symmetric redox-flow battery

Tino Hagemann^{1,2}, Jan Winsberg^{1,2}, Bernhard Häupler^{1,2}, Tobias Janoschka^{1,2}, Jeremy J Gruber^{1,2,3}, Andreas Wild^{1,2} and Ulrich S Schubert^{1,2}

An all-organic symmetric redox-flow battery (RFB) that employs nitronyl nitroxide (NN) units as a bipolar redox-active charge-storage material was designed and investigated. An organic molecule possessing two bipolar redox-active NN units connected via a tetraethylene glycol chain was synthesized for this purpose. Owing to the ethylene glycol chain, this molecule demonstrates good solubility in organic solvents. The electrochemical behavior of the obtained compound was investigated via cyclic voltammetry (CV) measurements and it features quasi-reversible redox reactions of the NN[•]/NN redox couple at $E_{1/2} = 0.37$ V and the NN/NN^{•-} redox couple at $E_{1/2} = -1.25$ V versus AgNO₃/Ag, which led to a promising cell voltage of 1.62 V in a subsequent battery application. A static solution-based battery exhibits a stable charge/discharge performance over 75 consecutive cycles with a high energy efficiency of 82% and an overall energy density of the electrolyte system of 0.67 Wh l⁻¹. In addition, a pumped RFB test demonstrates an overall energy density of the electrolyte system of 4.1 Wh l⁻¹ and an energy efficiency of 79%.

NPG Asia Materials (2017) 9, e340; doi:10.1038/am.2016.195; published online 13 January 2017

INTRODUCTION

State-of-the-art redox-flow batteries (RFBs) such as the well-investigated all-vanadium RFB^{1–4} contain metal salts and corrosive acidic electrolytes. As these metals are generally obtained as products of mining, their relative abundance in the lithosphere does not represent their actual availability and the process to achieve pure materials such as cobalt and vanadium is expensive. As part of the global energy transition, new energy-storage technologies such as RFBs will increase in popularity. Therefore, the demand for charge-storage materials will grow significantly and, consequently, the price of these metals will rise.^{5,6} Further disadvantages of classical RFBs are the deficient civil and environmental standards associated with ore mining, the applied hazardous and highly corrosive acidic electrolytes, and the expensive membranes such as the commonly used Nafion (DuPont, Wilmington, DE, USA) cation-exchange membrane.^{6–10}

The development of an all-organic RFB with inexpensive and sustainable redox-active materials and low-cost membranes may overcome these drawbacks.^{7,10–14} Among others, Darling *et al.*¹⁵ conducted cost analyses, which revealed that the price of the active material itself and the membrane represent the main costs of these systems. Cost-efficient organic charge-storage materials can feature a price advantage compared with metal-based RFBs; in particular, if the raw materials are affordable, no synthesis or fewer synthesis

procedures are required and the avoidance of elaborate purification steps can be achieved. For example, a brief calculation for the anthraquinone disulphonate/bromine system yields a price of \$27 per kW h for the redox-active organic charge-storage materials used, which is significantly lower than the price of \$81 per kW h for vanadium systems.¹⁶

In recent years, several semi-organic,^{17–29} metal-free organic/inorganic^{16,30} and all-organic RFBs^{7,11–13,31–35} have been reported. Commonly, two different redox-active materials are used as charge-storage materials, one within the catholyte and the other within the anolyte. To the best of our knowledge, along with Oh *et al.*,³⁵ Potash *et al.*¹⁴ and Duan *et al.*,³⁶ we are the only researchers that have used one organic bipolar material simultaneously as both the catholyte and anolyte. Oh *et al.*³⁵ fabricated a polythiophene microparticle suspension-based electrolyte using polythiophene as the bipolar charge-storage material and at a current density of 0.5 mA cm⁻² they demonstrated a non-aqueous all-organic RFB with 20 stable charge/discharge cycles, an energy efficiency of 60.9% and an energy density of 2.7 Wh l⁻¹. Potash *et al.*,¹⁴ on the other hand, described the bipolar redox-active molecule Disperse Blue 134, a diaminoanthraquinone derivative, and reported a symmetric all-organic solution-based battery in an H-cell glass setup, which exhibits three charge/discharge cycles with an energy efficiency between 43 and 28%, and an energy density

¹Laboratory of Organic and Macromolecular Chemistry, Institute of Organic Chemistry and Macromolecular Chemistry (IOMC), Jena Center for Soft Matter (JCSM), Friedrich Schiller University Jena, Jena, Germany and ²Center for Energy and Environmental Chemistry Jena (CEEC Jena), Friedrich Schiller University Jena, Jena, Germany

³Current address: Department of Chemical Engineering, 158 Fenske Laboratory, The Pennsylvania State University, University Park, PA 16802, USA.

Correspondence: Professor Dr US Schubert, Laboratory of Organic and Macromolecular Chemistry, Institute of Organic Chemistry and Macromolecular Chemistry (IOMC), Jena Center for Soft Matter (JCSM), Center for Energy and Environmental Chemistry Jena (CEEC Jena), Friedrich Schiller University Jena, Humboldtstrasse 10, D-07743 Jena, Germany.

E-mail: ulrich.schubert@uni-jena.de

Received 16 August 2016; revised 29 September 2016; accepted 13 October 2016

of 0.94 Wh l^{-1} . Similar to our work, Duan *et al.*³⁶ used a nitronyl nitroxide (NN) radical as the charge-storage material. The reported flow battery that used 0.5 M of the commercially available 2-phenyl-4,4,5,5-tetramethylimidazoline-1-oxyl-oxide with 1 M TBAPF₆/acetonitrile as the supporting electrolyte demonstrated over 15 consecutive charge/discharge cycles at a current density of 20 mA cm^{-2} , a coulombic efficiency of $\sim 90\%$, a voltage efficiency of 67% , an energy efficiency of 60% , an energy density of 9 Wh l^{-1} during the charging procedure and an energy density of 5 Wh l^{-1} during the discharging procedure, which are far better results than those of the two previously reported symmetric RFBs.³⁶

The application of a bipolar redox-active charge-storage material in an RFB has significant advantages, such as the considerably reduced synthesis effort, the simplified flow cell design (as both cell compartments use the same material) and a solution to the problematic cross-contamination, which prevents long-term capacity decay.^{1,14,35,37,38} The redox-active unit for our approach is the well-known NN radical, which was first described by Osiecki *et al.*³⁹ The electrochemical behavior of NN radicals and diradicals has been investigated in detail.^{40–44} NNs have been used as organic magnetic materials⁴⁵ and ligands for single-chain magnets⁴⁶ or single-molecule magnets;⁴⁷ furthermore, they have been used as organic memory elements⁴¹ and the charge-storage material in an RFB application due to their *n*- and *p*-type properties.³⁶ In addition, NN-containing polymers are used as bipolar active electrode materials in all-organic radical batteries.^{40,48} Owing to their high chemical reversibility, high cell voltage and electrochemical reversibility, NN-containing molecules represent potential charge-storage materials that can be used as the active material in RFBs. To achieve a high theoretical specific capacity (C_{spec}) and to enhance the solubility in solvents preferred for RFB applications, we designed and synthesized a small molecule with two redox-active NN units connected via a tetraethylene glycol chain.

Consequently, the redox-active molecule **4** was electrochemically characterized and its performance as an active material in a static solution-based and a pumped RFB setup was investigated.

MATERIALS AND METHODS

Materials and chemicals

All starting materials were purchased from commercial sources and were used as obtained. The graphite felt ($2.25 \times 2.25 \times 0.4 \text{ cm}^3$, Sigracell GFA6 EA, SGL Carbon, Wiesbaden, Germany) used and the anion-exchange membrane fumasep FAP-PK-3130 (FuMA-Tech, Bietigheim-Bissingen, Germany) were cut into appropriate pieces.

Methods

The reactions were monitored by thin layer chromatography on 0.2 mm silica gel plates (60 F254, Merck Chemicals GmbH, Darmstadt, Germany) and by gas chromatography–mass spectrometry using a Shimadzu (Kyoto, Japan) GCMS-1-system with a GC-QP2010S-detector and an Agilent DB-5 ms-column. Column chromatography was performed on silica gel 60 (Macherey-Nagel, Düren, Germany). ^1H and ^{13}C nuclear magnetic resonance (NMR) spectra were recorded on a Bruker (Billerica, MA, USA) AC 300 (300 and 75 MHz) spectrometer at 298 K . Chemical shifts are reported in parts per million (p.p.m., δ scale) relative to the residual signal of the deuterated solvent. Elemental analyses were carried out using a Vario ELIII-Elementar Euro (Elementar, Langensfeld, Germany) and an EA-Hekatech (HEKATECH GmbH, Wegberg, Germany). Electrospray ionization (ESI) mass spectrometry measurements were performed on a microTOF (Bruker) ESI time-of-flight (ESI-TOF) system.

Electrochemical characterization

The radical content of **4** was determined via X-band electron paramagnetic resonance (EPR) spectroscopy. The measurements were conducted on an EMXmicro CW-EPR spectrometer from Bruker using powdered samples and

10^{-4} M solutions in toluene. Samples were investigated at room temperature and data handling was performed on the Bruker Xenon software package, version 1.1b86. The Spin Count software module (Bruker) was used for quantitative measurements. The spectrometer was calibrated using TEMPO (99% (high-performance liquid chromatography) purity, Sigma-Aldrich (St Louis, MO, USA)) as a reference standard. The total spin count provided in this contribution is the average of four measurements. Cyclic voltammetry (CV) and rotating disc electrode (RDE) measurements were conducted on a Model SP-50 potentiostat/galvanostat (Bio-Logic, Seyssinet-Pariset, France), with a glassy carbon tip (5 mm diameter), an AgNO_3/Ag reference electrode for organic-based electrolytes and a platinum wire counter electrode. The rotation speed was controlled externally by a Model CTV 101 ring-disk electrode system (Radiometer Analytical SAS, Lyon, France). Evaluation of the RDE analysis via Levich plots (limiting current i_{lim} versus square root of rotation speed ω) yields the diffusion coefficient D by using the Levich equation, $i_{\text{lim}} = 0.62 n F A D^{2/3} \omega^{1/2} v^{-1/6} c_0$, with $n = 1$, Faraday's constant $F = 96485 \text{ C mol}^{-1}$, electrode surface area $A = 0.2 \text{ cm}^2$, the kinematic viscosity of the solution $\nu = 4.48 \times 10^{-7} \text{ m}^2 \text{ s}^{-1}$ at 298.3 K ⁴⁹ and the bulk concentration c_0 of the redox-active NN units. As the peak current i_p grows linearly with the square root of the scan rate, the diffusion coefficient D was calculated using the Randles–Sevcik equation, $i_p = 0.4463 n F A c (n F v D)^{1/2} (RT)^{-1/2}$, with $n = 1$, Faraday's constant $F = 96485 \text{ C mol}^{-1}$, electrode surface area $A = 0.2 \text{ cm}^2$, the bulk concentration c of the redox-active NN units at a temperature $T = 298.3 \text{ K}$ and gas constant $R = 8.314 \text{ J K}^{-1} \text{ mol}^{-1}$.

Cell assembly

The static laboratory cell was designed and constructed into a flat cell type with a membrane active area of 5 cm^2 (JenaBatteries GmbH, Jena, Germany). Supplementary Figure S4 gives a detailed overview of the cell structure. The graphite felt ($2.25 \times 2.25 \times 0.4 \text{ cm}^3$, Sigracell GFA6 EA, SGL Carbon) and anion-exchange membrane fumasep FAP-PK-3130 (FuMA-Tech) were cut into appropriate pieces. Charge/discharge tests were conducted on a VMP3 potentiostat/galvanostat (Bio-Logic). To study the impact of the current density on the battery performance, dynamic measurements were performed. The electrolyte was circulated between the electrochemical cell and the storage tanks with a peristaltic pump (Hei-Flow Value 01 Multi, Heidolph, Schwabach, Germany). Typically, 4 or 10 ml of the electrolyte was used with a flow rate of 10 ml min^{-1} . All measurements were carried out at 25°C under argon atmosphere in a glove box. The batteries were charged/discharged with constant current and the resulting potential was measured over time.

Synthesis of the NN containing compound **4**

Compound **1** was prepared with slight modifications according to the procedure from Hirel *et al.*⁵⁰

2,3-Dimethyl-2,3-dinitrobutane (17.85 g , 0.1 mol) was suspended in concentrated hydrochloric acid (37% , 150 ml). The suspension was heated up to 50°C and granular tin (100 g , 0.84 mol) was added in portions over a period of one hour. Subsequently, the suspension was heated to 90°C for 4 h and stirred at 110°C until the mixture became a clear solution. After cooling to room temperature, the solution was extracted with diethyl ether (100 ml , three times), to remove residual 2,3-dimethyl-2,3-dinitrobutane. Afterwards, saturated sodium hydroxide solution (150 ml) was added to the aqueous phase under cooling in an ice bath. The resulting black precipitate was removed by filtration and the clear solution obtained was extracted with CH_2Cl_2 (100 ml , three times). The combined organic phases were dried over MgSO_4 and then the solvent was removed under reduced pressure to obtain **1** as a colorless solid (5.24 g , 0.045 mol) in a yield of 45% . ^1H NMR (300 MHz , CDCl_3 , δ): 1.24 (brs, 4H , NH_2), 1.08 (s, 12H , CH_3); ^{13}C NMR (75 MHz , CDCl_3 , δ): 54.66 (CC), 26.41 (CH_3); ESI-TOF MS m/z (%): 117.14 (100) [$\text{M}^+ + \text{H}$]; high resolution mass spectrometry (ESI) m/z : [$\text{M} + \text{H}$]⁺ calcd for $\text{C}_6\text{H}_{16}\text{N}_2$, 117.1386 ; found, 117.1383 .

Compound **2** was prepared with slight modifications according to the procedure from Wang *et al.*⁵¹

Under inert conditions, K_2CO_3 (42.1 g , 0.305 mol) and 4-hydroxybenzaldehyde (18.6 g , 0.152 mol) were dissolved in dry dimethylformamide (230 ml) and 1-chloro-2-[2-(2-(2-chloroethoxy)ethoxy)ethoxy]ethane (13.6 ml ,

0.069 mol) was added dropwise. The solution was stirred at 120 °C for 20 h. After cooling to room temperature, the solvent was removed under reduced pressure. The oily residue was diluted in CHCl_3 (10 ml), whereby the remaining K_2CO_3 precipitated as a white solid. The K_2CO_3 was filtered off and the filtrate was dried over Na_2SO_4 . The solvent was removed under reduced pressure to obtain the crude product, which was purified via column chromatography (SiO_2 ; ethyl acetate: *n*-heptane 5:1) to obtain the pure product **2** (21.35 g, 0.053 mol) in a yield of 77%. ^1H NMR (300 MHz, CDCl_3 , δ): 9.85 (s, 2H; CHO), 7.79 (d, $J = 9$ Hz, 4H, Ar H), 6.99 (d, $J = 9$ Hz, 4H, Ar H), 4.18 (t, $J = 6$ Hz, 4H, CH_2), 3.86 (t, $J = 6$ Hz, 4H, CH_2), 3.70–3.68 (m, 8H, CH_2); ^{13}C NMR (75 MHz, CDCl_3 , δ): 190.85 (C=O), 163.88 (CO), 132.00 (CC), 130.11 (CC), 114.93 (CC), 70.58 (CO), 70.72 (CO), 69.53 (CO), 67.82 (CO); ESI-TOF MS m/z (%): 425.36 (100) [$\text{M}^+ + \text{Na}$], 403.83 (16) [$\text{M}^+ + \text{H}$]; high resolution mass spectrometry (ESI) m/z : [$\text{M} + \text{Na}$] $^+$ calcd for $\text{C}_{22}\text{H}_{26}\text{O}_7$, 425.1570; found, 425.1561; Anal. calcd. for $\text{C}_{22}\text{H}_{26}\text{O}_7$: C 65.66, H 6.51; found: C 65.76, H 6.54.

Compound **3** was prepared as follows.

Compound **1** (5.2 g, 0.045 mol) was dissolved in tetrahydrofuran (100 ml) and a solution of **2** (8.6 g, 0.021 mol) in tetrahydrofuran (50 ml) was added dropwise. The reaction mixture was stirred at room temperature until the condensation was completed (monitored via thin layer chromatography). The solvent was removed *in vacuo* to obtain a yellowish oil, which solidified overnight at 5 °C. The solid was washed with diethyl ether (30 ml, three times) to obtain **3** as a white powder (10.3 g, 0.017 mol) in a yield of 81%. ^1H NMR (300 MHz, CDCl_3 , δ): 7.43 (d, $J = 9$ Hz, 4H, Ar H), 6.85 (d, $J = 9$ Hz, 4H, Ar H), 5.12 (s, 2H, CH), 4.09 (t, $J = 6$ Hz, 4H, CH_2), 3.83 (t, $J = 6$ Hz, 4H, CH_2), 3.69 to 3.68 (m, 8H, CH_2), 2.09 (s, 4H, CH_2), 1.17 (s, 12H, CH_3), 1.09 (s, 12H, CH_3); ^{13}C NMR (75 MHz, CDCl_3 , δ): 158.33 (CO), 136.37 (CC), 127.61 (CC), 114.52 (CC), 73.05 (CC), 70.93 (CO), 70.78 (CO), 69.85 (CO), 67.56 (CO), 62.92 (CC), 25.6 (CH $_3$), 23.77 (CH $_3$); ESI-TOF MS m/z (%): 599.40 (8) [$\text{M}^+ + \text{H}$], 300.21 (100) [$\text{M}^{2+} + \text{H}$]; high resolution mass spectrometry (ESI) m/z : [$\text{M} + \text{H}$] $^{2+}$ calcd for $\text{C}_{34}\text{H}_{54}\text{N}_4\text{O}_5$, 300.2119; found, 300.2113; Anal. calcd. for $\text{C}_{34}\text{H}_{54}\text{N}_4\text{O}_5$: C 68.20; H 9.09; N 9.36; found: C 68.20; H 9.07; N 8.91.

Compound **4** was prepared as follows.

A mixture of 4,4'-[oxybis(2,1-ethanedioxy-2,1-ethanedioxy)]bis-4,4,5,5-tetramethylimidazolidine (**3**, 10 g, 0.017 mol), CH_2Cl_2 (500 ml) and saturated NaHCO_3 solution (300 ml) was cooled to 0 °C. Over a period of 1 h, a solution of *m*-chloroperbenzoic acid ($\leq 77\%$, 14.64 g, 0.085 mol) in CH_2Cl_2 (180 ml) was added dropwise to the reaction mixture. Subsequently, a solution of NaO_4 (10.89 g, 0.051 mol) in water (180 ml) was added dropwise. The mixture was allowed to reach room temperature and was stirred for an additional hour. Then, the organic phase was separated from the aqueous phase and the aqueous solution was extracted with CH_2Cl_2 (three times). Subsequently, the combined organic phases were extracted with saturated NaHCO_3 (200 ml). The organic phase was dried over Na_2SO_4 , filtered and concentrated under reduced pressure. The resulting crude purple residue was purified *via* column chromatography (SiO_2 ; ethyl acetate) to yield **4** (3.65 g, 0.0056 mol, 33%) as a purple oil. ESI-TOF MS m/z (%): 656.34 (100) [M^{2+}]; high resolution mass spectrometry (ESI) m/z : [M] $^+$ calcd for $\text{C}_{34}\text{H}_{48}\text{N}_4\text{O}_9^{2+}$, 656.3415; found, 656.3402; Anal. calcd. for $\text{C}_{34}\text{H}_{48}\text{N}_4\text{O}_9^{2+}$: C 62.18, H 7.37, N 8.53; found: C 62.63; H 7.38; N 7.60; EPR: calcd spin-activity for $\text{C}_{34}\text{H}_{48}\text{N}_4\text{O}_9^{2+}$: 97.31%.

RESULTS AND DISCUSSION

Synthesis and electrochemical behavior of **4**

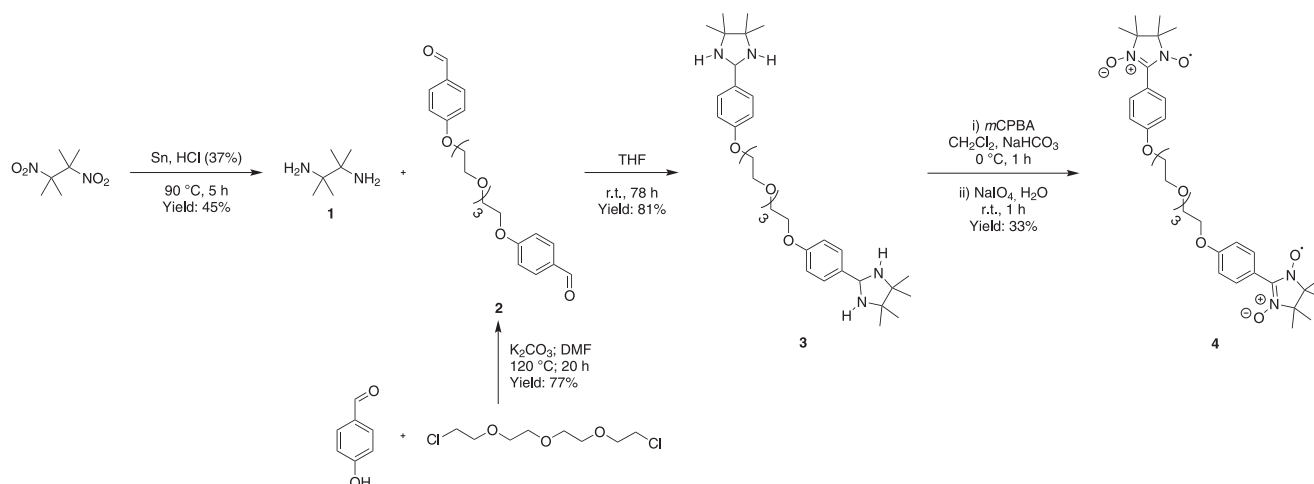
For battery applications, the active material used should possess a high energy density. Therefore, the theoretical specific capacity, the cell voltage and, in particular, the solubility of the redox-active material in the applied solvent should be maximized. Unfortunately, most aromatic NNs exhibit a moderate to poor solubility in nitrile- and carbonate-based solvents, which are preferred for RFB applications due to their electrochemical stability. To improve the solubility and thereby the energy density, even compared with the commercial available 2-phenyl-4,4,5,5-tetramethylimidazoline-1-oxyl-oxide, an ethylene glycol chain was introduced as a linker between two NN

molecules. It is noteworthy that due to the presence of two NN units per molecule, the theoretical capacity and the solubility compared with the single NN units is doubled. The introduction of two redox-active NN units was performed to achieve a high theoretical specific capacity by improving the solubility of molecule **4** in preferred organic solvents, such as acetonitrile (3.8 molal). Furthermore, the synthesis of the active dimeric material was beneficial in comparison with a monomeric active material. The starting material used, 1-chloro-2-[2-(2-chloroethoxy)ethoxy]ethoxyethane, has several benefits such as a reasonable price per kg or the absence of interfering hydroxyl end groups, for example, 1-chloro-2-[2-(2-methoxyethoxy)ethoxy]ethane, 1-chloro-2-[2-(2-ethoxyethoxy)ethoxy]ethane or 2-[2-[2-(2-chloroethoxy)ethoxy]ethoxy]ethanol. Based on its good chemical stability in acetonitrile, benzonitrile and carbonate-based solvents, a fumasep FAP-PK-3130 (FuMA-Tech) anion-exchange membrane was used to separate the electrolyte circuits. In contrast to commonly used Nafion membranes, this simpler membrane presents a high cost-saving potential. Acetonitrile was selected for all static and pumped flow battery tests, as it demonstrated the highest solubility of **4** and the best PF_6^- ion transport across the membrane, which resulted in a low electric cell resistance (determined by electrochemical impedance spectroscopy (Supplementary Figure S6a and b).

A higher theoretical specific capacity may be achieved by using 2,2'-[oxybis(2,1-ethanedioxy)]bisacetaldehyde as the linker unit to obtain an NN-containing molecule with a theoretical specific capacity of 120.7 mA h g $^{-1}$. Unfortunately, this compact NN-containing molecule is not practical for battery applications due to its poor chemical stability in solution in the presence of air. Various studies show that the introduction of an aromatic ring ($\text{C}_6\text{H}_4\text{R}$) at the 2-position of the NN moiety leads to a significantly enhanced stability of the radicals against the presence of air.^{52–54} Therefore, it is essential to introduce a phenyl spacer between the NN units and the solubility-promoting tetraethylene glycol linker to engineer stable NN-containing small molecules. With 1-chloro-2-[2-(2-(2-chloroethoxy)ethoxy)ethoxy]ethane as the starting compound, this is, in the simplest case, the 4,4'-[oxybis(2,1-ethanedioxy-2,1-ethanedioxy)]bisnitronyl nitroxide (**4**) with a theoretical specific capacity of 81.7 mA h g $^{-1}$ (Scheme 1).

Compound **4** was obtained from inexpensive commercially available starting materials in four synthesis steps (Scheme 1). Here, 2,3-dimethyl-2,3-dinitrobutane was completely reduced (Sn/conc. HCl, reflux) to achieve the corresponding diamino compound **1** in a moderate yield of 45%.⁵⁰ The bisaldehyde **2** was prepared from 4-hydroxybenzaldehyde and 1-chloro-2-[2-(2-(2-chloroethoxy)ethoxy)ethoxy]ethane under inert conditions in dry dimethylformamide. K_2CO_3 was used as a base to obtain **2** in a yield of 77%.⁵¹ The subsequent condensation reaction of **1** and **2** in tetrahydrofuran produced compound **3** in a yield of 81%. In the last reaction step, the bisimidazolidine **3** was oxidized in a one-pot reaction, first by *meta*-chloroperbenzoic acid to the bishydroxyimidazolidine and, subsequently, by sodium periodate to the NN redox-active material **4** in a moderate yield of 33%.⁵⁰ A brief calculation of the costs of this bipolar redox-active charge-storage material can be found in the Supplementary Information.

The unpaired electrons of the two NN groups of molecule **4** were characterized by EPR spectroscopy. The EPR spectrum, obtained in 10 $^{-4}$ M toluene solution, displays a nine-line pattern in the hyperfine structure (Figure 1a). According to the literature, a five-line pattern with an intensity ratio of 1:2:3:2:1 is expected due to the interaction between the two identical nitrogens of the NN group. However, because of the close proximity of the two NN units in compound **4**, a spin–spin interaction between both NN units occurs, which results in



Scheme 1 Schematic representation of the synthesis route for the nitronyl nitroxide-containing compound **4**.

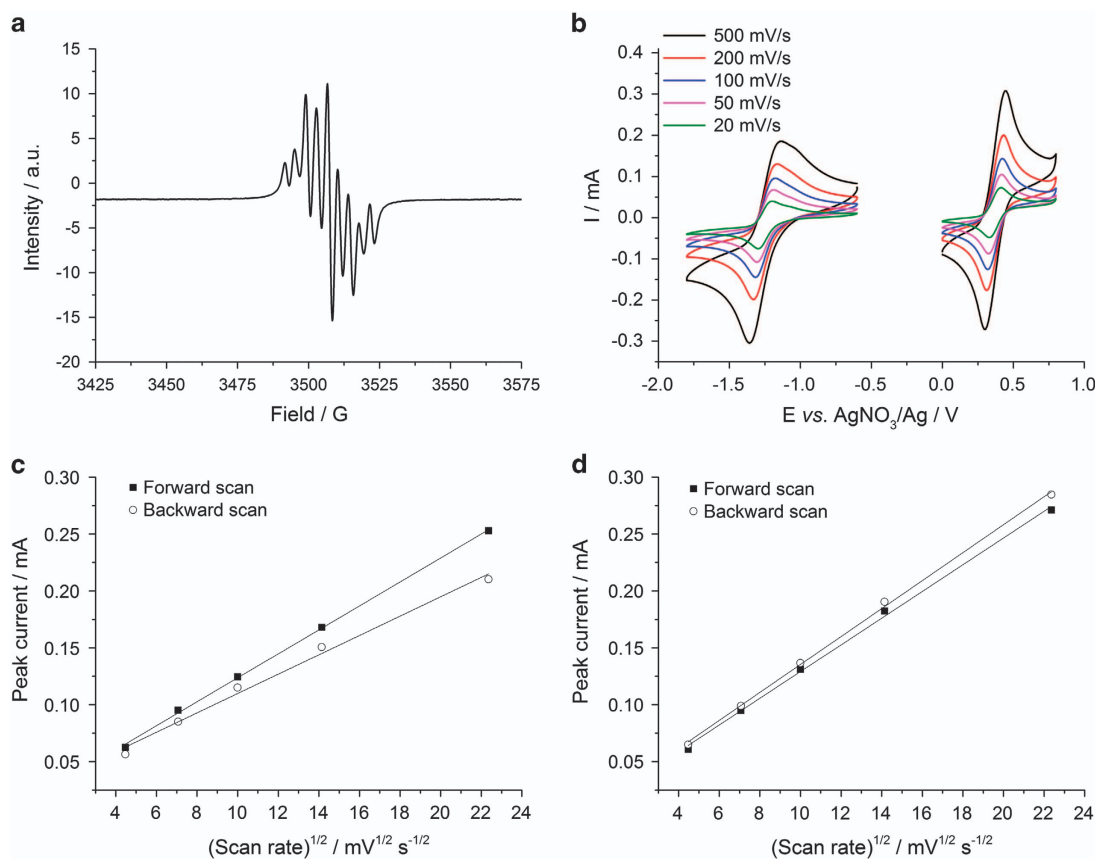


Figure 1 Characterization of **4**: (a) EPR spectrum of **4** in 10^{-4} M toluene solution, (b) cyclic voltammogram obtained for 2.1 mM CH_3CN solution of **4** with 0.1 M TBAPF_6 as the supporting electrolyte at different scan rates, (c) plot of the reduction and the re-oxidation peak current versus square root of the scan rate and (d) plot of the oxidation and the re-reduction peak current versus square root of the scan rate.

a nine-line pattern.^{40,55} The absolute spin activity of compound **4**, obtained from the EPR spectrum in solid state (Supplementary Figure S1), was 1.79×10^{18} spins per mg, which equals a radical content of above 97% and indicates a complete oxidation of bisimidazolidine.

The electrochemical properties of NN radicals and diradicals are well known, and they have been investigated in detail in previous reports.^{40–44} Several studies show that the electrochemical behavior of

the NNs strongly depends on the substituent. For example, Sukegawa *et al.*⁴⁰ reported a phenyl-substituted NN diradical that can undergo reversible oxidation and reduction reactions.

The electrochemical properties of compound **4** were investigated via CV, to determine the formal potentials of the NN redox couples, and RDE measurements, to obtain the diffusion coefficient and the rate constant. The CV measurements of compound **4** were performed in acetonitrile solution with 0.1 M TBAPF_6 as a conductive salt. The cyclic

voltammogram (Figure 1b) displays a quasi-reversible oxidation and re-reduction of the NN to the oxoammonium cation (NN^+) at $E_{1/2} = 0.37$ V versus AgNO_3/Ag with a peak split of 146 mV and a quasi-reversible reduction and re-oxidation of the NN to the aminoxyl anion (NN^-) at $E_{1/2} = -1.25$ V versus AgNO_3/Ag with a peak split of 218 mV, which would lead to a cell voltage of 1.62 V in a subsequent battery application. At approximately -1 V at the re-oxidation of the reduction of the NN to the NN^- , a second minor peak is visible, which indicates possible side reactions and/or consecutive reactions of the NN^- . A more extensive investigation of the CV curves (Figure 1c and d) for both redox couples, the NN^+/NN and the NN/NN^- , exhibits a linear relation between the peak currents and the square root of the scan rate, which reveals a diffusion-controlled behavior and the non-appearance of precipitates. Using the Randles–Sevcik equation, the diffusion coefficients D of 1.08×10^{-5} and $0.81 \times 10^{-5} \text{ cm}^2 \text{ s}^{-1}$ were calculated for the NN^+/NN and NN/NN^- redox couples, respectively. The obtained diffusion coefficient D for both these redox couples is in the same magnitude as the diffusion coefficient D subsequently calculated by using the Levich equation from the evaluation of the RDE measurements.

RDE measurements of **4** were performed in acetonitrile solution with 0.1 M TBAPF₆ as the supporting electrolyte for the oxidation to the oxoammonium cation (NN^+ , Supplementary Figure S2 and Supplementary Information) and the reduction to the

NN^- (Supplementary Figure S3 and Supplementary Information). The NN^+/NN redox couple exhibits a diffusion-controlled behavior of **4** with a diffusion coefficient D of $4.74 \times 10^{-6} \text{ cm}^2 \text{ s}^{-1}$ (Supplementary Figure S2a and b, and Supplementary Information). Subsequently, the Koutecký–Levich analysis performed displays mass-transport-independent currents and the following Tafel analysis (Supplementary Figure S2c and d, and Supplementary Information) presents an electron-transfer rate constant (k^0) of $1.42 \times 10^{-2} \text{ cm s}^{-1}$ and a transfer coefficient α of 0.59, which is close to the α -value of an ideal reversible redox-reaction of 0.5.

The NN/NN^- redox couple also exhibits a diffusion-controlled behavior of **4** in acetonitrile with 0.1 M TBAPF₆ and a diffusion coefficient D of $3.45 \times 10^{-6} \text{ cm}^2 \text{ s}^{-1}$ (Supplementary Figure S3a and b, and Supplementary Information). Unfortunately, both the Koutecký–Levich analysis and the Tafel analysis could not be performed. We assume that the calculation of the kinetics of the redox-reaction was impossible due to the non-defined redox-reaction of the NN/NN^- redox couple. The cyclic voltammogram (Figure 1b) of the reduction of the NN to the NN^- and the corresponding re-oxidation, in contrast to the NN^+/NN redox couple, displays a broader peak split, a large peak width and, at lower scan rates, a slight potential shift, which leads to a non-defined redox reaction. This issue can be caused by side reactions and/or consecutive reactions of the NN^- . To summarize, the diffusion coefficient D obtained for the NN/NN^+ and the NN/NN^- redox couple, and the electron-transfer rate constant k^0 and the transfer coefficient α for the NN/NN^+ redox couple are similar to the values reported in the literature for other organic charge-storage materials, such as the comparable 2-phenyl-4,4,5,5-tetramethylimidazoline-1-oxyl-oxide material,³⁶ DBBB^{32,56} and several quinone derivatives;^{16,33,57} thereby, they enable the application of **4** in a battery test cell.

Battery tests

The use of compound **4** as a bipolar charge-storage material for RFB applications was initially investigated in a static battery setup (Supplementary Figure S4 and Supplementary Information). Here, acetonitrile with 0.5 M TBAPF₆ was used as the supporting electrolyte and a fumasep anion-exchange membrane was applied to separate the cathode and anode compartments.

The static solution-based battery comprised a 16 mm (32 mm active NN units) solution of **4** within the anolyte and catholyte. This results in a theoretical capacity of 0.88 Ah l^{-1} for both solutions and an overall energy density of the electrolyte system of 0.67 Wh l^{-1} . The charge/discharge experiments were conducted in a voltage range of 1.10–1.95 V and a stable battery cycling was performed for 75 consecutive charge/discharge cycles at a current density of 1 mA cm^{-2} . Representatively, cycles 3 to 5 are shown in Figure 2a.

The NN-containing static solution-based battery exhibits well-defined charge and discharge plateaus at 1.67 and 1.45 V, respectively. Coulombic efficiencies up to 95% were attained, which indicate a good chemical reversibility of the redox reactions of the bipolar charge-storage material and a low membrane crossover. A voltage efficiency of 86% and an energy efficiency of 82% were exemplarily calculated for the 75th cycle. For the static battery setup used, a theoretical discharge capacity of 1.97 mA h is possible, whereas a discharge capacity of 0.53 mA h (27%) could be achieved in the first cycle (Figure 2b) at a current density of 1 mA cm^{-2} . This moderate material activity originates from the use of un-pumped battery setup, where only a limited amount of the redox-active NN units can be transported to the active electrode area by diffusion. In addition to this kinetic limitation, a high overpotential further reduces the material

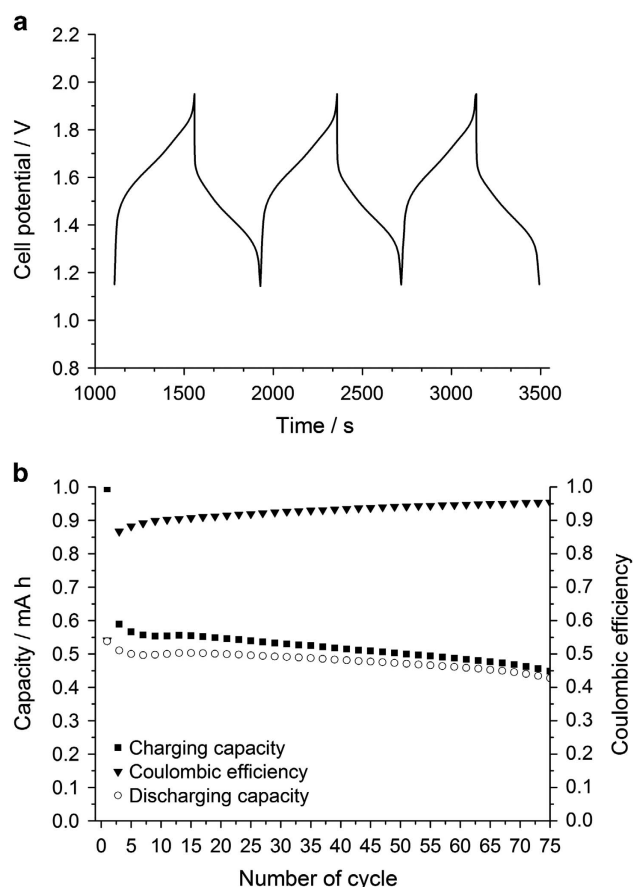


Figure 2 Charge/discharge experiments in a 5 cm^2 electrochemical static test cell with 16 mm (32 mm NN units) **4** and 0.5 M TBAPF₆ in acetonitrile, (a) representative third to fifth charge/discharge cycles at a current density of 1 mA cm^{-2} and (b) long-time stability: charge and discharge capacity and coulombic efficiency at a current density of 1 mA cm^{-2} .

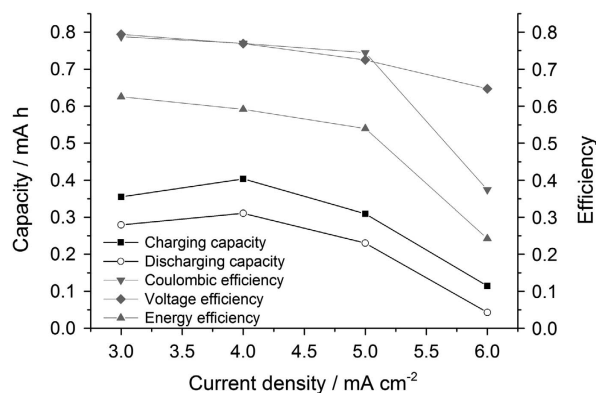


Figure 3 Electric performance of a pumped 5 cm² test cell with 16 mm (32 mm NN units) **4** and 0.5 M TBAPF₆ in acetonitrile (with a theoretical capacity of 0.83 A h l⁻¹ for both solutions); capacity, coulombic, voltage and energy efficiency with respect to the current density for 10 ml electrolyte per half-cell, with the flow rate adjusted to 10 ml min⁻¹.

activity and the cell design allows only a rough estimation of the electrolyte volume. Furthermore, after 75 consecutive charge/discharge cycles, a capacity decay of ~20% was observed (Figure 2a), which is probably caused by side reactions of the charged species or decomposition by the reaction of radicals with each other.

To determine the impact of the current density on the performance of the flow battery, charge/discharge measurements in a pumped flow battery (Supplementary Figure S5 and Supplementary Information) were performed (Figure 3).

Four different current densities (3, 4, 5 and 6 mA cm⁻²) were applied, and the charge/discharge capacity and the coulombic, voltage and energy efficiency were determined. The capacity decreases linearly as the current density increases, except for the current density of 3 mA cm⁻², due to the limited mass transport to the electrode, which leads to an increasing overpotential. Charging/discharging was possible up to current densities of 6 mA cm⁻². At this current density, the coulombic efficiency drops significantly under 40% because of kinetic limitations in the discharging process. In addition, with increasing current densities, a linear decline of the voltage efficiency was observed, which is presumably induced by the restricted ion conductivity in the applied electrolyte and, therefore, by the increasing potential gap between the charging and discharging plateaus.

In addition, further pumped flow battery tests with a higher concentration of the active material **4** were performed (Figure 4). This battery comprised 0.1 M (0.2 M active NN units) **4** and 0.5 M TBAPF₆ in acetonitrile, as the anolyte and catholyte, respectively, resulting in a theoretical capacity of 5.4 A h l⁻¹ for both solutions and an overall energy density of the electrolyte system of 4.1 W h l⁻¹. The charge/discharge experiments were conducted in a voltage range from 1.10 to 1.95 V and battery cycling was performed for 20 consecutive charge/discharge cycles at a current density of 1 mA cm⁻².

At an active material concentration of 0.1 M (0.2 M active NN units), the electrolyte viscosity increased during the charging process, which resulted in an impaired mass transport and a high overvoltage and eventually caused a low material utilization (~20%) and a steep voltage profile (Figure 4a). The change in viscosity is attributed to a decrease in the solubility of the charged species in contrast to the pristine active material **4**. Furthermore, after 11 consecutive charge/discharge cycles, a capacity fade of approximately 50%, probably due to side reactions of the charged species or decomposition by the reaction of radicals with each other, was observed (Figure 4b). It is noteworthy that up to

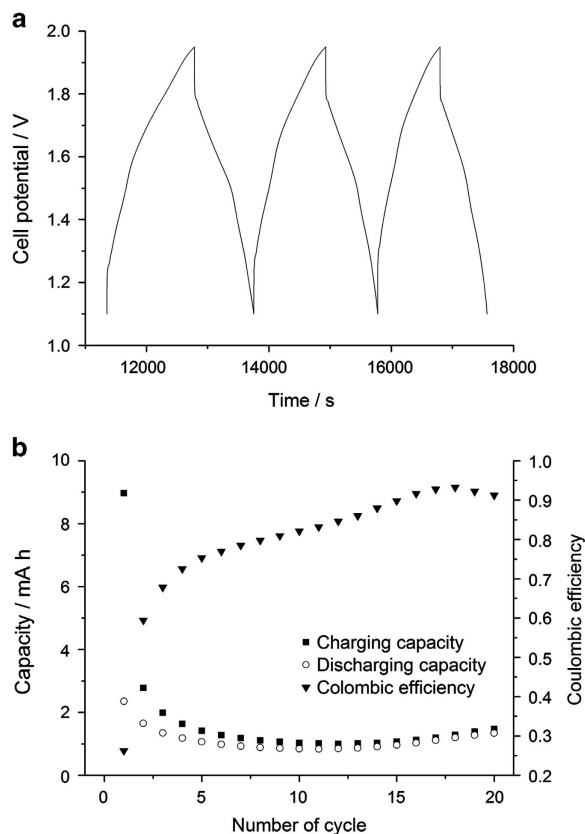


Figure 4 Charge/discharge experiments in a pumped 5 cm² electrochemical test cell with 0.1 M (0.2 M NN units) **4** and 0.5 M TBAPF₆ in acetonitrile, (a) representative third to fifth charge/discharge cycles at a current density of 1 mA cm⁻², and (b) charge and discharge capacity and coulombic efficiency at a current density of 1 mA cm⁻² over 20 charge/discharge cycles.

cycle 20, the capacity recovers to ~60% of the original value because the pumped cell requires some time to reach the ideal operational conditions. This can be attributed to the decrease of the area-specific resistance, from 2.58 Ω before cycling to 1.91 Ω after cycling (Supplementary Figure S6 and Supplementary Information), which results in a subsequently achieved cutoff voltage that leads to a higher material utilization. At 0.5 M (1 M active NN units) **4**, the charged species precipitated and therefore the charged active material (Supplementary Figure S7) cannot be discharged at higher concentrations.

The maximum solubility limit (3.8 M in acetonitrile) of **4** in pumped flow battery experiments was not attained. This was probably because the two charged NN units reduced the solubility of **4** in the electrolyte used. The use of a longer ethylene glycol chain, a detailed optimization of the electrolyte and an improvement in the cell design may solve this limitation.

CONCLUSION

An all-organic RFB with a bipolar molecule containing two redox-active NN units was successfully demonstrated. Compound **4** was synthesized in four synthesis steps from inexpensive commercially available materials. Two NNs were connected via a tetraethylene glycol chain, which improves the solubility behavior to 3.8 molal in the preferred organic solvent, acetonitrile. Compound **4** was electrochemically characterized via CV, which shows a quasi-reversible redox reaction at $E_{1/2} = 0.37$ V for the NN⁺/NN and at $E_{1/2} = -1.25$ V versus AgNO₃/Ag for the NN/NN⁻ redox couple, leading to a high cell

voltage of 1.62 V and RDE measurements, which display a diffusion-controlled behavior. Furthermore, its potential as a bipolar charge-storage material for RFB applications was demonstrated in a static and pumped laboratory test cell. The static flow battery was charged/discharged at a current density of 1 mA cm^{-2} for 75 consecutive cycles and it achieved coulombic efficiencies of up to 95%, a voltage efficiency of 86% and an energy efficiency of 82%. The pumped battery test revealed stable capacity retention and efficiencies for current densities in the range of 3 to 5 mA cm^{-2} .

According to these preliminary static and pumped battery tests, which exhibit far better results than those from the previously reported symmetric RFBs by Oh *et al.*³⁵ and Potash *et al.*¹⁴ and are comparable to values for symmetric RFB described by Duan *et al.*,³⁶ compound **4** appears to possess a high potential for the application as a bipolar organic charge-storage material in non-aqueous all-organic RFBs. However, further investigations are required to improve certain properties, for example, the solubility of the charged species, to achieve higher energy densities and performance parameters. This can be conducted by a detailed optimization of the electrolyte.

CONFLICT OF INTEREST

The authors declare no conflict of interest.

ACKNOWLEDGEMENTS

We thank the European Regional Development Fund (EFRE), the Thuringian Ministry for Economic Affairs, Science and Digital Society (TMWdG), the Zentrales Innovationsprogramm Mittelstand (ZIM) and the Fonds der Chemischen Industrie (FCI) for the financial support, René Burgés for electrospray ionization mass spectrometry measurements, Sabine Morgenstern for EPR measurements, Christian Friebe for help with the electrochemical characterization and JenaBatteries GmbH for the redox-flow cell assembly.

- 1 Skyllas-Kazacos, M., Rychcik, M., Robins, R. G. & Fane, A. G. New all-vanadium redox flow cell. *J. Electrochem. Soc.* **133**, 1057–1058 (1986).
- 2 Vijayakumar, M., Wang, W., Nie, Z., Sprenkle, V. & Hu, J. Elucidating the higher stability of vanadium(V) cations in mixed acid based redox flow battery electrolytes. *J. Power Sources* **241**, 173–177 (2013).
- 3 Roe, S., Menicetas, C. & Skyllas-Kazacos, M. A high energy density vanadium redox flow battery with 3 M vanadium electrolyte. *J. Electrochem. Soc.* **163**, A5023–A5028 (2016).
- 4 Sun, C., Chen, J., Zhang, H., Han, X. & Luo, Q. Investigations on transfer of water and vanadium ions across Nafion membrane in an operating vanadium redox flow battery. *J. Power Sources* **195**, 890–897 (2010).
- 5 Barnhart, C. J. & Benson, S. M. On the importance of reducing the energetic and material demands of electrical energy storage. *Energy Environ. Sci.* **6**, 1083–1092 (2013).
- 6 Armand, M. & Tarascon, J. M. Building better batteries. *Nature* **451**, 652–657 (2008).
- 7 Janoschka, T., Martin, N., Martin, U., Friebe, C., Morgenstern, S., Hiller, H., Hager, M. D. & Schubert, U. S. An aqueous, polymer-based redox-flow battery using non-corrosive, safe, and low-cost materials. *Nature* **527**, 78–81 (2015).
- 8 Weber, A., Mench, M., Meyers, J., Ross, P., Gostick, J. & Liu, Q. Redox flow batteries: a review. *J. Appl. Electrochem.* **41**, 1137–1164 (2011).
- 9 Zhang, X., Yang, L., Li, Y., Li, H., Wang, W. & Ye, B. Impacts of lead/zinc mining and smelting on the environment and human health in China. *Environ. Monit. Assess.* **184**, 2261–2273 (2012).
- 10 Winsberg, J., Hagemann, T., Janoschka, T., Hager, M. D. & Schubert, U. S. Redox flow batteries: from metals to organics. *Angew. Chem. Int. Ed.* doi:10.1002/anie.201604925R201604921 (2016).
- 11 Janoschka, T., Morgenstern, S., Hiller, H., Friebe, C., Wolkersdorfer, K., Haeupler, B., Hager, M. D. & Schubert, U. S. Synthesis and characterization of TEMPO- and viologen-polymers for water-based redox-flow batteries. *Polym. Chem.* **6**, 7801–7811 (2015).
- 12 Liu, T., Wei, X., Nie, Z., Sprenkle, V. & Wang, W. A Total organic aqueous redox flow battery employing a low cost and sustainable methyl viologen anolyte and 4-HO-TEMPO catholyte. *Adv. Energy Mater.* **6**, 1501449 (2016).
- 13 Wei, X., Xu, W., Huang, J., Zhang, L., Walter, E., Lawrence, C., Vijayakumar, M., Henderson, W. A., Liu, T., Cosimbescu, L., Li, B., Sprenkle, V. & Wang, W. Radical compatibility with nonaqueous electrolytes and its impact on an all-organic redox flow battery. *Angew. Chem. Int. Ed.* **54**, 8684–8687 (2015).
- 14 Potash, R. A., McKone, J. R., Conte, S. & Abrufia, H. D. On the benefits of a symmetric redox flow battery. *J. Electrochem. Soc.* **163**, A338–A344 (2016).
- 15 Darling, R. M., Gallagher, K. G., Kowalski, J. A., Ha, S. & Brushett, F. R. Pathways to low-cost electrochemical energy storage: a comparison of aqueous and nonaqueous flow batteries. *Energy Environ. Sci.* **7**, 3459–3477 (2014).
- 16 Huskinson, B., Marshak, M. P., Suh, C., Er, S., Gerhardt, M. R., Galvin, C. J., Chen, X., Aspuru-Guzik, A., Gordon, R. G. & Aziz, M. J. A metal-free organic-inorganic aqueous flow battery. *Nature* **505**, 195–198 (2014).
- 17 Xu, Y., Wen, Y., Cheng, J., Cao, G. & Yang, Y. Study on a single flow acid Cd-chloranil battery. *Electrochem. Commun.* **11**, 1422–1424 (2009).
- 18 Xu, Y., Wen, Y.-H., Cheng, J., Cao, G.-P. & Yang, Y.-S. A study of tiron in aqueous solutions for redox flow battery application. *Electrochim. Acta* **55**, 715–720 (2010).
- 19 Wang, W., Xu, W., Cosimbescu, L., Choi, D., Li, L. & Yang, Z. Anthraquinone with tailored structure for a nonaqueous metal-organic redox flow battery. *Chem. Commun.* **48**, 6669–6671 (2012).
- 20 Wei, X., Xu, W., Vijayakumar, M., Cosimbescu, L., Liu, T., Sprenkle, V. & Wang, W. TEMPO-based catholyte for high-energy density nonaqueous redox flow batteries. *Adv. Mater.* **26**, 7649–7653 (2014).
- 21 Huang, J., Cheng, L., Assary, R. S., Wang, P., Xue, Z., Burrell, A. K., Curtiss, L. A. & Zhang, L. Liquid catholyte molecules for nonaqueous redox flow batteries. *Adv. Energy Mater.* **5**, 1401782 (2015).
- 22 Huang, J., Su, L., Kowalski, J. A., Barton, J. L., Ferrandon, M., Burrell, A. K., Brushett, F. R. & Zhang, L. A subtractive approach to molecular engineering of dimethoxybenzene-based redox materials for non-aqueous flow batteries. *J. Mater. Chem. A* **3**, 14971–14976 (2015).
- 23 Lin, K., Chen, Q., Gerhardt, M. R., Tong, L., Kim, S. B., Eisenach, L., Valle, A. W., Hardee, D., Gordon, R. G., Aziz, M. J. & Marshak, M. P. Alkaline quinone flow battery. *Science* **349**, 1529–1532 (2015).
- 24 Takechi, K., Kato, Y. & Hase, Y. A highly concentrated catholyte based on a solvate ionic liquid for rechargeable flow batteries. *Adv. Mater.* **27**, 2501–2506 (2015).
- 25 Zhao, Y., Si, S. & Liao, C. A single flow zinc/polyaniline suspension rechargeable battery. *J. Power Sources* **241**, 449–453 (2013).
- 26 Nagarajana, G., Hui, J., Cheng, K. J., Lichtenstein, T., Shen, M., Moore, J. S. & Rodríguez-López, J. Impact of redox-active polymer molecular weight on the electrochemical properties and transport across porous separators in nonaqueous solvents. *J. Am. Chem. Soc.* **136**, 16309–16316 (2014).
- 27 Sukegawa, T., Masuko, I., Oyaizu, K. & Nishide, H. Expanding the dimensionality of polymers populated with organic robust radicals toward flow cell application: synthesis of TEMPO-crowded bottlebrush polymers using anionic polymerization and ROMP. *Macromolecules* **47**, 8611–8617 (2014).
- 28 Winsberg, J., Muench, S., Hagemann, T., Janoschka, T., Morgenstern, S., Billing, M., Schacher, F. H., Hauffman, G., Gohy, J.-F., Hoepfener, S., Hager, M. D. & Schubert, U. S. Polymer/zinc hybrid-flow battery using block copolymer micelles featuring a TEMPO corona as catholyte. *Polym. Chem.* **7**, 1711–1718 (2016).
- 29 Winsberg, J., Janoschka, T., Morgenstern, S., Muench, S., Hagemann, T., Hauffman, G., Gohy, J.-F., Hager, M. D. & Schubert, U. S. Poly(TEMPO)/zinc hybrid-flow battery: a novel, 'green', high voltage, and safe energy storage system. *Adv. Mater.* **28**, 2238–2243 (2016).
- 30 Chen, Q., Gerhardt, M. R., Hartle, L. & Aziz, M. J. A quinone-bromide flow battery with 1 W cm^{-2} power density. *J. Electrochem. Soc.* **163**, A5010–A5013 (2016).
- 31 Li, Z., Li, S., Liu, S., Huang, K., Fang, D., Wang, F. & Peng, S. Electrochemical properties of an all-organic redox flow battery using 2,2,6,6-tetramethyl-1-piperidinyloxy and N-methylphthalimide. *Electrochem. Solid State Lett.* **14**, A171–A173 (2011).
- 32 Brushett, F. R., Vaughey, J. T. & Jansen, A. N. An all-organic non-aqueous lithium-ion redox flow battery. *Adv. Energy Mater.* **2**, 1390–1396 (2012).
- 33 Yang, B., Hooper-Burkhardt, L., Wang, F., Surya Prakash, G. K. & Narayanan, S. R. An inexpensive aqueous flow battery for large-scale electrical energy storage based on water-soluble organic redox couples. *J. Electrochem. Soc.* **161**, A1371–A1380 (2014).
- 34 Kaur, A. P., Holubowitch, N. E., Ergun, S., Elliott, C. F. & Odom, S. A. A highly soluble organic catholyte for non-aqueous redox flow batteries. *Energy Technol.* **3**, 446–446 (2015).
- 35 Oh, S. H., Lee, C. W., Chun, D. H., Jeon, J. D., Shim, J., Shin, K. H. & Yang, J. H. A metal-free and all-organic redox flow battery with polythiophene as the electroactive species. *J. Mater. Chem. A* **2**, 19994–19998 (2014).
- 36 Duan, W., Vemuri, R. S., Milshtein, J. D., Laramie, S., Drmelio, R. D., Huang, J., Zhang, L., Hu, D., Vijayakumar, M., Wang, W., Liu, J., Darling, R. M., Thompson, L., Smith, K., Moore, J. S., Brushett, F. R. & Wei, X. A symmetric organic-based nonaqueous redox flow battery and its state of charge diagnostics by FTIR. *J. Mater. Chem. A* **4**, 5448–5456 (2016).
- 37 Rasmussen, P. G. Electrical Storage Device Vinazene Inc. (Ann Arbor, MI, USA, 2011).
- 38 Rychcik, M. & Skyllas-Kazacos, M. Characteristics of a new all-vanadium redox flow battery. *J. Power Sources* **22**, 59–67 (1988).
- 39 Osiecki, J. H. & Ullman, E. F. a-Nitronyl nitroxides, a new class of stable radicals. *J. Am. Chem. Soc.* **90**, 1078–1079 (1968).
- 40 Sukegawa, T., Kai, A., Oyaizu, K. & Nishide, H. Synthesis of pendant nitronyl nitroxide radical-containing poly(norbornene)s as ambipolar electrode-active materials. *Macromolecules* **46**, 1361–1367 (2013).

- 41 Lee, J., Lee, E., Kim, S., Bang, G. S., Shultz, D. A., Schmidt, R. D., Forbes, M. D. E. & Lee, H. Nitronyl nitroxide radicals as organic memory elements with both n- and p-type properties. *Angew. Chem. Int. Ed.* **50**, 4414–4418 (2011).
- 42 Ziesel, R., Ulrich, G., Lawson, C. R. & Echegoyen, L. Oligopyridine bis(nitronyl nitroxides): synthesis, structures, electrochemical, magnetic and electronic properties. *J. Mater. Chem.* **9**, 1435–1448 (1999).
- 43 Coronado, E., Gimenez-Saiz, C., Nicolas, M., Romero, F. M., Rusanov, E. & Stoeckli-Evans, H. Synthesis, crystal structures and electronic properties of imidazoline nitroxide radicals bearing active groups in electropolymerisation. *New J. Chem.* **27**, 490–497 (2003).
- 44 Nakano, Y., Yagyu, T., Hirayama, T., Ito, A. & Tanaka, K. Synthesis and intramolecular magnetic interaction of triphenylamine derivatives with nitronyl nitroxide radicals. *Polyhedron* **24**, 2141–2147 (2005).
- 45 Caneschi, A., Gatteschi, D., Lalioti, N., Sangregorio, C., Sessoli, R., Venturi, G., Vindigni, A., Rettori, A., Pini, M. G. & Novak, M. A. Cobalt(II)-nitronyl nitroxide chains as molecular magnetic nanowires. *Angew. Chem. Int. Ed.* **40**, 1760–1763 (2001).
- 46 Zhou, S. Y., Li, X., Li, T., Tian, L., Liu, Z. Y. & Wang, X. G. A series of heterospin complexes based on lanthanides and pyridine biradicals: synthesis, structure and magnetic properties. *RSC Adv.* **5**, 17131–17139 (2015).
- 47 Li, L.-L., Liu, S., Zhang, Y., Shi, W. & Cheng, P. Three new mononuclear tri-spin lanthanide-nitronyl nitroxide radical compounds: syntheses, structures and magnetic properties. *Dalton Trans.* **44**, 6118–6125 (2015).
- 48 Suga, T., Sugita, S., Ohshiro, H., Oyaizu, K. & Nishide, H. p- and n-Type bipolar redox-active radical polymer: toward totally organic polymer-based rechargeable devices with variable configuration. *Adv. Mater.* **23**, 751–754 (2011).
- 49 DDBST GmbH http://www.ddbst.com/en/EED/PCP/VSK_C3.php Accessed on 10 August 2016.
- 50 Hirel, C., Vostrikova, K. E., Pécaut, J., Ovcharenko, V. I. & Rey, P. Nitronyl and Imino nitroxides: improvement of ullman's procedure and report on a new efficient synthetic route. *Chem. Eur. J.* **7**, 2007–2014 (2001).
- 51 Wang, W. & Li, A. D. Q. Design and synthesis of efficient fluorescent dyes for incorporation into DNA backbone and biomolecule detection. *Bioconjugate Chem.* **18**, 1036–1052 (2007).
- 52 Ullman, E. F., Call, L. & Osiecki, J. H. Stable Free radicals. VIII. New imino, amidino, and carbamoyl nitroxides. *J. Org. Chem.* **36**, 3623–3631 (1970).
- 53 Ullman, E. F., Osiecki, J. H., Boockcock, D. G. B. & Darcy, R. Studies of stable free radicals. X. Nitronyl nitroxide monoradicals and biradicals as possible small molecule spin labels. *J. Amer. Chem. Soc.* **94**, 7049–7059 (1972).
- 54 Dulog, L. & Kim, J. S. Stable free radical paramagnetic monomers containing aminoxylamine oxide moieties. An intermediate step toward organic ferromagnetic polyradicals. *Die Makromol. Chem.* **190**, 2609–2614 (1989).
- 55 Nishide, H., Hozumi, Y., Nii, T. & Tsuchida, E. Poly(1,2-phenylenevinylene)s bearing nitronyl nitroxide and galvinoxyl at the 4-position: π -conjugated and non-kekulé-type polyradicals with a triplet ground state. *Macromolecules* **30**, 3986–3991 (1997).
- 56 Su, L., Ferrandon, M., Kowalski, J. A., Vaughey, J. T. & Brushett, F. R. Electrolyte development for non-aqueous redox flow batteries using a high-throughput screening platform. *J. Electrochem. Soc.* **161**, A1905–A1914 (2014).
- 57 Zhang, S., Li, X. & Chu, D. An organic electroactive material for flow batteries. *Electrochim. Acta* **190**, 737–743 (2016).



This work is licensed under a Creative Commons Attribution 4.0 International License. The images or other third party material in this article are included in the article's Creative Commons license, unless indicated otherwise in the credit line; if the material is not included under the Creative Commons license, users will need to obtain permission from the license holder to reproduce the material. To view a copy of this license, visit <http://creativecommons.org/licenses/by/4.0/>

© The Author(s) 2017

Supplementary Information accompanies the paper on the NPG Asia Materials website (<http://www.nature.com/am>)

Bipolar Nitronyl Nitroxide Small-Molecule for an All-Organic Symmetric Redox-Flow Battery

Tino Hagemann^{ab}, Jan Winsberg^{ab}, Bernhard Häupler^{ab}, Tobias Janoschka^{ab}, Jeremy J. Gruber^c, Andreas Wild^{ab}, Ulrich S. Schubert^{ab,*}

^a Laboratory of Organic and Macromolecular Chemistry (IOMC), Friedrich Schiller University Jena, Humboldtstrasse 10, 07743 Jena, Germany

E-mail: ulrich.schubert@uni-jena.de

^b Center for Energy and Environmental Chemistry Jena (CEEC Jena), Friedrich Schiller University Jena, Philosophenweg 7a, 07743 Jena, Germany

[#] Current address: Department of Chemical Engineering, 158 Fenske Laboratory, The Pennsylvania State University, University Park, PA 16802

EXPERIMENTS

Electrochemical characterization

The radical content of **4** was determined *via* X-Band electron paramagnetic resonance (EPR) spectroscopy. The measurements were conducted on an EMXmicro CW-EPR spectrometer from Bruker using powdered samples as well as 10^{-4} M solutions in toluene. Samples were investigated at room temperature and data handling was done on the Bruker Xenon software package, version 1.1b86. The SpinCount™ software module was used for quantitative measurements. The spectrometer was calibrated using TEMPO (99% (HPLC) purity, Sigma-Aldrich Chemie GmbH) as a reference standard. The total spin count provided in this contribution is the average of four measurements. Cyclic voltammetry (CV) and rotating disc electrode (RDE) measurements were conducted on a Model SP-50 potentiostat/galvanostat (Bio-Logic, France), with a glassy carbon disc electrode (diameter 5 mm), an AgNO₃/Ag reference electrode for organic-based electrolytes and a platinum wire counter electrode. The rotation speed was controlled externally by a Model CTV 101 ring-disk electrode system (Radiometer analytica, France). Evaluation of the RDE analysis *via* Levich plot (limiting current i_{lim} vs. square root of rotation speed ω) yields the diffusion coefficient D by using Levich equation, $i_{lim} = 0.62nFAD^{\frac{2}{3}}\omega^{\frac{1}{2}}\nu^{-\frac{1}{6}}c_0$, with $n = 1$, Faraday's constant $F = 96,485$ C mol⁻¹, electrode surface of 0.2 cm², the solutions kinematic viscosity $\nu = 4.48 \times 10^{-7}$ m² s⁻¹ at 298.3 K¹ and the bulk concentration c_0 of the redox-active nitronyl nitroxide units.

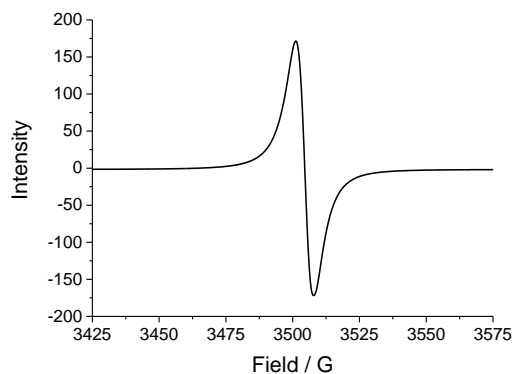


Figure S1. EPR spectrum of **4** in solid state. In contrast to the spectrum measured in 10^{-4} M toluene solution (**Figure 1a**), the powder spectrum displays only a single line without hyperfine structure due to the high concentration of the nitronyl nitroxide radicals and the resulting line broadening.

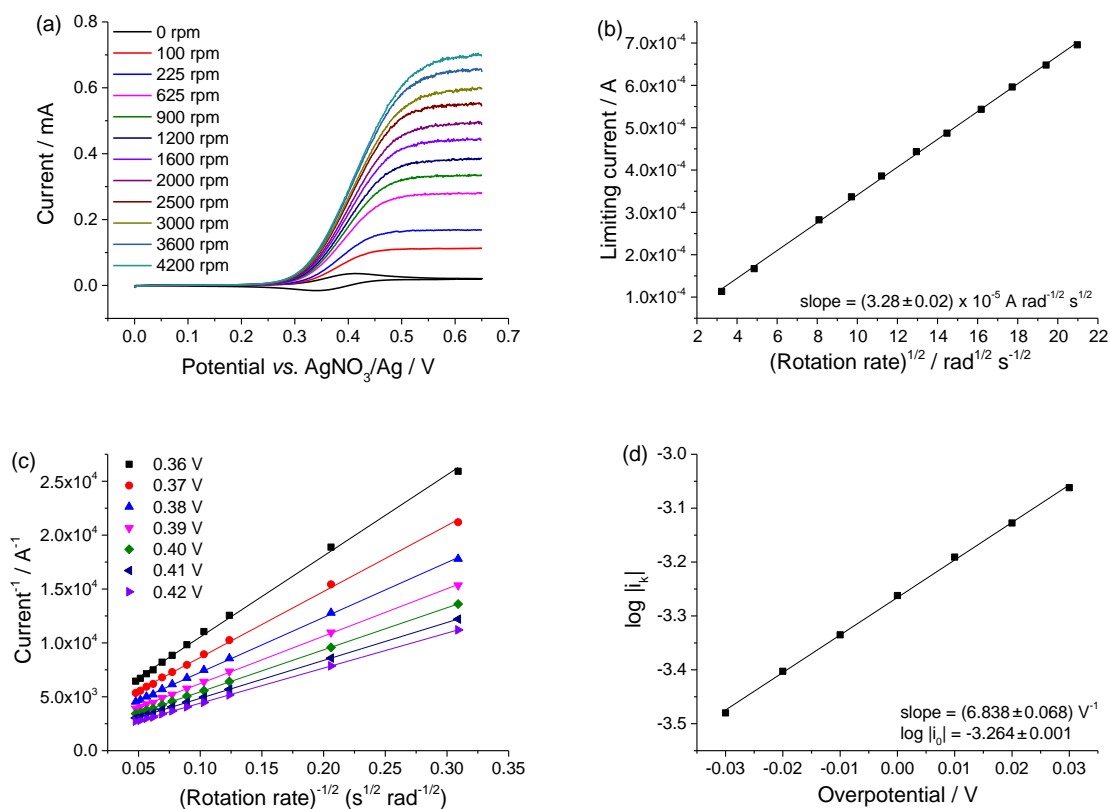


Figure S2: (a) Rotating disk electrode measurement of **4** (2×10^{-3} mol L $^{-1}$), 0.1 M TBAPF $_6$ in acetonitrile, scan rate 5 mV s $^{-1}$, at rotating rates from 0 to 4200 rpm, (b) Levich-plot from the obtained limiting currents at 650 mV vs. AgNO $_3$ /Ag; application of Levich-equation yields a diffusion coefficient $D = 4.74 \times 10^{-6}$ cm 2 s $^{-1}$, (c) Koutecký-Levich plot for different overpotentials yielding the mass-transfer-independent current i_k , (d) Tafel plot yielding $k_0 = 1.42 \times 10^{-2}$ cm s $^{-1}$ and $\alpha = 0.59$.

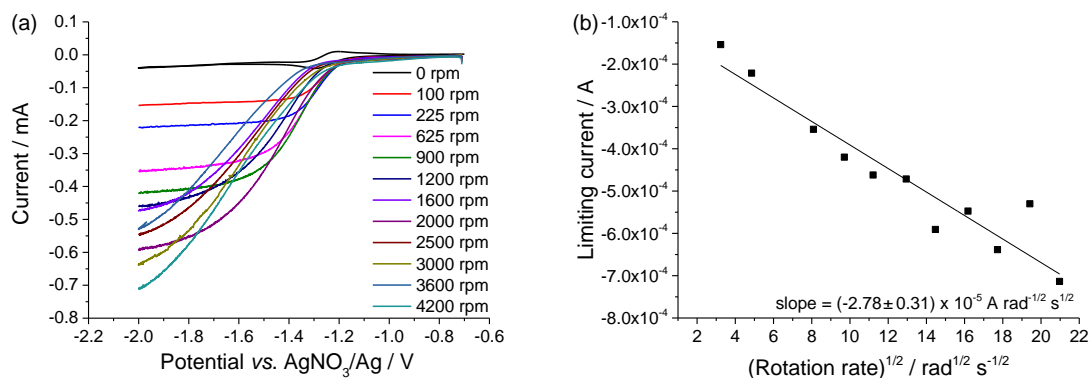


Figure S3:(a) Rotating disk electrode measurement of **4** ($2.1 \times 10^{-3} \text{ mol L}^{-1}$), 0.1 M TBAPF₆ in acetonitrile, scan rate 5 mV s^{-1} , at different rotating rates from 0 to 4200 rpm, (b) Levich-plot from the obtained limiting currents at 2000 mV vs. AgNO_3/Ag ; application of Levich-equation yields a diffusion coefficient $D = 3.45 \times 10^{-6} \text{ cm}^2 \text{ s}^{-1}$.

BATTERIE TESTS

Cell assembly

The static laboratory cell was designed and constructed in a flat cell type with a membrane active area of 5 cm^2 (JenaBatteries GmbH, Germany). See **Figure S4** for a detailed overview. The graphite felt ($2.25 \times 2.25 \times 0.4 \text{ cm}^3$, sigracell® GFA6 EA, SGLCarbon, Germany), as well as the anion-exchange membrane fumasep® FAP-PK-3130 (FuMA-Tech, Germany) were cut into appropriate pieces. Electrochemical impedance spectroscopy (EIS) and charge/discharge tests were conducted on a VMP3 potentiostat/galvanostat (Bio-Logic, France). To study the impact of the current density on the battery performance, dynamic measurements were performed. The electrolyte was circulated between the electrochemical cell and the storage tanks with a peristaltic pump (Hei-FLOW Value 01 Multi, Heidolph, Germany). Typically, 4 or 10 mL of electrolyte were used with a flow rate of 10 mL min^{-1} . All measurements were carried out at 25°C under argon atmosphere in a glove box. The batteries were charged/discharged with constant current and the resulting potential was measured over time. Cut-off voltages of 1.10 V and 1.95 V were employed.

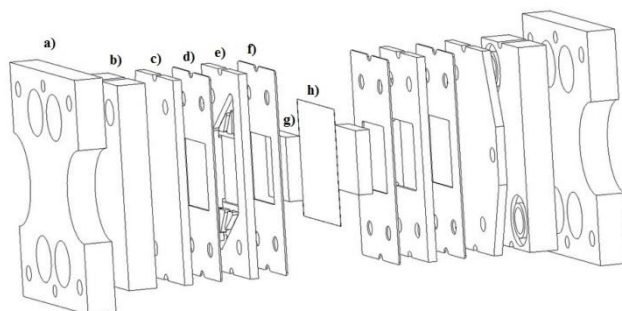


Figure S4: Schematic representation of the 5 cm^2 test cell. One half-cell consists of a frame a), PTFE block with hose connections and rubber seal b), graphite current collector c), Teflon sealing d), PTFE flow frame e), Teflon sealing f), surface enhancing graphite felt g). Both half cells are separated by an anion-exchange membrane h).

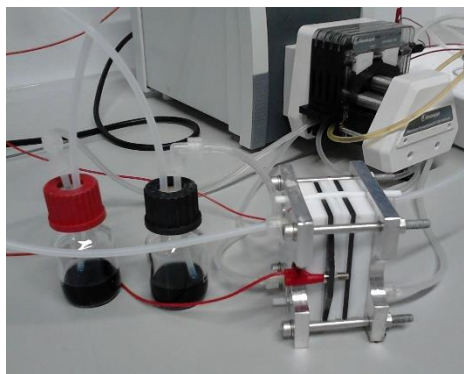


Figure S5: Photograph of a laboratory RFB (5 cm²), comprising the electrochemical cell, two reservoir tanks and a peristaltic pump, used for charge/discharge experiments.

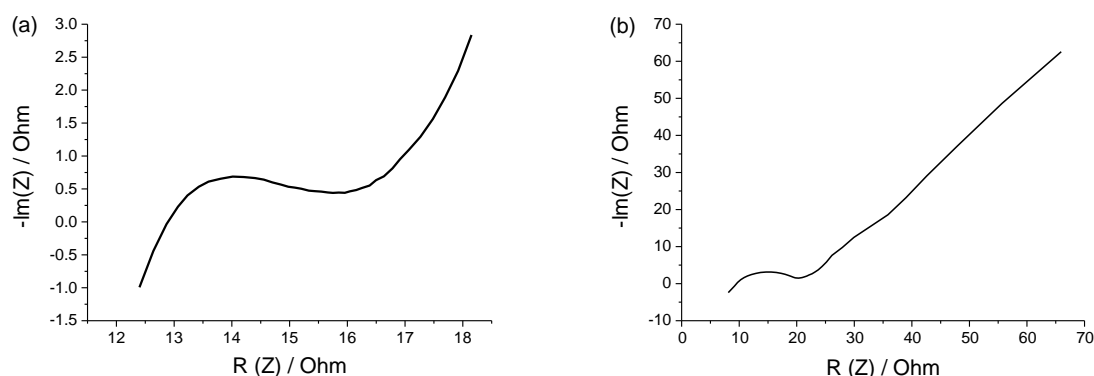


Figure S6: Nyquist plot of an electrochemical impedance spectroscopy (EIS) measurement of a pumped 5 cm² test cell with 0.1 M **4**, 0.5 M TBAPF₆ in acetonitrile, (a) between 100 MHz and 200 kHz at 0 V in potentiostatic mode prior cycling, (b) between 100 MHz and 400 kHz at 0 V in potentiostatic mode after cycling.

As example, the area-specific resistance of the pumped flow cell with 0.1 mM **4**, 0.5 M TBAPF₆ in acetonitrile before and after cycling was calculated. With a cell area of 5 cm² the area-specific resistance before the cycling is 2.58 Ohm and after cycling 1.91 Ohm. The decrease of the cell resistance is caused by the fact that the utilized membrane needs some time to reach the ideal operational conditions.

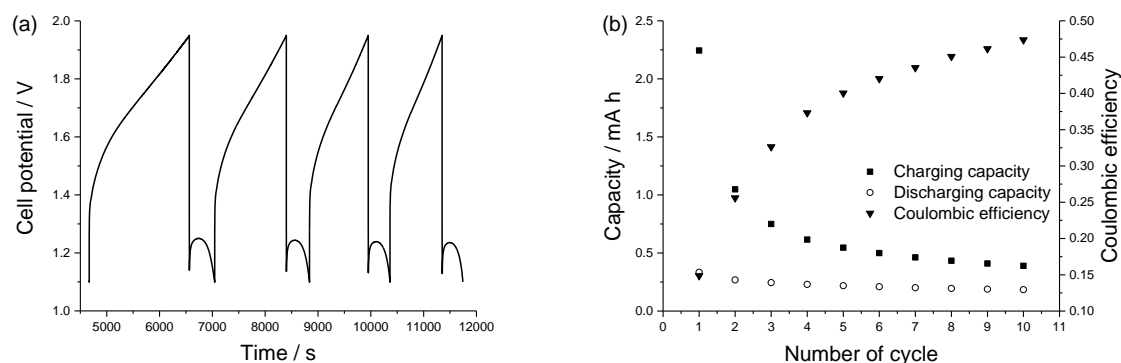


Figure S7: Charge/discharge experiments in a pumped RFB test cell with 0.5 M **4**, 1.13 M TBAPF₆ in acetonitrile, (a) exemplary 2nd to 5th charge/discharge cycle at a current density of 0.4 mA cm⁻², (b) charge and discharge capacity and coulombic efficiency at a current density of 0.4 mA cm⁻² over 10 charge/discharge cycles. At this high active material concentration the charged species precipitated in the graphite felts, impairing the material transport and finally impeding the discharging process.

CALCULATION OF THE ACTIVE MATERIAL COSTS

The utilized bipolar organic charge-storage material was obtained in four synthesis steps. The starting material 2,3-dimethyl-2,3-dinitrobutane can be purchased at prices in the range of \$1 to 5 per kg, 1-chloro-2-[2-[2-(2-chloroethoxy)ethoxy]ethoxy]ethane for \$1 per kg and the 4-hydroxybenzaldehyde for \$0.1 per kg. All wholesale prices were obtained from Alibaba.com for a purchase at industrial scale. In the following synthesis steps further materials were used: Tin for \$10 per kg, hydrochloric acid for \$0.2 per kg, K_2CO_3 for \$0.82 per kg, DMF for \$0.65 per kg, THF for \$1 per kg, CH_2Cl_2 for \$0.35 per kg, *m*-chloroperbenzoic acid for \$0.09 per kg, $NaHCO_3$ for \$0.18 per kg and $NaIO_4$ for \$0.5 per kg. In combination with an addition of 20% for the incidental synthesis cost and a cell voltage of 1.53 V costs of the active material of \$725 per kW h is determined, which is significantly higher than the price of \$81 kW h for the vanadium systems.² However, the calculated price for the active material **4** can be reduced considerably through an optimized synthesis route and the utilization of cheaper materials. For example to synthesize the diamino compound **1**, 2,3-dimethyl-2,3-dinitrobutane was completely reduced with Sn/conc. HCl. With the high tin price (\$10 per kg) in mind catalytic hydrogenation or other reducing agents, like Zn (\$3 per kg), iron(III)acetylacetonate (\$1 per kg) or hydrazine hydrate (\$1 to 1.8 per kg) may be used for a scale up.

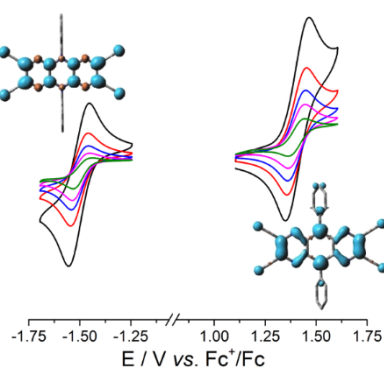
REFERENCES

1. DDBST GmbH. http://www.ddbst.com/en/EED/PCP/VSK_C3.php. Accessed 10 August 2016.
2. Huskinson, B., Marshak, M. P., Suh, C., Er, S., Gerhardt, M. R., Galvin, C. J., Chen, X., Aspuru-Guzik, A., Gordon, R. G., Aziz, M. J. A metal-free organic-inorganic aqueous flow battery. *Nature* **505**, 195-198 (2014).

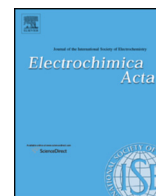
Publication P3

Synthesis and electrochemical study of a TCAA derivative – A potential bipolar redox-active material

T. Hagemann, J. Winsberg, A. Wild, U. S. Schubert,
Electrochim. Acta. **2017**, 228, 494-502.



Reproduced with permission of Elsevier, Copyright © 2017.



Synthesis and Electrochemical Study of a TCAA Derivative – A potential bipolar redox-active material



Tino Hagemann^{a,b}, Jan Winsberg^{a,b}, Andreas Wild^{a,b}, Ulrich S. Schubert^{a,b,*}

^a Laboratory of Organic and Macromolecular Chemistry (IOMC), Friedrich Schiller University Jena, Humboldtstraße 10, 07743 Jena, Germany

^b Center for Energy and Environmental Chemistry Jena (CEEC Jena), Friedrich Schiller University Jena, Philosophenweg 7a, 07743 Jena, Germany

ARTICLE INFO

Article history:

Received 30 September 2016

Received in revised form 21 December 2016

Accepted 10 January 2017

Available online 11 January 2017

Keywords:

Bipolar redox-active

2,3,7,8-tetracyano-1,4,5,6,9,10-hexazaanthracene

ABSTRACT

The 2,3,7,8-tetracyano-1,4,5,6,9,10-hexazaanthracene (TCAA) derivatives represent an interesting substance class for future research on organic electronic devices, such as solar cells, organic batteries or redox-flow batteries (RFBs). Because of their multivalent redox behavior they are potentially “bipolar”, usable both as cathode and anode active charge-storage materials. Furthermore, they show a strong absorption and fluorescence behavior both in solution and solid state, rendering them a promising emitter for electroluminescence devices, like lamps or displays. In order to evaluate a TCAA for electrochemical applications the derivative 2,3,7,8-tetracyano-5,10-diphenyl-5,10-dihydrodipyrzino [2,3-*b*:2',3'-*e*]pyrazine (**2**) was synthesized in two straightforward synthesis steps. The electrochemical behavior of **2** was initially determined by density functional theory (DFT) calculation and afterwards investigated via rotating disc electrode (RDE), UV–vis–NIR spectroelectrochemical as well as cyclic voltammetry (CV) measurements. It features a quasi-reversible oxidation and re-reduction at $E_{1/2} = 1.42$ V vs. Fc^+/Fc with a peak split of 96 mV and a quasi-reversible reduction and re-oxidation at $E_{1/2} = -1.49$ V vs. Fc^+/Fc with a peak split of 174 mV, which lead to a theoretical potential difference of 2.91 V.

© 2017 Elsevier Ltd. All rights reserved.

1. Introduction

As a direct consequence of the climate change the general energy production is shifting to ‘greener’ and more sustainable sources, such as geothermal and solar energy, hydroelectricity and wind power [1–4]. Because of several disadvantages and the restriction to certain geographical circumstances hydroelectricity and geothermal energy are inferior in comparison to solar energy and wind power, which seem to be the most promising candidates to meet the global energy demand in the future [5–8]. However, to render the “Energiewende” an adjusted electricity grid combining renewable power sources and energy storage systems is essential [4,9]. Among all possible storage technologies, in particular redox-flow batteries seem to be tailor-made for the storage of wind and solar electricity. They can be independently scaled in capacity as well as in power—in contrast to most other electrochemical energy-storage technologies—and furthermore precisely adjusted to the generator unit [4]. State-of-the-art RFBs, like the

commercially available and well investigated all-vanadium [10–13] and Fe/Cr [14–17] RFBs systems utilize toxic and expensive metal salts and corrosive acidic electrolytes as well as commonly high-cost cation-exchange membranes like NafionTM [18–21]. Due to the high environmental impact as well as the economical aspects metal-based RFBs will most likely not be a profound energy-storage solution. Therefore, the development of organic RFBs, which utilize low cost and sustainable redox-active charge-storage materials, water-based electrolyte systems as well as inexpensive membranes, can overcome these obstacles and enabling a competitive electrochemical energy-storage technology [19,22–25].

As a consequence, current research in this field is focused on the investigation and evaluation of several redox-active materials as potential charge-storage materials. Among others, the substance class TCAA is, due to the reported electrochemical reversibility and in particular due to their high voltage between the oxidation and reduction reactions, highly interesting for the application both as cathode as well as anode active material in organic RFBs. The electrochemical properties can easily be adjusted by the introduction of functional groups and, furthermore, the solubility of these derivatives can be enhanced by the introduction of solubility promoting substituents during the two-step synthesis.

* Corresponding author at: Laboratory of Organic and Macromolecular Chemistry (IOMC), Friedrich Schiller University Jena, Humboldtstraße 10, 07743 Jena, Germany.

E-mail address: ulrich.schubert@uni-jena.de (U.S. Schubert).

The multivalent, redox-active 2,3,7,8-tetracyano-1,4,5,6,9,10-hexazaanthracenes (TCAAs) were first mentioned in 1993 by Matsuoka et al. [26] and investigated in more detail in 1997 by Jaung et al. [27]. Beside first incomplete electrochemical investigations via cyclic voltammetry, Jaung and co-workers [27] studied the electronic properties of several 2,3,7,8-tetracyano-1,4,5,6,9,10-hexazaanthracene derivatives using UV–vis spectroscopy and the Pariser–Parr–Popel molecular orbital calculation method. Due to the reported reversibility of the redox reaction and the high potential difference between oxidation and reduction, the TCAA derivatives represent highly interesting materials for the potential application in symmetric electrochemical energy-storage devices. In addition, this substance class features a chromophoric system in solution, with a strong intramolecular charge-transfer (Fig. 1), in which the amino groups act as donor and the two dicyanopyrazine rings as acceptor moieties. Consequently, they possess a strong fluorescence in solution and for several derivatives also in the solid state, potentially caused by aggregation-induced emission whereby due to an aggregate formation a higher photoemission efficiency of faint luminescent chromogens is induced [28], making them potential candidates as emitter for electroluminescence devices, such as organic light emitting diodes (OLEDs) [27].

Furthermore, cyanoheteroaromatics are known as drug intermediates [29–31], as materials of pharmaceutical interest [32,33], or precursors for the synthesis of thermally stable and oxidation-resistant polymers [34] as well as nonlinear optical materials [35,36].

To evaluate the substance class of TCAAs as potential charge storage materials for the application in electrochemical energy-storage devices like RFBs, the known 2,3,7,8-tetracyano-5,10-diphenyl-5,10-dihydrodipyrazino[2,3-*b*:2',3'-*e*]pyrazine (**2**, Fig. 2) was synthesized with slight modifications according to literature procedures [26,27]. The presence of two individual redox pairs of TCAA derivatives render these an interesting potential material for symmetric battery applications.

Density functional theory (DFT) calculations of compound **2** and an electrochemically characterization via cyclic voltammetry (CV), rotating disc electrode (RDE) and UV–vis–NIR spectroelectrochemical measurements were performed.

2. Experimental part

2.1. Materials and chemicals

All starting materials were purchased from commercial sources and were used as obtained.

2.2. Methods

Reactions were monitored by thin-layer chromatography (TLC) on 0.2 mm Merck Millipore (Germany) silica gel plates (60 F254) and by GC–MS using a Shimadzu (Japan) GCMS-1-system with a

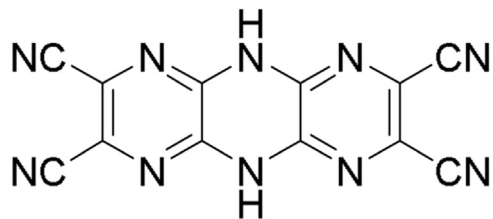


Fig. 1. Schematic representation of chemical structure of 2,3,7,8-tetracyano-5,10-dihydrodipyrazino[2,3-*b*:2',3'-*e*]pyrazine, the fundamental structure of the 2,3,7,8-tetracyano-1,4,5,6,9,10-hexazaanthracene derivatives.

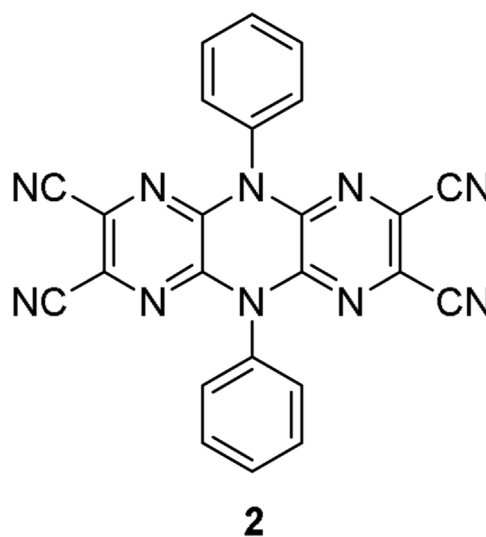


Fig. 2. Schematic representation of the chemical structure of 2,3,7,8-tetracyano-5,10-diphenyl-5,10-dihydrodipyrazino[2,3-*b*:2',3'-*e*]pyrazine (**2**).

GC–QP2010S-detector and an Agilent (USA) DB-5ms-column. Column chromatography was performed on silica gel 60 (Macherey–Nagel, Germany). ^1H and ^{13}C NMR spectra were recorded on a AC 300 (300 and 75 MHz; Bruker, USA) spectrometer at 298 K. Chemical shifts are reported in parts per million (ppm, δ scale) relative to the residual signal of the deuterated solvent. Elemental analyses were carried out using a Vario ELIII-Elementar Euro (Elementar, Germany) and an EA-HekaTech (HekaTech GmbH, Germany). Electrospray ionization mass spectrometry (ESI–MS) measurements were performed on a microTOF (Bruker, USA) electrospray ionization time-of-flight (ESI–TOF) system.

2.3. Synthesis of 2,3,7,8-tetracyano-5,10-diphenyl-5,10-dihydrodipyrazino[2,3-*b*:2',3'-*e*]pyrazine (**2**)

2.3.1. 2-Anilino-3-chloro-5,6-dicyanopyrazine (1) was prepared with slight modifications according to the procedure by Jaung et al. [27]

Under argon atmosphere 2,3-dichloro-5,6-dicyanopyrazine (6.18 g, 31.24 mmol) was dissolved in dry THF (65 mL). The solution was cooled to 0 °C in an ice bath, and aniline (5.71 mL, 62.49 mmol), diluted in dry THF (15 mL), was added dropwise. Subsequently, the reaction mixture was allowed to reach room temperature and stirred for 4 h, till TLC showed a complete conversion of the starting material. The solution was poured into 700 mL deionized water. The formed solid was filtered off and washed carefully with deionized water (five times, each 100 mL) to obtain **1** as a white solid (7.91 g, 30.99 mmol) in a yield of 99.2%. ^1H NMR (300 MHz, DMSO- d_6 , δ): 10.23 (s, 1H, NH), 7.56 (d, J = 6 Hz, 2H, Ar H), 7.45 (t, J = 7 Hz, 2H, Ar H), 7.27 (t, J = 7 Hz, 1H, Ar H); ^{13}C NMR (75 MHz, DMSO- d_6 , δ): 149.95 (CNH), 138.26 (CNH), 136.69 (CCI), 130.20 (CCN), 128.80 (CC), 126.07 (CC), 123.71 (CC), 118.17 (CCN), 114.15 (CN), 113.84 (CN); HRMS (ESI) m/z : $[\text{M} + \text{Na}]^+$ calcd. for $\text{C}_{12}\text{H}_6\text{ClN}_5$, 278.0204; found, 278.0204; Anal. calcd. for $\text{C}_{12}\text{H}_6\text{ClN}_5$: C 56.38; H 2.37; Cl 13.87; N 27.39; found: C 56.52; H 2.39; Cl 13.61; N 27.20.

2.3.2. The synthesis of compound 2 was carried out following **a**) a method by Jaung et al. with slight modifications [27]

Compound **1** (5 g, 19.56 mmol) was dissolved in DMF (100 mL) and heated up to 140 °C. Triethylamine (6.78 mL, 48.89 mmol) was added dropwise and the solution was stirred at this temperature. After 8 h, once the TLC monitoring showed no further changes, the reaction mixture was cooled to room temperature and poured into a 1 M hydrochloride acid solution (300 mL). The formed solid was

removed and carefully washed with 1 M hydrochloride acid solution as well as deionized water (25 mL, each three times). The brown crude product was purified *via* column chromatography (SiO₂; ethyl acetate/*n*-heptane, 2:1) and afterwards recrystallized from a mixture of ethyl acetate/*n*-heptane (2:1) to obtain the pure yellowish product **2** (2.91 g, 6.65 mmol) in a yield of 34%. ¹H NMR (300 MHz, DMSO-*d*₆, δ): 7.66 (t, *J* = 7.5 Hz, 4H, Ar H), 7.56 (t, *J* = 7.5 Hz, 2H, Ar H), 7.35 (d, *J* = 7.5 Hz, 2H, Ar H); ¹³C NMR (75 MHz, DMSO-*d*₆, δ): 146.11 (ArCCN), 133.06 (NCN), 130.43 (ArC), 129.76 (ArC), 128.10 (ArC), 124.61 (CCN), 113.78 (CN); ESI-TOF MS *m/z* (%): 899.19 (100) [2 M⁺ + Na], 461.16 (65) [M⁺ + Na]; HRMS (ESI) *m/z*: [M + Na]⁺ calcd. for C₂₄H₁₀N₁₀, 461.0982; found, 461.0974.

2.3.3. Synthesis of compound **2** by the alternate method **b**) [37]

Compound **1** (0.44 g, 1.71 mmol) was dissolved in 1-methoxy-2-(2-methoxyethoxy)ethane (diglyme, 8.5 mL). *N,N*-Diisopropylethylamine (DIPEA, 0.64 mL, 3.76 mmol) was added dropwise and the solution was stirred for 12 h under reflux. Afterwards the reaction mixture was cooled to room temperature and poured into a 1 M hydrochloride acid solution (100 mL). The suspension was centrifugated and the formed solid was washed with 1 M hydrochloride acid solution and deionized water (15 mL, each three times). The brown crude product was purified *via* column chromatography (SiO₂; ethyl acetate/*n*-heptane, 2:1) to obtain compound **2** (0.1 g, 0.25 mmol) in a yield of 15%. ¹H NMR (300 MHz, DMSO-*d*₆, δ): 7.66 (t, *J* = 7.8 Hz, 4H, Ar H), 7.56 (t, *J* = 7.2 Hz, 2H, Ar H), 7.35 (d, *J* = 7.2 Hz, 2H, Ar H); ¹³C NMR (75 MHz, DMSO-*d*₆, δ): 146.10 (ArCCN), 133.05 (NCN), 130.42 (ArC), 129.75 (ArC), 128.09 (ArC), 124.60 (CCN), 113.77 (CN).

2.4. Electrochemical measurements

2.4.1. Electrochemical characterization

Cyclic voltammetry (CV) was conducted on a VMP3 potentiostat/galvanostat (Bio-Logic, France). For CV measurements, a standard three-electrode setup with a glassy-carbon disk working electrode (diameter 2 mm), AgNO₃/Ag reference electrode and a platinum wire counter electrode was utilized. Because the peak current *i_p* grows linearly with the square root of the scan rate, the diffusion coefficient *D* was calculated from the measured CV curves using Randles-Sevcik equation, $i_p = 0.4463nFAC(nFvD)^{1/2}(RT)^{-1/2}$, with *n* = 1, Faraday's constant *F* = 96,485 C mol^{−1}, electrode surface *A* = 0.0078 cm², the bulk concentration *c* of the redox-active TCAA derivative **2** at a temperature *T* = 298.3 K and the gas constant *R* = 8.314 J K^{−1} mol^{−1}.

UV–vis–NIR spectroelectrochemical experiments were performed in a quartz cuvette containing a platinum grid working electrode, a platinum wire auxiliary electrode and a AgNO₃/Ag reference electrode. The potential was controlled using a VMP3 potentiostat/galvanostat (Bio-Logic, France). The redox process

was monitored by UV–vis spectroscopy using a PerkinElmer (USA) Lambda 750 UV–vis–NIR spectrophotometer and considered complete when there was no further spectral change.

Rotating disc electrode (RDE) measurements were conducted on a Model SP-50 potentiostat/galvanostat (Bio-Logic, France), with a glassy-carbon tip (diameter 5 mm), an AgNO₃/Ag reference electrode and a platinum wire counter electrode. The rotation speed was controlled externally by a Model CTV 101 ring-disk electrode system (Radiometer analytical, Hach, USA). Evaluation of the RDE analysis *via* Levich plot (limiting current *i_{lim}* vs. square root of rotation speed ω) yields the diffusion coefficient *D* by using Levich equation, $i_{lim} = 0.62nFAD^{2/3}\omega^{1/2}\nu^{-1/6}c_0$, with *n* = 1, Faraday's constant *F* = 96,485 C mol^{−1}, electrode surface *A* = 0.2 cm², the solutions kinematic viscosity ν = 4.48 × 10^{−7} m² s^{−1} at 298.3 K [38] and the bulk concentration *c*₀ of the bipolar redox-active TCAA derivative **2**.

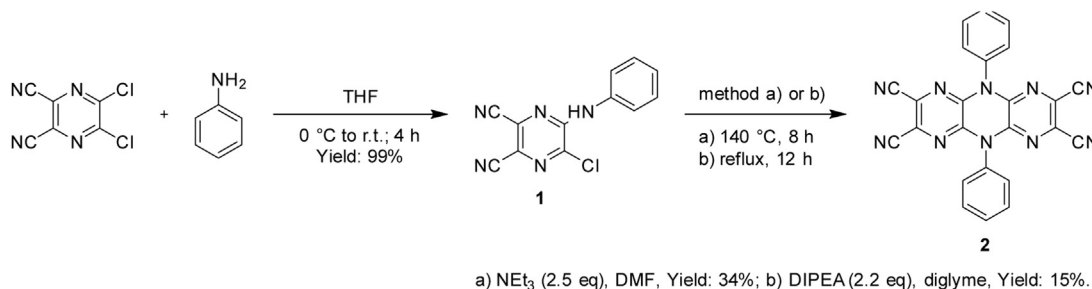
3. Results and discussion

3.1. Synthesis of compound **2**

The two-step synthesis of 2,3,7,8-tetracyano-5,10-diphenyl-5,10-dihydrodipyrazino[2,3-*b*:2',3'-*e*]pyrazine (**2**, Scheme 1) as well as other 2,3,7,8-tetracyano-1,4,5,6,9,10-hexazaanthracene derivatives was described in detail by Juang and coworkers [27].

The inexpensive and commercially available starting material 2,3-dichloro-5,6-dicyanopyrazine undergoes a nucleophilic substitution reaction, in which, depending on the molar ratio, one (two equivalents of amines) or both (four equivalents of amines) chlorine atoms are replaced. By adding two equivalents of an amine to the starting compound, the monosubstituted 2-arylamino-3-chloro-5,6-dicyanopyrazines can be synthesized [26,27]. Finally, through a subsequent intermolecular cyclization of the 2-arylamino-3-chloro-5,6-dicyanopyrazine a 5,10-disubstituted-2,3,7,8-tetracyano-5,10-dihydrodipyrazino[2,3-*b*:2',3'-*e*]pyrazine can be synthesized [27].

Compound **1** was obtained in a high yield above 99% by adding two equivalents of aniline dropwise to an ice-cooled solution (~0 °C) of 2,3-dichloro-5,6-dicyanopyrazine in THF (Scheme 1). The multivalent, redox-active 2,3,7,8-tetracyano-5,10-diphenyl-5,10-dihydrodipyrazino[2,3-*b*:2',3'-*e*]pyrazine (**2**) could be prepared in moderate yields of 34% and 15%, respectively, *via* an intermolecular cyclization of the 2-arylamino-3-chloro-5,6-dicyanopyrazine in two different methods (Scheme 1): a) With DMF as solvent and triethylamine (2.5 eq) as base as well as b) with bis(2-methoxyethyl) ether (diglyme) as solvent and *N,N*-diisopropylethylamine (DIPEA) (2.2 eq) as base. Due to the less expensive chemicals and the higher obtained yield, method a) was chosen for further investigations and a scale-up.



Scheme 1. Schematic representation of the two-step synthesis route to molecule **2**.

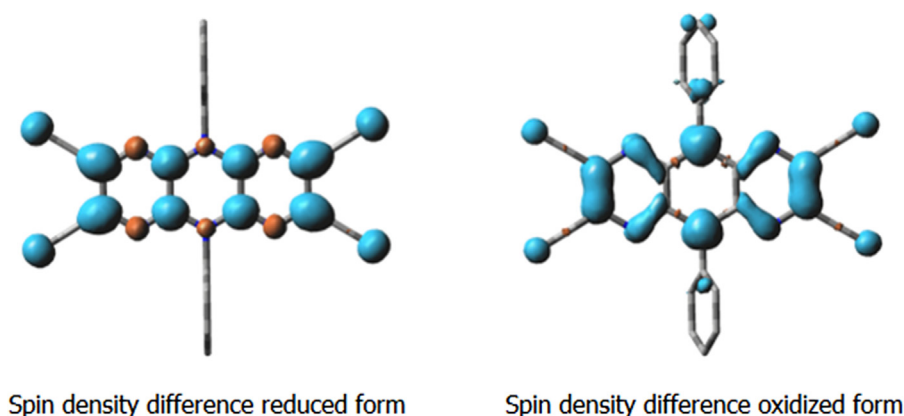


Fig. 3. Schematic representation of the spin density difference of the reduced species (left) and the oxidized species (right), drawn at an isovalue of 0.002, which were determined by DFT using the Gaussian09 program package (Version A.02) [39]. The hybrid functional B3LYP [40,41] was selected in combination with the 6-31G* basis set. For all calculation, the solvent environment was modelled for acetonitrile using the implemented polarization continuum model (PCM) [42,43].

3.2. Density functional theory (DFT) calculation and electrochemical behavior of **2**

To the best of our knowledge, the electrochemical properties of 2,3,7,8-tetracyano-1,4,5,6,9,10-hexazaanthracene derivatives are, up to now, only studied by basic CV measurements, only of the reduction reaction. Jaung et al. [27] investigated this redox reaction of a few TCAA derivatives and reported reversible electrochemical properties with a reduction potential in the range of -1.30 to -1.34 V (depending on the substituent) vs. Ag^+/Ag [27].

To receive an initial understanding of the structure of **2** in its oxidized and reduced form (Figs. 3, S7 and S8), as well as its redox potentials, density functional theory (DFT) calculations were performed (detailed description in the Supporting information).

As indicated in Fig. 3 the spin density of both redox states is in each case spread over major areas of the whole molecule, which is an indication that both redox species are relatively stable, since no position in the molecule should reveal an increased reactivity due to a high or low spin density. This behavior is beneficial in view of a potential application as charge-storage material. In other schematic representations such as in Fig. S7, where the spin density difference of the reduced species (left) and the oxidized species (right), mapped with H-atoms, was drawn at an isovalue of 0.008 and Fig. S8, where the spin density difference of the reduced species (left) and the oxidized species (right) was drawn at an isovalue of 0.005 with the electrostatic potential (-0.3 to 0.3) mapped onto the total density, a more accurate distribution of the spin density becomes apparent. The spin density is relatively evenly spread over the carbon atoms of the three fused pyrazine rings in the spin density difference reduced form (Fig. S8, left) as well as the four nitrile groups, which indicates as we mentioned above essentially a stabilization of this redox species. However, there is a probability of a radical recombination, which counteracting the stability. On the other hand, the spin density in the spin density difference oxidized form (Fig. S8, right) is also delocalized over the three fused pyrazine rings, but with an emphasis on the six nitrogen atoms, in particular (the probability is twice as high) on the two central nitrogen atoms. This behavior indicates a good stability of this redox state, because a nucleophilic attack is only possible on these positions, which are sterically shielded. Furthermore, the formal absolute redox potential of both redox-couples were calculated from the difference in energy (including zero-point vibrational energy), i.e. the formal oxidation were calculated between S_0 and D^+ (-6.09 V), and S_0 and D^- (-3.28 V). The absolute potentials were referenced vs. the calculated potentials of Fc^+/Fc in acetonitrile (-4.57 V) according to Batista

and coworkers, i.e. on the basis of the absolute SHE potential (-4.60 V), and the calculated potential of Fc^+/Fc vs. SHE ($+0.51$ V) and the systematic offset caused by the B3LYP functional (-0.48 V) in combination with the 6-31G* basis set [44]: The oxidation and re-reduction at $E_{1/2} = +1.52$ V and the reduction and re-oxidation at $E_{1/2} = -1.29$ V, which lead to a corresponding cell voltage of 2.81 V.

Subsequently, the electrochemical properties of compound **2** were investigated via cyclic voltammetry to determine the actual potentials of the two redox-couples. Additionally, cyclic voltammetry measurements with IR drop compensation were performed (detailed description in the Supporting information) to determine n (number of transferred electrons) for both the oxidation/re-reduction and reduction/re-oxidation redox-couple.

The CV measurements were performed in acetonitrile solution with 0.1 M TBAPF₆ as supporting electrolyte. The cyclic voltammogram (Fig. 4) displays a quasi-reversible oxidation and re-reduction at $E_{1/2} = 1.42$ V vs. Fc^+/Fc with a peak split of 96 mV, as well as a quasi-reversible reduction and re-oxidation at $E_{1/2} = -1.49$ V vs. Fc^+/Fc with a peak split of 169 mV, which leads to a theoretical cell voltage of 2.91 V in a subsequent battery application. The experimentally determined potentials are in fair agreement with the calculated values.

A detailed investigation of the obtained CV curves (Fig. 5a and b) exposes a linear relation of the peak currents and the square root of the scan rate for the oxidation/re-reduction redox-couple (Fig. 5a) and for the reduction/re-oxidation redox-couple (Fig. 5b). This is an indication for a diffusion-controlled behavior and the

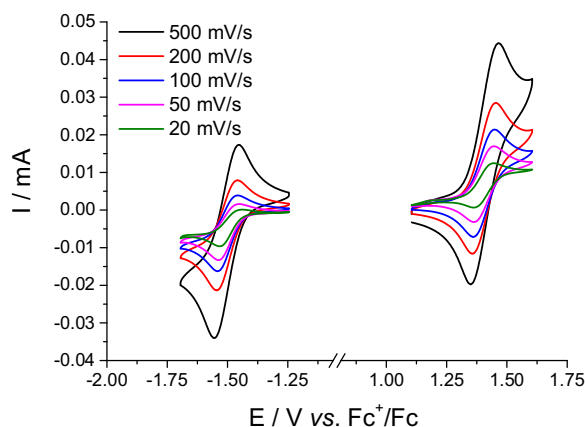


Fig. 4. Cyclic voltammogram obtained for 3.8 mM CH_3CN solution of **2** with 0.1 M TBAPF₆ as supporting electrolyte at different scan rates.

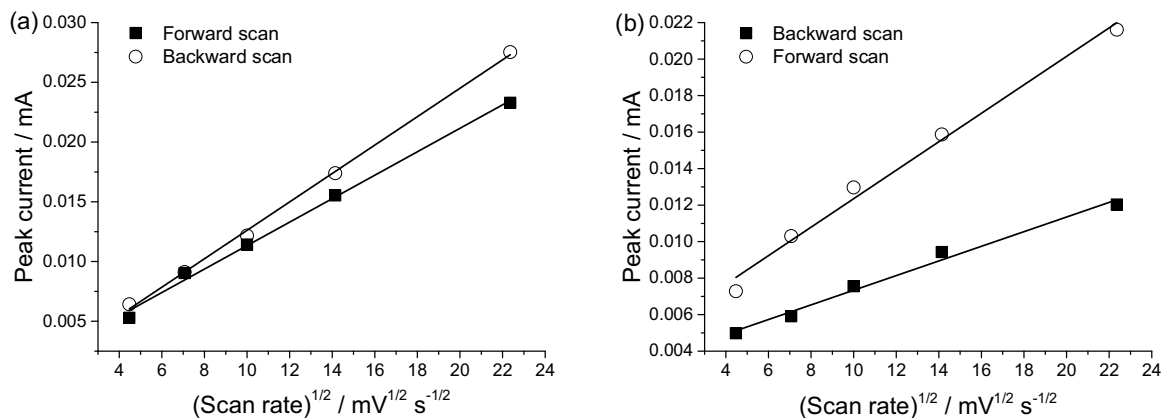


Fig. 5. Cyclic voltammogram obtained for 3.8 mM CH₃CN solution of **2** with 0.1 M TBAPF₆ as supporting electrolyte: (a) Plot of the oxidation and the re-reduction peak current vs. square root of the scan rate as well as (b) plot of the reduction and the re-oxidation peak current vs. square root of the scan rate.

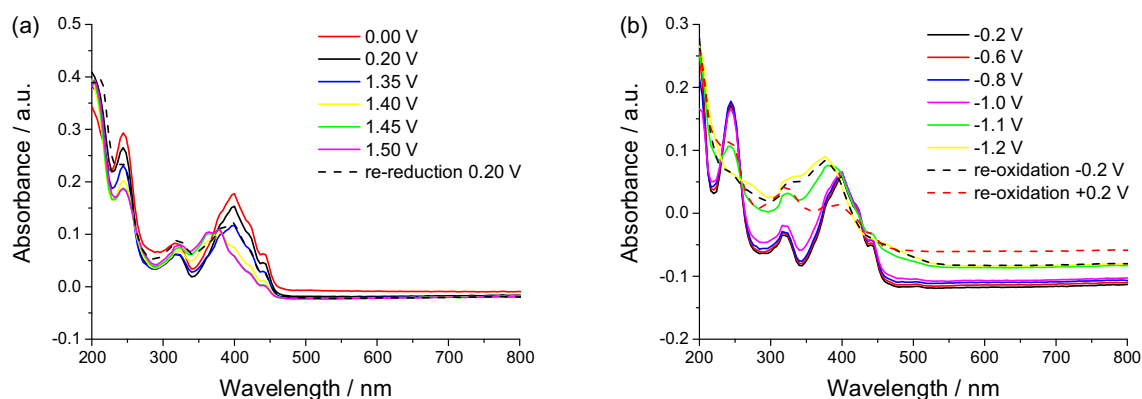


Fig. 6. Spectroelectrochemical measurements of **2** in acetonitrile with 0.1 M TBAPF₆ as supporting electrolyte (E vs. AgNO₃/Ag, about -0.084 V vs. Fc⁺/Fc): (a) Oxidation reaction and (b) reduction reaction.

nonappearance of precipitates. Afterwards, the diffusion coefficient D was calculated to be $4.1 \times 10^{-5} \text{ cm}^2 \text{ s}^{-1}$ for the oxidation and re-reduction as well as $2.6 \times 10^{-5} \text{ cm}^2 \text{ s}^{-1}$ for the reduction and re-oxidation experiment by the use of the Randles-Sevcik equation.

To investigate the chemical reversibility of both redox reactions UV-vis-NIR spectroelectrochemical measurements (Fig. 6a and b) were performed in a highly diluted acetonitrile solution of **2** with 0.1 M TBAPF₆ as supporting electrolyte. In contrast to the CV measurements, the potentials were determined against an AgNO₃/Ag pseudoreference electrode (about -0.084 V vs. Fc⁺/Fc).

After the oxidation of **2** at potentials up to 1.5 V (vs. AgNO₃/Ag) the intensity of the most characteristic absorption bands at 400, 322 and 244 nm as well as the small absorption band at 441 nm decreases slightly. Noticeable is a hypsochromic shift of the main absorbance signal at 400 nm, beginning with potentials of 1.4 V, to 378 nm (Fig. 6a). Furthermore, also starting at a potential of 1.4 V a new absorption band at 362 nm appears, whose intensity rises with increasing potentials up to 1.5 V (Fig. 6a). Over the following re-reduction at 0.2 V the original signals are restored qualitatively and the occurred signal at 362 nm disappears, which is an

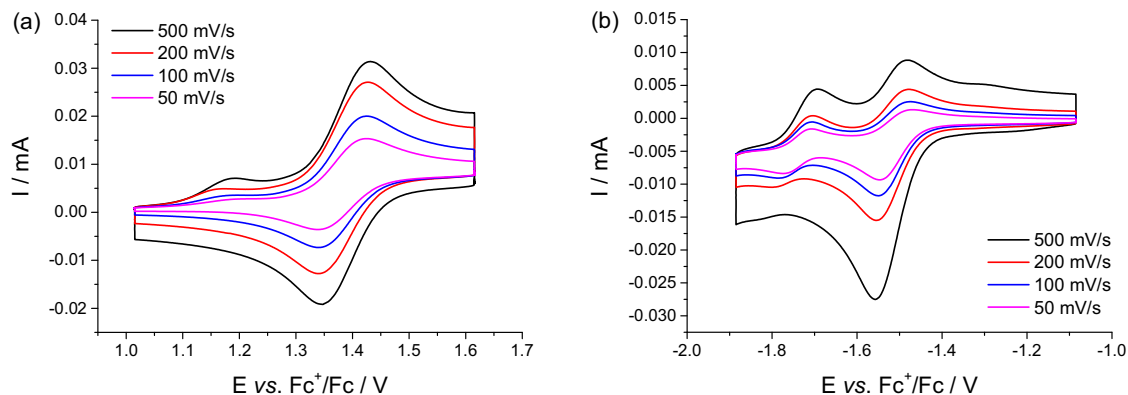


Fig. 7. Cyclic voltammogram obtained for 2.5 mM CH₃CN solution of **2** with 0.1 M TBAPF₆ as supporting electrolyte at different scan rates via an advanced CV method (hold time of five minutes at each scan rate): (a) Oxidation and re-reduction as well as (b) reduction and re-oxidation.

indication for the chemical reversibility of this redox reaction. During the reduction reaction of **2** at potentials up to -1.2 V the absorbance signal at 400 nm also displays a hypsochromic shift to 376 nm, while the band at 319 nm recedes and the signals at 441 and 244 nm fully disappears (Fig. 6b). After the subsequent re-oxidation at -0.2 V the original absorbance spectrum was not re-established. Indeed, this spectrum looks very similar to the one at -1.2 V. Only at 0.2 V the original absorbance spectrum could roughly be restored, but still revealed slight differences such as the intensity of the characteristic absorption bands. This behavior may indicate side reactions for this redox-couple.

To examine the chemical reversibility of both redox reactions as well as to investigate a potential side reaction for the reduction/re-oxidation redox-couple, which is lightly implied due to the shown behavior during the spectroelectrochemical measurements, advanced cyclic voltammetry (CVA) measurements were performed. In contrast to common CV measurements a hold time of five minutes was introduced after each forward scan (oxidation and re-reduction as well as reduction and re-oxidation) to study the chemical reversibility in an environment which is closer to a battery operation. The CVA measurements were also performed in acetonitrile solution with 0.1 M TBAPF₆ as supporting electrolyte.

The cyclic voltammogram, obtained for the oxidation of **2** (Fig. 7a) via the advanced CV method, displays a quasi-reversible oxidation and re-reduction at $E_{1/2} = 1.39$ V vs. Fc⁺/Fc with a peak split of 86 mV and, therefore, no significant differences to the original cyclic voltammogram (Fig. 4, right). In contrast, the cyclic

voltammogram obtained for the reduction reaction of **2** (Fig. 7b) exhibits a different behavior than in the original spectrum (Fig. 4, left). Indeed, the original reduction and re-oxidation at $E_{1/2} = -1.51$ V vs. Fc⁺/Fc is identifiable, but a new signal at -1.69 V and, in particular visible at lower scan rates, at -1.79 V vs. Fc⁺/Fc appears, which probably indicates a consecutive or side-reaction. This compound seems to undergo another reduction and re-oxidation reaction particularly obvious at a scan rate of 50 and 100 mV s⁻¹, which consequently leads to a non-stable redox behavior of the reduction of **2** during extended electrolysis conditions.

For further investigations of the redox behavior, in particularly to study the diffusion behavior and to obtain the electron-transfer rate constant k^0 and the transfer coefficient α of both redox-couples, RDE measurements of **2** were performed in acetonitrile solution with 0.1 M TBAPF₆ as supporting electrolyte.

For the oxidation/re-reduction redox-couple a diffusion coefficient D of 1.42×10^{-5} cm² s⁻¹ (Fig. 8a and b) was calculated. The following performed Koutecký-Levich analysis revealed mass-transport-independent currents and the Tafel analysis (Fig. 8c and d) exhibited an electron-transfer rate constant (k^0) of 1.08×10^{-2} cm s⁻¹ as well as a transfer coefficient α of 0.86 . However, the obtained transfer coefficient α deviates to the value of an ideal reversible redox reaction of 0.5 . These observation can probably be explained by the deviating values at the rotating rates 225 and 1200 rpm, which is for example visible in the Koutecký-Levich plot (Fig. 8c) and in particular through the occurred side reaction at 1.0 and 1.3 V, which resulted in an overlap of the individual curves (Fig. 8a).

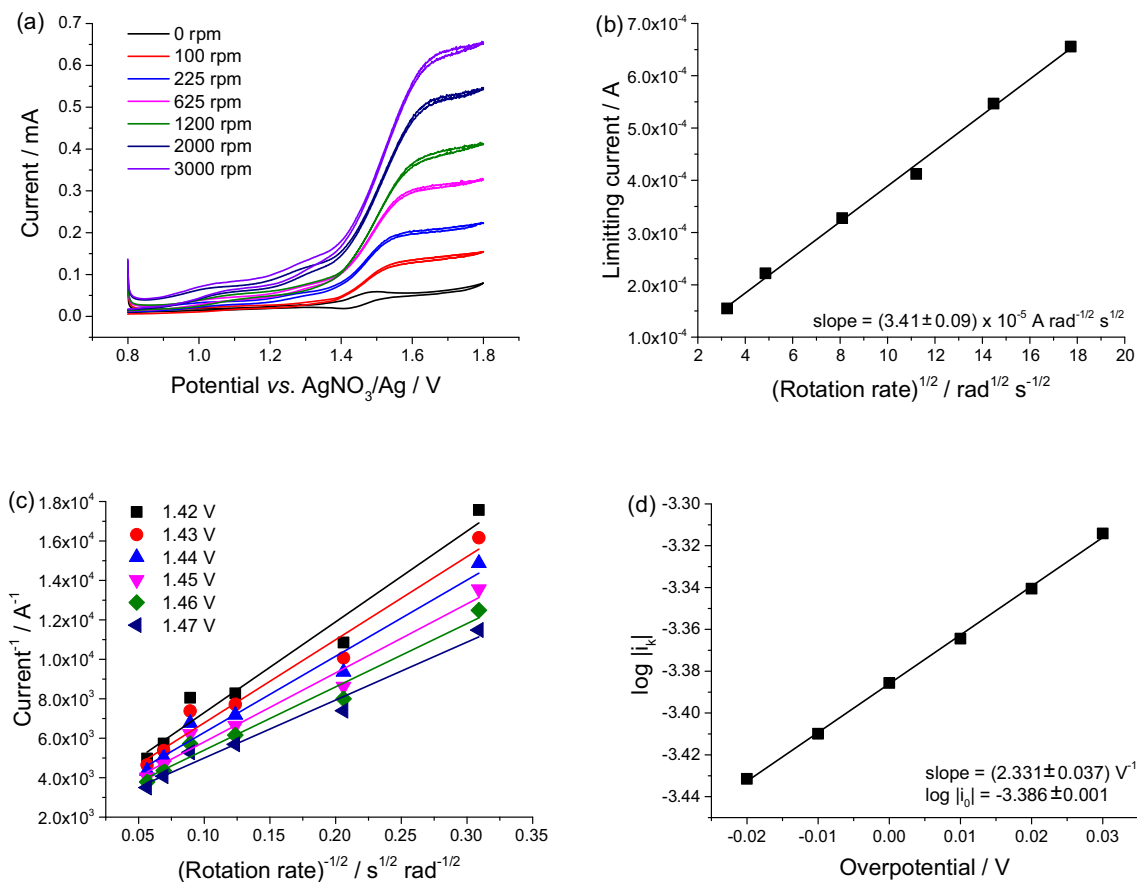


Fig. 8. (a) Rotating disk electrode measurement of **2** (2×10^{-3} mol L⁻¹), 0.1 M TBAPF₆ in acetonitrile, scan rate 5 mV s⁻¹, at rotating rates from 0 to 3000 rpm, (b) Levich-plot from the obtained limiting currents at 1.8 V vs. AgNO₃/Ag; application of Levich-equation yields a diffusion coefficient $D = 1.42 \times 10^{-5}$ cm² s⁻¹, (c) Koutecký-Levich plot for different overpotentials yielding the mass-transfer-independent current i_k , (d) Tafel plot yielding $k^0 = 1.08 \times 10^{-2}$ cm s⁻¹ and $\alpha = 0.86$.

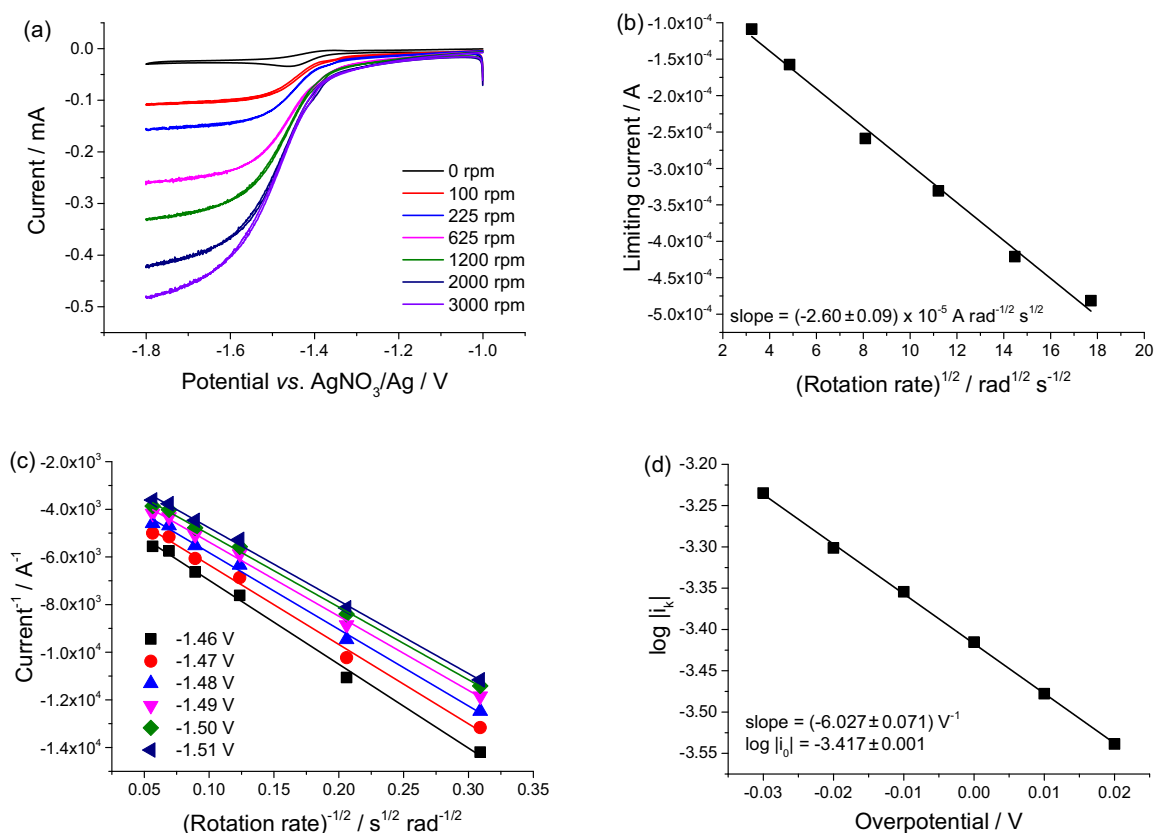


Fig. 9. (a) Rotating disk electrode measurement of **2** ($2 \times 10^{-3} \text{ mol L}^{-1}$), 0.1 M TBAPF₆ in acetonitrile, scan rate 5 mV s^{-1} , at rotating rates from 0 to 3000 rpm, (b) Levich-plot from the obtained limiting currents at $-1.8 \text{ V vs. AgNO}_3/\text{Ag}$; application of Levich-equation yields a diffusion coefficient $D = 9.43 \times 10^{-6} \text{ cm}^2 \text{ s}^{-1}$, (c) Koutecký-Levich plot for different overpotentials yielding the mass-transfer-independent current i_k , (d) Tafel plot yielding $k^0 = 1.00 \times 10^{-2} \text{ cm s}^{-1}$ and $\alpha = 0.65$.

The reduction/re-oxidation redox-couple showed a diffusion-controlled behavior of **2** with a diffusion coefficient D of $9.43 \times 10^{-6} \text{ cm}^2 \text{ s}^{-1}$ (Fig. 9a and b). Similarly, the subsequently performed Koutecký-Levich analysis revealed mass-transport-independent currents and the Tafel analysis (Fig. 9c and d) revealed an electron-transfer rate constant (k^0) of $1.00 \times 10^{-2} \text{ cm s}^{-1}$ as well as a transfer coefficient α of 0.65, which is nearly the α value of an ideal reversible redox reaction of 0.5. To recapitulate, the received diffusion coefficient D for both redox-couples is in the same magnitude as the subsequently calculated diffusion coefficient D by using the Randles-Sevcik equation from the evaluation of the CV measurements. Furthermore the diffusion coefficients D of both redox-couples are similar to literature values of known organic charge-storage materials like 2-phenyl-4,4,5,5-tetramethylimidazoline-1-oxyl-3-oxide (PTIO) [45], 2,5-di-*tert*-butyl-1,4-bis(2-methoxy-ethoxy)benzene (DBBB) [46,47], and several quinone derivatives [48–50] with typical values in the range of 1.4 to $6.2 \times 10^{-6} \text{ cm}^2 \text{ s}^{-1}$.

To summarize all results from the different electrochemical investigations, the good electrochemical properties of **2**, an electrochemically stable quasi-reversible oxidation and re-reduction as well as reduction and re-oxidation, respectively, determined by DFT calculation and validated by CV measurements could not unequivocally be confirmed via UV-vis-NIR spectroelectrochemical, CVA and RDE measurements for both redox-couples. Whereas the oxidation/re-reduction redox-couple features a chemically stable species and a reversible and diffusion-controlled redox behavior, the results of the CVA and UV-vis-NIR spectroelectrochemical measurements indicate an irreversible consecutive or side-

reaction under bulk electrolysis conditions for the reduction/re-oxidation redox-couple.

4. Conclusion

The multivalent, redox-active 2,3,7,8-tetracyano-5,10-diphenyl-5,10-dihydropyrazino[2,3-*b*:2',3'-*e*]pyrazine (**2**) was synthesized in two synthesis steps from inexpensive, commercially available compounds and its electrochemical properties were studied by DFT calculations and afterwards investigated via CV, which exhibited quasi-reversible redox reactions at $E_{1/2} = 1.42 \text{ V}$ and at $E_{1/2} = -1.49 \text{ V vs. Fc}^+/\text{Fc}$, which led to a theoretical cell voltage of 2.91 V .

To evaluate the 2,3,7,8-tetracyano-1,4,5,6,9,10-hexazaanthracene derivatives as potential bipolar charge-storage materials for energy storage applications, the electrochemical behavior of compound **2** was further investigated via UV-vis-NIR spectroelectrochemical and RDE measurements, which revealed for the oxidation/re-reduction redox-couple a chemically stable reversible redox behavior, but for the reduction/re-oxidation several concerns regarding the chemical and electrochemical stability of this redox-couple were obtained. However, by the simple introduction of various functional groups during the two-step synthesis, the electrochemical properties can be adjusted. Therefore, further studies will focus on the synthesis of a tailor-made 2,3,7,8-tetracyano-1,4,5,6,9,10-hexazaanthracene derivative with two stable redox-couples and the investigation of several other electrolytes, in terms of their ability to stabilize the reduced TCAA species.

Nevertheless, the extensive electrochemical studies of molecule 2 display the potential usability of this substance class as charge-storage material in electrochemical energy-storage devices.

Acknowledgements

The authors thank the European Regional Development Fund (EFRE), the Thuringian Ministry for Economic Affairs, Science and Digital Society (TMWWdG), the Zentrales Innovationsprogramm Mittelstand (ZIM) and the Fonds der Chemischen Industrie (FCI) for the financial support, Nicole Fritz for ESI-MS measurements, as well as the support from Dr. Michael Jäger for the DFT calculation.

Appendix A. Supplementary data

Supplementary data associated with this article can be found, in the online version, at <http://dx.doi.org/10.1016/j.electacta.2017.01.055>.

References

- [1] S. Solomon, G.-K. Plattner, R. Knutti, P. Friedlingstein, Irreversible climate change due to carbon dioxide emissions, *Proc. Natl. Acad. Sci.* 106 (2009) 1704–1709.
- [2] P.M. Cox, R.A. Betts, C.D. Jones, S.A. Spall, I.J. Totterdell, Acceleration of global warming due to carbon-cycle feedbacks in a coupled climate model, *Nature* 408 (2000) 184–187.
- [3] J.T. Houghton, L.G.M. Filho, B.A. Callander, N. Harris, A. Kattenberg, K. Maskell, *Climate Change 1995, The Science of Climate Change*, Cambridge Univ. Press, 1996.
- [4] J. Winsberg, T. Hagemann, T. Janoschka, M.D. Hager, U.S. Schubert, Redox-Flow Batteries: from metals to organic redox-active materials, *Angew. Chem. Int. Ed.* 56 (2017) 686–711.
- [5] D. Cook, B. Davidsdottir, J.G. Petursson, Accounting for the utilisation of geothermal energy resources within the genuine progress indicator – A methodological review, *Renew. Sust. Energ. Rev.* 49 (2015) 211–220.
- [6] D.M. Rosenberg, R.A. Bodaly, P.J. Usher, Environmental and social impacts of large scale hydroelectric development: who is listening? *Global Environ. Chang.* 5 (1995) 127–148.
- [7] O. Edenhofer, K. Seyboth, F. Creutz, S. Schlömer, On the sustainability of renewable energy sources, *Annu. Rev. Environ. Resour.* 38 (2013) 169–200.
- [8] S. Weitemeyer, D. Kleinhan, T. Vogt, C. Agert, Integration of renewable energy sources in future power systems: the role of storage, *Renew. Energ.* 75 (2015) 14–20.
- [9] C. Budischak, D. Sewell, H. Thomson, L. Mach, D.E. Veron, W. Kempton, Cost-minimized combinations of wind power, solar power and electrochemical storage, powering the grid up to 99.9% of the time, *J. Power Sources* 225 (2013) 60–74.
- [10] M. Skyllas-Kazacos, M. Rychcik, R.G. Robins, A.G. Fane, New all-vanadium redox flow cell, *J. Electrochem. Soc.* 133 (1986) 1057–1058.
- [11] M. Vijayakumar, W. Wang, Z. Nie, V. Sprenkle, J. Hu, Elucidating the higher stability of vanadium(V) cations in mixed acid based redox flow battery electrolytes, *J. Power Sources* 241 (2013) 173–177.
- [12] S. Roe, C. Menicatas, M. Skyllas-Kazacos, A high energy density vanadium redox flow battery with 3 M vanadium electrolyte, *J. Electrochem. Soc.* 163 (2016) A5023–A5028.
- [13] C. Sun, J. Chen, H. Zhang, X. Han, Q. Luo, Investigations on transfer of water and vanadium ions across Nafion membrane in an operating vanadium redox flow battery, *J. Power Sources* 195 (2010) 890–897.
- [14] H.L. Thaller, Electrically rechargeable redox flow cell, US 3996064, 1976.
- [15] N.H. Hagedorn, L.H. Thaller, Design flexibility of redox flow systems, National Aeronautics and Space Administration, Lewis Research Center, 1982.
- [16] M. Lopez-Atalaya, G. Codina, J.R. Perez, J.L. Vazquez, A. Aldaz, Optimization studies on a Fe/Cr redox flow battery, *J. Power Sources* 39 (1992) 147–154.
- [17] M. Lopez-Atalaya, G. Codina, J.R. Perez, J.L. Vazquez, A. Aldaz, M.A. Climent, Behaviour of the Cr(III)/Cr(II) reaction on gold graphite electrodes. Application to redox flow storage cell, *J. Power Sources* 35 (1991) 225–234.
- [18] M. Armand, J.M. Tarascon, Building better batteries, *Nature* 451 (2008) 652–657.
- [19] T. Janoschka, N. Martin, U. Martin, C. Friebe, S. Morgenstern, H. Hiller, M.D. Hager, U.S. Schubert, An aqueous, polymer-based redox-flow battery using non-corrosive, safe, and low-cost materials, *Nature* 527 (2015) 78–81.
- [20] J. Winsberg, T. Hagemann, S. Muench, C. Friebe, B. Häupler, T. Janoschka, S. Morgenstern, M.D. Hager, U.S. Schubert, Poly(boron-dipyrromethene) – A redox-active polymer class for polymer redox-flow batteries, *Chem. Mater.* 28 (2016) 3401–3405.
- [21] C.J. Barnhart, S.M. Benson, On the importance of reducing the energetic and material demands of electrical energy storage, *Energy Environ. Sci.* 6 (2013) 1083–1092.
- [22] T. Janoschka, S. Morgenstern, H. Hiller, C. Friebe, K. Wolkersdorfer, B. Häupler, M.D. Hager, U.S. Schubert, Synthesis and characterization of TEMPO- and viologen-polymers for water-based redox-flow batteries, *Polym. Chem.* 6 (2015) 7801–7811.
- [23] T. Liu, X. Wei, Z. Nie, V. Sprenkle, W. Wang, A total organic aqueous redox flow battery employing a low cost and sustainable methyl viologen anolyte and 4-HO-TEMPO catholyte, *Adv. Energy Mater.* 6 (2016) 1501449.
- [24] X. Wei, W. Xu, J. Huang, L. Zhang, E. Walter, C. Lawrence, M. Vijayakumar, W.A. Henderson, T. Liu, L. Cosimbescu, B. Li, V. Sprenkle, W. Wang, Radical compatibility with nonaqueous electrolytes and its impact on an all-organic redox flow battery, *Angew. Chem. Int. Ed.* 54 (2015) 8684–8687.
- [25] R.A. Potash, J.R. McKone, S. Conte, H.D. Abruña, On the benefits of a symmetric redox flow battery, *J. Electrochem. Soc.* 163 (2016) A338–A344.
- [26] D. Hou, M. Matsuoka, Reaction of 2,3-dichloro-5,6-dicyanopyrazine with amines, *Dyes Pigm.* 22 (1993) 57–68.
- [27] J.-Y. Jaung, K. Fukunishi, M. Matsuoka, Syntheses and spectral properties of 2,3,7,8-tetracyano-5,10-dihydropyrazino[2,3-b:2',3'-e]pyrazine, *J. Heterocycl. Chem.* 34 (1997) 653–657.
- [28] J. Mei, Y. Hong, J.W.Y. Lam, A. Qin, Y. Tang, B.Z. Tang, Aggregation-induced emission: the whole is more brilliant than the parts, *Adv. Mater.* 26 (2014) 5429–5479.
- [29] D.W. Robertson, E.E. Beedle, J.K. Swartzendruber, N.D. Jones, T.K. Elzey, R.F. Kauffman, H. Wilson, J.S. Hayes, Bipyridine cardiotonics: the three-dimensional structures of amrinone and milrinone, *J. Med. Chem.* 29 (1986) 635–640.
- [30] S. Goswami, A.C. Maity, N.K. Das, D. Sen, S. Maity, Triselenium dicyanide (TSD) as a new cyanation reagent: synthesis of cyano pterins and quinoxalines along with library of cyano N-heterocyclic compounds, *Synth. Commun.* 39 (2009) 407–415.
- [31] S. Ancizu, E. Moreno, E. Torres, A. Burguete, S. Pérez-Silanes, D. Benítez, R. Villar, B. Solano, A. Marín, I. Aldana, H. Cerecetto, M. González, A. Monge, Heterocyclic-2-carboxylic acid (3-cyano-1,4-di-N-oxidequinoxalin-2-yl) amide derivatives as hits for the development of neglected disease drugs, *Molecules* 14 (2009) 2256–2272.
- [32] G. Brahmachari, B. Banerjee, Facile and one-pot access to diverse and densely functionalized 2-amino-3-cyano-4H-pyrans and pyran-annulated heterocyclic scaffolds via an eco-friendly multicomponent reaction at room temperature using urea as a novel organo-catalyst, *ACS Sustai. Chem. Eng.* 2 (2014) 411–422.
- [33] H.Z. Shams, R.M. Mohareb, M.H. Helal, A.E. Mahmoud, Novel synthesis and antitumor evaluation of polyfunctionally substituted heterocyclic compounds derived from 2-cyano-N-(3-cyano-4,5,6,7-tetrahydrobenzo[b]thiophen-2-yl)-acetamide, *Molecules* 16 (2011) 52–73.
- [34] K. Kanakarajan, A.W. Czarnik, Synthesis and some reactions of hexaazatriphenylenehexanitride, a hydrogen-free polyfunctional heterocycle with D_{3h} symmetry, *J. Org. Chem.* 51 (1986) 5241–5243.
- [35] H.E. Katz, M.L. Schilling, Head-to-tail assemblies of dipolar, piperazine-linked chromophores: synthesis, x-ray structure, and dielectric characterization, *JACS* 111 (1989) 7554–7557.
- [36] M.L. Schilling, H.E. Katz, Synthetic approaches to head-to-tail linked azo dyes for nonlinear optical applications, *Chem. Mater.* 1 (1989) 668–673.
- [37] P.G. Rasmussen R.G. Lawton, Process for manufacturing bis(2-methoxy ethyl)-2, 3, 6, 7-tetracyano-1, 4, 5, 8, 9, 10-hexazaanthracene, US 8742107 B1, 2012.
- [38] http://www.ddbst.com/en/EED/PCP/VSK_C3.php. (Accessed 10 August 2016).
- [39] M.J. Frisch, G.W. Trucks, H.B. Schlegel, G. Scuseria, M.A. Robb, J.R. Cheeseman, G. Scalmani, V. Barone, B. Mennucci, G.A. Petersson, H. Nakatsuji, M. Caricato, X. Li, H.P. Hratchian, A.F. Izmaylov, J. Bloino, G. Zheng, J.L. Sonnenberg, M. Hada, M. Ehara, K. Toyota, R. Fukuda, J. Hasegawa, M. Ishida, T. Nakajima, Y. Honda, O. Kitao, H. Nakai, T. Vreven, J. Montgomery Jr., J.E. Peralta, F. Ogliaro, M. Bearpark, J.J. Heyd, E. Brothers, K.N. Kudin, V.N. Staroverov, R. Kobayashi, J. Normand, K. Raghavachari, A. Rendell, J.C. Burant, S.S. Iyengar, J. Tomasi, M. Cossi, N. Rega, N. J. Millam, M. Klene, J.E. Knox, J.B. Cross, V. Bakken, C. Adamo, J. Jaramillo, R. Gomperts, R.E. Stratmann, O. Yazyev, A.J. Austin, R. Cammi, C. Pomelli, J.W. Ochterski, R.L. Martin, K. Morokuma, V.G. Zakrzewski, G.A. Voth, P. Salvador, J.J. Dannenberg, S. Dapprich, A.D. Daniels, Ö. Farkas, J.B. Foresman, J.V. Ortiz, J. Cioslowski, D.J. Fox, Gaussian 09, Gaussian, Inc, Wallingford, CT, 2010.
- [40] A.D. Becke, Density-functional thermochemistry 3. The role of exact exchange, *J. Chem. Phys.* 98 (1993) 5648–5652.
- [41] C.T. Lee, W.T. Yang, R.G. Parr, Development of the Colle-Salvetti correlation-energy formula into a functional of the electron-density, *Physical Review B* 37 (1988) 785–789.
- [42] E. Cancès, B. Mennucci, J. Tomasi, A new integral equation formalism for the polarizable continuum model: theoretical background and applications to isotropic and anisotropic dielectrics, *J. Chem. Phys.* 107 (1997) 3032–3041.
- [43] J. Tomasi, B. Mennucci, R. Cammi, Quantum mechanical continuum solvation models, *Chem. Rev.* 105 (2005) 2999–3093.
- [44] L.E. Roy, E. Jakubikova, M.G. Guthrie, E.R. Batista, Calculation of one-electron redox potentials revisited. Is it possible to calculate accurate potentials with density functional methods? *J. Phys. Chem. A* 113 (2009) 6745–6750.
- [45] W. Duan, R.S. Vemuri, J.D. Milshtein, S. Laramie, R.D. Dmello, J. Huang, L. Zhang, D. Hu, M. Vijayakumar, W. Wang, J. Liu, R.M. Darling, L. Thompson, J.S. Moore, F.R. Brushett, X. Wei, A symmetric organic-based nonaqueous redox flow battery and its state of charge diagnostics by FTIR, *J. Mater. Chem. A* 4 (2016) 5448–5456.
- [46] F.R. Brushett, J.T. Vaughey, A.N. Jansen, An all-organic non-aqueous lithium-ion redox flow battery, *Adv. Energy Mater.* 2 (2012) 1390–1396.

- [47] L. Su, M. Ferrandon, J.A. Kowalski, J.T. Vaughey, F.R. Brushett, Electrolyte development for non-aqueous redox flow batteries using a high-throughput screening platform, *J. Electrochem. Soc.* 161 (2014) A1905–A1914.
- [48] B. Yang, L. Hooper-Burkhardt, F. Wang, G.K. Surya Prakash, S.R. Narayanan, An inexpensive aqueous flow battery for large-scale electrical energy storage based on water-soluble organic redox couples, *J. Electrochem. Soc.* 161 (2014) A1371–A1380.
- [49] B. Huskinson, M.P. Marshak, C. Suh, S. Er, M.R. Gerhardt, C.J. Galvin, X. Chen, A. Aspuru-Guzik, R.G. Gordon M.J. Aziz, A metal-free organic-inorganic aqueous flow battery, *Nature* 505 (2014) 195–198.
- [50] S. Zhang, X. Li, D. Chu, An organic electroactive material for flow batteries, *Electrochim. Acta* 190 (2016) 737–743.

Supporting Information

Synthesis and Electrochemical Study of a TCAA Derivative – A potential bipolar redox-active material

Tino Hagemann^{a,b}, Jan Winsberg^{a,b}, Andreas Wild^{a,b}, Ulrich S. Schubert^{a,b*}

1. Experiments

Nuclear magnetic resonance (NMR) spectroscopy. The ^1H and ^{13}C NMR spectra were recorded on a AC 300 (300 and 75 MHz; Bruker, USA) spectrometer at 298 K. Chemical shifts are reported in parts per million (ppm, δ scale) relative to the residual signal of the deuterated solvent.

^1H and ^{13}C NMR spectra of 2-anilino-3-chloro-5,6-dicyanopyrazine (**1**):

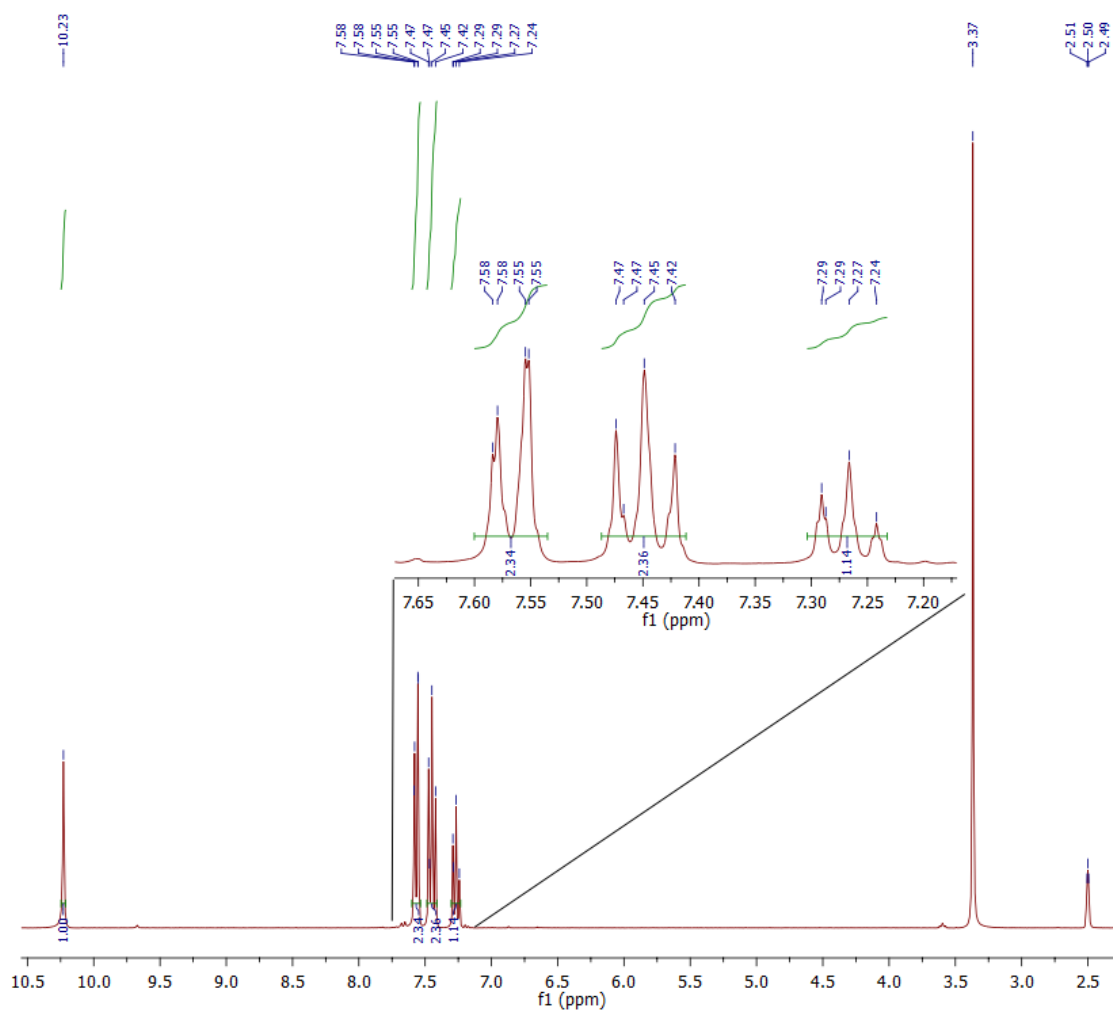


Figure S1. ^1H NMR spectra (300 MHz, DMSO- d_6 , δ): 10.23 (s, 1H, NH), 7.56 (d, J = 6 Hz, 2H, Ar H), 7.45 (t, J = 7 Hz, 2H, Ar H), 7.27 (t, J = 7 Hz, 1H, Ar H), obtained for molecule **1**. The signal (δ) at 3.37 (s) belongs to water and 2.50 (s) is the solvent residual peak of DMSO.

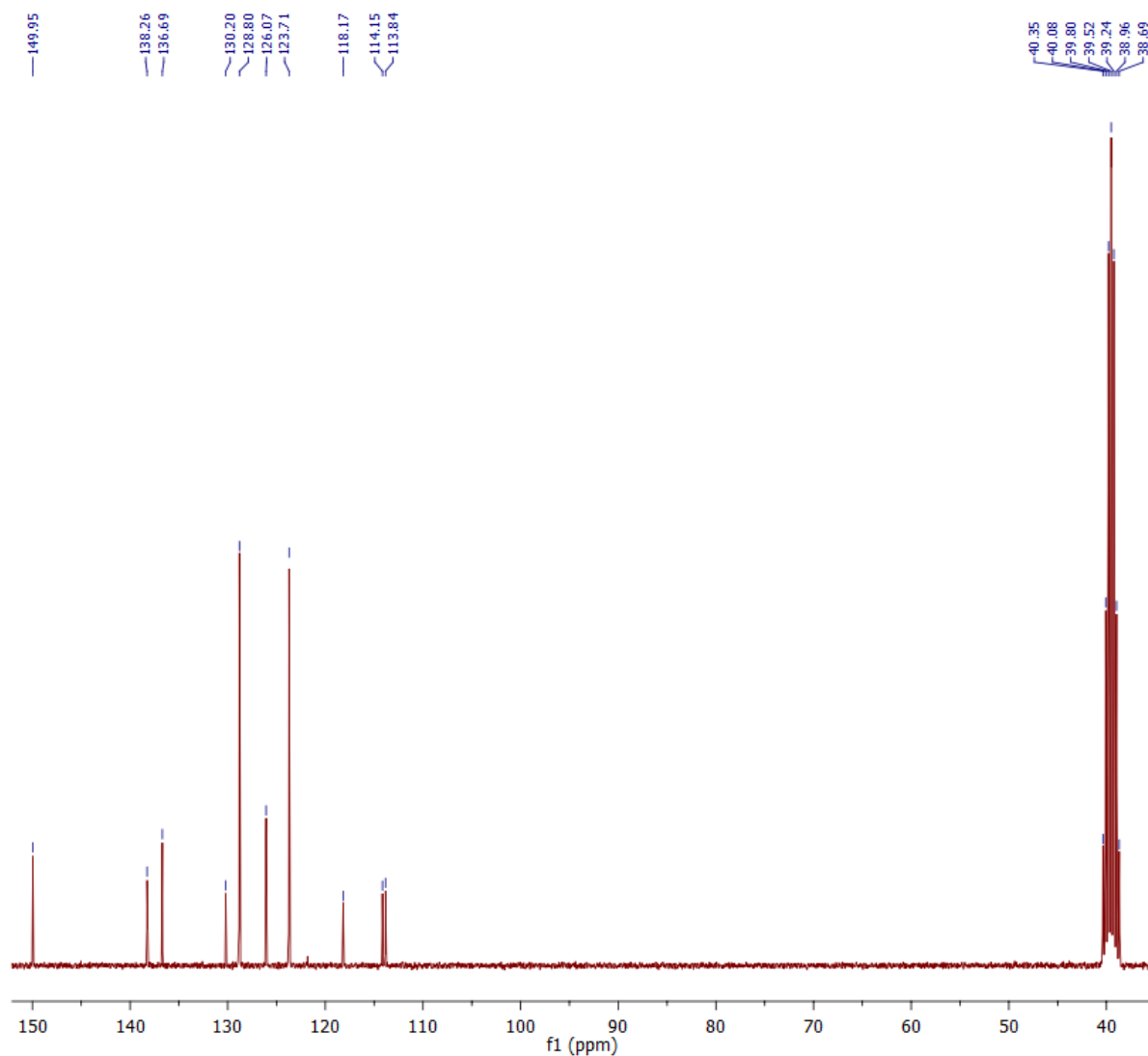


Figure S2. ^{13}C NMR spectra (75 MHz, DMSO-d_6 , δ): 149.95 (CNH), 138.26 (CNH), 136.69 (CCI), 130.20 (CCN), 128.80 (CC), 126.07 (CC), 123.71 (CC), 118.17 (CCN), 114.15 (CN), 113.84 (CN), obtained for molecule **1**. The signal (δ) at 39.52 (sep) is the solvent signal of DMSO.

^1H and ^{13}C NMR spectra of 2,3,7,8-tetracyano-5,10-diphenyl-5,10-dihydrodipyrzino[2,3-*b*:2',3'-*e*]pyrazine (**2**), synthesized by method **a**):

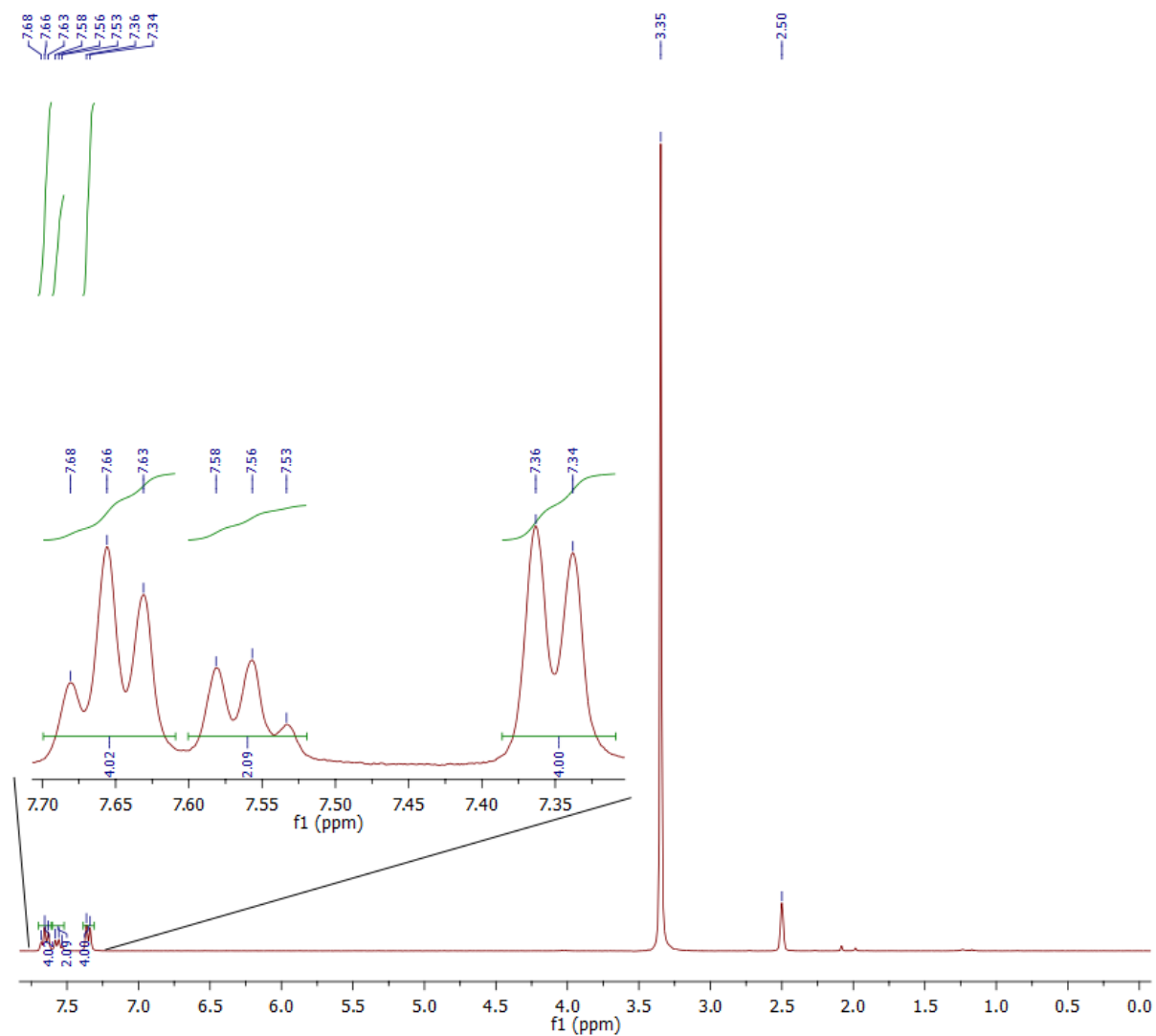


Figure S3. ^1H NMR spectra (300 MHz, DMSO-d_6 , δ): 7.66 (t, $J = 7.5$ Hz, 4H, Ar H), 7.56 (t, $J = 7.5$ Hz, 2H, Ar H) 7.35 (d, $J = 7.5$ Hz, 2H, Ar H), obtained for molecule **2** synthesized by method **a**). The signal (δ) at 3.35 (s) belongs to water and 2.50 (s) is the solvent residual peak of DMSO.

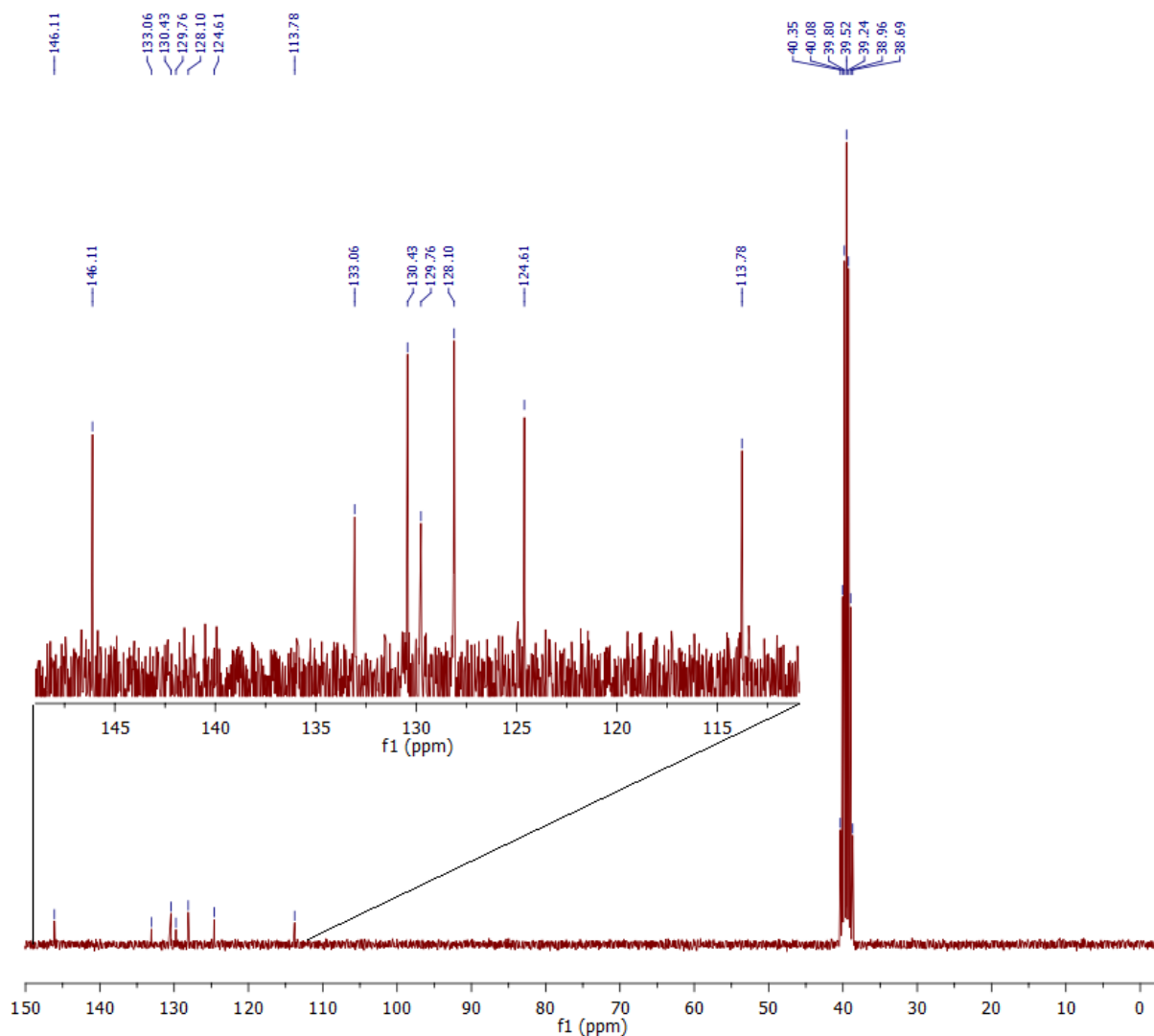


Figure S4. ^{13}C NMR spectra (75 MHz, DMSO- d_6 , δ): 146.11 (ArCCN), 133.06 (NCN), 130.43 (ArC), 129.76 (ArC), 128.10 (ArC), 124.61 (CCN), 113.78 (CN), obtained for molecule **2** synthesized by method **a**). The signal (δ) at 39.52 (sep) is the solvent signal of DMSO.

^1H and ^{13}C NMR spectra of 2,3,7,8-tetracyano-5,10-diphenyl-5,10-dihydrodipyrzino[2,3-*b*:2',3'-*e*]pyrazine (**2**), synthesized by method **b**):

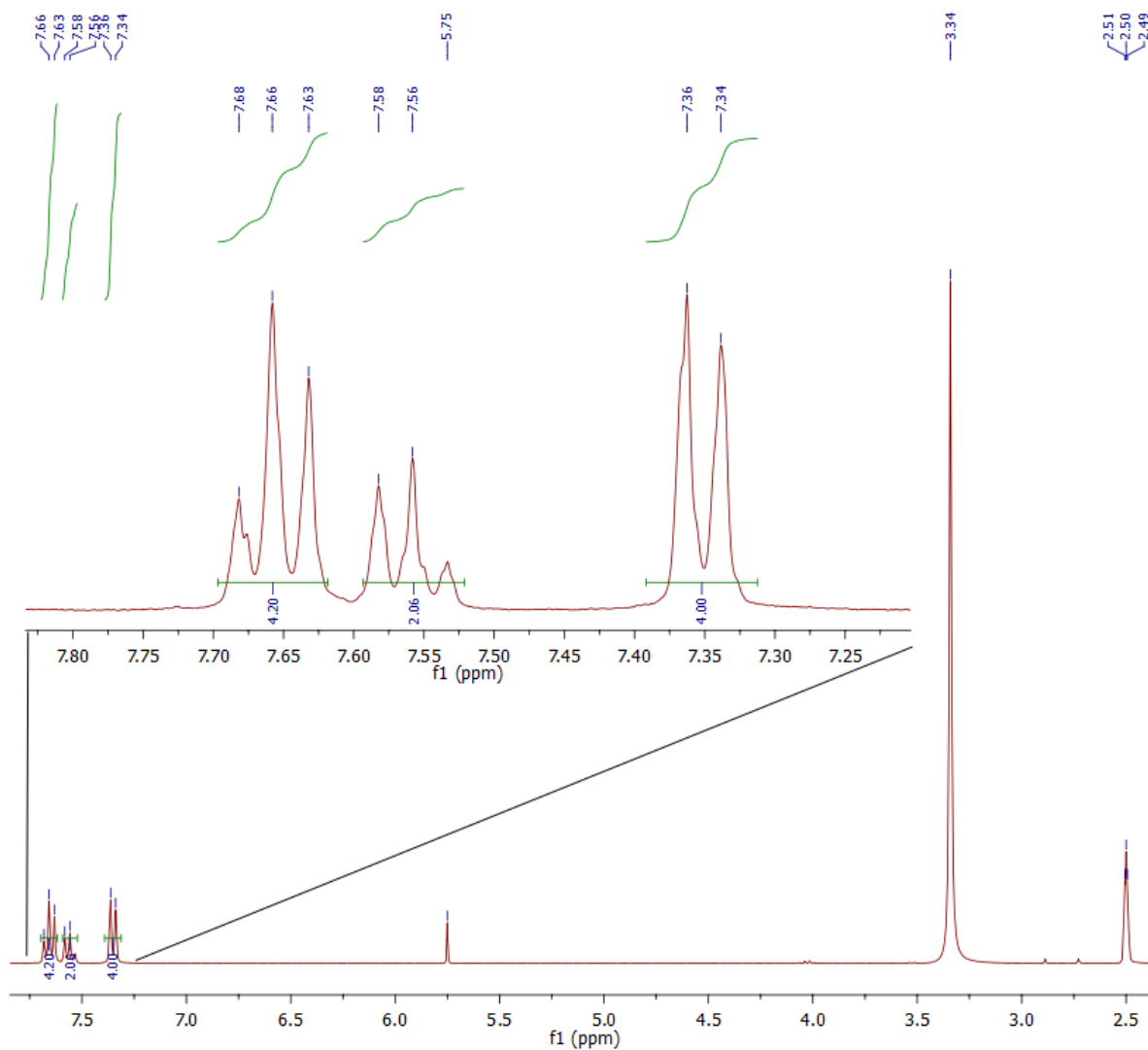


Figure S5. ^1H NMR spectra (300 MHz, DMSO-d_6 , δ): 7.66 (t, $J = 7.5$ Hz, 4H, Ar H), 7.56 (t, $J = 7.5$ Hz, 2H, Ar H) 7.35 (d, $J = 7.5$ Hz, 2H, Ar H), obtained for molecule **2** synthesized by method **b**). The signal (δ) at 5.75 belongs to dichloromethane, at 3.34 (s) belongs to water and 2.50 (s) is the solvent residual peak of DMSO.

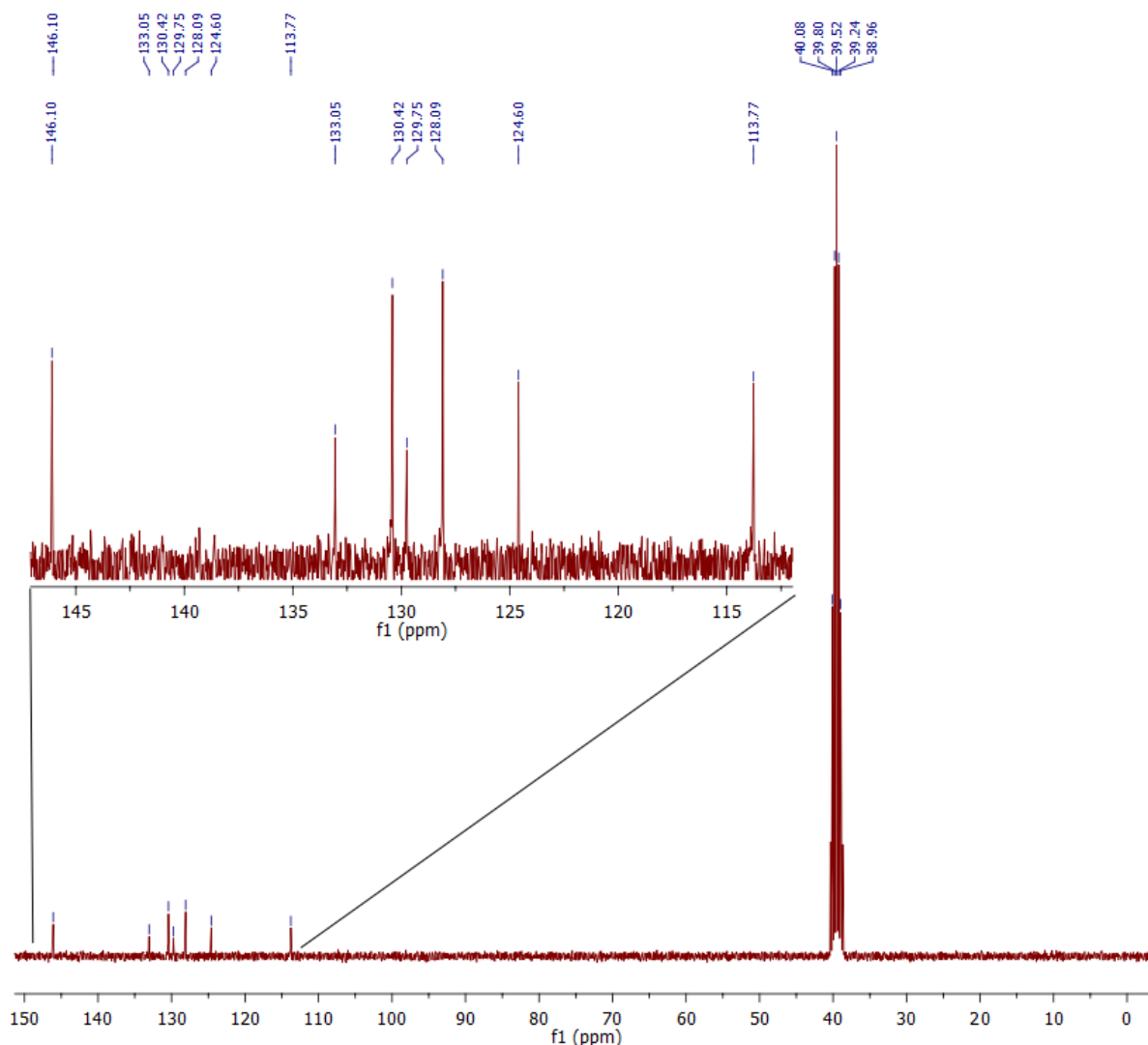


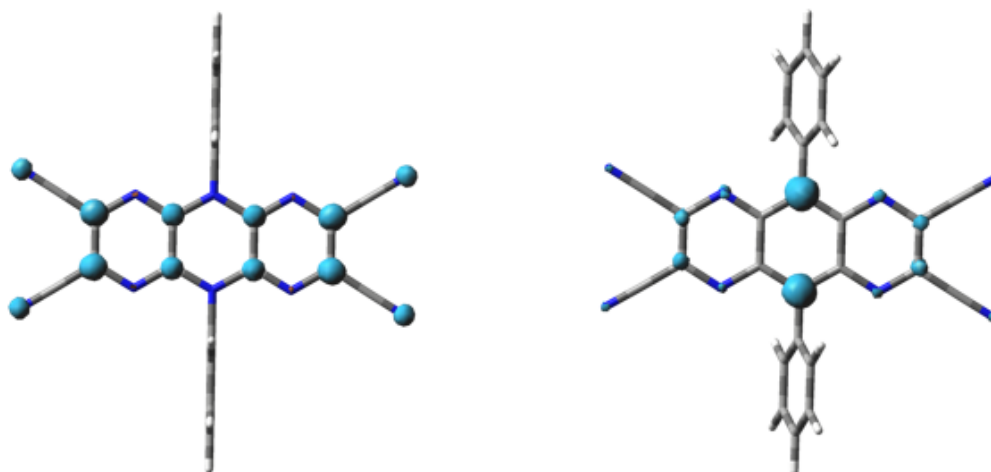
Figure S6. ^{13}C NMR spectra (75 MHz, DMSO-d_6 , δ): 146.10 (ArCCN), 133.05 (NCN), 130.42 (ArC), 129.75 (ArC), 128.09 (ArC), 124.60 (CCN), 113.77 (CN), obtained for molecule **2** synthesized by method **b**). The signal (δ) at 39.52 (sep) is the solvent signal of DMSO.

Density functional theory (DFT). The theoretical calculations are based on density functional theory using the Gaussian09 program package (Version A.02).[1] The hybrid functional B3LYP[2, 3] was selected in combination with the 6-31G* basis set. For all calculations, the solvent environment was modelled for acetonitrile using the implemented polarization continuum model (PCM).[4, 5] The geometries of the singlet ground state (S_0) were first optimized, which serve as the starting point for the optimization of the corresponding oxidized (D^+) or reduced (D^-) doublet states. In cases of difficult SCF convergence, additional extra quadratic (xqc) functions were used. The true nature of all minima structures was confirmed by vibrational analysis showing no imaginary frequencies. The formal absolute

redox potentials were calculated from the difference in energy (including zero-point vibrational energy), *i.e.* the formal oxidation were calculated between S_0 and D^+ (−6.09 V), and S_0 and D^- (−3.28 V). The absolute potentials were referenced *versus* the calculated potentials of $Fc^{+/0}$ in acetonitrile (−4.57 V) according to Batista and coworkers, *i.e.* on the basis of the absolute SHE potential (−4.60 V), and the calculated potential of $Fc^{+/0}$ *vs.* SHE (+0.51 V) and the systematic offset caused by the B3LYP functional (−0.48 V).[6] Hence, the theoretical redox potentials of the title compound are +1.52 V (oxidation) and −1.29 V (reduction) in acetonitrile *vs.* ferrocene. The graphical visualizations were generated by GaussView5.0.8,[7] *i.e.* isovalues were drawn at 0.002, 0.005 or 0.008 (spin-density calculations).

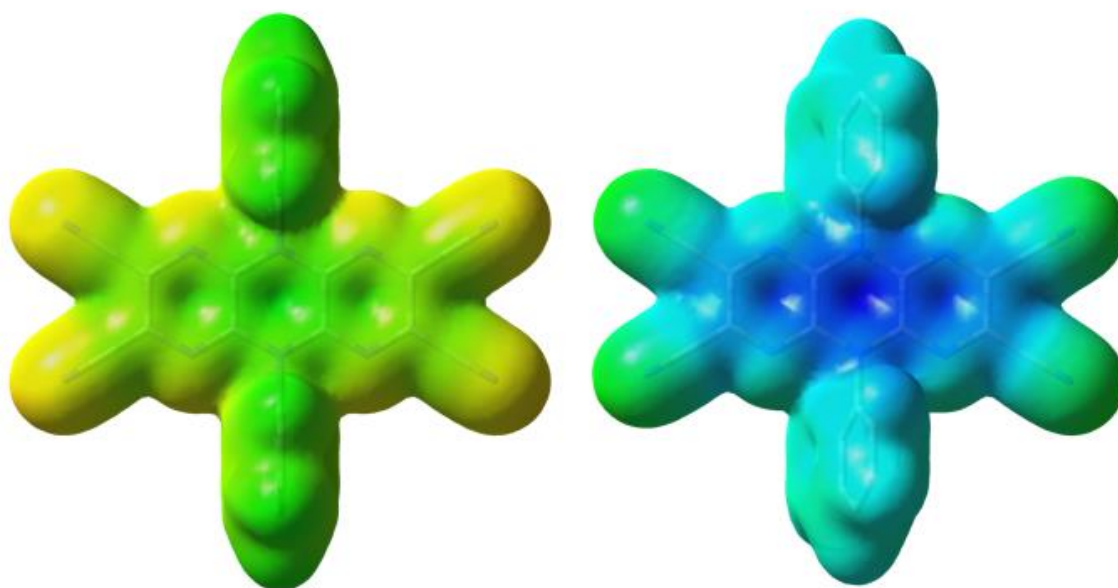
The hybrid functional B3LYP in combination with the 6-31G* basis set as well as the implemented polarized continuum model (PCM) was utilized for all calculations, due to the pleasing study of seven different density functionals combined with three different basis sets, under consideration of additional necessary assumptions such as solvation effects, published by Batista *et al.*[6] In particular, the calculation of the redox potentials in acetonitrile can be best performed by the combination of the hybrid functional B3LYP with the 6-31G* basis set and reveals a promising approach to achieve the most comparable results to the experimental values. Furthermore, the solvent environment was modeled for acetonitrile using the implemented polarization continuum model (PCM), because in consideration of the interaction between the molecule and solvent probably only the PCM model supplies a rough estimate of the changes in the electronic distribution. Batista and coworkers further recommend to utilize a calculated absolute potential of a standard reference (as the case may be with a correction term of −0.48 V) like ferrocene, when the calculated redox potentials are compared to experimental values. However, – under allowance of the standard reference (ferrocene) and the solvent (acetonitrile) – the combination of the hybrid functional B3LYP with the 6-31G* basis set as well as the implemented polarization continuum model (PCM) had the most accordance of the calculated redox potentials with the experimentally determined ones.

	S ₀ (-1468.03933336 hartree)			D ⁺ (-1467.81566541 hartree)			D ⁻ (-1468.15588080 hartree)		
Atom	x	y	z	x	y	z	x	y	z
C	-1.202120	0.719050	-0.000012	-2.041550	-0.524730	0.711550	-1.207190	-0.729610	0.000000
C	-1.202330	-0.718690	0.000005	-1.838310	0.136330	-0.543240	-1.207180	0.729620	0.000002
N	-0.000211	-1.412850	0.000000	-2.908030	0.658500	-1.245070	0.000007	1.416220	0.000000
C	1.202120	-0.719050	-0.000005	-4.177210	0.524540	-0.715390	1.207190	0.729610	-0.000002
C	1.202330	0.718690	0.000011	-4.379080	-0.144330	0.535540	1.207180	-0.729620	0.000000
N	0.000211	1.412850	0.000000	-3.308920	-0.656060	1.239940	-0.000007	-1.416220	0.000000
N	-2.328780	1.398270	-0.000026	-1.020910	-1.044100	1.383640	-2.332900	-1.403480	-0.000002
C	-3.484870	0.698200	-0.000026	0.193830	-0.923120	0.858550	-3.499420	-0.712580	0.000000
C	-3.485070	-0.697160	0.000012	0.395260	-0.271680	-0.391080	-3.499410	0.712620	0.000006
N	-2.329190	-1.397570	0.000031	-0.625190	0.239520	-1.071680	-2.332890	1.403500	0.000007
N	2.328780	-1.398270	-0.000032	-5.198300	1.051860	-1.379570	2.332900	1.403480	-0.000007
C	3.484870	-0.698200	-0.000013	-6.413770	0.920320	-0.858620	3.499420	0.712590	-0.000007
C	3.485070	0.697160	0.000025	-6.615110	0.247350	0.379530	3.499410	-0.712620	0.000000
N	2.329190	1.397570	0.000025	-5.593690	-0.264580	1.058030	2.332890	-1.403500	0.000002
C	0.000432	2.864460	0.000000	-3.512980	-1.315170	2.523180	-0.000014	-2.863180	0.000000
C	-0.000432	-2.864460	0.000000	-2.701640	1.329910	-2.517430	0.000014	2.863180	0.000000
C	-0.000537	-3.545560	1.216510	-2.006670	2.540800	-2.538120	-0.000019	3.549940	-1.214000
C	-0.000746	-4.941170	1.211050	-1.814180	3.175750	-3.763380	-0.000011	4.945870	-1.210320
C	-0.000855	-5.637870	0.000001	-2.301980	2.598870	-4.939480	0.000028	5.643930	0.000000
C	-0.000753	-4.941170	-1.211050	-2.992030	1.384040	-4.896750	0.000060	4.945870	1.210320
C	-0.000538	-3.545560	-1.216510	-3.202690	0.739800	-3.679420	0.000054	3.549940	1.214000
C	0.000559	3.545560	-1.216510	-4.088280	-2.585290	2.545800	-0.000039	-3.549940	1.214000
C	0.000768	4.941180	-1.211050	-4.279950	-3.204910	3.780090	-0.000048	-4.945870	1.210320
C	0.000855	5.637870	0.000001	-3.906090	-2.555030	4.959370	-0.000028	-5.643930	0.000000
C	0.000731	4.941170	1.211050	-3.333300	-1.281300	4.912370	-0.000001	-4.945870	-1.210320
C	0.000516	3.545560	1.216510	-3.127970	-0.649360	3.686690	0.000004	-3.549940	-1.214000
C	-4.705780	1.453400	-0.000059	1.294310	-1.486980	1.588710	-4.704460	-1.466180	-0.000004
C	-4.706210	-1.452000	0.000045	1.705130	-0.159010	-0.968740	-4.704440	1.466230	0.000011
N	-5.699660	-2.055650	0.000080	2.771250	-0.074670	-1.421910	-5.704110	2.071610	0.000009
N	-5.699050	2.057350	-0.000079	2.194790	-1.936940	2.168120	-5.704130	-2.071560	-0.000014
C	4.705780	-1.453400	-0.000046	-7.513930	1.494970	-1.580670	4.704460	1.466180	-0.000012
C	4.706210	1.452000	0.000057	-7.926890	0.112960	0.948410	4.704440	-1.466230	0.000004
N	5.699660	2.055650	0.000077	-8.994400	0.011550	1.394710	5.704110	-2.071610	0.000014
N	5.699050	-2.057350	-0.000081	-8.414290	1.953010	-2.153940	5.704130	2.071550	-0.000010
H	-0.000476	-2.990540	2.149280	-1.638920	2.982080	-1.618250	-0.000057	2.994910	-2.147030
H	-0.000823	-5.481420	2.152860	-1.283810	4.121860	-3.796340	-0.000027	5.485870	-2.152660
H	-0.001020	-6.723890	0.000001	-2.144160	3.097000	-5.891000	0.000034	6.730180	0.000000
H	-0.000842	-5.481430	-2.152860	-3.366270	0.933840	-5.810420	0.000082	5.485870	2.152660
H	-0.000431	-2.990540	-2.149280	-3.730840	-0.206080	-3.633050	0.000087	2.994910	2.147030
H	0.000514	2.990540	-2.149280	-4.369170	-3.080270	1.622480	-0.000045	-2.994910	2.147030
H	0.000861	5.481430	-2.152860	-4.721020	-4.195750	3.816850	-0.000078	-5.485870	2.152660
H	0.001020	6.723890	0.000002	-4.061480	-3.042220	5.916980	-0.000034	-6.730180	0.000000
H	0.000803	5.481420	2.152860	-3.046240	-0.775110	5.828380	0.000023	-5.485870	-2.152660
H	0.000393	2.990540	2.149280	-2.689910	0.341530	3.634780	0.000016	-2.994910	-2.147030



Spin density difference reduced form Spin density difference oxidized form

Figure S7. Schematic representation of the spin density difference of the reduced species (left) and the oxidized species (right) with mapped H-atoms, drawn at an isovalue of 0.008, which were determined by DFT using the Gaussian09 program package (Version A.02).[1] The hybrid functional B3LYP[2, 3] was selected in combination with the 6-31G* basis set. For all calculation, the solvent environment was modelled for acetonitrile using the implemented polarization continuum model (PCM).[4, 5]



Spin density difference reduced form Spin density difference oxidized form

Figure S8. Schematic representation of the spin density difference of the reduced species (left) and the oxidized species (right) with the electrostatic potential (−0.3 to 0.3) mapped onto the total density, drawn at an isovalue of 0.005, which were determined by DFT using the Gaussian09 program package (Version A.02).[1] The hybrid functional B3LYP[2, 3] was selected in combination with the 6-31G* basis set. For all calculation, the solvent environment was modelled for acetonitrile using the implemented polarization continuum model (PCM).[4, 5]

Cyclic voltammetry (CV) measurements with IR drop compensation. To the best of our knowledge there exists no information about the electron transfer processes of the TCAA

derivatives. To determine n (number of electrons) for both the oxidation/re-reduction and reduction/re-oxidation redox-couple, cyclic voltammetry measurements with IR drop compensation were performed, because for a reversible redox process the peak potential separation ($E_{pa} - E_{pc}$) is equal to $59 \text{ mV} / n$.

At an scan rate of 50 mV/s the reduction/re-oxidation redox-couple show a peak split ($E_{pa} - E_{pc}$) of 68.23 mV and the oxidation/re-reduction redox-couple a peak split ($E_{pa} - E_{pc}$) of 75.32 mV , which results in $n = 0.86$ for the reduction and $n = 0.78$ for the oxidation redox process. Including the fact of non ideal reversible redox-reactions, the investigated TCAA derivative 2 features for the oxidation and reduction, respectively, a one electron process.

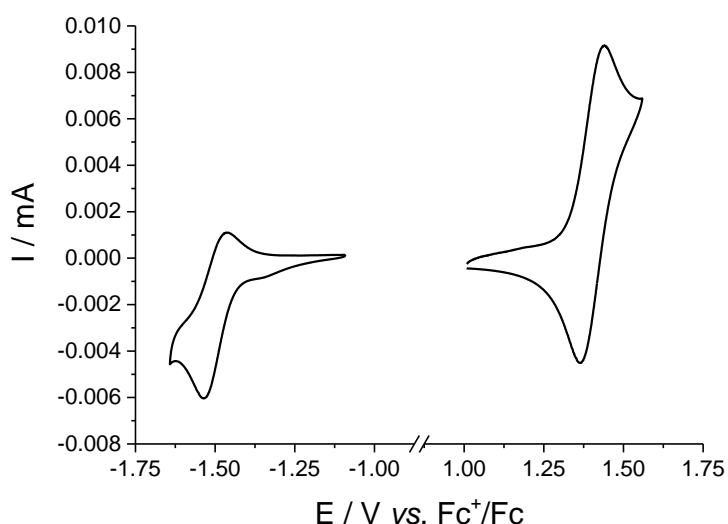


Figure S9. Cyclic voltammogram obtained for 3.5 mM CH_3CN solution of **2** with 0.1 M TBAPF_6 as supporting electrolyte at a scan rate of 50 mV/s .

References

- [1] M.J. Frisch, G.W. Trucks, H.B. Schlegel, G. Scuseria, M.A. Robb, J.R. Cheeseman, G. Scalmani, V. Barone, B. Mennucci, G.A. Petersson, H. Nakatsuji, M. Caricato, X. Li, H.P. Hratchian, A.F. Izmaylov, J. Bloino, G. Zheng, J.L. Sonnenberg, M. Hada, M. Ehara, K. Toyota, R. Fukuda, J. Hasegawa, M. Ishida, T. Nakajima, Y. Honda, O. Kitao, H. Nakai, T. Vreven, J. Montgomery, Jr., J.E. Peralta, F. Ogliaro, M. Bearpark, J.J. Heyd, E. Brothers, K.N. Kudin, V.N. Staroverov, R. Kobayashi, J. Normand, K. Raghavachari, A. Rendell, J.C. Burant, S.S. Iyengar, J. Tomasi, M. Cossi, N. Rega, N.J. Millam, M. Klene, J.E. Knox, J.B. Cross, V. Bakken, C. Adamo, J. Jaramillo, R. Gomperts, R.E. Stratmann, O. Yazyev, A.J. Austin, R. Cammi, C. Pomelli, J.W. Ochterski, R.L. Martin, K. Morokuma, V.G. Zakrzewski, G.A. Voth, P. Salvador, J.J. Dannenberg, S. Dapprich, A.D. Daniels, Ö. Farkas, J.B. Foresman, J.V. Ortiz, J. Cioslowski, D.J. Fox, Gaussian 09, Gaussian, Inc., Wallingford, CT, 2010.

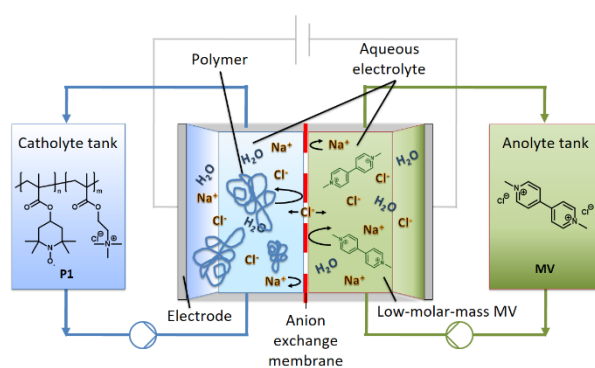
- [2] A.D. Becke, Density-functional thermochemistry 3. The role of exact exchange, *J. Chem. Phys.*, 98 (1993) 5648-5652.
- [3] C.T. Lee, W.T. Yang, R.G. Parr, Development of the Colle-Salvetti correlation-energy formula into a functional of the electron-density, *Physical Review B*, 37 (1988) 785-789.
- [4] E. Cancès, B. Mennucci, J. Tomasi, A new integral equation formalism for the polarizable continuum model: theoretical background and applications to isotropic and anisotropic dielectrics, *J. Chem. Phys.*, 107 (1997) 3032-3041.
- [5] J. Tomasi, B. Mennucci, R. Cammi, Quantum mechanical continuum solvation models, *Chem. Rev.*, 105 (2005) 2999-3093.
- [6] L.E. Roy, E. Jakubikova, M.G. Guthrie, E.R. Batista, Calculation of one-electron redox potentials revisited. Is it possible to calculate accurate potentials with density functional methods?, *J. Phys. Chem. A*, 113 (2009) 6745-6750.
- [7] R. Dennington, T. Keith, J.M. Millan, GaussView 5.0, Semicchem, Inc., Wallingford, CT, 2008.

Publication P4

An aqueous all-organic RFB employing a (2,2,6,6-tetramethylpiperidin-1-yl)oxyl-containing polymer as catholyte and dimethyl viologen dichloride as anolyte

T. Hagemann, J. Winsberg, M. Grube, I. Nischang, T. Janoschka, N. Martin, M. D. Hager, U. S. Schubert,

J. Power Sources **2018**, 378, 546-554.



Reproduced with permission of Elsevier, Copyright © 2018.



An aqueous all-organic redox-flow battery employing a (2,2,6,6-tetramethylpiperidin-1-yl)oxyl-containing polymer as catholyte and dimethyl viologen dichloride as anolyte

Tino Hagemann^{a, b}, Jan Winsberg^{a, b}, Mandy Grube^{a, c}, Ivo Nischang^{a, c}, Tobias Janoschka^d, Norbert Martin^d, Martin D. Hager^{a, b}, Ulrich S. Schubert^{a, b, c, *}

^a Laboratory of Organic and Macromolecular Chemistry (IOMC), Friedrich Schiller University Jena, Humboldtstrasse 10, 07743 Jena, Germany

^b Center for Energy and Environmental Chemistry Jena (CEEC Jena), Friedrich Schiller University Jena, Philosophenweg 7a, 07743 Jena, Germany

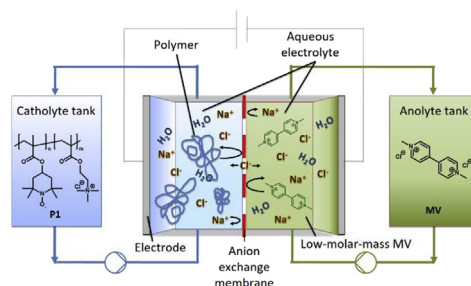
^c Jena Center for Soft Matter (JCSM), Friedrich Schiller University Jena, Philosophenweg 7, 07743 Jena, Germany

^d JenaBatteries GmbH, Botzstrasse 5, 07743 Jena, Germany

HIGHLIGHTS

- A redox-flow battery utilizing polymer and low-molar-mass compound was manufactured.
- Safe aqueous sodium chloride solution and cheap anion-exchange membranes were used.
- A TEMPO copolymer and paraquat were employed as active materials.
- Various flow conditions, conductive salt concentrations, membranes were investigated.

GRAPHICAL ABSTRACT



ARTICLE INFO

Article history:

Received 26 May 2017

Received in revised form

30 August 2017

Accepted 2 September 2017

Keywords:

Aqueous all-organic

Combined polymer-/low-molar-mass redox-flow battery

Dimethylviologene

TEMPO

ABSTRACT

Herein we present a new redox-flow battery (RFB) that employs a (2,2,6,6-tetramethylpiperidin-1-yl)oxyl (TEMPO) containing copolymer (**P1**) as catholyte and the viologen derivative *N,N'*-dimethyl-4,4'-bipyridinium dichloride (**MV**) as anolyte in an aqueous sodium chloride solution. This is the first time that a combination of an organic polymer and a low-molar-mass organic redox-active material is presented. The electrochemical behavior of the utilized charge-storage materials were investigated by cyclic voltammetry (CV) and feature reversible redox-reactions at $E_{1/2} = 0.7$ V (TEMPO/TEMPO⁺) and $E_{1/2} = -0.6$ V vs. AgCl/Ag (MV²⁺/MV^{•+}), which lead to a promising cell voltage of 1.3 V in the subsequent battery application.

Studies were performed to determine the most suitable anion-exchange membrane (AEM), the ideal conducting salt concentration and the optimal flow rate. The resulting battery reveals a stable charge/discharge performance over 100 consecutive cycles with coulombic efficiencies of up to 95%, a high energy efficiency of 85% and an overall energy density of the electrolyte system of 3.8 W h L⁻¹.

© 2017 Elsevier B.V. All rights reserved.

* Corresponding author. Laboratory of Organic and Macromolecular Chemistry (IOMC), Friedrich Schiller University Jena, Humboldtstrasse 10, 07743 Jena, Germany.

E-mail address: ulrich.schubert@uni-jena.de (U.S. Schubert).

1. Introduction

The climate change, caused primarily by greenhouse gas emissions, provoked a rethinking of the world energy production [1–4].

In order to reduce CO₂ emissions, research is directed towards 'greener' and more sustainable sources such as solar and geothermal energy as well as hydroelectricity and wind power [5–7]. Thereby, solar energy and wind power, which are in comparison to hydroelectricity and geothermal energy not limited by several crucial preconditions such as certain geographical circumstances, will become the most relevant renewable energy source for the future [8–10]. Unfortunately, the present electricity grids are not suitable for this kind of intermittent electricity production, and have to be advanced by the incorporation of flexible and scalable energy-storage systems to render the energy transition successful [5,11].

In particular, redox-flow batteries (RFBs) are convenient for the storage of wind and solar electricity, since they can be adapted to the generator unit. Unlike most electrochemical energy-storage technologies, flow batteries exhibit the benefit of independent scalability in capacity and in power [5,12]. State-of-the-art, commercially available systems such as the all-vanadium [13–16] and Fe/Cr [17–19] RFB have the disadvantage of utilizing critical and high-priced metal salts and/or corrosive electrolyte solutions (e.g., sulfuric acid) together with expensive cation-exchange membranes such as Nafion® [12,20–22]. Therefore, current research focuses on aqueous electrolyte systems, inexpensive membranes and organic charge-storage materials featuring safety, environmental, and cost benefits. Low-molar-mass compounds such as quinones [23–27], stable nitroxide radicals [28–33], and *N,N'*-disubstituted 4,4'-bipyridine (viologen) derivatives [12,30,33,34] as well as polymers bearing these functionalities [22,35–41] were investigated for this purpose [5].

For aqueous electrolyte systems, viologen species are better suited as anolytes than anthraquinones because of their high water solubility and low reduction potential [5,12]. Care however, should be taken to use these viologen derivatives, in particular the *N,N'*-dimethyl-4,4'-bipyridinium dichloride (**MV**), since they are widely used herbicides and known for their phytotoxicity. Notwithstanding, due to their chemical reversibility, fast reaction kinetics and economical aspects (2,2,6,6-tetramethyl-piperidin-1-yl)oxyl (TEMPO) derivatives are attractive catholyte materials. Consequently, aqueous all-organic RFBs with high capacity and power utilizing TEMPO/viologen derivatives as active materials were published in the last few years. For example, Janoschka et al. [22] developed a novel RFB concept based on TEMPO- and viologen-containing polymers and utilized pH-neutral sodium chloride solution as well as affordable dialysis membranes [22]. In addition, Liu et al. [30] and Janoschka et al. [12] utilized *N,N'*-dimethyl-4,4'-bipyridinium dichloride as well as the TEMPO derivatives 4-HO-TEMPO [30] and TEMP-TMA [12] as a low-molar-mass-compound based version of this aqueous all-organic RFB.

To determine whether an organic polymer and a low-molar-mass organic compound can be used as charge-storage materials, a combined all-organic aqueous RFB utilizing sodium chloride as conducting salt and low cost AEMs was developed. The system was investigated in detail. Particular focus was on electrochemical performance and long-term stability in comparison to low-molar-mass- and polymer-based RFBs. As active materials and for comparability, the well-known low-molar-mass **MV** [12,30,34] in combination with the TEMPO-containing copolymer poly(2,2,6,6-tetramethylpiperidinyloxy-4-yl methacrylate-co-[2-(methacryloyl-oxy)ethyl]trimethylammonium chloride) [22] (**P1**) were utilized. Particular advantage of this combined system for cost benefits results from the low cost of the AEMs and the utilized **MV**, which is a well-known herbicide produced on 100,000 ton-scale. The flow rate of the electrolytes, the concentration of the supporting electrolyte, the behavior without the use of additional conducting salt and the type of anion-exchange membrane (AEM)

are key factors addressed in the present study. Except the latter, these important factors in terms of the battery performance have only partially been addressed in previously published studies so far.

2. Experimental

2.1. Materials, chemicals and methods

All starting materials were purchased from commercial sources and were used as obtained. Poly(2,2,6,6-tetramethylpiperidinyloxy-4-yl methacrylate-co-[2-(methacryloyloxy)ethyl]trimethylammonium chloride) (**P1**) was a test sample provided as aqueous solution (capacity of 8.3 Ah L⁻¹) by Polymaterials AG (Germany). For the dialysis of **P1**, a regenerated cellulose-based dialysis membrane (Spectra/Por® 6, Spectrum Laboratories, Inc., USA) with a molecular-weight cut-off (MWCO) of 1000 g mol⁻¹ and a flat width of 45 mm was utilized. The used graphite felt (2.25 × 2.25 × 0.4 cm³, sigrancell® GFA6 EA, SGL Carbon, Germany), as well as the utilized anion-exchange membranes fumasep® FAA-3-PE30, FAP-PK-3130, FAS-30 and FAA-3-50 (all Fumatech BWT, Germany), were cut into appropriate pieces.

Reactions were monitored by using a Shimadzu (Japan) GCMS-1-system with a GC-QP2010S-detector and an Agilent (USA) DB-5ms-column. ¹H NMR spectra were recorded on a Bruker (USA) AC 300 (300 MHz) spectrometer at 298 K. Chemical shifts are reported in parts per million (ppm, δ scale) relative to the residual signal of the deuterated solvent. Electrospray ionization (ESI) mass spectrometry measurements were performed on a micrOTOF Q-II (Bruker Daltonics Inc., USA) ESI time-of-flight (ESI-TOF) system. Asymmetric flow field-flow fractionation (AF4) coupled to a refractive index and multi angle laser light scattering (MALLS) detector (PN3621, Postnova Analytics GmbH, Germany) was used to determine the absolute molar mass and dispersity of **P1** with independently determined values of the refractive index increment dn/dc by an Optilab rEX system (Wyatt, Germany) (see [Supporting Information](#) for complete experimental details). The radical content of **P1** was determined via X-Band electron paramagnetic resonance (EPR) spectroscopy. The measurements were conducted on an EMXmicro CW-EPR spectrometer from Bruker (USA) using powdered samples. The total spin count was estimated by an average of nine measurements. The calculated errors of the determined theoretical charge storage capacities, including the volume errors, mass errors and errors of the measured EPR activities, are around 10%.

2.2. Synthesis and characterization of **MV** and **P1**

4,4'-Bipyridine (100 g, 0.64 mol) was dissolved in dimethylformamide (600 mL). Afterwards, chloroacetic acid (163.4 g, 1.72 mol) was added [42] and the suspension was heated to 140 °C, whereas the chloroacetic acid dissolved, followed by stirring at 130 °C overnight. After cooling to room temperature, the formed precipitate was filtered off and washed with hot dimethylformamide, chloroform, dichloromethane (each two times) to obtain the yellowish pure product **MV** (160.64 g, 0.63 mol) in a yield of 98%. ¹H NMR (Fig. S1, 300 MHz, D₂O, δ in ppm): 9.03 (d, *J* = 6.8 Hz, 4H, Ar H), 8.49 (d, *J* = 6.7 Hz, 4H, Ar H), 4.48 (s, 6H, CH₃); ESI-TOF MS (Fig. S2) *m/z* (%): 93 (100) [M²⁺], 171 (23) [M⁺ - CH₃].

Poly(2,2,6,6-tetramethylpiperidinyloxy-4-yl methacrylate-co-[2-(methacryloyloxy)ethyl] trimethylammonium chloride) (**P1**) was a test sample provided as aqueous solution (capacity of 8.3 Ah L⁻¹) in a molar ratio (2,2,6,6-tetramethylpiperidin-4-yl-methacrylate:[2-(methacryloyloxy)ethyl]trimethylammonium chloride) of 1:1 by Polymaterials AG (Germany). The aqueous solution was dialysed against water (MWCO = 1000 g mol⁻¹) and lyophilized to

yield an orange powder. The number-average $M_n = 20,600 \text{ g mol}^{-1}$ and weight average molar mass $M_w = 35,300 \text{ g mol}^{-1}$, resulting in a relatively broad dispersity of $\bar{D} = 1.71$, was determined by AF4-MALLS (Fig. S3); ^1H NMR (Fig. S4, 300 MHz, D_2O , δ in ppm): 5.02 (s, br, 1H), 4.49 (s, br, 2H), 3.77 (s, br, 2H), 3.22 (s, br, 9H), 2.15–1.06 (m, 36H), (radical quenched by phenylhydrazine, for the multiplett at 2.15–1.06 ppm after integration an amount of 26 protons was expected; however, 36 protons were calculated, which belong to the hydrolysis of the methacrylic ester in the backbone of the copolymer); absolute spin-activity: $6.93 \times 10^{17} \text{ spins mg}^{-1}$ (equals a radical content of $50 \pm 4\%$ of the TEMPO moiety of **P1**), capacity (given error corresponds to the error propagation calculated from the theoretical capacity and the measured EPR activities): $30 \pm 3 \text{ mA h g}^{-1}$ (both determined by EPR, Fig. S5).

2.3. Electrochemical characterization

Cyclic voltammetry (CV) measurements were conducted on a VMP3 potentiostat/galvanostat (Bio-Logic, France), with a glassy-carbon disk (diameter 2 mm), an AgCl/Ag reference electrode for aqueous electrolytes and a platinum wire counter electrode.

2.4. Cell assembly

The static laboratory cell was designed and constructed in a flat cell type with a membrane active area of 5 cm^2 (JenaBatteries GmbH, Germany), see Fig. S6 for a detailed overview. Charge/discharge tests were conducted on a VMP3 potentiostat/galvanostat (Bio-Logic, France). The electrolyte was circulated between the electrochemical cell and the storage tanks with a peristaltic pump (Hei-FLOW Value 01 Multi, Heidolph, Germany). Typically, 10 mL of electrolyte were used with a flow rate from 4 up to 16 mL min^{-1} . All pumped flow cell measurements were carried out at room temperature under argon atmosphere. For static flow cell measurements 4 mL of electrolyte, whereby the active usable volume is 1.84 mL (see Supporting Information for calculation of the effective usable volume), per half-cell were utilized. The batteries were charged/discharged with constant current and the resulting potential was measured over time. The electric cell resistance (R_I with and R_2 without the FAA-3-50 AEM) was determined by electrochemical impedance spectroscopy (EIS). Afterwards, the area resistance (R) was calculated by using the equation, $R = (R_I - R_2) \cdot A$ in $[\Omega \text{ cm}^2]$ with $A =$ area of the used 5 cm^2 test cell.

3. Results and discussion

3.1. Synthesis, characterization, and electrochemical behavior

To investigate the general applicability of a combined all-organic aqueous RFB, a suitable organic polymer as well as a low-molar-mass-based charge-storage material is required. Therefore, we used the N,N' -dimethyl-4,4'-bipyridinium dichloride (**MV**) as anolyte and a TEMPO-containing copolymer **P1** as catholyte. In particular, this active material combination was chosen with regard to a further application on a large-scale and for future commercialization. On the one hand, **MV** (also known as paraquat) is produced in a two-step synthesis from inexpensive educts on the multi-ton scale by Syngenta® (Switzerland), therefore being much cheaper than respective polymers and readily available for battery production. On the other hand, the only commercially available and water-soluble TEMPO molecule (4-HO-TEMPO; TEMPOL) is comparatively more expensive and poorly suitable for RFB application due to side reactions. The long-term usability of 4-HO-TEMPO as active material is restricted by the auto-oxidation of the OH-functionality forming the 4-keto-TEMP-hydroxylamine [43].

Hence, co-polymers working without OH-functionalities and being water soluble represent a suitable alternative.

The synthesis of the anode material **MV** (Scheme 1, Fig. S1) started from 4,4'-bipyridine and was carried out according to the literature [12,42].

The basic electrochemical behavior of **MV** was studied by cyclic voltammetry (CV) and advanced cyclic voltammetry (CVA). In contrast to CV a hold time after each forward scan is implemented at CVA measurements. This experimental design is used to investigate the chemical reversibility of the redox-process in an environment, which is more representative to a battery operation. Both measurements (Fig. 1) were performed in 1 M aqueous sodium chloride solution with a low concentration of the redox-active material of 10 mM. In general, viologens can undergo a two-step reduction. The first reduction yields a monocationic radical species **MV^{•+}** (Scheme 1), which shows a characteristic intense blue color. The following second reduction step yields the neutral colorless species **MV⁰**. However, for battery application only the first reduction, which is completely chemically reversible, is usable due to occurring side reactions and insolubility of **MV⁰** [12,44,45].

The cyclic voltammogram (Fig. 1a), obtained for 10 mM **MV**, shows a chemically reversible reduction and re-oxidation at $E_{1/2} = -0.6 \text{ V}$ vs. AgCl/Ag for the **MV^{•+}/MV^{•+}** redox couple. The cyclic voltammogram (Fig. 1b), obtained with the CVA under the same conditions, exhibits no significant differences to the original voltammogram.

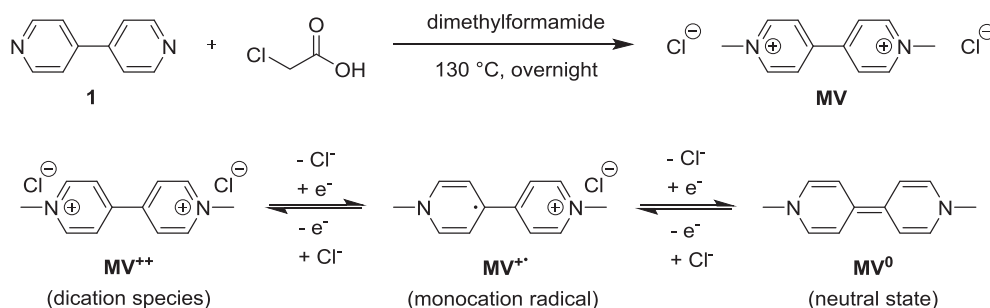
The utilized copolymer **P1** (see Scheme 2), which contains the radical TEMPO as well as a quaternary ammonium cation moiety in a 1:1 ratio to increase the solubility in water, was prepared via a free radical copolymerization of 2,2,6,6-tetramethylpiperidin-4-yl-methacrylate and [2-(methacryloyloxy)ethyl]trimethyl ammonium chloride, followed by oxidation with $\text{H}_2\text{O}_2/\text{Na}_2\text{WO}_4$ [22]. An industrial sample solution of this material was dialysed against water ($\text{MWCO} = 1000 \text{ g mol}^{-1}$) and lyophilized to obtain an orange powder for further applications. Its weight-average molar mass (M_w) was determined to be $35,300 \text{ g mol}^{-1}$ ($\bar{D} = 1.71$) in an absolute manner by AF4-MALLS, since size-exclusion chromatography did not provide adequate estimations of the molar mass. The radical content of **P1** was determined by EPR spectroscopy, indicating an absolute spin-activity of $6.93 \times 10^{17} \text{ spins mg}^{-1}$ and, hence, a capacity of $30 \pm 3 \text{ mA h g}^{-1}$ (given error corresponds to the error propagation calculated from the theoretical capacity and the measured EPR activities). Afterwards, the electrochemical behavior of **P1** was studied by cyclic voltammetry as well as advanced cyclic voltammetry, with a low active-material concentration of 5 mM **P1** in 1 M NaCl_{aq} solution (Fig. 2).

The cyclic voltammogram (Fig. 2a) shows a chemically reversible oxidation and re-reduction at a half-wave potential of 0.7 V vs. AgCl/Ag for the TEMPO/TEMPO^{•+} redox couple. The spectrum (Fig. 2b), obtained by CVA measurements under the same conditions, also displays a chemically reversible redox wave at $E_{1/2} = 0.7 \text{ V}$ vs. AgCl/Ag and, therefore, no significant differences.

3.2. Battery tests

3.2.1. Membrane tests

The separator represents a crucial component of a RFB, because of economic aspects (besides the fact that the active material is one of the main cost elements [34,46]) and associated performance parameters such as lifetime, current, and energy density. Therefore, it should be tailor-made for RFB applications and ideally exhibit a low ohmic resistance in the utilized electrolyte as well as a good permeability for the supporting electrolyte ions to allow a high counterion mobility. At the same time, it should prevent cross-contamination of the redox-active species, which would



Scheme 1. Schematic representation of the synthesis route to **MV** (top) and its two possible reductions steps of **MV⁺⁺** (bottom).

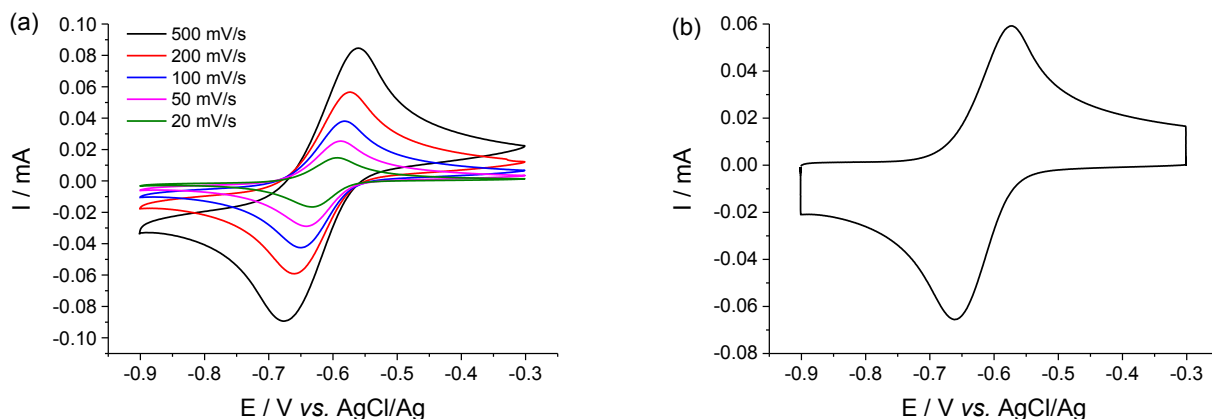
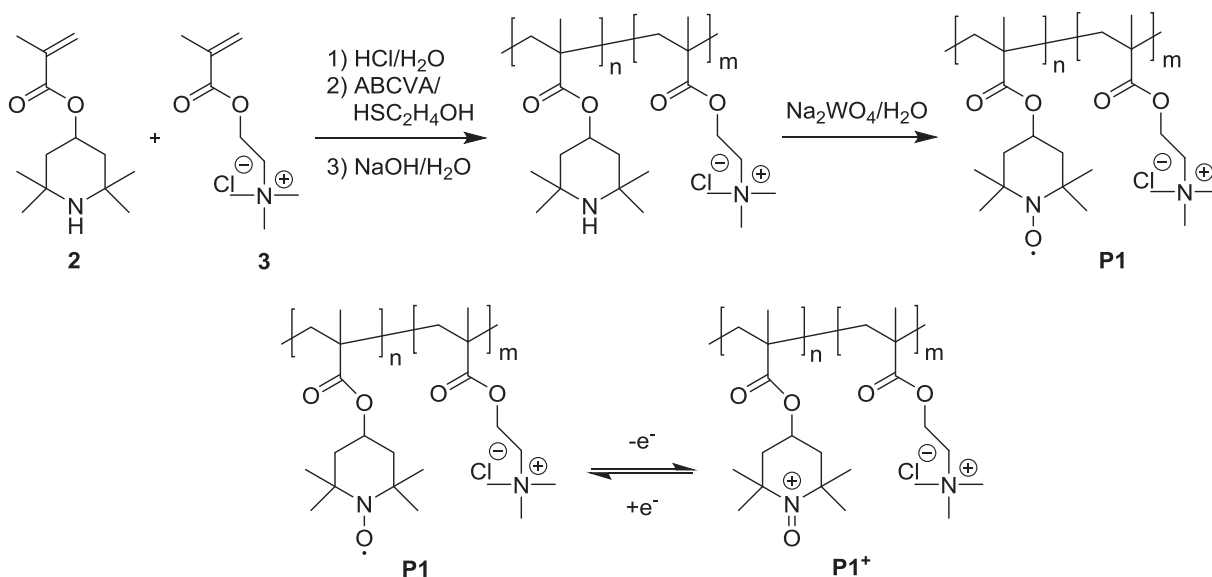


Fig. 1. Characterization of **MV**: Cyclic voltammogram obtained for 10 mM aqueous solution of **MV** with 1 M NaCl as supporting electrolyte, (a) at different scan rates and (b) via an advanced method including a hold time of 5 min at the inversion potential (exemplary at 200 mV s⁻¹).



Scheme 2. Schematic representation of the synthesis route and the redox-reaction of **P1**. The TEMPO containing copolymer **P1** was originally prepared by Janoschka et al. [22] via a free radical polymerization followed by a polymer-analogous oxidation (top); redox reaction of **P1** (bottom). ABCVA = 4,4'-azobis(4-cyanovaleric acid).

otherwise result in a low coulombic efficiency and in a long-term capacity decay. Furthermore, a good mechanical stability and chemical inertness are essential for a long lifetime [5]. Commonly used perfluorinated Nafion® (DuPont, USA) membranes should be replaced due to economic aspects (ca. US\$ 500/m²) [30,34], while lower-priced dialysis membranes are not suitable for separation of

low-molar-mass materials such as **MV**.

Since both utilized active materials exhibit a positive charge in all occurring redox-states, inexpensive anion-exchange membranes were chosen for all battery tests. These AEMs (all Fumatech BWT, Germany) offer cost saving versus Nafion® membranes by around 30–70%. Four different types, namely the FAA-3-PE30, FAP-

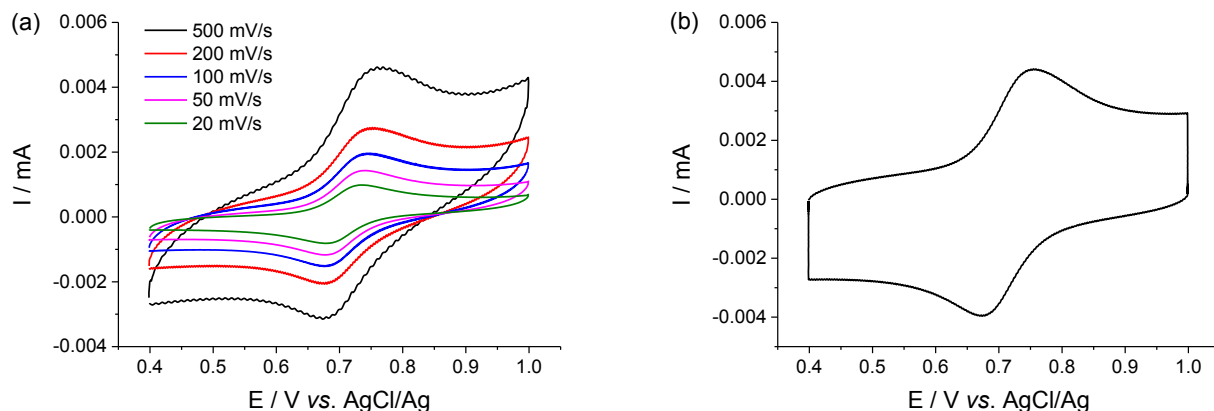


Fig. 2. Characterization of **P1**: Cyclic voltammogram obtained for 5 mM aqueous solution of **P1** with 1 M NaCl as supporting electrolyte, (a) at different scan rates and (b) via an advanced method including a hold time of 5 min (exemplary at 200 mV s⁻¹).

PK-3130, FAS-30 and FAA-3-50 (detailed technical data in Table S1) were investigated in a flow cell (Fig. S7) employing 0.5 M **MV** and **P1** (each in a 1.5 M NaCl_{aq} solution) as well as graphite felt electrodes.

To determine the electric cell resistance and to study the impact of the current density on the performance, the four cells were charged/discharged in a voltage window of 0.80–1.35 V (Fig. 3, Table S2). No apparent degradation of the electrolyte that would result in hydrogen-, oxygen- or chlorine-formation, was noticed.

The FAS-30 and the FAA-3-50 AEM show the lowest area resistance with 3.32 and 1.67 Ω cm² (calculated after determination of the electric cell resistance by electrochemical impedance spectroscopy, EIS), respectively and therefore the best ion mobility. Furthermore, nine different current densities (1, 2, 3, 4, 6, 8, 10, 12 and 16 mA cm⁻²) could be applied. In contrast, for the flow cells employing the FAA-3-PE30 or the FAP-PK-3130 membrane lower maximum current densities of only 8 and 12 mA cm⁻² were applicable and higher area resistances of 9.62 and 7.77 Ω cm² were

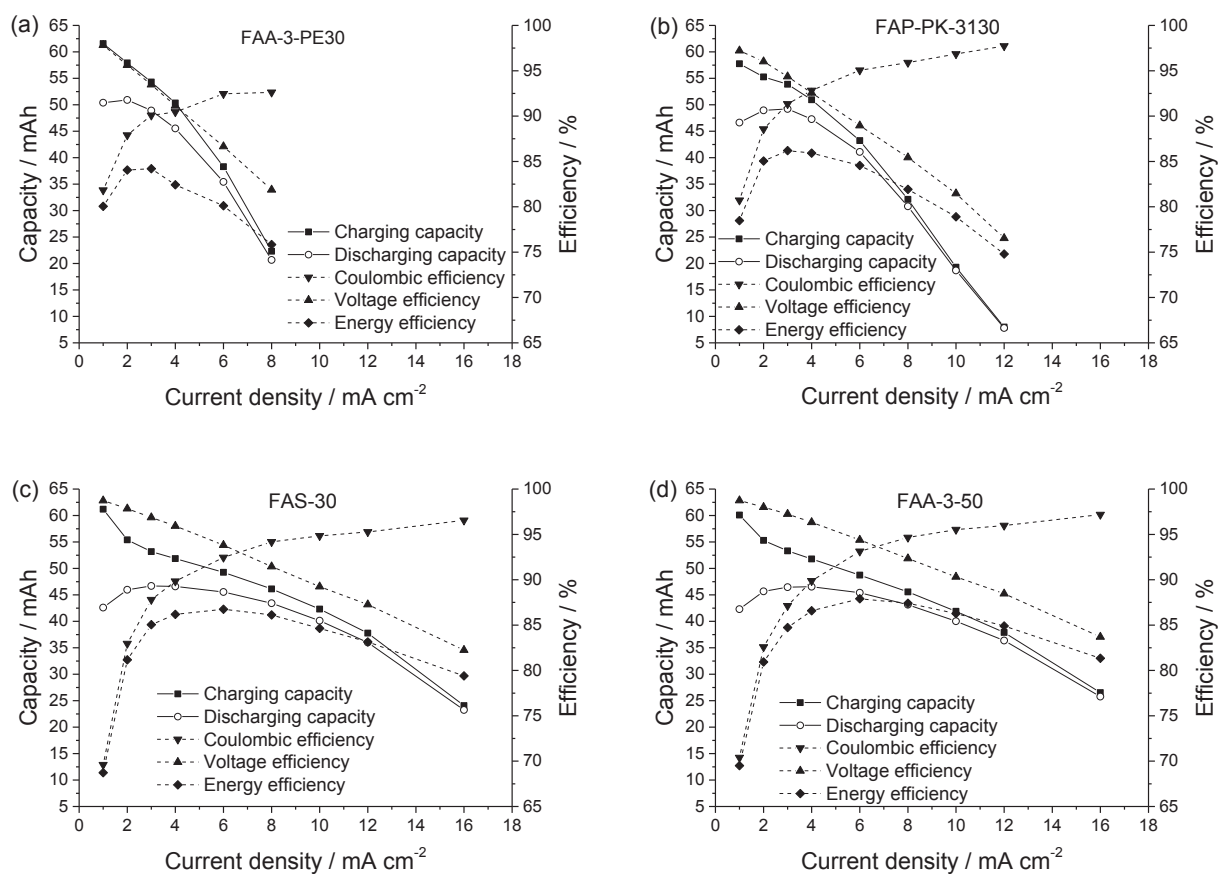


Fig. 3. Electric performance of a pumped 5 cm² test cell including capacity, coulombic, voltage, and energy efficiency depending on the current density (0.5 M **MV** and **P1** in 1.5 M NaCl_{aq}; 10 mL electrolyte per half-cell; flow rate adjusted to 16 mL min⁻¹; theoretical charge storage capacity of 6.5 Ah L⁻¹); a) fumasep® FAA-3-PE30, b) fumasep® FAP-PK-3130, c) fumasep® FAS-30 and d) fumasep® FAA-3-50 AEM.

found. Comparing the values for the charging/discharging capacity as well as the coulombic, voltage and energy efficiency (Fig. 3a–d) similar results were achieved. In particular, Fig. 3c and d (FAS-30 and FAA-3-50 AEM) display a high conformity with coulombic efficiencies up to 97%, energy efficiencies of 80–87% (except for a current density of 1 mA cm^{-2}) and charging capacities of 62 to 42 mAh at current densities of $1\text{--}10 \text{ mA cm}^{-2}$. Nevertheless, also the flow cell tests of FAA-3-PE30 and FAP-PK-3130 present appreciably good results with coulombic efficiencies of up to 92/98%, energy efficiencies of 75/85%, and charging capacities of 61 to 32 mAh at current densities of $1\text{--}6 \text{ mA cm}^{-2}$.

To summarize, in all cell tests a parabolic rise of the coulombic efficiency and a linear drop of the voltage efficiency with increasing current densities can be observed. This may be caused by the increasing potential gap between the charging and discharging plateaus. The charging capacities decrease with increasing current densities. Furthermore, it was shown that all four employed AEMs are suitable for this low-molar-mass/polymer combined aqueous RFB. However, due to the lowest electric cell resistance and best performance parameters the fumasep® FAA-3-50 AEM is utilized for all following flow cell experiments.

3.2.2. Influence of the conducting salt concentration on the electric cell resistance

Commonly, supporting electrolytes (conducting salts) are used for charge balancing and to increase the conductivity of the electrolyte solution [5]. For example, Hu et al. [34] investigated the influence of the conducting salt concentration on the conductivity of the electrolytes. In terms of safety and economic aspects, the utilization of sodium chloride in aqueous solution as the supporting electrolyte is favored.

However, due to the high mobility of chloride counterions of **MV** [12], it is an interesting consideration whether the utilization of a conducting salt such as NaCl is generally essential for this combined RFB. Therefore, a flow cell without additional conducting salt was charged/discharged in a voltage window of 0.80–1.35 V (Fig. 4a) and the impact on the current rating investigated (Fig. 4b).

The obtained results (Fig. 4a and b) verify that the usage of a conducting salt is not mandatory. However, the achieved performance parameters are inferior compared to those of the same flow cell (Fig. 3d) using additional 1.5 M NaCl_{aq} conducting salt. For example, it exhibits a three times higher area resistance ($10.1 \Omega \text{ cm}^2$) and only current densities of up to 6 mA cm^{-2} are achievable. Therefore, the utilization of NaCl_{aq} as conducting salt

for the combined aqueous RFB is highly recommended. To determine its optimal concentration, a flow cell was cycled with electrolytes containing 0–5 M NaCl (Fig. 5, Table S3).

With increasing NaCl concentration (up to 1.5 M) the electric cell and area resistance decreases nearly linear until a plateau at 1.5 M is reached. At even higher concentrations over 3 M the resistance slightly rises again. This behavior is attributed to an increase in the viscosity of the NaCl_{aq} solution, leading to a decline in their mobility.

On the basis of these results, a 1.5 M NaCl_{aq} solution was utilized as electrolyte for all pumped flow cell tests, because the best compromise between a high counterion mobility and solution viscosity is accomplished at this concentration.

3.2.3. Investigation of the influence of the flow rate on the battery performance

In contrast to previous publications that studied the active material design, the optimization of flow conditions has, surprisingly, not been addressed so far. Since the flow rate used to pump the electrolyte through a cell stack has a significant influence on a battery's overall efficiency and on the performance of the cell itself, the discharge capacity on the utilized electrolyte flow rate was investigated. The flow cell was charged/discharged in a voltage

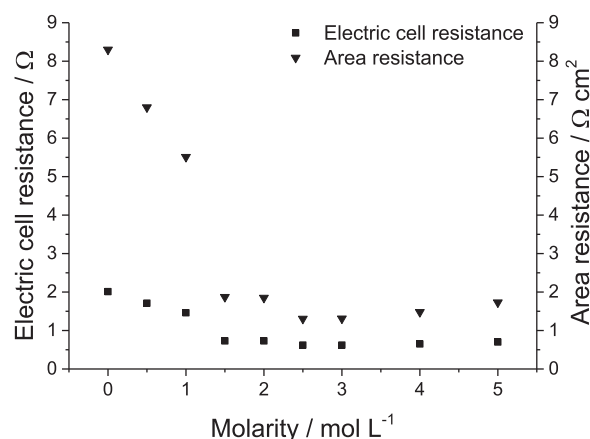


Fig. 5. Electric cell and area resistance of a 5 cm^2 test cell as a function of the utilized concentration of the NaCl_{aq} solution (10 mL solution per half-cell, flow rate adjusted to 16 mL min^{-1} , FAA-3-50 AEM).

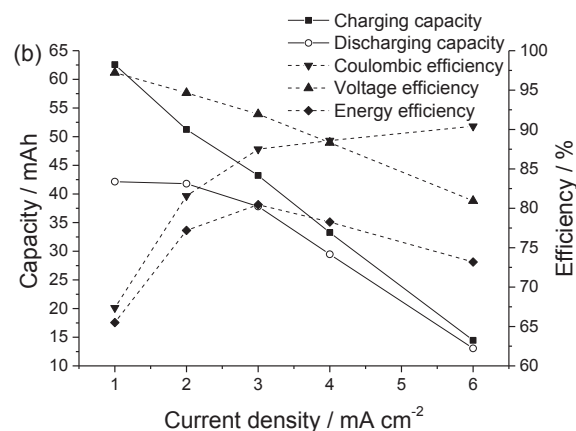
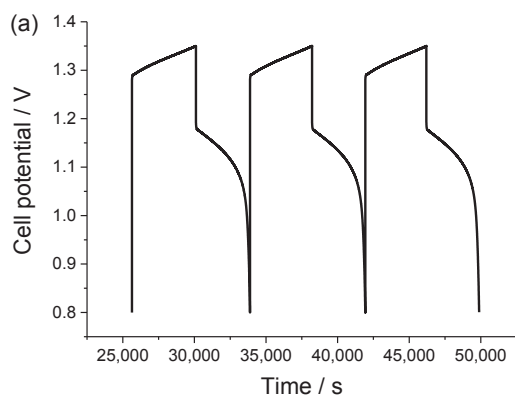


Fig. 4. Pumped 5 cm^2 test cell, employing the FAA-3-50 AEM, with 0.5 M of **MV** and **P1** in aqueous solutions (with a theoretical charge storage capacity of 6.7 Ah L^{-1}), 10 mL electrolyte per half-cell, flow rate adjusted to 16 mL min^{-1} ; a) exemplary 3rd to 5th charge/discharge cycle at a current density of 5 mA cm^{-2} , b) capacity, coulombic-, voltage-, and energy efficiency depending on the current density.

window of 0.80–1.35 V at a current density of 10 mA cm^{-2} . In a first experiment, the flow rate of the anolyte and catholyte solutions were increased from 4 mL min^{-1} to 8 and 12 mL min^{-1} , reaching up to 16 mL min^{-1} (Fig. 6). This equals a full exchange of the solution within the cell of two up to eight times per minute.

When comparing a static with a dynamic flow cell, the overall efficiency and the performance of the pumped cell itself is incomparably better, because in a static set-up only a restricted amount of the redox-active materials diffuses to the active electrode area. Furthermore, the utilized cell design allows only a partial assessment of the available electrolyte volume. However, by utilizing a dynamic set-up an increase of the flow rate improves the overall efficiency and performance of the cell only to a moderate extent. Therefore, as obvious in Fig. 6 the discharge capacity only slightly rises with increasing flow rate (up to 16 mL min^{-1}). For the next experiment, the flow rate of the anolyte and the catholyte were changed independently of each other. First, the **P1** containing catholyte was set at a constant rate of 4 mL min^{-1} while the flow rate of **MV** was altered (Fig. S8a). Second, the flow rate of the **P1** containing catholyte was studied at constant flow rate of **MV** (Fig. S8b). Compared to the previous experiment, with increasing flow rate of only one electrolyte solution (other electrolyte solution constant at 4 mL min^{-1} flow rate during the test) the discharge capacity only imperceptibly changed.

To summarize, both experiments indicate that the influence of the flow rate compared to other important factors, such as the conducting salt concentration or the employed AEM, appears less significant.

3.2.4. Investigation of the long-term cycling stability

Based on the results of the applicability of four different AEMs, the influence of the conducting salt concentration, the flow rate, as well as the voltage window, the following conditions were chosen for a final long-term cycling stability test, carried out in a static test cell (Fig. 7) and pumped (Fig. 8) 5 cm^2 flow cell: fumasep® FAA-3-50 AEM, 0.5 M MV and **P1**, each in a $1.5 \text{ M NaCl}_{\text{aq}}$ solution, charging/discharging with a constant current density of 5 mA cm^{-2} in a voltage window of 0.80–1.35 V and a constant flow rate of 16 mL min^{-1} for the pumped flow cell.

The static test cell was charged/discharged for 2,500 consecutive cycles. A capacity of 6.8 mAh was achieved in the fifth cycle (Fig. 7). The theoretical possible discharge capacity is 12.3 mAh, this equals

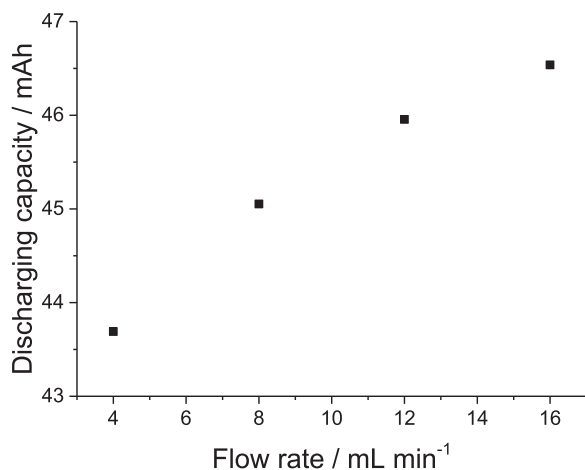


Fig. 6. Discharging capacity of a pumped 5 cm^2 test cell, employing the FAA-3-50 AEM, with 0.5 M MV and **P1** (both in $1.5 \text{ M NaCl}_{\text{aq}}$ solution, with a theoretical charge storage capacity of 6.7 Ah L^{-1} , 10 mL electrolyte per half-cell, as a function of the utilized electrolyte flow rate.

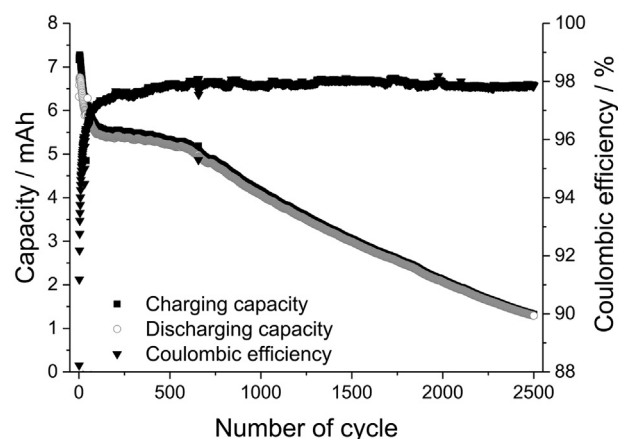


Fig. 7. Long-term cycling stability test in a static electrochemical 5 cm^2 test cell with 0.5 M MV and **P1** (each in $1.5 \text{ M NaCl}_{\text{aq}}$ solution, theoretical charge storage capacity 6.7 Ah L^{-1}): charge/discharge capacity and coulombic efficiency over 2,500 consecutive charge/discharge cycles at a constant current density of 5 mA cm^{-2} .

a material utilization of 55%. This low value can be attributed, as previously described, to the use of a static test cell set-up. The coulombic efficiencies rise within the first 60 cycles from 88 up to 97% and remain constant at 97–98% afterwards. After an initial capacity drop, the capacity is almost constant for 500 cycles before a linear decay in capacity occurs. During the 2,500 consecutive charge/discharge cycles, the maximal discharge capacity of 6.8 mAh decreases to 1.3 mAh, which represents a capacity decay of 81%. This major capacity decay is possibly caused by side reactions, induced by atmospheric oxygen that slowly permeates into the cell and oxidizes the viologen monoradical cation $\text{MV}^{+\bullet}$. Exemplarily for the 5th, 500th and 2,500th cycle a voltage efficiency of ~90% as well as an energy efficiency of 84 and twice 88% were calculated.

A pumped flow battery (Fig. 8) was cycled for 500 consecutive charge/discharge cycles and revealed a maximum discharge capacity of 44.4 mAh, which correlates to 66% of the theoretical possible discharge capacity of 67 mAh. A stable battery cycling was possible for 100 consecutive charge/discharge cycles. Afterwards the discharge capacity rapidly decreased to 2.8 mAh within 400 cycles. This major capacity decay is caused by an osmotic process.

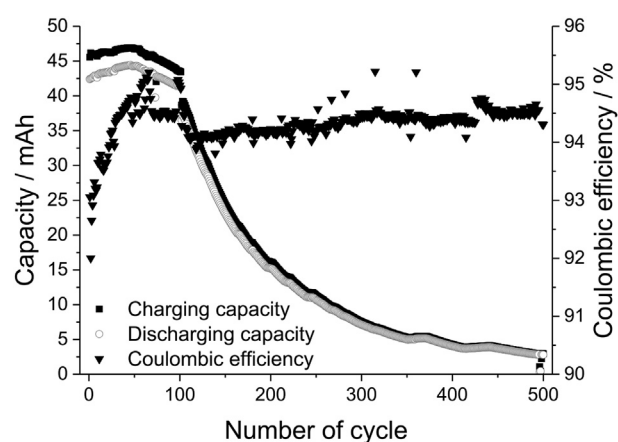


Fig. 8. Long-term cycling stability test in a pumped electrochemical 5 cm^2 test cell with 0.5 M MV and **P1** (each in $1.5 \text{ M NaCl}_{\text{aq}}$ solution, theoretical charge storage capacity 6.7 Ah L^{-1} , 10 mL electrolyte per half-cell, flow rate adjusted to 16 mL min^{-1}): charge/discharge capacity and coulombic efficiency over 500 consecutive charge/discharge cycles at a constant current density.

During the long period of this experiment, it was observed that the electrolyte volume of the **P1** containing half-cell slowly decreased, whereas the volume of the **MV** containing half-cell slowly increased. We assume, that after the 100th cycle the solubility limit of **P1** was achieved, whereby the active material refined on the surface of the electrode (Fig. S9), which results in a pronounced decline of the capacity. To confirm this assumption the osmotic pressure of the catholyte and anolyte, respectively was investigated in an osmosis chamber with determined densities of the catholyte and anolyte solutions (Fig. S10, detailed description in the Supplementary information).

Exemplarily for the 10th and 100th cycle a voltage efficiency of 90 and 91%, as well as an energy efficiency of both times 85% was calculated.

4. Conclusion

A combined aqueous all-organic RFB, which for the first time utilized a polymer as well as low-molar-mass-compound as active materials was manufactured and investigated in detail. A TEMPO-containing copolymer poly(2,2,6,6-tetramethylpiperidinyloxy-4-yl methacrylate-co-[2-(methacryloyloxy)ethyl]trimethyl ammonium chloride) (**P1**) whose absolute molar mass was detailed via solution light scattering and the viologen derivative *N,N'*-dimethyl-4,4'-bipyridinium dichloride (**MV**) dissolved in a safe aqueous sodium chloride solution and affordable AEMs were used. Both redox-active materials are widely considered as suitable charge-storage materials in RFBs and are, due to their economic and environmental benefits, the most promising organic alternatives to the commonly used metal-based active materials. **MV** and **P1** were electrochemically characterized via cyclic voltammetry, which shows a chemically reversible redox-reaction at a half-wave potential of 0.7 V for the TEMPO/TEMPO⁺ redox couple and −0.6 V vs. AgCl/Ag for the MV²⁺/MV^{•+} redox couple, leading to a cell voltage of 1.3 V in a subsequent battery application.

Furthermore, several key factors such as the concentration of the conducting salt, the flow rate of the electrolytes and the applicability of four different AEMs were investigated in detail to approach the best battery performance. With the acquired insights (1.5 M NaCl_{aq} solution, constant flow rate of 16 mL min^{−1}, fumasep[®] FAA-3-50 AEM), long-term cycling stability tests in a static and subsequently in a pumped battery set-up were performed. The final flow cell exhibits a stable charge/discharge performance over 100 consecutive cycles with a discharge capacity of over 44 mAh, coulombic efficiencies up to 95%, a high energy efficiency of 85% as well as an overall energy density of the electrolyte system of 3.8 Wh L^{−1}.

Acknowledgements

We thank the European Regional Development Fund, the Thuringian Ministry for Economic Affairs, Science and Digital Society (TMWWdG) (2015 FE 9112) and the Zentrales Innovationsprogramm Mittelstand (ZIM) (KF 2258008ZG4) for the financial support, René Burgés for electrospray ionization mass spectrometry measurements, and JenaBatteries GmbH for help with the redox-flow cell assembly. Furthermore, the authors acknowledge support of this study from the Thüringer Ministerium für Wirtschaft, Wissenschaft und Digitale Gesellschaft (TMWWdG, ProExzellenz II, NanoPolar).

Appendix A. Supplementary data

Supplementary data related to this article can be found at <https://doi.org/10.1016/j.jpowsour.2017.09.007>.

References

- [1] R.K.P. Tans, NOAA ESRL data: recent global monthly mean CO₂ (accessed 07 april 2017), <https://www.esrl.noaa.gov/gmd/ccgg/trends/global.html#global>, 2017.
- [2] P. Friedlingstein, R.A. Houghton, G. Marland, J. Hackler, T.A. Boden, T.J. Conway, J.G. Canadell, M.R. Raupach, P. Ciais, C. Le Quere, Nat. Geosci. 3 (2010) 811–812.
- [3] Z.J.N. Steinmann, A. Venkatesh, M. Hauck, A.M. Schipper, R. Karupiah, I.J. Laurenzi, M.A.J. Huijbregts, Environ. Sci. Technol. 48 (2014) 5282–5289.
- [4] S. Solomon, G.-K. Plattner, R. Knutti, P. Friedlingstein, Proc. Natl. Acad. Sci. 106 (2009) 1704–1709.
- [5] J. Winsberg, T. Hagemann, T. Janoschka, M.D. Hager, U.S. Schubert, Angew. Chem. Int. Ed. 56 (2017) 686–711.
- [6] P.M. Cox, R.A. Betts, C.D. Jones, S.A. Spall, I.J. Totterdell, Nature 408 (2000) 184–187.
- [7] J.T. Houghton, L.G.M. Filho, B.A. Callander, N. Harris, A. Kattenberg, K. Maskell, Climate Change 1995: the Science of Climate Change, Cambridge Univ. Press, 1996.
- [8] D. Cook, B. Davidsdottir, J.G. Petursson, Renew. Sust. Energy Rev. 49 (2015) 211–220.
- [9] O. Edenhofer, K. Seyboth, F. Creutz, S. Schlömer, Annu. Rev. Environ. Resour. 38 (2013) 169–200.
- [10] S. Weitemeyer, D. Kleinhans, T. Vogt, C. Agert, Renew. Energy 75 (2015) 14–20.
- [11] C. Budischak, D. Sewell, H. Thomson, L. Mach, D.E. Veron, W. Kempton, J. Power Sources 225 (2013) 60–74.
- [12] T. Janoschka, N. Martin, M.D. Hager, U.S. Schubert, Angew. Chem. Int. Ed. 55 (2016) 14427–14430.
- [13] M. Skyllas-Kazacos, M. Rychcik, R.G. Robins, A.G. Fane, J. Electrochem. Soc. 133 (1986) 1057–1058.
- [14] M. Vijayakumar, W. Wang, Z. Nie, V. Sprenkle, J. Hu, J. Power Sources 241 (2013) 173–177.
- [15] S. Roe, C. Menictas, M. Skyllas-Kazacos, J. Electrochem. Soc. 163 (2016) A5023–A5028.
- [16] C. Sun, J. Chen, H. Zhang, X. Han, Q. Luo, J. Power Sources 195 (2010) 890–897.
- [17] N.H. Hagedorn, L.H. Thaller, National Aeronautics and Space Administration, Lewis Research Center, 1982.
- [18] M. Lopez-Atalaya, G. Codina, J.R. Perez, J.L. Vazquez, A. Aldaz, J. Power Sources 39 (1992) 147–154.
- [19] H.L. Thaller, United States Patent Application 3996064, (1976).
- [20] M. Armand, J.M. Tarascon, Nature 451 (2008) 652–657.
- [21] P. Alotto, M. Guarnieri, F. Moro, Renew. Sust. Energy Rev. 29 (2014) 325–335.
- [22] T. Janoschka, N. Martin, U. Martin, C. Friebe, S. Morgenstern, H. Hiller, M.D. Hager, U.S. Schubert, Nature 527 (2015) 78–81.
- [23] W. Wang, W. Xu, L. Cosimbescu, D. Choi, L. Li, Z. Yang, Chem. Commun. 48 (2012) 6669–6671.
- [24] B. Huskinson, M.P. Marshak, C. Suh, S. Er, M.R. Gerhardt, C.J. Galvin, X. Chen, A. Aspuru-Guzik, R.G. Gordon, M.J. Aziz, Nature 505 (2014) 195–198.
- [25] B. Yang, L. Hooper-Burkhardt, F. Wang, G.K. Surya Prakash, S.R. Narayanan, J. Electrochem. Soc. 161 (2014) A1371–A1380.
- [26] K. Lin, Q. Chen, M.R. Gerhardt, L. Tong, S.B. Kim, L. Eisenach, A.W. Valle, D. Hardee, R.G. Gordon, M.J. Aziz, M.P. Marshak, Science 349 (2015) 1529–1532.
- [27] S. Zhang, X. Li, D. Chu, Electrochim. Acta 190 (2016) 737–743.
- [28] X. Wei, W. Xu, M. Vijayakumar, L. Cosimbescu, T. Liu, V. Sprenkle, W. Wang, Adv. Mat. 26 (2014) 7649–7653.
- [29] Z. Li, S. Li, S. Liu, K. Huang, D. Fang, F. Wang, S. Peng, Electrochem. Solid-State Lett. 14 (2011) A171–A173.
- [30] T. Liu, X. Wei, Z. Nie, V. Sprenkle, W. Wang, Adv. Energy Mat. 6 (2016) 1501449.
- [31] W. Duan, R.S. Vemuri, J.D. Milshtein, S. Laramie, R.D. Dmello, J. Huang, L. Zhang, D. Hu, M. Vijayakumar, W. Wang, J. Liu, R.M. Darling, L. Thompson, K. Smith, J.S. Moore, F.R. Brushett, X. Wei, J. Mat. Chem. A 4 (2016) 5448–5456.
- [32] T. Hagemann, J. Winsberg, B. Häupler, T. Janoschka, J.J. Gruber, A. Wild, U.S. Schubert, NPG Asia Mater 9 (2017) e340.
- [33] T. Janoschka, C. Friebe, M.D. Hager, N. Martin, U.S. Schubert, ChemistryOpen 6 (2017) 216–220.
- [34] B. Hu, C. DeBruler, Z. Rhodes, T.L. Liu, J. Am. Chem. Soc. 139 (2017) 1207–1214.
- [35] J. Winsberg, S. Muench, T. Hagemann, T. Janoschka, S. Morgenstern, M. Billing, F.H. Schacher, G. Hauffman, J.-F. Gohy, S. Hoeppe, M. Hager, U.S. Schubert, Polym. Chem. 7 (2016) 1711–1718.
- [36] J. Winsberg, T. Hagemann, S. Muench, C. Friebe, B. Häupler, T. Janoschka, S. Morgenstern, M.D. Hager, U.S. Schubert, Chem. Mat. 28 (2016) 3401–3405.
- [37] J. Winsberg, T. Janoschka, S. Morgenstern, S. Muench, T. Hagemann, G. Hauffman, J.-F. Gohy, M.D. Hager, U.S. Schubert, Adv. Mat. 28 (2016) 2238–2243.
- [38] T. Janoschka, S. Morgenstern, H. Hiller, C. Friebe, K. Wolkersdorfer, B. Häupler, M.D. Hager, U.S. Schubert, Polym. Chem. 6 (2015) 7801–7811.
- [39] S.H. Oh, C.W. Lee, D.H. Chun, J.D. Jeon, J. Shim, K.H. Shin, J.H. Yang, J. Mat. Chem. A 2 (2014) 19994–19998.
- [40] Y. Zhao, S. Si, C. Liao, J. Power Sources 241 (2013) 449–453.

- [41] G. Nagarjuna, J. Hui, K.J. Cheng, T. Lichtenstein, M. Shen, J.S. Moore, J. Rodríguez-López, J. Am. Chem. Soc. 136 (2014) 16309–16316.
- [42] C. Yang, M.-S. Wang, L.-Z. Cai, X.-M. Jiang, M.-F. Wu, G.-C. Guo, J.-S. Huang, Inorg. Chem. Commun. 13 (2010) 1021–1024.
- [43] E. Fritz-Langhals, Org. Process Res. Dev. 9 (2005) 577–582.
- [44] K. Murugavel, Polym. Chem. 5 (2014) 5873–5884.
- [45] C.L. Bird, A.T. Kuhn, Chem. Soc. Rev. 10 (1981) 49–82.
- [46] R.M. Darling, K.G. Gallagher, J.A. Kowalski, S. Ha, F.R. Brushett, Energy Environ. Sci. 7 (2014) 3459–3477.

Supporting Information

An aqueous all-organic redox-flow battery employing a (2,2,6,6-tetramethylpiperidin-1-yl)oxyl-containing polymer as catholyte and dimethyl viologen dichloride as anolyte

Tino Hagemann^{a,b}, Jan Winsberg^{a,b}, Mandy Grube^{a,c}, Ivo Nischang^{a,c}, Tobias Janoschka^d, Norbert Martin^d, Martin D. Hager^{a,b}, Ulrich S. Schubert^{a,b,c,}*

1. Experimental

1.1. Materials, chemicals and methods

All starting materials were purchased from commercial sources and were used as obtained. Poly(2,2,6,6-tetramethylpiperidinyloxy-4-yl methacrylate-*co*-[2-(methacryloyloxy) ethyl]trimethylammonium chloride) (**P1**) was a test sample provided as aqueous solution (capacity of 8.3 Ah L⁻¹) by Polymaterials AG (Germany). For the dialysis of **P1** a regenerated cellulose-based dialysis membrane (Spectra/Por[®] 6, Spectrum Laboratories, Inc., USA) with an molecular-weight cut-off (MWCO) of 1,000 g mol⁻¹ and a flat width of 45 mm was utilized. The used graphite felt (2.25 × 2.25 × 0.4 cm³, sigracell[®] GFA6 EA, SGL Carbon, Germany), as well as the utilized anion-exchange membranes fumasep[®] FAA-3-PE30, FAP-PK-3130, FAS-30 and FAA-3-50 (all Fumatech BWT, Germany), were cut into appropriate pieces. Reactions were monitored by using a Shimadzu (Japan) GC-MS-1-system with a GC-QP2010S-detector and an Agilent (USA) DB-5ms-column. ¹H NMR spectra were recorded on a Bruker (USA) AC 300 (300 MHz) spectrometer at 298 K. Chemical shifts are reported in parts per million (ppm, δ scale) relative to the residual signal of the deuterated solvent. Electrospray ionization (ESI) mass spectrometry measurements were performed on a micrOTOF Q-II (Bruker Daltonics Inc., USA) ESI time-of-flight (ESI-TOF) system. Asymmetric flow field-flow fractionation (AF4) (Postnova Analytics, Germany) was used to determine molar masses.[1] The radical content of **P1** was determined *via* X-Band electron paramagnetic resonance (EPR) spectroscopy. The measurements were conducted on an EMXmicro CW-EPR spectrometer from Bruker (USA) using powdered samples. The total spin count was the average of nine measurements. Cyclic voltammetry (CV) measurements were conducted on a VMP3 potentiostat/galvanostat (Bio-Logic, France), with a glassy-carbon disk (diameter 2 mm), an AgCl/Ag reference electrode for aqueous electrolytes and a platinum wire counter electrode. The densities of the anolyte and catholyte solutions needed for estimations

of the osmotic and hydrostatic pressure were measured with a DMA4100 density meter (Anton Paar, Austria) at a temperature of 20 °C. The accuracy of the obtained density values were enabled by appropriate calibration and verified by a control measurement of the density of pure water arriving at exactly known literature values ($\rho = 0.9982 \text{ g cm}^{-3}$).[2]

1.2. Characterization of the utilized *N,N*-dimethyl-4,4'-bipyridinium dichloride (**MV**)

¹H NMR spectrum of *N,N*-dimethyl-4,4'-bipyridinium dichloride (**MV**).

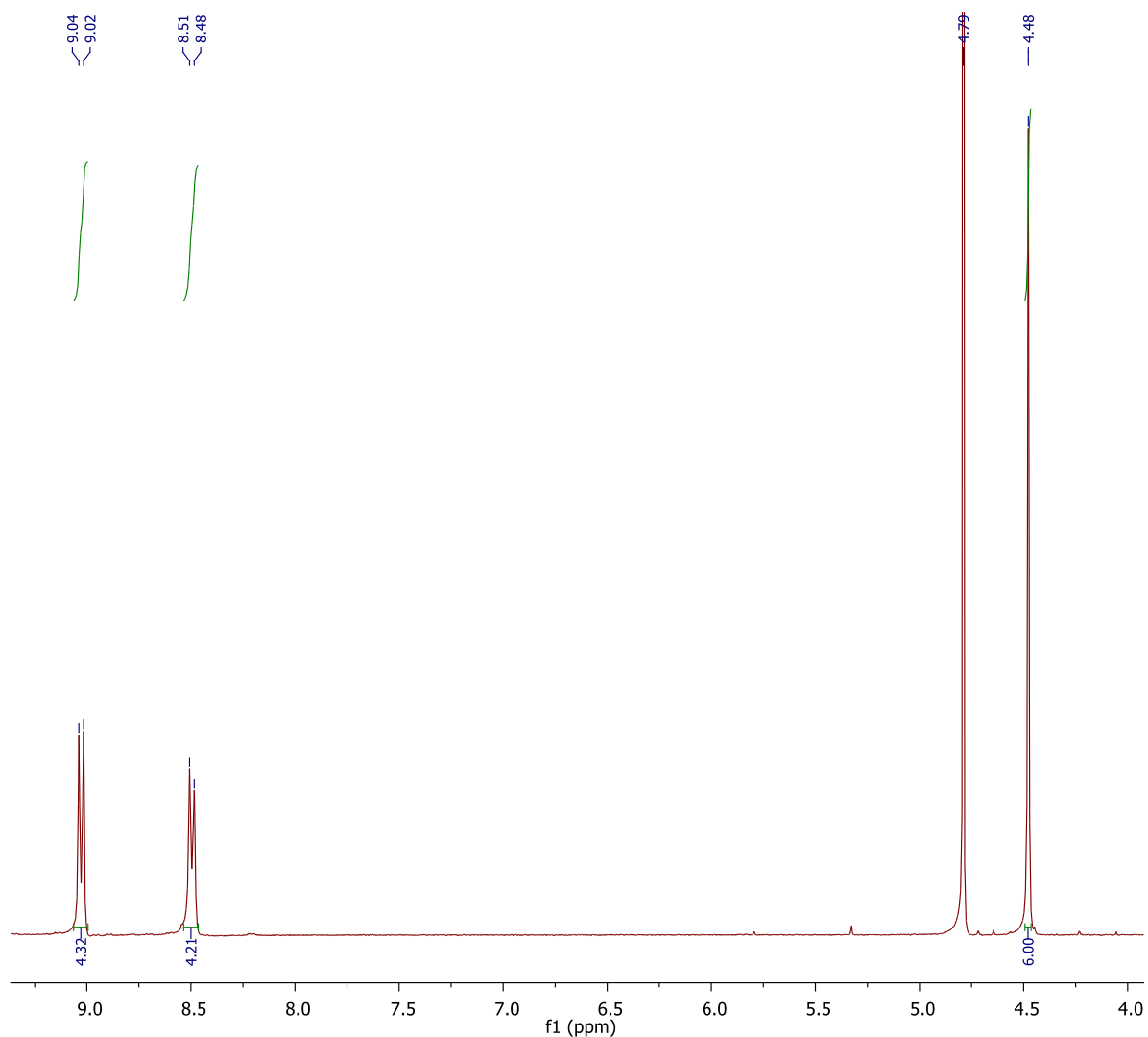


Figure S1. ¹H NMR spectrum (300 MHz, D₂O, δ): 9.03 (d, $J = 6.8 \text{ Hz}$, 4H, Ar H), 8.49 (d, $J = 6.7 \text{ Hz}$, 4H, Ar H), 4.48 (s, 6H, CH₃), obtained for **MV**. The signal (δ in ppm) at 4.79 (s) belongs to the solvent residual peak of D₂O.

ESI-TOF MS spectrum of *N,N*-dimethyl-4,4'-bipyridinium dichloride (**MV**).

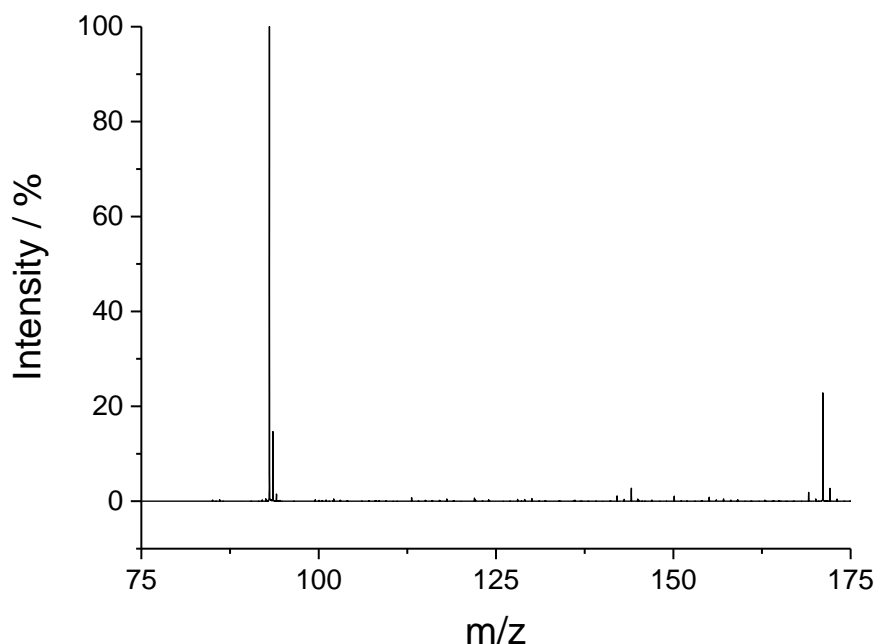


Figure S2. ESI-TOF MS spectrum (positive ion mode, $\text{H}_2\text{O}/\text{CH}_3\text{CN}$, $c = 0.5 \mu\text{g mL}^{-1}$) m/z (%): 93 (100) [M^{2+}], 171 (23) [$\text{M}^+ - \text{CH}_3$], obtained for **MV**.

1.3. Characterization of the utilized poly(2,2,6,6-tetramethylpiperidinyloxy-4-yl methacrylate-co-[2-(methacryloyloxy) ethyl]trimethylammonium chloride) (**P1**)

Asymmetric flow field-flow fractionation (AF4) coupled to multi angle laser light scattering (MALLS)

AF4 was performed on an AF2000 MT System (Postnova Analytics, Germany) coupled to a refractive index (RI) detector as concentration detector (PN3150) and a MALLS detector (PN3621) equipped with a 532 nm laser. Molar mass estimations were performed *via* Zimm-plot. The AF4 system is equipped with a tip and focus pump (PN1130), an autosampler (PN5300), and a channel oven unit (PN4020). The channel had a trapezoidal geometry with an overall footprint area of 31.6 cm^2 . The nominal height of the spacer was $350 \mu\text{m}$ and a 10 kDa molar mass cut off membrane made of regenerated cellulose (Postnova Analytics GmbH, Germany) was used as accumulation wall. All experiments were carried out at a channel oven temperature of $T = 25 \text{ }^\circ\text{C}$ with a fluid phase of 0.9% (w/w) aqueous sodium chloride solution. For the measurements, the focusing time was set to 4 min and $20 \mu\text{L}$ of sample at a concentration of 14.1 mg mL^{-1} were injected with an injection flow rate of 0.2 mL min^{-1} . The cross-flow was set to 2.8 mL min^{-1} and the focus flow rate was set to 3.3 mL min^{-1} , resulting in a detector flow rate of 0.7 mL min^{-1} . After switching to elution, the cross-flow was hold constant for 30 minutes. Afterwards, it was decreased linearly to 0 mL min^{-1} within 5 minutes.

After the cross-flow reached zero, the tip flow was kept constant for at least 5 minutes and elution further monitored. The elution measurement with the corresponding MALLS signal at an angle of 90° are shown in **Figure S3**.

Refractive index increment

Accurate values of the refractive index increment dn/dc needed to estimate appropriate values of the molar mass were determined independently with an Optilab rEX system (Wyatt, Germany) by manual delivery of six known concentrations of **P1** in 0.9% (w/w) aqueous sodium chloride solution, i.e. identical to that used as the liquid phase in AF4. Delivery of solutions was enabled *via* a plastic syringe. The temperature was set to $T = 25^\circ\text{C}$. The dn/dc was calculated by the slope of the plot from the refractive index against the concentration. A value of the dn/dc of 0.160 mL g^{-1} was estimated.

AF4 fractogram of **P1**

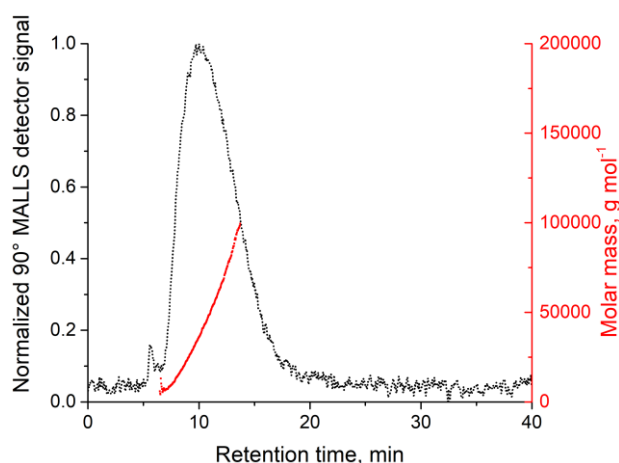


Figure S3. AF4 elugram with elution monitored *via* the MALLS detector at an angle of 90° and the corresponding molar mass trace shown in red for **P1**. Fluid phase in the experiment: 0.9% (w/w) NaCl_{aq} solution. Conditions: concentration: $c = 14.1\text{ mg mL}^{-1}$, Injection volume: $V_{\text{injection}} = 20\text{ }\mu\text{L}$, recovery: 73%.

^1H NMR spectrum of **P1**

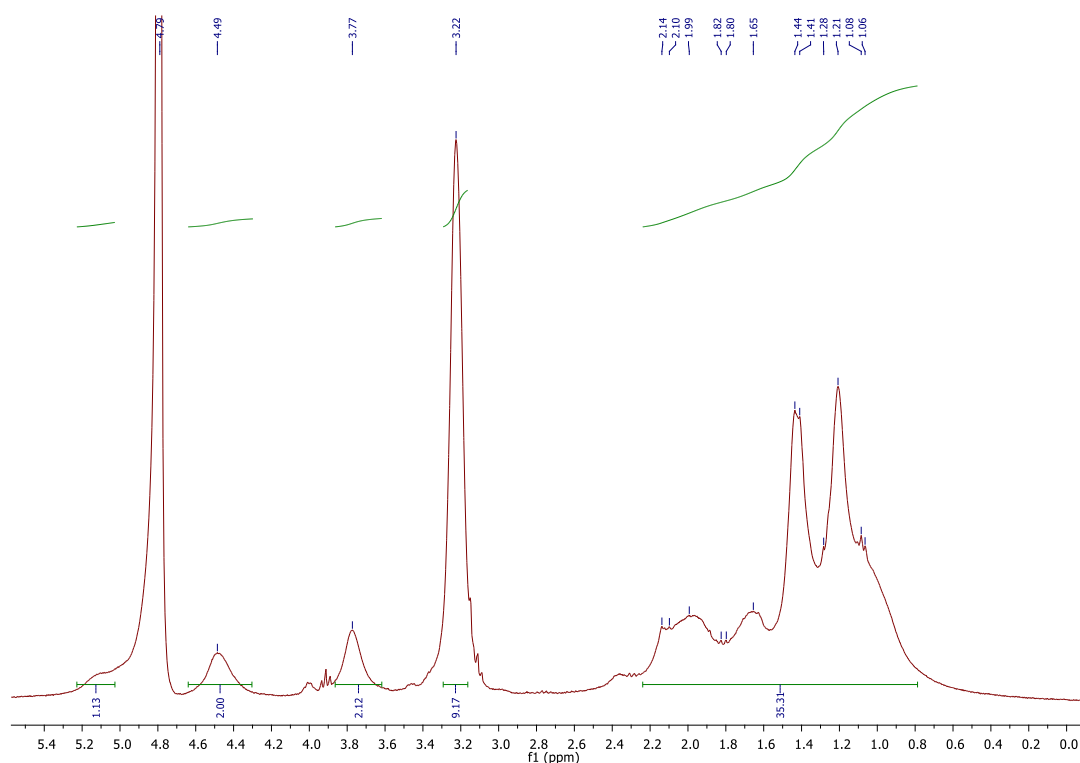


Figure S4. ^1H NMR spectra (300 MHz, D_2O , δ): 5.10 (s, br, 1H), 4.49 (s, br, 2H), 3.77 (s, br, 2H), 3.22 (s, br, 9H), 2.2-0.8 (m, 36H), (radical quenched by phenylhydrazine), obtained for **P1**. The signal (δ in ppm) at 4.79 (s) belongs to the solvent residual peak of D_2O . For the multiplett at 2.15-1.06 ppm after integration a amount of 26 protons was expected, however 36 protons were calculated, which belongs to the hydrolysis product of the methacrylic ester in the backbone of the copolymer.

EPR spectrum of **P1**

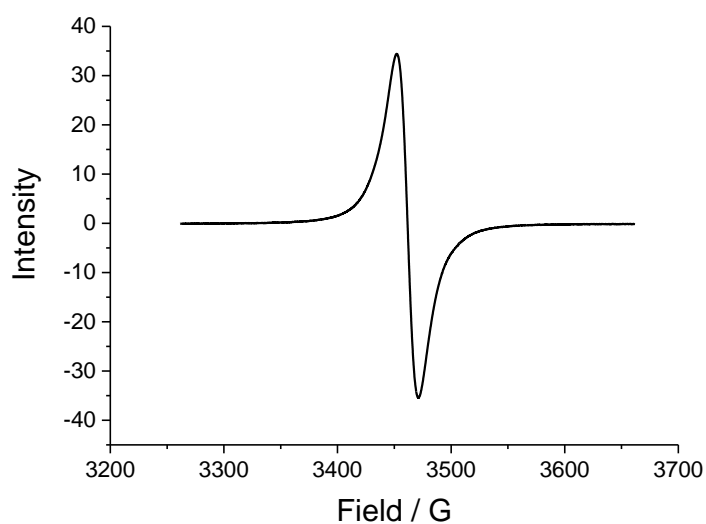


Figure S5. EPR spectrum of **P1** in solid state. According to literature[3, 4] a three-line pattern with an intensity ratio of 1:1:1 is anticipated in aqueous solution, due to the free electron interaction with the ^{14}N nucleus of the nitroxide group. Indeed, the powder spectrum displays only a single line without hyperfine structure due to the high concentration of the nitroxide radicals and the resulting line broadening.

2. Cell assembly

The static laboratory cell was designed and constructed in a flat cell type with a membrane active area of 5 cm² (JenaBatteries GmbH, Germany), see **Figure S6** for a detailed overview. The used graphite felt (2.25 × 2.25 × 0.4 cm³, sigracell[®] GFA6 EA, SGL Carbon, Germany), as well as the utilized anion-exchange membranes fumasep[®] FAA-3-PE30, FAP-PK-3130, FAS-30 and FAA-3-50 (all Fumatech BWT, Germany), were cut into appropriate pieces. Charge/discharge tests were conducted on a VMP3 potentiostat/galvanostat (Bio-Logic, France). The electrolyte was circulated between the electrochemical cell and the storage tanks with a peristaltic pump (Hei-FLOW Value 01 Multi, Heidolph, Germany). Typically, 10 mL of electrolyte were used with a flow rate from 4 up to 16 mL min⁻¹. All pumped flow cell measurements were carried out at room temperature under argon atmosphere. For static flow cell measurements 4 mL of electrolyte per half-cell were utilized, whereby the effective volume is 1.84 mL. The effective volume (V_E) was calculated by using the equation, $V_E = A_g \cdot \tau \cdot \varnothing$ in [mL] with A_g (geometric area of the electrode) = 5 cm², τ (thickness of the electrode) = 4 mm and \varnothing (porosity of the electrode) = 0.92. The batteries were charged/discharged with constant current and the resulting potential was measured over time. The electric cell resistance (R_1 with and R_2 without the FAA-3-50 AEM) was determined by electrochemical impedance spectroscopy (EIS). Afterwards, the area resistance (R) was calculated by using the equation, $R = (R_1 - R_2) \cdot A$ in [Ω cm²] with A = area of the used 5 cm² test cell.

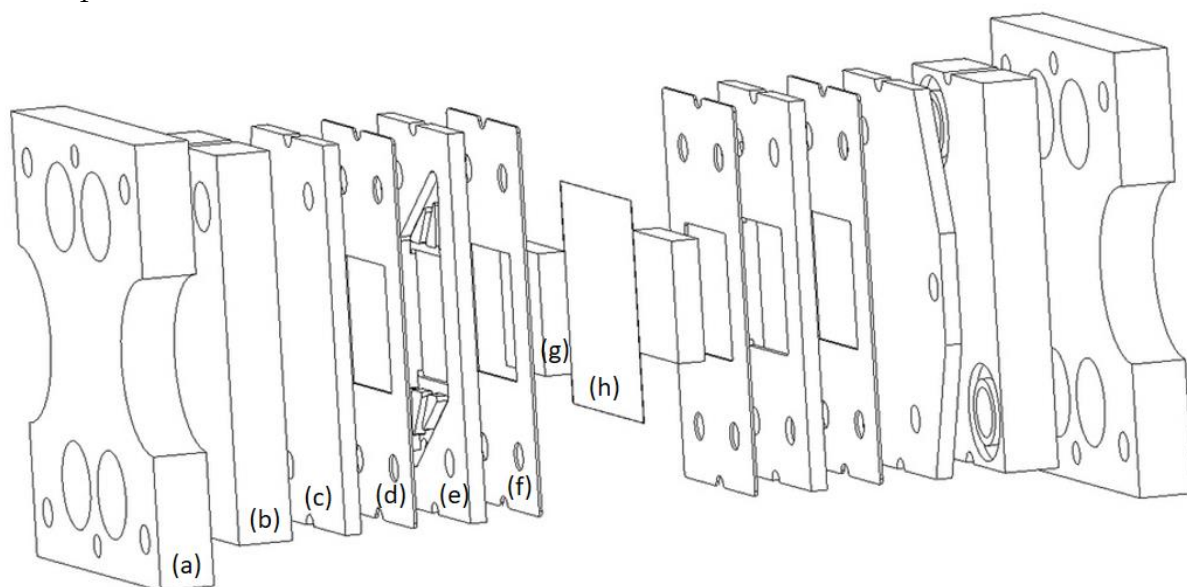


Figure S6. Schematic representation of the 5 cm² test cell. One half-cell consists of a frame (a), PTFE block with hose connections and rubber seal (b), graphite current collector (c), Teflon sealing (d), PTFE flow frame (e), Teflon sealing (f), surface enhancing graphite felt (g). Both half cells are separated by an anion-exchange membrane (h).[5]

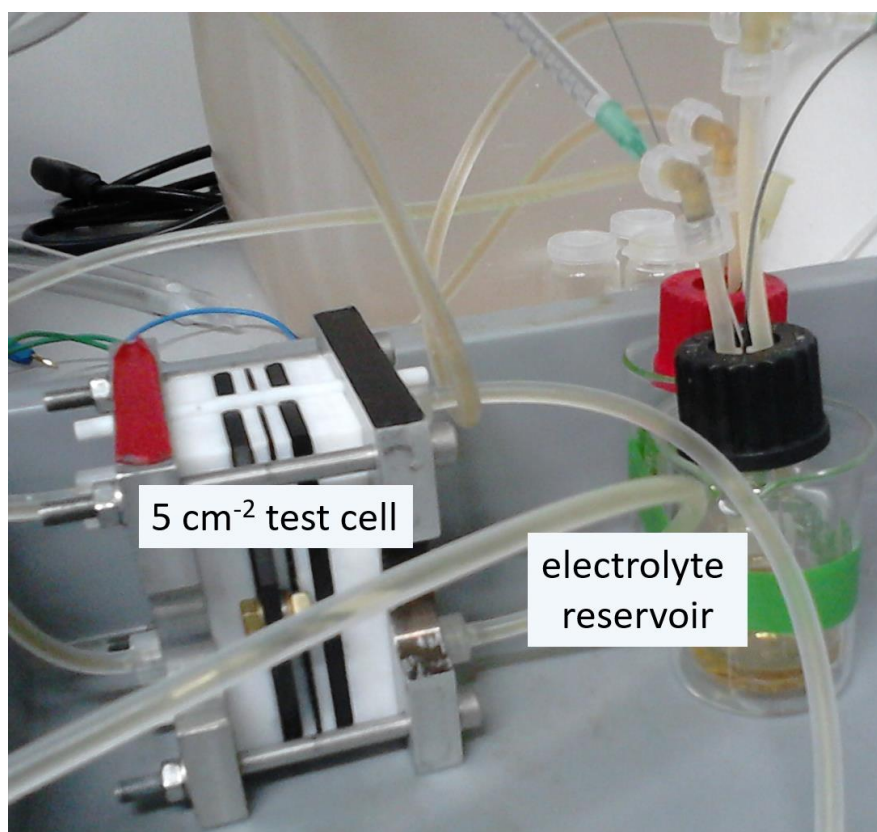


Figure S7. Photograph of the utilized pumped battery set-up (5 cm² test cell, electrolyte reservoirs, and tubes) for charge/discharge experiments. The peristaltic pump is absent in the photograph.

2.1. Membrane tests

Table S1. Selected technical data of the employed fumasep[®] AEM membranes.

	<i>FAA-3-PE30</i>	<i>FAP-PK-3130</i>	<i>FAS-30</i>	<i>FAA-3-50</i>
<i>Backing foil</i>	PET	PET	PET	PET
<i>Reinforcement</i>	PE	PK	none	none
<i>Counter ion</i>	bromide	chloride / sulfate	bromide	bromide
<i>Thickness (dry) / μm</i>	30	110-130	28-31	40-45
<i>Area resistance* (Cl^- form) / $\Omega \text{ cm}^2$</i>	0.48	1.20	0.80	<2.50

*In Cl^- form in 0.5 M NaCl_{aq} at 25 °C, measured in standard measuring cell (through-plane).

Table S2. Performance parameter of the employed fumasep® AEM membranes in a dynamic flow cell.

Membrane	Electric cell resistance / Ω	Current density / mA cm^{-2}	Capacity (charge/discharge) / mAh	Coulombic efficiency / %
FAA-3-PE30	2.28	1 to 8	54.29/48.91 at 3 mA cm^{-2}	82 to 93
FAP-PK-3130	1.91	1 to 12	53.87/49.21 at 3 mA cm^{-2}	81 to 98
FAS-30	1.02	1 to 16	53.17/46.69 at 3 mA cm^{-2}	70 to 97
FAA-3-50	0.69	1 to 16	53.31/46.45 at 3 mA cm^{-2}	70 to 97

2.2. Investigation of the influence of the conductive salt concentration on the electric cell resistance

Table S3. Influence of the conducting salt concentration on the electric cell and area resistance.*

Molarity NaCl_{aq} / mol L^{-1}	Electric cell resistance (R_1) / Ω	Electric cell resistance without AEM (R_2) / Ω	Area resistance (R) / $\Omega \text{ cm}^2$
0.0	2.01	0.350	8.30
0.5	1.71	0.350	6.80
1.0	1.46	0.358	5.51
1.5	0.73	0.356	1.87
2.0	0.73	0.360	1.85
2.5	0.62	0.359	1.31
3.0	0.62	0.358	1.31
4.0	0.65	0.354	1.48
5.0	0.70	0.354	1.73

*The influence of the conducting salt concentration on the electric cell and area resistance was investigated in a 5 cm^2 test cell: 10 mL solution per half-cell, flow rate adjusted to 16 mL min^{-1} , FAA-3-50 AEM.

2.3. Investigation of the influence of the flow rate on the battery performance

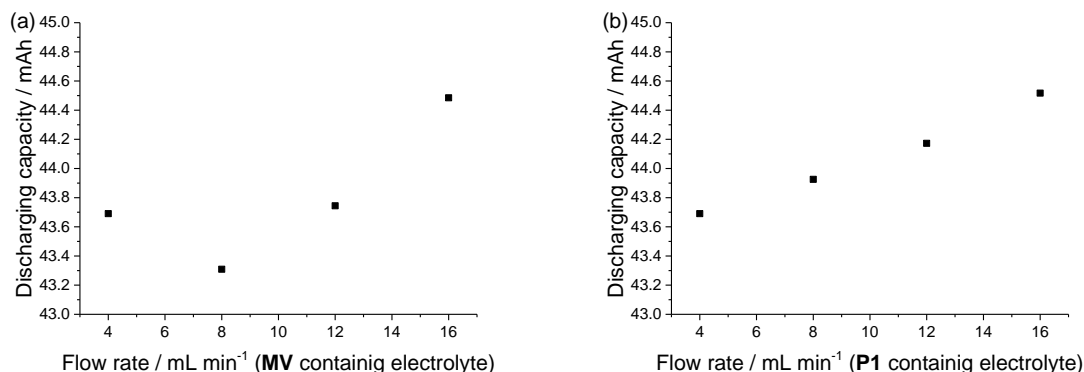


Figure S8. Discharging capacity of a pumped 5 cm² test cell, employing the FAA-3-50 AEM, with 10 mL of 0.5 M **MV** and **P1** (both in 1.5 M NaCl_{aq} solution, with a theoretical charge storage capacity of 6.42 Ah L⁻¹), 10 mL electrolyte per half-cell, as a function of the utilized electrolyte flow rate; a) with constant 4 mL min⁻¹ flow rate of the **P1** containing electrolyte and b) with constant 4 mL min⁻¹ flow rate of the **MV** containing electrolyte.

2.4. Investigation of the long-term cycling stability

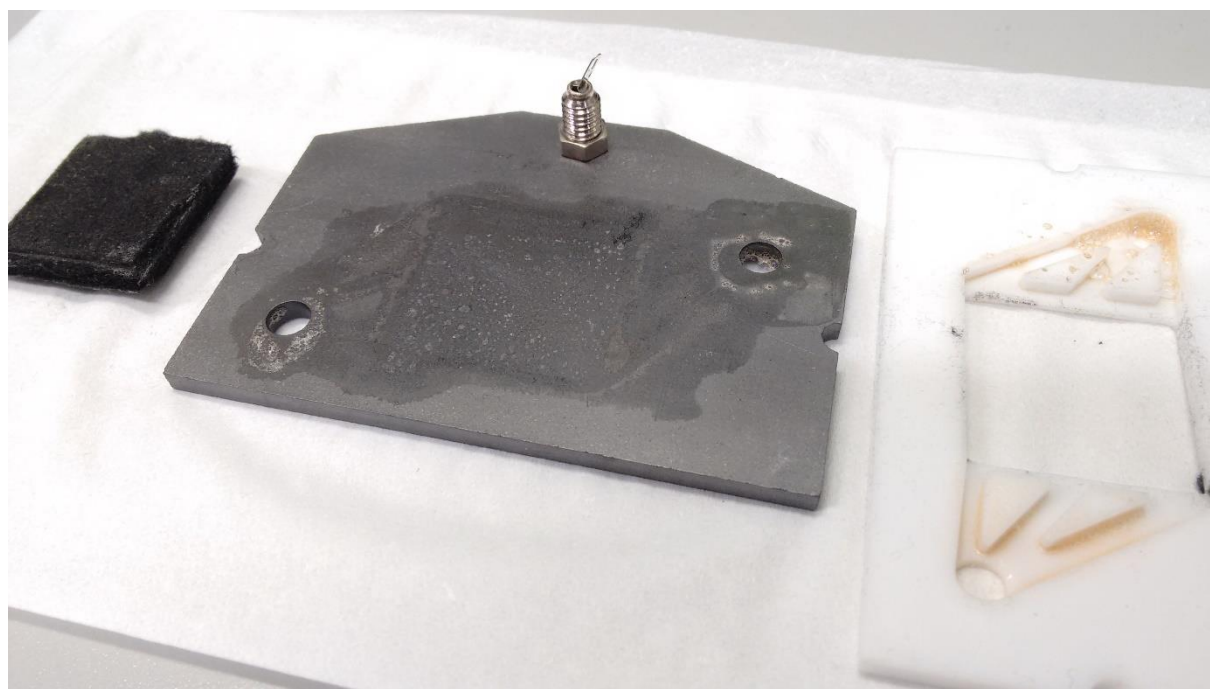


Figure S9. Photograph of utilized graphite felt, graphite current collector and PTFE flow frame (from left to right) after the long-term cycling stability test of a pumped electrochemical 5 cm² test cell with 0.5 M **MV** and **P1** (each in 1.5 M NaCl_{aq} solution, theoretical charge storage capacity 6.44 Ah L⁻¹), 10 mL electrolyte per half-cell, flow rate adjusted to 16 mL min⁻¹.

2.5. Investigation of the osmotic process

To confirm the assumption that the major capacity decay, which occurred after 100 cycles during the long-term cycling stability test in a pumped electrochemical 5 cm² test cell (**Figure 8, Chapter 3.2.4**), is caused by an osmotic process, the osmotic pressure of the anolyte and catholyte was investigated in an osmotic chamber (**Figure S10**). To create conditions, which

are as close as possible to the ones in the long-term cycling stability test, the left side of the osmosis chamber was filled with 0.5 M **MV** in 1.5 M NaCl_{aq} solution (60 mL), the right side with 0.5 M **P1** in 1.5 M NaCl_{aq} solution (60 mL). The half-cells were separated by a fumasep® FAA-3-50 AEM.

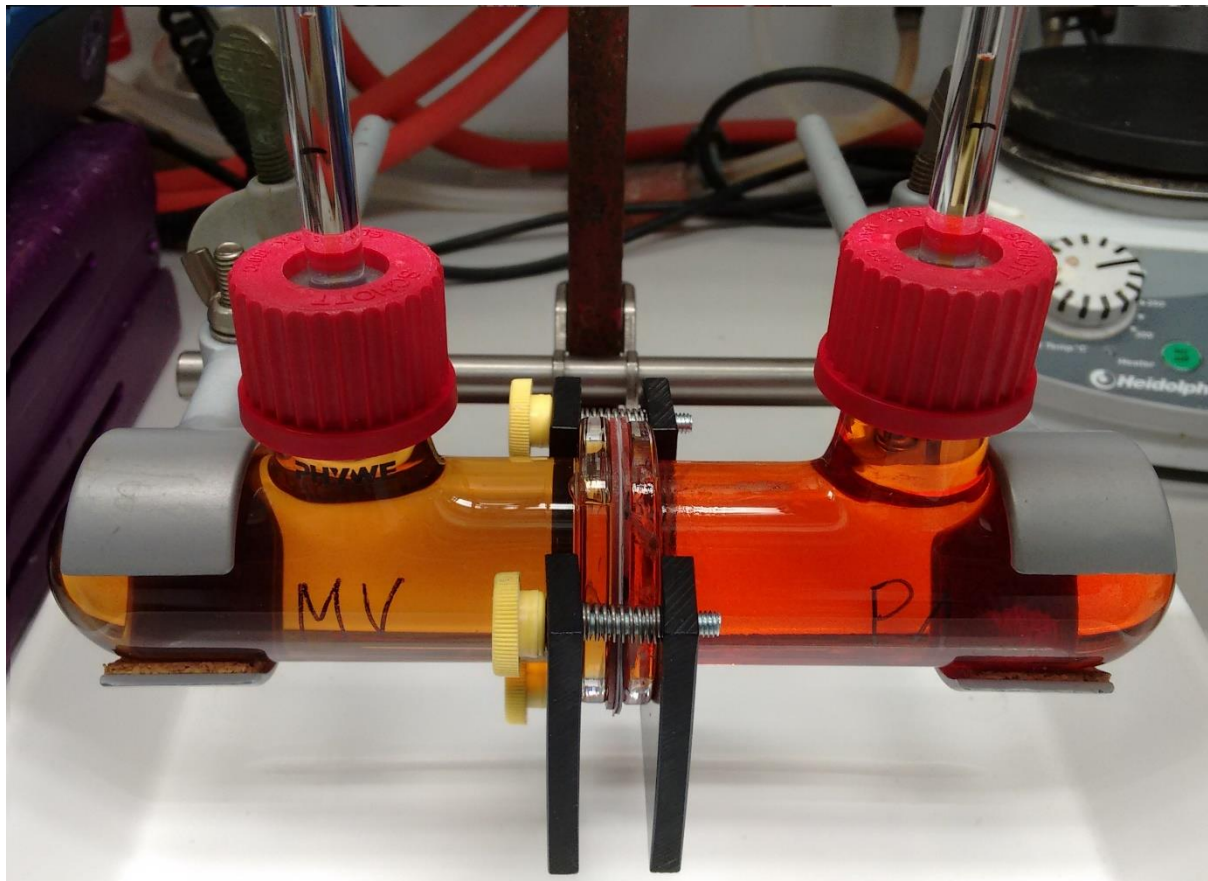


Figure S10. Photograph of utilized osmosis chamber. Left chamber: 0.5 M **MV** in 1.5 M NaCl_{aq} solution (60 mL); right chamber: 0.5 M **P1** in 1.5 M NaCl_{aq} solution (60 mL). Both chambers are separated through a fumasep® FAA-3-50 AEM.

After the osmotic (p_{osmo}) and the hydrostatic pressure (p_{hydro}) have balanced out, it was observed (**Figure S10**) that the capillary rise (h) of the left cell (0.5 M **MV** in 1.5 M NaCl_{aq} solution) was higher than the one of the right cell (0.5 M **P1** in 1.5 M NaCl_{aq} solution), which indicates a different osmotic pressure and therefore a different concentration of the dissolved material. With the observed capillary rise (h) the osmotic pressure difference (Δp_{osmo}) was calculated by using the equation, $\Delta p_{\text{osmo}} = \rho \cdot g \cdot h = \Delta p_{\text{hydro}}$ with ρ = density of the liquid, g = gravitational acceleration and h = capillary rise. The density of both the anolyte (0.5 M **MV** in 1.5 M NaCl_{aq}, $\rho = 1.0773 \text{ g cm}^{-3}$) and catholyte (0.5 M **P1** in 1.5 M NaCl_{aq}, $\rho = 1.0922 \text{ g cm}^{-3}$) was measured with a DMA4100 densitometer (Anton Paar, Austria) at 20 °C and verified by a subsequently measurement of the density of water ($\rho = 0.9982 \text{ g cm}^{-3}$, which is equal to the literature value).[2] With an observed capillary rise of 5.6 cm an osmotic pressure of $p_{\text{osmo}} = p_{\text{hydro}} = 591.83 \text{ Pa}$ of the **MV** containing anolyte (left half-cell) as well as

$p_{osmo} = p_{hydro} = 460.72$ Pa of the **P1** containing catholyte (capillary rise of 4.3 cm, right half-cell) was calculated resulting a osmotic pressure difference of $\Delta p_{osmo} = 131.11$ Pa. This results prove that the concentration of dissolved material of the anolyte is higher than these of the catholyte, whereas over time *e.g.*, during long-term cycling stability tests in a pumped flow cell, water flows from the catholyte half-cell through the semipermeable AEM to the anolyte half-cell.

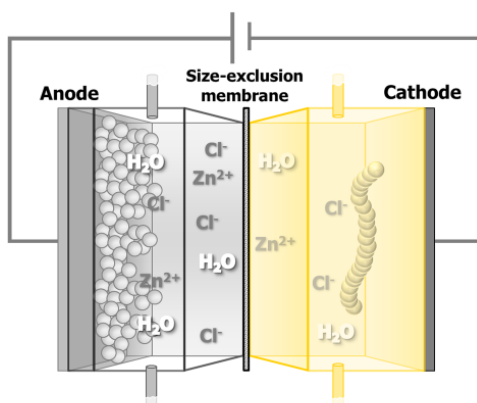
References

- [1] M. Wagner, C. Pietsch, L. Tauhardt, A. Schallon, U.S. Schubert, J. Chromatogr. A, 1325 (2014) 195-203.
- [2] Die naturwissenschaftliche Wissensdatenbank. <http://www.internetchemie.info/chemielexikon/daten/w/wasser-dichtetabelle.php>, 2017 (accessed 25.08.2017).
- [3] S. Yi, B. Captain, M.F. Ottaviani, A.E. Kaifer, Langmuir, 27 (2011) 5624-5632.
- [4] O. Swiech, R. Bilewicz, E. Megiel, RSC Adv., 3 (2013) 5979-5986.
- [5] T. Hagemann, J. Winsberg, B. Häupler, T. Janoschka, J.J. Gruber, A. Wild, U.S. Schubert, NPG Asia Mater, 9 (2017) e340.

Publication P5

Poly(TEMPO)/zinc hybrid-flow battery: A novel, “green,” high voltage, and safe energy storage system

J. Winsberg, T. Janoschka, S. Morgenstern, T. Hagemann, S. Muench, G. Hauffman,
J.-F. Gohy, M. D. Hager, U. S. Schubert,
Adv. Mater. **2016**, 28, 2238-2243.



Reproduced with permission of Wiley VCH, Copyright © 2017.

Poly(TEMPO)/Zinc Hybrid-Flow Battery: A Novel, “Green,” High Voltage, and Safe Energy Storage System

Jan Winsberg, Tobias Janoschka, Sabine Morgenstern, Tino Hagemann, Simon Muench, Guillaume Hauffman, Jean-François Gohy, Martin D. Hager, and Ulrich S. Schubert*

The amount of electric energy, produced from renewable sources like wind power and solar radiation, increases globally every year.^[1–3] Therefore, intelligent energy storage systems have to be developed. Interesting candidates for the storage of electric energy from renewable sources are redox-flow batteries (RFBs).^[4–9] In contrast to “classical” batteries, the active material of RFBs does not form solid electrodes, but is dissolved in an electrolyte. Besides the all-vanadium RFB,^[10–14] hybrid-flow batteries, which combine a zinc anode with a halogen cathode, have attained much attention, e.g., zinc-bromine and zinc-polyiodide batteries.^[15–18] The special characteristic of a hybrid-flow battery is that at least one redox state of one active species is insoluble. Typically $\text{Zn}^{2+}_{(\text{aq})}$ is reduced to $\text{Zn}^0_{(\text{s})}$ during the charging process forming a solid anode. Inherent of a halogen cathode is the toxicity of I_2 and particularly of bromine, which are generated during battery cycling.^[17,19,20] Expensive complexing agents are required to maintain the solubility of bromine and to increase the safety of halogen-based RFBs.^[20,21] In recent years research on organic active materials experienced a significant upturn;^[5,22–26] e.g., Zhao et al. reported a polyaniline-particle/zinc flow battery.^[27] With the polymer-based redox-flow battery (pRFB), a new, metal-free concept was demonstrated recently. Organic polymers were used as redox-active materials in combination with a simple size exclusion membrane as separator.^[7] The pRFB tries to reduce acquisition costs and the environmental impact of RFBs, by replacing toxic and expensive heavy metal salts, the critical sulfuric acid electrolyte, and also expensive Nafion membranes by more cost-efficient and less corrosive components. Both, the zinc-halogen

and the pRFB system still have potential for further improvements. Combining the benefits of both systems by applying a 2,2,6,6-tetramethylpiperidiny-1-oxyl (TEMPO) containing polymer as catholyte and a $\text{Zn}^{2+}/\text{Zn}^0$ anode, together with an inexpensive size exclusion membrane, leads to a new type of a semi-organic hybrid-flow battery. TEMPO containing polymers show a lower toxicity compared with other ionic polymers (e.g., poly-L-lysine and poly(ethylene imine)) as well as vanadium salts.^[7] Various zinc compounds, e.g., zinc chloride, -gluconate, and -oxide, are approved as nutrients and dietary supplements by the US Food and Drug Administration. Therefore, a better environmental sustainability of a TEMPO/zinc hybrid-flow battery against state-of-the-art RFB technologies is evident. Nishide and co-workers investigated TEMPO containing polymers, mainly with the focus as cathode-active material for semi- and all-organic thin-film batteries.^[28–32] TEMPO containing catholytes for application in RFBs were previously investigated;^[23,33–35] however, all of these systems suffered from considerable drawbacks. For instance they rely on lithium anodes strictly limited to organic solvents and anhydrous conditions. From an economic and ecological point of view lithium represents an unfavored active material for RFB applications, due to its high price and serious safety issues. The requirement of strictly anhydrous and oxygen-free conditions results in low applicable current densities and high manufacturing efforts and costs.

With regard to the standard redox-potentials of the two redox couples, a TEMPO/zinc battery should exhibit a cell-potential of about 1.69 V.^[36,37] Considering thermodynamics, such high voltages are not attainable in aqueous solution, as water electrolysis would initiate above 1.2 V. However, the application of a zinc-anode with a very high overpotential for hydrogen evolution expands the applicable potential window up to 2 V. An additional benefit is the robustness of the novel battery system. The presence of oxygen, commonly causing self-discharge, does not lead to any side reactions and, therefore, an elaborate inertization of the battery is not required.

The hybrid-flow battery consists of two half cells separated by a size-exclusion membrane derived from regenerated cellulose. The membrane is permeable for small ions like Zn^{2+} , chloride, and perchlorate, as well as the solvent (water), but retains the polymeric active material. The main advantages of this membrane are the high stability in many solvents as well as the low cost compared to state-of-the-art Nafion membranes. The anolyte contains a Zn^{2+} -salt as active species, which acts simultaneously as supporting electrolyte. The catholyte is basically the same solution as the anolyte, but comprises additionally the polymeric TEMPO cathode active material (Figure 1).

J. Winsberg, T. Janoschka, S. Morgenstern,
T. Hagemann, S. Muench, Dr. M. D. Hager,
Prof. U. S. Schubert
Laboratory of Organic and Macromolecular
Chemistry (IOMC)
Friedrich Schiller University Jena
Humboldtstraße 10, 07743 Jena, Germany
E-mail: ulrich.schubert@uni-jena.de



J. Winsberg, T. Janoschka, S. Morgenstern, T. Hagemann, S. Muench,
Dr. M. D. Hager, Prof. U. S. Schubert
Center for Energy and Environmental Chemistry Jena (CEEC Jena)
Friedrich Schiller University Jena
Philosophenweg 7a, 07743 Jena, Germany
G. Hauffman, Prof. J.-F. Gohy
Institute of Condensed Matter and Nanoscience
Bio- and Soft Matter
Université Catholique de Louvain
Louvain-la-Neuve 1348, Belgium

DOI: 10.1002/adma.201505000

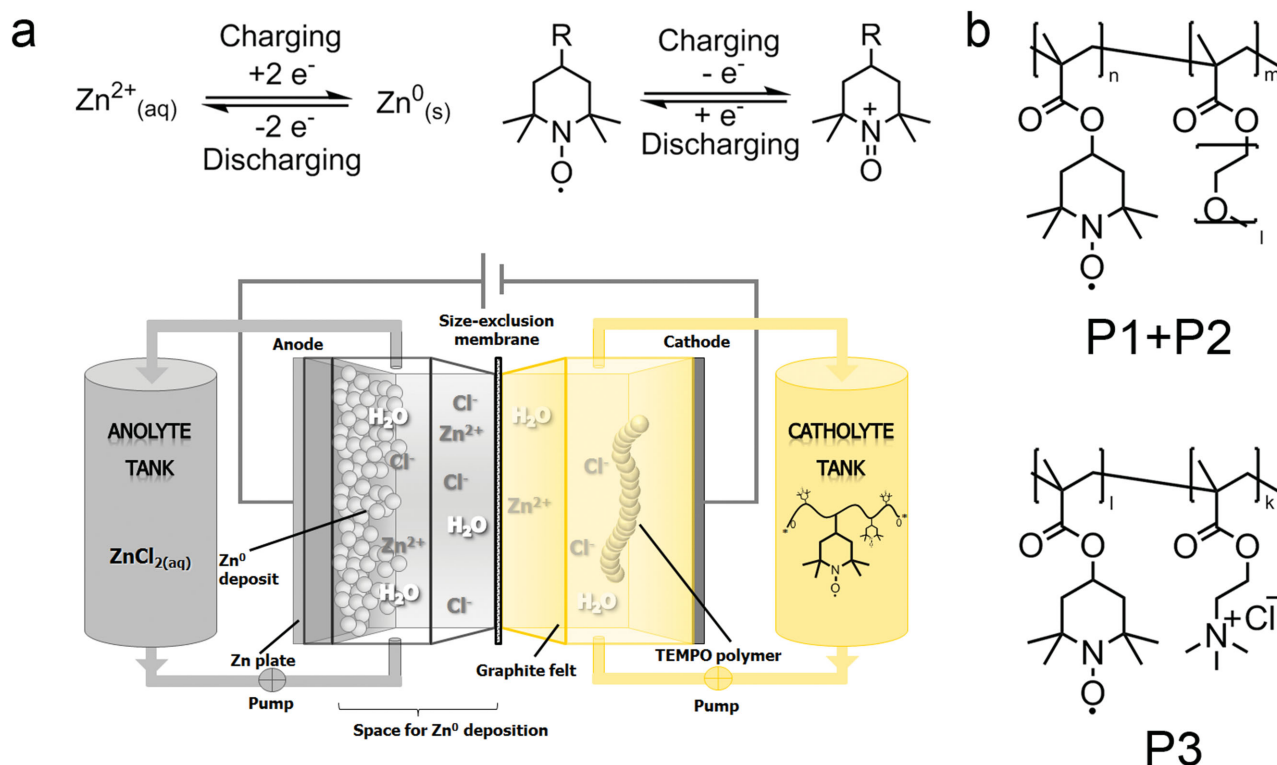


Figure 1. a) A water-based poly(TEMPO)/zinc hybrid-flow battery. The battery contains an electrochemical cell with an anode and a cathode compartment, separated by a size exclusion membrane. Catholyte and anolyte are circulated between the electrochemical cell and the storage tanks. Zinc chloride is used simultaneously as anode active material and as supporting electrolyte. The polymeric TEMPO is the cathode active material. b) Schematic representation of the copolymer structures: P(TEMPO-co-PEGMA) (**P1** and **P2**) in different molar ratios and P(TEMPO-co-METAC) (**P3**).^[38]

In this study, three types of different TEMPO copolymers were investigated (Table 1). Each polymer was designed in particular for either application in organic or aqueous media and was used as active material in a corresponding electrolyte solution (Table 2). Detailed description of the polymer synthesis and characterization can be found in the Supporting Information.

The catholytes can be divided into two groups: organic carbonate-based (A and B) and water-based (C and D) catholytes. Organic carbonates are widely used solvents in various battery applications, because of the good electrochemical stability and low vapor pressures.^[39] For this study a mixture of ethylene carbonate (EC), dimethyl carbonate (DMC), and diethyl carbonate (DEC) was utilized showing a good ion conductivity compared with other carbonate-based electrolytes (Table S1, Supporting

Information). $\text{Zn}(\text{ClO}_4)_2 \times 6\text{H}_2\text{O}$ served as supporting electrolyte and anode active material, respectively.

Water-based electrolytes reveal the highest ionic conductivity and are, therefore, used with preference (Table S1, Supporting Information). The group of aqueous catholytes employs **P2** and **P3**. Zinc chloride was used as supporting electrolyte and anode active material. The chloride salt was selected because of its superior solubility and electrochemical stability compared to other zinc salts. To prevent the formation of zinc hydroxide, ammonium chloride was added.^[30] Solutions of **P3** precipitated in zinc chloride solutions above 0.1 M, therefore, sodium chloride was utilized as main supporting electrolyte.

Cyclic voltammetry (CV) measurements of 0.1 M $\text{Zn}(\text{ClO}_4)_2 \times 6\text{H}_2\text{O}$ dissolved in a carbonate mixture (EC/DMC/DEC, v:v:v, 1:1:1) were performed to determine potentials of the $\text{Zn}^{2+}/\text{Zn}^0$

Table 1. Polymers used in this study.

Polymer	M_w [kg mol ⁻¹]	PDI	Molar ratio (TEMPO:Comonomer)	Radical content ^{f)} [mole fraction x]
P1	70 ^{a)}	1.3	3.5:1 ^{c)}	0.77 ^{f)} (theoretical value 0.77)
P2	54 ^{a)}	2.6	1:1 ^{d)}	0.49 ^{f)} (theoretical value 0.5)
P3	37 ^{b)}	2.4	1:1 ^{e)}	0.28 ^{f)} (theoretical value 0.5)

^{a)}SEC DMAc + 0.21 wt-% LiCl, poly(styrene) standard; ^{b)}Asymmetric flow field flow fractionation (AF4); comonomers: ^{c)}Poly(ethylene glycol) methacrylate $M_n = 450$ g mol⁻¹; ^{d)}Poly(ethylene glycol) methacrylate $M_n = 950$ g mol⁻¹; ^{e)}[2-(methacryloyloxy)ethyl]trimethylammonium chloride; ^{f)}Calculated from EPR spin count (see Figure S4, Supporting Information, for EPR spectra).

Table 2. Polymeric catholytes used in this study

Catholyte	Polymer	Solvent	Supporting electrolyte	Energy density ^{b)} [Wh L ⁻¹]
A	P1	EC/DMC/DEC ^{a)}	0.75 M Zn(ClO ₄) ₂ × 6H ₂ O	8.1
B	P1	EC/DMC/DEC ^{a)}	0.5 M Zn(ClO ₄) ₂ × 6H ₂ O	1.2
C	P2	Water	1.0 M ZnCl ₂ , 1.0 M NH ₄ Cl	4.1
D	P3	Water	0.71 M NaCl, 0.08 M ZnCl ₂ , 0.08 M NH ₄ Cl	1.9

^{a)}Mixture (v:v:v 1:1:1); ^{b)}energy density as product of capacity and OCV at 50% SOC (carbonate-based electrolytes: 1.3 V, aqueous electrolyte: 1.7 V, see Figure S7 (Supporting Information) for OCVs depending on SOC).

redox couple. Zinc precipitation at potentials lower than −1.25 V versus AgNO₃/Ag and dissolution at potentials above −1.0 V versus AgNO₃/Ag were observed on a glassy carbon electrode (Figure 2a, dashed line). The special shape of the voltammogram is typical for zinc electrodeposition and illustrates a large peak split of 1.8 V. Likely, a limited ionic conductivity going along with finite diffusion of zinc cations in the carbonate electrolyte is the reason for the large peak split. As far as a battery application is concerned, this effect is disadvantageous

as it decreases the cell potential. The cyclic voltammogram of **P1** shows the quasi-reversible oxidation and rereduction of the radical TEMPO moiety to the oxammonium cation (TEMPO⁺) at 0.4 V versus AgNO₃/Ag with a peak split of 120 mV in the previously investigated electrolyte (Figure 2a, solid line). Rotating disc electrode (RDE) measurements were performed to investigate the redox properties of **P1**. Levich-analysis reveals a diffusion-controlled behavior of **P1** in zinc perchlorate solution and a diffusion coefficient of $1.65 \times 10^{-7} \text{ cm}^2 \text{ s}^{-1}$

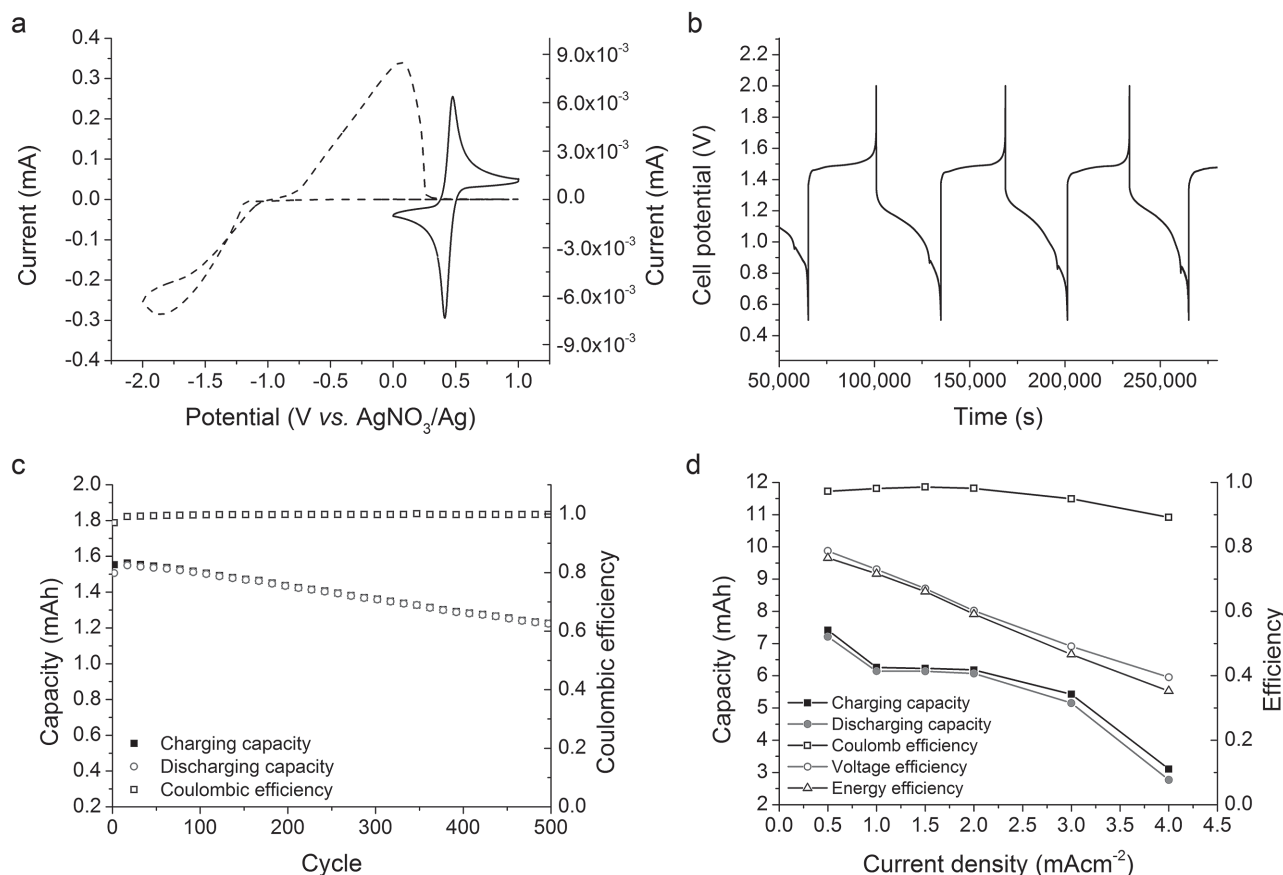


Figure 2. a) Cyclic voltammogram of 0.1 M Zn(ClO₄)₂ × 6H₂O (dashed line) and 0.01 M **P1** (solid line) in EC/DMC/DEC (v:v:v, 1:1:1), scan rate 50 mV s⁻¹, b) charging/discharging curve of a poly(TEMPO)/zinc hybrid-flow battery, catholyte: **A** 0.75 M Zn(ClO₄)₂ × 6H₂O EC/DMC/DEC (v:v:v, 1:1:1), 8 mL electrolyte per half-cell, 6.1 Ah L⁻¹, current density 1 mA cm⁻², flow rate 20 mL min⁻¹, c) long-term cycling of a static poly(TEMPO)/zinc hybrid-flow battery utilizing catholyte **B** with constant current of 1.4 mA cm⁻², cycles 2–501, after 500 cycles 81% of initial discharge capacity were retained, coulombic efficiency above 99.7%, and d) capacity, coulombic-, voltage-, and energy efficiency depending on the current density, catholyte **B** with a capacity of 0.91 Ah L⁻¹, 8 mL electrolyte per half-cell, flow rate adjusted to 20 mL min⁻¹.

(Figure S3a,b, Supporting Information). Subsequent Koutecký–Levich analysis illustrates mass-transport-independent currents. The electron-transfer rate constant k^0 of $9.93 \times 10^{-4} \text{ cm s}^{-1}$ and a transfer coefficient α of 0.443, which is close to the value of an ideal reversible redox reaction of 0.5, were derived by Tafel analysis (Figure S3c,d, Supporting Information).

A hybrid-flow battery was setup by utilizing zinc-foil as anode, a 0.75 M $\text{Zn}(\text{ClO}_4)_2 \times 6\text{H}_2\text{O}$ solution in EC/DMC/DEC (v:v:v, 1:1:1) as anolyte, and catholyte **A** with a capacity of 6.1 Ah L^{-1} . This configuration leads to a theoretical energy density of 8.1 Wh L^{-1} . Both half-cells were separated by a dialysis membrane (regenerated cellulose, molecular weight cut-off (MWCO) of $1,000 \text{ g mol}^{-1}$; see Figure S8b, Supporting Information, for a representative setup). A simple charging/discharging experiment (Figure 2b) illustrates reversible charging and discharging, but also shows a potential drop of 350 mV between the charging and discharging plateau. The cell resistance, determined by electrochemical impedance spectroscopy (EIS), was 27.3Ω prior to charging. After 227 charging/discharging cycles a second EIS measurement revealed the formation of a semi-circle, which indicates a charge transfer resistance of 79Ω and implies an evidence for the internal resistance drop (Figure S5b, Supporting Information). Also the kinetically restricted redox reaction of $\text{Zn(II)}/\text{Zn(0)}$ in the carbonate-based electrolyte, determined prior via CV, and a low ionic conductivity of 6.9 mS cm^{-1} substantiate this observation. Continuous cycling of a static nonpumped battery with steady current (Figure 2c) revealed very slow capacity decay of only 0.04% per cycle and high coulombic efficiencies ($>99.7\%$). Investigations of the battery performance at various current densities were conducted with catholyte **B**, with a capacity of 0.91 Ah L^{-1} (Figure 2d). Various current densities were applied and the charging/discharging capacity as well as the potentials of the corresponding plateau were determined. A material activity of 99% for current densities of 0.5 mA cm^{-2} was reached. For higher current densities the discharge capacity drops to a plateau level of around 6 mAh (82% activity). Charging was possible up to 4 mA cm^{-2} . The coulombic efficiency stayed always above 89% with a peak efficiency of 99% at a current density of 1.5 mA cm^{-2} . A linear decline of the voltage efficiency was observed with increasing current densities. This behavior was probably caused by the restricted ion conductivity in the applied electrolytes and the consequential increasing potential gap between charging and discharging plateaus. Charging times for catholytes **A** and **B** are summarized in Tables S2 and S3 in the Supporting Information.

In conclusion, poly(TEMPO)/zinc hybrid-flow batteries based on organic carbonate electrolytes could be established successfully. Energy densities of up to 8.1 Wh L^{-1} were achieved with catholyte **A**, due to the high solubility of **P1** in organic carbonates. In comparison, energy densities of water insensitive redox-flow batteries already reported in literature range from 5 to 16 Wh L^{-1} .^[5,40] Also, a good long-term stability with 500 consecutive charging/discharging cycles was obtained. In the charging process, zinc-cations are reduced at the anode to $\text{Zn}^0_{(\text{s})}$ and a deposit is formed on the electrode. The long-term cycling tests revealed the formation of dendrites (Figure S8a, Supporting Information), which can potentially limit the long-term stability. In order to prevent shortenings by dendrite growth

through the pores of the membrane, additional space for the Zn^0 deposit was established in the anode half-cell. Carbon paper is used to increase the surface area of the anode and allows the application of higher current densities. According to the limited ionic conductivity of organic electrolytes applicable current densities are limited to 4 mA cm^{-2} . Higher current densities can be applied in aqueous electrolytes.

Polymer **P3** shows low solubility in concentrated solutions of various zinc salts, independent of the applied anion (chloride, perchlorate, sulfate, and nitrate). Therefore, the amount of zinc chloride was reduced to a twofold molar excess related to TEMPO units and sodium chloride was employed as essential supporting electrolyte. Ammonium chloride was added to suppress the formation of zinc hydroxide during battery cycling.^[30] CV analysis revealed an improved behavior of the $\text{Zn}^{2+}/\text{Zn}^0$ redox couple in water-based electrolytes compared to organic carbonates (Figure 3a). The peak separation of the redox couple is reduced to 0.53 V at a scan rate of 50 mV s^{-1} . Determination of the diffusion coefficient for **P3** by RDE analysis was not possible, due to a nonlinear curve in the Levich-plot (see Figure S3a,b, Supporting Information, for voltammograms and Levich-plot).^[41]

A water-based hybrid-flow battery with catholyte **D** showed an excellent battery cycling. Well-defined flat charging/discharging plateaus with a narrow potential drop were achieved. Current densities up to 12 mA cm^{-2} could be applied and, thus, increased by factor three compared to organic electrolytes. Varying the current density did not have a significant effect on the capacity (Figure 3d). The discharging capacity maintained stable for current densities between 1 and 10 mA cm^{-2} . Starting from 12 mA cm^{-2} , a decrease in capacity was observed. Catholyte **D** showed 73% of the theoretical discharging capacity. The coulombic efficiency remained always above 90% with a maximum of 99% at 12 mA cm^{-2} ; the energy efficiency never dropped below 80%. Charging times for different current densities are summarized in Table S5 in the Supporting Information. The improved battery performance is caused by the accelerated reaction of the zinc redox couple in aqueous media and by a substantially reduced cell resistance of 1.35Ω (see Figure S5a, Supporting Information, for impedance spectrum). A long-term cycling test revealed good stability (Figure 3c). After 1,000 consecutive charging/discharging cycles 78.6% of initial discharging capacity was retained, which indicates a stable redox behavior of the active species. Water electrolysis or the formation of gaseous chlorine did not occur.

A precipitation of **P2** in zinc chloride solutions could not be observed up to salt concentrations of 1 M. Thus, zinc chloride could be used as supporting electrolyte without the additional usage of sodium chloride. As noted before, the addition of ammonium chloride improved the cycling stability due to the suppression of zinc hydroxide formation. Higher concentrations of **P2** could be achieved in water compared to **P3**, so that a capacity of 2.39 Ah L^{-1} was reached with catholyte **C**. Current densities of up to 20 mA cm^{-2} were applicable; however, going along with a significantly reduced capacity (Figure S6c, Supporting Information). Charging times depending on the applied current density are summarized in Table S4 in the Supporting Information. In general, a linear decrease of the capacity was observed with increasing current density. This is induced

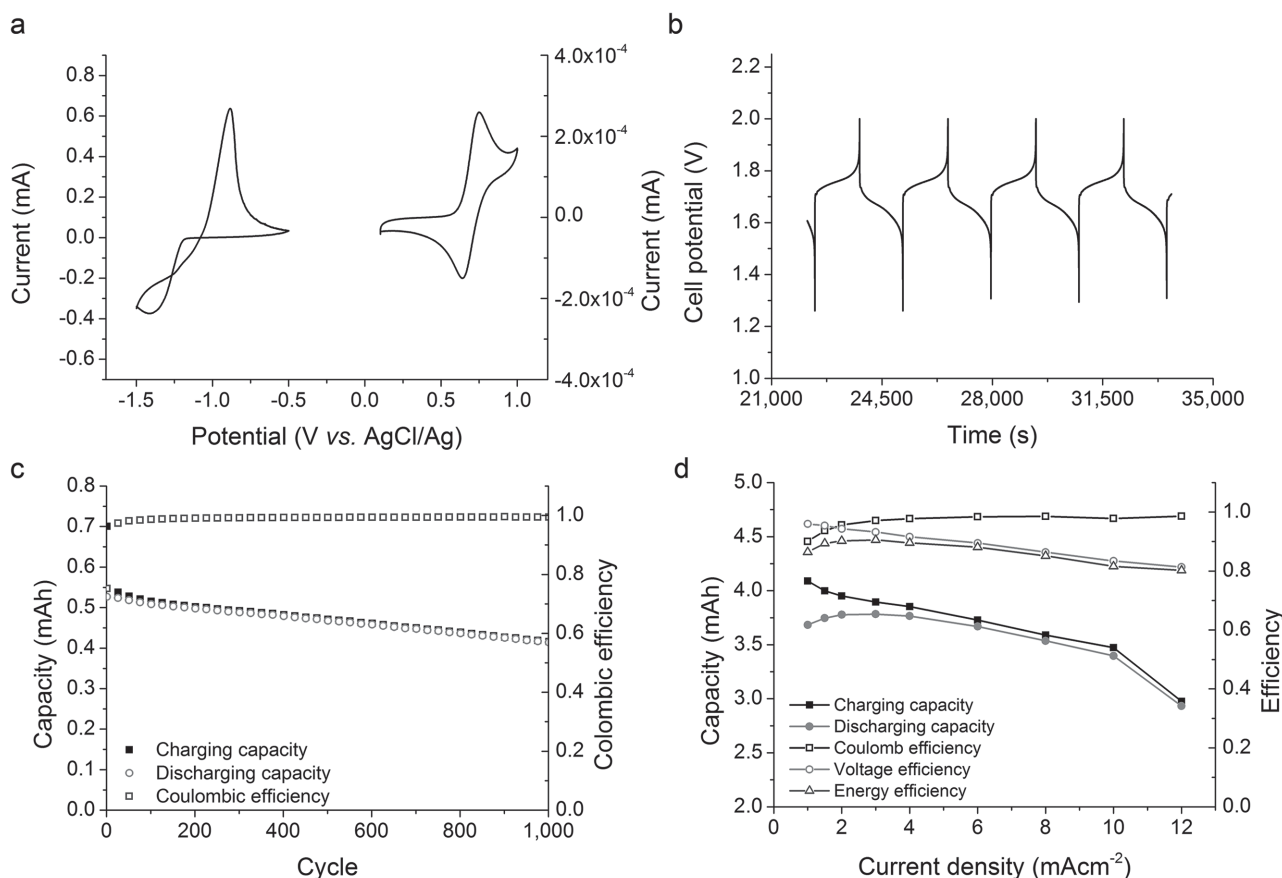


Figure 3. a) Cyclic voltammogram of an aqueous 0.1 M zinc chloride 0.01 M **P3** solution. Scan rate 50 mV s^{-1} , b) exemplary charging/discharging curves at a current density of 2 mA cm^{-2} , aqueous catholyte **D**: **P3** solution in NaCl, ZnCl_2 , NH_4Cl with a capacity of 1.1 Ah L^{-1} , flow rate 20 mL min^{-1} , c) long-term stability test, cycling of a static cell, catholyte **D**, and d) electrical performance: capacity, coulombic-, voltage-, and energy efficiency depending on the applied current density.

by a limited mass transport to the electrode and leads to an increasing overpotential. Nevertheless, the system benefits significantly from the increased Zn^{2+} concentration in catholyte **C** compared to catholyte **D**, as the applicable current density was nearly doubled. A maximum material activity of 87.6% was reached at 2 mA cm^{-2} , which also is a significant improvement compared to catholyte **C**. The coulombic efficiency was not affected by the decreasing behavior of the capacity and stayed mostly above 90%. Charging/discharging curves, long-term stability test, and electrical performance analysis can be found in Figure S6a–c (Supporting Information). The stable potential window of 2 V is of importance for the charging process with high current densities, as the potential of the charging plateau increases with increasing current density (Figure S6d, Supporting Information). For densities of, e.g., 20 mA cm^{-2} a charging up to 2 V was observed, while charging with relatively slow densities of, e.g., 6 mA cm^{-2} , is completed at 1.9 V.

In reference to the investigated hybrid-flow batteries utilizing carbonate-based electrolytes, the electrical performance could be increased by the use of an aqueous electrolyte. Thus, the environmental impact could be reduced as well. Despite of the high cut-off voltage of 2 V, no water electrolysis could be detected and stable battery cycling was performed. Particular worth mentioning is the difference between the two

open circuit voltage (OCV) curves (Figure S7a,b, Supporting Information). In the aqueous system an OCV of 1.7 V at 50% state of charge (SOC) was observed, in contrast to the organic system, where an OCV of 1.3 V at 50% SOC was reached.

A novel type of zinc hybrid-flow battery was successfully implemented. The application of several TEMPO-containing polymers, as active cathode material, leads to significant improvements concerning corrosion and environmental impact compared to already known zinc-halogen hybrid-flow batteries. The different applied catholytes comprised P(TEMPO-co-PEGMA)s, synthesized via RAFT polymerization and P(TEMPO-co-METAC), which was designed particularly for aqueous solutions. To the best of our knowledge, it is the first reported type of flow battery, which enables a stable potential window of up to 2 V in aqueous media, without utilization of toxic and expensive heavy metals. Furthermore, a contamination with oxygen is unproblematic rendering the expensive inertization of the battery unnecessary. In carbonate-based electrolytes, high-energy densities of 8.1 Wh L^{-1} were achieved, while water-based electrolytes allow application of higher current densities of up to 20 mA cm^{-2} , as well as a stable energy efficiency of over 80%. Furthermore, water-based TEMPO/zinc HFBs feature an elevated OCV of 1.7 V compared to organic-based ones with an OCV of 1.3 V. Both systems showed very good

long-term stability of 500 and 1,000 consecutive charging and discharging cycles, respectively. When comparing the investigated TEMPO-copolymers with one another, P(TEMPO-co-PEGMA)s are the copolymers of choice for poly(TEMPO)/zinc hybrid-flow batteries. The reported poly(TEMPO)/zinc HFB features high applicable current densities, compared to previously reported TEMPO containing RFBs, low acquisition costs for both active materials as well as the membrane. The robustness of the employed redox couples leads to high cycle stabilities and, in general, to low intrinsic hazards. This enables the suitability as energy storage system in large scales.

Supporting Information

Supporting Information is available from the Wiley Online Library or from the author.

Acknowledgements

The authors acknowledge the European Regional Development Fund (EFRE), the Thüringer Aufbaubank (TAB), the Thuringian Ministry for Economic Affairs, Science and Digital Society (TMWdG), and the Fonds der Chemischen Industrie (FCI), as well as the support from JenaBatteries GmbH. G.H. is grateful to FRIA for financial support. J.-F.G. acknowledges the CFB for support in the frame of the ARC 14/19-057 BATTAB.

Received: October 11, 2015

Revised: December 5, 2015

Published online: January 26, 2016

- [1] A. T. Gullberg, D. Ohlhorst, M. Schreurs, *Renew. Energ.* **2014**, 68, 216.
- [2] R. Sen, S. C. Bhattacharyya, *Renew. Energ.* **2014**, 62, 388.
- [3] H. Ahlborg, L. Hammar, *Renew. Energ.* **2014**, 61, 117.
- [4] P. Alotto, M. Guarnieri, F. Moro, *Renew. Sust. Energ. Rev.* **2014**, 29, 325.
- [5] B. Huskinson, M. P. Marshak, C. Suh, S. Er, M. R. Gerhardt, C. J. Galvin, X. Chen, A. Aspuru-Guzik, R. G. Gordon, M. J. Aziz, *Nature* **2014**, 505, 195.
- [6] K. Lin, Q. Chen, M. R. Gerhardt, L. Tong, S. B. Kim, L. Eisenach, A. W. Valle, D. Hardee, R. G. Gordon, M. J. Aziz, M. P. Marshak, *Science* **2015**, 349, 1529.
- [7] T. Janoschka, N. Martin, U. Martin, C. Friebe, S. Morgenstern, H. Hiller, M. D. Hager, U. S. Schubert, *Nature* **2015**, 527, 78.
- [8] J. Noack, N. Roznyatovskaya, T. Herr, P. Fischer, *Angew. Chem. Int. Ed.* **2015**, 54, 9776.
- [9] M. Skyllas-Kazacos, M. H. Chakrabarti, S. A. Hajimolana, F. S. Mjalli, M. Saleem, *J. Electrochem. Soc.* **2011**, 158, R55.
- [10] M. Skyllas-Kazacos, M. Kazacos, R. J. C. McDermott (U.-A. Limited), *WO8905528*, **1989**.
- [11] S. Kim, M. Vijayakumar, W. Wang, J. Zhang, B. Chen, Z. Nie, F. Chen, J. Hu, L. Li, Z. Yang, *Phys. Chem. Chem. Phys.* **2011**, 13, 18186.
- [12] G. Kear, A. A. Shah, F. C. Walsh, *Int. J. Energ. Res.* **2012**, 36, 1105.
- [13] H. Liu, Q. Xu, C. Yan, Y. Qiao, *Electrochim. Acta* **2011**, 56, 8783.
- [14] H. Zhang, H. Zhang, X. Li, Z. Mai, J. Zhang, *Energ. Environ. Sci.* **2011**, 4, 1676.
- [15] B. Li, Z. Nie, M. Vijayakumar, G. Li, J. Liu, V. Sprenkle, W. Wang, *Nat. Commun.* **2015**, 6, 6303.
- [16] Q. Lai, H. Zhang, X. Li, L. Zhang, Y. Cheng, *J. Power Sources* **2013**, 235, 1.
- [17] S. Suresh, T. Kesavan, Y. Munaiah, I. Arulraj, S. Dheenadayalan, P. Ragupathy, *RSC Adv.* **2014**, 4, 37947.
- [18] J. H. Yang, H. S. Yang, H. W. Ra, J. Shim, J.-D. Jeon, *J. Power Sources* **2015**, 275, 294.
- [19] E. Lancry, B.-Z. Magnes, I. Ben-David, M. Freiberg, *ECS Trans.* **2013**, 53, 107.
- [20] J.-D. Jeon, H. S. Yang, J. Shim, H. S. Kim, J. H. Yang, *Electrochim. Acta* **2014**, 127, 397.
- [21] M. E. Easton, P. Turner, A. F. Masters, T. Maschmeyer, *RSC Adv.* **2015**, 5, 83674.
- [22] A. P. Kaur, N. E. Holubowitch, S. Ergun, C. F. Elliott, S. A. Odom, *Energ. Tech.* **2015**, 3, 476.
- [23] Z. Li, S. Li, S. Liu, K. Huang, D. Fang, F. Wang, S. Peng, *Electrochem. Solid St.* **2011**, 14, A171.
- [24] S. H. Oh, C. W. Lee, D. H. Chun, J. D. Jeon, J. Shim, K. H. Shin, J. H. Yang, *J. Mater. Chem. A* **2014**, 2, 19994.
- [25] W. Wang, W. Xu, L. Cosimbescu, D. Choi, L. Li, Z. Yang, *Chem. Commun.* **2012**, 48, 6669.
- [26] L. M. Zhu, A. W. Lei, Y. L. Cao, X. P. Ai, H. X. Yang, *Chem. Commun.* **2013**, 49, 567.
- [27] Y. Zhao, S. Si, C. Liao, *J. Power Sources* **2013**, 241, 449.
- [28] K. Koshika, N. Sano, K. Oyaizu, H. Nishide, *Chem. Commun.* **2009**, 7, 836.
- [29] W. Choi, S. Ohtani, K. Oyaizu, H. Nishide, K. E. Geckeler, *Adv. Mater.* **2011**, 23, 4440.
- [30] K. Koshika, N. Chikushi, N. Sano, K. Oyaizu, H. Nishide, *Green Chem.* **2010**, 12, 1573.
- [31] K. Koshika, N. Sano, K. Oyaizu, H. Nishide, *Macromol. Chem. Phys.* **2009**, 210, 1989.
- [32] H. Nishide, S. Iwasa, Y.-J. Pu, T. Suga, K. Nakahara, M. Satoh, *Electrochim. Acta* **2004**, 50, 827.
- [33] X. Wei, W. Xu, M. Vijayakumar, L. Cosimbescu, T. Liu, V. Sprenkle, W. Wang, *Adv. Mater.* **2014**, 26, 7649.
- [34] T. Sukegawa, I. Masuko, K. Oyaizu, H. Nishide, *Macromolecules* **2014**, 47, 8611.
- [35] K. Takechi, Y. Kato, Y. Hase, *Adv. Mater.* **2015**, 27, 2501.
- [36] T. Janoschka, M. D. Hager, U. S. Schubert, *Adv. Mater.* **2012**, 24, 6397.
- [37] D. R. Lide, *CRC Handbook of Chemistry and Physics*, Taylor and Francis Group LLC, Florence, Kentucky, USA **2007**.
- [38] T. Janoschka, S. Morgenstern, H. Hiller, C. Friebe, K. Woltersdoerfer, B. Haeupler, M. D. Hager, U. S. Schubert, *Polym. Chem.* **2015**, 6, 7801.
- [39] R. Naejus, R. Coudert, P. Willmann, D. Lemordant, *Electrochim. Acta* **1998**, 43, 275.
- [40] B. Yang, L. Hooper-Burkhardt, F. Wang, G. K. Surya Prakash, S. R. Narayanan, *J. Electrochem. Soc.* **2014**, 161, A1371.
- [41] S. Treimer, A. Tang, D. C. Johnson, *Electroanalysis* **2002**, 14, 165.

ADVANCED MATERIALS

Supporting Information

for *Adv. Mater.*, DOI: 10.1002/adma. 201505000

Poly(TEMPO)/Zinc Hybrid-Flow Battery: A Novel, “Green,”
High Voltage, and Safe Energy Storage System

*Jan Winsberg, Tobias Janoschka, Sabine Morgenstern, Tino
Hagemann, Simon Muench, Guillaume Hauffman, Jean-
François Gohy, Martin D. Hager, and Ulrich S. Schubert**

Supporting Information

Poly(TEMPO)/Zinc Hybrid-Flow Battery - A Novel ‘Green’, High Voltage and Safe Energy Storage System

Jan Winsberg, Tobias Janoschka, Sabine Morgenstern, Tino Hagemann, Simon Muench, Guillaume Hauffman, Jean-François Gohy, Martin D. Hager, Ulrich S. Schubert*

Chemicals and materials: Ethylene carbonate (99%, Alfa Aesar), dimethyl carbonate (anhydrous $\geq 99\%$, Aldrich), diethyl carbonate (anhydrous $\geq 99\%$, Aldrich), zinc perchlorate hexahydrate (Aldrich), zinc chloride (reagent grade $\geq 98\%$, Aldrich), sodium chloride (VWR) and ammonium chloride (Carl Roth) were used as received. Zinc foil (99.98%, thickness 250 μm Alfa Aesar) was used to build zinc electrodes. Dialysis membrane derived from regenerated cellulose with a MWCO of 1,000 Da (Spectra/Por® 6, Spectrum Laboratories, USA) received as pre-wetted dialysis tubing was cut, rinsed with water/propylene carbonate and stored in the electrolyte solution for at least 24 hours. Graphite felt was cut in appropriate pieces (2.25×2.25×0.4 cm, GFA6, SGL, Germany).

Polymer description: The synthesis of polymers **P1**, **P2** and **P3** is described in literature.^[38] Analytical data such as molar masses and radical content are given in Table 1. 2,2,6,6-Tetramethyl-4-piperidyl methacrylate (TEMPMA) was used as precursor of the redox-active TEMPO moiety and was copolymerized with a comonomer unit, increasing the solubility and capacity of the polymer electrolyte. Therefore, TEMPMA was copolymerized with [2-(methacryloyloxy)ethyl]trimethylammonium chloride (METAC) or poly(ethylene glycol) methyl ether methacrylate (PEGMA) and subsequently oxidized in a polymer analogous reaction to the TEMPO radical. P(TEMPO-co-PEGMA)s (**P1** and **P2**) were synthesized via reversible addition-fragmentation chain transfer (RAFT) polymerization.^[38] Both polymers differ in the PEGMA/TEMPO ratio. Polymer **P1** contains PEGMA ($M_n = 450 \text{ g mol}^{-1}$) as comonomer in a ratio of 3.5:1 TEMPO:PEGMA; **P2** incorporates PEGMA ($M_n = 950 \text{ g mol}^{-1}$)

in a ratio of 1:1. For **P2**, the PEGMA content is higher, to achieve a better water solubility. P(TEMPO-*co*-METAC) (**P3**) is especially designed for aqueous solutions and polymerized *via* free radical polymerization initiated by azo-*bis*-isobutyronitrile (AIBN). **P1**, **P2** and **P3** are statistically distributed copolymers.

Molar masses (M_w) $< 100 \text{ kg mol}^{-1}$ were aimed to ensure low viscosities of the electrolytes. Approximate molar masses were determined *via* size exclusion chromatography (SEC). For **P1** and **P2** molar masses (M_w) of 54 and 70 kg mol^{-1} were reached with PDI values of 1.3 and 2.6, respectively. Polymer **P3** has a molar mass (M_w) of 37 kg mol^{-1} and a PDI value of 2.4. The radical content was determined *via* electron paramagnetic resonance (EPR) spectroscopy (Figure S4). For **P1** $1.7 \times 10^{18} \text{ spins mg}^{-1}$ (107% of theoretical activity, mole fraction: 77% (based on 100% of theoretical activity)), for **P2** $5.2 \times 10^{17} \text{ spins mg}^{-1}$ (97% of theoretical activity, mole fraction: 49%) and for **P3** $7.5 \times 10^{17} \text{ spins mg}^{-1}$ (55.3% of theoretical activity, mole fraction: 27.5%) was measured.

Synthesis: Poly(2,2,6,6-tetramethylpiperidin-4-yl methacrylate-*co*-poly(ethylene glycol) methyl ether methacrylate)

In a representative example for the precursor polymer of **P1** and **P2**, 2,2,6,6-tetramethylpiperidin-4-yl methacrylate (100 g; 443.8 mmol) and poly(ethylene glycol) methyl ether methacrylate (57.06 g; 126.8 mmol) as well as 2-cyano-2-butyl dithiobenzoate (895.3 mg; 3.8 mmol) and 4,4'-azobis(4-cyanovaleric acid) (533.1 mg; 1.9 mmol) were dissolved in a mixture of methanol and water (3:1; 380 mL). The mixture was deaerated by flushing with argon for 20 min and subsequently stirred at 70 °C for 24 h, after which full monomer conversion was achieved. The reaction mixture was used for the subsequent oxidation without further purification.

Poly(2,2,6,6-tetramethylpiperidin-4-yl methacrylate-*co*-2-(methacryloyloxy)-*N,N,N*-trimethylethane ammonium chloride)

In a representative example for the precursor polymer of **P3**, 2,2,6,6-tetramethylpiperidin-4-yl methacrylate (100 g; 443.8 mmol) was dispersed in water. After the addition of hydrochloric acid (45 mL; 37%), the mixture was stirred at room temperature until the monomer was completely dissolved. 2-(Methacryloyloxy)-*N,N,N*-trimethylethane ammonium chloride (106.7 mL; 80% solution in water; 443.8 mmol), 4,4'-azobis(4-cyanovaleric acid) (12.4 g; 44.38 mmol) and 2-mercaptoethanol (4.98 mL; 70.7 mmol) were added. The mixture was deaerated by flushing with argon for 20 min and stirred at 80 °C for 6 h, after which full monomer conversion was achieved. After cooling to room temperature, the solution was alkalized with sodium hydroxide and used for the subsequent oxidation without further purification.

General procedure for preparation of **P1**, **P2** and **P3** (oxidation)

To the reaction mixture, three equivalents hydrogen peroxide (30%) and 0.03 equivalents sodium tungstate dihydrate were added. The mixture was stirred for 24 h at room temperature and subsequently dialyzed against water. The solvent was removed by lyophilization to yield the polymer as orange powder.

Polymer characterization: Size exclusion chromatography (SEC) was performed on an Agilent 1200 series system (degasser, PSS; pump, G1310A; auto sampler, G1329A; oven, Techlab; DAD detector, G1315D; RI detector, G1362A; eluent, DMAc + 0.21% LiCl, 1 mL/min; temperature, 40 °C; column, PSS GRAM guard/1000/30 Å). Asymmetric flow field flow fractionation (AF4) was conducted on an AF2000 MT System (Postnova Analytics, Landsberg, Germany) coupled to an UV (PN3211, 260 nm), RI (PN3150), MALLS (PN3070,

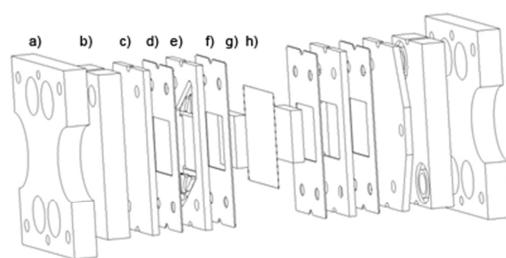
633 nm). X-band electron paramagnetic resonance (EPR) measurements were conducted on a EMXmicro CW-EPR spectrometer from Bruker using powdered samples. The total spin count was the average of five measurements.

Cell assembly: The electrochemical cell was designed and constructed in a flat cell type with a membrane active area of 5 cm² (JenaBatteries GmbH, Germany). See **Scheme S1** for a detailed overview. Zinc electrodes were cut out of zinc foil (50×65 mm, 5.7 g) and brushed with sandpaper directly before cell assembly.

Electrochemical characterization: Cyclic voltammetry (CV), electrochemical impedance spectroscopy (EIS) and charging-/discharging tests were conducted on a VMP3 potentiostat/galvanostat (Biologic, France). For CV measurements, a standard three electrode setup with a glassy-carbon disk working electrode (diameter 2 mm), a AgNO₃/Ag reference electrode for carbonate based electrolytes, a AgCl/Ag/water reference electrode for aqueous electrolytes and a platinum wire counter electrode were used. Rotating disc electrode (RDE) measurements were conducted on a VersaSTAT potentiostat/galvanostat (Princeton Applied Research, USA), with a glassy carbon tip (diameter 5 mm), the rotation speed was controlled externally by a Model 636A ring-disk electrode system (Princeton Applied Research, USA). Evaluation of the RDE analysis *via* Levich plot (limiting current i_{lim} vs. square root of rotation speed ω) yields the diffusion coefficient D by using Levich equation, $i_{lim} = 0.62nFAD^{\frac{2}{3}}\omega^{\frac{1}{2}}\nu^{-\frac{1}{6}}c_0$, with $n = 1$, Faraday's constant $F = 96,485 \text{ C mol}^{-1}$, electrode surface of 0.2 cm², the solutions kinematic viscosity $\nu = 1.0 \times 10^{-6} \text{ m}^2 \text{ s}^{-1}$ ^[37] and the bulk concentration c_0 of the redox-active TEMPO repeating unit. The ion conductivity of the electrolytes was measured with a Cond 3110 SET 1 incl. TetraCon 325 (WTW, Germany) at 20 °C.

Membrane description: In this study dialysis membranes derived from standard regenerated cellulose were applied as separator in battery application. Spectra/Por® 6 (Spectrum Labs, USA) with a MWCO 1,000 g/mol were received as pre-wetted dialysis tubing. The membrane is characterized by a symmetric porosity, a thickness of 62.5 μm and is manufactured from natural cellulose reconstituted from cotton linters. With this separator a retention of the cathode active polymer (molar masses $>10,000$ g/mol) but a diffusion of the low molecular mass conductive additive is possible.

Battery tests: For static, non-pumped long-term charging/discharging experiments, both half cells were filled with 3 mL electrolyte solution using a syringe. To study the influence of the current density on the electrical performance of the battery, dynamic measurements were performed, whereat the electrolyte was circulated between the electrochemical cell and the storage tanks with a peristaltic pump (Hei-FLOW Value 01 Multi, Heidolph, Germany). Typically, 8 mL of electrolyte were used with a flow rate of 20 mL min^{-1} . All measurements were carried out at 25°C under normal atmosphere. The batteries were charged/discharged with constant current and the resulting potential was measured over time. EIS was measured between 100 mHz and 200 kHz at 0 V in potentiostatic mode, zero crossing determined cell resistance. Coulombic efficiencies were calculated by the quotient of discharging current and charging current of the same cycle, voltage efficiencies by the quotient of mean potential of discharging- and charging plateau, energy efficiency by the product of voltage efficiency and coulombic efficiency. State of charge (SOC) vs. open circuit voltage (OCV) was conducted with alternating charging and resting periods. A current of 0.5 mA cm^{-2} was applied for 30 s subsequently followed by a resting period of 60 s, where the OCV was measured.



Scheme S1: Schematic representation of the electrochemical cell. One half-cell consists of a frame (a), PTFE block with hose connections and rubber seal (b), graphite/zinc current collector (c), rubber sealing (d), PTFE flow frame (e), rubber sealing (f), surface enhancing graphite felt/carbon paper (g). Both half cells are separated by a size exclusion membrane (h).

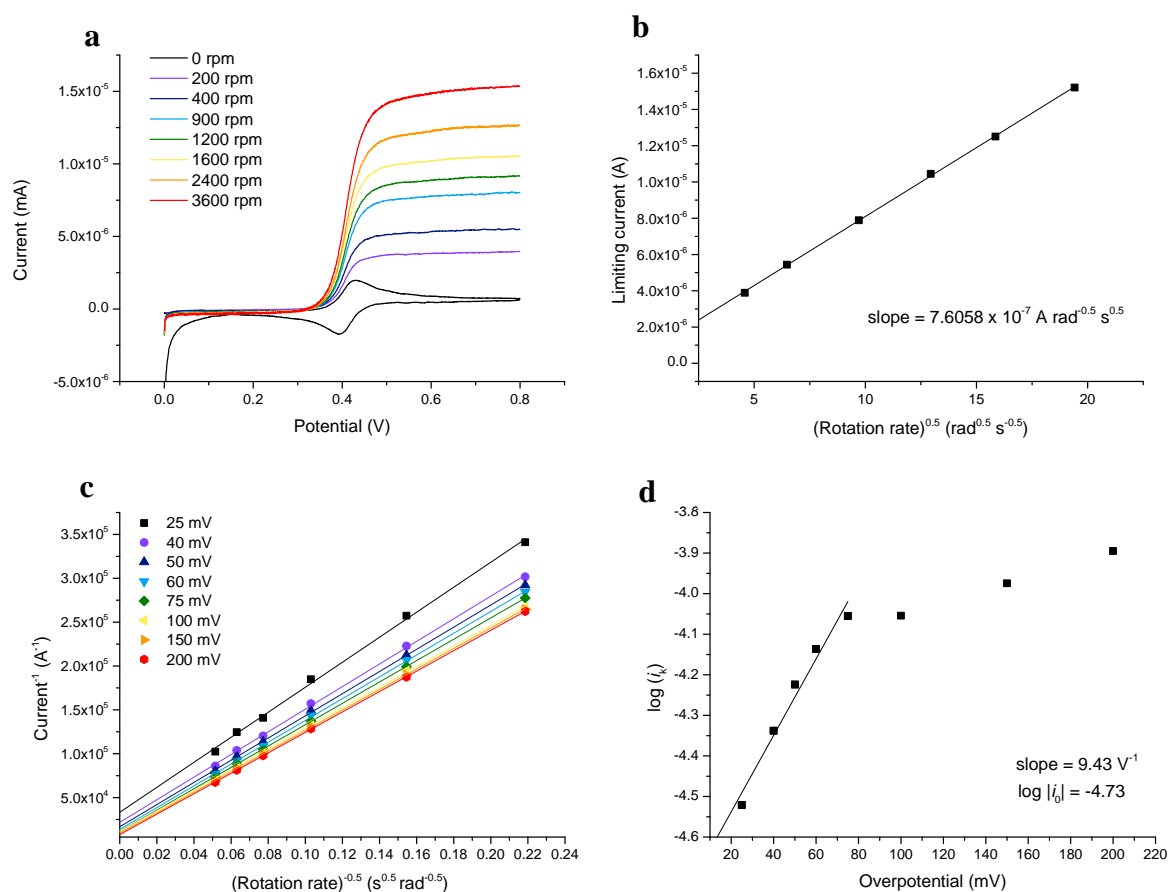


Figure S2: a) Rotating disc electrode measurement of **P1** ($1 \times 10^{-3} \text{ mol L}^{-1}$ (repeating unit), $0.1 \text{ M Zn}(\text{ClO}_4)_2 \cdot 6\text{H}_2\text{O}$ in EC/DMC/DEC v:v:v, 1:1:1, scan rate 5 mV s^{-1}) at different rotating rates from 0 to 3600 rpm, b) Levich-plot from the obtained limiting currents at $700 \text{ mV vs. AgNO}_3/\text{Ag}$; application of Levich-equation yields a diffusion coefficient $D = 1.65 \times 10^{-7} \text{ cm}^2 \text{ s}^{-1}$, c) Koutecký-Levich plot for different overpotentials yielding the mass-transfer-independent current i_k , d) Tafel plot yielding $k^0 = 9.93 \times 10^{-4} \text{ cm s}^{-1}$ and $\alpha = 0.443$.

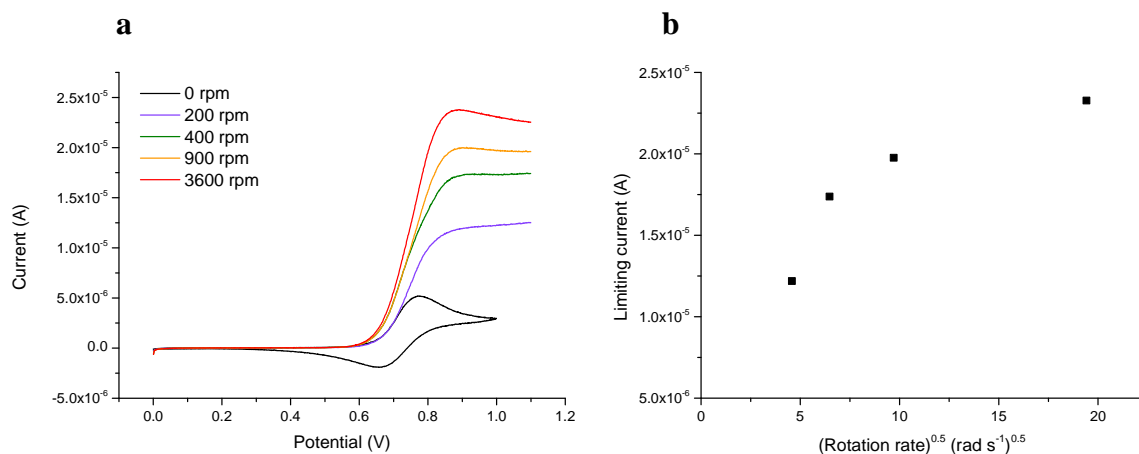


Figure S3: a) Rotating disc electrode measurements of **P3** (33 mM) in 710 mM NaCl, 8 mM ZnCl₂ and 8 mM NH₄Cl in H₂O. b) Levich-plot from the obtained limiting currents at 900 mV vs. AgCl/Ag.

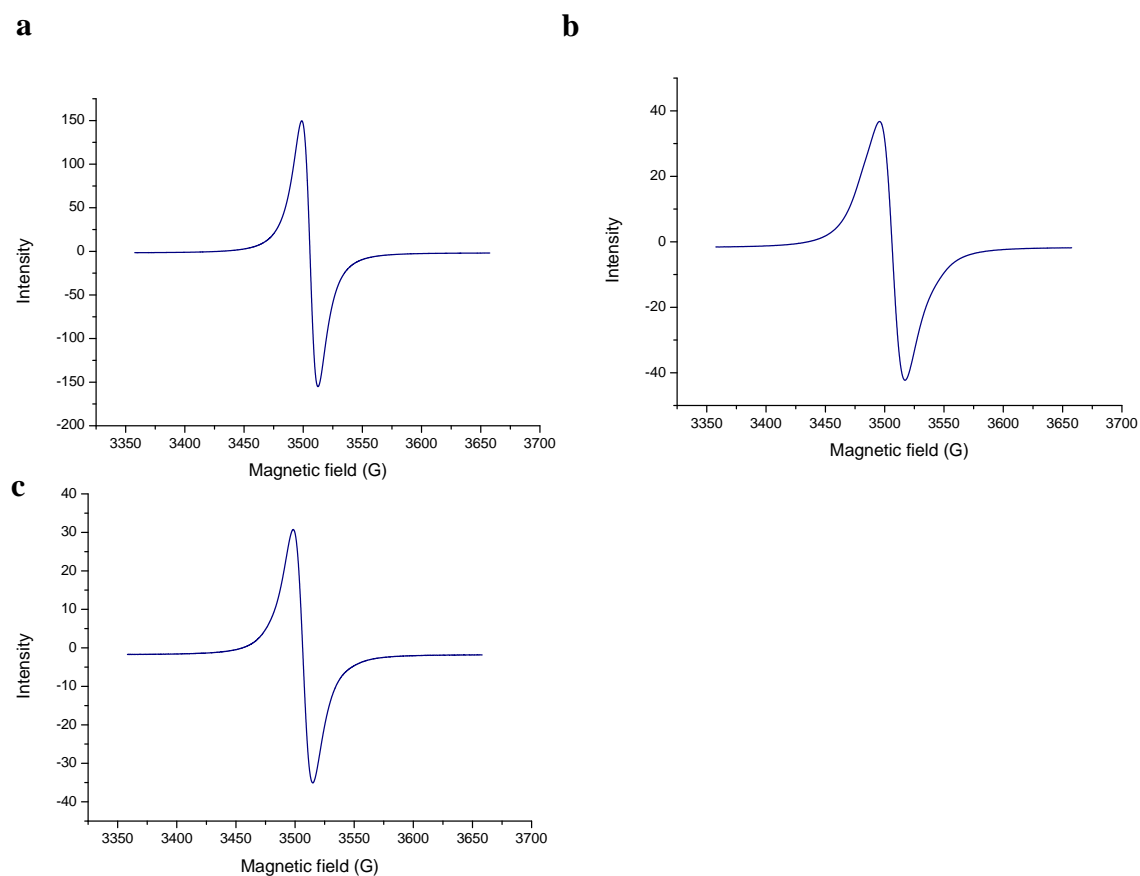


Figure S4: Solid state EPR measurements of a) **P1** (1.7x10¹⁸ spins mg⁻¹, radical content $x=0.77$), b) **P2** (5.2x10¹⁷ spins mg⁻¹, radical content $x=0.49$) and c) **P3** (7.5x10¹⁷ spins mg⁻¹, radical content $x=0.28$).

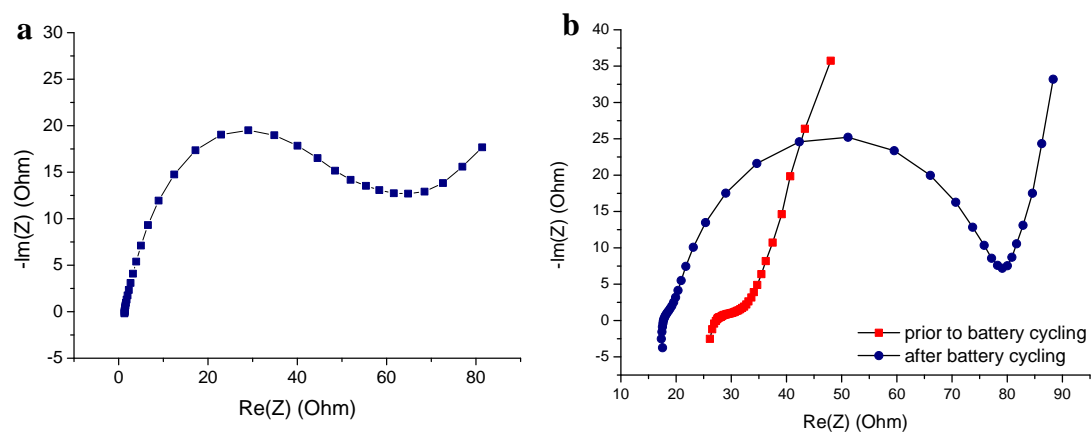


Figure S5: EIS measurements of poly(TEMPO)/zinc hybrid-flow batteries; a) catholyte **D** (**P3**) (recorded prior to cycling) and b) catholyte **B** (**P1**).

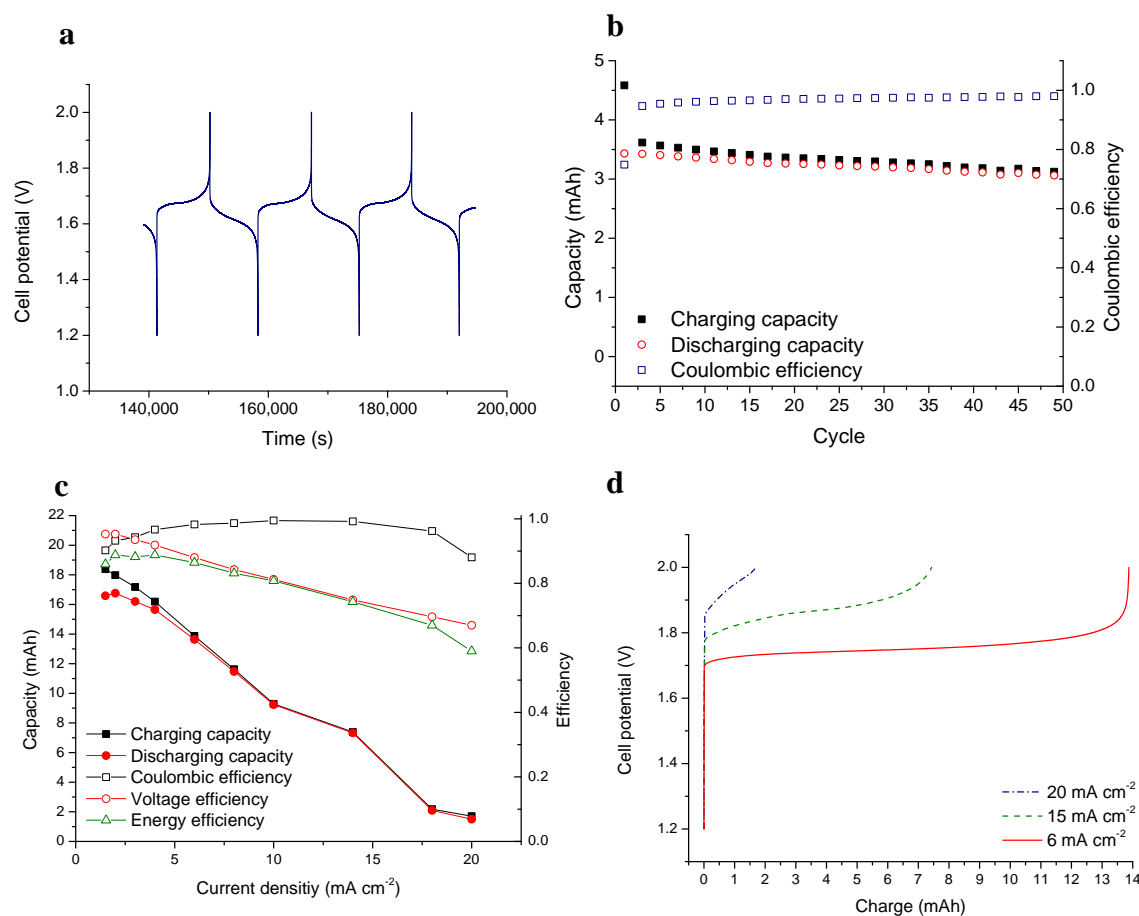


Figure S6: Poly(TEMPO)/zinc hybrid-flow battery utilizing catholyte **C** (**P2**, P(TEMPO-co-PEGMA), a) exemplary charging-/discharging curves, 1.5 mA cm^{-2} , 8 mL electrolyte per half-cell, flow rate 20 mL min^{-1} , b) long-term stability test in a static, non-pumped hybrid-flow-cell, 3 mA cm^{-2} , at room temperature, c) electrical performance, varied current density, 8 mL electrolyte per half-cell, flow rate 20 mL min^{-1} and d) cell potential over charge for different current densities.

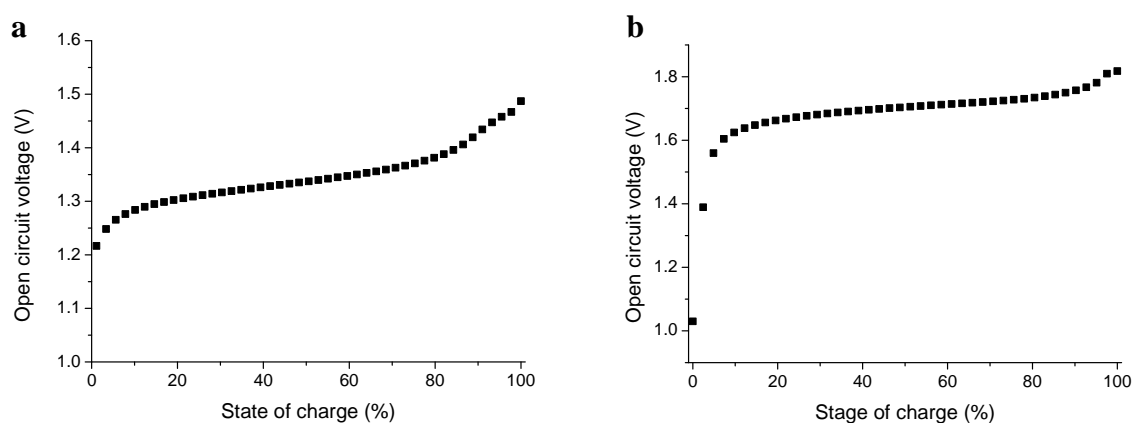


Figure S7: Open circuit voltage (OCV) vs. state of charge (SOC) for a) catholyte **B**, at 50% SOC the OCV was 1.3 V and b) catholyte **D**, at 50% SOC the OCV was 1.7 V.

Table S1: Ion conductivities of the applied electrolytes.

Electrolyte	Ion conductivity [mS cm^{-1}]
0.71 M NaCl, 0.08 M ZnCl_2 , 0.08 M NH_4	60.4
1 M ZnCl_2 , 1 M NH_4Cl	144.0
0.5 M TBAClO ₄	5.9
0.75 M TBAClO ₄	6.9

Table S2: Charging times of a poly(TEMPO)/zinc hybrid-flow battery utilizing catholyte **A** depending on the applied current density.

Current density [mA cm^{-2}]	Full charge/discharge time [s]
6	2,700
5	3,000
4	3,300
3	4,700
2	8,200

Table S3: Charging times of a poly(TEMPO)/zinc hybrid-flow battery utilizing catholyte **B** depending on the applied current density.

Current density [mA cm^{-2}]	Full charge/discharge time [s]
4	1,100
3	2,500
2	4,400
1.5	5,900
1	8,900
0.5	21,100
0.2	68,700

Table S4: Charging times of a poly(TEMPO)/zinc hybrid-flow battery utilizing catholyte **C** depending on the applied current density.

Current density [mA cm^{-2}]	Full charge/discharge time [s]
20	115
18	170
16	440
14	720
12	840
10	1,380
8	2,080
6	3,310
4	5,770
3	8,010
2	12,520
1	24,760
0.5	46,390

Table S5: Charging times of a poly(TEMPO)/zinc hybrid-flow battery utilizing catholyte **D** depending on the applied current density.

Current density [mA cm^{-2}]	Full charge/discharge time [s]
12	380
10	500
8	640
6	890
4	1,380
3	1,840
2	2,780
1.5	3,720
1	5,600

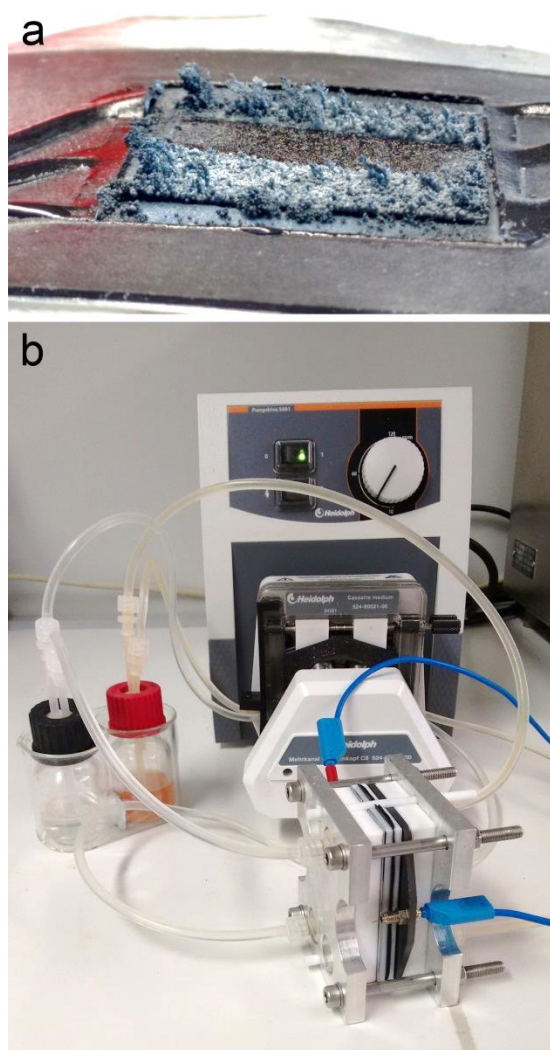
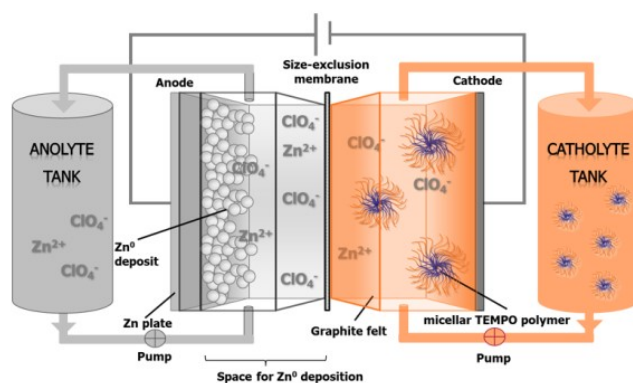


Figure S8: a) Dendrite formation inside the anode half-cell after battery cycling and b) pumped HFB battery setup, comprising the electrochemical cell, two reservoir tanks (catholyte & anolyte) and a peristaltic pump.

Publication P6

Polymer/zinc hybrid-flow battery using block copolymer micelles featuring a TEMPO corona as catholyte

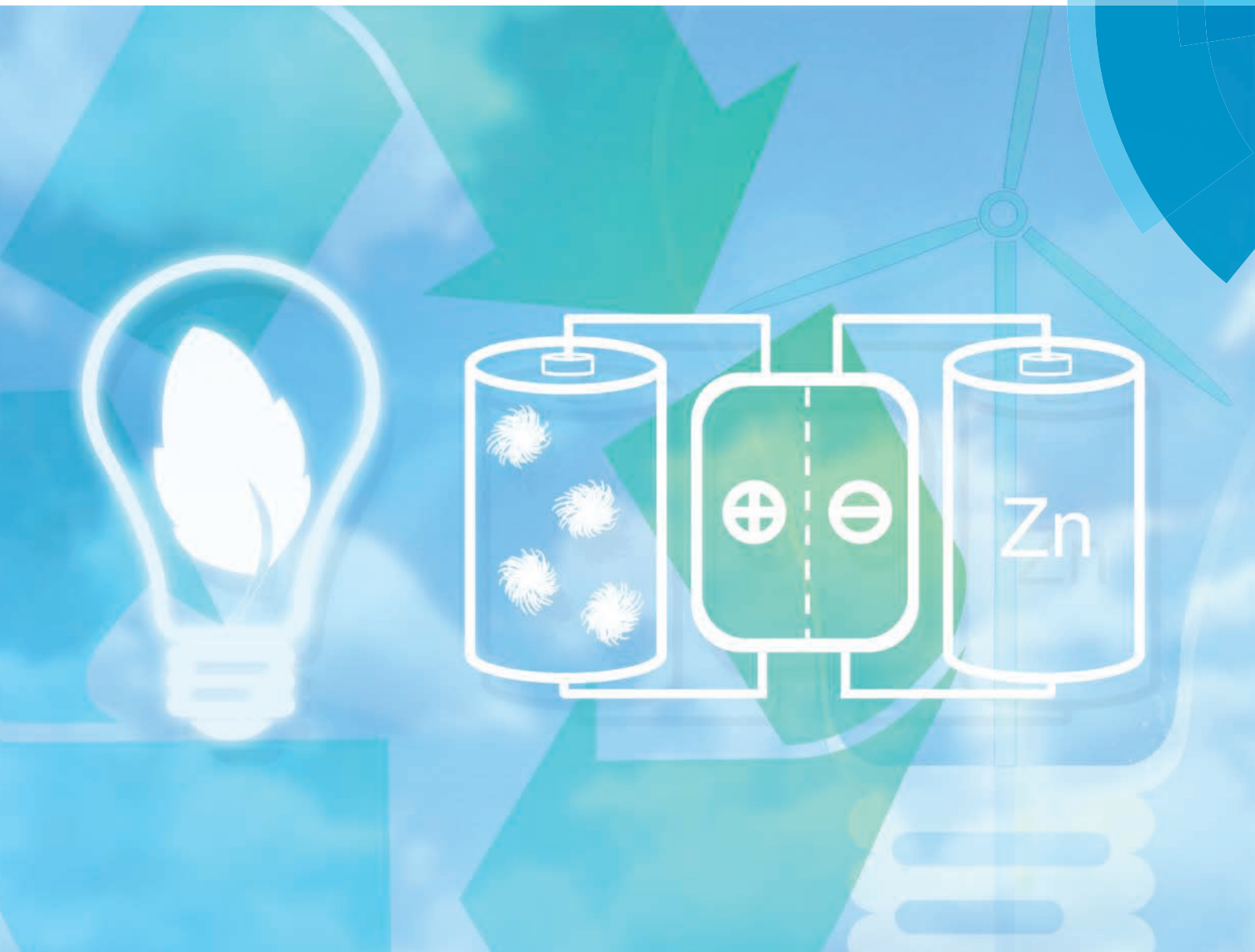
J. Winsberg, S. Muench, T. Hagemann, S. Morgenstern, T. Janoschka, M. Billing, F. H. Schacher, G. Hauffman, J.-F. Gohy, S. Hoeppeener, M. D. Hager, U. S. Schubert, *Polym. Chem.* **2016**, 7, 1711-1718.



Reproduced with permission of the Royal Society of Chemistry, Copyright © 2017.

Polymer Chemistry

www.rsc.org/polymers



ISSN 1759-9954



PAPER

Ulrich S. Schubert *et al.*

Polymer/zinc hybrid-flow battery using block copolymer micelles featuring a TEMPO corona as catholyte

175 YEARS



Cite this: *Polym. Chem.*, 2016, 7, 1711

Polymer/zinc hybrid-flow battery using block copolymer micelles featuring a TEMPO corona as catholyte†

Jan Winsberg,^{a,b} Simon Muench,^{a,b} Tino Hagemann,^{a,b} Sabine Morgenstern,^{a,b} Tobias Janoschka,^{a,b} Mark Billing,^a Felix H. Schacher,^{a,b} Guillaume Hauffman,^c Jean-François Gohy,^c Stephanie Hoeppener,^a Martin D. Hager^{a,b} and Ulrich S. Schubert^{*a,b}

A well-defined block copolymer was applied in a semi-organic polymer hybrid-flow battery (pHFB). A 2,2,6,6-tetramethylpiperidiny-*N*-oxyl (TEMPO) containing polymer was utilised as cathode active material. Micellar structures of the active material were achieved by utilising a diblock copolymer composed of a polar poly(TEMPO methacrylate) (PTMA) and an unpolar poly(styrene) (PS) block, which enables the formation of core-corona micelles in organic carbonates. The synthesised PTMA-*b*-PS was electrochemically investigated and subsequently utilised as catholyte in polymer/Zn pHFBs. The constructed flow batteries feature an excellent cycling stability of 1000 consecutive charge/discharge cycles with 95% retention of initial discharge capacity and a stable voltage range of 2 V. Further, the charging process leads to slight changes in the micellar structure combined with an increased solubility.

Received 22nd December 2015,
Accepted 18th January 2016

DOI: 10.1039/c5py02036k

www.rsc.org/polymers

Introduction

The energy transition from an ecologically problematic electricity generation mainly based on fossil fuels and nuclear power to a sustainable and 'green' electricity production faces several problems concerning grid stability and temporal shifts between energy production and consumption.^{1–3} Intelligent energy storage and management technologies are required to overcome these problems and to ensure a stable electricity supply. Smart grids combine sustainable electricity production from renewable sources, like wind power and solar energy, with storage systems. One of the most promising storage technologies for decentralised grids is the redox-flow battery (RFB) technology.² RFBs utilise solvated redox-active materials that are circulated between an electrochemical cell and storage tanks. Accordingly, RFBs are one of a few battery technologies where power and capacity can be scaled independently from each other, by sizing the volume of the electrolyte (capacity) or

the active area of the electrochemical cell (power). All-vanadium redox-flow batteries (VRFB) are the state of the art and the ones closest to market penetration. They utilise vanadium ions dissolved in sulfuric acid as redox-active material and supporting electrolyte, respectively.^{4,5} Consequently, the VRFB faces several problems concerning acquisition costs, environmental impact and corrosion.^{6,7} These drawbacks can be reduced with zinc hybrid-flow batteries (HFB), which feature a $\text{Zn}^{2+}_{(\text{aq})}/\text{Zn}^0_{(\text{s})}$ anode, but also a problematic halogen-based cathode, *e.g.*, bromine or polyiodide.^{8–12} In recent years, research focused increasingly on organic active materials for RFB applications.^{13–25} Several polymeric redox-active materials for the utilisation in flow batteries were reported,^{22,26} *e.g.*, Sukegawa *et al.* presented a 2,2,6,6-tetramethylpiperidiny-*N*-oxyl (TEMPO) crowded bottlebrush polymer for flow battery applications.¹⁷ A promising next generation of aqueous-based all-organic polymer redox-flow batteries (pRFB) was recently reported by Janoschka *et al.* and employed statistically distributed TEMPO- and *N*-methyl-4,4'-bipyridinium-based copolymers as catholyte and anolyte, respectively.^{15,24} Thus, a substitution of the dangerous halogen-based cathode in zinc HFBs with a safer organic-based, *e.g.*, polymeric TEMPO is meaningful and was reported by us, recently.²⁷ However, one major challenge pRFBs have to deal with is the viscosity of the electrolyte. Dissolved polymeric species lead to an increased viscosity of the electrolyte compared to low molar mass compounds. Special shaped polymers

^aLaboratory of Organic and Macromolecular Chemistry (IOMC), Friedrich Schiller University Jena, Humboldtstraße 10, 07743 Jena, Germany.

E-mail: ulrich.schubert@uni-jena.de

^bCenter for Energy and Environmental Chemistry Jena (CEEC Jena), Friedrich Schiller University Jena, Philosophenweg 7a, 07743 Jena, Germany

^cInstitute of Condensed Matter and Nanoscience, Bio- and Soft Matter, Université catholique de Louvain, Louvain-la-Neuve, 1348 Belgium

†Electronic supplementary information (ESI) available. See DOI: 10.1039/c5py02036k

can counteract this phenomenon, so that dendrimeric or micellar structures are preferred architectures over regular, linear polymers. Micellar TEMPO-containing block copolymers were previously reported by Hauffman *et al.* and were applied as active material in semi-organic thin-film batteries.^{28,29} The aim of this study is the application of well-defined TEMPO-methacrylate/styrene block copolymers, self-assembling into micellar structures in organic carbonate-based electrolytes, as cathode active material in semi-organic polymer/Zn hybrid-flow batteries (pHFB) and the investigation of the electrochemical behaviour as well as the structure of the charged micelles.

Experimental

Chemicals and materials

Ethylene carbonate (99%, Alfa Aesar), dimethyl carbonate (anhydrous $\geq 99\%$, Aldrich), diethyl carbonate (anhydrous $\geq 99\%$, Aldrich) and zinc perchlorate hexahydrate (Aldrich) were used as received. Zinc foil (99.98%, thickness 250 μm , Alfa Aesar) was used to build zinc electrodes. Dialysis membrane derived from regenerated cellulose with a molecular weight cut-off (MWCO) of 1000 Da (Spectra/Por® 6, Spectrum Laboratories), received as pre-wetted dialysis tubing, was cut, rinsed with water/propylene carbonate and stored in the electrolyte solution for at least 24 hours. Graphite felt was cut in appropriate pieces ($2.25 \times 2.25 \times 0.4$ cm, GFA6, SGL).

Synthesis

The synthesis of PTMA₆₃-*b*-PS₃₅ is described in literature and was conducted in a two-step reaction.^{24,28} First, tosylchloride initiated the synthesis of the poly(2,2,6,6-tetramethyl-4-piperidyl methacrylate) chloride (PTEMPMA-Cl) block. In a second reaction step, PTEMPMA-Cl was used as macro initiator for the polymerisation of a second nonpolar styrene block. The subscripted number reflects the average degree of polymerisation of the respective blocks (determined *via* ^1H NMR analysis). An exemplary synthesis procedure is described as follows:

In a first reaction step, PTEMPMA-Cl was synthesised *via* atom transfer radical polymerisation (ATRP). A solution of *N,N,N',N'',N'''*-pentamethyldiethylenetriamine (PMDETA; 57.8 mg, 0.333 mmol, 1.1 equiv.) and CuCl (30 mg, 0.303 mmol, 1 equiv.) in anisole was added to a solution of 2,2,6,6-tetramethyl-4-piperidyl methacrylate (TEMPMA) (30.727 g, 136.36 mmol, 450 equiv.) and 4-toluenesulfonyl chloride (57.8 mg, 0.303 mmol, 1 equiv.) in anisole and stirred at 80 °C for 16 min. The polymerisation was quenched by cooling in an ice bath and exposing the reaction mixture to air. In a second reaction step, the block copolymer PTEMPMA₆₃-*b*-PS₃₅ was synthesised *via* ATRP. A solution of PMDETA (30.8 mg, 0.178 mmol, 1.1 equiv.) and CuCl (16 mg, 0.1616 mmol, 1 equiv.) in anisole was added to a solution of PTEMPMA-Cl ($M_n = 14\,400$ g mol⁻¹, $\bar{D} = 1.18$; 2.327 g, 0.1616 mmol, 1 equiv.) and styrene (7.416 g, 80.808 mmol, 500 equiv.) in anisole and stirred at 100 °C for 16 h. The polymerisation was quenched by cooling in an ice bath and exposing the

reaction mixture to air. The subsequent oxidation to the TEMPO free radical was conducted by the addition of *meta*-chloroperoxybenzoic acid (463.9 mg, 2.688 mmol, 1.5 equiv.) to a solution of PTEMPMA₆₃-*b*-PS₃₅ (2 g, 0.0284 mmol, 0.0284 equiv.) in dichloromethane at 0 °C and stirred for 1 h. The accordingly obtained PTMA₆₃-*b*-PS₃₅ diblock copolymer was precipitated in hexane and dried under reduced pressure.

Polymer characterisation

Dynamic light scattering (DLS) measurements were performed on an ALV CGS-3 (ALV-Laser GmbH, Langen, Germany) equipped with a He-Ne laser (633 nm) at 25 °C (viscosity of the electrolyte mixture $\eta = 1.92$ mPas, refractive index $n = 1.4004$). Determination of the refractive index was conducted on a Optilab rEX at 25 °C (Wyatt Technology, USA). Size exclusion chromatography (SEC) was performed on an Agilent 1200 series system (degasser, PSS; pump, G1310A; auto sampler, G1329A; oven, Techlab; DAD detector, G1315D; RI detector, G1362A; eluent, DMAc + 0.21% LiCl, 1 mL min⁻¹; temperature, 40 °C; column, PSS GRAM guard/1000/30 Å). Transmission electron microscopy (TEM) was performed on a Tecnai G² 20 (FEI, USA) at an acceleration voltage of 120 kV. Samples were prepared on a carbon coated TEM grid (Quantifoil, Germany) by depositing 2 μL of the solutions onto the grid. Solutions were allowed to adhere to the grid for 5 min. After that, the solution was removed with filter paper and allowed to dry. Finally, the grids were rinsed with the pure electrolyte solution and dried. X-band electron paramagnetic resonance (EPR) measurements were performed on an EMXmicro CW-EPR spectrometer (Bruker, USA) using powdered samples. The total spin count was determined *via* the SpinCountT software module taking the average of five measurements.

Cell assembly

The electrochemical cell was designed and constructed in a flat cell type with an active membrane area of 5 cm² (Jena-Batteries, Germany; see Scheme S1†). Zinc electrodes were cut out of zinc foil (50 \times 65 mm, 5.7 g) and brushed with sandpaper directly before cell assembly.

Electrochemical characterisation

Cyclic voltammetry (CV), electrochemical impedance spectroscopy (EIS) and charge/discharge experiments were conducted using a VMP3 potentiostat/galvanostat (Biologic, France). For CV measurements, a standard three-electrode setup with a glassy-carbon disk working-electrode (diameter 2 mm), a AgNO₃/Ag reference electrode and a platinum wire counter electrode were used. Rotating disc electrode (RDE) measurements were conducted on a VersaSTAT potentiostat/galvanostat (Princeton Applied Research, USA), with a glassy-carbon tip (diameter 5 mm), the rotation speed was controlled externally by a Model 636A ring-disk electrode system (Princeton Applied Research, USA). Evaluation of the RDE analysis *via* Levich plot (limiting current i_{lim} vs. square root of rotation speed ω) reveals the diffusion coefficient D by using Levich equation: $i_{\text{lim}} = 0.62nFAD^{2/3}\omega^{1/2}v^{-1/6}c_0$, with $n = 1$, Faraday's constant $F = 96\,485$ C mol⁻¹, electrode surface of 0.2 cm², the solu-

tions kinematic viscosity $\nu = 1.0 \times 10^{-6} \text{ m}^2 \text{ s}^{-1}$ (ref. 30) and the bulk concentration c_0 of the redox-active TEMPO repeating unit.

Battery tests

For static, non-pumped long-term charge/discharge experiments, both half cells were filled with electrolyte solution (3 mL) using a syringe. Dynamic measurements were performed to study the influence of the current density on the electrical performance of the battery, whereas the electrolyte was circulated between the electrochemical cell and the storage tanks with a peristaltic pump (Hei-FLOW Value 01 Multi, Heidolph, Germany). Typically, 8 mL of electrolyte were used with a flow rate of 20 mL min^{-1} (Fig. S4b†). All measurements were carried out at 25°C under normal atmosphere. The batteries were charged/discharged with constant current and the resulting potential was measured over time. EIS was measured between 100 mHz and 200 kHz at 0 V in potentiostatic mode, zero crossing determined cell resistance. Coulombic efficiencies were calculated by the quotient of discharging current and charging current of the same cycle, voltage efficiencies by the quotient of mean potential of discharging and charging plateau, energy efficiency by the product of voltage efficiency and coulombic efficiency. State of charge (SOC) vs. open circuit voltage (OCV) was determined with alternating charging and resting periods. A current of 0.5 mA cm^{-2} was applied for 30 s, subsequently followed by a resting period of 60 s, where the OCV was measured.

Results and discussion

The detailed synthesis of TEMPO-methacrylate/styrene block copolymers (PTMA-*b*-PS) was previously reported.^{28,29} Since a radical polymerisation of TEMPO-methacrylate cannot be performed, 2,2,6,6-tetramethyl-4-piperidyl methacrylate (TEMPMA) is polymerised as precursor and afterwards oxidised to the TEMPO free-radical in a polymer analogous reaction. In this study PTMA₆₃-*b*-PS₃₅ was used for all experiments. The number in the subscript reflects the average degree of polymerisation of the respective blocks and was determined *via* ^1H NMR analysis prior to oxidation to the TEMPO free-radical. The TEMPMA to comonomer ratio was 1.8 and the actual radical content of the polymer was investigated *via* electron paramagnetic resonance (EPR) spectroscopy. A spin count of $1.7 \times 10^{18} \text{ spins mg}^{-1}$ (Fig. S1†) was measured, which correlates to a radical content of 82% of the theoretical maximal value (mole fraction $x = 0.53$). According to SEC measurements, the polymer has a molar mass (M_n) of 41 kg mol^{-1} (poly(styrene) standards) and a dispersity (D) of 1.1 (Fig. S2†). This deviation can be attributed to the used calibration standards.

Since PTMA₆₃-*b*-PS₃₅ contains an nonpolar styrene block and a polar TEMPO block, it aggregates into micellar structures when dissolved in organic carbonates, presumably into micelles featuring a PS core and a PTMA corona.²⁸ Because of their good electrochemical stability and low vapour pressures organic carbonates are widely used solvents in various battery

applications.³¹ For this study a mixture of ethylene carbonate (EC), dimethyl carbonate (DMC) and diethyl carbonate (DEC) was utilised revealing a good ion conductivity compared to other carbonate-based electrolytes and a previously verified formation of micelles for PTMA₆₃-*b*-PS₃₅.²⁸ $\text{Zn}(\text{ClO}_4)_2 \cdot 6\text{H}_2\text{O}$ with a concentration of 0.5 M served as supporting electrolyte and anode active material, respectively. In a subsequent battery application the redox couples TEMPO⁺/TEMPO and $\text{Zn}^{2+}_{(\text{aq})}/\text{Zn}^0_{(\text{s})}$ were employed (Fig. 1a).

$\text{Zn}^{2+}_{(\text{aq})}$ is reduced to $\text{Zn}^0_{(\text{s})}$ in the charging process and forms a deposit on the anode. This process is characteristic to a hybrid flow battery (HFB), always featuring one active material with one insoluble species. Hence, additional space for the $\text{Zn}^0_{(\text{s})}$ deposit is required to prevent a short circuit, caused by dendrites growing through the pores of the membrane. Dialysis membranes, derived from regenerated cellulose, with a molar mass cut-off (MWCO) of 1000 g mol^{-1} were employed as separator. This membrane is permeable for the supporting electrolyte but retains the cathode active micelles (Fig. 1c). An additional benefit of Zn pHFB is the robustness of the utilised anode active material, since Zn shows no side-reactions with oxygen, which typically lead to self-discharge in battery applications. Expensive treatment with an inert gas is, therefore, rendered unnecessary.

Electrochemical analysis of PTMA₆₃-*b*-PS₃₅

Cyclic voltammetry (CV) measurements of 0.01 M PTMA₆₃-*b*-PS₃₅ (referred to the weighted average repeating unit of TEMPO-methacrylate and styrene) were conducted in EC/DMC/DEC ($v:v:v$ 1:1:1) with 0.1 M $\text{Zn}(\text{ClO}_4)_2 \cdot 6\text{H}_2\text{O}$ and revealed a quasi-reversible redox reaction of the TEMPO⁺/TEMPO redox-couple at 0.4 V vs. AgNO_3/Ag with a peak-split of 90 mV (Fig. 2, solid line). Additionally the electrodeposition of Zn^{2+} on the glassy-carbon electrode was observed for potentials lower than -1.18 V and dissolution at potentials above -1 V vs. AgNO_3/Ag (Fig. 2, dashed line). The redox reaction reveals a large peak split of 2.1 V. This is attributed to the restricted ionic conductivity of Zn^{2+} in organic carbonate-based electrolytes.

Further electrochemical analyses were performed *via* rotating disc electrode (RDE) measurements of 1.6 mM PTMA₆₃-*b*-PS₃₅ (based on the weighted average repeating unit of TEMPO-methacrylate and styrene) in EC/DMC/DEC ($v:v:v$ 1:1:1) with 0.1 M $\text{Zn}(\text{ClO}_4)_2 \cdot 6\text{H}_2\text{O}$. Levich-analysis reveals a diffusion-controlled behaviour of the micellar polymer in zinc perchlorate solution and a diffusion coefficient D of $1.8 \times 10^{-7} \text{ cm}^2 \text{ s}^{-1}$. Subsequent Koutecký-Levich analysis illustrates mass-transport-independent currents. The electron-transfer rate constant k^0 of $7 \times 10^{-4} \text{ cm s}^{-1}$ and a transfer coefficient α of 0.49, which is close to the value of an ideal reversible redox reaction of 0.5, were derived by Tafel analysis (Fig. 3).

In a subsequent pHFB application zinc foil was utilised as anode and a 0.5 M solution of $\text{Zn}(\text{ClO}_4)_2 \cdot 6\text{H}_2\text{O}$ in EC/DMC/DEC ($v:v:v$ 1:1:1) was used as anolyte, in which zinc perchlorate serves both as supporting electrolyte and anode active material. The catholyte additionally contains the block copolymer micelles with a concentration of 13 mg mL^{-1} . This con-

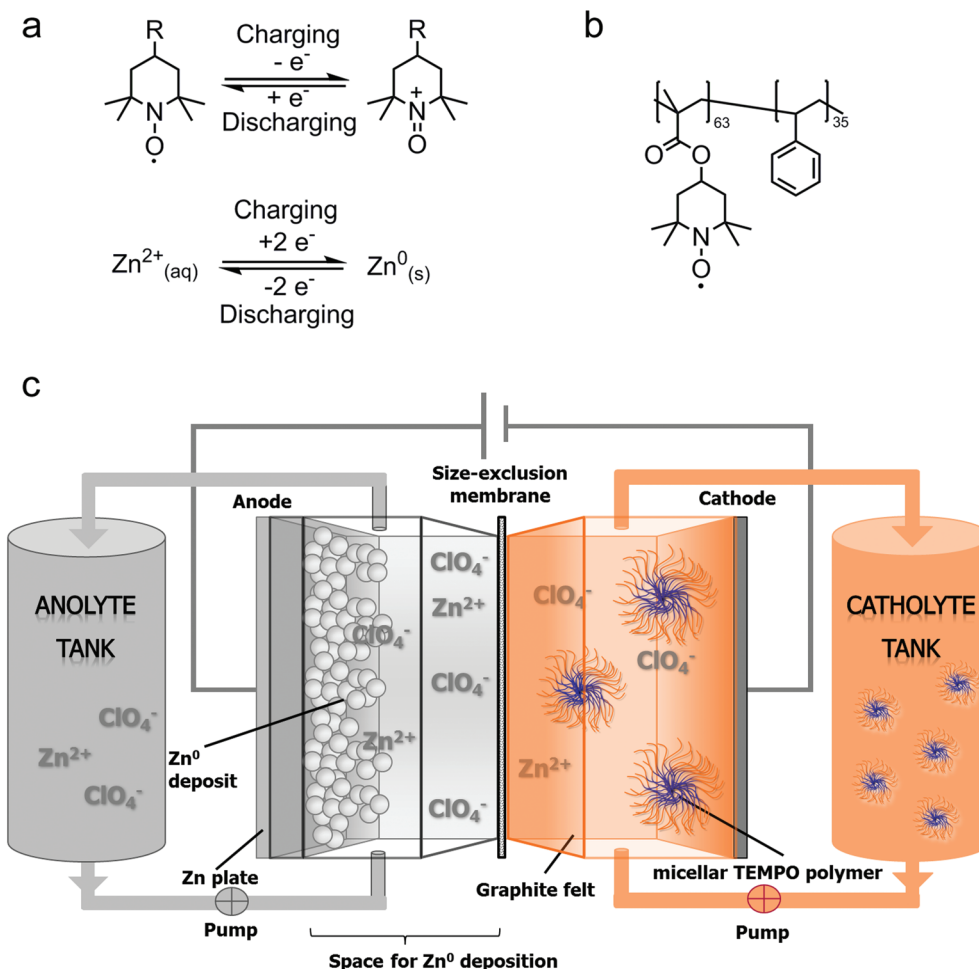


Fig. 1 (a) Redox reaction of the TEMPO⁺/TEMPO and the Zn²⁺/Zn⁰ redox couple, (b) schematic representation of the copolymer structure of PTMA₆₃-*b*-PS₃₅ and (c) schematic representation of a micellar poly(TEMPO)/zinc hybrid-flow battery (pHFB): the battery contains an electrochemical cell with an anode and a cathode compartment, separated by a size-exclusion membrane. Catholyte and anolyte are circulated between the electrochemical cell and the storage tanks. Zinc perchlorate is used simultaneously as anode active material and as supporting electrolyte. The micellar PTMA₆₃-*b*-PS₃₅ acts as cathode active material.

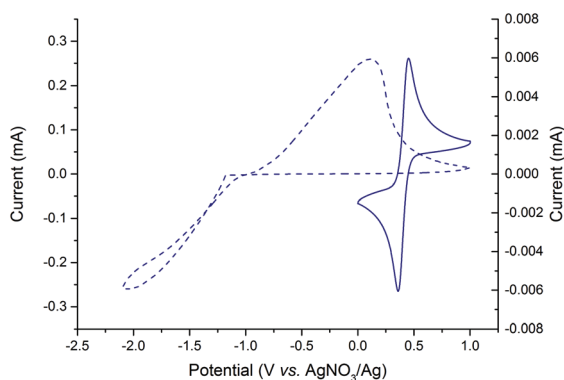


Fig. 2 Cyclic voltammogram of PTMA₆₃-*b*-PS₃₅ in EC/DMC/DEC (v:v:v 1:1:1) with 0.1 M Zn(ClO₄)₂·6H₂O as supporting electrolyte, scan rate 50 mV s⁻¹ (solid line: TEMPO⁺/TEMPO, right y-axis; dashed line: Zn²⁺/Zn⁰, left y-axis).

centration represents the maximum solubility of PTMA₆₃-*b*-PS₃₅ in the electrolyte solution and leads to a capacity of 1.2 Ah L⁻¹ and 1.6 Wh L⁻¹ at 50% state of charge (SOC). A stable battery cycling was performed in a voltage range between 0.5 and 2 V. Well-defined charge/discharge plateaus were achieved but illustrate a voltage drop of 280 mV at a current density of 1 mA cm⁻² (Fig. 4a). This effect is related to a relatively high solution resistance of 29 Ω (see Fig. S3† for EIS measurement) and the restricted ionic conductivity of the organic electrolyte, which causes a finite Zn²⁺-diffusion to the anode. This effect is also evident in the behaviour of the voltage efficiency (VE), which decreases linearly with increasing current densities. However, coulombic efficiencies (CE) above 90% were achieved for all applied current densities, with a maximum of 98% at 2 mA cm⁻². A maximal discharge capacity of 8.7 mA h was reached at 0.2 mA cm⁻², which correlates to a material utilisation of 93%. A constant discharge capacity of 6.1 mA h was attained for current densities in the

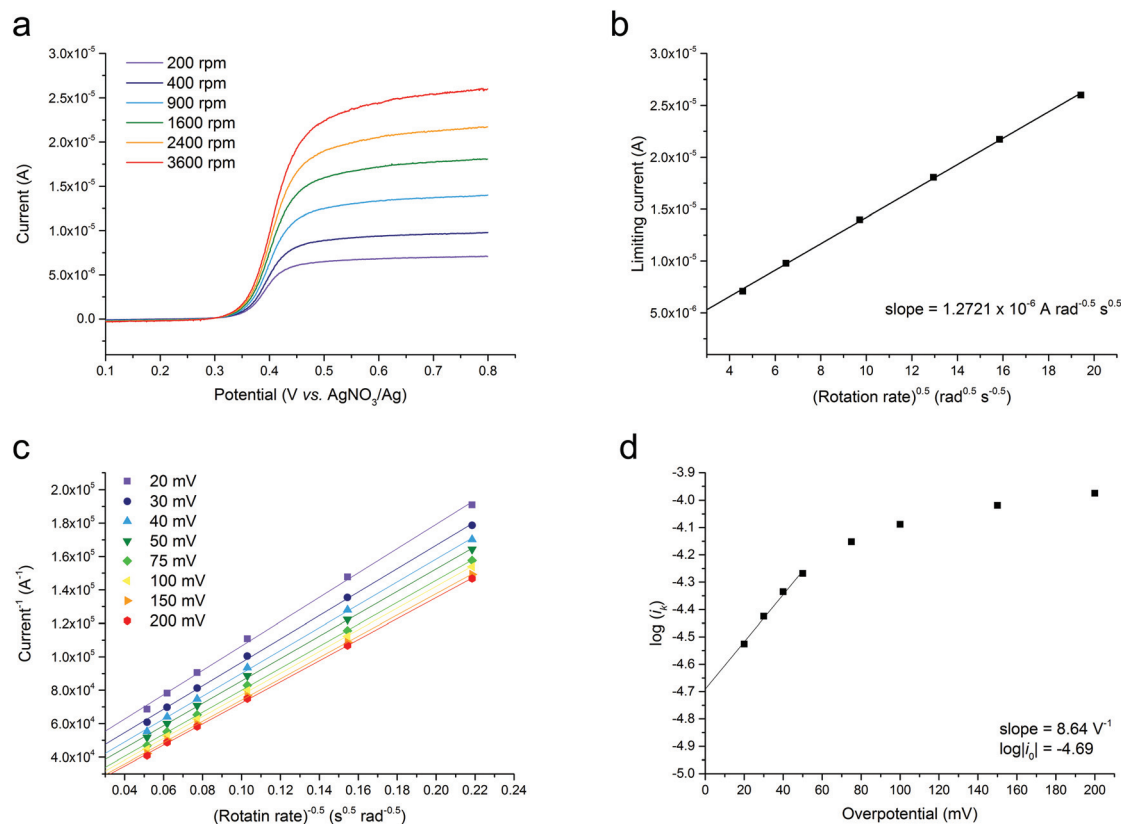


Fig. 3 Electrochemical characterisation of PTMA₆₃-*b*-PS₃₅ in EC/DMC/DEC (v:v:v 1:1:1): (a) rotating disc electrode (RDE) measurements of 1.6 mM PTMA₆₃-*b*-PS₃₅ with 0.1 M Zn(ClO₄)₂·6H₂O as supporting electrolyte at different rotation rates; (b) Levich-analysis using previously obtained limiting currents for different rotation rates; (c) Koutecký–Levich analysis and (d) Tafel-plot for different overpotentials.

range of 1 to 3 mA cm⁻² (Fig. 4b). Carbon paper is used to increase the surface area of the anode and allows the application of higher current densities. Due to the limited ionic conductivity of organic electrolytes, applicable current densities are still limited to 5 mA cm⁻². This is comparable to previously reported flow battery systems based on organic electrolytes, where maximal current densities in the range of 0.06 and 10 mA cm⁻² were achieved.^{18,22,25,26,32,33} Investigations on the reversibility of the employed redox couples were performed by long-term battery cycling in a non-pumped cell-setup at constant current of 1.5 mA cm⁻². Over 1000 consecutive charge/discharge cycles with excellent discharge capacity retention of 95% and coulombic efficiencies of 99.8% were reached (Fig. 4c). During the charging process zinc-cations are reduced at the anode to Zn_(s) and a deposit is formed onto the electrode. This led to a formation of dendrites in the long-term cycling tests (Fig. S4b†), potentially limiting the long-term stability. Additional space for the Zn⁰ deposit is required in the anode half-cell to prevent short circuits by dendrite growth through the pores of the membrane. All battery tests were conducted under regular atmosphere and neither oxygen nor traces of water lead to side reactions of the employed redox couples, despite the elevated voltage of 2 V and the low reduction potential of Zn²⁺_(aq).

Micellar structure of PTMA₆₃-*b*-PS₃₅

Rheological measurements of polymeric catholytes revealed non-Newtonian, shear thinning behaviour, for polymer concentrations of 13 mg mL⁻¹ in EC/DMC/DEC (v:v:v 1:1:1) with 0.5 M Zn(ClO₄)₂·6H₂O. A comparison of the dynamic viscosities between the micellar PTMA₆₃-*b*-PS₃₅ and a statistically distributed copolymer P(TMA-*co*-PEGMA)²⁴ (equal ratio of TEMPO active-unit and comonomer) indicates a lower viscosity of the catholyte comprising the micellar polymer in the relevant shear rate window >10⁰ s⁻¹ (Fig. 5a). Therefore, the micellar structure of the polymer has a positive effect on the overall viscosity of the electrolyte.

We also investigated the structure of the charged block copolymer micelles in solution. After the charging procedure a change of the structure was observed. Prior to charging, a Tyndall effect was observed by clouding of the catholyte (Fig. S5†). This indicates a certain agglomeration of the uncharged micelles, at a concentration of 13 mg mL⁻¹ in the applied electrolyte. After complete charging *via* chronoamperometry at 1.9 V (Fig. S6†), a clear catholyte solution was obtained. The subsequent characterisation *via* dynamic light scattering (DLS) measurements detected one population of micelles with an average apparent hydrodynamic radius

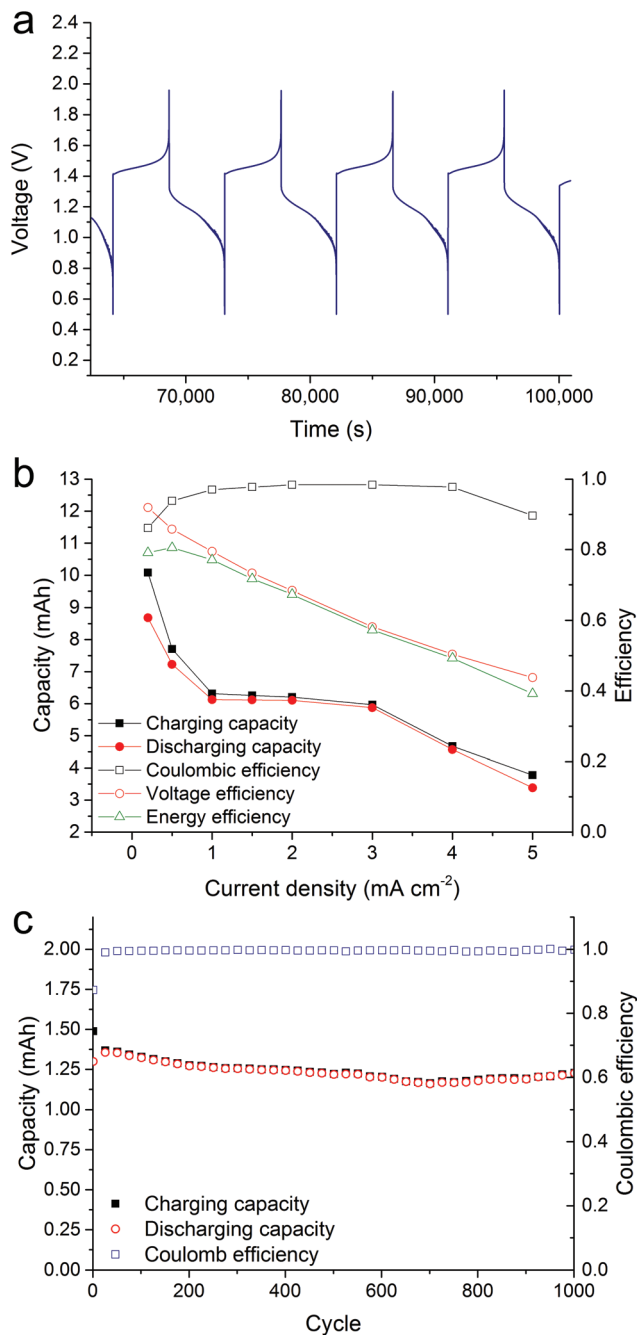


Fig. 4 Polymer/zinc hybrid-flow battery utilising PTMA₆₃-*b*-PS₃₅ as cathode active material in EC/DMC/DEC (v:v:v 1:1:1) with 0.5 M Zn(ClO₄)₂·6H₂O as supporting electrolyte and anode active material, respectively; energy density 1.6 W h L⁻¹ (a) exemplary charge/discharge curves, 1 mA cm⁻², 8 mL electrolyte per half-cell, flow rate 20 mL min⁻¹, (b) electrical performance for varied current densities, 8 mL electrolyte per half-cell, flow rate 20 mL min⁻¹, (c) long-term stability test in a non-pumped cell-setup, constant current of 1.5 mA cm⁻².

($R_{h,app}$) of 40 nm. Furthermore, the intensity weighted distribution ($R_{z,app}$) revealed two populations, one with a radius of 55 nm and a second population with a radius of 310 nm. This signal is likely induced by secondary aggregation (Fig. 5b).

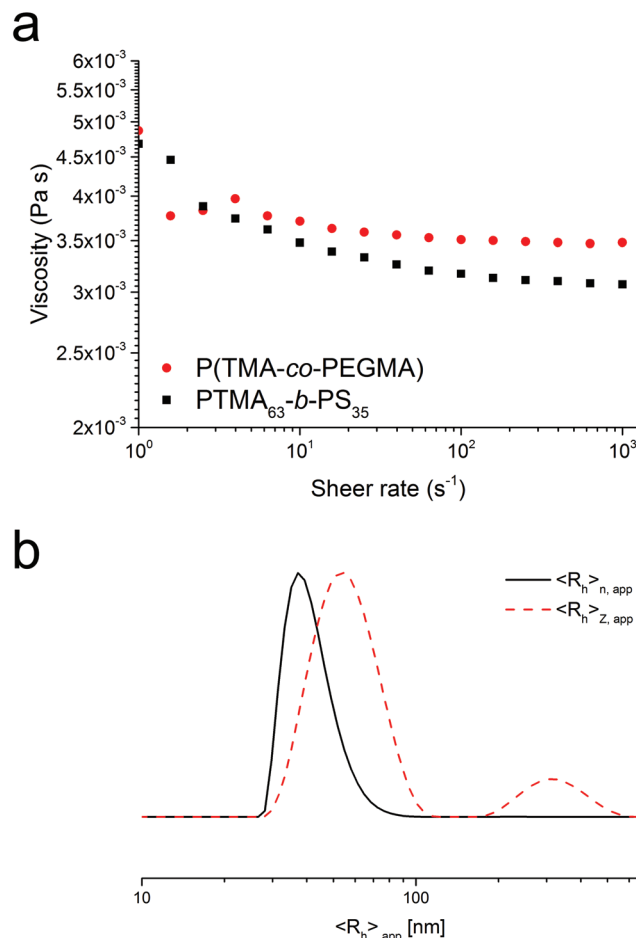


Fig. 5 (a) Rheological measurements of 13 mg mL⁻¹ PTMA₆₃-*b*-PS₃₅ and P(TMA-co-PEGMA)²⁴ in EC/DMC/DEC (v:v:v 1:1:1) with 0.5 M Zn(ClO₄)₂·6H₂O, (b) dynamic light scattering (DLS) measurement of charged PTMA₆₃-*b*-PS₃₅ micelles 13 mg mL⁻¹ in EC/DMC/DEC (v:v:v 1:1:1), distributions $\langle R_h \rangle_{n,app}$: mean number weighted and $\langle R_h \rangle_{z,app}$: mean intensity weighted distribution; the characterisation of the uncharged catholyte was not feasible due to the clouding within the electrolyte.

The enhanced solubility of the micelles after charging is induced by the positively charged corona. Additional transmission electron microscopy (TEM) images were acquired to confirm these observations. The clouded electrolyte solutions contain a large number of sheet-like structures, which are rather unstable under TEM imaging conditions (Fig. 6a). Occasionally also individual micellar structures can be found (Fig. 6b), however, the majority of the observed structures resembles the form of extended sheet-like structures. In contrast, TEM imaging of the charged micellar solution revealed the presence of a large number of individual micelles with a typical diameter of 50 to 75 nm (Fig. 6c). A zoom-in on individual micelles reveals the core-corona structure, due likely to electrolyte residues in the corona of the structures. Contrast is obscured in this case by small needle-like features, which presumably stem from the electrolyte itself (as revealed by the rather dark contrast). Next to the micellar structures larger

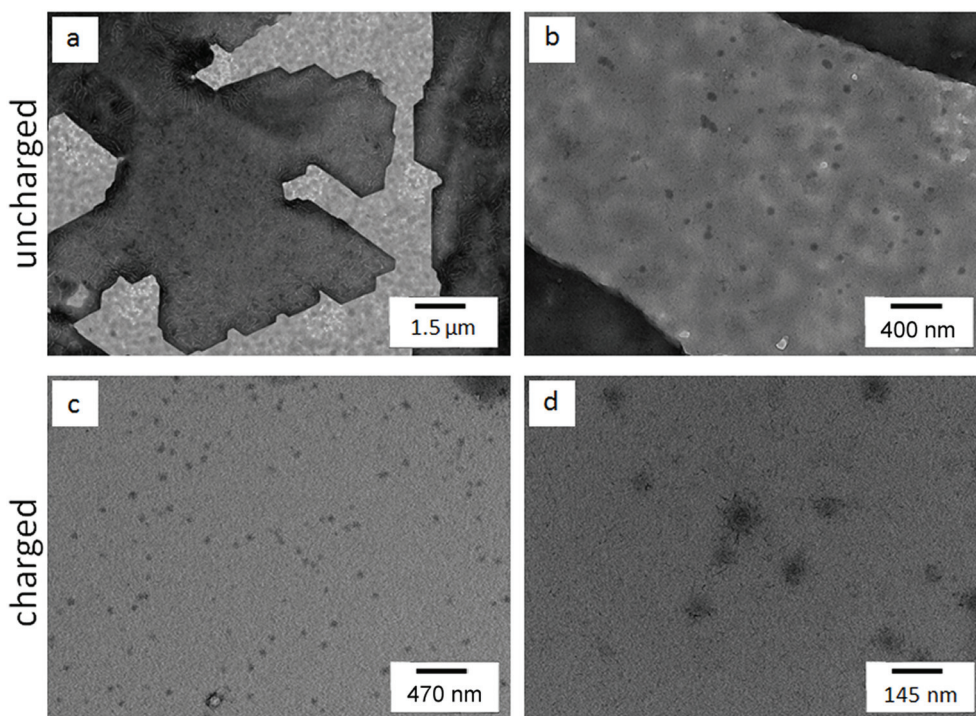


Fig. 6 Transmission electron microscopy (TEM) images of PTMA₆₃-*b*-PS₃₅ prior and after charging, 13 mg mL⁻¹ active polymer in EC/DMC/DEC (v : v : v 1 : 1 : 1) with 0.5 M Zn(ClO₄)₂·6H₂O, (a) imaging of the uncharged catholyte, (b) zoom-in of Fig. 6(a), (c) imaging of the charged catholyte, (d) zoom-in of Fig. 6(c).

aggregates with a diameter of ~ 300 nm are formed (Fig. S7a†). These were observed also by DLS measurements. Additionally, structures with a similar diameter, but an immense contrast, were observed (Fig. S7b†). It is apparent that these structures are significantly darker compared to the micellar systems, thus, it is assumed that they consist of rather heavy elements, which can be found in the electrolyte solution. Thus, it is concluded that these high contrast aggregates assemble by accumulation of the supporting electrolyte in the preparation process.

The TEMPO-containing micelles revealed excellent stability during all experiments, indicated by stable voltage curves over hundreds of charge/discharge cycles. No significant change in the micellar structure between the oxidised and neutral redox-state was observed. However, an enhanced solubility of the charged, more polar, micelles was apparent and a precipitation or proceeding formation of agglomerates can be excluded.

Conclusions

A novel type of TEMPO-containing catholyte was utilised successfully in a semi-organic polymer/zinc hybrid-flow battery (pHFB), combining the well-defined block copolymer PTMA₆₃-*b*-PS₃₅ as redox-active cathode and Zn²⁺_(aq)/Zn⁰_(s) as anode active material as well as EC/DMC/DEC (v : v : v 1 : 1 : 1) with 0.5 M Zn(ClO₄)₂·6H₂O as solvent and supporting electrolyte,

respectively. Electrochemical investigations *via* cyclic voltammetry (CV) and rotating disc electrode (RDE) measurements revealed a quasi-reversible oxidation at 0.4 V *vs.* AgNO₃/Ag, as well as a diffusion coefficient D of 1.8×10^{-7} cm² s⁻¹. The semi-organic pHFBs showed well-defined potential curves with flat charge/discharge plateaus. A stable cycling in the range of 0.5 and 2.0 V was observed with coulombic efficiencies of 99.8% and 1000 consecutive charge/discharge cycles, indicating stable and fully reversible redox reactions of the anode and cathode active material, even in the presence of oxygen and water. With increasing current densities up to 5 mA cm⁻² a linear decrease of the energy efficiency was observed. The micellar catholyte features a maximum material utilisation of 93%. Investigations on the structure of the oxidised catholyte *via* dynamic light scattering measurements (DLS) were conducted and confirmed the preservation of micellar structures for the charged polymer. Radii of 40 and 55 nm were detected for single micelles as well as a radius of 310 nm for secondary agglomerates. Transmission electron microscopy (TEM) images confirmed these observations. Micelles with a diameter in the range of 50 and 75 nm as well as agglomerates with ~ 300 nm were observed. The viscosity of the electrolyte was reduced by the utilisation of a micellar catholyte in comparison to previously reported catholytes based on linear, statistically distributed TEMPO-containing copolymers. Thus, an implementation of special shaped polymers for flow battery applications is a consequential advancement by compensating one of the largest challenges this technology has to overcome.

Acknowledgements

The authors acknowledge the European Regional Development Fund (EFRE), the Thüringer Aufbaubank (TAB), the Thuringian Ministry for Economic Affairs, Science and Digital Society (TMWWdG), the Thuringian Ministry for Education, Science, and Culture (TMBWK, #B515-10065), and the Fonds der Chemischen Industrie (FCI), as well as the support from Jena-Batteries GmbH. G. H. is grateful to FRIA for financial support. J.-F. G. acknowledges the CfB for support in the frame of the ARC 14/19-057 BATTAB. TEM facilities were funded with grants of the Deutsche Forschungsgemeinschaft (DFG) and the European Fond for Regional Development (EFRE).

Notes and references

- R. M. Darling, K. G. Gallagher, J. A. Kowalski, S. Ha and F. R. Brushett, *Energy Environ. Sci.*, 2014, **7**, 3459–3477.
- P. Alotto, M. Guarnieri and F. Moro, *Renewable Sustainable Energy Rev.*, 2014, **29**, 325–335.
- B. Dunn, H. Kamath and J.-M. Tarascon, *Science*, 2011, **334**, 928–935.
- M. Skyllas-Kazacos, M. Kazacos and R. J. C. McDermott, *Australia Pat.*, WO8905528, 1989.
- M. Skyllas-Kazacos, M. H. Chakrabarti, S. A. Hajimolana, F. S. Mjalli and M. Saleem, *J. Electrochem. Soc.*, 2011, **158**, R55–R79.
- H. Liu, Q. Xu, C. Yan and Y. Qiao, *Electrochim. Acta*, 2011, **56**, 8783–8790.
- G. Kear, A. A. Shah and F. C. Walsh, *Int. J. Energy Res.*, 2012, **36**, 1105–1120.
- B. Li, Z. Nie, M. Vijayakumar, G. Li, J. Liu, V. Sprenkle and W. Wang, *Nat. Commun.*, 2015, **6**, 6303.
- Q. Lai, H. Zhang, X. Li, L. Zhang and Y. Cheng, *J. Power Sources*, 2013, **235**, 1–4.
- S. Suresh, T. Kesavan, Y. Munaiah, I. Arulraj, S. Dheenadayalan and P. Ragupathy, *RSC Adv.*, 2014, **4**, 37947–37953.
- J.-D. Jeon, H. S. Yang, J. Shim, H. S. Kim and J. H. Yang, *Electrochim. Acta*, 2014, **127**, 397–402.
- J. H. Yang, H. S. Yang, H. W. Ra, J. Shim and J.-D. Jeon, *J. Power Sources*, 2015, **275**, 294–297.
- K. Lin, Q. Chen, M. R. Gerhardt, L. Tong, S. B. Kim, L. Eisenach, A. W. Valle, D. Hardee, R. G. Gordon, M. J. Aziz and M. P. Marshak, *Science*, 2015, **349**, 1529–1532.
- B. Huskinson, M. P. Marshak, C. Suh, S. Er, M. R. Gerhardt, C. J. Galvin, X. Chen, A. Aspuru-Guzik, R. G. Gordon and M. J. Aziz, *Nature*, 2014, **505**, 195–198.
- T. Janoschka, N. Martin, U. Martin, C. Friebe, S. Morgenstern, H. Hiller, M. D. Hager and U. S. Schubert, *Nature*, 2015, **527**, 78–81.
- J. Noack, N. Roznyatovskaya, T. Herr and P. Fischer, *Angew. Chem., Int. Ed.*, 2015, **54**, 9776–9809.
- T. Sukegawa, I. Masuko, K. Oyaizu and H. Nishide, *Macromolecules*, 2014, **47**, 8611–8617.
- X. Wei, W. Xu, M. Vijayakumar, L. Cosimbescu, T. Liu, V. Sprenkle and W. Wang, *Adv. Mater.*, 2014, **26**, 7649–7653.
- Z. Li, S. Li, S. Liu, K. Huang, D. Fang, F. Wang and S. Peng, *Electrochem. Solid-State Lett.*, 2011, **14**, A171–A173.
- A. P. Kaur, N. E. Holubowitch, S. Ergun, C. F. Elliott and S. A. Odom, *Energy Technol.*, 2015, **3**, 476–480.
- B. Yang, L. Hoober-Burkhardt, F. Wang, G. K. Surya Prakash and S. R. Narayanan, *J. Electrochem. Soc.*, 2014, **161**, A1371–A1380.
- S. H. Oh, C. W. Lee, D. H. Chun, J. D. Jeon, J. Shim, K. H. Shin and J. H. Yang, *J. Mater. Chem. A*, 2014, **2**, 19994–19998.
- Y. Zhao, S. Si and C. Liao, *J. Power Sources*, 2013, **241**, 449–453.
- T. Janoschka, S. Morgenstern, H. Hiller, C. Friebe, K. Wolkersdörfer, B. Häupler, M. D. Hager and U. S. Schubert, *Polym. Chem.*, 2015, **6**, 7801–7811.
- F. R. Brushett, J. T. Vaughey and A. N. Jansen, *Adv. Energy Mater.*, 2012, **2**, 1390–1396.
- G. Nagarjuna, J. Hui, K. J. Cheng, T. Lichtenstein, M. Shen, J. S. Moore and J. Rodríguez-López, *J. Am. Chem. Soc.*, 2014, **136**, 16309–16316.
- J. Winsberg, T. Janoschka, S. Morgenstern, S. Muench, T. Hagemann, G. Hauffman, J.-F. Gohy, M. D. Hager and U. S. Schubert, *Adv. Mater.*, 2016, DOI: 10.1002/adma.201505000.
- G. Hauffman, Q. Maguin, J.-P. Bourgeois, A. Vlad and J.-F. Gohy, *Macromol. Rapid Commun.*, 2014, **35**, 228–233.
- G. Hauffman, J. Rolland, J.-P. Bourgeois, A. Vlad and J.-F. Gohy, *J. Polym. Sci., Part A: Polym. Chem.*, 2013, **51**, 101–108.
- D. R. Lide, *CRC Handbook of Chemistry and Physics*, Taylor and Francis Group LLCT, Florence, Kentucky, USA, 2007.
- R. Naejus, R. Coudert, P. Willmann and D. Lemordant, *Electrochim. Acta*, 1998, **43**, 275–284.
- Z. Li, S. Li, S. Liu, K. Huang, D. Fang, F. Wang and S. Peng, *Electrochem. Solid-State Lett.*, 2011, **14**, A171–A173.
- W. Wang, W. Xu, L. Cosimbescu, D. Choi, L. Li and Z. Yang, *Chem. Commun.*, 2012, **48**, 6669–6671.

Electronic Supplementary Material (ESI) for Polymer Chemistry. This journal is © of The Royal Society of Chemistry 2014

Supporting information

Polymer/Zinc Hybrid-Flow Battery Using Block Copolymer Micelles featuring a TEMPO Corona As Catholyte

Jan Winsberg,^{ab} Simon Muench,^{ab} Tino Hagemann,^{ab} Sabine Morgenstern,^{ab} Tobias Janoschka,^{ab} Mark Billing,^a Felix H. Schacher,^{ab} Guillaume Hauffman,^c Jean-François Gohy,^c Stephanie Hoeppener,^a Martin D. Hager,^{ab} Ulrich S. Schubert^{ab *}

a Laboratory of Organic and Macromolecular Chemistry (IOMC), Friedrich Schiller University Jena, Humboldtstraße 10, 07743 Jena, Germany ulrich.schubert@uni-jena.de

b Center for Energy and Environmental Chemistry Jena (CEEC Jena), Friedrich Schiller University Jena, Philosophenweg 7a, 07743 Jena, Germany

c Institute of Condensed Matter and Nanoscience, Bio- and Soft Matter, Université catholique de Louvain, Louvain-la-Neuve, 1348 Belgium.

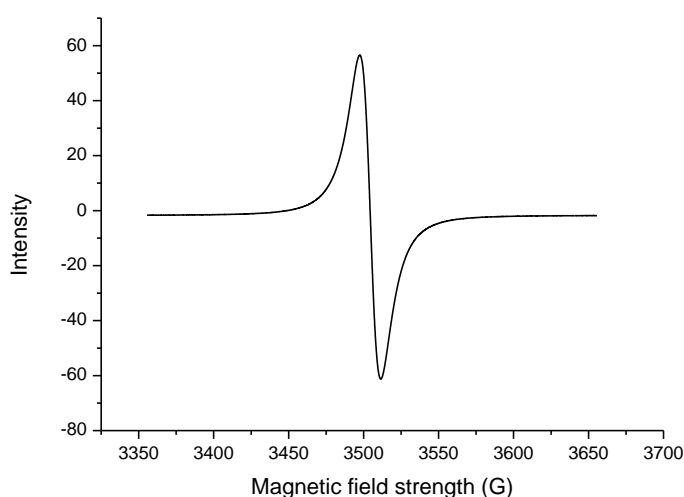


Figure S1: Electron paramagnetic resonance (EPR) measurement of PTMA₆₃-*b*-PS₃₅ in the solid state, spin count: 1.657×10¹⁸ spins mg⁻¹.

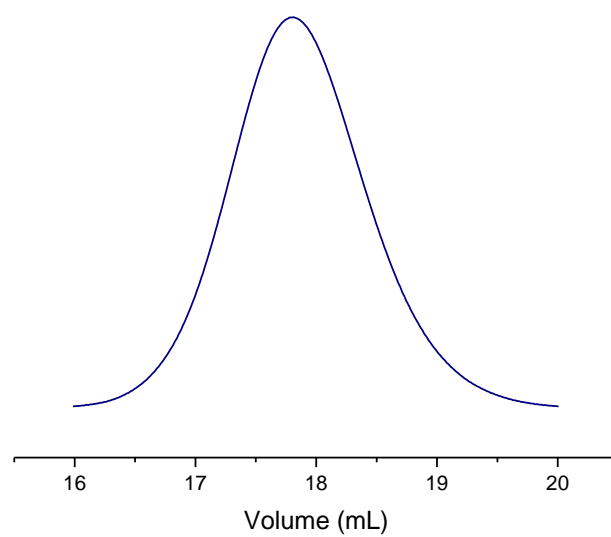


Figure S2: Size exclusion chromatography (SEC) elugram of PTMA₆₃-*b*-PS₃₅, eluent: DMAc + 0.21 wt-% LiCl, poly(styrene) standard.

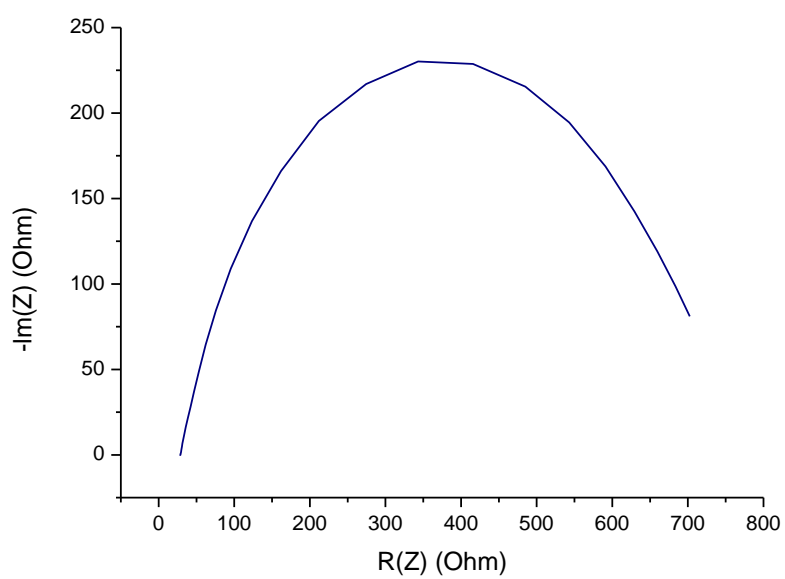
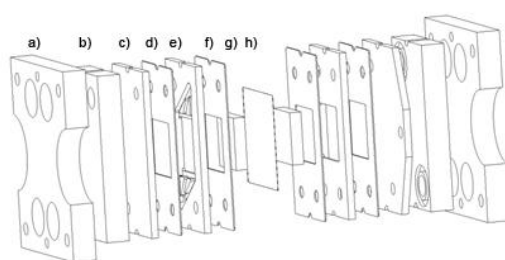


Figure S3: Electrochemical impedance spectroscopy (EIS) of a polymer TEMPO/zinc hybrid-flow battery (pHFB) between 100 mHz and 200 kHz at 0 V in potentiostatic mode.



Scheme S1: Schematic representation of the electrochemical cell. One half-cell consists of a frame (a), PTFE block with hose connections and rubber seal (b), graphite or zinc current collector (c), rubber sealing (d), PTFE flow frame (e), rubber sealing (f) and a surface enhancing graphite felt/carbon paper (g). Both half cells are separated by a size exclusion membrane (h).

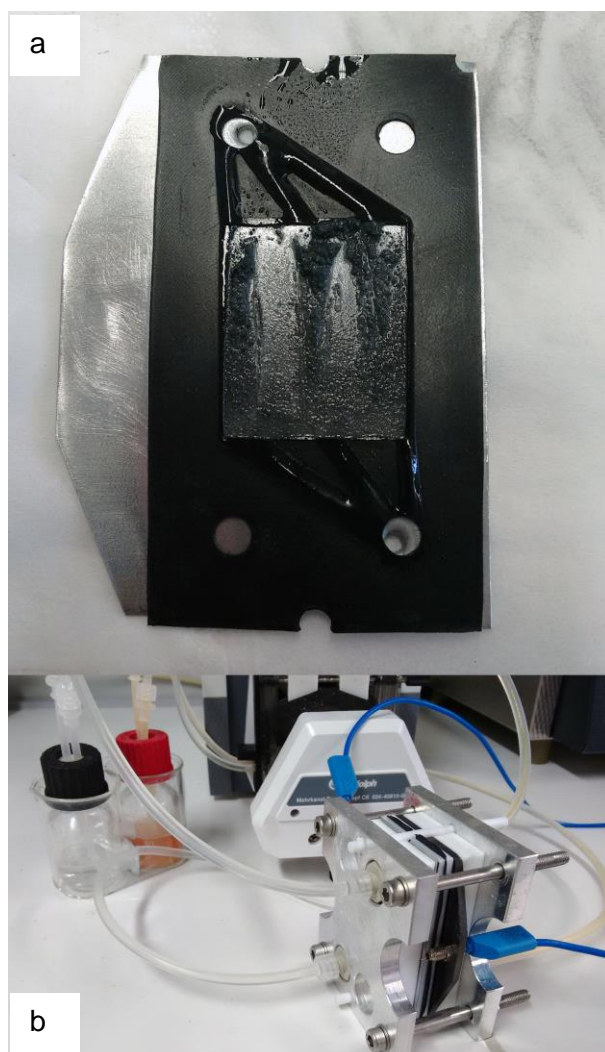


Figure S4: a) Dendrite formation inside the anode half-cell after battery cycling and b) pumped pHFB setup, comprising the electrochemical cell, two reservoir tanks (catholyte & anolyte) and a peristaltic pump.

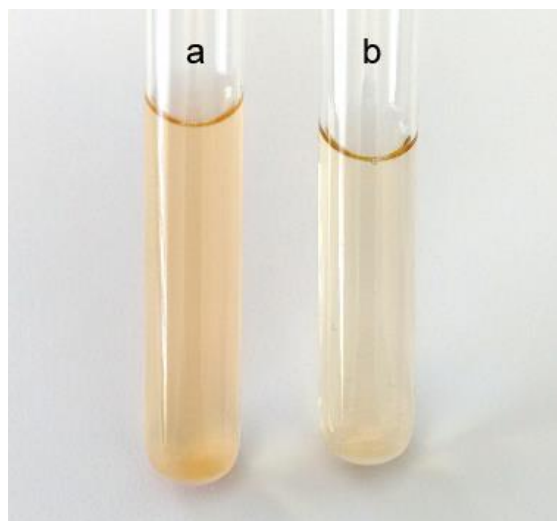


Figure S5: Micellar catholyte a) prior to charging (cloudy dispersion) and b) after charging (clear solution).

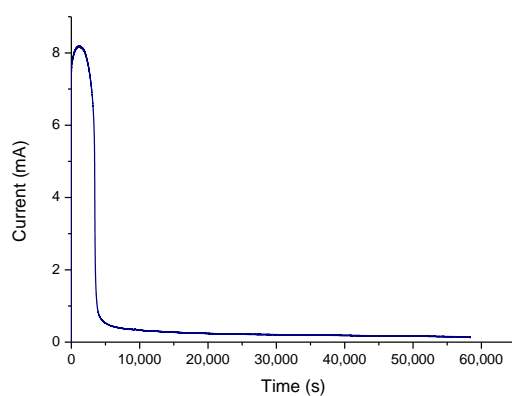


Figure S6: Chronoamperometry for charging of the pHFB, potential 1.9 V. The resulting current was measured over time.

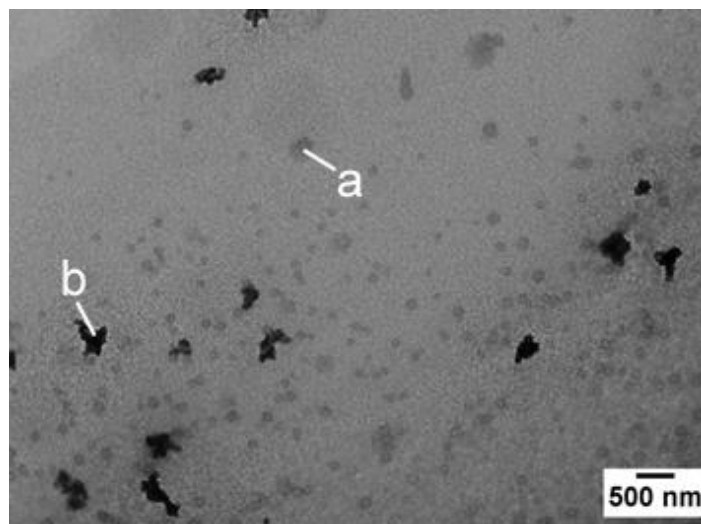


Figure S7: Transmission electron microscopy (TEM) image of PTMA₆₃-*b*-PS₃₅ after charging, catholyte: 13 mg mL⁻¹ active polymer in EC/DMC/DEC (v:v:v 1:1:1) with 0.5 M Zn(ClO₄)₂·6H₂O; secondary agglomerate ~300 nm diameter (a), high contrast agglomerate with an elevated content of heavy metal supporting electrolyte (b).

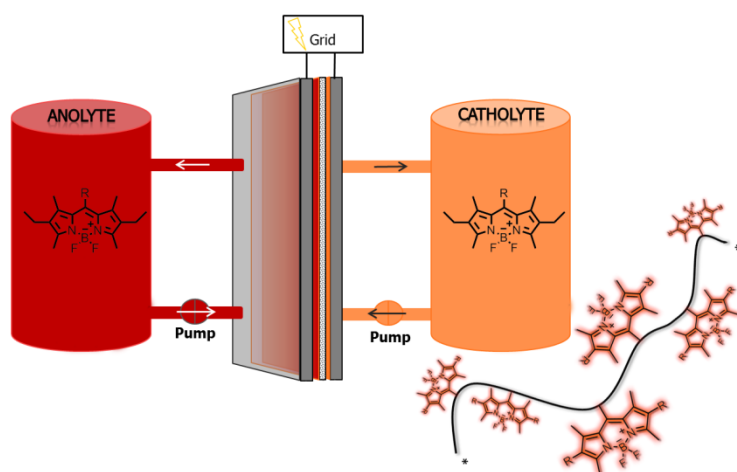
Table S1: Ion conductivity of the applied electrolyte.

Electrolyte	Ion conductivity [mS cm ⁻¹]
0.5 M Zn(ClO ₄) ₂ ·6H ₂ O	5.9

Publication P7

Poly(boron-dipyrromethene) – A redox-active polymer class for polymer redox-flow batteries

J. Winsberg, T. Hagemann, S. Muench, C. Friebe, B. Häupler, T. Janoschka, S. Morgenstern,
M. D. Hager, U. S. Schubert,
Chem. Mater. **2016**, 28, 3401-3405.



Poly(boron-dipyrromethene)—A Redox-Active Polymer Class for Polymer Redox-Flow Batteries

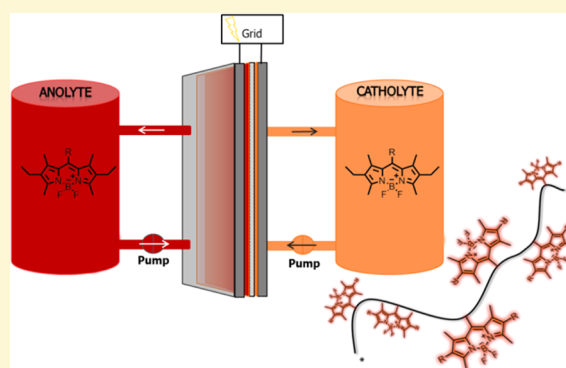
Jan Winsberg,^{†,‡} Tino Hagemann,^{†,‡} Simon Muench,^{†,‡} Christian Friebe,^{†,‡} Bernhard Häupler,^{†,‡} Tobias Janoschka,^{†,‡} Sabine Morgenstern,^{†,‡} Martin D. Hager,^{†,‡} and Ulrich S. Schubert^{*,†,‡}

[†]Laboratory of Organic and Macromolecular Chemistry (IOMC), Friedrich Schiller University Jena, Humboldtstraße 10, 07743 Jena, Germany

[‡]Center for Energy and Environmental Chemistry Jena (CEEC Jena), Friedrich Schiller University Jena, Philosophenweg 7a, 07743 Jena, Germany

Supporting Information

ABSTRACT: The utilization of boron-dipyrromethene (BODIPY) as active group for the charge storage process in a battery application is reported. Two BODIPY-containing copolymers were synthesized and electrochemically characterized. The polymers feature redox processes at 0.7 V and −1.5 V vs AgNO₃/Ag, which enable the application in a redox-flow battery setup.



The amount of electricity generated from renewable sources, like wind power and solar energy, increases year by year.^{1,2} The basis of energy supply changes from fossil fuels and nuclear power to a sustainable, renewable, and more decentralized production.^{3,4} Since most of the renewable sources cannot provide energy continuously, storage technologies are required to ensure a stable supply by closing the gap between energy production and consumption.^{5,6} One of the most promising storage technologies that fulfils these demands is the redox-flow battery (RFB).^{7–9} The development of RFBs started in the 1940s by Kangro and co-workers.¹⁰ Skyllas-Kazacos et al. improved the RFB technology by the development of the all-vanadium redox-flow battery (VRFB).^{11–13} It utilizes vanadium ions as both cathode and anode active material. Sulfuric acid serves as solvent and supporting electrolyte.¹⁴ Both half cells are separated by a proton-permeable Nafion membrane. From an ecological and economic perspective, the VRFB is not the storage technology of choice, as the toxic and expensive heavy metal and the highly corrosive electrolyte have a significant ecological impact, with regard to disposal and fabrication. Additionally, the relatively low cell voltage of <1.4 V represents a limitation of this technology. Research focused increasingly on organic redox-active materials for RFB applications,^{15–18} e.g., Potash et al. reported a symmetric RFB featuring diaminoanthraquinones as active materials, recently.¹⁹ First attempts on organic polymer RFBs were conducted by Nishide et al. proposing a polymeric TEMPO-crowded bottlebrush polymer²⁰ and by Nagarjuna et al. investigating a poly(viologen)/lithium system.²¹ A promising

next generation RFB technology, the all-organic polymer RFB (pRFB), was developed by Janoschka et al.; it utilizes water-soluble redox-active polymers as active materials in combination with an aqueous sodium chloride solution as electrolyte.²² Thus, the use of rare and expensive heavy metals can be avoided. Additionally, the Nafion membrane was replaced by a more cost-efficient dialysis membrane, derived from regenerated cellulose. However, the potential long-term capacity decay by cross contamination of cathode- and anode-active polymers (e.g., by side reactions) and a relatively low cell voltage of 1.2 V are inherent properties of this system. Additionally polymer/zinc hybrid-flow batteries were reported by us, recently.^{23,24} With the VRFB as a model, a bipolar redox-active unit that can be used as both cathode and anode active material is desired, since it reduces the synthetic effort and counteracts the long-term capacity decay by cross contamination, which then affects only the Coulombic efficiency.¹⁹ Also, a potential gap between the two redox reactions of around 2 V would be favored to achieve high power densities. Oh et al. presented the first attempt using a polythiophene-particle-based RFB,²⁵ but the conjugated polymer led to unstable cell voltages, ranging from 1 to 3 V, and agglomerated particles, which can clog flow channels in the cell stack. To overcome these drawbacks, a nonconjugated polymer solution is the material of

Received: February 12, 2016

Revised: April 15, 2016

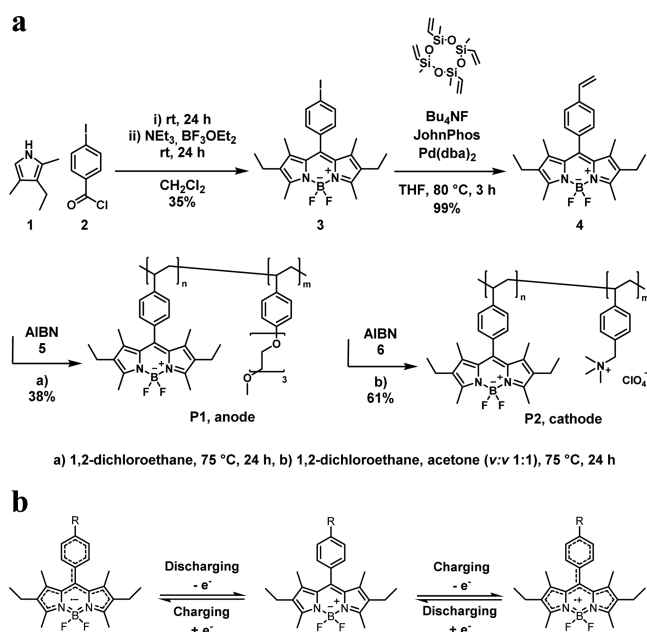
Published: May 6, 2016

choice. Boron-dipyrromethenes (BODIPYs), typically used as LASER and fluorescent dyes,^{26–28} are promising candidates for organic battery applications, because tailored BODIPY derivatives feature reversible oxidation and reduction reactions.²⁹ The potential gap between the oxidized and reduced state, as well as their stability and reversibility, can be controlled by the choice of the substituents decorating the BODIPY core.^{30,31} In comparison to other organic bipolar active groups (e.g., nitronyl nitroxides, thiophene, etc.), BODIPYs represent the best compromise with regard to the synthetic effort and voltage between the two redox reactions as well as the stability of all three redox states.

The aim of this study is the synthesis of BODIPY-containing polymers that are tailored for RFB applications, as well as the investigation of their electrochemical behavior and their ability to be utilized as active group in all-organic redox-flow batteries (see Figure S1 for a schematic representation of an all-BODIPY pRFB). The substitution of all hydrogen atoms of the BODIPY core impedes side reactions and, thus, ensures the reversibility of all redox reactions, which is mandatory for the charge storage process.

Hence, the styrene-based, alkyl-functionalized derivative **4** was used as monomer (Scheme 1). A five-step synthesis of **4**

Scheme 1. (a) Schematic Representation of the Synthesis of Monomer **4** and the Polymers **P1** and **P2** and (b) Redox Mechanism of **4**^a



^aA detailed investigation of the redox mechanism was performed earlier.³³

was recently developed by Gazon et al., with an overall yield of 7%.³⁴ We advanced the procedure toward a two-step route with an overall yield of 34%. The first step comprises the condensation of 3-ethyl-2,4-dimethylpyrrole **1** and 4-iodobenzoyl chloride **2** to an iodophenyl BODIPY derivative **3**. Subsequent Hiyama cross-coupling reaction, utilizing Pd(dba)₃ (dba = dibenzylideneacetone) as palladium source and JohnPhos ((2-biphenyl)di-*tert*-butylphosphine) as ligand, leads to the styrene-containing monomer **4**.

The capacities of pRFB electrolytes mainly depend on the solubility of the active polymer in the electrolyte and, therefore, monomer **4** was copolymerized with solubility-enhancing comonomers. The polymerizations were performed by free radical polymerization procedures and initiated by 2,2'-azo-bis-(2-methylpropionitrile) (AIBN). Relatively low molar masses ($M_n = 3\text{--}100\text{ kg mol}^{-1}$) and a good solubility were aspired. Because polar solvents, like organic carbonates, are preferred for battery applications, polymers with polar comonomers are required to increase the solubility. Thus, (vinylbenzyl)-triethylene glycol monomethyl ether (TEGST) **5**³⁵ and (vinylbenzyl)trimethylammonium perchlorate (TAS⁺t) **6** were applied as comonomers, leading to highly soluble copolymers, poly(BODIPY-*co*-TEGST) **P1** ($M_n = 17\text{ kg mol}^{-1}$, $\bar{D} = 2.3$) and poly(BODIPY-*co*-TAS⁺t) **P2** ($M_n = 4\text{ kg mol}^{-1}$, $\bar{D} = 1.5$). The compositions (determined via ¹H NMR) and molar-mass characteristics are summarized in Table 1. Both polymers differ mainly in the polarity of the comonomer unit, as TEGSt is partially negatively charged and TAS⁺t is positively charged.

Table 1. Compositions, Molar Masses, and Dispersities of the Poly(BODIPY)s **P1** and **P2** as well as of Poly(TEMPO) **P3**

polymer	comonomer	molar ratio ^a	M_n^b	M_w^b	\bar{D}	Y ^c
P1	6	0.20	17	40	2.3	0.38
P2	7	0.20	4	6	1.5	0.61
P3 ^d	n.a.	0.78	55	70	1.3	0.96

^aRatios determined via ¹H NMR spectroscopy, quotient of redox-active monomer and comonomer. ^bSEC: DMAc + 0.21 wt % LiCl, poly(styrene) standard, in kg mol⁻¹. ^cY: yield. ^dPoly(TEMPO-*co*-PEGMA)³² (see Supporting Information for synthesis procedure and schematic representation).

The electrochemical behavior of **4** was analyzed by cyclic voltammetry (CV) measurements and revealed two quasi-reversible redox reactions at -1.51 and 0.69 V vs AgNO₃/Ag in 0.1 M Bu₄NClO₄ in propylene carbonate (see Figure S2 for CV measurements and Scheme 1b for the redox mechanism). This leads to a high possible cell voltage of over 2 V for a respective battery.

Further investigations on the chemical reversibility of the redox couples were conducted via UV-vis-NIR spectro-electrochemical measurements. After oxidation to BODIPY⁺, the intensity of all characteristic absorption bands at 520, 370, and 256 nm decreases (Figure S3a). During the subsequent rereduction, all signals are restored qualitatively. This is an indication for a chemically reversible redox reaction. During the reduction reaction to BODIPY⁻, the intensity of the main absorbance signals at 521 and 371 nm decreases, and a new signal at 432 nm arises (Figure S3b). After subsequent reoxidation, the initial absorbance spectrum is re-established, confirming the stable redox behavior of the monomeric BODIPY species for both oxidation and reduction.

However, the electrochemical behavior of the polymers differs. CV measurements of **P1** and **P2** in propylene carbonate (PC) with 0.1 M Bu₄NClO₄ (Figure 1) revealed a quasi-reversible redox couple in the cathodic and anodic region. The peak splits of the redox reactions are 90 mV (**P1**) and 100 mV (**P2**); the corresponding integrals are summarized in Table S1. A linear increase of the peak current against the scan rate indicates a precipitation on the glassy carbon electrode in case of the oxidation reaction of **P1** (Figure 1a, inset). This effect

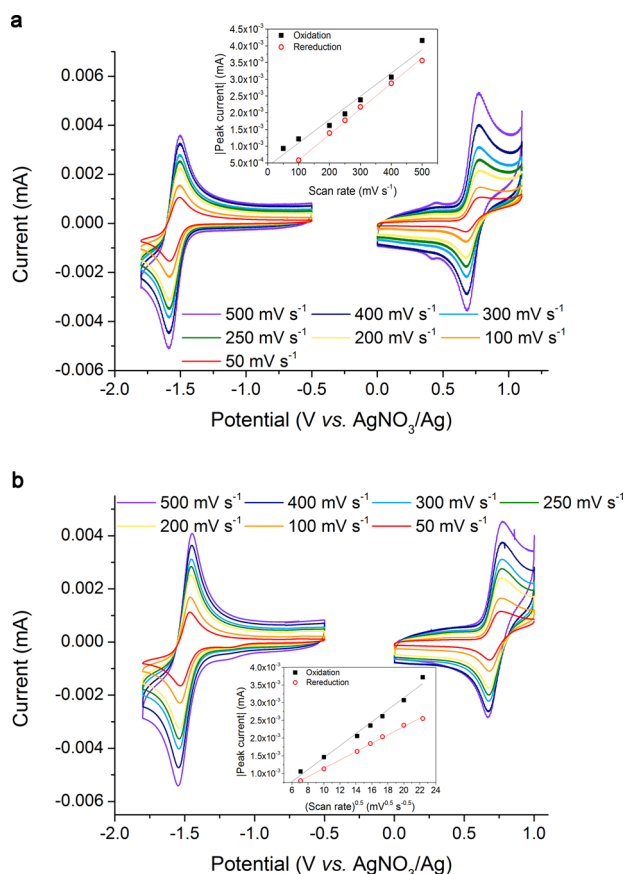


Figure 1. Cyclic voltammograms of **P1** (a) and **P2** (b) in propylene carbonate 0.1 M Bu_4NClO_4 at different scan rates. Inset: (a) peak current vs scan speed, oxidation reaction, (b) peak current vs square root of scan speed, oxidation reaction.

was not observed for **P2**, where a linear increase of the peak current vs the square root of the scan rate was observed (Figure 1b, inset). This behavior was also apparent for the reduction reaction of both polymers (Figure S4). Hence, it is assumed that **P1** is not ideally suited as cathode active material, but **P2** is an appropriate choice.

The capability of **P1** and **P2** as active material in battery applications was investigated in two static test setups (Figure S5). PC and 0.5 M Bu_4NClO_4 served as electrolyte. Cathode and anode compartment are separated by a size-exclusion membrane with a molecular weight cutoff (MWCO) of 1,000 g mol^{-1} . An all-organic pRFB comprising poly(TEMPO-*co*-PEGMA) **P3**³² (TEMPO = 2,2,6,6-tetramethylpiperidinyloxy, PEGMA = poly(ethylene glycol)methacrylate, see Supporting Information for synthesis procedure and schematic polymer structure) as catholyte and **P1** as anolyte was investigated first to study the capability of the BODIPY polymer as anode-active material. A second all-BODIPY battery, which utilized **P2** as catholyte and **P1** as anolyte, was investigated afterward.

The TEMPO/BODIPY battery (**P3/P1**) revealed well-defined charge and discharge plateaus at 2.04 and 1.82 V, respectively. The low potential voltage difference leads to a voltage efficiency (VE) of 89% and an energy efficiency (EE) of 88% (Figure 2a). A long-term stability test with 100 consecutive charge/discharge cycles showed Coulombic efficiencies of 99%, indicating good reversibility of the employed redox couples (Figure 2b). A total of 70% of initial discharge capacity could be preserved. The slowly decreasing

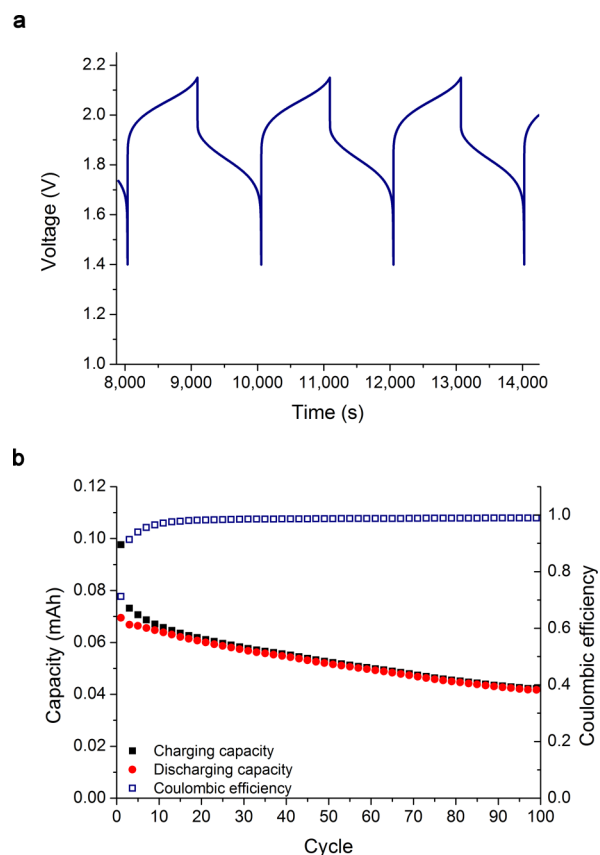


Figure 2. (a) Representative charge/discharge voltage curves of an all-organic pRFB comprising **P1** and **P3**, operating voltage in the range of 1.4 and 2.15 V, electrolyte energy density 0.5 Wh L^{-1} , cycles 3rd to 5th. (b) Long-term battery cycling, with a constant current of 0.25 mA. PC with 0.5 M Bu_4NClO_4 served as electrolyte.

discharge capacity can be attributed to a moderately proceeding electrolyte crossover. The material activity was 64 mAh L^{-1} ; an activity on this scale was expected for charge/discharge experiments in nonpumped setups, since the charging process proceeded exclusively diffusion controlled.

The applied comonomers in **P1** and **P2** are optimized for either utilization as cathode or anode active material. Therefore, an all-BODIPY battery was fabricated using **P2** as cathode and **P1** as anode active material. Flat charging plateaus at 2.06 V were observed, while the mean discharge voltage was 1.28 V. Therefore, a VE of 62% and an EE of 55% were achieved. In a long-term stability test, a discharge capacity decay of 30% was observed during an initialization period over the first 10 cycles, followed by a stable period over the next 90 cycles with steady capacity retention (Figure 3b); Coulombic efficiencies reached 89%. The material activity was 6 mAh L^{-1} . With regard to the results of the TEMPO/BODIPY RFB, the high potential difference between the charge/discharge plateaus represents an indication of a hindered rereduction of **P2** (Figure 3a), although CV measurements revealed no indication for irreversible redox processes. Further investigations on the discharge process were conducted using a three electrode setup (AgNO_3/Ag reference; Figure S6). The discharge process can be divided in two separate stages at a half-cell potential of 0.5 and 0.1 V vs AgNO_3/Ag . Nevertheless, constant discharge capacities were reached. The applied current was 0.25 mA, which was limited by the ionic conductivity of the electrolyte,

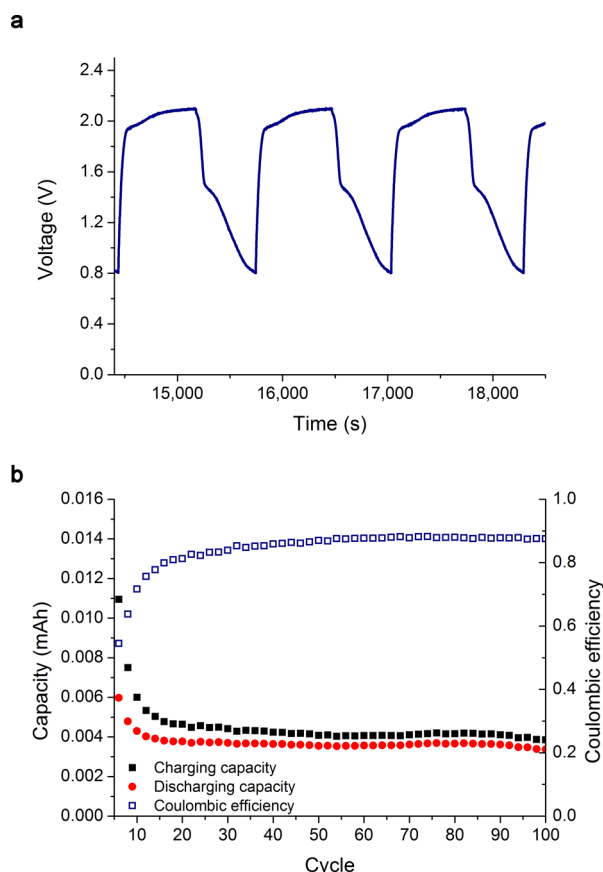


Figure 3. (a) Representative charge/discharge voltage curves of an all-BODIPY pRFB comprising **P1** and **P2**, operating voltage in the range of 0.8 and 2.1 V, electrolyte energy density 0.5 Wh L^{-1} , cycles 13 to 15. (b) Long-term battery cycling with constant current of 0.025 mA . PC $0.5 \text{ M Bu}_4\text{NClO}_4$ served as electrolyte.

but is in the typical range other systems, based on organic electrolytes, could achieve.^{16,17,19,21,36–39}

CONCLUSION

The utilization of a BODIPY compound as active group in an energy storage application was demonstrated successfully. The synthesis of the BODIPY styrene derivative **4** was improved with respect to the known literature procedure (from 7% to 34% yield). Two different BODIPY copolymers were synthesized and electrochemically characterized, and their suitability as active material in a redox-flow battery was demonstrated. Poly(BODIPY-*co*-TEGSt) **P1** and poly(BODIPY-*co*-TASSt) **P2** were synthesized and revealed good electrochemical stability. **P1** and **P2** were successfully applied in a static battery setup. The first battery utilized **P1** as anolyte and poly(TEMPO-*co*-PEGMA) **P3** as catholyte. This high-voltage, all-organic redox-flow battery shows a good Coulombic efficiency of 99% and a high average discharge voltage of 1.82 V. A second, all-BODIPY flow battery was prepared where, **P1** was utilized as anolyte and **P2** as catholyte. After a short induction phase of 10 cycles, a stable battery cycling was achieved for an additional 90 cycles. The demonstration of one bipolar copolymer, which can be used as both cathode and anode active material could not be demonstrated in the present work. Further investigations on the anodic redox reaction as well as the development of a bipolar copolymer and the application in a pumped battery would be part of future

research. Nevertheless, BODIPYs could demonstrate their capability as potential bipolar material in RFB applications, therefore being an organic alternative to all-vanadium redox-flow batteries.

ASSOCIATED CONTENT

Supporting Information

The Supporting Information is available free of charge on the ACS Publications website at DOI: [10.1021/acs.chemmater.6b00640](https://doi.org/10.1021/acs.chemmater.6b00640).

Experimental methods, synthesis procedures, a schematic representation of a pRFB, additional electrochemical measurements, and a photograph of the utilized test cell (PDF)

AUTHOR INFORMATION

Corresponding Author

*U.S.S.: Laboratory of Organic and Macromolecular Chemistry (IOMC), Friedrich Schiller University Jena, Humboldtstraße 10, 07743 Jena, Germany. E-mail: ulrich.schubert@uni-jena.de.

Author Contributions

The manuscript was written through contributions of all authors, and all authors have given approval to the final version of the manuscript.

Funding

The authors acknowledge the European Regional Development Fund (EFRE), the Thüringer Aufbaubank (TAB), the Thuringian Ministry for Economic Affairs, Science and Digital Society (TMWWdG), and the Fonds der Chemischen Industrie (FCI).

Notes

The authors declare no competing financial interest.

REFERENCES

- Gullberg, A. T.; Ohlhorst, D.; Schreurs, M. Towards a low carbon energy future – Renewable energy cooperation between Germany and Norway. *Renewable Energy* **2014**, *68*, 216–222.
- Sen, R.; Bhattacharyya, S. C. Off-grid electricity generation with renewable energy technologies in India: An application of HOMER. *Renewable Energy* **2014**, *62*, 388–398.
- Hiremath, R. B.; Shikha, S.; Ravindranath, N. H. Decentralized energy planning; modeling and application—a review. *Renewable Sustainable Energy Rev.* **2007**, *11*, 729–752.
- Ibrahim, H.; Ilinca, A.; Perron, J. Energy storage systems—Characteristics and comparisons. *Renewable Sustainable Energy Rev.* **2008**, *12*, 1221–1250.
- Lund, H. Large-scale integration of wind power into different energy systems. *Energy* **2005**, *30*, 2402–2412.
- Harsha, P.; Dahleh, M. Optimal Management and Sizing of Energy Storage Under Dynamic Pricing for the Efficient Integration of Renewable Energy. *IEEE T. Power. Syst.* **2015**, *30*, 1164–1181.
- Alotto, P.; Guarnieri, M.; Moro, F. Redox flow batteries for the storage of renewable energy: A review. *Renewable Sustainable Energy Rev.* **2014**, *29*, 325–335.
- Ha, S.; Gallagher, K. G. Estimating the system price of redox flow batteries for grid storage. *J. Power Sources* **2015**, *296*, 122–132.
- Joerissen, L.; Garche, J.; Fabjan, C.; Tomazic, G. Possible use of vanadium redox-flow batteries for energy storage in small grids and stand-alone photovoltaic systems. *J. Power Sources* **2004**, *127*, 98–104.
- Kangro, W. Verfahren zur Speicherung von elektrischer Energie. DE914264, 1949.
- Skyllas-Kazacos, M.; Kazacos, M.; McDermott, R. J. C. Vanadium Charging Cell and Vanadium Dual Battery System. WO8905528, 1989.

- (12) Rychcik, M.; Skyllas-Kazacos, M. Characteristics of a new all-vanadium redox flow battery. *J. Power Sources* **1988**, *22*, 59–67.
- (13) Kear, G.; Shah, A. A.; Walsh, F. C. Development of the all-vanadium redox flow battery for energy storage: a review of technological, financial and policy aspects. *Int. J. Energy Res.* **2012**, *36*, 1105–1120.
- (14) Skyllas-Kazacos, M.; Chakrabarti, M. H.; Hajimolana, S. A.; Mjalli, F. S.; Saleem, M. Progress in Flow Battery Research and Development. *J. Electrochem. Soc.* **2011**, *158*, R55–R79.
- (15) Huskinson, B.; Marshak, M. P.; Suh, C.; Er, S.; Gerhardt, M. R.; Galvin, C. J.; Chen, X.; Aspuru-Guzik, A.; Gordon, R. G.; Aziz, M. J. A metal-free organic-inorganic aqueous flow battery. *Nature* **2014**, *505*, 195–198.
- (16) Kaur, A. P.; Holubowitch, N. E.; Ergun, S.; Elliott, C. F.; Odom, S. A. A Highly Soluble Organic Catholyte for Non-Aqueous Redox Flow Batteries. *Energy Technol.* **2015**, *3*, 476–480.
- (17) Li, Z.; Li, S.; Liu, S.; Huang, K.; Fang, D.; Wang, F.; Peng, S. Electrochemical Properties of an All-Organic Redox Flow Battery Using 2,2,6,6-Tetramethyl-1-Piperidinyloxy and N-Methylphthalimide. *Electrochem. Solid-State Lett.* **2011**, *14*, A171–A173.
- (18) Lin, K.; Chen, Q.; Gerhardt, M. R.; Tong, L.; Kim, S. B.; Eisenach, L.; Valle, A. W.; Hardee, D.; Gordon, R. G.; Aziz, M. J.; Marshak, M. P. Alkaline quinone flow battery. *Science* **2015**, *349*, 1529–1532.
- (19) Potash, R. A.; McKone, J. R.; Conte, S.; Abruña, H. D. On the Benefits of a Symmetric Redox Flow Battery. *J. Electrochem. Soc.* **2016**, *163*, A338–A344.
- (20) Sukegawa, T.; Masuko, I.; Oyaizu, K.; Nishide, H. Expanding the Dimensionality of Polymers Populated with Organic Robust Radicals toward Flow Cell Application: Synthesis of TEMPO-Crowded Bottlebrush Polymers Using Anionic Polymerization and ROMP. *Macromolecules* **2014**, *47*, 8611–8617.
- (21) Nagarjuna, G.; Hui, J.; Cheng, K. J.; Lichtenstein, T.; Shen, M.; Moore, J. S.; Rodríguez-López, J. Impact of Redox-Active Polymer Molecular Weight on the Electrochemical Properties and Transport Across Porous Separators in Nonaqueous Solvents. *J. Am. Chem. Soc.* **2014**, *136*, 16309–16316.
- (22) Janoschka, T.; Martin, N.; Martin, U.; Friebe, C.; Morgenstern, S.; Hiller, H.; Hager, M. D.; Schubert, U. S. An aqueous, polymer-based redox-flow battery using non-corrosive, safe, and low-cost materials. *Nature* **2015**, *527*, 78–81.
- (23) Winsberg, J.; Janoschka, T.; Morgenstern, S.; Muench, S.; Hagemann, T.; Gohy, J.-F.; Hauffman, G.; Hager, M. D.; Schubert, U. S. Poly(TEMPO)/Zinc Hybrid-Flow Battery: A Novel, "Green," High Voltage, and Safe Energy Storage System. *Adv. Mater.* **2016**, *28*, 2238.
- (24) Winsberg, J.; Muench, S.; Hagemann, T.; Morgenstern, S.; Janoschka, T.; Billing, M.; Schacher, F. H.; Gohy, J.-F.; Hauffman, G.; Hoepfner, S.; Hager, M. D.; Schubert, U. S. Polymer/zinc hybrid-flow battery using block copolymer micelles featuring a TEMPO corona as catholyte. *Polym. Chem.* **2016**, *7*, 1711.
- (25) Oh, S. H.; Lee, C. W.; Chun, D. H.; Jeon, J. D.; Shim, J.; Shin, K. H.; Yang, J. H. A metal-free and all-organic redox flow battery with polythiophene as the electroactive species. *J. Mater. Chem. A* **2014**, *2*, 19994–19998.
- (26) Boens, N.; Verbelen, B.; Dehaen, W. Postfunctionalization of the BODIPY Core: Synthesis and Spectroscopy. *Eur. J. Org. Chem.* **2015**, *2015*, 6577–6595.
- (27) Kowada, T.; Maeda, H.; Kikuchi, K. BODIPY-based probes for the fluorescence imaging of biomolecules in living cells. *Chem. Soc. Rev.* **2015**, *44*, 4953–4972.
- (28) Singh, S. P.; Gayathri, T. Evolution of BODIPY Dyes as Potential Sensitizers for Dye-Sensitized Solar Cells. *Eur. J. Org. Chem.* **2014**, *2014*, 4689–4707.
- (29) Harnisch, F.; Schröder, U. P. D.; Bröring, M. P. D. Use of metal-free organonitrogen compound as redox-active substance used in redox electrolyte for energy storage accumulator, fuel cell and redox flow battery, contains two five- or six- diatomic annealed rings. DE102012015176A1, 2014.
- (30) Kim, S.; Bouffard, J.; Kim, Y. Tailoring the Solid-State Fluorescence Emission of BODIPY Dyes by meso Substitution. *Chem. - Eur. J.* **2015**, *21*, 17459–17465.
- (31) Nepomnyashchii, A. B.; Cho, S.; Rossky, P. J.; Bard, A. J. Dependence of Electrochemical and Electrogenerated Chemiluminescence Properties on the Structure of BODIPY Dyes. Unusually Large Separation between Sequential Electron Transfers. *J. Am. Chem. Soc.* **2010**, *132*, 17550–17559.
- (32) Janoschka, T.; Morgenstern, S.; Hiller, H.; Friebe, C.; Wolkersdörfer, K.; Häupler, B.; Hager, M. D.; Schubert, U. S. Synthesis and characterization of TEMPO- and viologen-polymers for water-based redox-flow batteries. *Polym. Chem.* **2015**, *6*, 7801–7811.
- (33) Nepomnyashchii, A. B.; Pistner, A. J.; Bard, A. J.; Rosenthal, J. Synthesis, Photophysics, Electrochemistry and Electrogenerated Chemiluminescence of PEG-Modified BODIPY Dyes in Organic and Aqueous Solutions. *J. Phys. Chem. C* **2013**, *117*, 5599–5609.
- (34) Gazon, C.; Rieger, J.; Méallet-Renault, R.; Charleux, B.; Clavier, G. Ultrabright Fluorescent Polymeric Nanoparticles Made from a New Family of BODIPY Monomers. *Macromolecules* **2013**, *46*, 5167–5176.
- (35) Zhao, B.; Li, D.; Hua, F.; Green, D. R. Synthesis of Thermosensitive Water-Soluble Polystyrenics with Pendant Methoxyoligo(ethylene glycol) Groups by Nitroxide-Mediated Radical Polymerization. *Macromolecules* **2005**, *38*, 9509–9517.
- (36) Huang, J.; Su, L.; Kowalski, J. A.; Barton, J. L.; Ferrandon, M.; Burrell, A. K.; Brushett, F. R.; Zhang, L. A subtractive approach to molecular engineering of dimethoxybenzene-based redox materials for non-aqueous flow batteries. *J. Mater. Chem. A* **2015**, *3*, 14971–14976.
- (37) Wei, X.; Xu, W.; Huang, J.; Zhang, L.; Walter, E.; Lawrence, C.; Vijayakumar, M.; Henderson, W. A.; Liu, T.; Cosimbescu, L.; Li, B.; Sprenkle, V.; Wang, W. Radical Compatibility with Nonaqueous Electrolytes and Its Impact on an All-Organic Redox Flow Battery. *Angew. Chem., Int. Ed.* **2015**, *54*, 8684–8687.
- (38) Takechi, K.; Kato, Y.; Hase, Y. A Highly Concentrated Catholyte Based on a Solvate Ionic Liquid for Rechargeable Flow Batteries. *Adv. Mater.* **2015**, *27*, 2501–2506.
- (39) Brushett, F. R.; Vaughey, J. T.; Jansen, A. N. An All-Organic Non-aqueous Lithium-Ion Redox Flow Battery. *Adv. Energy Mater.* **2012**, *2*, 1390–1396.

Supporting information

Poly(BODIPY) – A Redox-Active Polymer Class for Polymer Redox-Flow Batteries

Jan Winsberg,^{a,b} Tino Hagemann,^{a,b} Simon Muench,^{a,b} Christian Friebe,^{a,b} Bernhard Häupler,^{a,b} Tobias Janoschka,^{a,b} Sabine Morgenstern,^{a,b} Martin D. Hager,^{a,b} Ulrich S. Schubert^{a,b,*}

a Laboratory of Organic and Macromolecular Chemistry (IOMC), Friedrich Schiller University Jena, Humboldtstraße 10, 07743 Jena, Germany

b Center for Energy and Environmental Chemistry Jena (CEEC Jena), Friedrich Schiller University Jena, Philosophenweg 7a, 07743 Jena, Germany

Experimental

Materials: 4-Iodobenzoyl chloride (97%, Apollo Scientific), 3-ethyl-2,4-dimethyl pyrrole (97%, fused in glass ampule, TCI), boron trifluoride diethyl etherate (Aldrich), triethylamine (VWR), JohnPhos (ABCR), 2,4,6,8-tetramethyl-2,4,6,8-tetravinyl-cyclotetrasiloxane (ABCR), *bis*(dibenzylideneacetone)palladium(0) (Aldrich), tetrabutylammonium fluoride solution (1.0 M in THF, Aldrich), 4-vinylbenzyl chloride (Aldrich), triethylene glycol (VWR), propylene carbonate (anhydrous 99.7%, Aldrich), perchloric acid (70%, Aldrich) and tetrabutylammonium perchlorate (99%, Aldrich) were used as received, 2,2'-azobis(2-methylpropionitrile) (AIBN, Aldrich) was recrystallized from methanol prior to use. 4-Vinylbenzyl methoxytris(oxyethylene) ether (TEGSt) **6** was synthesized according to literature procedures.¹ Graphite felt (SGL Carbon, Germany) was cut in appropriate pieces. Dialysis membrane (SpectraPor 6, SpectrumLabs, USA) was received as pre-wetted dialysis tube, cut into squares (10×10 mm²) rinsed with deionized water, washed with dry propylene carbonate, and stored in the electrolyte solution over molecular sieves for at least 24 h.

Characterization: ¹H and ¹³C NMR measurements were performed on a Bruker RC AC 300 (300 MHz & 75 MHz) at 298 K. Chemical shifts are reported in parts per million (ppm, δ scale) referred to the residual signal of the deuterated solvent. Elemental analyses were performed using a Vario ELIII-Elementar Euro and an EA-HekaTech. Size-exclusion chromatography (SEC) was conducted on an Agilent 1200 series system (degasser, PSS; pump, G1310A; auto sampler, G1329A; oven, Techlab; DAD detector, G1315D; RI detector, G1362A; eluent, DMAc + 0.21% LiCl, 1 mL min⁻¹; temperature, 40 °C; column, PSS GRAM guard/1000/30 Å).

Electrochemical characterization: Cyclic voltammetry (CV) and charge/discharge tests were performed on a VMP3 potentiostat/galvanostat (Biologic, France). For CV

measurements, a standard three-electrode setup with a glassy-carbon disk working electrode (diameter 2 mm), a AgNO₃/Ag reference electrode for carbonate-based electrolytes and a platinum wire counter electrode was utilized. Spectro-electro-chemical experiments were performed in a quartz cuvette containing, a platinum grid working electrode, a platinum wire auxiliary electrode, and a AgCl/Ag reference electrode. The potential was controlled using a Metrohm Autolab PGSTAT30 potentiostat. The redox process was monitored by UV-vis spectroscopy using a PerkinElmer Lambda 750 UV-vis-NIR spectrophotometer and considered complete when there was no further spectral change

Battery tests: For static, non-pumped long-term charge/discharge experiments a custom-made PTFE-trough with a restrained membrane was utilized. The membrane was pinched between the two compartments. Graphite felt blocks (5×5×5 mm³) were put in the compartments and a platinum wire pierced in. One compartment was filled with 1 mL of catholyte, the other one with 1 mL of anolyte solution. Catholyte and anolyte were prepared with a concentration of 13 mg mL⁻¹ of active polymer and 0.5 M Bu₄NClO₄ in propylene carbonate. The polymers were previously dialyzed to remove oligomeric species. All measurements were carried out at 25 °C under argon atmosphere. The batteries were charged/discharged with constant current and the resulting potential was measured over time. Coulombic efficiencies were calculated by the quotient of discharging current and charging current of the same cycle, the voltage efficiency by the quotient of the mean discharging potential and the mean charging potential and the energy efficiency by the product of coulombic efficiency and voltage efficiency.

Synthesis

4,4-Difluoro-1,3,5,7-tetramethyl-2,6-diethyl-8-(4-iodophenyl)-4-bora-3a,4a,-diazas-indacene (**3**)

4-Iodobenzoyl chloride **2** (1.03 g, 3.9 mmol) was dissolved in dry CH₂Cl₂ (90 mL). The solution was deaerated with argon and 3-ethyl-2,4-dimethylpyrrole **1** (1 g, 8.1 mmol, 2.1 eq.) was added *via* a syringe. The reaction mixture was stirred at room temperature for 24 h. Triethylamine (2.5 mL, 18 mmol, 4.7 eq) and BF₃·OEt₂ (2.5 mL, 20.3 mmol, 5.2 eq) were added. After additional 24 h the reaction mixture was extracted three times with H₂O (100 mL). The organic phase was dried over MgSO₄ and the solvent removed in vacuum. The crude product was purified *via* column chromatography (eluent EtOAc:heptane, v:v, 1:1). The bright orange phase was collected. Yield: 710 mg, 36%. ¹H NMR (CD₂Cl₂, 300 MHz, ppm): δ 7.89 (d, *J* = 8.3 Hz, 2H), 7.1 (d, *J* = 8.3 Hz, 2H), 2.51 (s, 6H), 2.35 (q, *J* = 7.6 Hz, 4H), 1.37 (s, 6H), 1.01 (t, *J* = 7.6 Hz, 6H); ¹³C NMR (CDCl₃, 75 MHz, ppm): δ 154.2, 138.2,

135.4, 133.0, 130.5, 130.32, 94.5, 17.1, 14.6, 12.6, 12.0, EI-MS: m/z 506; elemental analysis: calc. C: 54.58%, H: 5.18%, N: 5.53%, found: C: 54.66%, H 5.18%, N: 5.59%.

4,4-Difluoro-1,3,5,7-tetramethyl-2,6-diethyl-8-(4-vinylphenyl)-4-bora-3a,4a,-diazas-indacene
(4)

$\text{Pd}(\text{dba})_2$ (dba = dibenzylideneacetone; 27.1 mg, 47.1 μmol), JohnPhos ((2-biphenyl)di-tert-butylphosphine; 17.7 mg, 59.3 μmol) and **3** (500 mg, 988 μmol) were dissolved in THF (5 mL) and purged with argon for 15 min. 2,4,6,8-Tetramethyl-2,4,6,8-tetravinylcyclotetrasiloxane (170.2 mg, 493.89 μmol) was added then followed by a 1 M solution of Bu_4NF in THF (1.09 mL, 1.09 mmol). The reaction mixture was purged with argon for additional 15 min and subsequently refluxed for 6 h. After cooling to room temperature, the solvent was evaporated under reduced pressure. Afterwards, the crude product was dissolved in EtOAc (50 mL) and extracted three times with H_2O (50 mL). The organic phase was dried over MgSO_4 and the solvent removed under reduced pressure. Purification of the crude product occurred *via* column chromatography on silica gel (eluent: EtOAc:Toluene, v:v, 1:1). Yield: 400 mg, 99%.

^1H NMR (CD_2Cl_2 , 300 MHz, ppm): δ 7.59 (d, J = 8.2 Hz, 2H), 7.29 (d, J = 8.1 Hz, 2H), 6.84 (dd, J = 17.7, 10.9 Hz, 1H), 5.9 (d, J = 17.7 Hz, 2H), 2.51 (s, 6H), 2.35 (q, J = 7.6 Hz, 4H), 1.37 (s, 6H), 1.01 (t, J = 7.5 Hz, 6H); ^{13}C NMR (CDCl_3 , 75 MHz, ppm): δ 153.8, 140.0, 138.4, 137.9, 136.3, 132.8, 130.8, 128.6, 126.8, 114.8, 17.1, 14.6, 12.5, 11.9; HR-ESI-MS: calculated m/z 429.2288, found m/z 429.2289, molecular formula $[\text{C}_{25}\text{H}_{29}\text{BF}_2\text{N}_2]^{\text{Na}+}$.

(Vinylbenzyl)trimethylammonium perchlorate (TAS_t) (7)

(Vinylbenzyl)trimethylammonium chloride (1 g, 6.55 mmol) was dissolved in H_2O (100 mL) and HClO_4 (5.6 mL, 65 mmol) was added. The precipitate was filtered off, washed with H_2O (3×50 mL), and dried under reduced pressure. Yield: 1.53 g, 86%.

^1H NMR (MeCN-d_3 , 300 MHz, ppm): δ 7.53 (dd, J = 30.2, 8.1 Hz, 4H), 6.81 (dd, J = 17.6, 11.0 Hz, 1H), 5.92 (d, J = 17.6 Hz, 1H), 5.38 (d, 11.0 Hz, 1H), 4.41 (s, 2H), 3.02 (s, 9H), ^{13}C NMR (CDCl_3 , 75 MHz, ppm): δ 139.8, 135.8, 133.2, 127.0, 126.8, 117.4, 115.9, 68.9, 52.3; ESI-MS: m/z 176.14.

Poly(BODIPY-co-TEGSt) **P1**

Monomer **4** (22 mg, 63 μmol), comonomer **6** (17.5 mg, 63 μmol) and AIBN (1 mg, 6 μmol) were dissolved in 1,2-dichloroethane (500 μL). The reaction solution was purged with argon until the volume was reduced to 100 μL and subsequently heated up to 75 $^{\circ}\text{C}$ for 24 h. After cooling to room temperature the polymer was precipitated from cold heptane, the solvent was decanted and the polymer dried under reduced pressure. Purification occurred *via* dialysis (acetone:acetone) using dialysis tubes with a molecular-weight cut-off of 1,000 g mol^{-1} . Yield: 38%

^1H NMR (CD_2Cl_2 , 300 MHz, ppm): δ 7.33-6.25 (br, 20H), 4.62-4.21 (br, 8H), 3.83-3.17 (br, 60H), 2.67-2.40 (br, 6H), 2.7-0.14 (br, 37H); SEC (DMAc + 0.21 wt-% LiCl, poly(styrene) standard): $M_n = 16,900 \text{ g mol}^{-1}$, $M_w = 39,600 \text{ g mol}^{-1}$, $\bar{D} = 2.3$.

Poly(BODIPY-co-TASSt) **P2**

Monomer **4** (50 mg, 123 μmol), comonomer **7** (135 mg, 492 μmol) and AIBN (5 mg, 31 μmol) were dissolved in 1,2-dichloroethane and acetone (2.6 mL, v:v, 5:8). The reaction solution was deaerated *via* three freeze-pump-thaw cycles and subsequently heated to 75 $^{\circ}\text{C}$ for 24 h. After cooling to room temperature the polymer was precipitated from cold heptane, the solvent was decanted, and the polymer dried under reduced pressure. Purification occurred *via* dialysis (acetone:acetone) using dialysis tubes with a molecular-weight cut-off of 1,000 g mol^{-1} . Yield: 61%

^1H NMR (MeCN-d_3 , 300 MHz, ppm): δ 7.52-6.37 (br, 19H), 4.69-4.16 (br, 9H), 3.41-2.77 (br, 36H), 2.43-2.08 (br, 19H) 1.89-0.7 (br, 19H); SEC (DMAc + 0.21 wt-% LiCl, poly(styrene) standard): $M_n = 3,900 \text{ g mol}^{-1}$, $M_w = 5,800 \text{ g mol}^{-1}$, $\bar{D} = 2.3$.

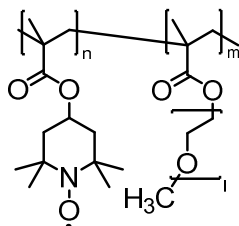
Poly(TMA-co-PEGMA) was synthesized according to literature.² An exemplary synthesis procedure as follows:

Poly(2,2,6,6-tetramethylpiperidin-4-yl methacrylate-co-poly(ethylene glycol) methyl ether methacrylate)

In a representative example for the precursor polymer of **P3**, 2,2,6,6-tetramethylpiperidin-4-yl methacrylate (100 g; 443.8 mmol) and poly(ethylene glycol) methyl ether methacrylate (57.06 g; 126.8 mmol) as well as 2-cyano-2-butyl dithiobenzoate (895.3 mg; 3.8 mmol) and 4,4'-azobis(4-cyanovaleric acid) (533.1 mg; 1.9 mmol) were dissolved in a mixture of methanol and water (3:1; 380 mL). The mixture was deaerated by flushing with argon for 20 min and subsequently stirred at 70 $^{\circ}\text{C}$ for 24 h, after which full monomer conversion was achieved. The reaction mixture was used for the subsequent oxidation without further purification.


General procedure for preparation of **P3** (oxidation)

To the reaction mixture, three equivalents hydrogen peroxide (30%) and 0.03 equivalents sodium tungstate dihydrate were added. The mixture was stirred for 24 h at room temperature and subsequently dialyzed against water. The solvent was removed by lyophilization to yield the polymer as orange powder.



Scheme 1: Schematic representation of the chemical structure of P3.

R = polymeric backbone



electrochemical cell with an anode- and a cathode compartment, which are separated by a size-exclusion membrane. Catholyte and anolyte contain the BODIPY-functionalized polymer, acting as active material, as well as a conductive additive. The electrolytes are circulated between the electrochemical cell and the storage tanks. In the catholyte BODIPY is oxidized to BODIPY⁺ and in the anolyte it is reduced to BODIPY⁻.

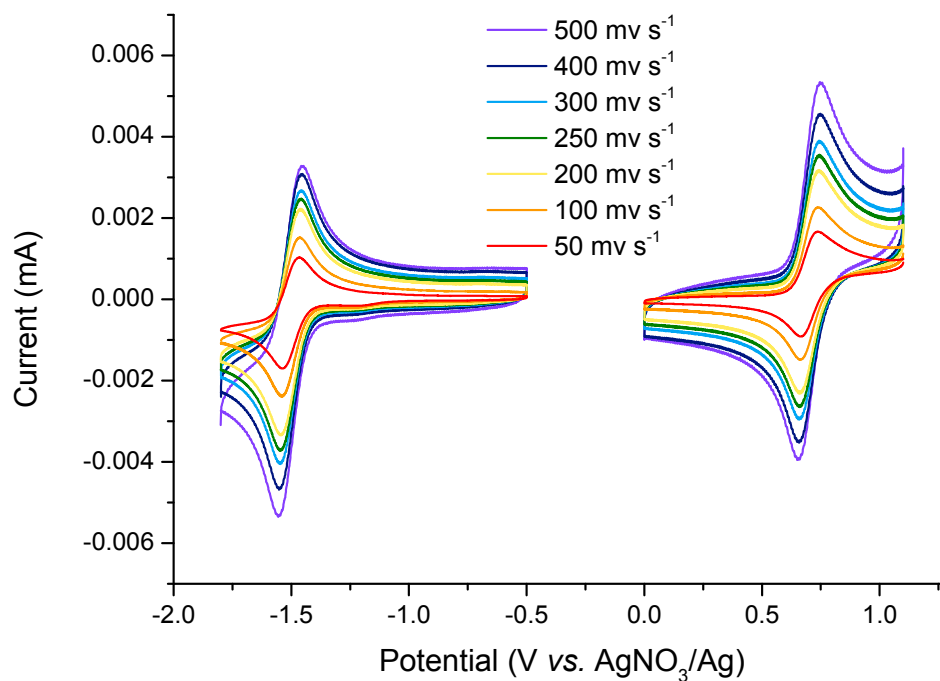


Figure S2: Cyclic voltammogram of BODIPY monomer **4** in PC 0.1 M TBAClO₄ at different scan rates.

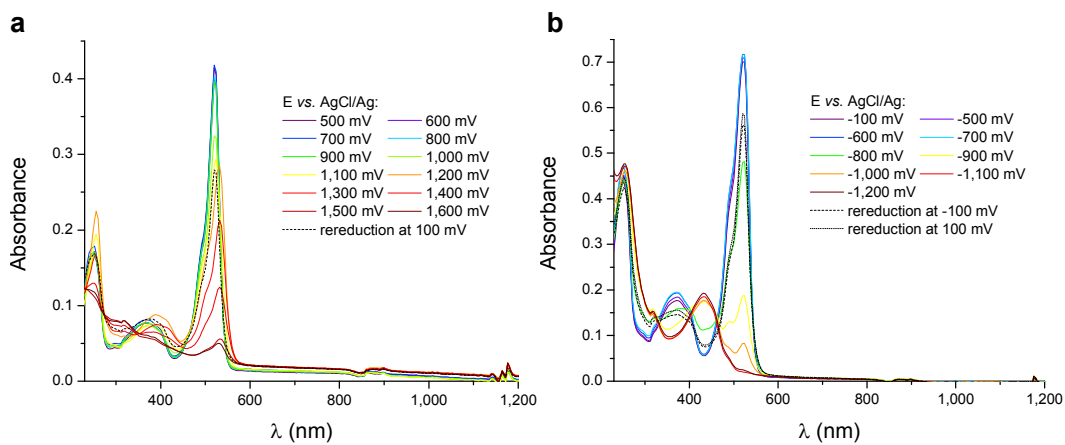


Figure S3: Spectro-electro-chemical measurements of the BODIPY monomer **4** in CH₂Cl₂ with 0.1 M TBAClO₄.

Table S1: Integrals of the redox peaks of **P1** and **P2** at a scan rate of 500 mV s⁻¹.

Polymer	Reaction	Integral (10 ⁻³ mC)
P1	Oxidation	1.22
P1	Re-reduction	1.11
P1	Reduction	1.10
P1	Re-oxidation	1.19
P2	Oxidation	0.88
P2	Re-reduction	0.85
P2	Reduction	1.25
P2	Re-oxidation	1.66

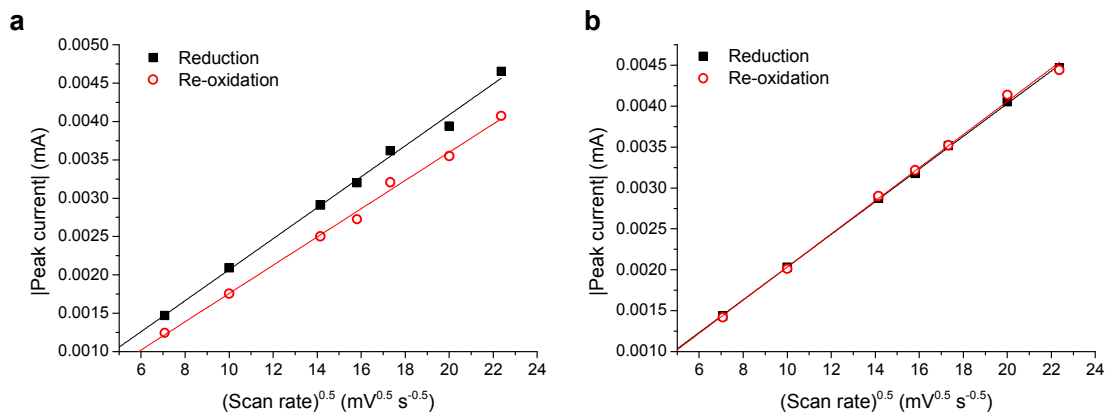


Figure S4: Absolute value of peak current against square root of scan speed of the reduction and re-oxidation reaction of (a) **P1** and (b) **P2**.

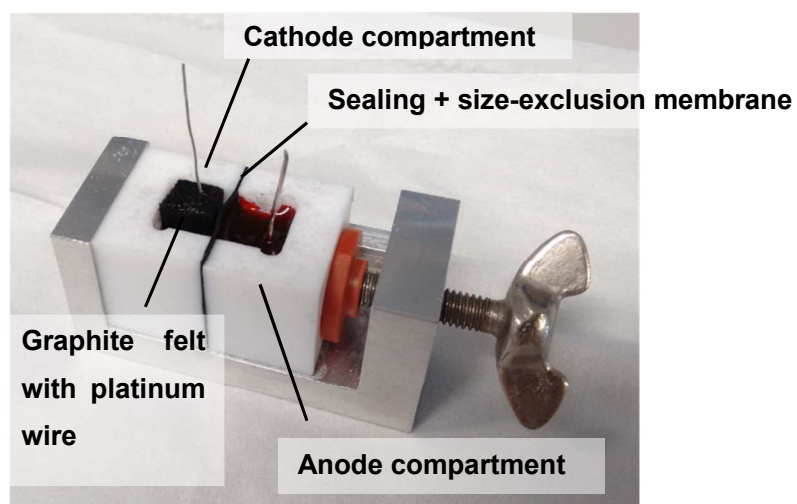


Figure S5: Photograph of the custom-made PTFE trough. The membrane can be pinched between the two sections.

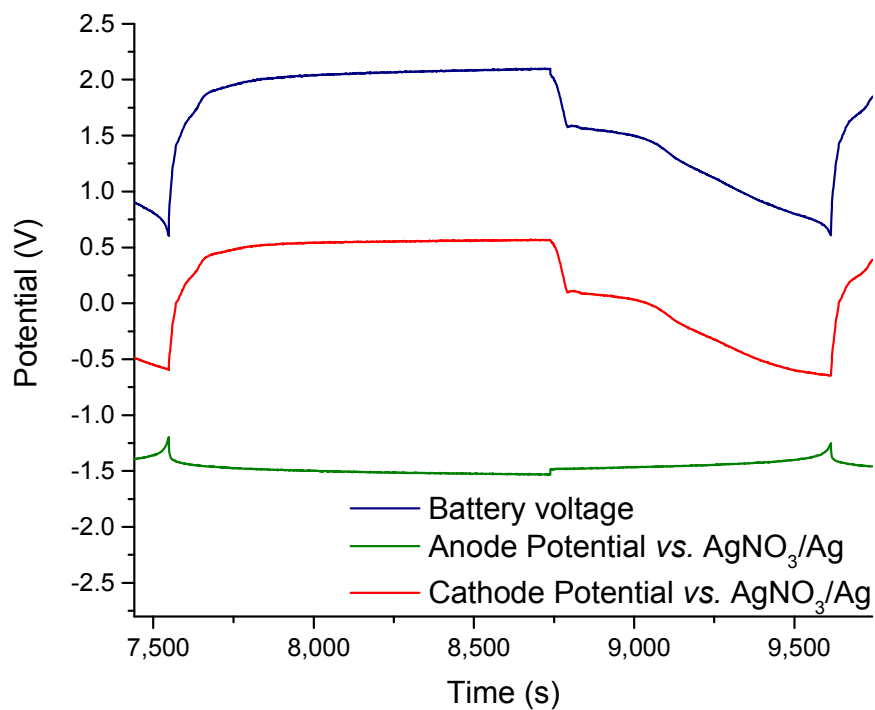


Figure S6: Discharging of an all-BODIPY **P1/P2** battery. Cathode and anode potentials are measured vs. AgNO_3/Ag .

References

1. Zhao, B.; Li, D.; Hua, F.; Green, D. R., Synthesis of Thermosensitive Water-Soluble Polystyrenics with Pendant Methoxyoligo(ethylene glycol) Groups by Nitroxide-Mediated Radical Polymerization. *Macromolecules* **2005**, *38*, 9509-9517.
2. Janoschka, T.; Morgenstern, S.; Hiller, H.; Friebe, C.; Wolkersdorfer, K.; Hapler, B.; Hager, M. D.; Schubert, U. S., Synthesis and characterization of TEMPO- and viologen-polymers for water-based redox-flow batteries. *Polymer Chemistry* **2015**, *6*, 7801-7811.